Heteromultivalent Glycomacromolecules Targeting Galectin-3

Inaugural-Dissertation

for the attainment of the title of doctor
in the Faculty of Mathematics and Natural Sciences
at the Heinrich Heine University Düsseldorf

presented by

Tanja Freichel
from Merzig

Düsseldorf, October 2019

From the Institute of Organic Chemistry and Macromolecular Chemistry
at the Heinrich Heine University Düsseldorf

Published by permission of the Faculty of Mathematics and Natural Sciences at the Heinrich Heine University Düsseldorf

Supervisor: Prof. Dr. Laura Hartmann
Co-supervisor: Prof. Dr. Jörg Pietruszka

Date of the oral examination: 28.10.2019

Statutory declaration

"I, Tanja Freichel, declare under oath that I have compiled my dissertation independently and without any undue assistance by third parties under consideration of the 'Principles for the Safeguarding of Good Scientific Practice at Heinrich Heine University Düsseldorf'".

Eidesstattliche Erklärung

„Ich, Tanja Freichel, versichere an Eides Statt, dass die Dissertation von mir selbständig und ohne unzulässige fremde Hilfe unter Beachtung der „Grundsätze zur Sicherung guter wissenschaftlicher Praxis an der Heinrich-Heine-Universität Düsseldorf" erstellt worden ist."

Düsseldorf,

Tanja Freichel

Table of Contents

Abstract

Protein-carbohydrate interactions are fundamental for various biochemical processes including cell-cell communications, cell proliferation and pathogen recognition. Dysregulated protein expression or changes in carbohydrate modifications are the cause for many diseases, and these changes can be used to develop new therapies to treat diseases such as cancer or viral infections.

The interaction of carbohydrates and proteins is generally quite weak, but nature overcomes this limitation by the presentation of different types of carbohydrates in multiple copies, a concept known as multivalency. This concept becomes the basis for the development of glycomimetic ligands, where multiple small fragments of naturally occurring larger oligo- or polysaccharide ligands are attached on a synthetic scaffold such as polymer chains, dendrimers or nanoparticles. Recently, Hartmann and coworkers introduced the synthesis of monodisperse, sequence-controlled oligo(amidoamines) as scaffolds for the multivalent presentation of carbohydrates to obtain glycomimetic ligands targeting bacterial and viral receptors. The high level of structural control in combination with straightforward variations of the structural parameters such as valency, ligand spacing and scaffold composition, have made these glycomacromolecules suitable model compounds to gain further insights into the fundamental aspects of multivalent interactions for the future development of new therapeutic approaches.

In this thesis, the platform of sequence-controlled oligo(amidoamines) is extended towards the development of glycomimetics targeting the tumor-associated carbohydrate recognizing receptor galectin-3, a lectin that is known to play an important role in *e.g.* tumor migration. More specifically, in order to obtain high affinity and potentially selective ligands, a new synthetic strategy was developed to give access to heteromultivalent glycomacromolecules combining glycosidic and non-glycosidic motifs.

In the first part of this thesis, a new functional building block, methyl-succinyl diethylenetriamine succinic acid (MDS), carrying a protected carboxylic side chain was developed. The design of MDS was inspired by other established building blocks based on a diethylenetriamine core (Fig. 1; A). After the first successful use in solid phase synthesis, the new building block was optimized for the implementation of a new conjugation reaction, the Staudinger ligation. The carboxylic side chain of MDS was used for the first

time for the Staudinger ligation with an azido-carbohydrate resulting in an amide-bond formation on solid support. This approach was then combined with the copper-catalyzed alkyne-azide cycloaddition (CuAAC) in an orthogonal conjugation approach as a method for the synthesis of heteromultivalent glycomacromolecules (Fig.1; B).

In the second part of this thesis, MDS was applied in the synthesis of lactose-functionalized homo- and heteromultivalent glycooligomers for studying their ability to bind to galectin-3 (Fig.1; C). The first generation of homomultivalent lactose-functionalized oligomers varying in the number and distance of carbohydrate ligands was evaluated via enzyme-linked immunosorbent assay (ELISA)-type and surface plasmon resonance (SPR) inhibition studies for galectin-3 interactions. In line with previous studies, an increase in valency from mono- to hexavalent showed a clear increase in binding. Additionally, through variations of both, distancing of lactose ligands along the scaffold as well as the linker between ligand and scaffold, an increase in binding was observed with decreasing density of the lactose-moieties. Based on the findings from this work, a first series of lactose-functionalized oligomers was conjugated onto lipids and used for multivalent presentation on liposomes by Miriam Hoffmann, showing a further increase in binding with nanomolar affinities. Such glycooligomer-functionalized liposomes could thus be used in the future for targeted drug delivery applications.

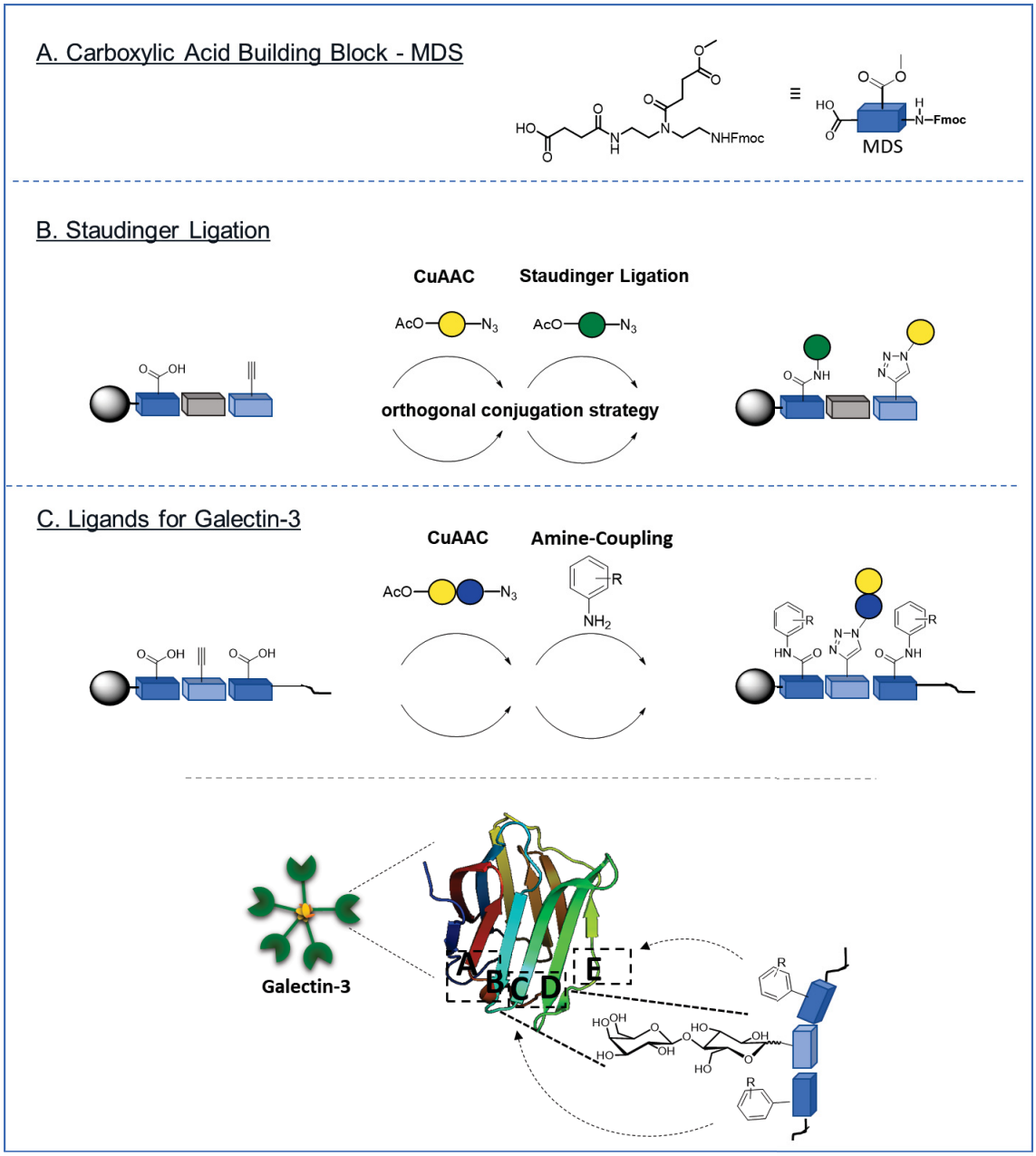

Figure 1: Schematic overview of the strategies established in this thesis. A. Structure of the new building block carrying a protected carboxylic acid side chain. B. Combination of the Staudinger ligation and the CuAAC for the orthogonal synthesis of heteromultivalent glycomacromolecules. C. Combination of the CuAAC and amine-coupling of non-glycosidic side chains for the synthesis of galectin-3 ligands and their potential site of action.

Extending on this first series of galectin-3 ligands, a second generation of ligands combining lactose and non-glycosidic-motifs was synthesized through the combination of a MDS building block for amide-coupling and the alkyne building block TDS for the CuAAC. Here, the carboxy-functionalized building block was used for the conjugation of amine-functionalized non-

glycosidic, aromatic moieties. In doing so, this building block was once more used in an orthogonal conjugation strategy for the conjugation of different phenyl-residues carrying different amine-, sulfonic acid- and hydroxy-group functionalities. Inhibition studies showed an enhanced binding for all heteromultivalent glycomacromolecules compared to their homomultivalent analogues. Comparing the different non-glycosidic motifs, sulfonic acid derivatives achieved the best binding with IC_{50} values in the lower micromolar range.

Based on these encouraging results, selected heteromultivalent glycomacromolecules were applied to human cancer cells in whole-cell assays in the third part of this thesis. In addition to toxicological (MTT), uptake (flow cytometry) and localization (fluorescence microscopy) studies, migration assays were performed with a galectin-3 positive MCF 7 breast cancer cell line using a "wound-healing" assay. Here, a slower cell-migration was observed after the treatment with glycomacromolecules in accordance with the galectin-3 avidity trend observed in the inhibition studies. This trend, in addition to results from control experiments, favors the hypothesis that galectin-3 inhibition is responsible for the delay, demonstrating for the first time, a selective biological outcome on human cells for this class of glycomacromolecules.

To summarize, in this thesis, the implementation of new synthetic strategies and their application for the synthesis of homo- and heteromultivalent lactose-functionalized glycomacromolecules was demonstrated. The obtained glycomimetics were subsequently used as ligands targeting the tumor-associated protein galectin-3. For the first time, the potential of those structures was demonstrated in whole-cell assays, which could be the basis for further cell studies and the development of glycomacromolecules as therapeutics.

Kurzzusammenfassung

Die Wechselwirkung von Proteinen und Kohlenhydraten ist die Grundlage vieler biochemischer Prozesse wie der Zell-Zell-Kommunikation, Zell-Proliferation und der Erkennung von Pathogenen. Die Ursache vieler Krankheiten liegt daher in einer Störung der Protein-Expression oder in einer Änderung der Kohlenhydrate-Modifikation von Glykoproteinen. Nichtdestotrotz, können die Wechselwirkungen zwischen Proteinen und Kohlenhydraten auch als Basis für die Entwicklung neuer Therapien zur Behandlung von Krebs oder viralen Infektionen genutzt werden.

Die Wechselwirkung zwischen Proteinen und Kohlenhydrat-Resten ist generell eher schwach, wird in der Natur jedoch durch die Präsentation verschiedener Typen von Kohlenhydraten und der vielfachen Präsentation dieser Liganden, auch Multivalenz genannt, erhöht. Auf diesem Konzept basierend können auch synthetische Glykoliganden entwickelt werden, welche in vielfacher Ausführung, kleine Fragment-Strukturen der natürlich-vorkommenden größeren Polysaccharide auf einem synthetischen Gerüst, wie Polymerketten, Dendrimeren oder Nanopartikeln, präsentieren. In diesem Kontext hat die Gruppe um L. Hartmann eine Strategie zur Synthese von monodispersen, sequenz-kontrollierten Oligo(amidoaminen), als synthetische Gerüste für die multivalente Präsentation von Kohlenhydraten zur Entwicklung von Glykomimetika für Anwendung auf bakteriellen und viralen Rezeptor-Proteinen, etabliert. Durch die hohe Kontrolle über die Struktur dieser Glykomimetika bei der gleichzeitig gegebenen Möglichkeit der einfachen Variation strukturrelevanter Parameter, wie der Valenz, dem Abstand der präsentierten Liganden und der Gerüst-Zusammensetzung, stellen diese Glykomakromoleküle geeignete Modellverbindungen dar, um weitere Einblicke in die grundlegenden Aspekte dieser multivalenten Wechselwirkung zu erhalten und darauf basierend potentielle neue Therapie-Anwendungen zu entwickeln.

In dieser Arbeit wurde daher die Plattform zur Synthese sequenz-kontrollierter Oligo(amidamine) für die Entwicklung von Glykomimetikern zur Anwendung auf Tumor-assoziierte Kohlenhydrate-Rezeptoren, insbesondere Galectin-3, welches beispielsweise eine Rolle bei der Migration von Tumorzellen spielt, erweitert. Des Weiteren wurde eine neue Synthesestrategie entwickelt, um den Zugang zur Synthese von heteromultivalenten Glykomakromolekülen, welche sowohl glykosidische als auch nicht-glykosidische Reste enthalten, zu ermöglichen und somit hoch-affine und potentiell selektive Liganden zu erhalten.

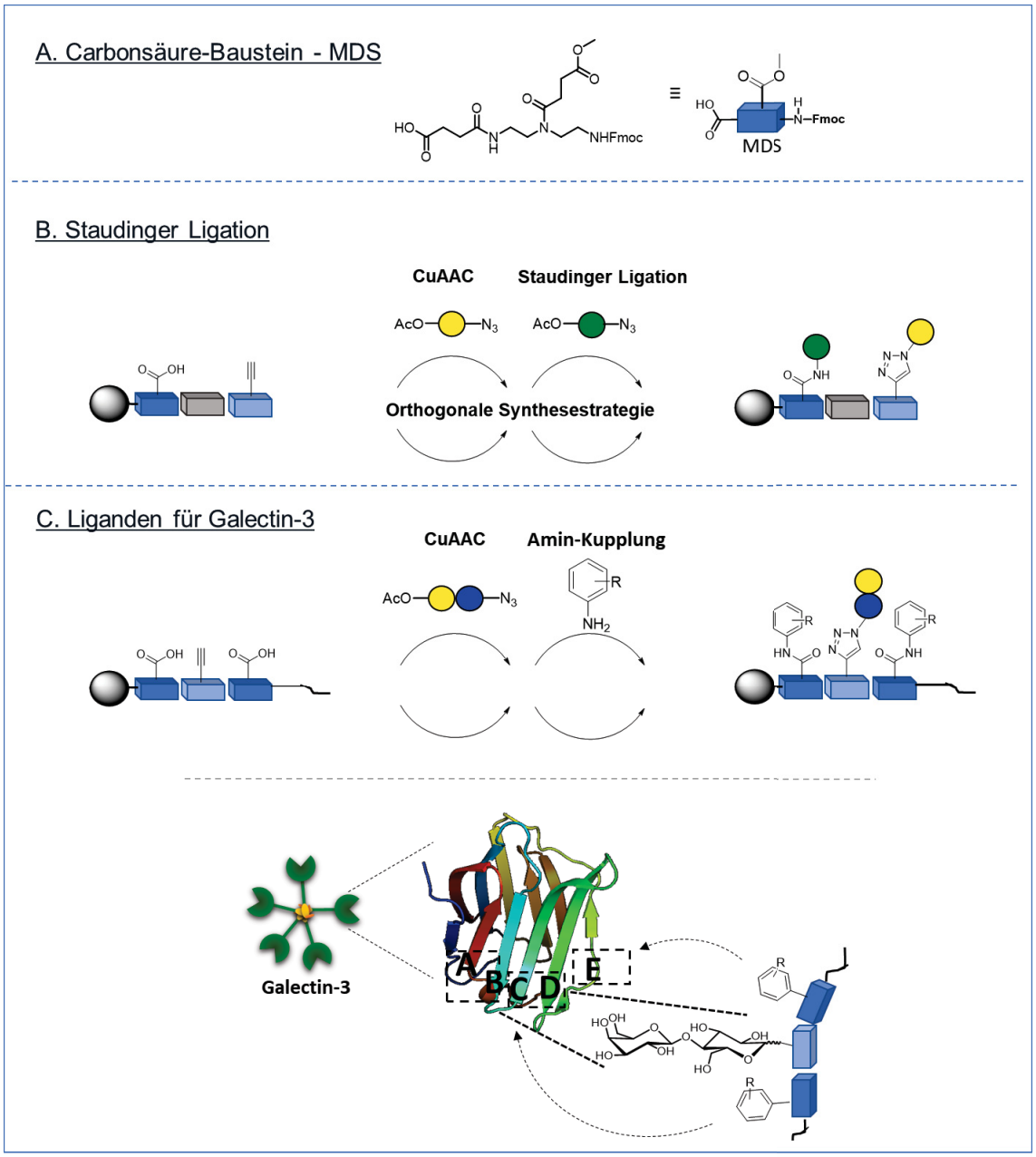

Abbildung 1: Schematische Übersicht über die, in dieser Arbeit, etablierten Strategien. A. Struktur des geschützten Carbonsäure-Bausteins MDS. B. Kombination aus der Staudinger Ligation und der CuAAC zur orthogonalen Synthese von Heteroglykomakromolekülen. C. Kombination aus der CuAAC und der Amin-Konjugation von nicht-glykosidischen Seitenketten zur gezielten Synthese von Galectin-3-Liganden und deren potenzielle Wechselwirkung.

Im ersten Teil dieser Arbeit wurde zunächst ein neuer funktioneller Baustein eingeführt, *methyl-succinyl diethylenetriamine succinic acid* (MDS), welcher an seiner Seitenkette über eine geschützte Carbonsäure-Funktion verfügt. Das Design des Bausteins lehnt sich dabei an bereits vorhandene Bausteine, basierend auf einem Diethylentriamin-Grundgerüst, an (Abb.1; A). Nach

der ersten, erfolgreichen Festphasensynthese konnte dieser Baustein zur Etablierung einer neuen Konjugationsmethode, der Staudinger Ligation, verwendet werden. Dabei konnte zum ersten Mal die Säure-Funktionalität durch die Tributylphosphin-vermittelte Staudinger Ligation mit einem Kohlenhydrat-Azid zur Bildung einer Amid-Bindung an der Festphase verwendet werden. Die optimierte Staudinger Ligation wurde daraufhin in Kombination mit der Kupfer-katalysierten Azid-Alkin Cycloaddition (CuAAC) in einer orthogonalen Synthese einer Heteroglykooligomer-Struktur demonstriert (Abb.1; B).

Im zweiten Teil der Arbeit wurde die Synthese von Lactose-funktionalisierten sowohl homo- als auch heteromultivalenten Glykomakromolekülen als Liganden für das Lectin, Galectin-3 durchgeführt (Abb.1; C).

Eine erste Generation von homomultivalenten Strukturen, welche sich in der Anzahl der Kohlenhydrate-Reste (Valenz) und dem Abstand der Reste zueinander unterschieden, wurde in Enzyme-linked Immunosorbent Assay (ELISA) und Oberflächenplasmonenresonanz (SPR) Inhibitionsstudien zur Binding an Galectin-3 untersucht. Wie in vorangegangenen Studien bereits an anderen Systemen gezeigt, führte eine Erhöhung der Valenz von mono- zu hexavalenten Strukturen zu einer klaren Bindungssteigerung. Zusätzlich konnte durch die Variation des Abstandes sowohl zwischen den Liganden entlang des Gerüstes, als auch der Variation des Linkers zwischen dem Liganden und dem Gerüst, gezeigt werden, dass eine Verringerung des Abstandes zu einer erhöhten Bindung führte. Basierend auf den Ergebnissen dieser Arbeit wurden, durchgeführt von Miriam Hoffmann, eine Serie Lactose-funktionalisierter Oligomere an Lipide konjugiert und diese multivalent auf der Oberfläche von Liposomen präsentiert. Diese Liposome zeigten einen weiteren Anstieg der Inhibitionsstärke mit Inhibitionskonzentrationen im nanomolaren Bereich. Solche Glykomakromolekül-funktionalisierten Liposome könnten daher in Zukunft für zielgerichtete Drug-Delivery-Anwendungen verwendet werden.

Zur Erweiterung der ersten Serie an Galectin-3 Liganden wurde eine zweite Generation an Liganden durch die Kombination von Lactose und nicht-glykosidische Resten unter Verwendung des Carbonsäure-Bausteins zur Amid-Kupplung und des Alkin-Bausteins TDS für die Kupfer-Click-Reaktion, synthetisiert. Dabei wurde der neue Baustein zur Konjugation Amin-funktionalisierter, aromatischer Reste verwendet.

Hier konnte erneut die Orthogonalität der Reaktion zur CuAAC genutzt werden, um eine Variation an phenylischen Resten mit verschiedenen Funktionalitäten (Amin, Sulfonsäure, Hydroxygruppe) zu konjugieren. In Inhibitionsstudien konnte dabei für alle Heterostrukturen eine erhöhte Bindung und damit Inhibierung zu Galectin-3, im Vergleich zu den entsprechenden homovalenten Strukturen mit gleicher Valenz, erzielt werden. Dabei konnte zusätzlich eine

Affinitätsabhängigkeit von der Funktionalität der Reste beobachtet und IC_{50} Werte im niedrigen mikromolaren Bereich erzielt werden.

Basierend auf diesen vielversprechenden Ergebnissen wurden im dritten Teil dieser Arbeit ausgewählte Glykooligomere an humanen Tumorzellen in Ganzzell-Studien untersucht. Dabei wurde neben toxikologischen (MTT), Wechselwirkungs- (Flow cytrometry) und Lokalisation-Studien (Fluoreszenz-Mikroskopie), auch die Migration von Galectin-3-positiven MCF 7 Brustkrebszellen in sogenannten „Wundheilungs"-Studien untersucht. Im Zuge der „Wundheilungs"-Studie konnte eine Verringerung der Migrationsgeschwindigkeit durch die Glykomakromoleküle, analog dem Trend der Ergebnisse aus den Bindungsstudien, beobachtet werden. Dieser kontinuierliche Trend und die Ergebnisse der Negativkontrollen lassen auf eine Galectin-3 basierende Inhibierung der Migration schließen und zeigen somit zum ersten Mal einen biologischen Effekt an humanen Zellen durch Glykooligo(amidoamine).

In dieser Arbeit wurde zusammenfassend, die Etablierung neuer Synthesestrategien und deren Anwendung zur Synthese von homo- und heteromultivalenten Glykomakromoleküle gezeigt. Die daraus resultierenden Glykomimetika wurden erfolgreich als Liganden für Galectin-3 getestet und konnten durch die Einführung nicht-glykosidischer Reste optimiert werden. Es konnte zum ersten Mal das Potenzial dieser Strukturen in Ganz-Zell Studien gezeigt werden und somit als Grundlage für weitere Optimierungen und folgende Studien dienen.

List of Publications

Publications included in this thesis

T. Freichel, V. Heine, D. Laaf, E. E. Mackintosh, S. Sarafova, L. Elling, N. L. Snyder and L. Hartmann

Sequence-defined Heteroglycomacromolecules Bearing Sulfated and Sulfonated Non-Glycosidic Moieties Selectively Bind Galectin-3 and Delay Wound Healing of a Galectin-3 Positive Tumor Cell Line

In preparation

T. Freichel, D. Laaf, M. Hoffmann, P. B. Konietzny, V. Heine, R. Wawrzinek, C. Rademacher, N. L. Snyder, L. Elling and L. Hartmann

Effects of linker and liposome anchoring on lactose-functionalized glycomacromolecules as multivalent ligands for binding galectin-3.

RSC Advances., **2019**, 9, 23484–23497.

T. Freichel, S. Eierhoff, N. L. Snyder and L. Hartmann

Toward Orthogonal Preparation of Sequence-Defined Monodisperse Heteromultivalent Glycomacromolecules on Solid Support Using Staudinger Ligation and Copper-Catalyzed Click Reactions

The Journal of Organic Chemistry, **2017**, 82, 9400-9409.

Publications not included in this thesis

K. Neuhaus, E.-C. Wamhoff, **T. Freichel**, A. Grafmueller, C. Rademacher and L. Hartmann

Asymmetrically Branched Precision Glycooligomers Targeting Langerin

Biomacromolecules, **2019***.*

K.S. Bücher, N. Babic, **T. Freichel**, F. Kovacic and L. Hartmann

Monodisperse Sequence-Controlled α-l-Fucosylated Glycooligomers and Their Multivalent Inhibitory Effects on LecB,

Macromolecular Bioscience, **2018**, 18, 1800337, 1-8.

C. Gerke, M. F. Ebbesen, D. Jansen, S. Boden, **T. Freichel** and L. Hartmann
Sequence-Controlled Glycopolymers via Step-Growth Polymerization of Precision Glycomacromolecules for Lectin Receptor Clustering
Biomacromolecules, **2017**, 18, 787-796.

Conferences

M. Hoffmann, **T. Freichel**, D. Laaf, R. Wawrzinek, Ch. Rademacher, S. Sarafova, L. Elling, N. L. Snyder and L. Hartmann
Lactose-Functionalized Precision Glycomacromolecules for Understanding the Role of Galectin-3 in Tumor Migration
Poster Macromolecular Colloquium Freiburg, **2019**.

T. Freichel, N. L. Snyder and L. Hartmann
Combining Staudinger ligation and copper-catalyzed click reactions for the synthesis of heteromultivalent glycomimetics
Abstracts of Papers of the American Chemical Society, **2018**, 255, Meeting Abstract: 586.

C. Gerke, M. Ebbesen, D. Jansen, S. Boden, **T. Freichel**, L. Goodwin, F. Pieper, A. C. de la Calle, S. Schmidt and L. Hartmann
Sequence-controlled polymeric glycomimetics for the investigation of epitope spacing on multivalent ligand/receptor interactions
Abstracts of Papers of the American Chemical Society, **2017**, 254, Meeting Abstract: 577.

Introduction

1. Carbohydrates and their role in nature

Carbohydrates together with proteins, lipids and nucleic acids are one of the major classes of natural biomacromolecules.[1] Carbohydrates are presented on nearly all cells, where they are linked to proteins or lipids forming glycoproteins and glycolipids, which together comprise 2-10 % of the plasma membrane.[2] Here, glycoproteins are the predominant glycoconjugates, as 80 % of the cell surface located carbohydrates are glycoproteins.[3, 4] Carbohydrates serve as recognition elements for carbohydrate-binding proteins (*e.g.* non-enzymatic lectins or antibodies), or in the case of glycogen as an energy source for the cell.[5, 6] Extracellularly, carbohydrates can be found as fibronectin, secreted collagen or heparan sulfates, for example in the extracellular matrix.[7] As a result, most biological processes occurring between cell surfaces such as cell-cell communication and pathogenic interactions, are based on carbohydrate-protein interactions on the glycocalyx of the cell (Figure 1). [3, 8]

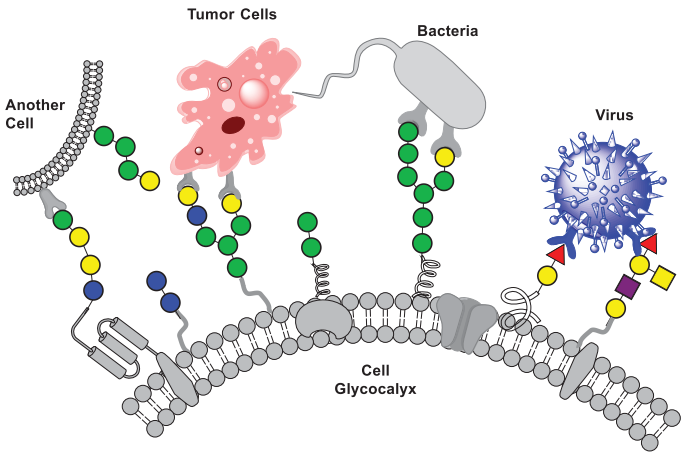

Figure 1: Schematic illustration of possible interactions occurring on the glycocalyx of a cell.

Glycosylation of proteins is a posttranslational modification which is not encoded in the genome.[6, 9] The result is a complex glycosylation pattern, due to the inherent molecular complexity of natural saccharides.[10] The structural characteristics of saccharides enable the assembly of oligo- or polysaccharides in multiple ways, for example, in comparison to amino acids where two identical amino acids can form only one dipeptide, two saccharides can form up to 11 different disaccharides.[8]

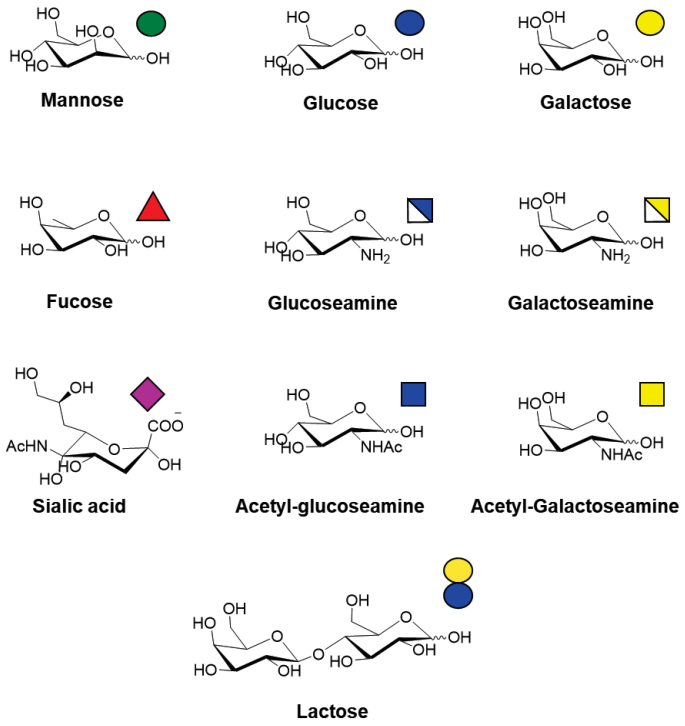

Figure 2: Structures of carbohydrates found in glycoconjugates occurring in human cell membranes and their symbol for representation in accordance with the Consortium for Functional Glycomics's (CFG) nomenclature.

In human cells, predominantly nine different monosaccharides are found, including mannose, fucose, sialic acid, glucose, galactose the amine derivatives glucosamine/galactosamine and the acetylated versions *N*-acetylglucosamine/*N*-acetlygalactosamine (Figure 2).[3, 11, 12]

The interaction of a single monosaccharide to its receptor *e.g.* a lectin, is in most cases relatively weak with binding constants in the high micromolar to millimolar range.[13] Nature circumvents this weak affinity by presenting multiple copies of the same saccharide on a surface.[14, 15] This multivalent presentation leads to an increased binding avidity, where the overall binding event is generally stronger than the sum of the individual binding events.[16, 17] The enhanced binding of multivalent ligands can be explained by different multivalency effects including chelate effect, cluster-glycosidic effect, statistical rebinding and sterical shielding (Figure 3).[15, 18, 19]

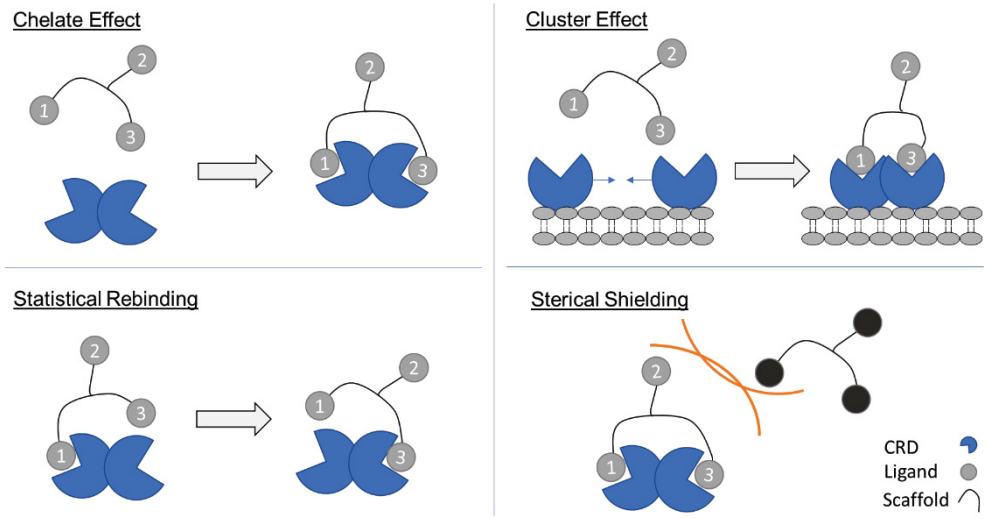

Figure 3: Possible mechanisms of interaction between a multivalent ligand and multivalent proteins.[20]

The chelate effect describes the multiple coordination of carbohydrates presented on one glycoligand to one protein containing more than one binding site, also called carbohydrate recognition domain (CRD).[21] The definition of this effect is also known from inorganic chemistry, where, for example, one metal ion is complexed by a multidentate ligand. For biological applications an important chelate complex is the Ni-NTA (nickel - nitrilotriacetic acid), which is used in its immobilized form for the purification of histidine (His)-tagged molecules.[22]

The second effect, the cluster effect, describes the possibility of multivalent ligands to simultaneously cross-link different receptor proteins. Sometimes signal transduction can only occur due to glycan-mediated receptor clustering on a membrane facilitating a successful signaling pathway.[23]

Statistical rebinding is based on the high local concentration of glycan ligands.[19] Through the binding of more than one ligand, the overall association and dissociation rate of the ligand is changed. The local concentration of the carbohydrates is enhanced after the first binding event, which can have a positive impact on the second binding. The proximity of the ligands furthermore allows a fast association and dissociation, where on average always one or more carbohydrates are in contact with the receptor, decreasing the overall dissociation of the ligand.[19, 24] The last listed effect, steric receptor shielding, is an effect which occurs in competition events. Through the binding of the first ligand, the same biomolecular scaffold can shield unoccupied binding sites from competing ligands.[25-28]

Beside multivalent effects, the presentation of different carbohydrates can further increase the ligand-receptor binding and the specificity of this binding event. [8, 29-31]

The presentation of different kinds of carbohydrates in a multivalent fashion is called heteromultivalency and has already been explored as an important characteristic for specific carbohydrate-protein interactions.[31, 32] Studies suggest that there is a so-called "heterocluster effect" or a synergic effect caused by secondary interactions of the lesser or non-active binding motifs.[33]

A dysregulation of glycan production and protein expression is often a reason for diseases like autoimmune disorders or cancer.[34] The role of carbohydrates in tumor biology is described in more detail in the following section.

1.1. Carbohydrates in tumor biology

Cancer was responsible for 8.8 million deaths in 2015, making it one of the leading causes of death worldwide.[35] In 1929/1930 Hirtsfeld and Thomsen first observed that tumor cells are often characterized through a change in the glycosylation pattern of glycoproteins and -lipids in both, type and quantity, of the occurring saccharides, relative to healthy cells.[34, 36, 37] Tumor cells are often surrounded by so-called tumor-associated carbohydrate antigens (TACA's) which are excessively expressed in this kind of tissue. Such antigens are the Tn (Thomson-nouveau), TF (Thomson-Friedenreich)-antigen and their corresponding sialylated derivatives STn and STF (Figure 4).[35]

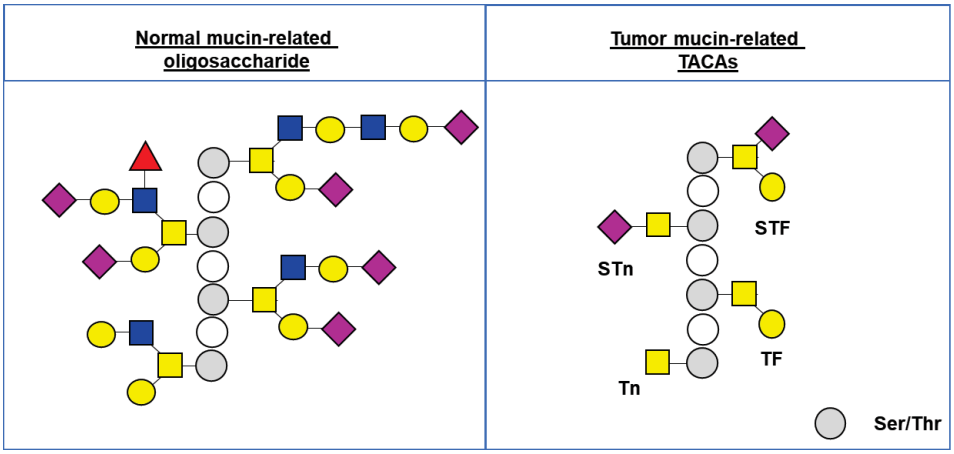

Figure 4: Schematic illustration of the difference between normal- and tumor-related oligosaccharides [adapted from [38]].

Researchers used these TACAs as starting points for the development of carbohydrate-based vaccines for cancer-therapy.[35, 39-42] For example, the group of Danishefsky, working in the field of semi-synthetic anticancer vaccines, synthesized mono-TACA structures which showed promising results in early clinical trials.[12]

Another approach is lectin-based drug targeting for drug delivery systems (DDS), where a drug is conjugated to a lectin or carbohydrate to guide the drug to its target location.[43, 44] This approach could lead to a higher therapeutic efficiency whilst also reducing side effects on healthy tissues. During the reverse targeting DDS, the lectin, which can recognize glycolipids or –proteins, is conjugated to the drug and during the direct targeting, the drug is conjugated to carbohydrate moieties, which can guide the drug to their target location by specific interactions with lectins. One important class of tumor-associated lectins are the galectins, which are described in the next section.[6, 43, 45-50]

1.2. Galectins: A family of human lectins and their ligands

Galectins are a family of human, tumor-associated proteins, which bind to glycans terminated by β-galactoside moieties and consist of 15 different members.[51] Galectins are relatively small lectins with a size between 14.5 to 38 kDa and are characterized by their conserved carbohydrate recognition domain (CRD). There are three subgroups of galectins: (i) homodimeric prototype like Gal-1, (ii) heterodimeric tandem-repeat type like Gal-9 and (iii) chimeric type protein like Gal-3 (Figure 5, A).[51] Gal-3 as the only chimeric member carries, in addition to the CRD, a non-carbohydrate binding N-terminus which enables the self-aggregation of galectin-3 from a monomeric to an oligomeric structure (Figure 5, B).[52, 53]

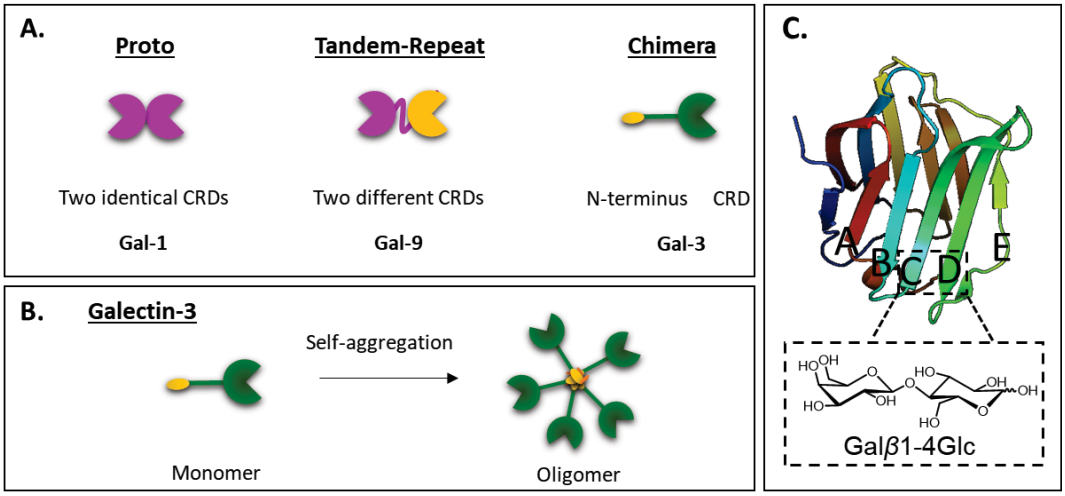

Figure 5: Galectins. A. Overview of the three classes of galectins: Proto-type, tandem-repeat and chimeric type. B. Scheme of the self-aggregation of the monomeric galectin-3 into galectin-3 oligomers. C: CRD of galectin-3 with the five subunits A-E and the interaction site of lactose (PDB: 4xbn.pdb). [54]

Although galectins can be secreted into the extracellular space, most of the expression takes place within the intracellular space and nucleus. Extracellular galectins serve as bridging elements of glycans on the same surface or they can cross-link different cells.[9, 52] Natural ligands of galectins include glycoproteins carrying polylactosamine glycans such as fibronectin and laminin, which can be found in the extracellular matrix.[7, 51] Because of these interactions, galectins play a role in tumor metastasis, a process, where a tumor cell is detached from the primary tumor, migrates into a blood vessel before circulating and residing in a new tissue. In this process, galectin-3 is known to act as a signaling molecule to promote the attachment of the cell to fibronectin, a crucial step of the migration (Figure 6). Because of the role of galectins in tumor-associated processes, researchers have focused on the synthesis of glycomimetics which can interact with galectins to serve as potential drugs or diagnostics.[55, 56]

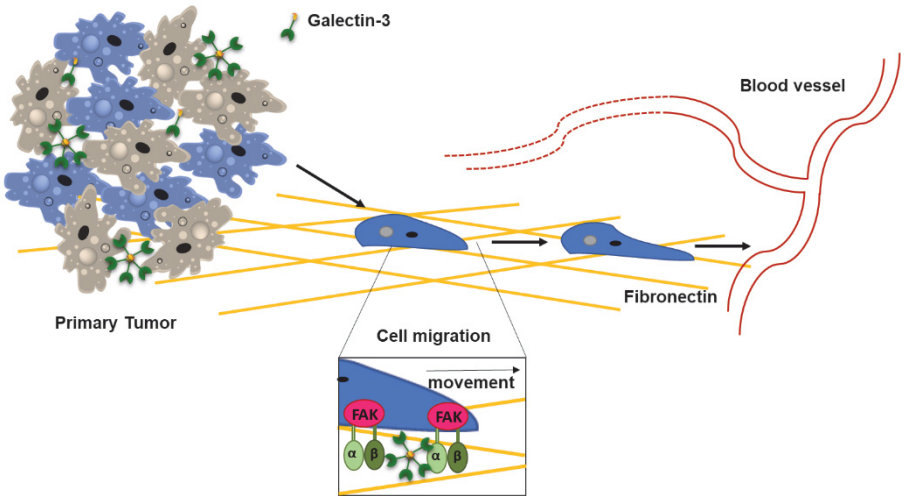

Figure 6: Scheme of the interactions of galectin-3 in tumor metastasis [adapted from [46] with Copyright © 2016 Cardoso, Andrade, Bustos and Chammas.]

The CRD of galectin-3 consists of five different subunits A-E, where subunit C binds to the galactose moiety and subunit D to the next attached carbohydrate, most often acetyl-glucosamine or glucose (Figure 5, C).[54]

The binding site of the CRD of galectin-3 consists of eight conserved amino acids which are responsible for the carbohydrate interaction. These are Trp181, Arg144, Asn160, His158, Arg162, Asn174, Glu184 and Glu165 (Figure 7).[45, 57] The major interactions of the amino acids with the carbohydrates are hydrogen bonds with Asn160, His158, Arg162, Asn174 and Glu184.[54] Furthermore, van der Waals interactions between Arg186 and Trp181 and galactose or acetyl-glucosamine are involved.

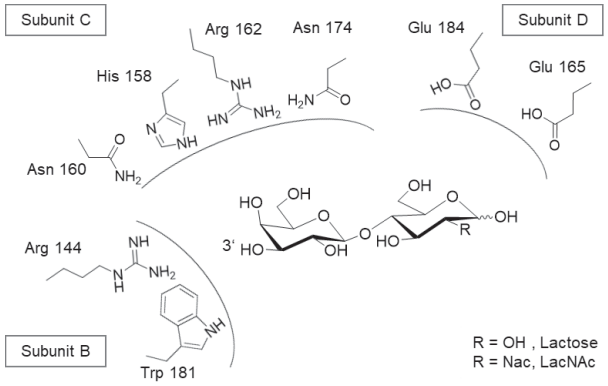

Figure 7:Representation of the binding site of galectin-3 with Lac/LacNAc.[20, 57]

Investigations have been performed addressing hydrophobic, secondary interactions towards high affinity and selective ligands. Regarding galectin-3 inhibitors, one approach engaged

interactions with subunits A-E through secondary binding motifs to enhance affinity and develop efficient galectin-3 inhibitors.[45, 58]

One strategy is the modification on the C3'-position of galactose of Lac/LacNAc for π-interactions with the Arg 144 and Trp 181 residues in subunit B.[59] Nilsson and Leffler synthesized different 3'-substituted LacNAc derivative bearing *e.g.* 3′-benzamido- and 3′-(4-methoxy-2,3,5,6-tetrafluorobenzamido)-residues for the investigation of the mentioned arginine interactions leading to galectin-3 inhibitors with k_d-values of 1.29 µM (Figure 8).[59]

Another approach involves modifications on the C1-position of galactose or on the glucose moiety through the introduction of an aromatic residue like a triazole motif, which subsequently led to increased binding of such synthetic ligands.[45, 60, 61] As an example, the synthesis of aldoxime derivatives of galactose with different aromatic residues at the anomeric center successfully increased galectin-3 binding of such carbohydrate ligands (Figure 8).[62, 63]

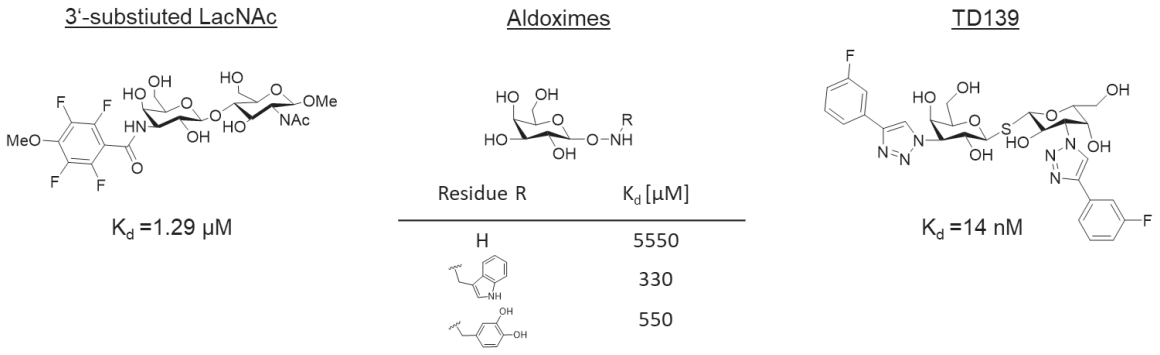

Figure 8: Examples of small molecule galectin-3 ligands known from literature: 3'-(Tetrafluoro-6-methoxybenzamido)-substituted LacNAc[64], aldoxime-derivatives[63] and the thiodigalactosid (TD139)[65].

C_2-symmetric thiodigalactosides (TDG) were also shown to serve as galectin-3 ligands with affinities comparable to the disaccharides Lac and LacNAc. The further development of a derivative of TDG through the introduction of two 4-fluorophenyl-triazoles at C3 and C3'-position yielded in TD139, with a ~1000-fold increase of binding to galectin-3.[66] Indeed, TD139 is currently tested in clinical trials as an galectin-3 inhibitor against idiopathic pulmonary fibrosis (IPF), showing the potential of such systems as future therapeutics (Figure 8).[67]

Sulfonation patterns of glycans are another tool that nature uses to achieve selectivity in carbohydrate-protein interactions.[68] Also studies on galectin-3 indicated that different sulfation patterns such as 2-O or 3-O-sulfation of the galactose of LacNAc increase galectin-3 binding. [69-71] Ölberg, Leffler and Nilsson showed, that the introduction of a sulfate-group at the C2-position of methyl-galactoside resulted in an increased binding with K_d values of 5900 µM for methyl-galactoside and 2800 µM for the sulfated counterpart. In the same study, they showed, that the

non-glycosidic 4-methylbenzaimdo residue on the C3-position in combination with the C2-sulfation on galactose led to an even higher galectin-3 binding with a K_d value of 87 µM and a relative inhibitory potency of 68.[72, 73]

As another example, in the work of Talaga *et al.*, the inhibition of galectin-3 by sulfated glycosaminoglycans and chondroitin was investigated showing minimum inhibitory concentrations of 14.2 µM for heparin and 3.9 µM to 7.0 µM for different chondroitin sulfates. These ligands were more potent inhibitors for galectin-3 compared to the standard ligand LacNAc with a minimum inhibitory concentration of 500 µM.[74]

Due to the ability of galectin-3 to oligomerize in the presence of multivalent glycans, the multivalent presentation of the carbohydrates on macromolecules is another approach to synthesize high affinity galectin-3 ligands.[49, 53, 75-82] Gouin *et al.* synthesized multivalent click-clusters containing 1-4 lactose residues with just low multivalent effects showing a K_d values of 72 µM for monovalent structure and 16-30 µM for the tetravalent structures.[61] Converting this to relative potencies, the tetravalent structures showed even a decrease in binding per carbohydrate with potencies of 2.4 to 4.6.

In contrast, Elling and Wang could show that the multivalent presentation of LacNAc-derivatives on neo-glycoproteins lead to effective galectin-3 inhibitors with IC_{50} values in the lower nanomolar range and inhibitory potencies of 100 or even higher (Figure 6).[80, 83, 84] Another example using multivalent constructs for targeting galectin-3 was introduced by Cloninger and coworkers. There, they demonstrated the potential of multivalent Lac and LacNAc functionalized PAMAM-dendrimers in galectin-3 mediated cancer cell aggregation assays, where in general, smaller LacNAc dendrimers showed higher inhibition of homotypic cancer cellular aggregation compared to the larger or lactose-functionalized ones.[49, 85] Gabius and Roy synthesized different type of glycomimetics like tetravalent glycoclusters[86] and a set of highvalent glycodendrimers [87] and evaluated those structures in solid phase, SPR or cell assays. The glycoclusters synthesized by Gabius and Roy resulted in IC_{50} values of 62-125 µM for the tetravalent structures and 700 µM for free lactose, resulting in a 6-11 times increase through the multivalent presentation. For the mentioned dendrimers, a variation in valency was applied going from 6 to 90 lactose residues (one example is shown in Figure 9). Whereas, the nonacontavalent dendrimer displayed the ligand with the lowest IC_{50} value of 0.16 µM and a relative inhibitory potency of 11 per carbohydrate, the decavalent derivative with an IC_{50} values of 0.31 µM showed with 53 the highest inhibitory potency per carbohydrate, pointing to the potential of such low-valency systems.

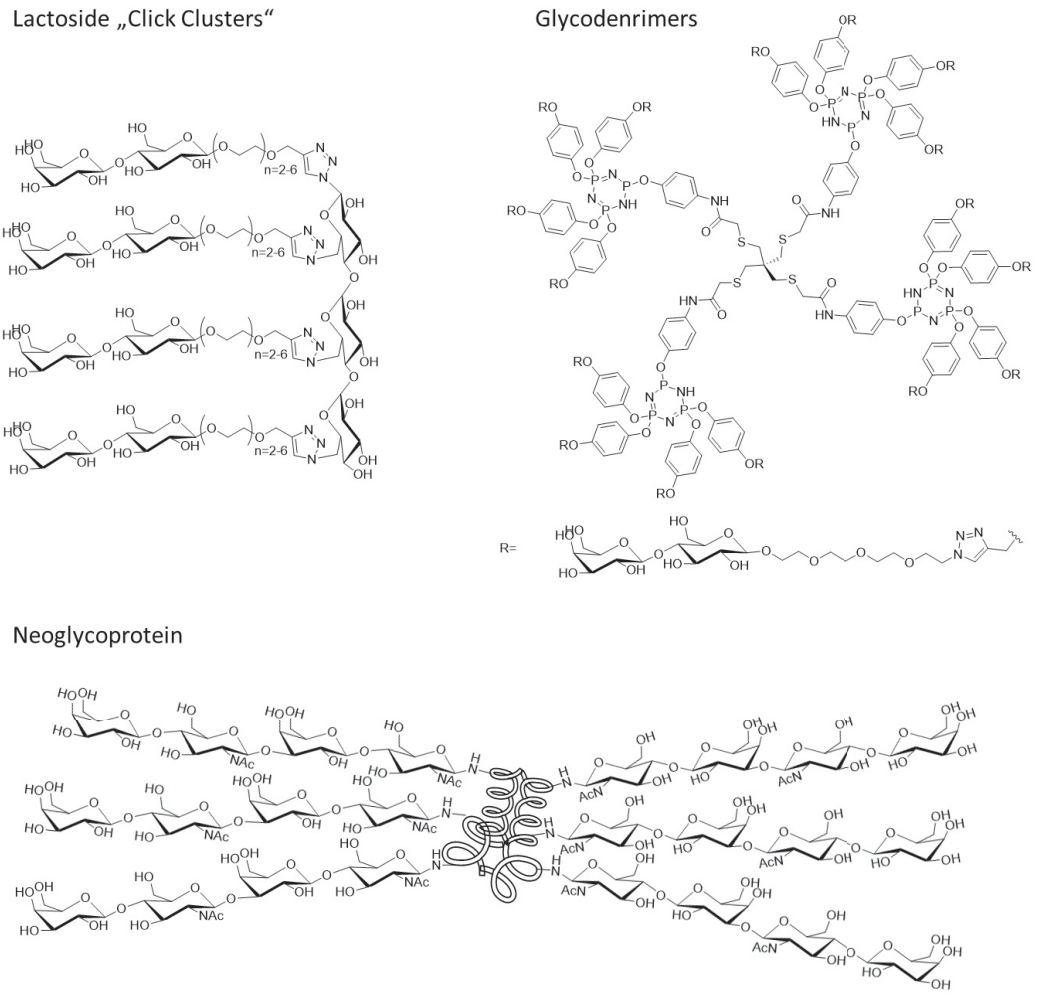

Figure 9: Examples of ligands for galectin: Multimeric lactose-functionalized “click-clusters”[61], glycodendrimers[87] and neoglycoproteins.[88]

As shown, the use of synthetic glycoligands to investigate the role and nature of lectin binding is a powerful tool towards potential carbohydrate-based pharmaceutics. The synthesis of various glycomimetics is thus described in the following chapter.

2. Glycomimetics

Understanding the nature of carbohydrate-protein interactions is a fundamental step in the development of carbohydrate-based pharmaceuticals. The above-mentioned complexity of natural polysaccharides complicates the investigation and understanding of the underlying processes, because the isolation of natural glycans is often challenging.[89, 90] In addition, the inhomogeneity of natural glycan presentation results in extraction of complex product mixtures which can be difficult to separate.[39] Therefore, researchers have focused on the development of simplified glycomimetics.[20] This strategy is based on the multivalent presentation of minimal binding motifs, usually the terminal fragments of oligosaccharides, to achieve ligands with high affinity and selectivity that are more easily accessible.

Multivalent presentation is realized through covalent attachment of the carbohydrates onto synthetic scaffolds.[15-18, 21, 31, 91, 92] Different synthetic strategies and scaffolds for the development of glycomimetics have been explored such as glycopolymers[93, 94], -dendrimers[95-97], -fullerenes[98, 99] or glycoconjugates like neoglycoproteins[4, 84], liposomes[100, 101], micelles[102] and glyconanoparticles[103, 104]. While all these systems have generally proven successful in generating high affinity glycomimetic ligands, it has been difficult to obtain structure-property correlations and compare results across the different scaffolds used, *e.g.* polymer and dendrimers.

A new class of glycomimetics was introduced by Hartmann and coworkers trying to develop a platform that allows for straightforward variation of the structural parameters of the scaffold and generate model compounds to investigate glycomimetic binding in a systematic fashion. The approach is based on the solid supported synthesis of sequence-controlled glycooligo(amidoamines) which demonstrated their ability to function as high-affinity glycomimetics in lectin binding studies as well as cell studies. [26, 92, 103, 105-111] The use of tailor-made building blocks in combination with already established solid supported coupling reactions enables the control over sequence, valency, inter-ligand spacing and architecture, all characteristics which are known to have an impact on the strength of lectin binding.

In the following section, the basics of the solid phase peptide synthesis as established by Merrifield, commonly used amide coupling reagents, and the adapted solid supported synthesis of glycooligo(amidoamines) are described in more detail.

2.1. Solid phase synthesis of sequence-defined glycooligo(amidoamines)

Solid phase peptide synthesis – a short overview

The solid supported synthesis of peptides was first reported by Merrifield.[112] Classic coupling reactions of amino acids in solution usually required numerous purification steps and thus were time-consuming and produced low yields.[113-115] Merrifield showed that through the fixation of the first amino acid onto a solid support these disadvantages can be circumvented, as reagents and solvents could easily be washed away while retaining the desired product on the support. This allowed for the use of excess of amino acids in the coupling steps, which then led to an increase in purity, yield and shorter reaction times laying the foundation work for what is known today as solid phase peptide synthesis (SPPS). [112, 116-118]

Since the first introduction by Merrifield, SPPS has been further developed.[117-124] In short, SPPS consists of three major steps: functionalization of the resin, deprotection of a temporary protecting group and coupling of an amino acid.[125] The repetition of the last two steps leads to an iterative coupling-deprotection approach building up a defined amino acid sequence (Figure 10). [124] Standard protocols typically employ peptide synthesis strategies from the C- to the N-terminus of the desired peptide, where the use of an amine functionalized solid support enables the attachment of a compound carrying a free carboxylic acid (Figure 10). [123]

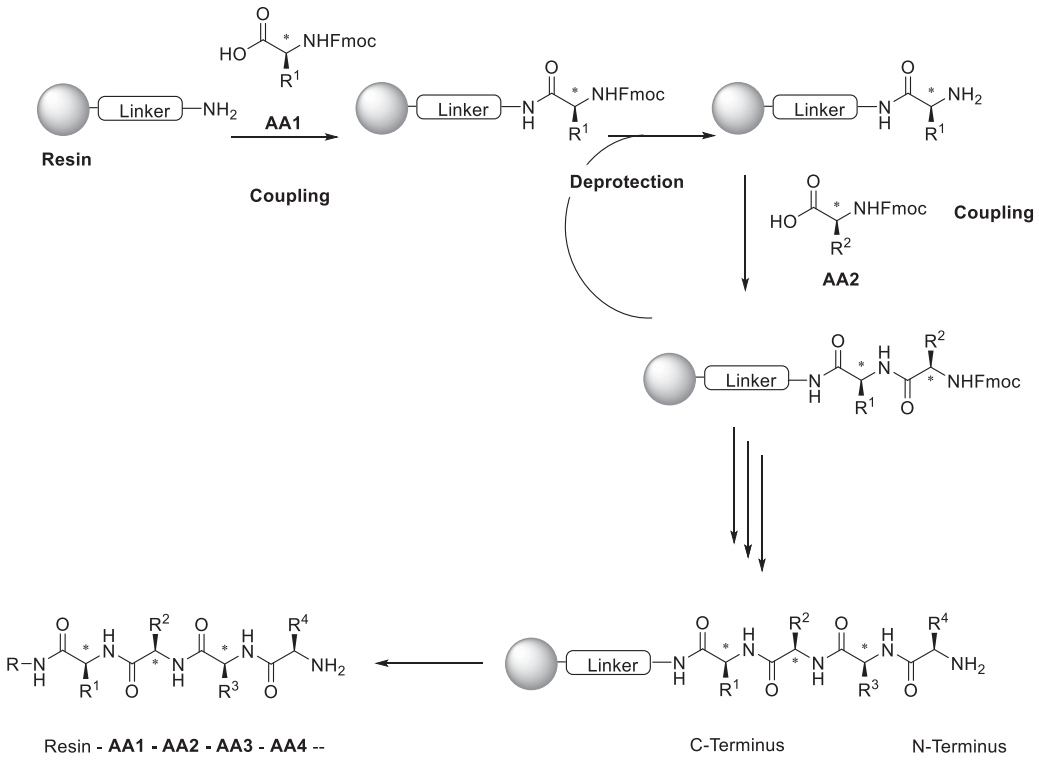

Figure 10: Illustration of solid phase peptide synthesis using amino acids in a sequential coupling-deprotection procedure building-up a peptide from the C- to the N-terminus.

The use of bifunctional amino acids as building blocks requires a temporary deactivation of the second functionality, here the amine, which is mostly realized by using temporary protecting groups such as *tert*-butyloxycarbonyl (Boc) or the 9-fluorenylmethoxycarbonyl (Fmoc) group.[126] [127] The choice of the protecting group depends on the resin and the linker where the first amino acid is appended. The resin linkage is decisive for the cleavage conditions and the functionality of the peptide after cleavage.[128, 129] Therefore, the choice of the protecting group strategy and the terminal linkage requirements dictates the overall strategy. A commonly used linker to produce an amide end group is the rink amide linker as shown in Figure 11. Normally, Fmoc is used together with acid-labile solid supports like the Rink amide resin or trityl-resins due to its base-sensitive character.[130]

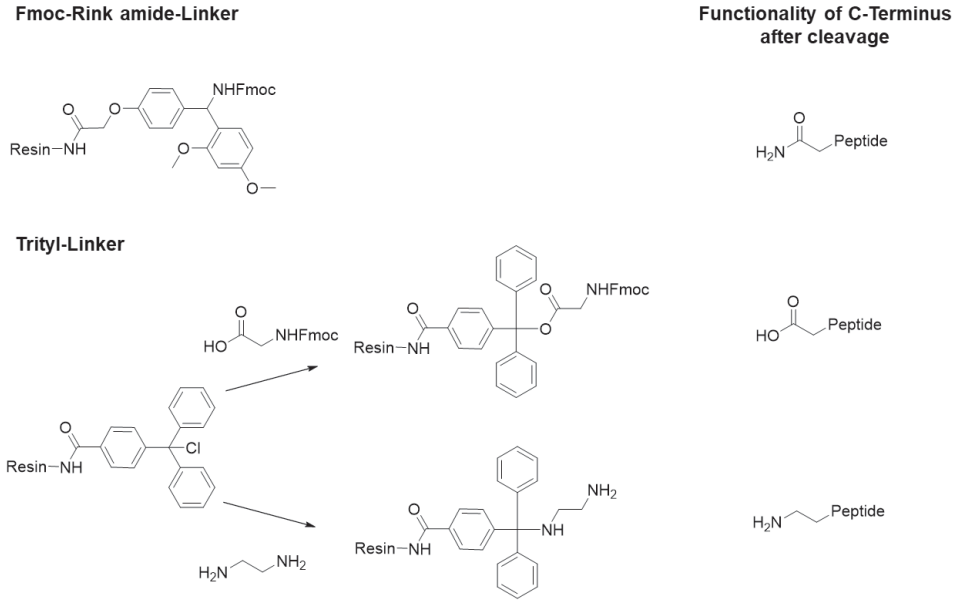

Figure 11: Structure of rink amide and trityl-linkers and the resulting functionality of the C-terminus after cleavage of the peptide. The functionality resulting from the trityl-linker is shown for a glycine and diamine functionalization resulting in a carboxylic acid and amine respectively.

The cleavage of the Fmoc-group is achieved using piperidine, as shown in (Figure 12). An important advantage of using Fmoc is the opportunity to monitor the cleavage due to the formation of a dibenzofulvene(DBF) adduct, a soluble side product.[131]

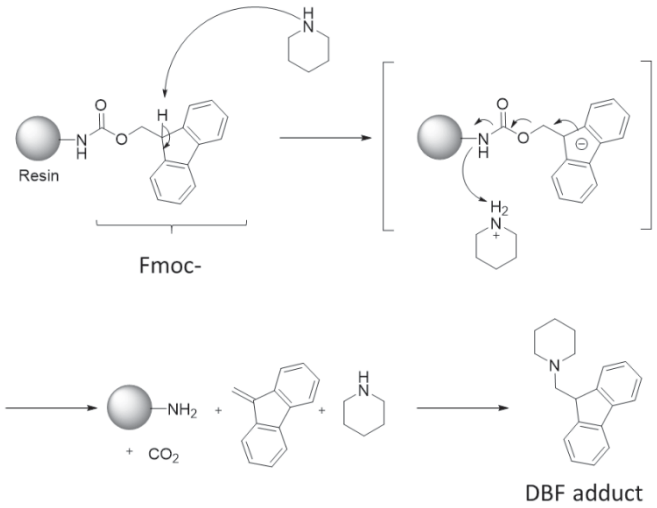

Figure 12: Proposed mechanism of the Fmoc-cleavage using piperidine.

After the deprotection of the amine group, the coupling step is initiated by the activation of the carboxylic acid using coupling reagents.[132, 133] There are different classes of coupling reagents available like the 1H-benzotriazole based phosphonium and uronium/guanidinium reagents and furthermore carbodiimides.[134] A widely used example of an activation reagent is PyBOP (benzotriazol-1-yloxy-tris pyrrolidino-phosphonium hexafluorophosphate), which is normally used together with DIPEA (diisoproylethylamine). The proposed mechanism of carboxylic acid activation using PyBOP is shown in Figure 13.[135]

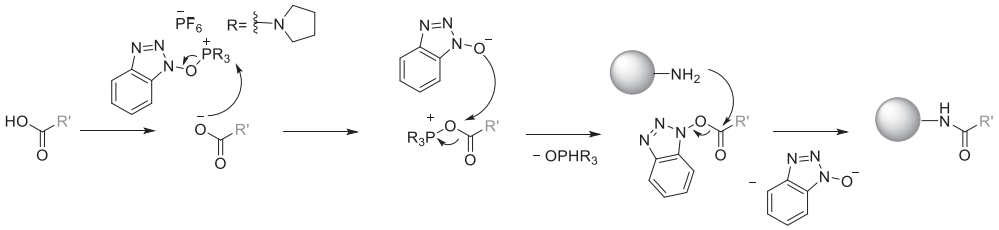

Figure 13: Proposed mechanism of the PyBOP mediated amide-bond formation used for assembly of building blocks on solid support.

The reaction of the carboxylate of the carboxylic acid with the oxophilic phosphonium species leads to an activated acyl oxyphosphonium salt intermediate, which liberates one equivalent of HOBt (1-hydroxybenzotriazole). HOBt itself is a commonly used additive in combination with other coupling reagents *e.g.* carbodiimides, where it can be used to reduce racemization of amino acids during coupling. [136, 137] For the PyBOP mediated reaction, the released HOBt attacks the acyl oxyphosphonium intermediate resulting in an less-labile activated ester, which enables the nucleophilic attack of the free amine achieving amide-bond formation.[122] Following this, the

Fmoc-group of the new building block can be cleaved enabling the coupling of another amino acid. A quite similar type of activation involves HATU (O-(7-Azabenzotriazol-1-yl)-N,N,N′,N′-tetramethyluronium-hexafluorphosphat.[138] HATU is often used in critical reactions because of its fast reaction rate, efficiency and no significant epimerization.[136] For base free coupling conditions and steric challenging reactions for example, diisopropylcarbodiimid (DIC), a member of the carbodiimide family can be used. A disadvantage of DIC is the high susceptibility to racemization, which can be suppressed, as said before, by using HOBt. [122]

Through all these developments, standard solid phase peptide synthesis can also be performed on an automated synthesizer these days, minimalizing time effort and enabling an easier scale up.[123, 139-141]

Challenges can occur for structures that contain an anomeric center. The basic conditions and basic nature of some of the coupling reagents can lead to racemization.[136, 142-144] For biological applications where stereocenters mediate function, this could potentially lead to unwanted biological outcomes (*e.g* immune response).[145, 146] One potential strategy to circumvent this disadvantage was established by Hartmann and coworkers. This strategy is based on a variety of tailor-made building blocks based on the Fmoc-protecting group strategy allowing for the synthesis of monodisperse, sequence-controlled oligo(amidoamine) scaffolds suitable for conjugation with ligands such as carbohydrates (Figure 14). This strategy is described in more detail in the following section.

Going from peptides to other scaffolds

While most of the reagents in solid phase peptide synthesis were developed for the synthesis of natural peptide structures, they can also be used for the synthesis of non-natural peptidomimetics or other amide-based macromolecules.[147-150] The most straightforward approach relies on bifunctional building blocks carrying a protected amine and free carboxylic acid that can be used instead of the amino acids.[151, 152] There are some requirements for such building blocks which have to be considered. First, regarding the synthesis of the building blocks, it must be possible to produce such building blocks in a high purity and large (gram) scales, because an excess of building blocks is often required to move the coupling on solid support to full conversion.[153] Second, the building blocks must be soluble in standard solvents like DMF or DCM. Furthermore, their coupling efficiency must be high to ensure a complete conversion, and in case of additional functionalities in the side chains, a selective, orthogonal protection/deprotection procedure must be installed to guarantee compatibility with Fmoc-group based standard conditions.[124] Orthogonal reactions are characterized through an

independent reaction sequence, without any cross-reactivity and thus no side product formation.[154, 155]

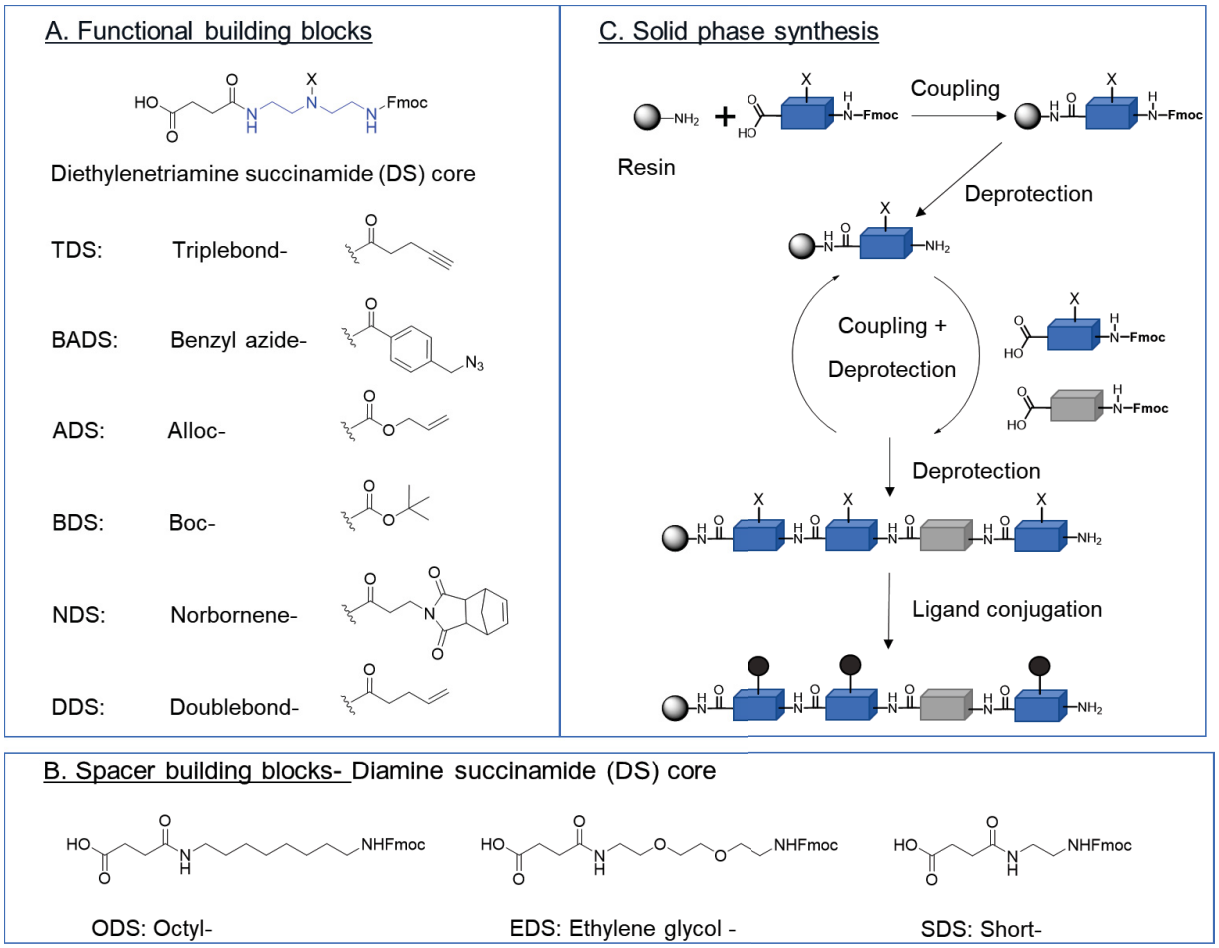

Figure 14: A: Overview of the functional building blocks and B: spacer building blocks developed in this group. C: Solid supported synthesis of oligo(amidoamines).

Dimer building blocks, which were developed and used for the synthesis of oligo(amidoamines), are derived by condensation of a diamine and a diacid unit introducing a Fmoc protecting group on the terminal amine group.[156, 157] Depending on their later use in scaffold assembly, they are differentiated into functional and spacer building blocks (Figure 14). Functional building blocks, usually based on a diethylenetriamine succinyl (DS) core, carry a side chain functionality on the center, secondary amine, allowing for post-modification of the scaffold using different conjugation strategies.[156] For example, the alkyne building block TDS (triple bond diethylenetriamine succinyl)[108] and the azide building block BADS (benzyl azide diethylenetriamine succinyl)[109] allow the modification via copper-catalyzed azide-alkyne cycloaddition (CuAAC) and the alkene derivatives DDS (double bond diethylenetriamine

succinyl)[111, 158] and NDS (norbornene diethylenetriamine succinyl)[159] can be further modified via thiol-ene chemistry (See also Chapter: 2.1.1).

The second group of building blocks are the spacer building blocks, introducing different main chain motifs. EDS (ethylene glycol diamine succinyl)[108] with an ethylene glycol core is the most commonly used spacer building block. In contrast, ODS (octyl diamine succinyl)[103] carrying a *n*-octyl core increases the spacer length and hydrophobicity, whereas SDS (short diamine succinimide) represents the shortest building block of the library so far, introducing an ethylene motif.[160]

Because of the C to N-terminus chain elongation, an end-functionalization through the reaction of the final amine-group is possible. Interesting end-functionalities are the conjugation of a fluorescence tag for localization in fluorescence studies like cellular localization and uptake, or the functionalization with biotin, which enables application in streptavidin-based assays. Furthermore, the amine can be used for the immobilization on the surface of particles[106] or sensor-chips[161], or finally it can be deactivated/capped through the reaction with acetic anhydride.

Through the iterative coupling of building blocks following standard protocols for Fmoc peptide chemistry, monodisperse sequence-controlled scaffolds are obtained, that can then be decorated with ligands using different conjugation strategies, which are described in the next section.

2.1.1.Conjugation strategies for the functionalization of oligo(amidoamines)

Different types of reactions can be used for the conjugation on solid support. Most of them belong to the class of so-called "click-reactions", which are reactions characterized by fast reaction times, simple set-ups, no side-products, high specificities, high product purities and yields.[162] Today, four major groups of "click-reactions" are employed: (I) cycloadditions *e.g.* Diels-Alder reactions, (II) non-aldol carbonyl reactions forming amides as the Staudinger ligation, (III) C-C-multi-bond addition as the thiol-ene[163] and (IV) nucleophilic ring-opening reactions *e.g.* with epoxides.[162, 164] One of the most widely used cycloaddition is the Huisgen 1,3-dipolar cycloaddition of azides and terminal alkynes forming 1,2,3-triazoles. This reaction is catalyzed by Cu^{I}, which can be directly added as Cu^{I} or *in situ* formed through the reduction of Cu^{II} from $CuSO_4$ using *e.g.* sodium ascorbate as reducing agent.[162] The proposed mechanism of the cycloaddition is shown in Figure 15.[165] Because of the use of copper, this reaction is also known as the copper-catalyzed azide-alkyne cycloaddition (CuAAC). A strain-promoted copper-free version of the

[3+2]cycloaddition was established by the Bertozzi group using cyclooctynes instead of terminal alkyne.[166]

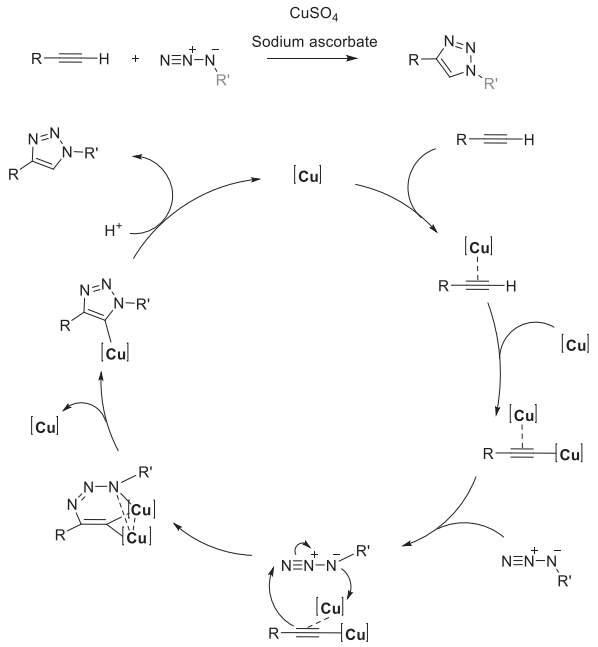

Figure 15: Proposed two copper ion mechanism of the CuAAC published by Fokin *et al*..[167]

In the Hartmann group, the CuAAC is used for the modification of the alkyne-functionalized building block TDS or the azide-functionalized building block BADS.[109] TDS can be conjugated with azide derivatives of carbohydrates, whose synthesis is well known from literature for most carbohydrates[108], whereas BADS can be used together with the corresponding propargyl derivatives.[168] A combination of the TDS and BADS building block on different scaffolds was furthermore used in a split-and-combine approach for the synthesis of branched structures.[109] The photoactivated thiol-ene reaction between a thiol and the double-bond of the DDS building block was demonstrated for the conjugation of thioglycosides in a continuous flow set-up, and furthermore, for the polymerization of larger glycopolymers. In additional work, a norbornene building block NDS was used as an alternative, more reactive ene-moiety for DDS.[107, 159]

Another “click-reaction” is the Staudinger ligation, a reaction evolved from the Staudinger reduction of azides in the presence of phosphines as first described by Staudinger in 1919.[169]

The reaction of an azide with a phosphine leads to the formation of an iminophosphorane intermediate with the release of nitrogen. During a Staudinger reduction, water leads to the formation of the free amine, whereas during a ligation, the reaction of the intermediate with a carboxylic acid leads to amide bond formation (Figure 16). Bertozzi and coworkers developed the methodology of a non-traceless Staudinger, where the phosphine species is integrated in the

starting material and also in the final product.[170] In a traceless Staudinger ligation, the phosphine is released during the reaction.[170]

The different types of Staudinger ligations were already shown as potential tools for the use on solid support, where the azide-derivative was attached to the resin. Nilsson *et al.* for examples used a traceless Staudinger ligation for the protein assembly on solid support, and Malkinson *et al.* a tributylphosphine, DIC and HOBt meditated Staudinger ligation for the synthesis of a glycopeptide. [171, 172]

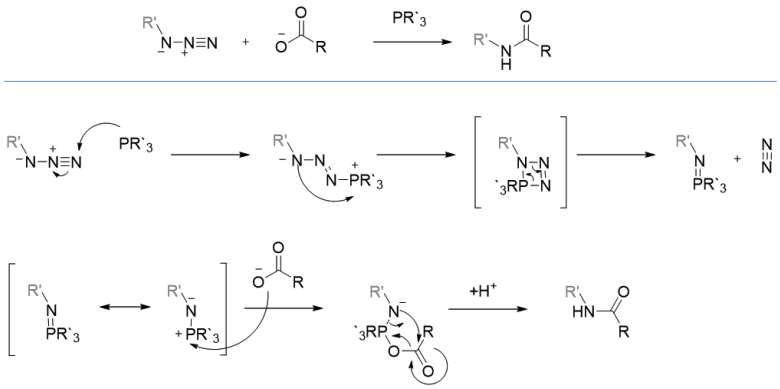

Figure 16: Proposed mechanism of the Staudinger ligation between an azide and a carboxylic acid mediated by a trialkylphosphine.[173]

In the following the use of one or more conjugation strategies for the synthesis of heteroglyco(amidoamines) is described in more detail.

2.1.2.Synthesis of heteromultivalent glyco(amidoamines)

The synthesis of nature inspired hetero-functionalized glycomimetics can provide powerful tools for the development of high affinity ligands, with a potential increase in specificity.[26, 32, 98] The name hetero-functionalized glycomimetic or hetero-glycoconjugate describes different types of glycomimetics where two or more different binding motifs are combined within one structure (Figure 17). The nature of such heteroglycoligands, bearing two or more different residues, requires a sophisticated synthetic approach to generate di- to polyvalent systems with a high density and simultaneously a control of the position of the presented motifs.[18]

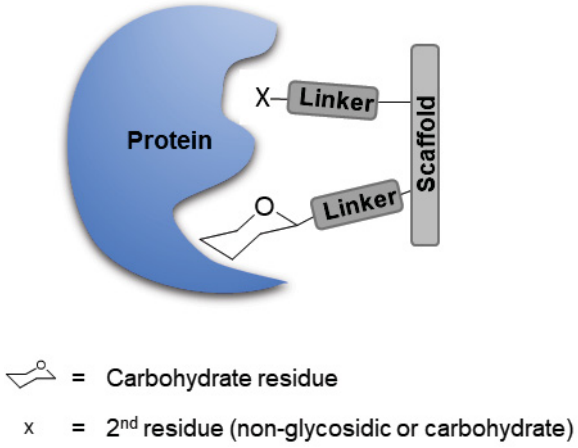

Figure 17:Principle of the binding mode and general design of heteroglycoligands bearing two different binding residues within one molecule.[174]

The combination of carbohydrates with non-glycosidic moieties can be listed as one class of hetero-glycomacromolecule. This kind of hetero-glycomacromolecule is interesting for the investigation of secondary binding motifs. For example, Nilsson and coworkers demonstrated that enhanced binding of small molecule ligands to galectin-3 could be achieved through the introduction of non-glycosidic moieties (see section 1.2).[63]

Tran *et al.* synthesized heterobifunctional polymers using amine functionalized polyacrylamide and dextran polymers for post-modification with a galactose-functionalized bifunctional residue, bearing an azido-functionality for the further conjugation of non-glycosidic moieties via copper-catalyzed cycloaddition as shown in Figure 18 and applied those structures as cholera toxin (CT) inhibitors with an increased affinity compared to the structures without the non-glycosidic moieties.[174] In another example, Haddleton and Gibson reported on the synthesis and application of galactose-functionalized glycopolymers bearing different non-glycosidic residues as secondary binding motifs to generate selectivity for cholera toxin and peanut agglutinin (PNA) as well. In their example, a post-polymerization modification approach was used to incorporate the two different residues into a polymer.[27, 28] This approach was also used to synthesize glycopolymers bearing two different types of carbohydrates, as another class of heteromultivalent glycomimetics.[111, 175]

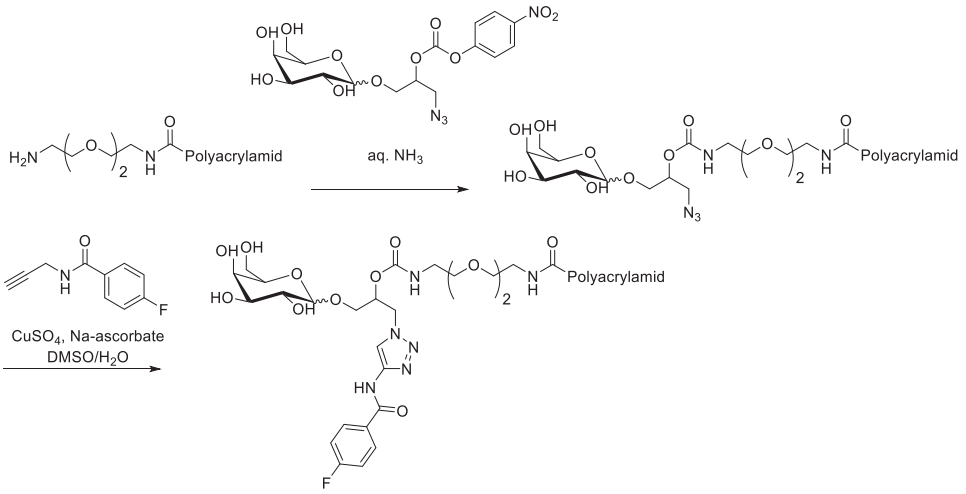

Figure 18: Synthetic strategy towards a heterobifunctional polymer as a ligand for CT applied by Tran et al..[174]

Natural glycans mostly consist of different types of carbohydrates, which are arranged in a specific order. Therefore, the presentation of different carbohydrate moieties within a structure is another way to mimic the complex natural polysaccharide structures.[176]

Lehn and coworkers established dynamic combinatorial chemistry (DCC) for the synthesis of carbohydrate-ligand libraries, including the synthesis of hetero-functionalized glycoligands.[177-179] The concept of DCC is based on functional building blocks which can undergo spontaneous and reversible connections in any possible combination. This has advantages regarding template-based ligand design, but the identification and purification of a single compound could be challenging.

Another possibility is the use of an orthogonal reaction procedure. Renaudet and coworkers for example established a multi-ligation strategy on cyclopeptides to generate hetero-functionalized glycomimetics.[32, 91, 180-182] As one example, they applied an orthogonal conjugation approach using oxime ligation in combination with CuAAC to generate cyclopeptide based heteroclusters as shown in Figure 19.[180] Applying this strategy, they were also able to synthesize Tn- and TF-antigen-functionalized heteroclusters as potential epitope carriers for antitumor vaccines.[32]

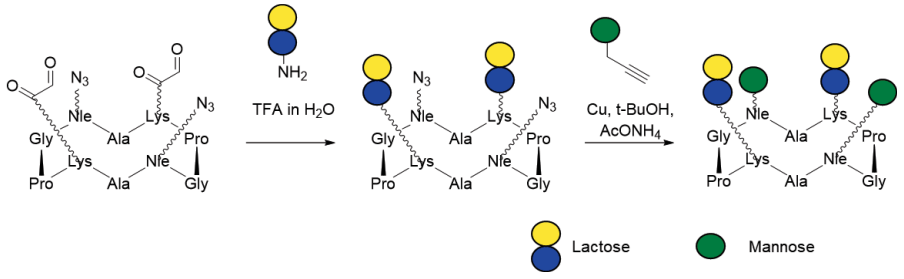

Figure 19: Synthetic strategy towards heteroglycoclusters using an orthogonal ligation approach applied by Renaudet and coworkers.[180]

The group of Fernández synthesized a series of different type of hetero-glycoclusters using a multistep approach involving a thiol-ene reaction between a thiol-carbohydrate derivative and allylated pentaerythritol derivatives, followed by the synthesis of a β-cyclodextrin (βCD) core. With these structures they demonstrated the impact of carbohydrate display on binding to different targets such as ConA, PNA and the glycosidases maltase, isomaltase and α-mannosidase.[18, 30] Chen and coworkers combined the Ugi reaction and CuAAC for the synthesis of mannose- and glucose-functionalized heteroglycopolymers and showed a higher affinity towards ConA compared to the homovalent counterparts in binding studies, as well as in bacterial adhesion studies.[183]

Another synthetic strategy is the combination of chemical synthesis and enzymatic catalysis, as applied by Cloninger and coworkers. This approach was used for the chemoenzymatic synthesis of hetero-functionalized dendrimers carrying lactosamine and glucosamine as ligands for galectins.[85]

One example for a synthetic strategy towards hetero-functionalized triantennary peptides based on solid phase synthesis was established by Lönnberg.[184] The use of a building block carrying three orthogonal protected amines, namely with a Fmoc-, Boc- and Alloc-group, enabled the stepwise coupling of different pentafluorophenyl-activated carbohydrates in a sequential deprotection and coupling procedure (Figure 20).

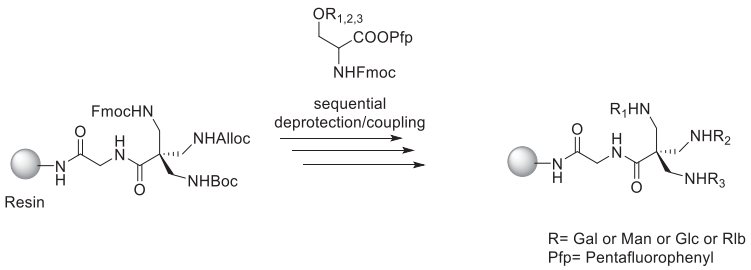

Figure 20: Orthogonal conjugation strategy on solid support towards hetero-functionalized triantennary glycopeptides.[184]

In the Hartmann group, different strategies towards the synthesis of heteromultivalent glyco(amidoamines) have been explored as presented in Figure 21 A and B.

The first approach by Wojcik *et al.* introduced pre-functionalized building blocks suitable for the direct assembly of heteromultivalent glycooligo(amidoamines) on solid support.[111] The advantage is the use of only a few reaction steps on solid support minimalizing material use and side product formation. The disadvantage is the synthesis of carbohydrate-incorporating building blocks, which is for some carbohydrates limited by their stability and synthetic effort.

Furthermore, this approach can be expensive when considering that the corresponding glycofunctionalized building blocks must be used in an excess during solid phase synthesis.

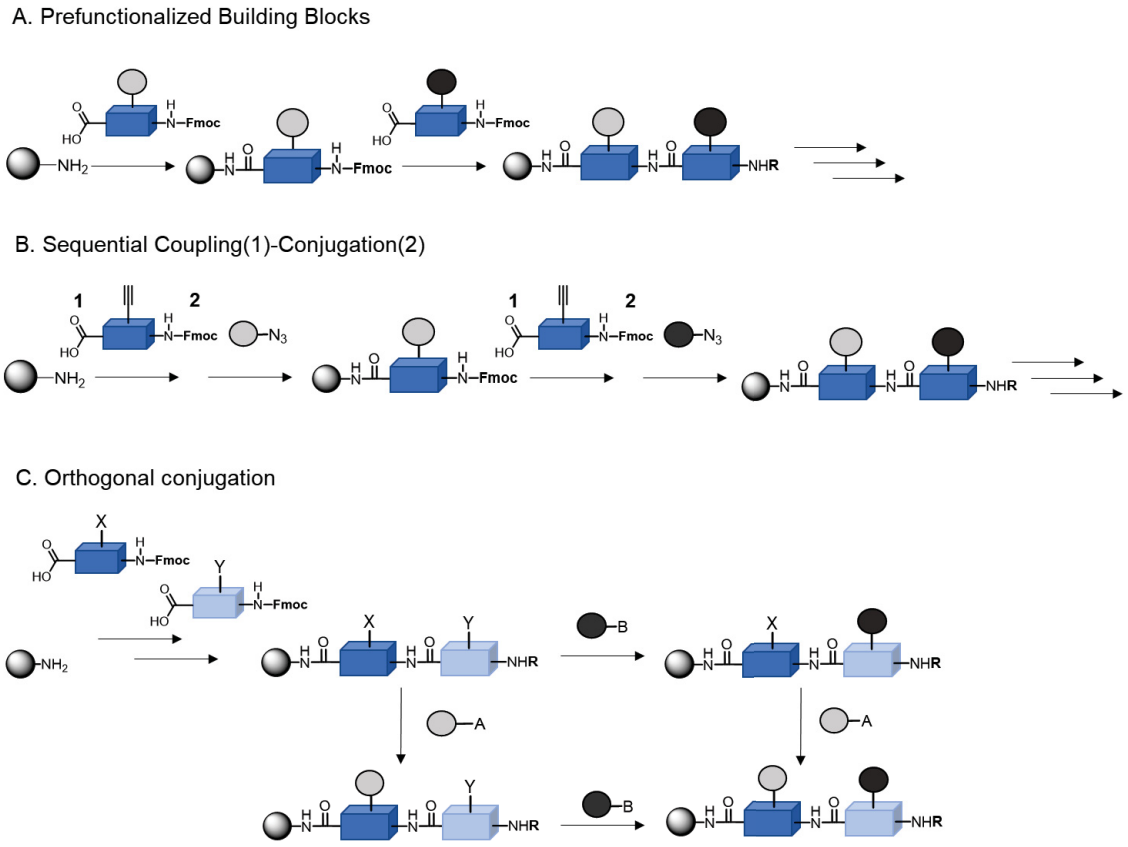

Figure 21: Possible synthetic route towards heteroglycooligo(amidoamines). A. Building block approach using pre-functionalized building blocks. B. Sequential coupling-conjugation: Usage of one functional building block, which is sequentially coupled and afterwards conjugated with a carbohydrate. C. Orthogonal conjugation: Usage of different functional building blocks and different conjugation reactions.

Another approach, which avoids pre-functionalized building blocks, is the sequential coupling and conjugation strategy introduced by Ponader *et al.*.[26] Here, TDS was used for the conjugation of azide-functionalized carbohydrates via CuAAC. The sequential coupling of the building block, followed by the carbohydrate conjugation, enables the stepwise build-up of the glycomacromolecules. In this case, just one functional building block is needed, which can be conjugated with different kinds of functionalized carbohydrates. A disadvantage is the need for several conjugation steps, which can lead to an increase in impurities, and reduced coupling efficiency through the higher steric hindrance of the growing glyco-functionalized chain.

An alternative approach involving the use of established orthogonal conjugation strategies that have been amended for use on solid support would allow for more easy access to heterofunctionalized scaffolds.[180-182] The combination of CuAAC with classic amide-coupling

reactions or CuAAC with the Staudinger ligation as examples for orthogonal conjugation reactions are the focus of the first part of this thesis (Figure 21, C).

Aims and Outline

Protein-carbohydrate interactions are known to mediate various important processes in biology. Indeed, many diseases such as virus or bacterial infections, autoimmune disorders and cancer, are based on protein-carbohydrate interactions and are often caused by a dysregulation of the corresponding glycan biosynthesis and protein expressions. The investigation and understanding of the underlying processes that govern this dysfunction is a crucial step towards developing carbohydrate-based pharmaceuticals that alleviate the corresponding pathologies associated with the aforementioned dysfunction. Due to the complex nature of natural glycans, research has focused on the design and synthesis of simplified glycomimetics, which enable the precise configuration of the characteristics of the glycoligand(s) and thus the systematic investigation of the ligand-protein interactions.

With this idea in mind, Hartmann and coworkers developed sequence-defined glycooligo(amidoamines) for the purpose of exploring carbohydrate-protein interactions of biological interest. Tailor-made building blocks bearing a protected amine-group and a free carboxylic acid, allow for the assembly of monodisperse, sequence-controlled oligo(amidoamine) scaffolds on solid support through a sequential coupling and deprotection procedure. Applying functional building blocks with reactive side-chains allows for the subsequent modification of the scaffold with glycoligands, creating glycomimetics with control over sequence, valency, functionality and spacing.

While glycooligo(amidoamines) have been shown to be suitable as glycomimetics targeting bacterial and viral lectins, thus far they have not been applied towards receptors related to tumor biology such as the galectins, particularly in the context of potential applications of glycomimetic ligands as therapeutics *in vivo*. Here, the introduction of non-glycosidic motifs addressing secondary binding sites of the targeted receptor might increase avidity as well as selectivity. Therefore, the goal of this thesis was to use heteromultivalent glycooligo(amidoamines) presenting both, glycan and non-glycosidic binding motifs for targeting galectin-3, a tumor-associated lectin. Such compounds will be compared to homomulivalent conjugates using a series of biophysical and biochemical approaches.

In the first part of this thesis, the development of an orthogonal conjugation approach for the synthesis of heteroglycomacromolecules will be introduced. Here, the CuAAC conjugation reaction will be combined with the Staudinger ligation as a new conjugation method for this class of glycomimetics. In realizing this goal, a carboxy functionalized building block will be designed and used for the synthesis of homomultivalent glycomacromolecules via Staudinger ligation. After

the development of the Staudinger ligation, the orthogonality of the CuAAC and Staudinger ligation as investigated to demonstrate proof of concept towards the synthesis of heteromultivalent glycomacromolecucles.

In the second part, lactose-functionalized glycooligomers varying in valency (mono- to hexavalent) and spacing will be synthesized as a first generation of ligands targeting galectin-3. The alkyne-building block TDS will be used for the conjugation of azide-functionalized lactose derivatives using CuAAC. The binding-characteristics of the synthesized glycomacromolecules will be evaluated in ELISA-type and SPR inhibition studies.

This lactose-functionalized ligand-library will be expanded in the third part of this work, to obtain heteromultivalent glycooligo(amidoamines) carrying non-glycosidic moieties as secondary binding motifs in the side chain. The introduction of those non-glycosidic fragments will be enabled using the carboxylic acid building block in an amine-coupling procedure. These structures will also be tested in ELISA-type and SPR inhibition studies.

Selected glycomacromolecules of the 1st and 2nd generation will be further tested in *in vitro* studies on human cancer cells. Preliminary studies using MTT-assay for the toxicity, flow cytometry and fluorescence microscopy demonstrate the ability of the glycomacromolecules to interact with these cells. In addition, the impact of the glycomacromolecules on the galectin-3 mediated cell migration of MCF 7 breast cancer cells will be explored in a “wound-healing” assay.

Conclusion

The aim of this thesis was the synthesis of homo- and heteromultivalent glycooligo(amidoamines) targeting the tumor-associated protein, galectin-3. Previously established solid phase polymer synthesis protocols were used as a platform for the implementation of new strategies to allow for the combination of non-glycosidic and glycosidic ligands within one glycomacromolecule. More specifically, orthogonal conjugation methods were implemented by introducing a novel building block carrying a temporarily protected carboxyl side chain allowing for both Staudinger ligation and amine-coupling in combination with CuAAC. Applying this methodology, two series of homo- and heteromultivalent lactose-functionalized glycomacromolecules were synthesized and evaluated for their binding to galectin-3 through inhibition/competition assays and *in vitro* cell studies on human cancer cells.

The first goal of this thesis was the design of a new building block that would enable orthogonal conjugation methods to CuAAC, the standard conjugation method for introduction of carbohydrate ligands, thereby giving access to heteromultivalent glycomacromolecules. Until now, two strategies towards hetero-functionalized glycooligo(amidoamine) were explored, using either pre-functionalized carbohydrate building blocks or a sequential coupling-conjugation approach via CuAAC. While pre-functionalized carbohydrate building blocks are expensive and time consuming, sequential coupling and conjugation strategies are often limited to shorter scaffolds due to side reactions and scaffold degradation. Using CuAAC as one conjugation strategy, orthogonal reactions such as direct amide coupling reactions between a carboxylic acid and an amine-functionality or through a Staudinger ligation between a carboxylic acid and an azide were envisioned, with the later route having the distinct advantage of using the same azido-functionalized carbohydrates as already synthesized for the CuAAC. For this reason, the design, synthesis and introduction of a new carboxy-functionalized building block called methyl succinyl diethylenetriamine succinyl (MDS) for the use in solid supported synthesis was successfully implemented in the first part of this thesis (Figure 23). This building block was designed as a methyl ester-protected carboxylic acid functionality for the deprotection on solid support releasing a free carboxylic acid for the further conjugation of the side chain.

The synthesis of MDS was established according to synthetic strategies, based on the diethylenetriamine core, which is already used for other functional building blocks in this working group.[26, 109, 111, 156] The final synthetic route is shown in Figure 22. By applying this route, the building block was synthesized in an overall yield of 43 % over 6 steps in gram scales and purities higher than 99 % determined by RP-HPLC, thus meeting all requirements for use in solid phase synthesis.

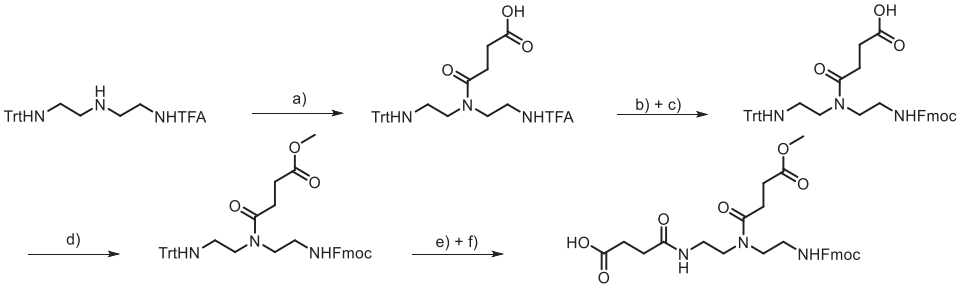

Figure 22: Synthetic route and structure of the new, carboxy functionalized methyl succinyl diethylenetriamine succinyl (MDS) building block: a.) Succinic anhydride, Et_3N, DCM; b) K_2CO_3, H_2O/MeOH; c) Fmoc-Cl, K_2CO_3, H_2O/ethyl acetate; d) MeI, K_2CO_3, DMF; e) TFA, TES, DCM; f) Succinic anhydride, Et_3N, DCM.

The aforementioned MDS building block was then applied to Fmoc-based SPPS coupling protocols. The deprotection of the sidechain was performed on solid support with conditions applicable for the oligo(amidoamine) scaffolds, demonstrating that the protecting group was stable during the scaffold assembly and could be selectively deprotected to expose the carboxylic acid using LiOH without an unintended cleavage or destroying of the scaffold (Figure 23, B). After demonstrating the suitability of the MDS building block for the solid phase synthesis, the establishment of a new conjugation reaction, namely the Staudinger ligation, for the reaction of the deprotected carboxylic side chain of the building block with commonly used azido-carbohydrates was successfully demonstrated, leading to the synthesis of the first homo-glycomacromolecules with amide linkages, as well as a heteroglyomacromolecule carrying a galactose and a mannose residue (Figure 23, C).

Though successful implementation was possible, for moving forward some optimization must be performed for reducing impurities in higher-valent structures. Notably, such amide-linker structures could be useful in further studies to investigate the impact of the triazole motifs on protein binding. The MDS building block also opens up the possibility for the synthesis of new classes of oligo(amidoamines). For example, P. Reuther was able to use this building block for the conjugation of amine-functionalized bisphosphonate ligands for the application on proteins, potentially binding to lysine residues.[185] In addition, the development of this building block also enabled the feasibility of the second part of this thesis which involved the introduction of non-glycosidic residues as a method to tune affinity to a new target protein galectin-3.

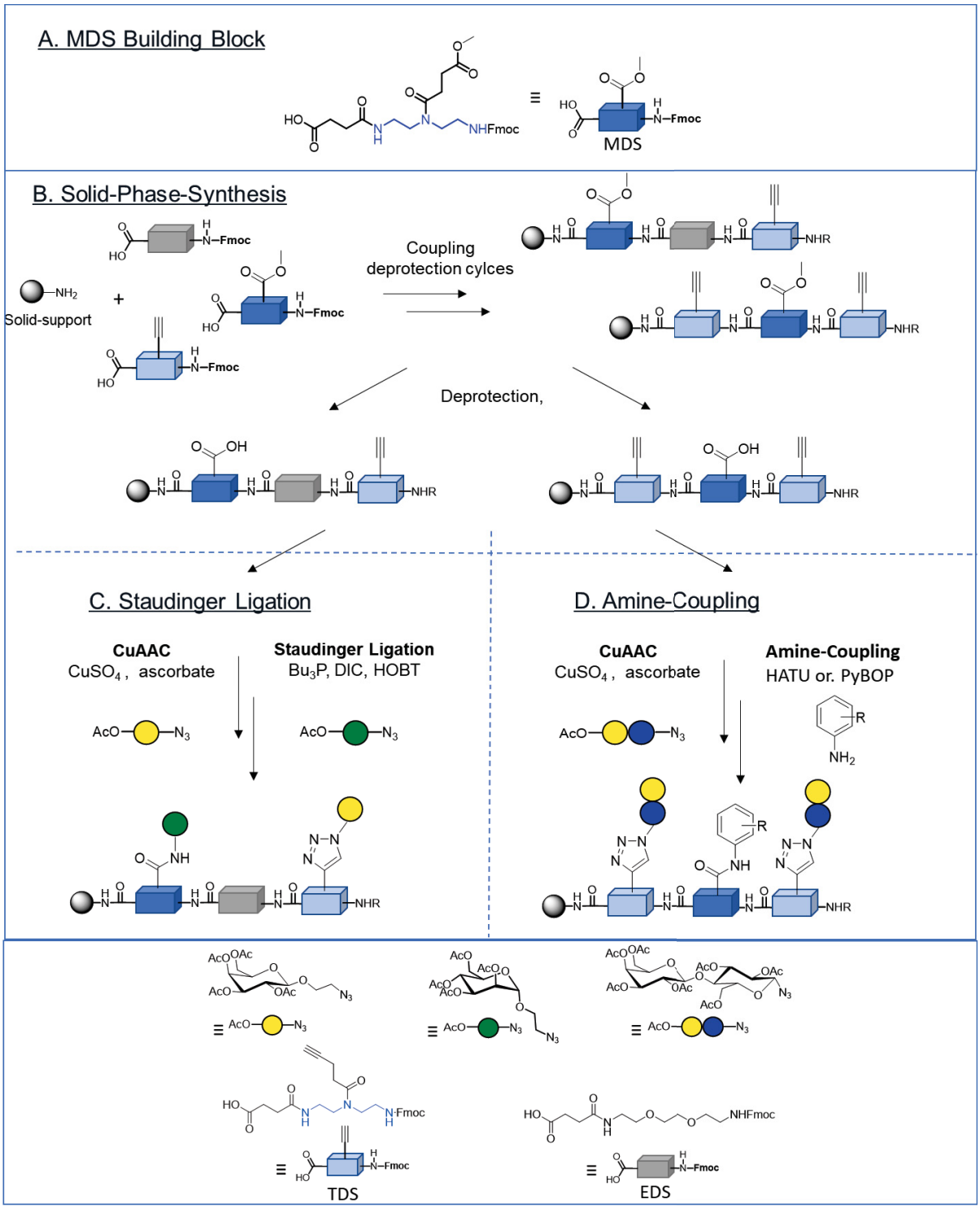

Figure 23: Overview of the synthetic strategies introduced in this work. A. Structure of the new building block MDS. B. Use of MDS in combination with the alkyne building block TDS to design exemplary hetero-functionalized scaffolds. C. Orthogonal modification of the scaffold using Staudinger ligation and CuAAC to synthesize the hetero-functionalized glycomacromolecule Man(1)-Gal(3)-3. D. Orthogonal conjugation approach using amine coupling for conjugation of non-glycosidic moieties on MDS and CuAAC for azido-lactose conjugation onto TDS.

The second goal of this thesis involved the combination of the novel MDS building block with established building blocks such as TDS for rational design of complex homo- and hetero-glycomacromolecules as ligands for galectin-3. Galectin-3 is known to play crucial roles in tumor-associated processes like proliferation and metastasis, and is therefore an interesting target for the development of therapeutics or diagnostic tools. It is well known from literature, that galectin-3 is able to oligomerize to flexible lattices with different distances between the CRDs which are dependent on the glycoligand target.[52, 53, 78] Furthermore, galectin-3 exhibits secondary binding sites next to the main carbohydrate-binding subunit, and is thus an interesting target for the application of sequence-controlled glycomimetics which can be designed to introduce both, glycosidic and non-glycosidic binding motifs addressing both types of binding in galectin-3 (Figure 24, a).

Initially, a first set of glycooligomers presenting either lactose (k_d ~0.2 mM) or galactose (k_d ~10 mM) as binding carbohydrates, or glucose as non-binding negative control of galectin-3 were synthesized. Within the series of lactose-functionalized macromolecules, different structural parameters such as the number and distance of carbohydrate ligands was varied to test for the influence on binding to galectin-3 (Figure 24 A).

ELISA-type inhibition studies were performed in cooperation with the group of Professor Lothar Elling from the RWTH Aachen. In short, galectin-3 binding to an ASF-coated surface was inhibited with different concentrations of the glycomacromolecules resulting in an inhibition curve giving the half maximum inhibition concentration (IC_{50}) of the glycomacromolecules in the case of a binding event. A higher binding results in a higher inhibition represented by lower IC_{50}-value. SPR-inhibition studies were performed as an additional binding assay to verify the trends obtained in the ELISA-type assay. For this, an assay was established, where a glycomacromolecule from this series was conjugated onto a carboxy-functionalized sensor chip surface using an amine-coupling procedure to allow for inhibition/competition assays with the full series of glycomacromolecules. Initial ELISA and SPR studies with the galactose glycooligomers showed no significant inhibition of the lectin, maybe due to the low affinity of galactose to galectin-3 (K_d ~10mM). As expected, both the evaluation in the ELISA-type and SPR inhibition studies of the lactose functionalized glycomacromolecules revealed that a higher valency results in a higher inhibition potency which is in agreement with previous studies from literature for various types of multivalent glycomimetics (Figure 24 B). [53, 56, 69, 77, 81, 86, 186, 187]

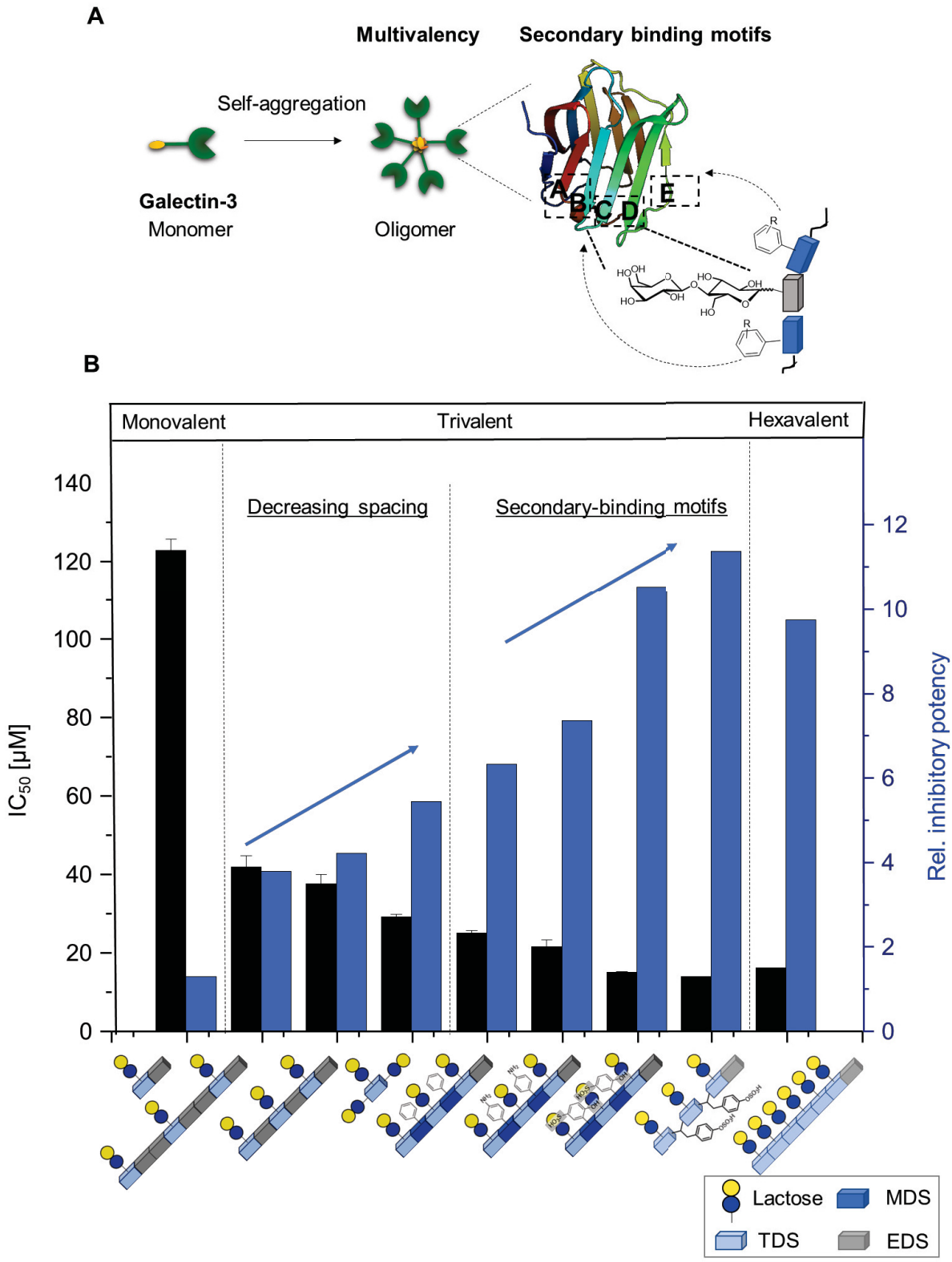

Figure 24: A. Overview of the strategies towards high affinity galectin-3 ligands used in this work: Multivalency addressing the oligomerization of galectin-3; spacing addressing the unknown distance of the CRDs in the oligomeric galectin-3; non-glycosidic moieties addressing secondary binding motifs next to the lactose binding site. B. Overview of selected results obtained from the ELISA-type inhibition studies of galectin-3. Relative inhibition potencies are calculated referencing the IC_{50} value of lactose resulting from the same assay.

Keeping the valency fixed, the influence of the distance between the lactose residues was investigated by sequentially increasing the number of EDS building blocks between the lactose moieties. The smallest structure of this series, Lac_3TPD (tripentynoic acid diethylenetriamine) consisting of just one building block, was synthesized in solution. The results of the ELISA-type inhibition studies showed slightly more effective inhibition and thus higher binding for the smaller structures with less spacer building blocks, with an IC_{50} value of 29 µM for the smallest, most rigid structure Lac_3TPD compared to 42 µM for one of the largest Lac(1,4,7)-8. This slight decrease in binding was also observed for lactose-functionalized glycomacromolecules with a longer linker between the carbohydrate and the scaffold, synthesized by P. Konietzny, and analyzed along with the glycomacromolecules of this thesis.

Based on these findings, selected mono- and trivalent glycooligomers from this thesis were conjugated to lipids for the formulation of liposomes by Miriam Hoffmann. This formulation allows for a further increase in valency to test for the effects of a so-called 'multivalency of multivalency' presentation where carbohydrate ligands are presented multivalently on two different length scales (the oligomer and the liposome). Indeed, attaching the glycooligomers to the liposome resulted in a further increase in inhibitory potency into the nanomolar range. Interestingly, presentation of the trivalent ligands on the liposome leads to a higher increase in inhibitory potency per sugar than the presentation of the monovalent ligands. This indicates that both levels of multivalency influence lectin binding.

After this first successful demonstration of lactose-functionalized glycooligomers as ligands for the new target protein galectin-3, non-glycosidic motifs were introduced to address additional secondary binding sites of the lectin with the goal of further increasing the affinity and potentially selectivity of the glycomimetics. Therefore, lactose-functionalized glycomacromolecules bearing different non-glycosidic aromatic moieties in the side chain were synthesized using the new carboxylic building block introduced in the first part of this thesis. The use of the MDS building block allowed the coupling of different amine-functionalized aromatic, non-glycosidic moieties through an amine-coupling procedure using HATU or PyBOP depending on the sterical hindrance of the residue. The residues used as non-glycosidic moieties were chosen to investigate the influence of the aromatic residues themselves as well as the charge of the residue. Therefore, benzyl was used as an uncharged residue, amino phenyl was used as a basic residue and sulfonic acid-functionalized phenyl residues were used to study sulfation which has also been shown to mediate galectin binding.[69, 70, 74] The TDS building block was used as before for the conjugation of the azido-lactose to generate, in combination with MDS, the desired heteromultivalent structures (Figure 23 D). It was found that steric hindrance of the sidechain to be introduced as

non-glycosidic motif impacted the orthogonal conjugation. Therefore, in some cases, it was necessary to reverse the order of the CuAAC and amine coupling to give the desired products. This demonstrates again the flexibility and benefits of the new building block in combination with the established building blocks, especially the commonly used TDS building block.

The ELISA-type inhibition studies of the heteromultivalent glycomacromolecules revealed that the presence of the non-glycosidic moieties led to higher avidities towards galectin-3 for all of the glycomacromolecules tested, with a decrease of the IC_{50} values down to 14 µM for the best binder, the lactose-sulfonic-acid derivative Lac(1,3,5)-(2-SO_3H-4-OH)Ph(2,4)-6, compared to 38 µM for the homomultivalent counterpart Lac(1,3,5)-6. This demonstrates, that even if the same amount of lactose is presented, a nearly three-times higher inhibition was obtained through additional interaction of galectin-3 with non-glycosidic moieties. Interestingly, the functionality of the residue also appeared to have an impact on the binding, since all structures tested with a sulfonic acid residue showed lower IC_{50} values (14-16 µM) compared to the uncharged benzyl (25 µM) or the amine derivative (22 µM). Using a sulfated derivative of tyrosine instead of the MDS building block leads to a smaller structure which was, as seen before in our previous studies, a slightly affiner binder compared to the larger MDS-sulfonic acid-derivative Lac(1,3,5)-(2-SO_3H-4-OH)Ph(2,4)-6. Glucose-functionalized heteromultivalent glycomacromolecules showed no binding to galectin-3, demonstrating the need for the lactose-residues to target this specific receptor.

In the third part of this thesis, selected homo- and heteromultivalent glycomacromolecules were evaluated in biological cell studies on human cancer cells for the first time. These studies were conducted in collaboration with Professor Nicole L. Snyder and Professor Sophia Sarafova during a research stay at Davidson College in North Carolina. For this purpose, glycomacromolecules were synthesized carrying amine end groups and were finally conjugated with a fluorophore.

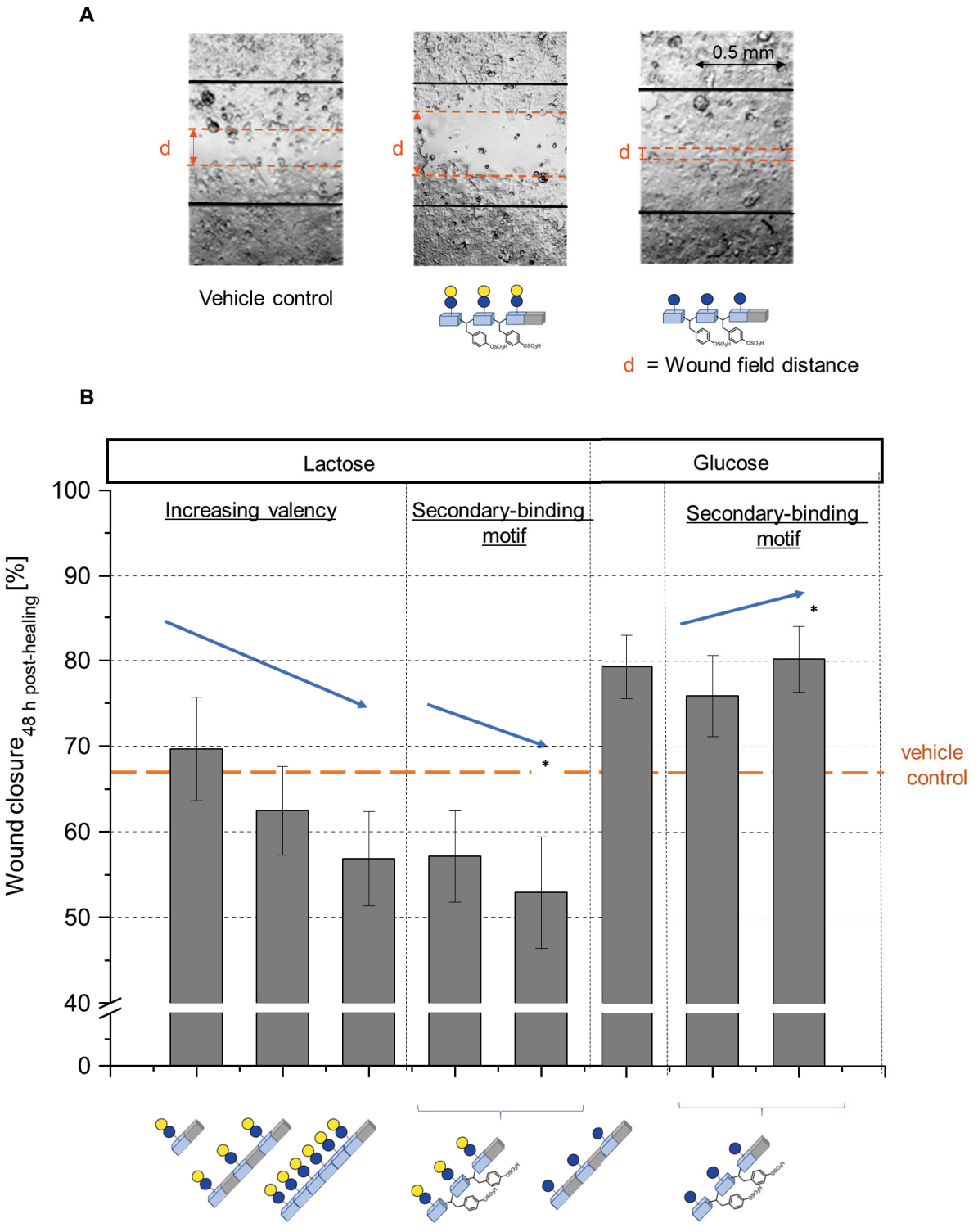

Figure 25: Overview of the results obtained from the wound healing assay. A. Example of wound field image of the MCF 7 cells treated with the vehicle control (left), lactose-functionalized sulfonic acid tyrosine derivative (middle) and glucose-functionalized sulfonic acid tyrosine (right). B. Overview of the wound closure in percentage after 48 h post-healing on MCF 7 breast cancer cells for different glycomacromolecules. Bars highlighted with a star (*) are the results of dosing experiments, meaning a higher concentration of the glycomacromolecules. Wound closure is given in [%] ± SD of two independent wound fields with at least 5 different distance measurements on wound field.

Cell studies were conducted on galectin-3 positive MCF 7 breast cancer cells and galectin-3 negative epithelia HEK 293 cells. The presence or absence of galectin-3 was confirmed by a galectin-3 antibody staining using flow cytometry, a fluorescence technique for quantification. This technique was further used in addition to fluorescence microscopy, to demonstrate the ability of the glycomacromolecules to interact with human cells. For these assays the FITC-derivatives of the glycomacromolecules were used, showing a dose dependent, but cell line and glycomacromolecule independent uptake pointing to a nonselective interaction, which was similarly observed in fluorescence microscopy. Interestingly, differences in cellular localization were observed for uncharged glycooligomers and the charged sulfonic acid containing heteromultivalent glycomacromolecules; slight enrichment of the negatively charged glycomacromolecules around the nucleus was observed in comparison to the uncharged glycomacromolecules. However, at this point it is not possible to differentiate between an enrichment in or on the nucleus. The possibility of the lactose-functionalized macromolecules to affect a biological outcome was successfully demonstrated in a "wound-healing" assay on MCF 7 cells in the next cell assay. There, a wound-field in a cell monolayer for both the MCF7 and HEK 293 cells was created and the wound-closure was observed under the influence of the lactose- and glucose-functionalized glycomacromolecules.

The incubation with lactose-functionalized macromolecules resulted in a delay of the wound closure up to 20 %, which is in the range of other studies known from literature.[68, 188-190] Furthermore, the observed trend is similar to the trends observed in the previous ELISA and SPR inhibition studies. An increased delay was observed when going from the mono- to hexavalent homomultivalent glycomacromolecules and furthermore an increase from the homo-trivalent to the hetero-trivalent structures bearing a sulfonic acid-functionalized aromatic residue (Figure 25). Notably, this was only observed for the galectin-3 positive MCF 7 cells. Furthermore, the glucose negative controls showed an even slightly faster migration compared to the vehicle control and comparing the results of the glucose and lactose counterparts for the higher concentrations, a difference of nearly 30 % was observed, indicating a delay caused by the inhibition of galectin-3 (Figure 25).

Based on the results obtained in this thesis future studies could be performed on the glycomacromolecules used in this thesis, exploring a potential specificity towards different galectins such as Gal-1, as an example for the homodimeric type which already showed promising results in literature. [191, 192] It would also be interesting to expand the library of glycomacromolecules, especially the hetero-glycomacromolecules, to evaluate more non-glycosidic moieties like nitro-groups or halogenated residues.[64] In addition to galectins this

approach could also be applied towards other target proteins showing different impacts of secondary binding motifs such as Langerin or DC-sign.[100, 193] Furthermore, such optimized hetero-glycomacromolecules could be explored as drug-delivery systems: One example could be their application in photo-dynamic therapy. Therefore, a photosensitizer, which can produce single oxygen and thus damage cancer cell tissue, should be conjugated to the glycomacromolecules.[194, 195] Through the specific interaction with cancer cell proteins, the side effect of the photosensitizer should be minimalized. Another similar approach could be the presentation of the hetero-glycomacromolecules on liposome surfaces, to generate high affinity supramolecular systems, which can be further tested as drug delivery systems in cancer cell-based assays as well.

Overall the work in this thesis demonstrated the usefulness of the platform of glycomacromolecules as obtained by solid phase polymer synthesis to develop glycomimetic ligands targeting tumor-related receptors. On the one hand they can serve as model compounds to further understand the underlying mechanisms in multivalent ligand receptor interactions. On the other hand, this study showed the successful application of the glycomacromolecules in cell studies and their potential in novel therapeutic approaches, specifically in that the design of heteromultivalent glycomacromolecules combining both glycosidic and non-glycosidic motifs can help to create ligands with higher affinity and selectivity, a key feature for their further development.

Publications and Author Contributions

1. Toward Orthogonal Preparation of Sequence-Defined Monodisperse Heteromultivalent Glycomacromolecules on Solid Support Using Staudinger Ligation and Copper-Catalyzed Click Reactions

Authors:	**T. Freichel**, S. Eierhoff, N. L. Snyder and L. Hartmann
Journal:	Journal of Organic Chemistry
Issue:	2017, 82, 9400-9409.
Type of paper:	Full Paper
Impact Factor:	4.805 (2018)

1st author contribution:

Collaborative design of the synthetic strategy and structures. Development and optimization of the synthetic route towards the methyl-succinyl diethylene triamine succinic acid building block (MDS). Development and optimization of the solid phase synthesis using the new MDS building block. Joined introduction of the Staudinger ligation on solid support. Optimization of a synthetic strategy using the Staudinger ligation in combination with the new building block and development and optimization of an orthogonal conjugation approach. Synthesis and analysis of all TDS and MDS based structures. Writing of the first manuscript draft followed by collaborative finalization of the manuscript.

JOC The Journal of Organic Chemistry

Article

pubs.acs.org/joc

Toward Orthogonal Preparation of Sequence-Defined Monodisperse Heteromultivalent Glycomacromolecules on Solid Support Using Staudinger Ligation and Copper-Catalyzed Click Reactions

Tanja Freichel,[†] Svenja Eierhoff,[†] Nicole L. Snyder,*[,‡] and Laura Hartmann*[,†]

[†]Department of Organic Chemistry and Macromolecular Chemistry, Heinrich-Heine-University Düsseldorf, 40225 Düsseldorf, Germany

[‡]Department of Chemistry, Davidson College, Davidson, North Carolina 28035, United States

Supporting Information

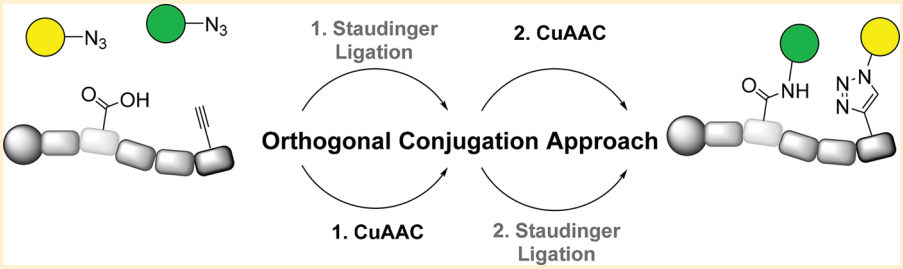

ABSTRACT: The investigation of heteromultivalent interactions of complex glycoligands and proteins is critical for understanding important biological processes and developing carbohydrate-based pharmaceutics. Synthetic glycomimetics, derived by mimicking complex glycoligands on a variety of scaffolds, have become important tools for studying the role of carbohydrates in chemistry and biology. In this paper, we report on a new synthetic strategy for the preparation of monodisperse, sequence-defined glycooligomers or so-called precision glycomacromolecules based on solid phase oligomer synthesis and the Staudinger ligation. This strategy employs a solid-supported synthetic approach using a novel carboxy-functionalized building block which bears a functional handle required for Staudinger ligation on solid support. Furthermore, we combined Staudinger ligation and copper catalyzed azide alkyne cycloaddition (CuAAC) reactions to synthesize heteromultivalent glycooligomers on solid support for the first time, demonstrating the utility of this approach for the synthesis of heterofunctional glycomacromolecules.

INTRODUCTION

Protein−carbohydrate interactions play a major role in biological processes including cell−cell communication, cell adhesion, and pathogen−host interactions.[1] Natural glycoligands are complex structures, consisting of different monosaccharides arranged in linear or branched fashions that are further conjugated to lipids or proteins. It has been shown that the orientation, spacing, and adjacent functionalities in the natural glycoligand structures have great impact on the affinity and selectivity of the glycan in protein binding and thereby their biological function.[2,3]

However, it has also been shown that despite their great complexity, natural glycoligands can be mimicked by more simplified structures such as the glycopolymers. Here, a carbohydrate motif, e.g. a mono- or disaccharide, is presented in the side chain of a synthetic polymer. Such structures mimic the multivalent structure of more complex carbohydrate or glycoconjugate ligands and still allow for selective binding to a protein receptor.[4] Several binding mechanisms have been identified to contribute to glycopolymer−protein binding, and a great variety of structurally diverse glycopolymers have helped to gain insight into their structure−property correlation.[5,6] Nevertheless, since most glycopolymers are still derived by means of classical polymer synthesis, their intrinsic polydispersity remains a limiting factor, e.g. hampering installation of a monomer sequence in the glycopolymer.

In an effort to overcome this limitation and obtain monodisperse, sequence-controlled glycooligo- and polymers, so-called precision glycomacromolecules were developed.[5] Through the stepwise addition of tailor-made building blocks following standard peptide coupling on solid support as first introduced by Merrifield, monodisperse and sequence-controlled oligo(amidoamine) scaffolds are obtained. A subset of building blocks has been introduced placing functional groups in the side chain of the scaffold allowing for functionalization with carbohydrate ligands e.g. via CuAAC or thiol−ene conjugation.[7,8] Through variation of the monomer sequence during solid phase assembly, control over the valency (number of ligands), interligand spacing, overall length, and the architecture of the precision macromolecules is realized. Furthermore, different carbohydrate ligands can be combined

Received: June 6, 2017
Published: August 28, 2017

DOI: 10.1021/acs.joc.7b01398
J. Org. Chem. 2017, 82, 9400−9409

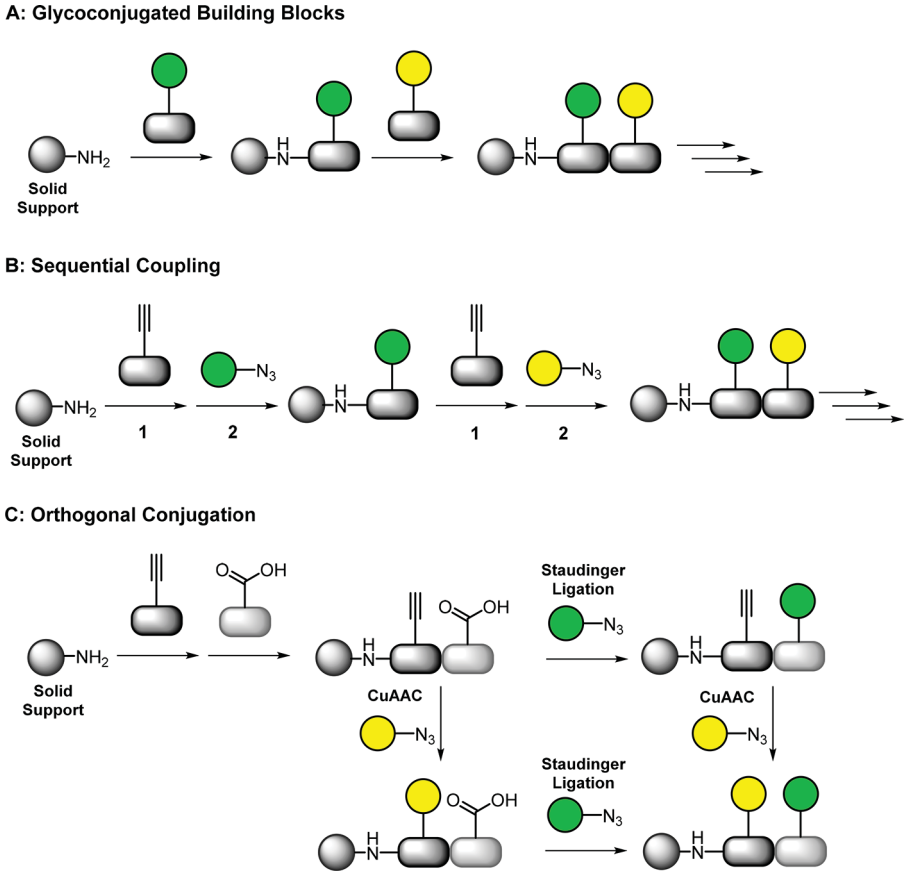

Figure 1. Scheme of different synthetic routes to heteromultivalent glycooligomers. (A) Glycoconjugated building block approach. Assembly of preconjugated building blocks. (B) Sequential coupling of one type of building block (1) and conjugation (2) with different types of carbohydrates. (C) Formation of heterofunctionalized scaffolds consisting of different building blocks for specific, orthogonal attachment of carbohydrates via different conjugation strategies (Here: Staudinger ligation and CuAAC).

within one glycomacromolecule giving so-called heteromultivalent structures.[11] Previously, we have introduced two different approaches for the synthesis of heteromultivalent glycomacromolecules: The "building block" approach, shown in Figure 1A, is based on the stepwise assembly of glycoconjugated building blocks,[9] while the "sequential coupling" approach, shown in Figure 1B, involves iterative coupling followed by CuAAC conjugation.[3]

While both approaches give access to heteromultivalent structures, they are limited in terms of the excess of synthetically expensive building blocks (building block approach) or by harsh reaction conditions (e.g., repeated exposure of scaffolds to copper salts can lead to scaffold degradation over time). One possible approach to avoid these drawbacks is the orthogonal conjugation strategy shown in Figure 1C. In this example, a multifunctionalized scaffold is modified by different, orthogonal conjugation strategies.[8,10]

We envisioned the use of a carboxy-functionalized building block to facilitate a Staudinger reaction with a glycosyl azide on solid support giving access to an orthogonal conjugation method to the previously established CuAAC. The Staudinger ligation has gained attention in recent years for its utility in *in vivo* and *in vitro* labeling experiments and the combination of small peptide fragments into larger peptides.[12] This is due to the fact that the Staudinger ligation is a so-called "click-reaction", which is known to be fast, selective, efficient, and traceless.[13] During the Staudinger ligation, an azide derivative is activated by alkyl or aryl phosphines for further reaction with carboxyl functionalities, resulting in amide bond formation.[14]

Despite the utility of the Staudinger ligation, there are just a few examples in literature that apply the Staudinger ligation on solid support. The majority of these examples bear a single azide functionality on solid support for reaction with activated acids in solution and lead to a single conjugated product in modest yields.[15−17] For example, Toth et al. demonstrated that a glycosyl azide functionalized solid support could undergo Staudinger ligation with short amino acid sequences to obtain monovalent glycoconjugates.[16,17] However, to the best of our knowledge, there are no reported attempts where multiple Staudinger ligations have been used to generate homo- or heteromultivalent constructs.

In this paper, we describe the use of a three-component Staudinger ligation on solid support to generate both homomultivalent and heteromultivalent glycoconjugates. In contrast to previous reports, we chose to prepare scaffolds functionalized with carboxyl functional groups so that readily accessible or even commercially available glycosyl azides could be used in the reaction. While our initial attempts used a commercially available Boc protected glutamic acid residue, our work quickly necessitated the development of a novel building block bearing a carboxy functionalized side chain suitable for our studies. The synthesis of this building block, its subsequent incorporation into scaffolds on solid support, and its application to the Staudinger ligation on solid support are reported herein.

DOI: 10.1021/acs.joc.7b01398
J. Org. Chem. 2017, 82, 9400−9409

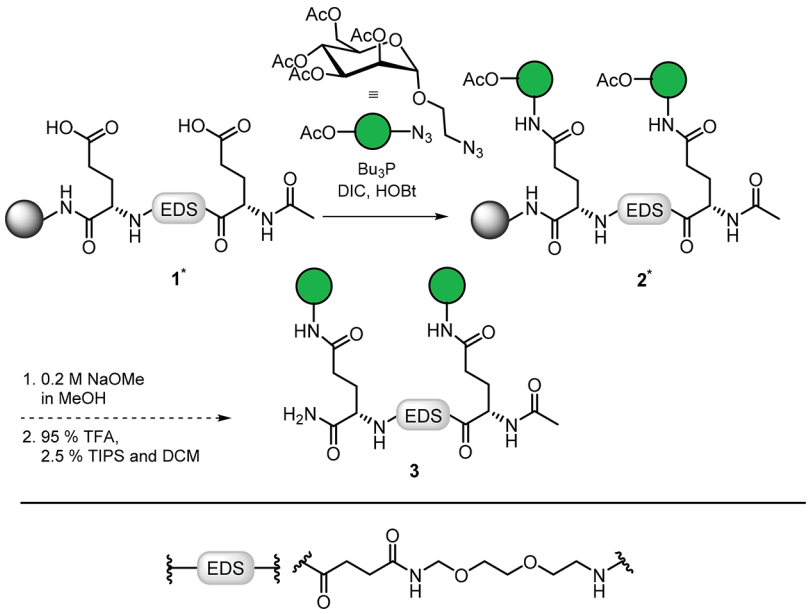

Figure 2. Initial synthetic approach using Glu and EDS.[3] Structures attached to the resin are denoted by an asterisk (*).

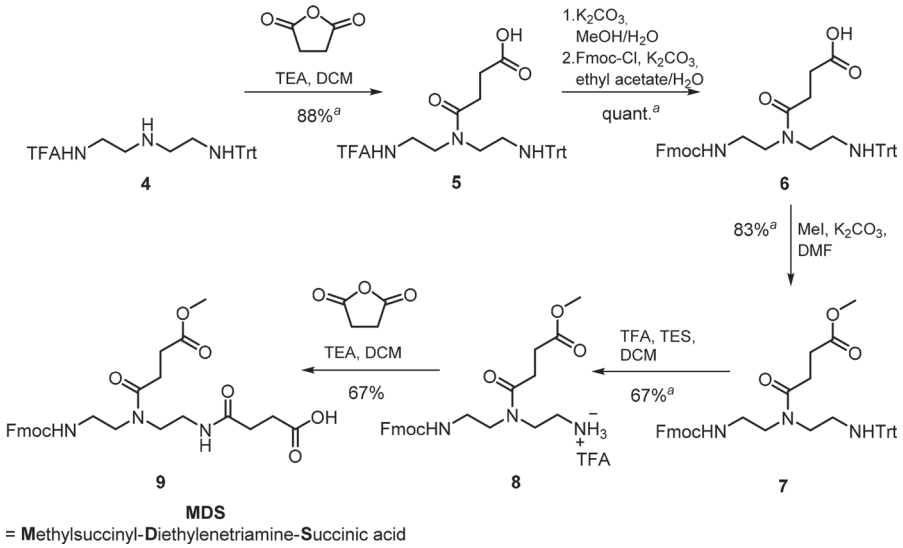

Figure 3. Synthesis of the new MDS (= Methyl-succinyl-Diethylenetriamine-Succinic acid) building block. [a] Crude yields.

RESULTS AND DISCUSSION

Our initial approach involved the solid supported synthesis of scaffolds bearing a carboxylic acid in the side chain using well-established peptide coupling, specifically a sequential procedure of acid activation, amine coupling and Fmoc deprotection. For simplicity, we selected a commercially available Boc protected glutamic acid residue (Glu) as a functionalizable building block and previously reported EDS (**E**thylene glycol-**D**iamine**S**uccinic acid)[3] as a spacer building block to generate a Glu-EDS-Glu (GEG, **1**) scaffold (Figure 2). A three-component Staudinger ligation was then performed on the scaffold with (2-azidoethyl)-2,3,4,6-tetra-*O*-α-D-mannopyranoside (Man-N_3) and tributyl phosphine (Bu_3P) in DMF on solid support. Since it has been well established that the ligation between azides and acids at room temperature only occurs in the presence of activation reagents, *N*,*N*-diisopropylcarbodiimide (DIC) and hydroxybenzyltriazole (HOBt) (2.5 equiv each) were used for this purpose. The reaction led to a mixture of products consisting predominantly of the fully glycosylated scaffold Man(1,3)GEG (**2**), along with a complex mixture of monoglycosylated scaffolds and starting material as shown by RP-HPLC analysis (Figure S26). While compound **2** could be isolated by RP-preparative HPLC to give pure **2**, further attempts to remove the acetyl protecting groups on solid support using Zemplén conditions led to significant epimerization of the α-carbons on the Glu residue leading to an inseparable mixture of products (data not shown).

While this approach allowed us to demonstrate the feasibility of the Staudinger ligation on solid support, the significant challenges we encountered, particularly with the epimerization reactions following ester hydrolysis, necessitated the development of a building block that would limit these unwanted side reactions. Therefore, we designed and developed the MDS (**M**ethyl-succinyl-**D**iethylenetriamine-**S**uccinic acid) building block for our further studies. The MDS building block, which bears a protected carboxylic acid, was inspired by other

DOI: 10.1021/acs.joc.7b01398
J. Org. Chem. 2017, 82, 9400−9409

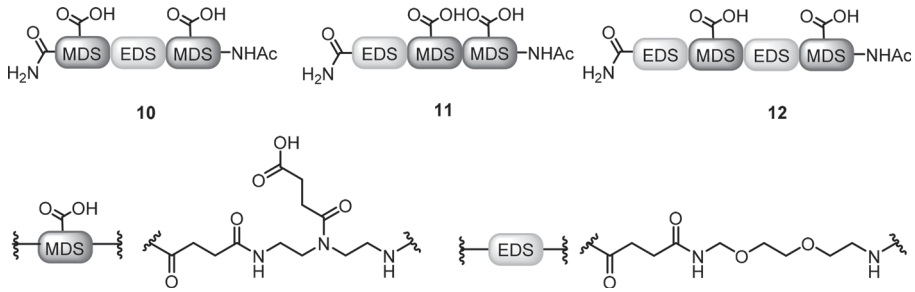

Figure 4. Scheme of scaffolds synthesized containing MDS and EDS building blocks.

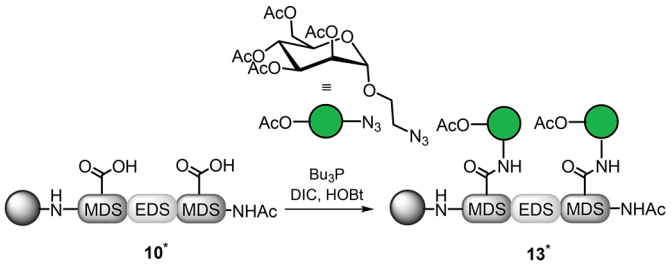

Structures	Mass Analysis
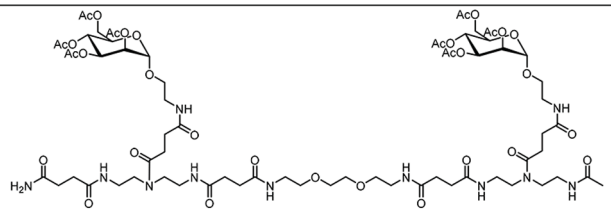 protected Man(1,3)-3 MEM, **13**	Expected Mass: 1605.70 Found Mass 803.95$[M+2H]^{2+}$
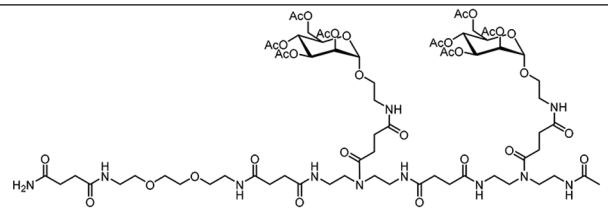 protected Man(2,3)-3 EMM, **14**	Expected Mass: 1605.70 Found Mass 803.95$[M+2H]^{2+}$
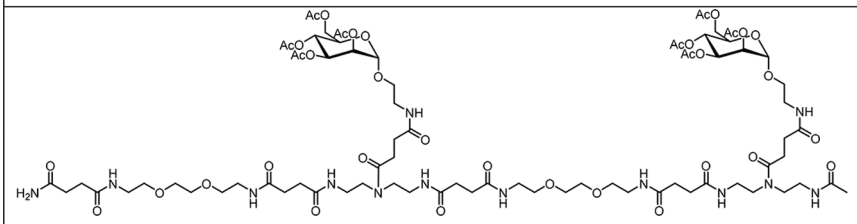 protected Man(2,4)-3 EMEM, **15**	Expected Mass: 1835.83 Found Mass: 919.00$[M+2H]^{2+}$

Figure 5. Reaction scheme of the Staudinger ligation on solid support, shown for MEM scaffold **10**. Below: Overview of syntheszied protected structures and ESI-MS analysis. Structures attached to the resin are denoted by an asterisk (*).

functionalizable building blocks used in our group.[7] The methyl ester protecting group was chosen because it is compatible with Fmoc (fluorenylmethyloxy-carbonyl)-based solid phase synthesis, stable against TFA, and cleavable on solid support.

The synthesis of the MDS-building block started from the reaction between succinic anhydride and asymmetrically protected compound **4** (Figure 3).[7] Cleavage of the TFA-protecting group of **5** with methanolic K_2CO_3, followed by the Fmoc protection of the resulting primary amine, led to compound **6**. Methylation of the carboxylic acid side chain with methyl iodide in the presence of K_2CO_3 provided compound **4**. TFA cleavage of the trityl group of **7** gave **8** in 67% yield over two steps. Coupling of the primary amine of **8** with succinic anhydride gave MDS **9** in 67% yield and an overall yield of 43% over five steps.

With the MDS building block in hand, solid phase synthesis was used to prepare three scaffolds: MDS-EDS-MDS (MEM, **10**), EDS-MDS-MDS (EMM, **11**), and EDS-MDS-EDS-MDS

DOI: 10.1021/acs.joc.7b01398
J. Org. Chem. 2017, 82, 9400−9409

(EMEM, **12**), shown in Figure 4. Deprotection of the methyl ester protecting group on solid support was performed with a solution of 2 M LiOH in THF/water to release the free carboxylic acid for further ligation.[18] Optimization of the Staudinger ligations was performed on MEM scaffold **10**.

The Staudinger ligation was performed on solid support with Man-N_3 and Bu_3P in DMF as shown in Figure 5. Initial results showed only low conversion to the desired product (~4%) and an appreciable amount of the monoconjugated derivative (~20%) as well as starting material (~70%). We hypothesized that higher conversions could be achieved using a multicoupling approach. In an effort to investigate this approach, the reaction was performed up to five times on the same scaffold. Reaction conversions were analyzed by RP-HPLC after each coupling, and the results are summarized in Table 1. The multicoupling approach led to higher product conversion; however, the appearance of an unknown side product also appeared to be growing over time. Spectroscopic analysis of the side product after preparative HPLC revealed a reaction between the carboxylic acid side chain of the MDS building block and methylamine formed from the hydrolysis of DMF (Figures S1 and S2).[19]

Table 1. Overview of the Conversion of the Staudinger Reaction after Five Couplings on MEM 10, EMM 11, and EMEM 12 Scaffold in DMF, ACN, and DMF/ACN[a]

	Diconjugated [%]			Side product [%]	
scaffold	DMF	ACN	DMF/ACN	DMF	DMF/ACN
MEM	65	60	70	20	10
EMEM	63	55	–	17	–
EMM	69	58	–	21	–

[a]Results are based on RP-HPLC data of the protected products after microcleavage by integration of the signals at 214 nm. HPLC: 100% A to 50% A in 30 min.

In an effort to circumvent the dimethylamide side product obtained by performing the Staudinger ligation in DMF, ACN was tested as a suitable solvent for our system.[20] Reactions carried out in ACN were performed as described for DMF, although a few drops of DMF were still necessary to dissolve the HOBt. The results of the initial coupling demonstrated that formation of the side product could be suppressed; however, conversion to the desired product was less efficient when compared to DMF. Surprisingly, applying a multicoupling approach in ACN did not appreciably improve the yields of the desired product (Table 1).

Side product formation in DMF and incomplete conversion in ACN motivated us to perform Staudinger ligation in a 1:1 DMF/ACN mixture. Figure 6 compares the results from Staudinger reactions on MEM scaffold **10** performed in DMF and DMF/ACN (1/1) after deprotection and isolation, giving Man(1,3)-3 MEM (**16**). Increasing the concentration of ACN in the reaction led to slower conversion but lower side product formation (10% in ACN compared to 20% in DMF), which made it easier to isolate the desired product from the crude mixture after cleavage by preparative RP-HPLC with a purity ≥99%.

Orthogonal strategies are particularly attractive for synthesis of heteromultivalent systems by an orthogonal coupling strategy. Therefore, we attempted to combine the optimized Staudinger ligation with the more commonly applied CuAAC reaction, which is used for the conjugation of azide functionalized carbohydrates to alkynes. For example, our group has previously reported the use of CuAAC to synthesize homo- and heteromultivalent glycooligomers using azide functionalized carbohydrates and scaffolds bearing TDS.[3,7] As a proof of concept, both conjugation strategies were first performed with Man-N_3 resulting in the protected Man(1,3)-3 MET **21*** as shown in Figure 7 (Table 2).

The MET scaffold **17*** was synthesized on solid support as described before, and the methyl ester side chain was deprotected before the first conjugation reaction resulting in structure **18*** (Figure 7). To develop an orthogonal strategy, both reactions should be independent from each other, so that the order of the conjugation steps is arbitrary. Therefore, two different reaction sequences were tested to verify the orthogonality of the Staudinger ligation and CuAAC reactions on solid support (Figure 7).

For pathway A, the Staudinger ligation was performed first giving structure **19***. Five couplings in ACN yielded nearly full conversion to the desired product with only a small amount of starting material remaining. CuAAC was then performed with $CuSO_4$ in the presence of sodium ascorbate in a DMF/water mixture overnight, resulting in complete addition of the carbohydrate to TDS as well as the unreacted starting material remaining from the incomplete Staudinger ligation (giving **20***). After the de-*O*-acetylation of the carbohydrates on solid support, the purity of Man(1,3)-3 MET **22** was determined by RP-HPLC to be 86%. It was also possible to purify the resulting

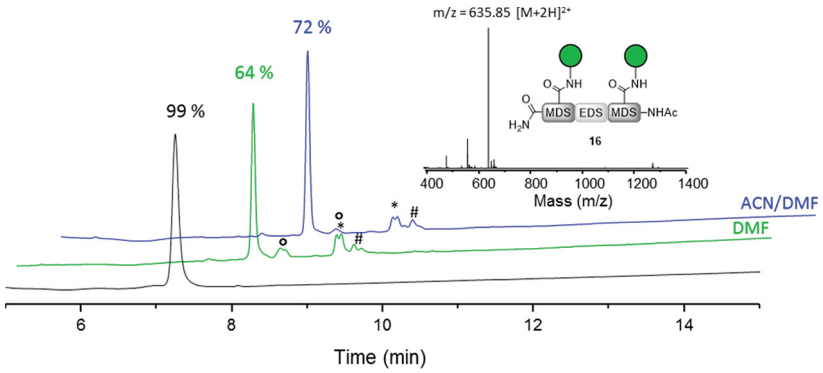

Figure 6. Comparison of RP-HPLC analysis of the deprotected products Man(1,3)-3 MEM **16** from the reaction in DMF (green), DMF/ACN (1/1) (blue), and purified product after preparative RP-HPLC (black). ° Monoconjugated derivative product; * Side product. # Unknown. ESI-MS spectrum of compound **16**.

DOI: 10.1021/acs.joc.7b01398
J. Org. Chem. 2017, 82, 9400−9409

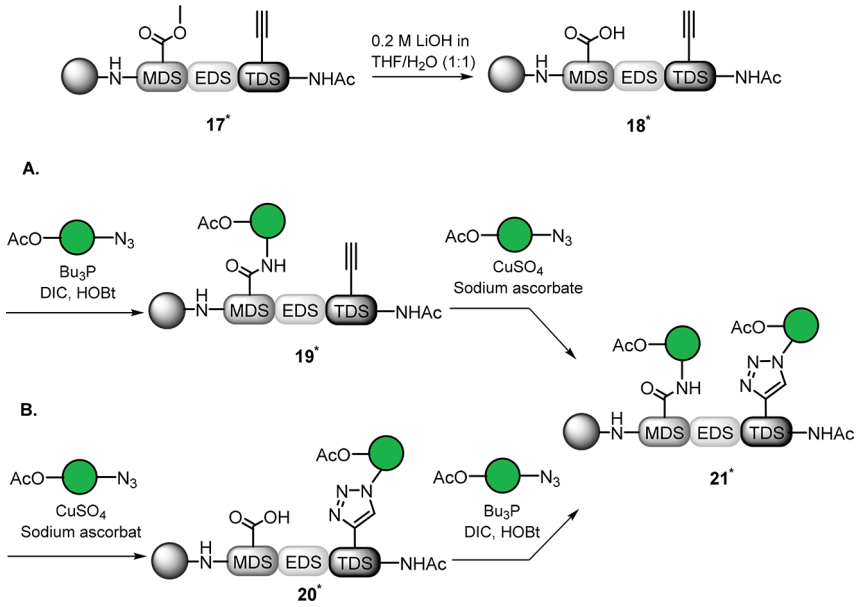

Figure 7. Scheme of the orthogonal conjugation on MDS-EDS-TDS scaffold. (A) Staudinger ligation in ACN, followed by CuAAC. (B) CuAAC, followed by Staudinger ligation in ACN. Structures attached to the resin are denoted by an asterisk (*).

Table 2. Overview of the Structures Synthesized with Orthogonal Conjugation Strategy: Homodivalent Man(1,3,)-3 MET 22 and Heterodivalent Man(1)-Gal(3)-3 MET 23

Structures	Mass Analysis
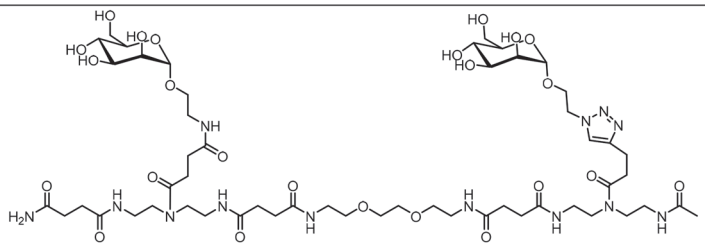 Man(1,3)-3 MET, **22**	Expected Mass: 1293.63 Found Mass 647.85$[M+2H]^{2+}$
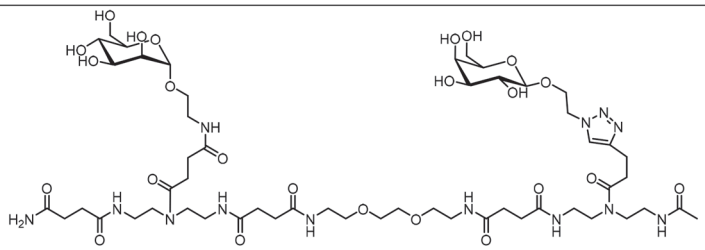 Man(1)-Gal(3)-3 MET, **23**	Expected Mass: 1293.63 Found Mass 648.00$[M+2H]^{2+}$

crude product by preparative RP-HPLC to >99% purity (Figure 8).

For pathway B, the CuAAC reaction was performed first giving structure **20***. The CuAAC reaction was performed overnight as described for pathway A resulting in full addition of the carbohydrate to TDS. Interestingly, the Staudinger ligation only required a triple coupling for nearly full conversion. Deprotection of the carbohydrate residues led to **22** in 88% purity as determined by RP-HPLC (Figure 8).

Comparison of pathway A and B demonstrated the orthogonality of our approach on solid support, and similar results were obtained with regard to the final purity of **22**. Nevertheless, pathway B was more efficient than pathway A based on the observation that full Staudinger ligation could be achieved with only three couplings. One possible explanation for this observation is that the copper preactivates the carboxylic acid so that the ligation is favored. However, attempts to try to increase the yield by pre-exposing the scaffold to CuAAC conditions in the absence of an azide prior to Staudinger ligation did not lead to appreciably higher conversions (data not shown). Another possibility is that the presence of the first sugar promotes the second attachment.

Next, we applied this strategy to prepare heteromultivalent structures such as Man(1)-βGal(3)-3 MET **23** using Man-N_3 and 2-azidoethyl-2,3,4,6-tetra-*O*-acetyl-β-galactopyranoside (βGal-N_3) (Table 2). The βGal-N_3 was conjugated to the deprotected MET scaffold **18*** via CuAAC as described before, resulting in the precursor **24*** (Figure S3). The conjugation of

DOI: 10.1021/acs.joc.7b01398
J. Org. Chem. 2017, 82, 9400−9409

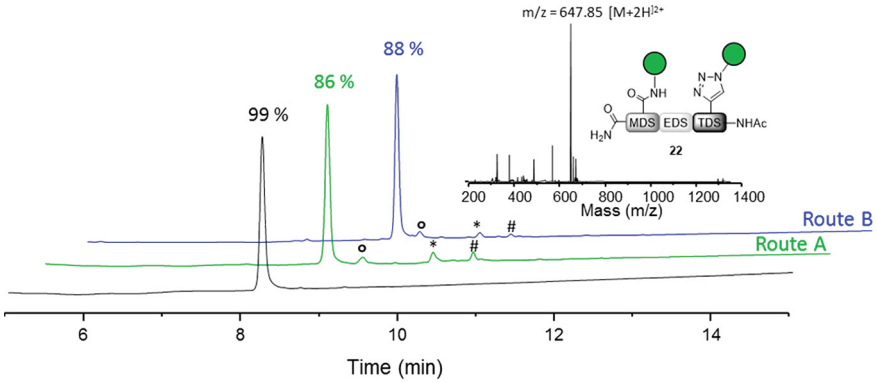

Figure 8. Comparison of the RP-HPLC analysis of deprotected Man(1,3)-3 MET **22** synthesized via Route A, purity of 86% (green); Route B, purity of 88% (blue) and after preparative HPLC, purity ≥99% (black) and ESI-MS spectrum of compound **17**. ° Monoconjugated product.

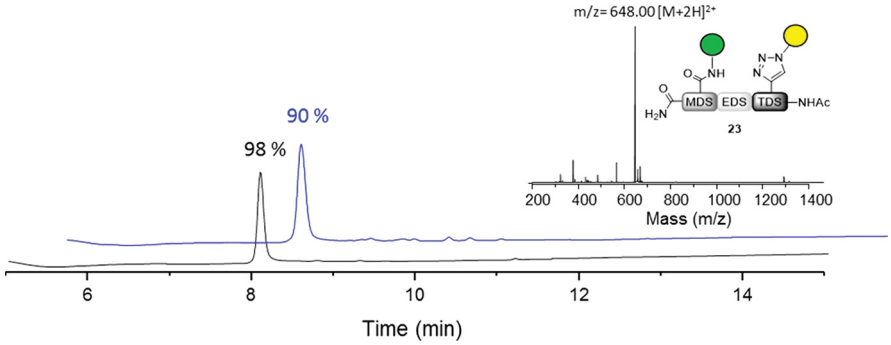

Figure 9. RP-HPLC analysis of deprotected Man(1)-Gal(3)-3 MET **23** synthesized via Route A, purity of 90% (blue) and after preparative HPLC, purity 98% (black) and ESI-MS spectrum of compound **23**.

Man-N_3 via Staudinger ligation gave protected compound **25***, which was globally deprotected to yield Man(1)-βGal(3)-3 MET **23** in 90% purity. Preparative HPLC yielded 98% pure compound determined by RP-HPLC as shown in Figure 9.

CONCLUSION

Within this work, Staudinger ligation for the conjugation of azide functionalized carbohydrates to carboxylic acids on solid support was introduced and successfully applied to an orthogonal synthetic approach for sequence-defined glycooligomers. Initial experiments with glutamic acid led to several synthetic challenges. Therefore, a methyl ester protected carboxy-functionalized building block (MDS) was synthesized to overcome the aforementioned limitations. The new building block was introduced into scaffolds using standard Fmoc based solid supported synthesis. Staudinger ligation in DMF could be forced to higher conversions through a multicoupling strategy. However, our results revealed the formation of a significant side product formed through the reaction of the acid with dimethylamine (a product of hydrolysis of DMF). Attempts to suppress this side reaction using ACN were successful; however, the desired product was achieved in slightly lower yields using this approach. Finally, the combination of the optimized Staudinger ligation in ACN with a CuAAC reaction was successfully applied for the orthogonal preparation of sequence-defined homo- and heteromultivalent glycooligomers demonstrating the potential of this method for the synthesis of heterofunctional systems.

EXPERIMENTAL SECTION

Materials and Methods. *N,N′*-Diisopropylcarbodiimide (DIC) and tributylphosphine were purchased from Sigma-Aldrich. Succinic anhydride, piperidine, and dimethylformamide (for peptide synthesis) were purchased from Acros Organics. Triethylamine and other solvents were purchased from Fisher Scientific. PyBOP and HOBt were purchased from Iris Biotech and methyl iodide from Merck. DIPEA was purchased from Carl Roth, lithium hydroxide, and potassium carbonate from PanReac AppliChem. Solid phase synthesis was performed on TentaGelSRam resin purchased from Rapp Polymere using polypropylene reactors with polyethylene frits closed with luerstoppers from MultiSyntech GmbH. All reagents and solvents were used without further purification. Building blocks TDS,[21] EDS,[7] and 2,2,2-trifluoro-*N*-(2-((2-(tritylamino)ethyl)amino)ethyl)-acetamide and (2-azidoethyl)-2,3,4,6-tetra-*O*-acetyl-α-D-mannopyranoside were synthesized as reported earlier.[7] (2-Azidoethyl)-2,3,4,6-tetra-*O*-acetyl-β-D-galactopyranoside was synthesized as described in the literature.[22] Reactions were monitored via analytical thin layer chromatography, performed on Merck silica gel 60 F254 plates, and visualized with ninhydrin staining.

^{1}H NMR, ^{13}C NMR, and HSQC NMR spectra were measured on a Bruker Avance III 300 or Bruker Avance III 600. High resolution ESI (HR-ESI) measurements were performed on UHR-QTOF maXis 4G (Bruker Daltonics). LC-MS measurements were performed on Agilent Technologies 6120 series coupled with an Agilent Quadrupol mass spectrometer. All LC-MS runs were performed with solvent A = 5% ACN in H_2O and solvent B = 95% ACN in H_2O as mobile phases. The solvents were used with 0.1% of formic acid. Purities of the compounds were determined by the integrations of the signals given at an absorption at 214 nm. Reversed phase HPLC (RP-HPLC) was performed on an Agilent 1200 series. For preparative HPLC, a gradient of 10% to 20% ACN in H_2O in 10 min was chosen. Yields of the final Staudinger products were determined after preparative purification and calculated in regard to the loading of the resin

DOI: 10.1021/acs.joc.7b01398
J. Org. Chem. 2017, 82, 9400−9409

provided by the supplier. Crude yields were determined after workup and without further purification. Melting point measurements were performed on Büchi Melting Point B-540.

Synthesis of Methylsuccinyl-Diethylenetriamine-Succinic Acid (MDS). *4-Oxo-4-((2-(2,2,2-trifluoroacetamido)ethyl)(2-(tritylamino)ethyl)amino)butanoic Acid (**5**).* To a solution of 2,2,2-trifluoro-*N*-(2-((2-(tritylamino)ethyl)amino)ethyl)acetamide[7] (14.90 g, 33.8 mmol, 1 equiv) in 270 mL of DCM were added Et_3N (10 g, 14 mL, 101 mmol, 3 equiv) and succinic anhydride (3.38 g, 33.8 mmol, 1 equiv). The reaction mixture was stirred for 1.5 h at room temperature, then diluted, and washed two times with 100 mL of citric acid (10%). After the mixture was dried with Na_2SO_4, the solvent was removed under reduced pressure to obtain the crude as a white foam. The crude was recrystallized from ethyl acetate to give a white solid (16.1 g; 88%). ^{1}H NMR (300 MHz, Methanol-d_4) δ 7.45−7.39 (m, 6H, **CH**−Trityl), 7.29−7.23 (m, 6H, **CH**−Trityl), 7.19−7.13 (m, 3H, **CH**−Trityl), 3.61 (t, J = 6.6 Hz, 1 H, −(CO)−NH−**CH$_2$**−CH$_2$), 3.51−3,45 (m, 4H, −**CH$_2$**−NHTFA, −(CO)−NH−**CH$_2$**−CH$_2$), 3.38 (t, J = 5.9 Hz, 1 H, −(CO)−NH−**CH$_2$**−CH$_2$), 2.75−2.66 (m, 2H, −CH$_2$−**CH$_2$**−COOH), 2.62−2.56 (m, 2H, −**CH$_2$**−CH$_2$−COOH), 2.35 (dt, J = 13.0, 6.1 Hz, 2H, −**CH$_2$**−NHTrt). ^{13}C NMR (75 MHz, Methanol-d_4) δ 176.6, 176.5, 175.2, 174.7, 147.3, 147.0, 129.8, 128.8, 127.5, 127.4, 72.2, 46.3, 43.9, 38.8, 30.3, 30.3, 29.2, 28.9. HRMS (ESI) m/z: [M + H]$^+$ calcd for $C_{29}H_{31}F_3N_3O_4$, 542.2261; found, 542.2260.

*4-((2-((((9H-Fluoren-9-yl)methoxy)carbonyl)amino)ethyl)(2-(tritylamino)ethyl)amino)-4-oxo-butanoic Acid (**6**).* K_2CO_3 (27.0 g, 195 mmol, 7 equiv) was dissolved in 30 mL of water and added to a solution of **5** (15.0 g, 28.0 mmol, 1 equiv) in 300 mL of MeOH. The reaction mixture was stirred for 18 h at room temperature.

The solvent was removed under reduced pressure and dried under high vacuum. The crude product was then redissolved in 90 mL of ethyl acetate and 70 mL of water. 9-Fluorenylmethoxycarbonyl chloride (7.5 g, 29.0 mmol, 1.05 equiv) was then added to the solution. After stirring for 18 h, the aqueous layer was separated and the organic layer was washed two times with 100 mL of citric acid (10%) and dried with Na_2SO_4. The solvent was removed under reduced pressure to obtain the product as a white solid (19.1 g; quant.). The product was used in the next step without further purification. ^{1}H NMR (600 MHz, Methanol-d_4) δ 7.78−7.74 (m, 2H **CH**−fluorene), 7.62−7.60 (m, 2H **CH**−fluorene), 7.43−7.33 (m, 8H, **CH**−fluorene, **CH**-trityl), 7.29−7.14 (m, 11H, **CH**−fluorene, **CH**−trityl), 4.20−4.16 (m, 1H, Fmoc−**CH**), 3.50 (t, J = 6.6 Hz, 1H, −CONH**CH$_2$**), 3.43 (t, J = 6.1 Hz, 1H, −CONH**CH$_2$**), 3.39 (dt, J = 12.1, 6.2 Hz, 2H, −CONH**CH$_2$**), 3.27 (t, J = 6.5 Hz, 1H, −CONH**CH$_2$**), 3.20 (t, J = 6.2 Hz, 1H, −CONH**CH$_2$**), 2.72 (t, J = 6.8 Hz, 1H, −CH$_2$−**CH$_2$**−COOH), 2.66 (t, J = 6.6 Hz, 1H, −CH$_2$−**CH$_2$**−COOH), 2.59−2.56 (m, 2H, −**CH$_2$**−CH$_2$−COOH), 2.37 (t, J = 6.1 Hz, 1H, −**CH$_2$**−NHTrt), 2.29 (t, J = 6.3 Hz, 1H, −**CH$_2$**−NHTrt). ^{13}C NMR (151 MHz, Methanol-d_4) δ 176.6, 176.5, 174.8, 174.8, 158.8, 147.3, 146.9, 145.3, 145.3, 142.6, 129.8, 129.8, 128.9, 128.8, 128.8, 128.7, 128.1, 127.5, 127.4, 126.1, 126.1, 120.9, 120.9, 72.3, 72.2, 67.7, 67.5, 50.3, 47.9, 47.3, 43.9, 43.5, 40.0, 39.6, 30.4, 30.4, 29.3, 29.0. HRMS (ESI) m/z: [M + H]$^+$ calcd for $C_{42}H_{42}N_3O_5$, 668.3119; found, 668.3124.

*Methyl 4-((2-((((9H-Fluoren-9-yl)methoxy)carbonyl)amino)ethyl)(2-(tritylamino)ethyl)amino)-4-oxo-butanoate (**7**).* Compound **6** (17.9 g, 26.1 mmol, 1 equiv) was dissolved in 140 mL of DMF under argon at room temperature. K_2CO_3 (7.2 g, 52.2 mmol, 2 equiv) was added, and the reaction mixture was stirred for 10 min. Methyl iodide (11.1 g, 4.9 mL, 78.3 mmol, 3 equiv) was then added, and the reaction was stirred overnight. The reaction mixture was precipitated using water (1.5 L) to produce a white solid. After decantation of the supernatant, the precipitation was extracted into DCM (300 mL) and the organic layer was washed three times with 100 mL of water and dried with Na_2SO_4. The solvent was removed under reduced pressure to obtain the crude as a white solid. The crude was used in the next step without further purification (14.9 g, 83%). ^{1}H NMR (300 MHz, $CDCl_3$) 7.78−7.70 (m, 2H, **CH**−fluorene), 7.62−7.56 (m, 2H, **CH**−fluorene) 7.47−7.36 (m, 8H, **CH**−fluorene, **CH**−trityl), 7.32−7.13 (m, 11H, **CH**−fluorene, **CH**−trityl), 5.42 (t, J = 5.9 Hz, 1H, N**H**), 4.44−4.33 (m, 2H, Fmoc−CH−C**H$_2$**), 4.19 (t, J = 7.0 Hz, 1H, Fmoc−C**H**), 3.64 (s, 2H, −C**H$_3$**), 3.60 (s, 1H, −C**H$_3$**), 3.46−3.41 (m, 4 H, −CONH**CH$_2$**), 3.32−3.26 (m, 2 H, −CONH**CH$_2$**), 2.78−2.61 (m, 4 H, −CONH**CH$_2$**, −C═OC**H$_2$**), 2.36−2.27 (m, 2H, −C═OC**H$_2$**), 1.71 (br s, 1H, −N**H**). ^{13}C NMR (75 MHz, $CDCl_3$) δ 173.6, 173.0, 156.7, 145.7, 144.1, 144.0, 141.4, 128.7, 128.5, 128.1, 128.0, 127.8, 127.8, 127.1, 126.6, 125.3, 120.0, 71.2, 66.8, 51.9, 49.1, 47.4, 45.8, 42.5, 39.8, 29.5, 28.2. HRMS (ESI) m/z: [M + H]$^+$ calcd for $C_{43}H_{44}N_3O_5$, 682.3275; found, 682.3280.

*Methyl 4-((2-((((9H-Fluoren-9-yl)methoxy)carbonyl)amino)ethyl)(2-aminoethyl)amino)-4-oxo-butanoate as TFA-Salt (**8**).* Compound **7** (14.7 g, 21.5 mmol, 1 equiv) was dissolved in 250 mL of DCM. TES (4.9 g, 6.7 mL, 45.0 mmol, 2 equiv) and TFA (24.5 g, 16.0 mL, 205.0 mmol; 10 equiv) were added dropwise, and the reaction was stirred at room temperature for 30 min. The solvent was removed under reduced pressure, and any remaining TFA was coevaporated with toluene. The crude product was redissolved in 100 mL of DCM and precipitated in 2 L of Et_2O to obtain the product as a white solid (9.35 g, 81%). ^{1}H NMR (300 MHz, Methanol-d_4) δ 7.81 (d, J = 7.7, 2H, C**H**−fluorene), 7.65 (d, J = 7.5 Hz, 2H, C**H**−fluorene), 7.41 (t, J = 7.5 Hz, 2H, C**H**−fluorene),7.32 (t, J = 7.4 Hz, 2H, C**H**−fluorene), 4.40 (d, J = 6.8 Hz, 2H, Fmoc−CH−C**H$_2$**), 4.21 (t, J = 6.7 Hz, 1H, Fmoc−C**H**), 3.65−3.61 (m, 5 H, −CONH**CH$_2$**, −C**H$_3$**), 3.51 (t, J = 6.3 Hz, 2H, −CONHC**H$_2$**), 3.36−3.31 (m, 2H, −CONHC**H$_2$**), 3.13 (t, J = 6.0 Hz, 2H, −CONH**CH$_2$**), 2.78−2.42 (m, 4H, −C═OC**H$_2$**−**CH$_2$**C═O). ^{13}C NMR (75 MHz, Methanol-d_4) δ 175.8, 175.4, 159.1, 145.3, 142.6, 128.8, 128.2, 126.1, 121.0, 67.9, 52.2, 45.2, 39.9, 39.7, 30.0, 28.8. HRMS (ESI) m/z: [M + H]$^+$ calcd for $C_{24}H_{30}N_3O_5$, 440.2180; found, 440.2180.

*1-(9H-Fluoren-9-yl)-7-(4-methoxy-4-oxobutanoyl)-3,11-dioxo-2-oxa-4,7,10-triazatetradecan-14-oic Acid (MDS) (**9**).* Compound **8** (9.3 g, 17.3 mmol, 1 equiv) was suspended in 170 mL of DCM, Et_3N (9.9 g, 7.2 mL, 51.8 mmol, 3 equiv) was added, and the reaction was stirred until the suspended solid was dissolved. Succinc anhydride (1.7 g, 17.3 mmol, 1 equiv) was then added and the reaction mixture was stirred for 1h. The reaction mixture was diluted with 50 mL of 10% citric acid, washed 3× with 50 mL of 10% citric acid, and dried with Na_2SO_4. After removal of the solvent under reduced pressure, the crude product was recrystallized from acetone to obtain the desired product as a white solid (6.1 g; 67%). Mp: 70−73 °C. ^{1}H NMR (300 MHz, Methanol-d_4) δ 7.79 (d, J = 7.4 Hz, 2H,**CH**−Aryl), 7.64 (d, J = 7.4 Hz, 2H, **CH**−Aryl), 7.39 (t, J = 7.2 Hz, 2H, **CH**−Aryl), 7.31 (t, J = 7.4 Hz, 2H, **CH**−Aryl), 4.37 (dd, J = 6.7, 1.5 Hz, 2H, Fmoc−CH−**CH$_2$**), 4.19 (t, J = 6.7 Hz, 1H, Fmoc−**CH**−CH$_2$), 3.62 (d, J = 6.9 Hz, 4H, −**CH$_3$**), 3.47−3.19 (m, 8H, −CONHC**H$_2$**), 2.72−2.63 (m, 2H, −COC**H$_2$**), 2.63−2.53 (m, 4H, COC**H$_2$**), 2.45 (m, 2H, COC**H$_2$**). ^{13}C NMR (75 MHz, $CDCl_3$) δ 175.4, 175.3, 174.4, 174.0, 173.7, 173.2, 157.3, 156.9, 144.0, 143.9, 141.4, 127.9, 127.2, 125.2, 120.1, 67.0, 66.0, 52.0, 47.3, 39.7, 38.9, 38.3, 30.8, 29.3, 28.0, 27.8, 15.4. HRMS (ESI) m/z: [M + H]$^+$ calcd for $C_{28}H_{34}N_3O_8$, 540.2340; found, 540.2335.

Solid-Supported Synthesis. *General Coupling Protocol.* Preparation of the resin: 0.1 mmol of resin (400 mg; 0.25 mmol/g loading) was swelled in DCM for 30 min. After that, the resin was washed ten times with 10 mL of DMF.

Fmoc Cleavage. The Fmoc protecting group was cleaved by treating the resin three times for 10 min with 10 mL of 25% piperidine in DMF. Between each step, the resin was washed three times with 10 mL of DMF. After the last cleavage, the resin was washed ten times with 10 mL of DMF.

Coupling. Building block (0.5 mmol, 5 equiv) and PyBOP (0.5 mmol, 5 equiv) were dissolved in 4 mL of DMF. After addition of DIPEA (1.0 mmol, 10 equiv), the mixture was flushed with nitrogen for 1 min. The yellow solution was added to the resin, and the reaction was shaken for 1.5 h. The resin was then washed ten times with 10 mL of DMF.

Capping. After the last Fmoc cleavage, the *N*-terminus of the resin was capped by treating the resin two times for 30 min with acetic 5 mL of anhydride. After that, the resin was washed ten times with 10 mL of DMF.

DOI: 10.1021/acs.joc.7b01398
J. Org. Chem. 2017, 82, 9400−9409

Deprotection of the Carboxylic Side Chain. The resin was washed ten times with 10 mL of THF/H_2O (1/1). The resin was then treated two times for 1 h with 10 mL of 0.2 M LiOH in THF/H_2O (1/1). After the first deprotection, the resin was washed three times with THF/H_2O (1/1). After the second deprotection, the resin was alternately washed three times each with 10 mL of H_2O, DMF, and DCM, and then with DMF and DCM. The resin was shaken overnight in fresh DMF to remove water.

Staudinger Ligation. The Staudinger ligation was performed in DMF and ACN under the same conditions. Resin (0.05 mmol, 1 equiv) were transferred into a 20 mL reactor. The resin was washed five times with 5 mL of DMF or ACN. (2-Azidoethyl)-2,3,4,6-tetra-*O*-α-D-mannopyranoside (112 mg, 0.25 mmol, 2.5 equiv/acid) and HOBt (42 mg, 0.25 mmol, 2.5 equiv/acid) were dissolved in 1.5 mL of DMF (or ACN + 15 drops DMF) and added to the resin. Then DIC (0.05 mL, 0.025 mmol 2.5 equiv/acid) was dissolved in 0.5 mL of DMF (or ACN) and added to the resin, and the reactor was placed on ice for 5 min. Tributylphosphine (0.25 mL, 1.0 mmol, 20 equiv) was dissolved in 0.5 mL of DMF (or ACN) and added to the resin. The syringe was closed tightly, softly shaken, and placed on ice for 10 min, and then at room temperature for 20 h. ***CAUTION:*** Nitrogen evolution occurs. Between the multicoupling reactions, the supernatant was removed and the resin was washed ten times with 5 mL of DMF or ACN and three times with 5 mL of DCM before performing a subsequent ligation. Upon completion of the last Staudinger ligation, the resin was alternately washed 5 × 5 times with 5 mL of H_2O, DMF, and DCM.

CuAAC. For 0.025 mmol resin, (2-azidoethyl)-2,3,4,6-tetra-*O*-α-D-mannopyranoside (56 mg, 0.13 mmol, 5 equiv/acid) were dissolved in 1 mL of DMF and flushed with nitrogen. Separately, 10 mg of $CuSO_4$ (20 mol %) and 10 mg of sodium ascorbate (20 mol %) were each dissolved in 0.1 mL of Milli-Q water. The azide solution was added to the resin, followed by sodium ascorbate and $CuSO_4$. After shaking the reaction mixture overnight, the supernatant was discarded and the resin was washed sequentially with 3 mL of DMF, 3 mL of a solution of 0.2 M sodium diethyldithiocarbamte in DMF and water, 3 mL of water, and 3 mL of DCM until no more color changes were observable after the treatment with 0.2 M sodium diethyldithiocarbamte in DMF and water.

Sugar Deprotection. The resin was treated with 5 mL of 0.2 M NaOMe in MeOH two times for 30 min. In between deprotections, the resin was washed with MeOH. After the second deprotection, the resin was washed with 5 mL of MeOH, DMF, and DCM.

Microcleavage. An aliquot of the resin was treated with 0.5 mL of a solution of 95% TFA, 2.5% TIPS, and 2.5% DCM for 30 min. The cleavage solution was added to 10 mL of Et_2O to precipitate the product. The mixture was then centrifuged, and the supernatant was discarded. After drying the residue under a stream of nitrogen, the product was dissolved in 0.5 mL of ACN/H_2O (1/2) and filtered to remove the resin prior to analytical analysis.

Macrocleavage. The resin was washed ten times with 5 mL of DCM and 5 mL of a solution of 95% TFA, 2.5% TIPS, and 2.5% DCM were added. The cleavage reaction was shaken for 1 h at room temperature. The supernatant was added dropwise to cooled Et_2O (40 mL). The mixture was centrifuged, the supernatant was decanted, and the white precipitation was dried under a stream of nitrogen. The resulting solid was redissolved in water and lyophilized.

Deprotected GEG Scaffold ***1***. ^{1}H NMR (600 MHz, D_2O) δ 4.34−4.27 (m, 2H, C**H**−CH_2−CH_2), 3.66−3.59 (m, 8H, O**C**H_2), 3.43−3.35 (m, 4H, N**C**H_2), 2.59−2.45 (m, 8H, NC═O**C**H_2, CH−CH_2−**C**H_2), 2.24−1.89 (m, 7H, NHC═O**C**H_3, CH−**C**H_2−CH_2). ^{13}C NMR (151 MHz, D_2O) δ 177.0, 176.9, 176.3, 175.0, 174.7, 174.2, 173.5, 69.6, 69.4, 68.8, 68.7, 53.2, 52.7, 38.9, 30.6, 30.0, 29.9, 26.3, 26.1, 21.6. HRMS (ESI) *m*/*z*: [M + H]$^+$ calcd for $C_{22}H_{38}N_5O_{11}$, 548.2562; found, 548.2564. Yield for 0.05 mmol batch: 17 mg (63%).

Man(1,3) GEG ***2***. ^{1}H NMR (300 MHz, D_2O) δ 5.37−5.25 (m, 6H, C**H** pyranose), 5.02−4.96 (m, 2H, C**H**$_{anomere}$ pyranose), 4.44 (dd, *J* = 13.1, 4.4 Hz, 2H, C**H** pyranose), 4.28 (m, 2H, C**H**−CH_2−CH_2), 4.21−4.16 (m, 4H, C**H**$_2$ pyranose), 3.87−3.80 (m, 2H, O**C**H_2), 3.71−3.60 (m, 10H, O**C**H_2), 3.49−3.37 (m, 8H, N**C**H_2), 2.63−2.56 (m, 4H NC═O**C**H_2), 2.43−2.35 (m, 4H, CH−CH_2−**C**H_2), 2.22 (s, 6H, OC═O**C**H_3), 2.18−2.10 (m Hz, 14H, OC═O**C**H_3, CH-C**H**$_2$), 2.08−1.90 (m, 11H, OC═O**C**H_3, NHC═O**C**H_3, CH−**C**H_2). ^{13}C NMR (75 MHz, D_2O) δ 176.1, 175.0, 174.9, 174.9, 174.7, 174.0, 173.6, 173.4, 173.0, 172.9, 172.7, 172.7, 97.1, 69.7, 69.6, 69.5, 69.3, 68.8, 68.8, 68.1, 66.5, 65.7, 62.0, 53.3, 52.8, 38.9, 38.8, 32.1, 31.9, 30.7, 30.6, 27.4, 27.3, 21.7, 20.1. HRMS (ESI) *m*/*z*: [M + H]$^+$ calcd for $C_{54}H_{84}N_7O_{29}$,1294.5308; found, 1294.5303. Yield for 0.1 mmol batch: 18 mg (14%).

Deprotected MEM Scaffold ***10***. ^{1}H NMR (300 MHz, D_2O) δ 3.69−3.66 (m, 5H, O**C**H_2), 3.62−3.58 (m, 3H, O**C**H_2), 3.53−3.33 (m, 20H, N**C**H_2), 2.71−2.60 (m, 8H, NC═O**C**H_2), 2.54−2.45 (m, 12H, NC═O**C**H_2), 1.95 (d, *J* = 10.4 Hz, NHC═O**C**H_3). ^{13}C NMR (151 MHz, D_2O) δ 177.1, 177.1, 177.0, 175.0, 174.8, 174.8, 174.7, 174.7, 174.7, 174.5, 174.2, 163.0, 162.8, 117.3, 115.3, 113.4, 69.6, 69.4, 68.8, 47.4, 46.9, 46.8, 46.8, 44.9, 44.8, 44.8, 44.8, 38.9, 37.2, 36.9, 35.8, 31.0, 30.9, 30.9, 30.8, 30.8, 30.7, 30.6, 30.2, 30.2, 30.1, 30.1, 29.1, 29.0, 28.7, 27.8, 21.8, 21.8. HRMS (ESI) *m*/*z*: [M + 2H]$^{2+}$ calcd for $C_{36}H_{63}N_9O_{15}$, 430.7216; found, 430.7214. Yield for 0.05 mmol batch: 33 mg (77%).

Man(1,3)-3 MEM ***16***. ^{1}H NMR (600 MHz, D_2O) δ 4.87 (d, *J* = 1.7 Hz, 2H, C**H**$_{anomere}$ pyranose), 3.95 (dd, *J* = 3.4, 1.7 Hz, 2H, C**H** pyranose), 3.89 (dd, *J* = 12.2, 1.8 Hz, 2H, C**H** pyranose), 3.81−3.74 (m, 6H, C**H** pyranose; C**H**$_2$−OH pyranose), 3.69−3.59 (m, 14H, C**H** pyranose, O**C**H_2), 3.55−3.51 (m, 4H, N**C**H_2), 3.49−3.45 (m, 6H, N**C**H_2), 3.44−3.33 (m, 14H, N**C**H_2), 2.72−2.69 (m, 4H, NC═O**C**H_2), 2.58−2.47 (m, 16H, NC═O**C**H_2), 1.98 (d, *J* = 20.9 Hz, 3H, NHC═O**C**H_3). ^{13}C NMR (151 MHz, D_2O) δ 177.6, 177.5, 175.0, 175.0, 174.8, 174.7, 174.7, 174.7, 174.4, 174.2, 99.7, 72.8, 70.5, 70.0, 69.4, 68.8, 66.7, 65.8, 60.9, 47.2, 47.1, 45.2, 45.1, 38.9, 38.9, 37.3, 36.9, 36.9, 31.0, 30.9, 30.8, 30.8, 30.7, 30.7, 30.7, 30.2, 30.1, 28.0, 28.0, 21.9, 21.8. HRMS (ESI) *m*/*z*: [M + 2H]$^{2+}$ calcd for $C_{52}H_{93}N_{11}O_{25}$, 635.8167; found, 635.8163. Yield: 15 mg (24%).

Deprotected MET Scaffold ***18***. ^{1}H NMR (300 MHz, D_2O) δ 3.69−3.65 (m, 4H, O**C**H_2), 3.62−3.58 (m, 4H, O**C**H_2), 3.53−3.35 (m, 20H, N**C**H_2), 2.71−2.60 (m, 8H, NC═O**C**H_2), 2.54−2.44 (m, 12H, NC═O**C**H_2), 2.34 (t, *J* = 2.6 Hz, C≡C**H**), 1.96 (d, *J* = 9.8 Hz, NHC═O**C**H_3). ^{13}C NMR (151 MHz, D_2O) δ 177.6, 177.6, 177.1, 177.1, 177.0, 176.8, 176.8, 175.1, 175.1, 175.0, 175.0, 174.8, 174.8, 174.8, 174.7, 174.7, 174.6, 174.5, 174.4, 174.2, 163.3, 163.0, 162.8, 162.6, 119.2, 117.3, 115.3, 113.4, 83.9, 69.7, 69.7, 69.6, 69.4, 68.8, 46.9, 46.9, 44.9, 44.8, 44.8, 44.8, 44.7, 38.9, 37.3, 37.2, 36.9, 36.9, 36.9, 35.8, 31.4, 31.4, 31.1, 31.1, 30.9, 30.8, 30.8, 30.7, 30.2, 30.2, 30.1, 30.1, 29.1, 29.0, 28.7, 27.8, 21.9, 21.9, 14.1. HRMS (ESI) *m*/*z*: [M + 2H]$^{2+}$ calcd for $C_{37}H_{63}N_9O_{13}$, 420.7267; found, 420.7266. Yield for 0.05 mmol batch: 35 mg (83%).

Man(1,3)-3 MET ***22***. ^{1}H NMR (300 MHz, D_2O) δ 7.87 (d, *J* = 1.5 Hz, 1H, Triazol−C**H**), 4.87 (d, *J* = 1.7 Hz, 1H, C **H**$_{anomere}$ pyranose), 4.69−4.59 (m, 2H, N−N−C**H**$_2$), 4.12−4.05 (m, 1H, C**H** pyranose), 3.95−3.85 (m, 4H, C**H** pyranose, C**H**$_2$-OH pyranose), 3.83−3.71 (m, 4H, C**H** pyranose, C**H**$_2$−OH pyranose), 3.70−3.58 (m, 14H, −O**C**H_2), 3.55−3.31 (m, 22H, C**H**, −N**C**H_2), 3.06−2.98 (m, 3H, C**H** pyranose, CH═C−C**H**$_2$), 2.80 (dt, *J* = 8.2, 4.1 Hz, 2H, −NC═O**C**H_2), 2.70 (t, *J* = 6.7 Hz, 2H, −NC═O**C**H_2), 2.59−2.47 (m, 14 H, −NC═O**C**H_2), 1.94 (d, *J* = 4.4 Hz, 3H, −NHC═O**C**H_3). ^{13}C NMR (75 MHz, D_2O) δ 177.6, 177.5, 175.0, 174.9, 174.9, 174.8, 174.8, 174.7, 174.7, 174.7, 174.6, 174.3, 174.1, 146.8, 123.9, 99.6, 99.4, 72.8, 72.7, 70.5, 70.4, 70.0, 69.9, 69.4, 68.8, 66.7, 66.3, 65.8, 65.4, 60.9, 60.6, 49.9, 47.1, 47.0, 45.2, 44.9, 38.9, 37.3, 36.9, 31.9, 31.0, 30.9, 30.8, 30.8, 30.8, 30.7, 30.7, 30.2, 30.1, 28.0, 21.8, 21.7, 20.6. HRMS (ESI) *m*/*z*: [M + 2H]$^{2+}$ calcd for $C_{53}H_{93}N_{13}O_{24}$, 647.8223; found, 647.8224. Yield: 19 mg (29%).

Man(1)-Gal(3)-3 MET ***23***. ^{1}H NMR (300 MHz, D_2O) δ 7.89 (s, 1H, Triazol−C**H**), 4.87 (d, *J* = 1.7 Hz, 1H, C**H**$_{anomere\ Man}$), 4.65 (t, *J* = 5.1 Hz, 2H, N−N−C**H**$_2$), 4.37 (d, *J* = 7.8 Hz, 1H, C**H**$_{anomere\ Gal}$), 4.29 (dt, *J* = 10.3, 4.8 Hz, 1H, C**H**−pyranose), 4.09 (dt, *J* = 11.2, 5.2 Hz, 1H, C**H**−pyranose,), 3.97−3.84 (m, 3H, C**H**−pyranose), 3.84−3.71 (m, 5H, C**H** pyranose, C**H**$_2$−OH pyranose), 3.71−3.57 (m, 13H, CH, −O**C**H_2), 3.56−3.30 (m, 23H, C**H**, −N**C**H_2), 3.01 (t, *J* = 7.2 Hz, 2H, CH═C−C**H**$_2$), 2.84−2.75 (m, 2H, −NC═O**C**H_2), 2.70 (t, *J* = 6.7 Hz, 2H, −NC═O**C**H_2), 2.60−2.43 (m, 14H, −NC═O**C**H_2), 1.93

DOI: 10.1021/acs.joc.7b01398
J. Org. Chem. 2017, 82, 9400−9409

(d, J = 6.2 Hz, 3H, C**H**$_3$). ^{13}C NMR (151 MHz, D_2O) δ 177.6, 177.5, 175.0, 175.0, 174.9, 174.9, 174.9, 174.8, 174.8, 174.8, 174.7, 174.7, 174.7, 174.7, 174.6, 174.3, 174.2, 146.6, 124.1, 103.0, 99.7, 75.1, 72.8, 72.6, 70.6, 70.5, 70.0, 69.4, 68.8, 68.5, 68.1, 66.7, 65.8, 60.9, 50.2, 47.2, 47.2, 47.1, 47.0, 45.2, 44.9, 44.9, 38.9, 38.9, 37.3, 37.3, 36.9, 36.9, 32.0, 31.0, 31.0, 30.9, 30.8, 30.8, 30.8, 30.8, 30.7, 30.7, 30.2, 30.1, 28.0, 21.8, 21.7, 20.7, 20.7. HRMS (ESI) m/z: $[M + 2H]^{2+}$ calcd for $C_{53}H_{93}N_{13}O_{24}$, 647.8223; found, 647.8224. Yield: 23 mg (35%).

Side Product Man(1)-Dimethylamine(3)-3 MEM or Dimethylamine(1)-Man(3)-3 MEM ***26***. ^{1}H NMR (300 MHz, D_2O) δ 4.87 (d, J = 1.8 Hz, 1H, C**H**$_{anomere}$), 3.95 (dd, 1H, J = 1.7; 1.7 Hz, C**H** pyranose), 3.89 (dd, J = 12.2; 1.7 Hz, 1H, C**H** pyranose), 3.83−3.75 (m, 3H, C**H** pyranose, C**H**$_2$−OH pyranose), 3.72−3.58 (m, 11H, C**H** pyranose, OC**H**$_2$), 3.57−3.31 (m, 22 H, NC **H**$_2$), 3.10 (s, 3H, NC**H**$_3$), 2.92 (s, 3H, NC**H**$_3$), 2.76−2.65 (m, 6H, −NC═OC**H**$_2$), 2.61−2.45 (m, 14H, NC═OC**H**$_2$), 1.98 (d, J = 10.7 Hz, 3H, NHC═OC**H**$_3$). ^{13}C NMR (151 MHz, D_2O) δ 175.2, 175.0, 174.8, 174.7, 174.7, 174.7, 174.4, 174.2, 99.7, 72.8, 70.5, 70.0, 69.4, 68.8, 66.7, 65.8, 60.9, 47.2, 45.1, 38.9, 38.9, 37.3, 37.2, 36.9, 35.4, 31.0, 30.9, 30.9, 30.8, 30.7, 30.7, 30.2, 30.1, 28.1, 27.9, 21.9, 21.8. HRMS (ESI) m/z: $[M + 2H]^{2+}$ calcd for $C_{46}H_{83}N_{11}O_{19}$, 546.7928; found, 546.7928. Yield for 0.05 mmol batch: 4 mg (8%).

■ ASSOCIATED CONTENT

Supporting Information

The Supporting Information is available free of charge on the ACS Publications website at DOI: 10.1021/acs.joc.7b01398.

NMR (^{1}H and ^{13}C NMR) and HRMS spectra for all new compounds, and RP-HPLC traces for select Staudinger ligation reactions and scaffolds (PDF)

■ AUTHOR INFORMATION

Corresponding Authors

*E-mail: nisnyder@davidson.edu.

*E-mail: laura.hartmann@hhu.de.

ORCID

Laura Hartmann: 0000-0003-0115-6405

Notes

The authors declare no competing financial interest.

■ ACKNOWLEDGMENTS

The authors would like to thank the Boehringer-Ingelheim Foundation for support through the 'Perspektivenprogramm Plus3'. N.L.S. would like to thank the Vice President for Academic Affairs and the Dean Rusk International Studies Program at Davidson College for sabbatical support. Furthermore, the authors would like to thank Julia Meisel for her technical assistance.

■ REFERENCES

(1) Kiessling, L. L.; Pohl, N. L. *Chem. Biol.* **1996**, *3*, 71−77.

(2) (a) François-Heude, M.; Méndez-Ardoy, A.; Cendret, V.; Lafite, P.; Daniellou, R.; Ortiz Mellet, C.; García Fernández, J. M.; Moreau, V.; Djedaïni-Pilard, F. *Chem. - Eur. J.* **2015**, *21*, 1978−1991. (b) Slavin, S.; Burns, J.; Haddleton, D. M.; Becer, C. R. *Eur. Polym. J.* **2011**, *47*, 435−446. (c) Ciuk, A. K.; Lindhorst, T. K. *Beilstein J. Org. Chem.* **2015**, *11*, 668−674. (d) Bergmann, M.; Michaud, G.; Visini, R.; Jin, X.; Gillon, E.; Stocker, A.; Imberty, A.; Darbre, T.; Reymond, J.-L. *Org. Biomol. Chem.* **2016**, *14*, 138−148.

(3) Ponader, D.; Maffre, P.; Aretz, J.; Pussak, D.; Ninnemann, N. M.; Schmidt, S.; Seeberger, P. H.; Rademacher, C.; Nienhaus, G. U.; Hartmann, L. *J. Am. Chem. Soc.* **2014**, *136*, 2008−2016.

(4) Ladmiral, V.; Melia, E.; Haddleton, D. M. *Eur. Polym. J.* **2004**, *40*, 431−449.

(5) Yilmaz, G.; Becer, C. R. *Eur. Polym. J.* **2013**, *49*, 3046−3051.

(6) Yilmaz, G.; Becer, C. R. *Front. Bioeng. Biotechnol.* **2014**, *2* (39), 1−18.

(7) Ponader, D.; Wojcik, F.; Beceren-Braun, F.; Dernedde, J.; Hartmann, L. *Biomacromolecules* **2012**, *13*, 1845−1852.

(8) Wojcik, F.; O'Brien, A. G.; Götze, S.; Seeberger, P. H.; Hartmann, L. *Chem. - Eur. J.* **2013**, *19*, 3090−3098.

(9) Wojcik, F.; Lel, S.; O'Brien, A. G.; Seeberger, P. H.; Hartmann, L. *Beilstein J. Org. Chem.* **2013**, *9*, 2395−2403.

(10) Gerke, C.; Ebbesen, M. F.; Jansen, D.; Boden, S.; Freichel, T.; Hartmann, L. *Biomacromolecules* **2017**, *18*, 787−796.

(11) (a) Gómez-García, M.; Benito, J. M.; Rodríguez-Lucena, D.; Yu, J.-X.; Chmurski, K.; Ortiz Mellet, C.; Gutiérrez Gallego, R.; Maestre, A.; Defaye, J.; García Fernández, J. M. *J. Am. Chem. Soc.* **2005**, *127*, 7970−7971. (b) Thomas, B.; Fiore, M.; Bossu, I.; Dumy, P.; Renaudet, O. *Beilstein J. Org. Chem.* **2012**, *8*, 421−427. (c) Gloe, T.-E.; Müller, A.; Ciuk, A.; Wrodnigg, T. M.; Lindhorst, T. K. *Carbohydr. Res.* **2016**, *425*, 1−9.

(12) (a) Saxon, E.; Bertozzi, C. R. *Science* **2000**, *287*, 2007−2010. (b) Köhn, M.; Breinbauer, R. *Angew. Chem., Int. Ed.* **2004**, *43*, 3106−3116.

(13) Tang, W.; Becker, M. L. *Chem. Soc. Rev.* **2014**, *43*, 7013−7039.

(14) Silva, L.; Affeldt, R. F.; Lüdtke, D. S. *J. Org. Chem.* **2016**, *81*, 5464−5473.

(15) (a) Tang, Z.; Pelletier, J. C. *Tetrahedron Lett.* **1998**, *39*, 4773−4776. (b) Jain, S.; Reiser, O. *ChemSusChem* **2008**, *1*, 534−541. (c) Nilsson, B. L.; Hondal, R. J.; Soellner, M. B.; Raines, R. T. *J. Am. Chem. Soc.* **2003**, *125*, 5268−5269. (d) Jain, S. L.; Sain, B. *Adv. Synth. Catal.* **2008**, *350*, 1479−1483.

(16) Malkinson, J. P.; Falconer, R. A.; Toth, I. *J. Org. Chem.* **2000**, *65*, 5249−5252.

(17) Kim, H.; Cho, J. K.; Aimoto, S.; Lee, Y.-S. *Org. Lett.* **2006**, *8*, 1149−1151.

(18) Toró, A.; Nowak, P.; Deslongchamps, P. *J. Am. Chem. Soc.* **2000**, *122*, 4526−4527.

(19) Hu, G. Z.; Nitze, F.; Jia, X.; Sharifi, T.; Barzegar, H. R.; Gracia-Espino, E.; Wagberg, T. *RSC Adv.* **2014**, *4*, 676−682.

(20) Doores, K. J.; Mimura, Y.; Dwek, R. A.; Rudd, P. M.; Elliott, T.; Davis, B. G. *Chem. Commun.* **2006**, 1401−1403.

(21) Ebbesen, M. F.; Gerke, C.; Hartwig, P.; Hartmann, L. *Polym. Chem.* **2016**, *7*, 7086−7093.

(22) Wu, L.; Sampson, N. S. *ACS Chem. Biol.* **2014**, *9*, 468−475.

DOI: 10.1021/acs.joc.7b01398
J. Org. Chem. 2017, 82, 9400−9409

Supporting Information

Towards Orthogonal Preparation of Sequence-Defined Monodisperse Heteromultivalent Glycomacromolecules on Solid Support Using Staudinger Ligation and Copper-Catalyzed Click Reactions

Tanja Freichel [†], Svenja Eierhoff [†], Nicole L. Snyder [‡,*] and Laura Hartmann [†,*]

[†] Department of Organic and Macromolecular Chemistry, Heinrich-Heine-University Düsseldorf, 40225 Düsseldorf, Germany

[‡] Department of Chemistry, Davidson College, North Carolina 28035.

*E-mail: laura.hartmann@hhu.de;

*E-mail: nisnyder@davidson.edu

Contents

1.) Schemes

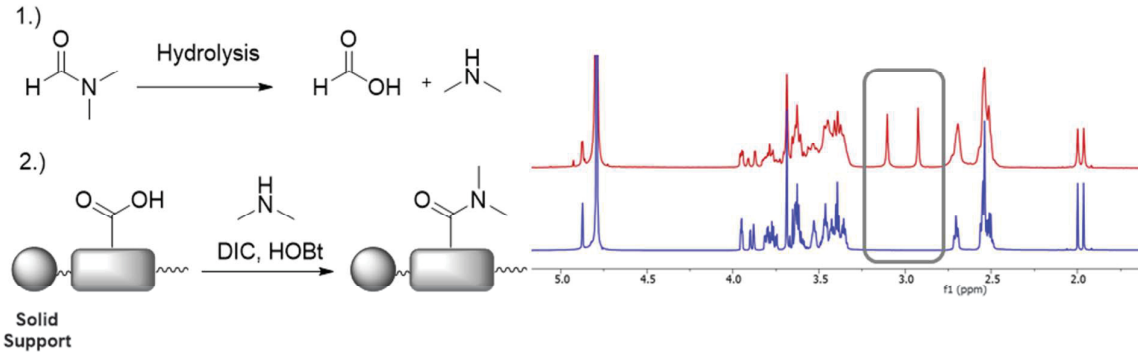

Figure S1: Left: Possible mechanism for the formation of the side product**.** Right: Comparison of ^{1}H-NMR analysis of the side product (red curve) and the product (blue curve). Red curve: ^{1}H-NMR contains characteristic signals of dimethylamine.

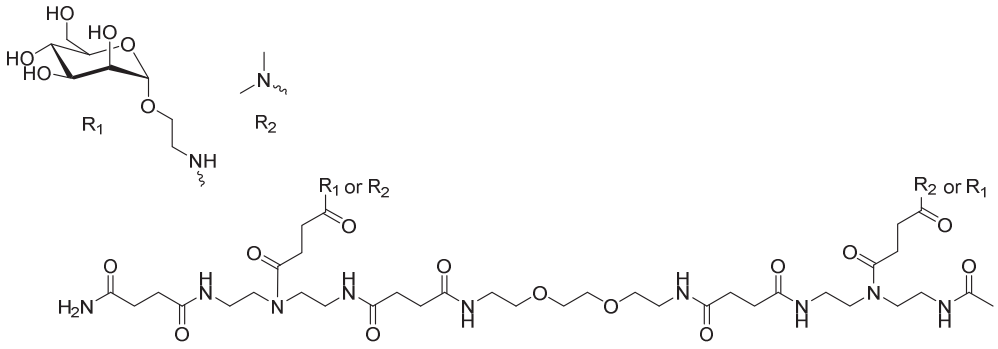

Figure S2: Possible structure of side product **26** from the reaction in DMF.

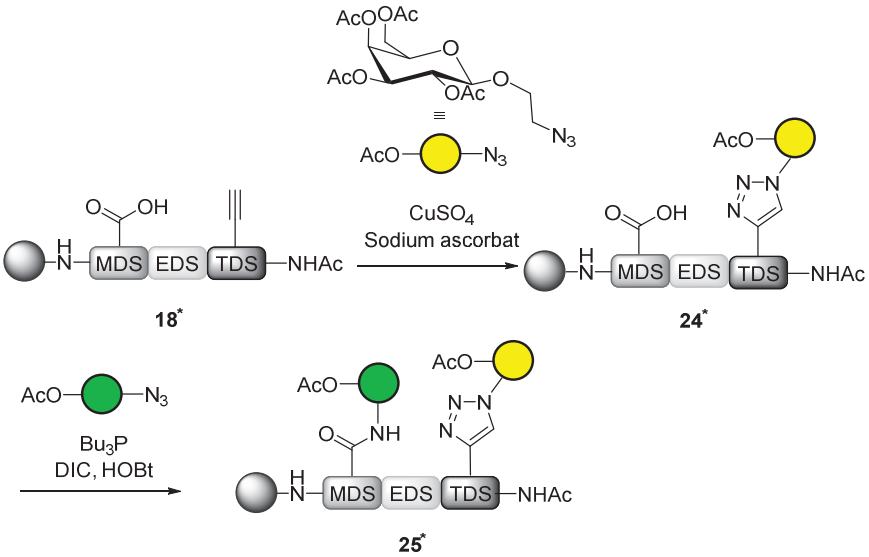

Figure S3: Scheme of the synthesis of the protected heterodivlanet Man(1)-Gal(3)-3 MET **25***. Structures attached to the resin are denoted by a *.

2.) Analytical Data for the MDS Building Block Synthesis

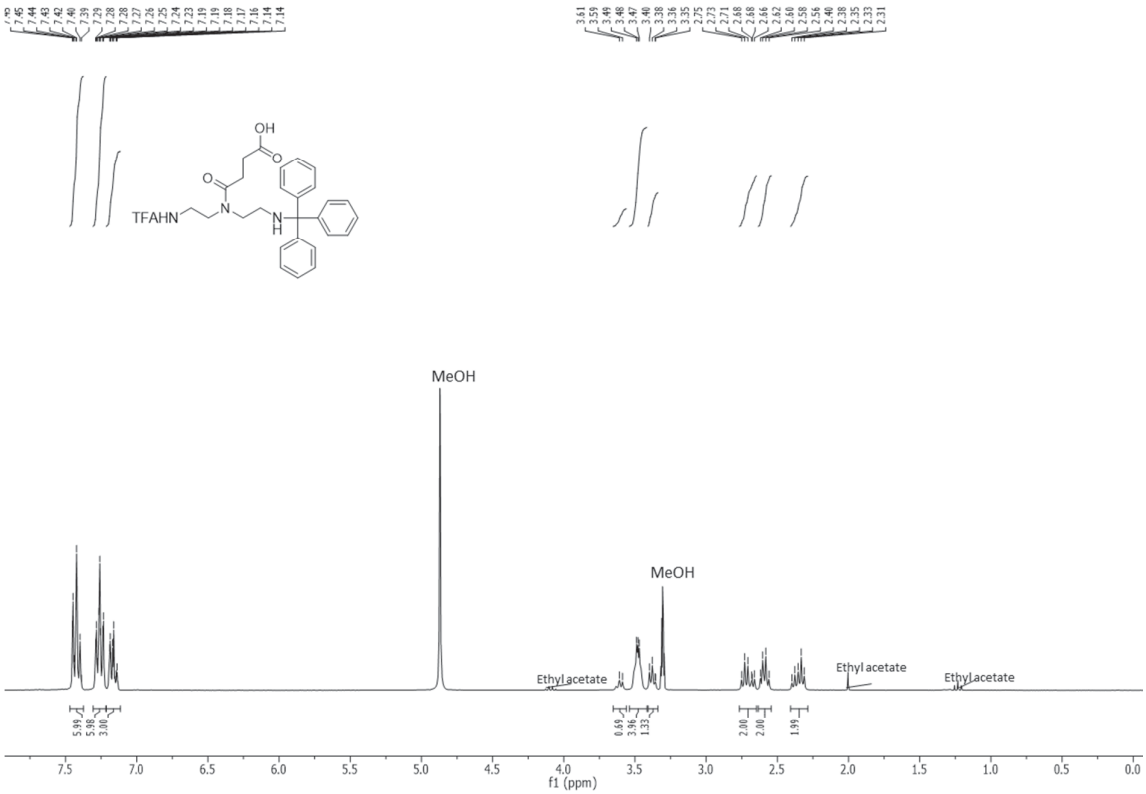

Figure S4: ^{1}H-NMR spectrum of compound **5** (MeOD, 600 MHz).

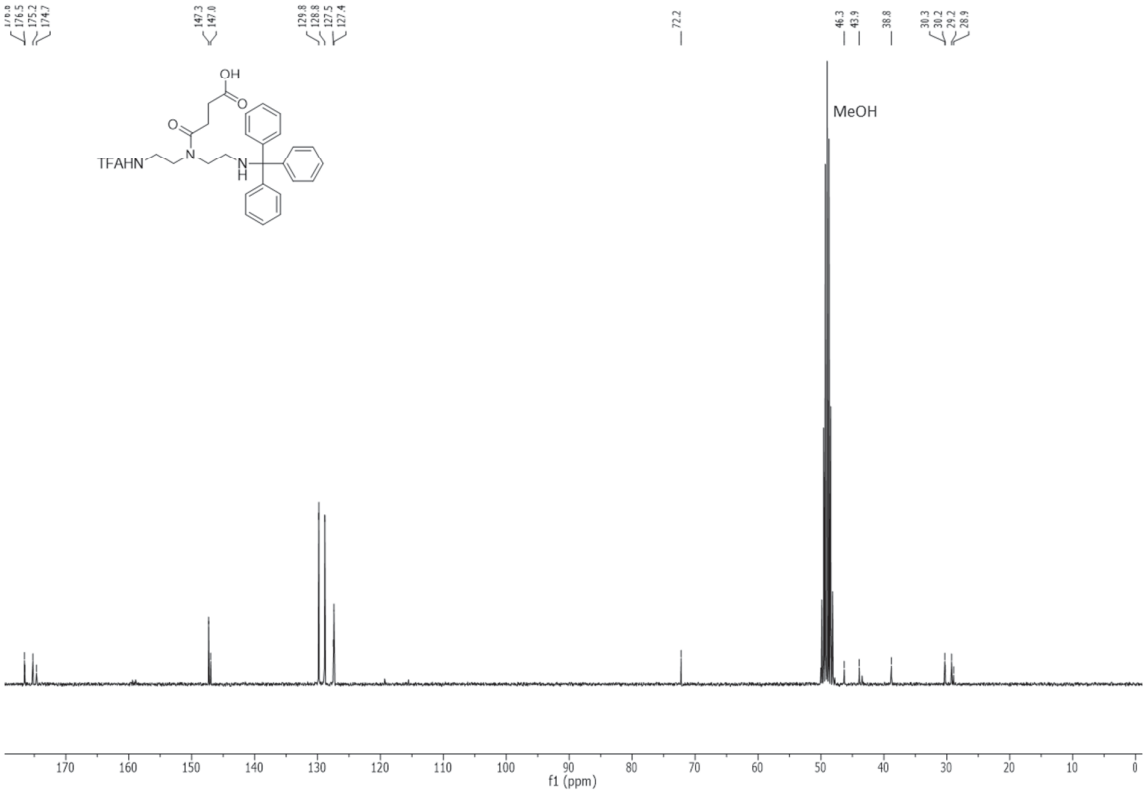

Figure S5: ^{13}C-NMR spectrum of compound **5** (MeOD, 75 MHz).

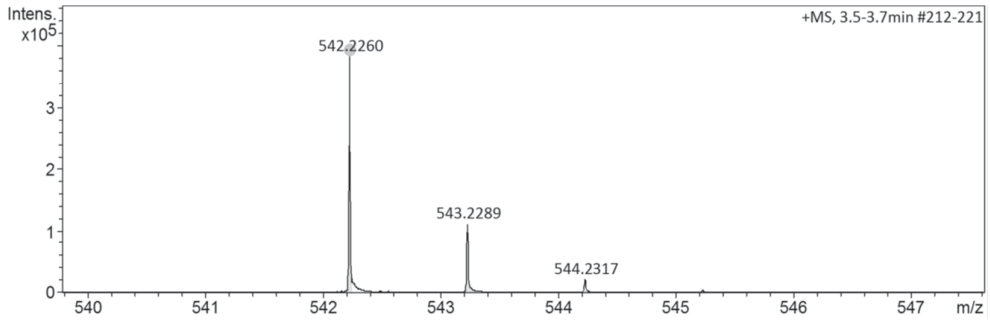

Figure S6: HR-ESI MS-spectrum of compound **5**.

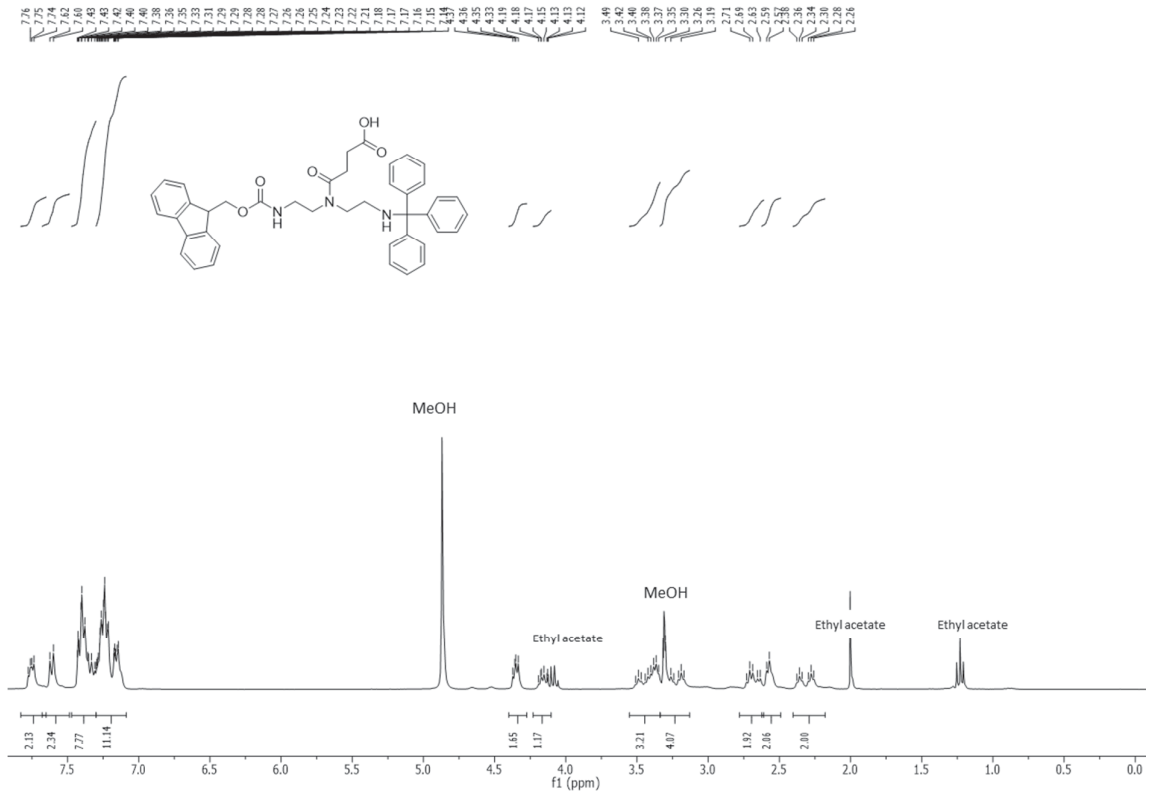

Figure S7: ^{1}H-NMR spectrum of compound **6** (MeOD, 300 MHz).

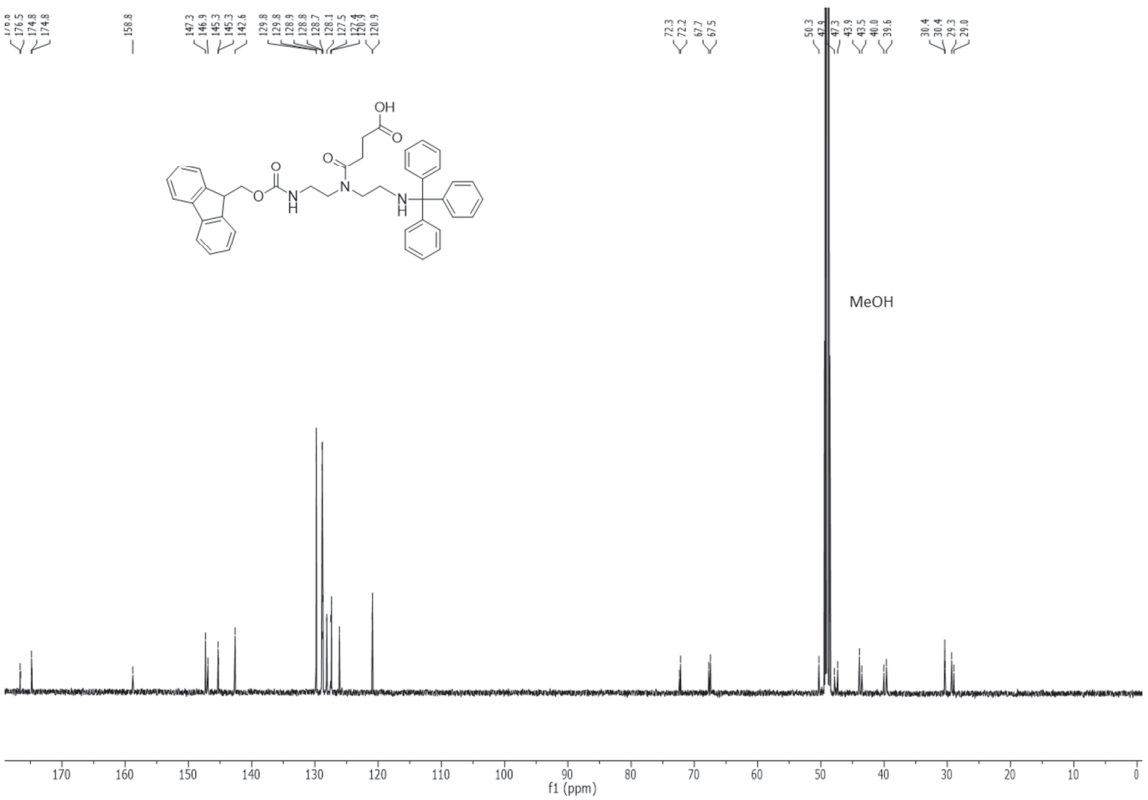

Figure S8: ^{13}C-NMR spectrum of compound **6** (MeOD, 151 MHz).

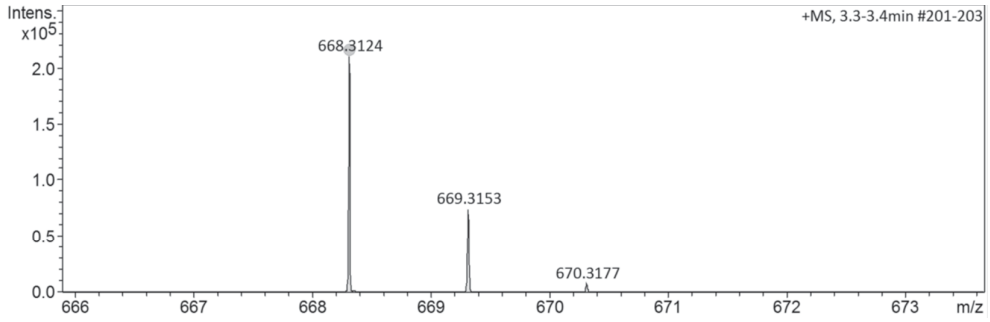

Figure S9: HR-ESI MS spectrum of compound **6**.

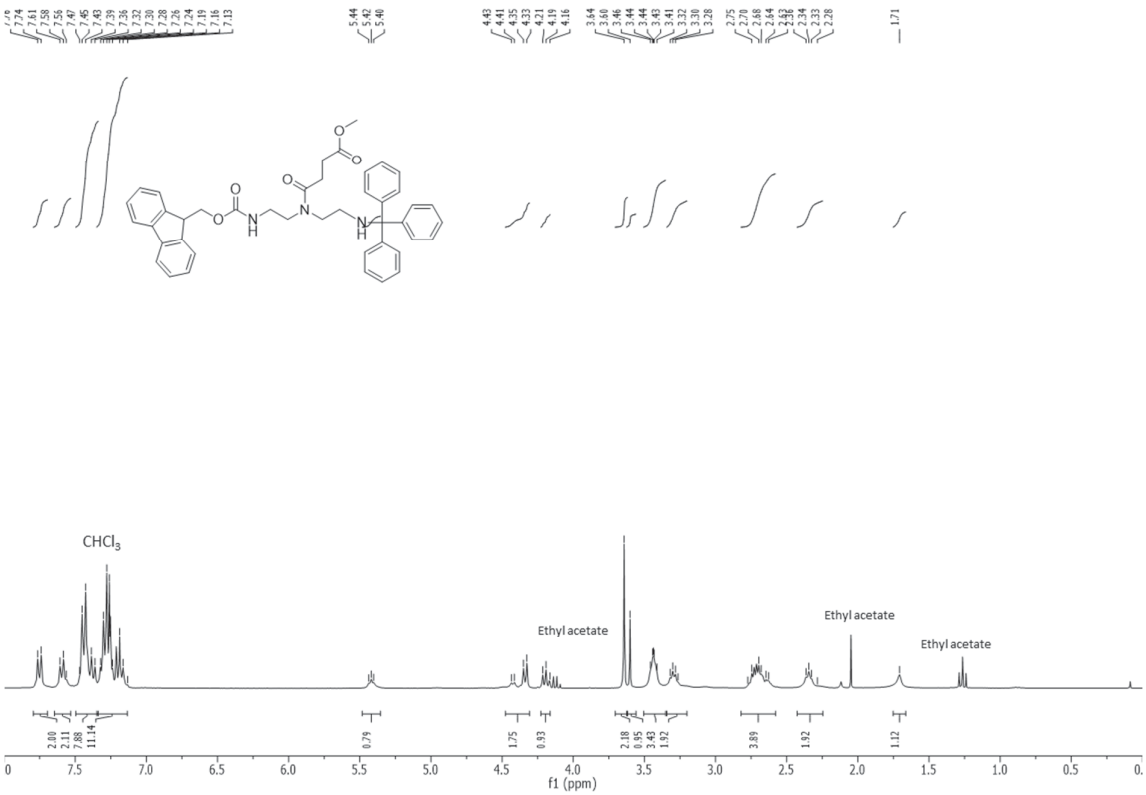

Figure S10: ^{1}H-NMR spectrum of compound **7** (MeOD, 300 MHz).

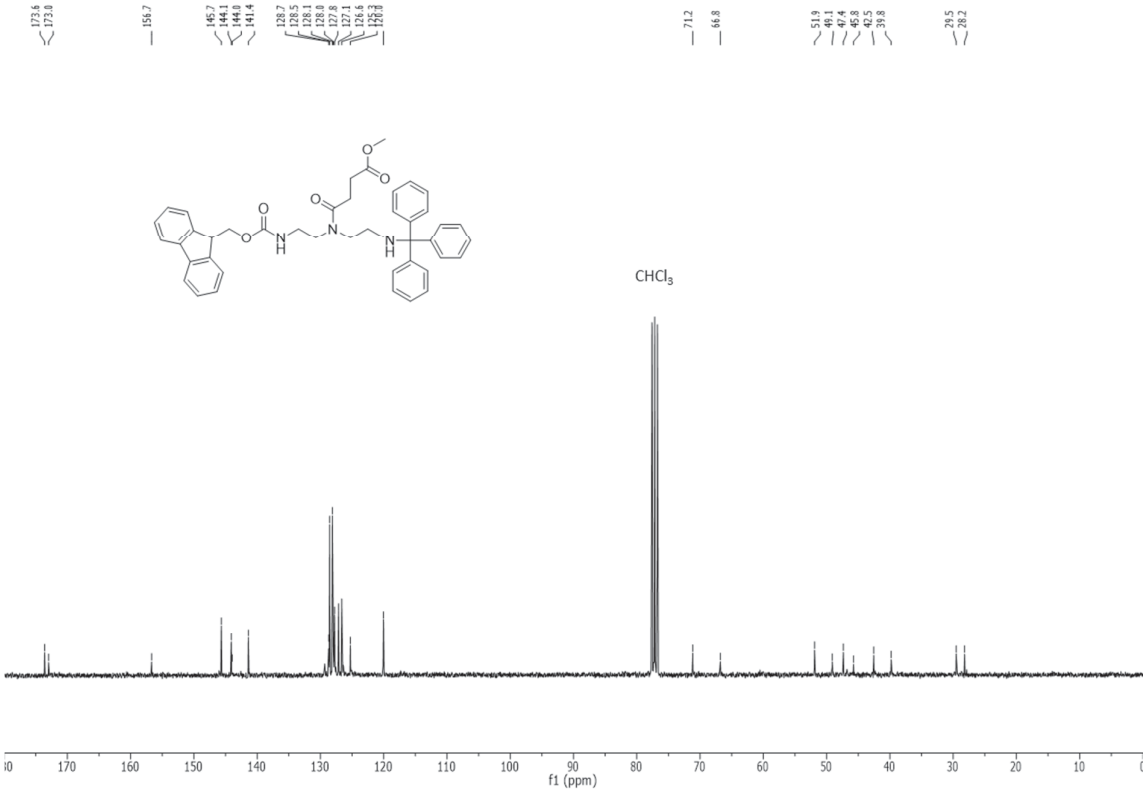

Figure S11: ^{13}C-NMR spectrum of compound **7** (MeOD, 75 MHz).

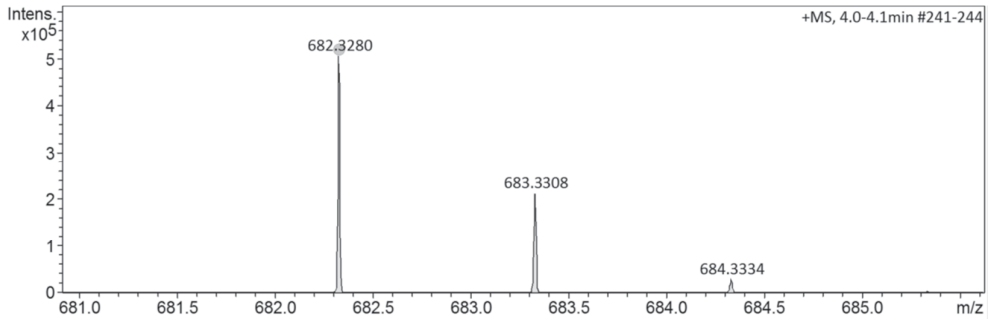

Figure S12: HR-ESI MS spectrum of compound **7**.

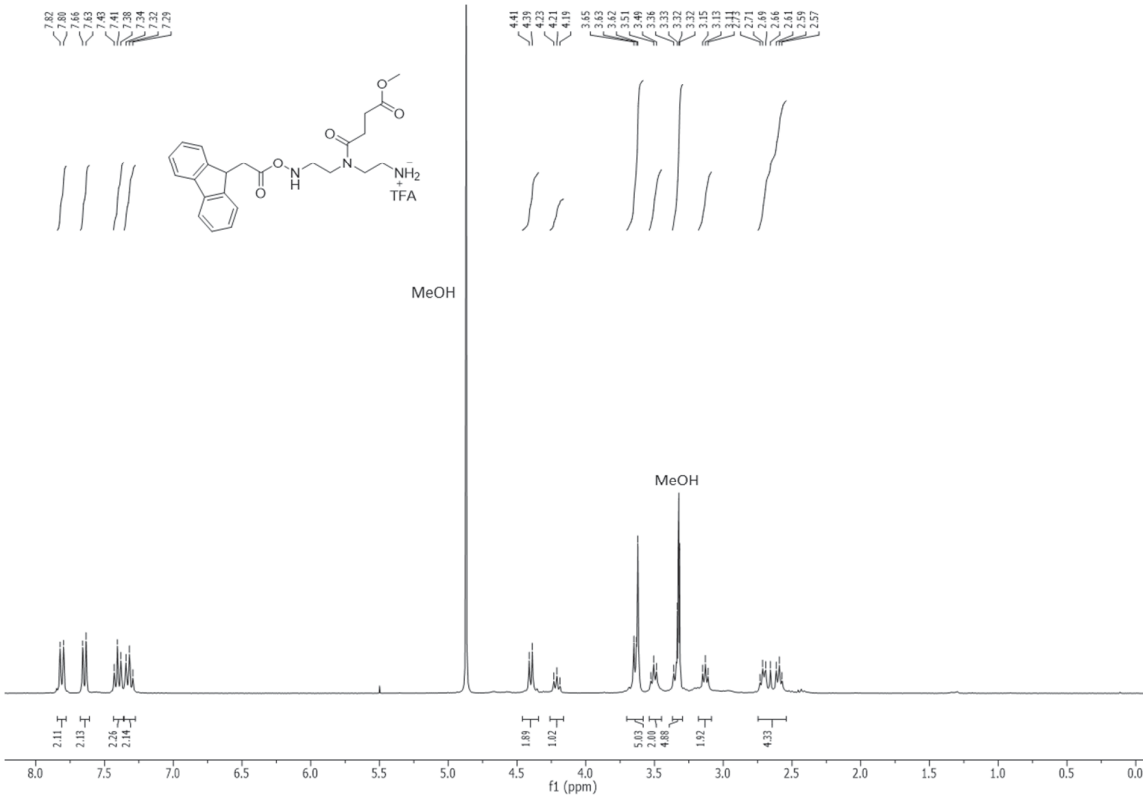

Figure S13: ^{1}H-NMR spectrum of compound **8** (MeOD, 300 MHz).

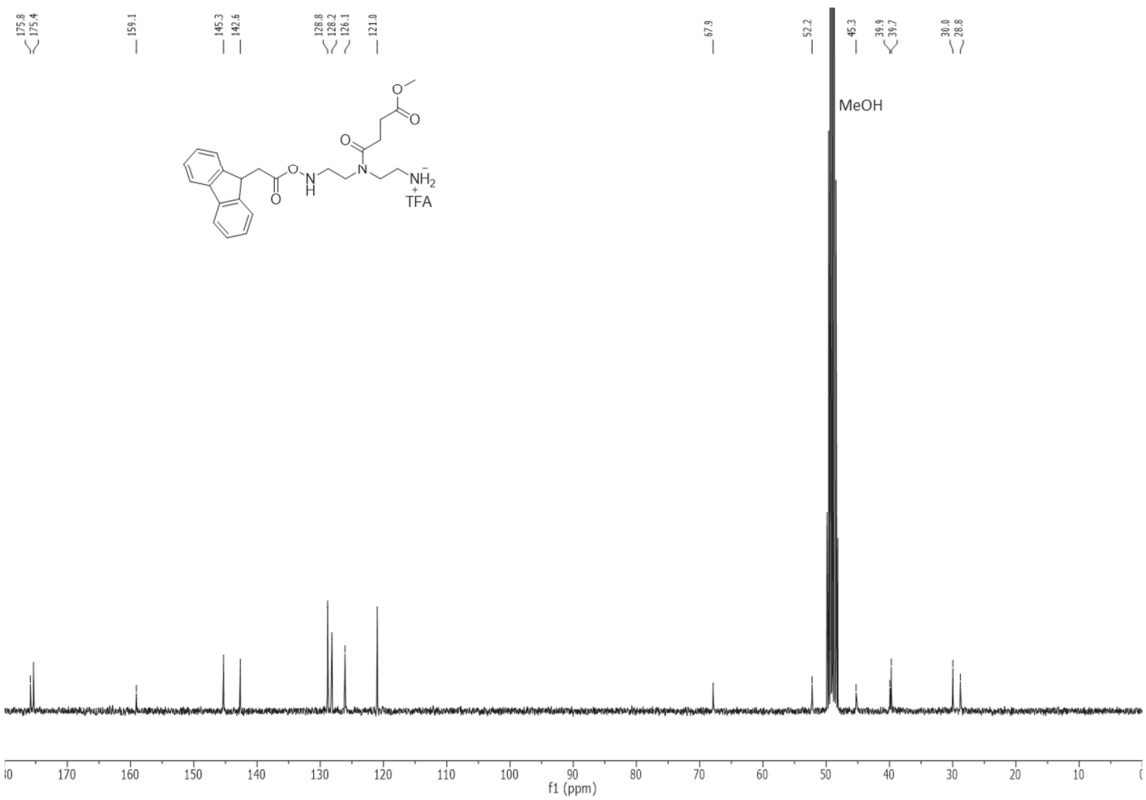

Figure S14: ^{13}C-NMR spectrum of compound **8** (MeOD, 75 MHz).

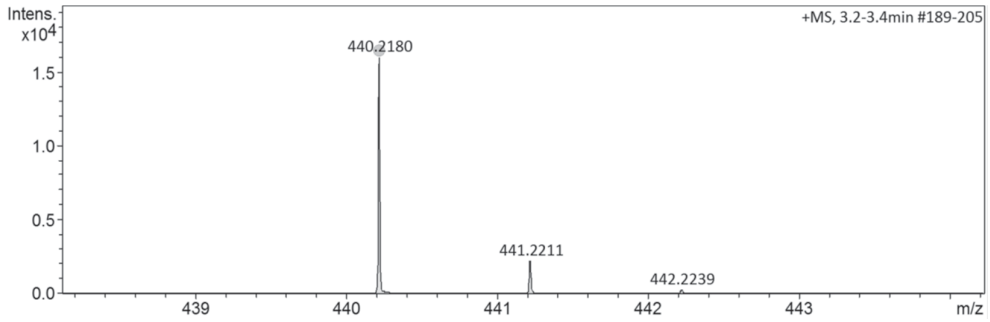

Figure S15: HR-ESI MS spectrum of compound **8**.

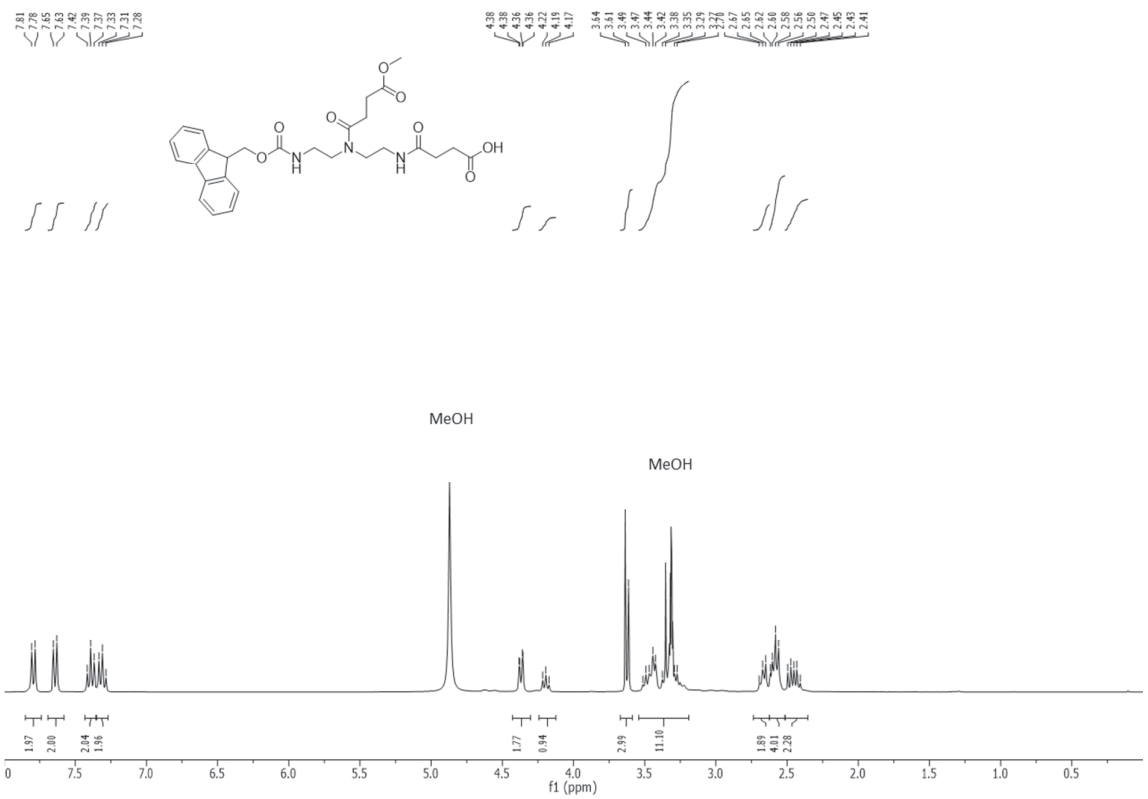

Figure S16: ^{1}H-NMR spectrum of MDS building block **9** (MeOD, 300 MHz).

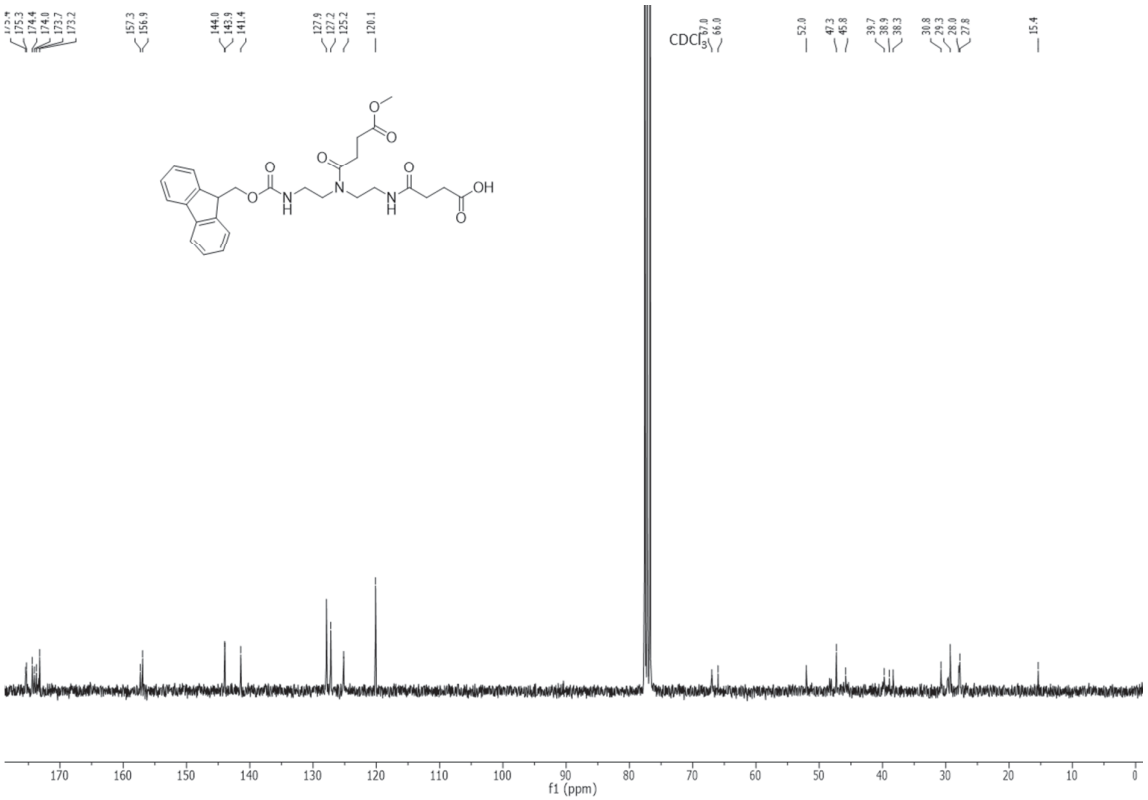

Figure S17: ^{13}C-NMR spectrum of MDS building block **9** ($CDCl_3$, 75 MHz).

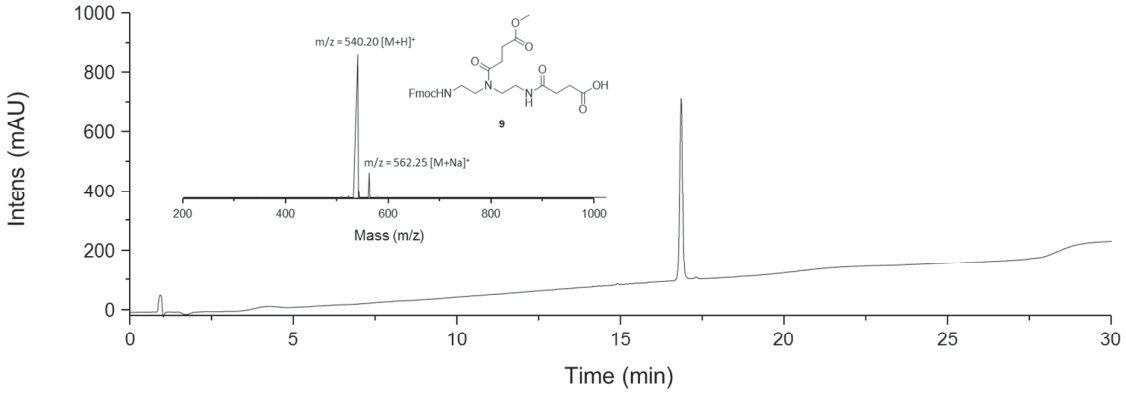

Figure S18: RP-HPLC and ESI-MS spectrum of MDS building block **9** (30 min, 25 °C, Gradient: 100 % A to 50 % A): t_R =16.8 min; Purity: 99 %.

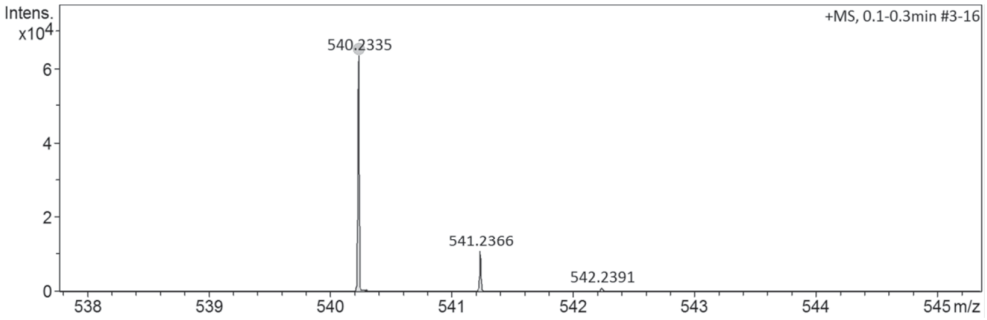

Figure S19: HR-ESI MS spectrum of MDS building block **9**.

3.) **Analytical Data for Solid Phase Synthesis**

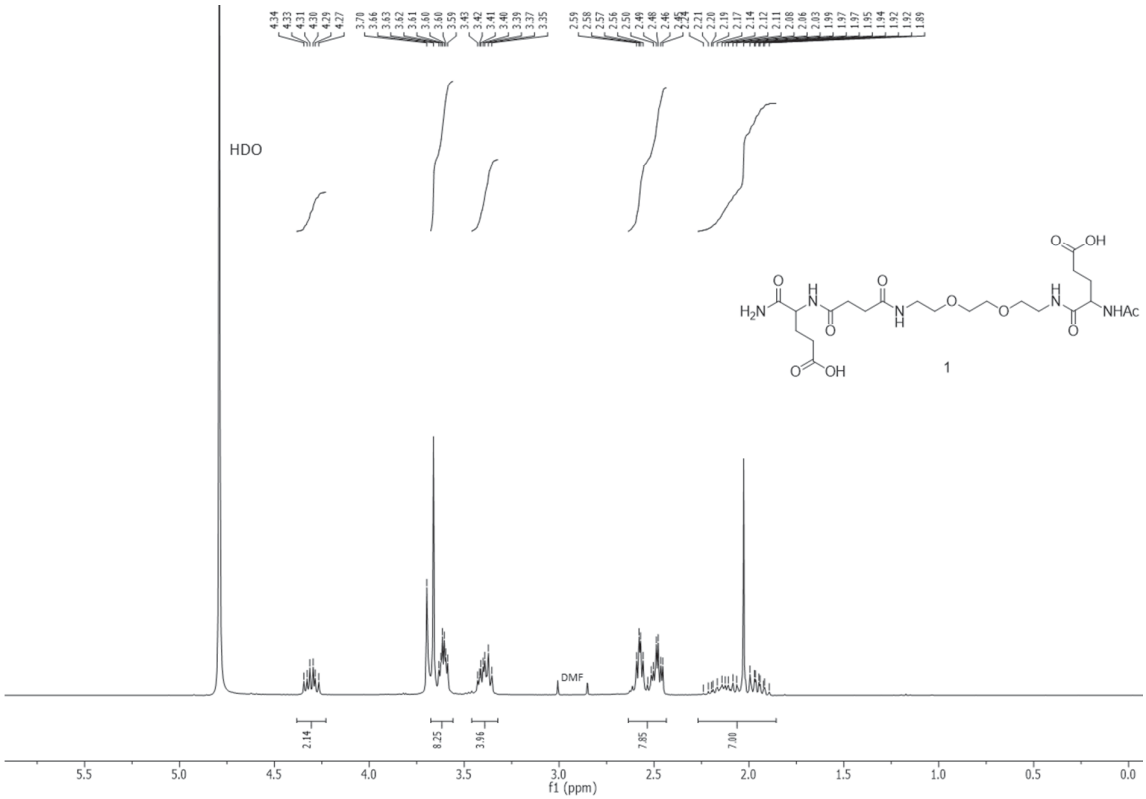

Figure S20: ^{1}H-NMR spectrum of scaffold GEG **1** (D_2O, 300 MHz).

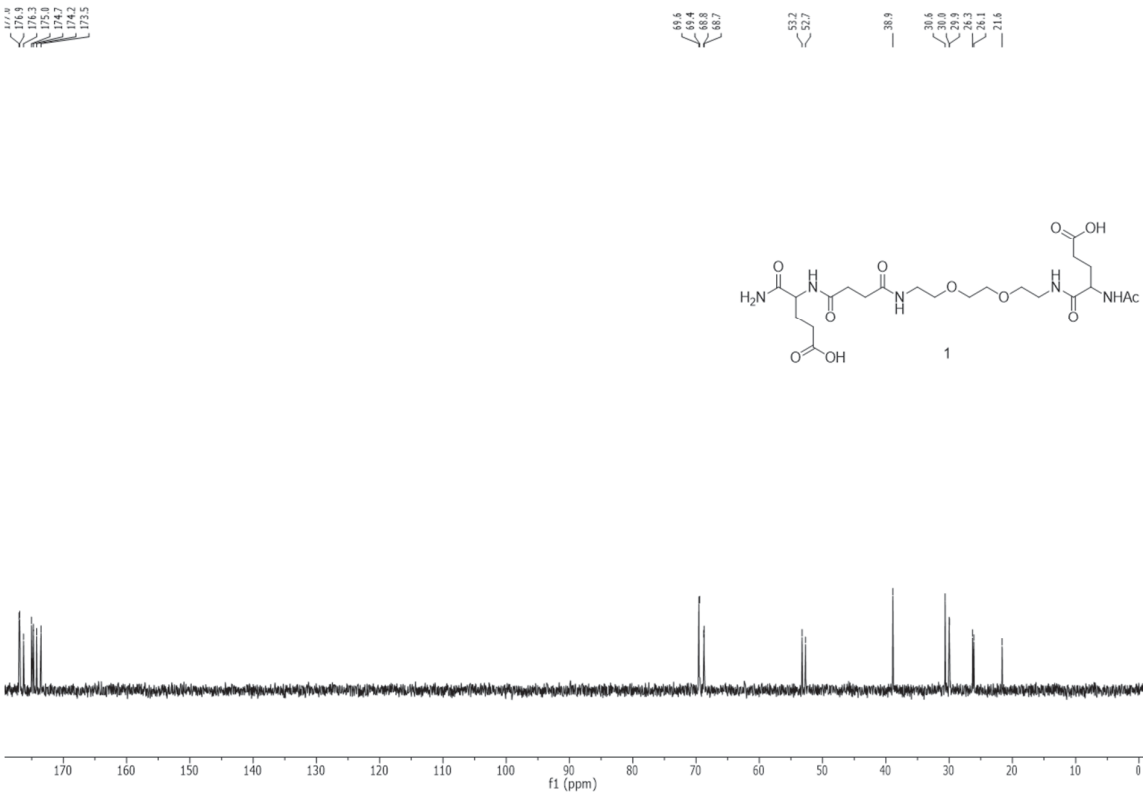

Figure S21: ^{13}C-NMR spectrum of scaffold GEG **1** (D_2O, 75 MHz).

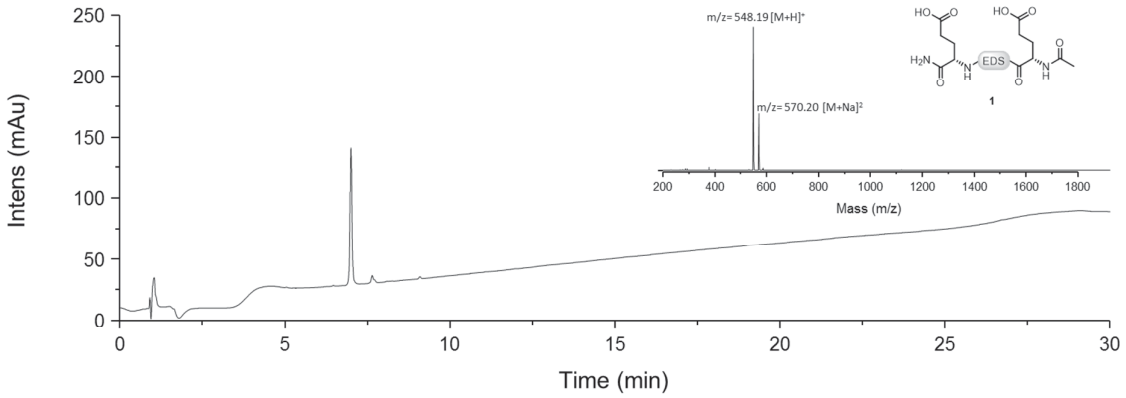

Figure S22: RP-HPLC and ESI-MS spectrum of scaffold GEG (**1)** (30 min, 25 °C, Gradient: 100 % A to 50 % A): t_R =7.0 min; Purity: 90 %.

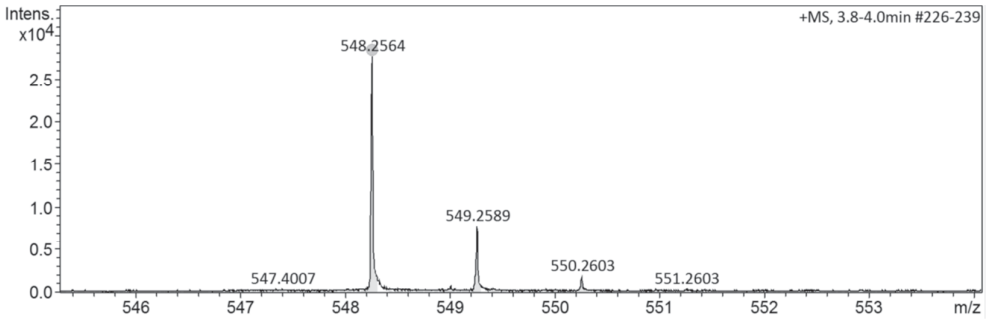

Figure S23: HR-ESI MS spectrum of deprotected scaffold GEG **1** (m/z for $[M+H]^+$).

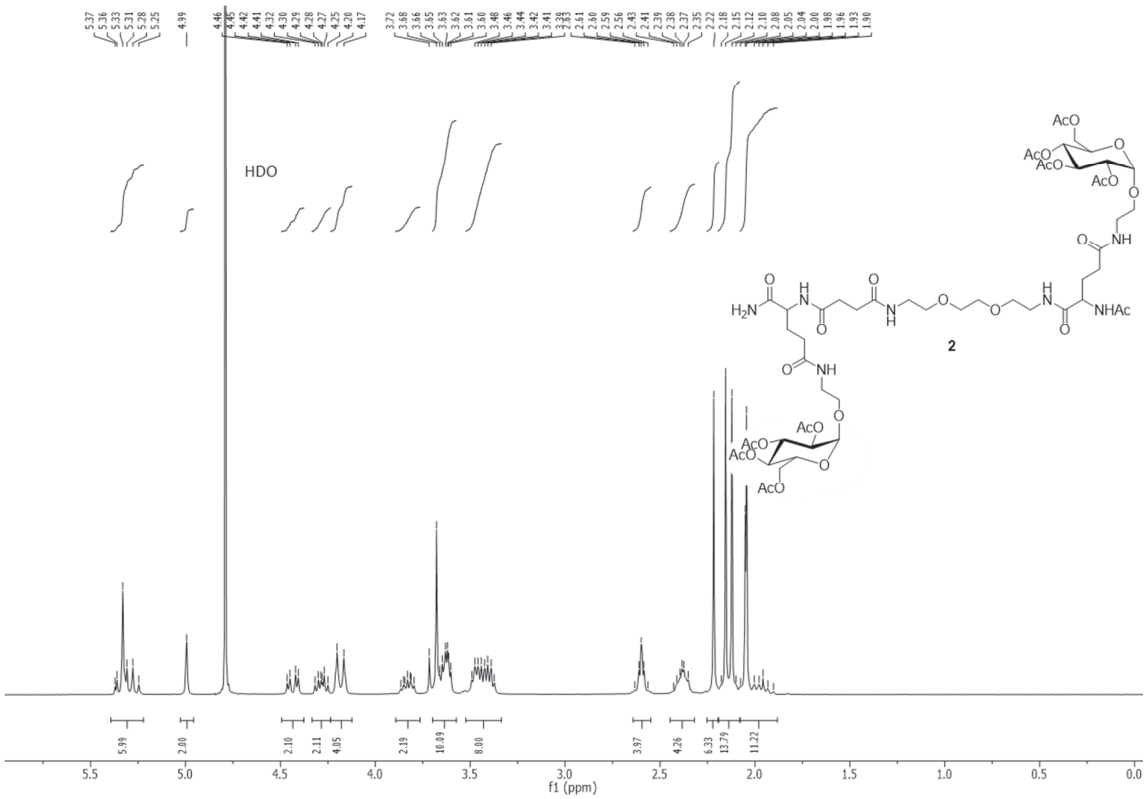

Figure S24:[1]H-NMR spectrum of protected Man(1,3)-3 GEG **2** (D_2O, 300 MHz).

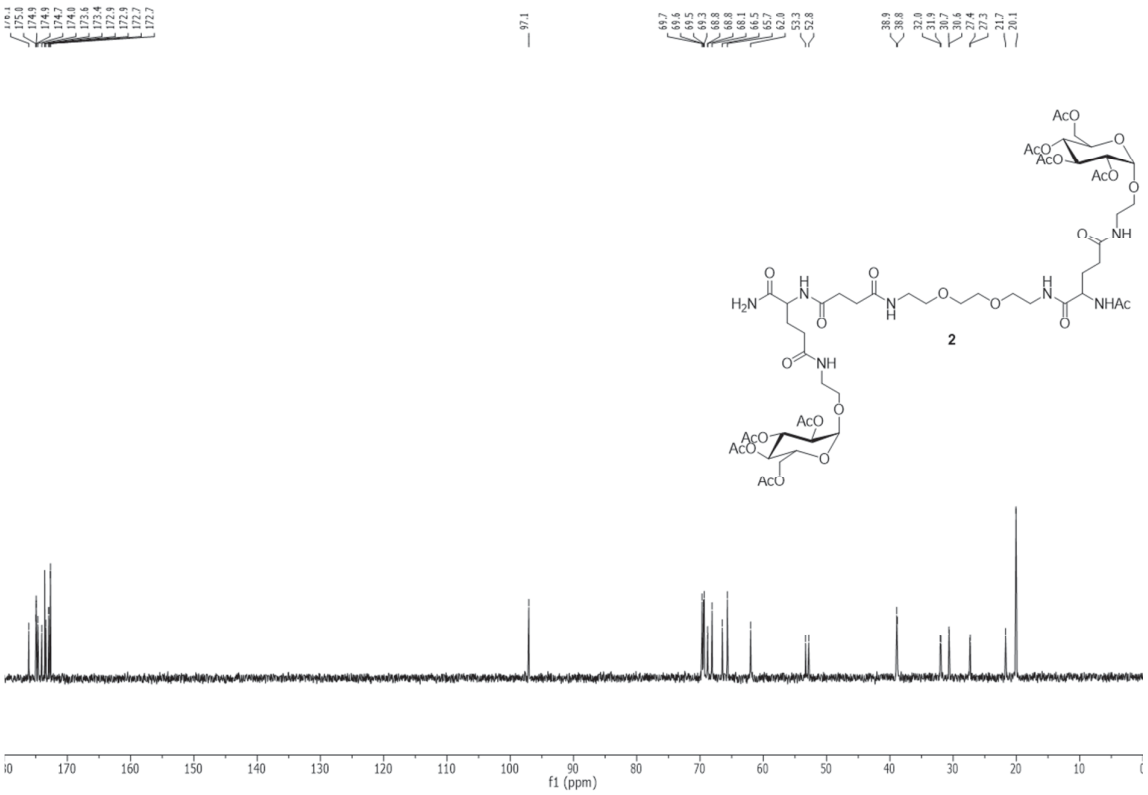

Figure S25: [13]C-NMR spectrum of protected Man(1,3)-3 GEG **2** (D_2O, 75 MHz).

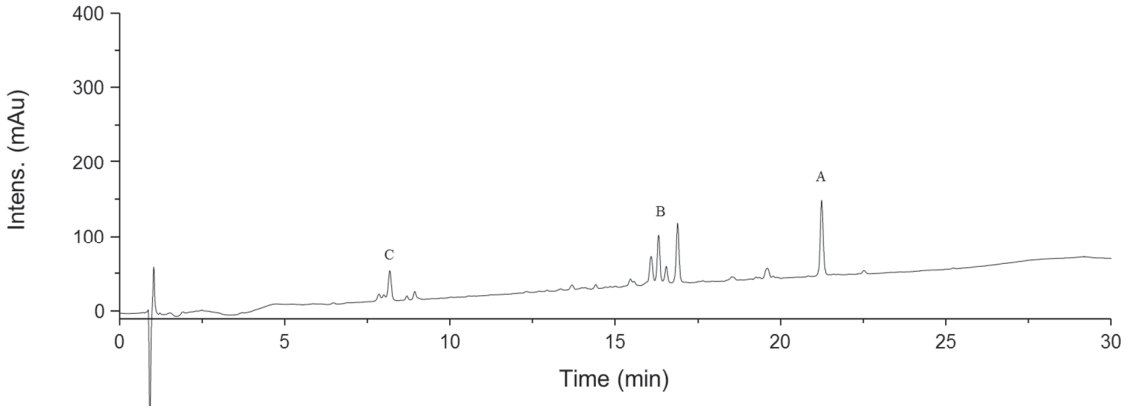

Figure S26: RP-HPLC of the crude from Staudinger ligation on GEG scaffold **1** (30 min, 25 °C, Gradient: 100 % A to 50 % A). A: Protected Man(1,3)-3 GEG (**2**), B: complex mixture of mono-glycosylated scaffolds and sideproducts, C: starting material.

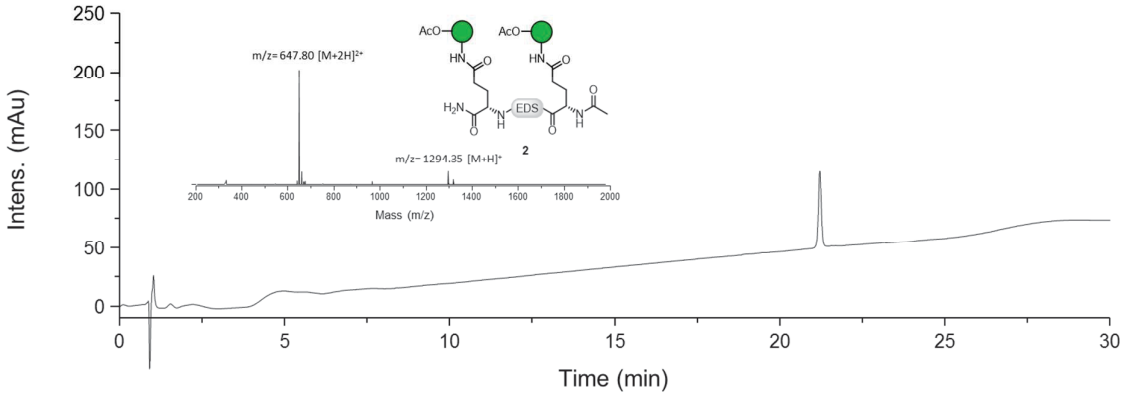

Figure S27: RP-HPLC and ESI-MS spectrum of protected Man(1,3)-3 GEG (**2**) after preparative purification (30 min, 25 °C, Gradient: 100 % A to 50 % A): t_R =21.2 min; Purity: 98 %.

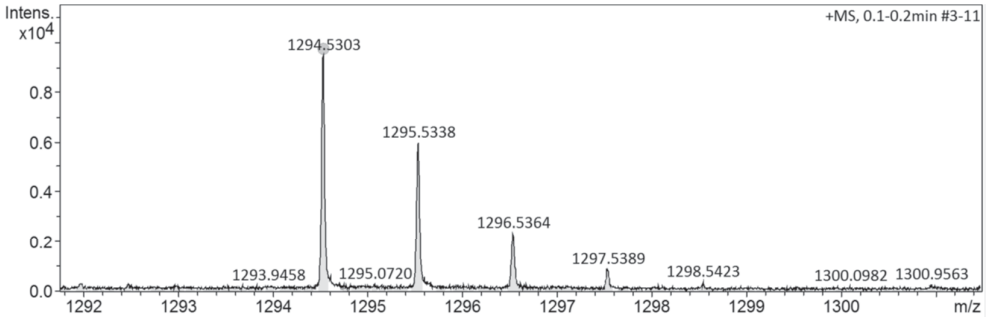

Figure S28: HR-ESI MS spectrum of protected Man(1,3)-3 GEG (**2**) (m/z for $[M+H]^+$).

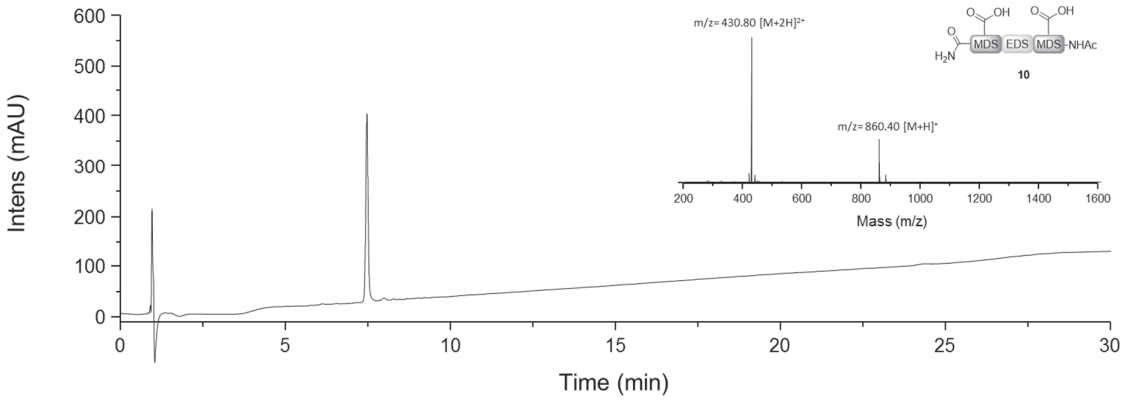

Figure S29: RP-HPLC and ESI-MS spectrum of deprotected scaffold MEM **10** (30 min, 25 °C, Gradient: 100 % A to 50 % A): t_R =7.5 min; Purity: 92 %.

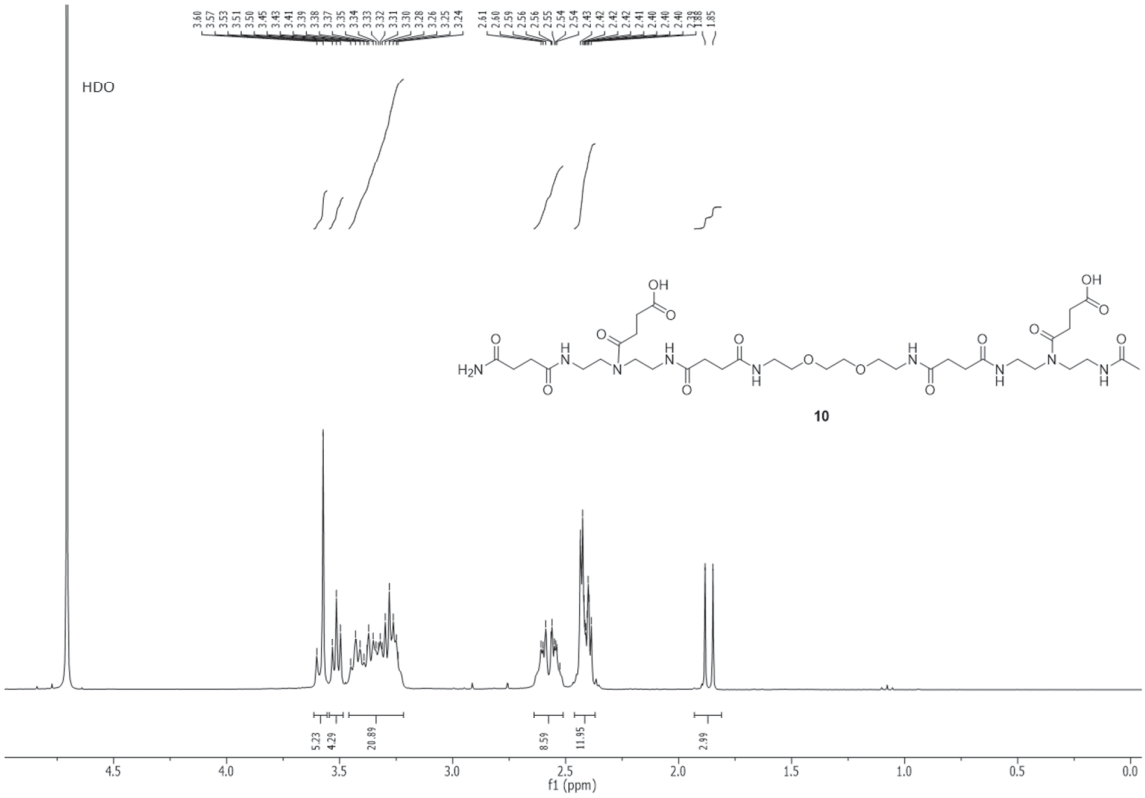

Figure S30: ^{1}H-NMR spectrum of deprotected scaffold MEM **10** (D_2O, 300 MHz).

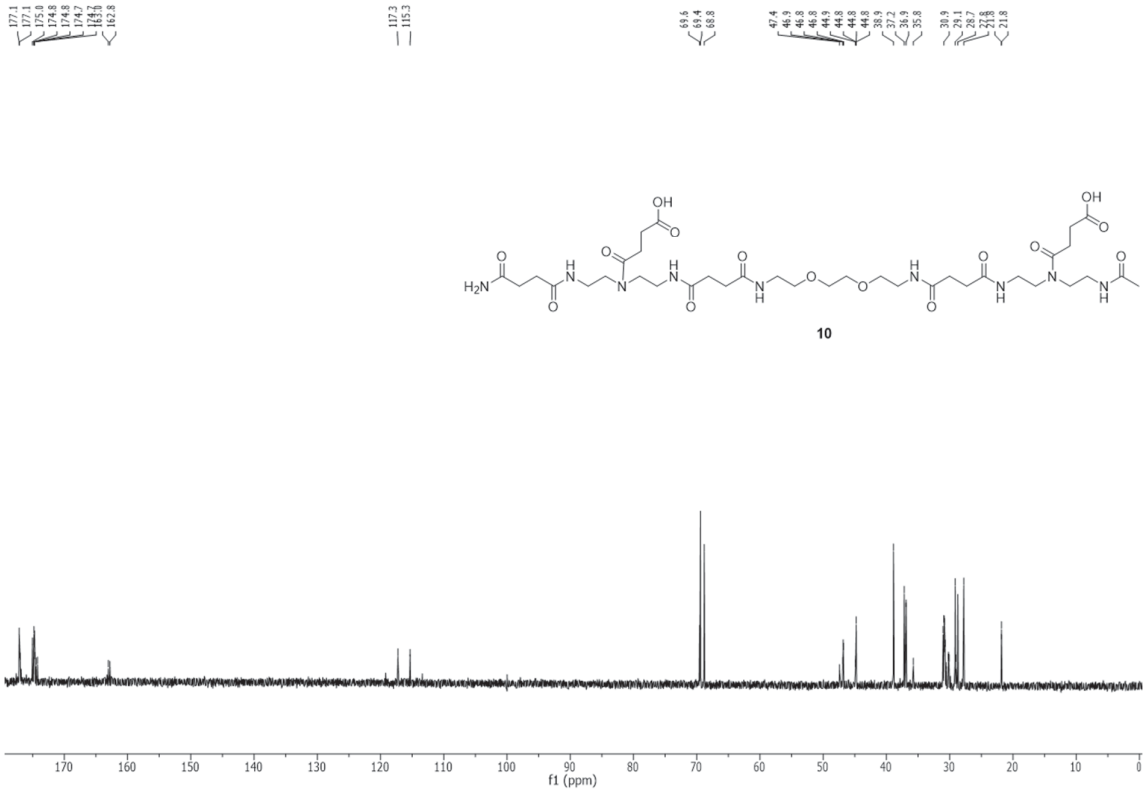

Figure S31: ^{13}C-NMR spectrum of deprotected scaffold MEM **10** (D_2O, 151 MHz).

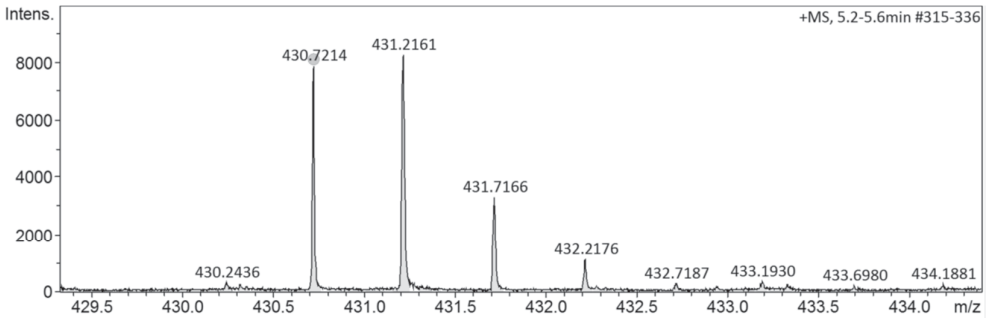

Figure S32: HR-ESI MS spectrum of deprotected scaffold MEM **10** (m/z for $[M+2H]^{2+}$).

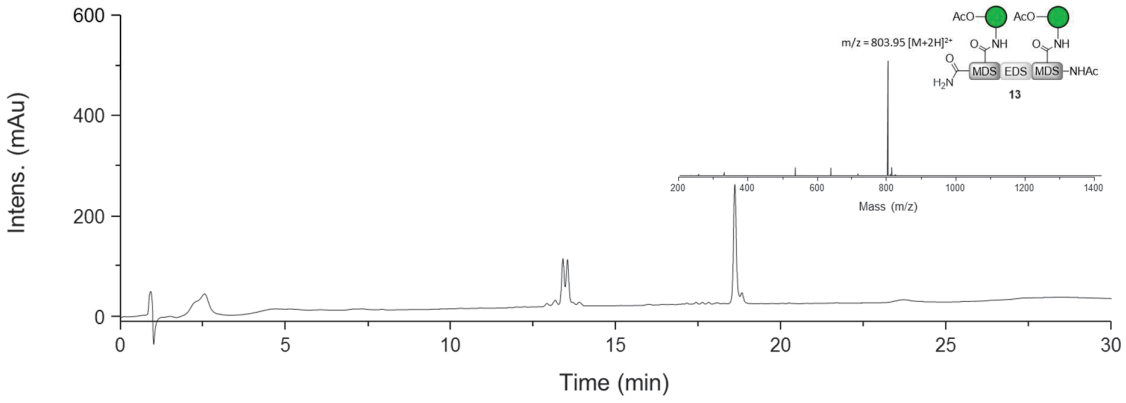

Figure S33: RP-HPLC and ESI-MS spectrum of protected Man(1,3)-3 MEM (**13)** from the reaction in ACN (30 min, 25 °C, Gradient: 100 % A to 50 % A): t_R =18.6 min; Purity: 53 %.

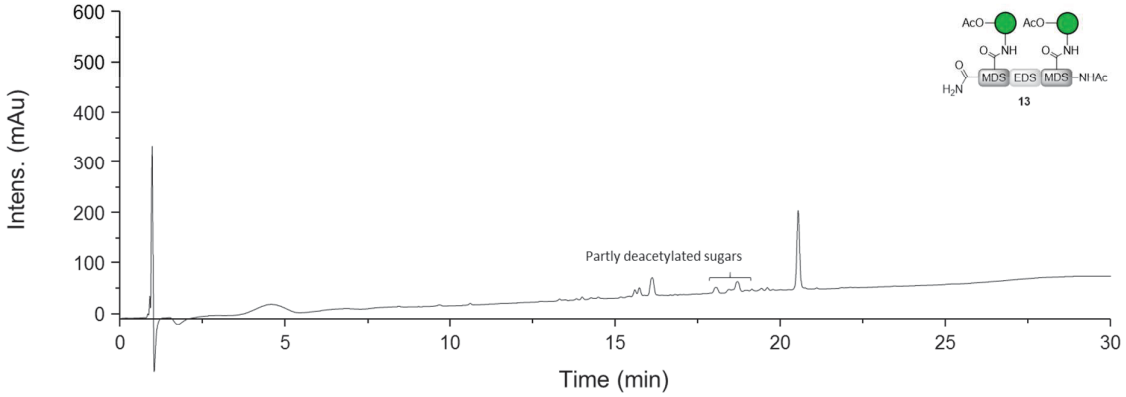

Figure S34: RP-HPLC spectrum of protected Man(1,3)-3 MEM (**13)** from the reaction in DMF (30 min, 25 °C, Gradient: 100 % A to 50 % A): t_R =20.5 min; Purity: 52 % + 21 % partly deprotected.

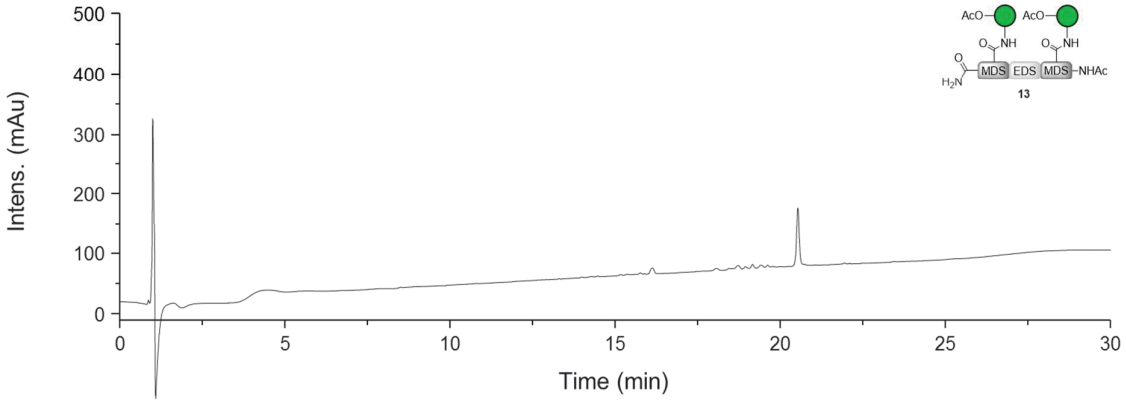

Figure S35: RP-HPLC spectrum of protected Man(1,3)-3 MEM (**13)** from the reaction in ACN/DMF (1/1) (30 min, 25 °C, Gradient: 100 % A to 50 % A)): t_R =20.5 min, Purity: 71 % .

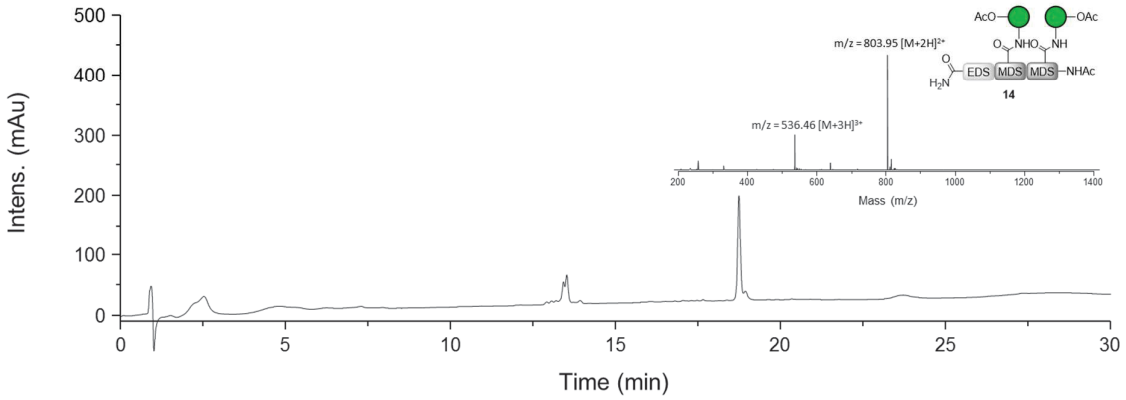

Figure S36: RP-HPLC and ESI-MS spectrum of protected Man(2,3)-3 EMM (**14)** from the reaction in ACN (30 min, 25 °C, Gradient: 100 % A to 50 % A) : t_R =18.7 min; Purity: 59 %.

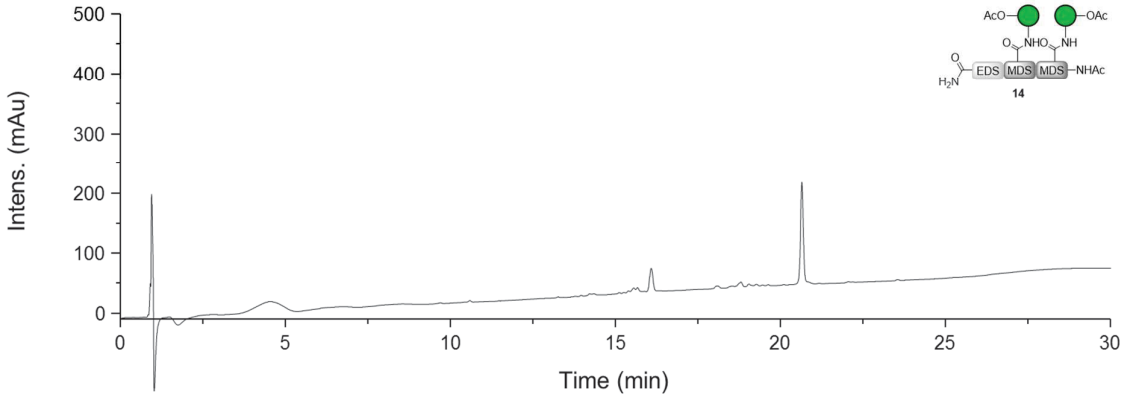

Figure S37: RP-HPLC of protected Man(2,3)-3 EMM (14) from the reaction in DMF (30 min, 25 °C, Gradient: 100 % A to 50 % A): t_R =20.5 min; Purity: 67 %.

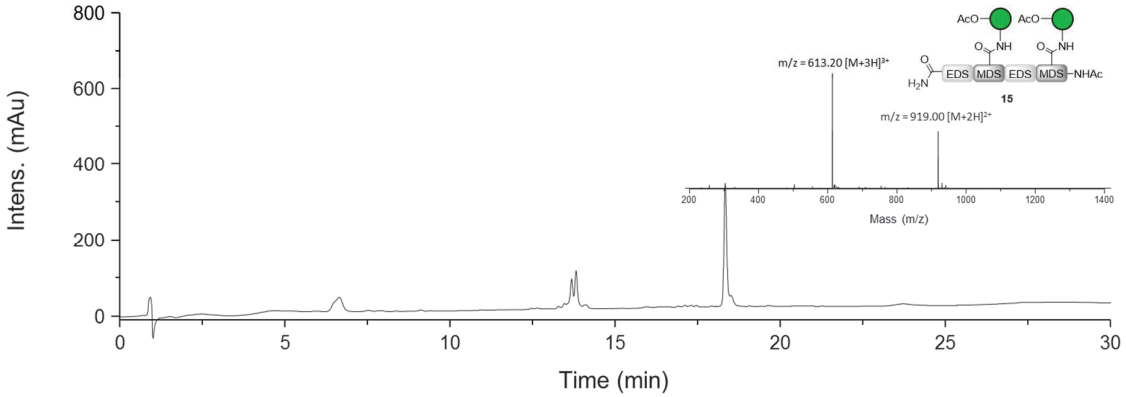

Figure S38: RP-HPLC and ESI-MS spectrum of protected Man(2,4)-4 EMEM (**15**) from the reaction in ACN (30 min, 25 °C, Gradient: 100 % A to 50 % A): t_R =18.3 min; Purity: 53 %**..**

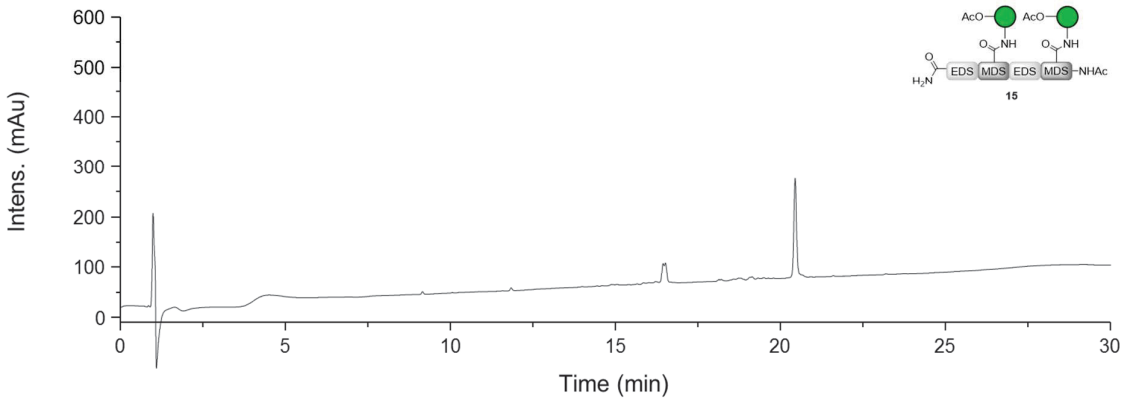

Figure S39: RP-HPLC of protected Man(2,4)-4 EMEM (**15**) from the reaction in DMF (30 min, 25 °C, Gradient: 100 % A to 50 % A): t_R =20.5 min; Purity: 68 %. **.**

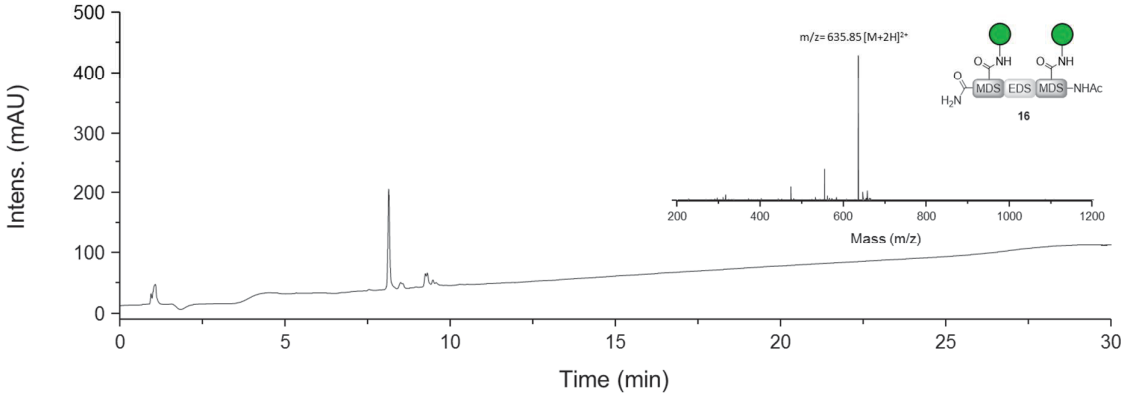

Figure S40: RP-HPLC and ESI-MS spectrum of Man(1,3)-3 MEM (**16**) from reaction in DMF (30 min, 25 °C, Gradient: 100 % A to 50 % A): t_R =7.9 min; Purity: 68 %.

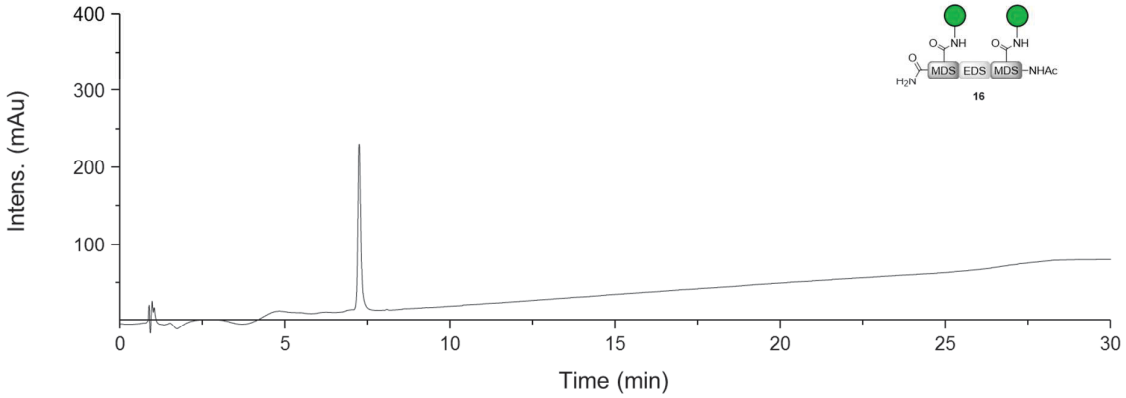

Figure S41: RP-HPLC and ESI-MS spectrum of Man(1,3)-3 MEM (**16**) after preparative purification (30 min, 25 °C, Gradient: 100 % A to 50 % A): t_R =7.3 min; Purity: 99 %.

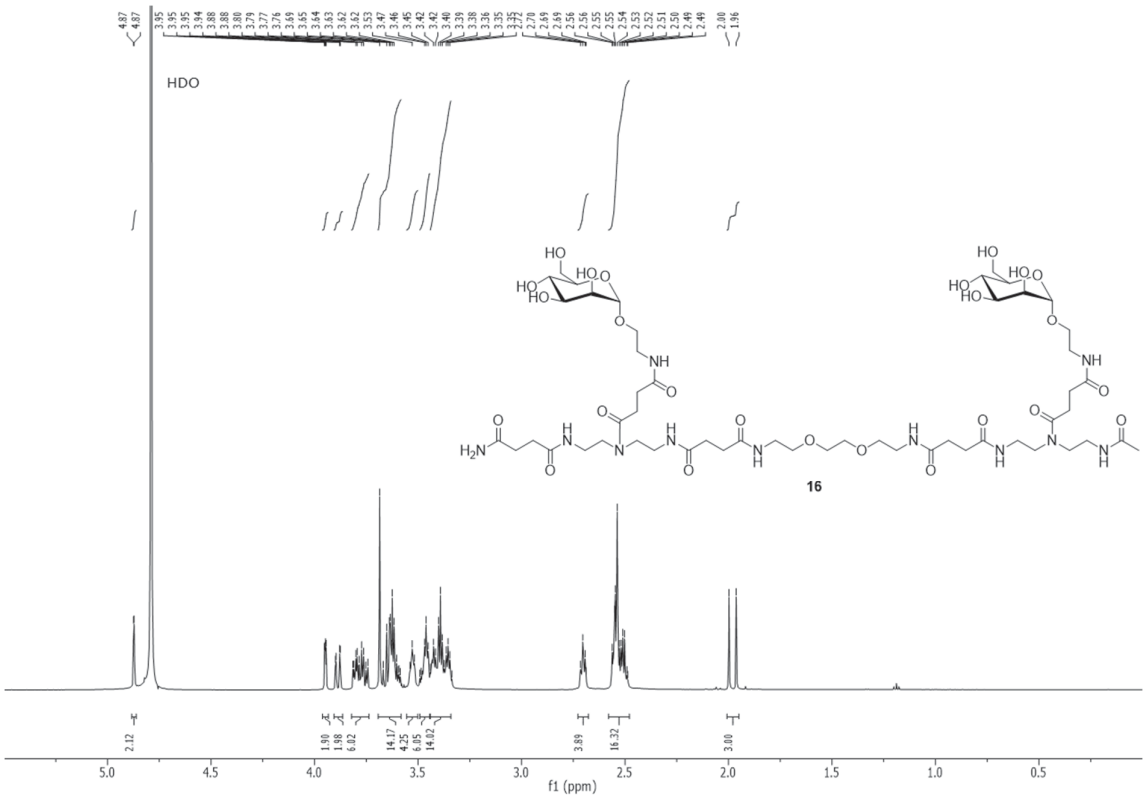

Figure S42: ^{1}H-NMR spectrum of Man(1,3)-3 MEM (**16**) (D_2O, 300 MHz).

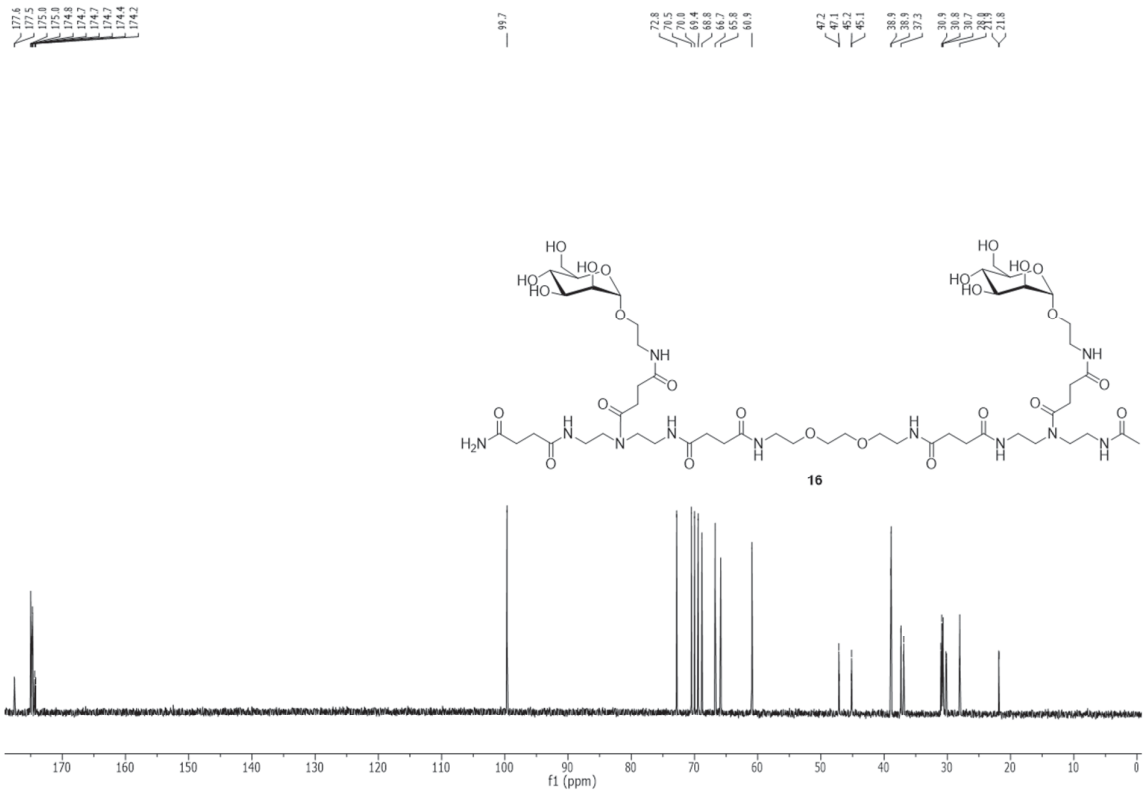

Figure S43: ^{13}C-NMR spectrum of Man(1,3)-3 MEM (**16**) (D_2O, 75 MHz).

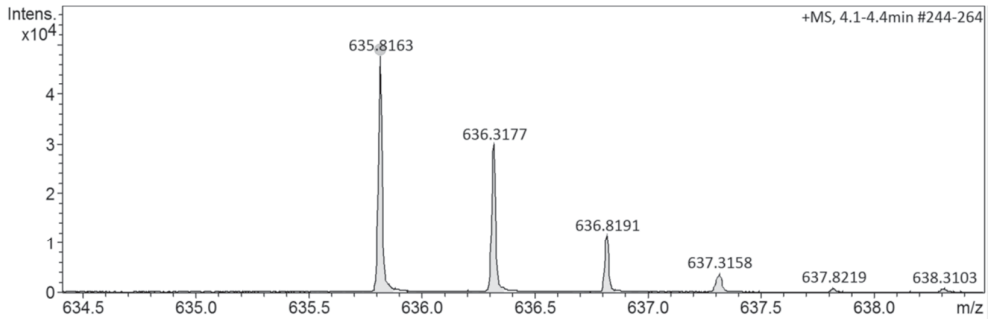

Figure S44: HR-ESI MS spectrum of Man(1,3)-3 MEM (**16**) (m/z for $[M+2H]^{2+}$).

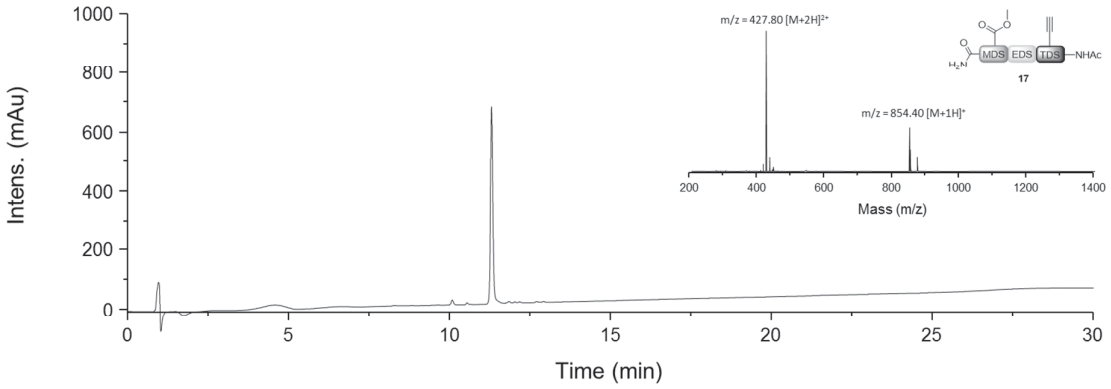

Figure S45: RP-HPLC and ESI-MS spectrum of compound **17** (30 min, 25 °C, Gradient: 100 % A to 50 % A): t_R =11.3 min; Purity: 94 %.

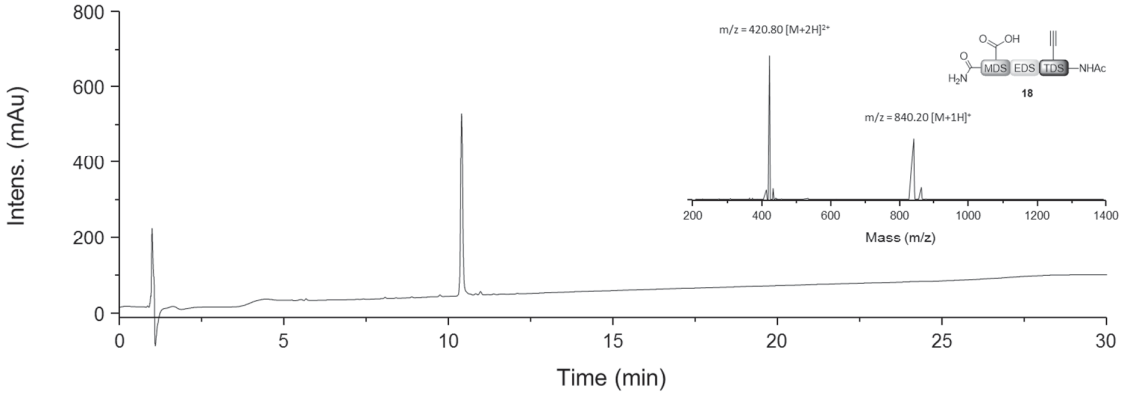

Figure S46: RP-HPLC and ESI-MS spectrum of compound **18** (30 min, 25 °C, Gradient: 100 % A to 50 % A): t_R =10.4 min; Purity: 94 %.

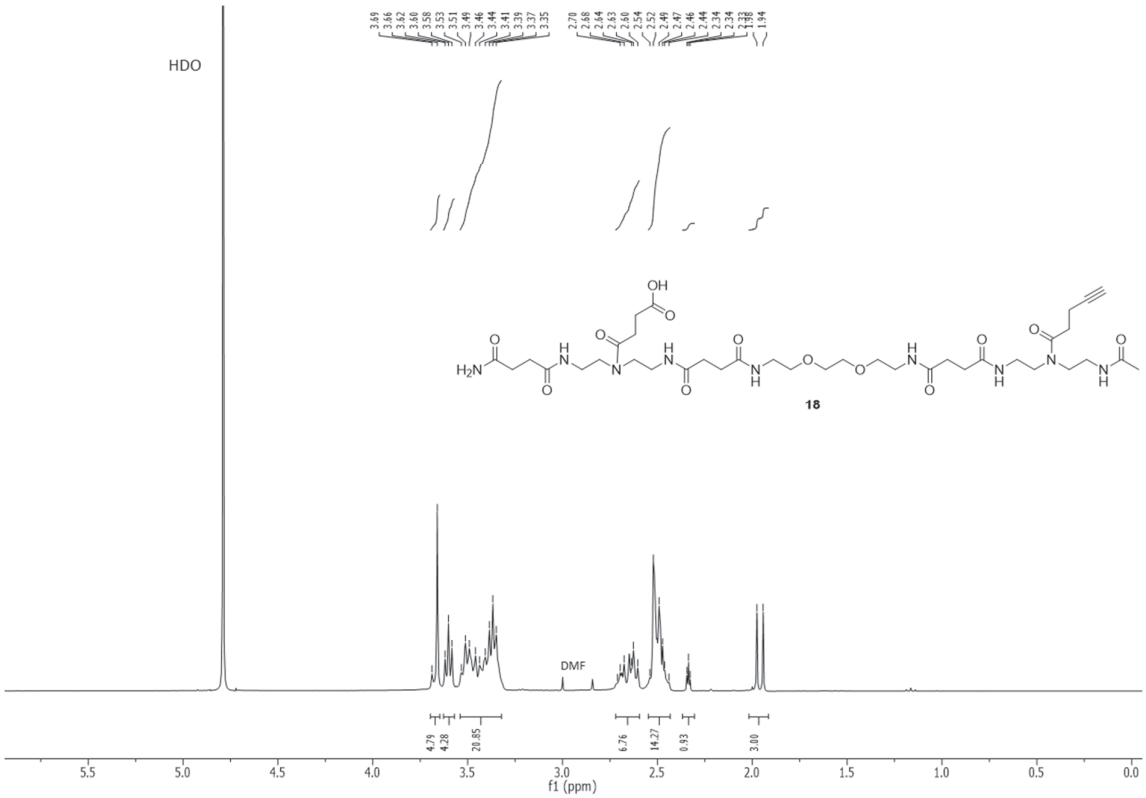

Figure S47: ^{1}H-NMR spectrum of deprotected MET scaffold **18** (D_2O, 300 MHz).

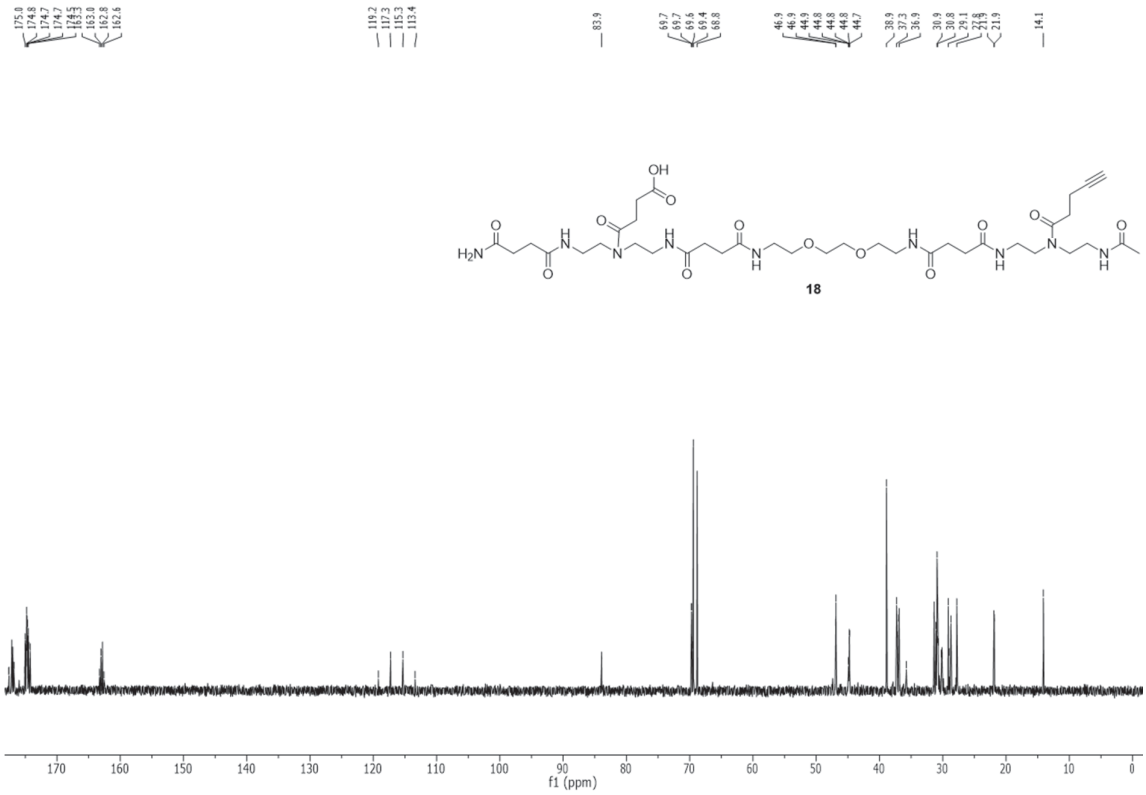

Figure S48: ^{13}C-NMR spectrum of deprotected MET scaffold **18** (D_2O, 151 MHz).

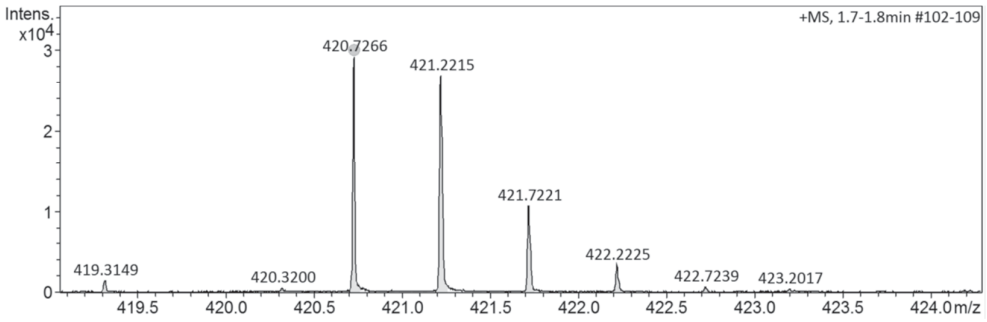

Figure S49: HR-ESI MS spectrum of deprotected MET scaffold **18** (m/z for $[M+2H]^{2+}$).

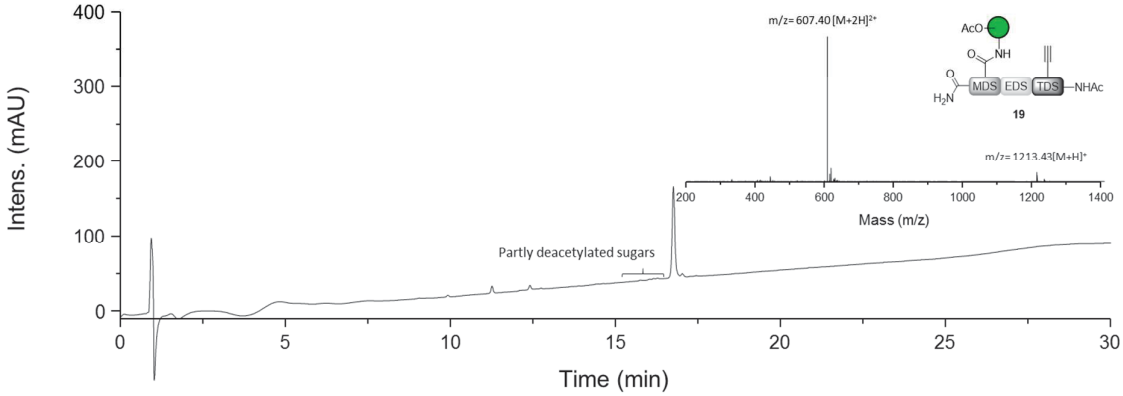

Figure S50: RP-HPLC and ESI-MS spectrum of Man(1)-3 MET **19** from Route A (30 min, 25 °C, Gradient: 100 % A to 50 % A): t_R =16.7 min; Purity: 88% (including partly deacetylated products).

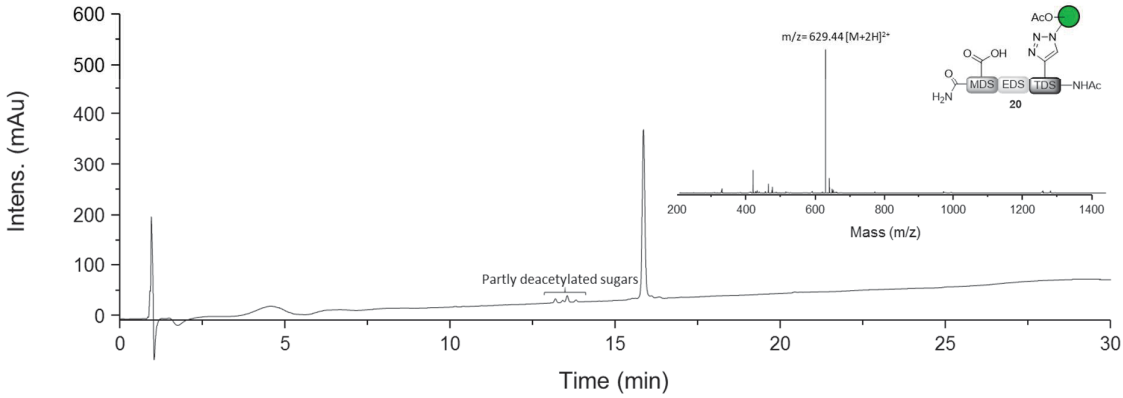

Figure S51: RP-HPLC and ESI-MS spectrum of Man(3)-3 MET **20** from Route B (30 min, 25 °C, Gradient: 100 % A to 50 % A): t_R =15.3 min; Purity: 94% (including partly deacetylated products).

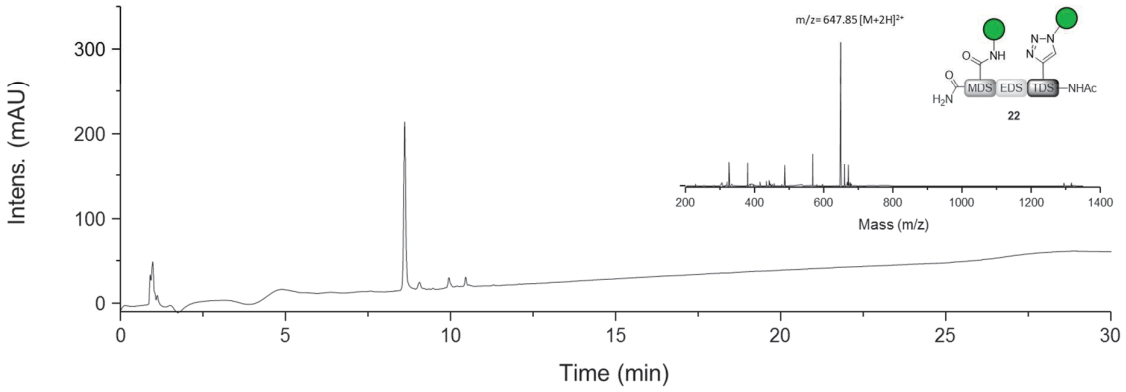

Figure S52: RP-HPLC and ESI-MS spectrum of Man(1,3)-3 MET from route A (**22**) (30 min, 25 °C, Gradient: 100 % A to 50 % A): t_R =8.6 min; Purity: 86 %.

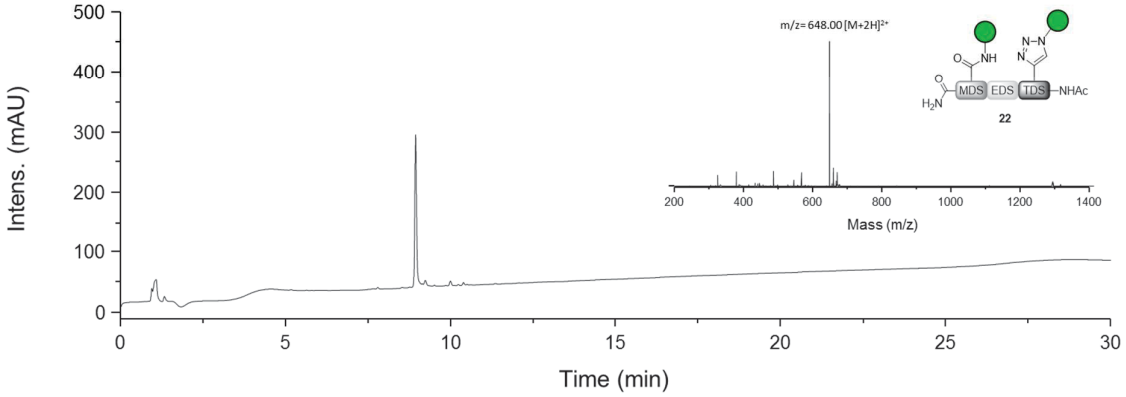

Figure S53: RP-HPLC and ESI-MS spectrum of Man(1,3)-3 MET from route B (**22**) (30 min, 25 °C, Gradient: 100 % A to 50 % A): t_R =8.9 min; Purity: 88 %.

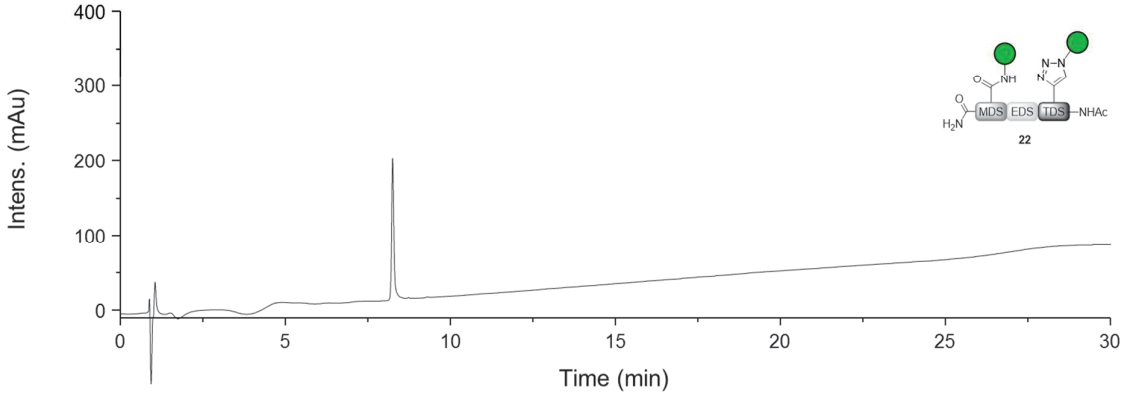

Figure S54: RP-HPLC and ESI-MS spectrum of Man(1,3)-3 MET (**22**) after preparative purification (30 min, 25 °C, Gradient: 100 % A to 50 % A): t_R =8.3 min; Purity: 99 %.

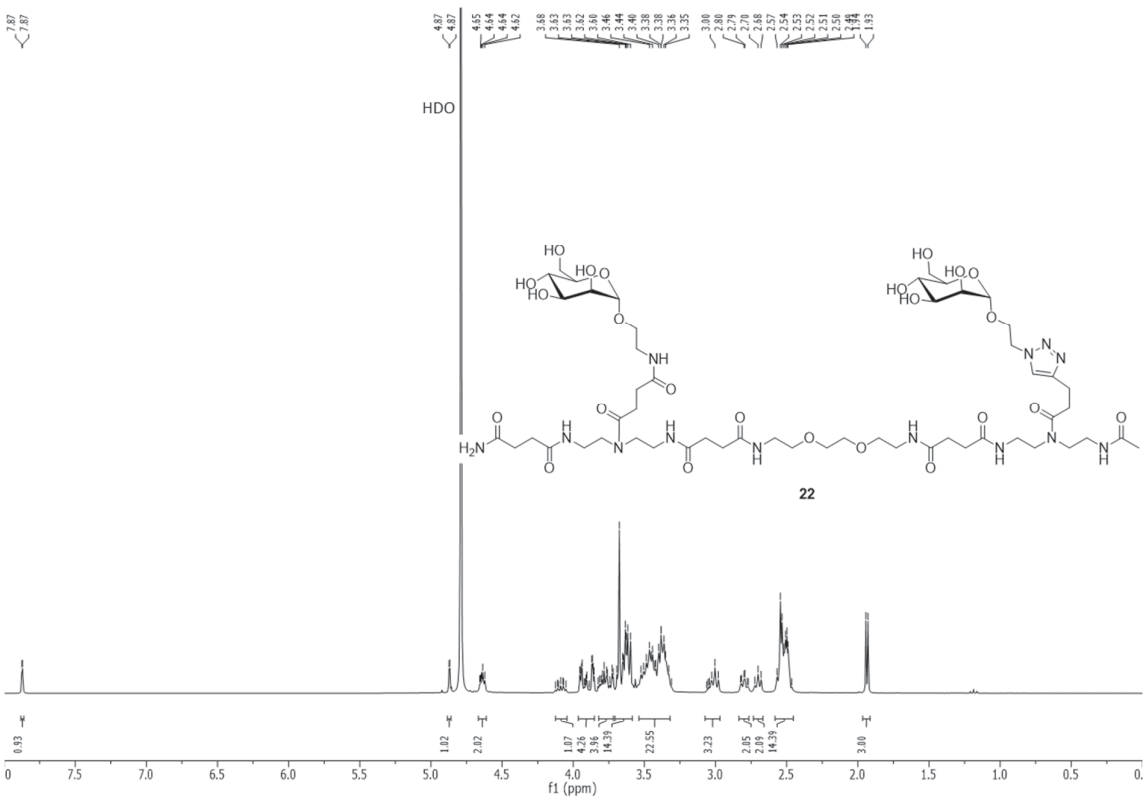

Figure S55: ^{1}H-NMR spectrum of Man(1,3)-3 MET (**22**) (D_2O, 300 MHz).

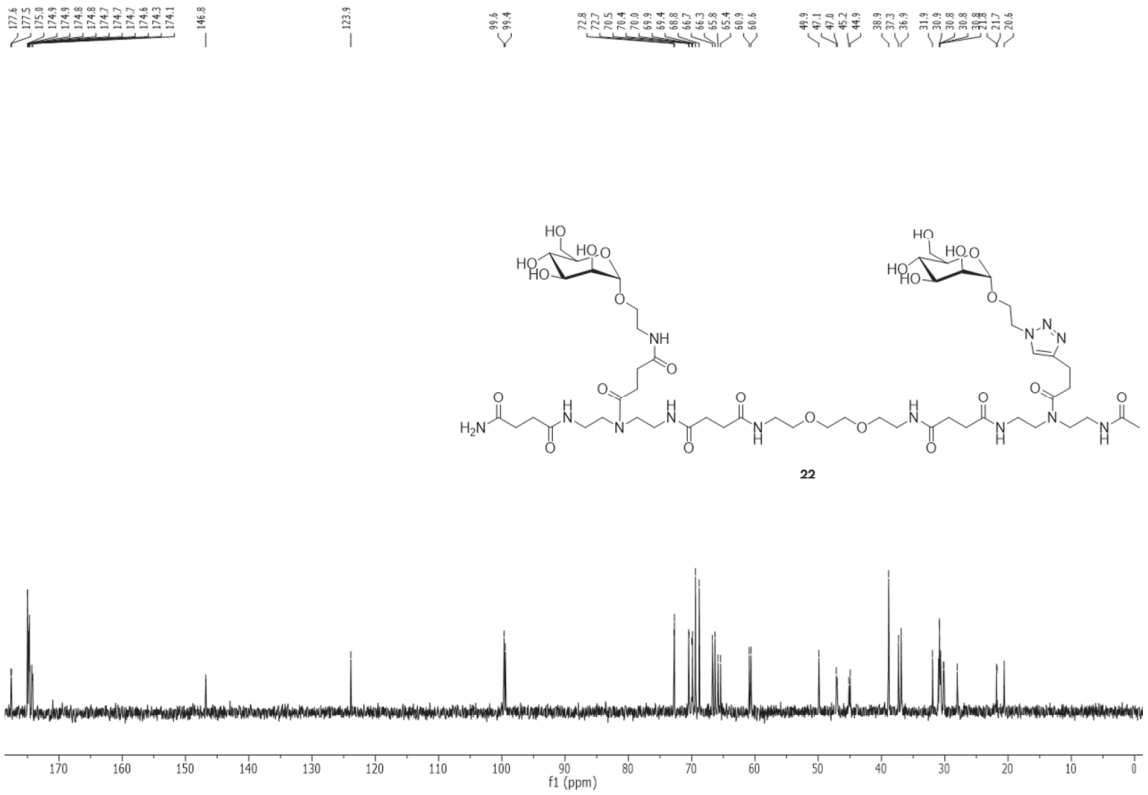

Figure S56: ^{13}C-NMR spectrum of Man(1,3)-3 MET (**22**) (D_2O, 75 MHz).

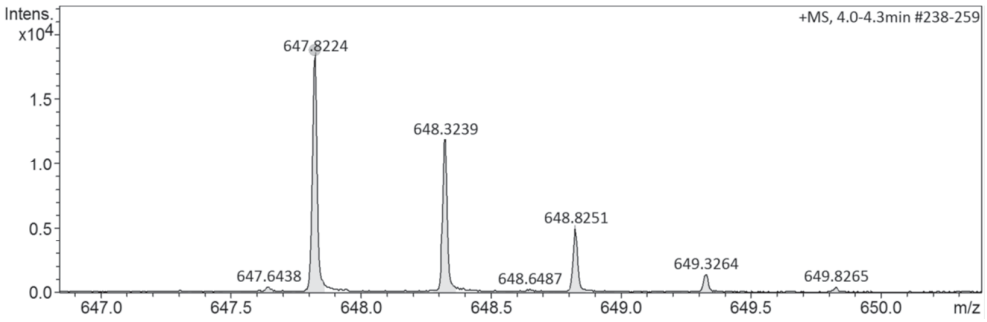

Figure S57: HR-ESI MS spectrum of Man(1,3)-3 MET (**22**) (m/z for $[M+2H]^{2+}$).

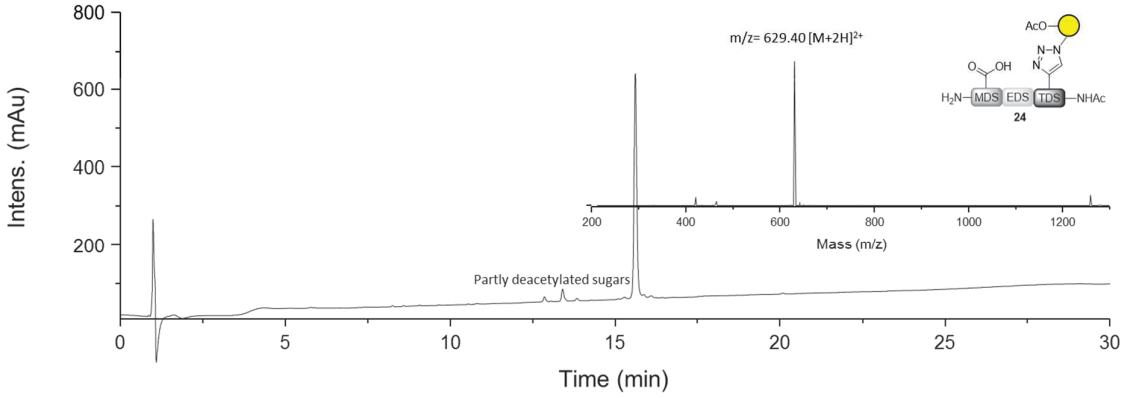

Figure S58: RP-HPLC and ESI-MS spectrum of Gal(3)-3 MET **24** (30 min, 25 °C, Gradient: 100 % A to 50 % A): t_R =15.6 min; Purity: 93 % (including partly deacetylated products).

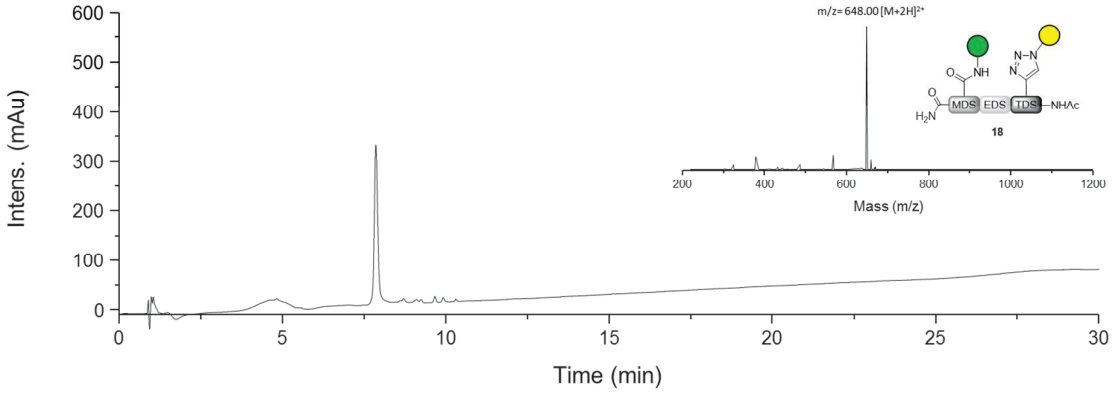

Figure S59: RP-HPLC and ESI-MS spectrum of Man(1)-Gal(3)-3 MET **23** (30 min, 25 °C, Gradient: 100 % A to 50 % A): t_R =7.9 min; Purity: 90 %.

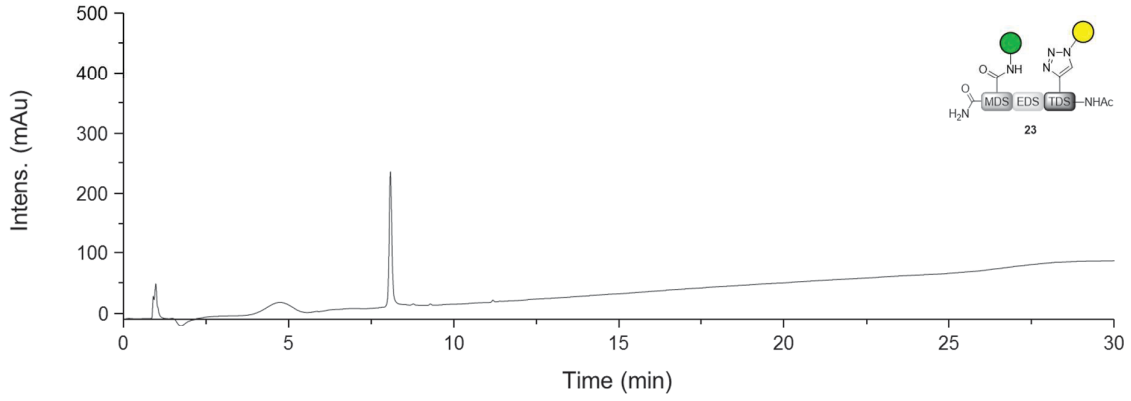

Figure S60: RP-HPLC and ESI-MS spectrum of Man(1)-Gal(3)-3 MET **23** after preparative purification (30 min, 25 °C, Gradient: 100 % A to 50 % A): t_R =8.0 min; Purity: 98 %.

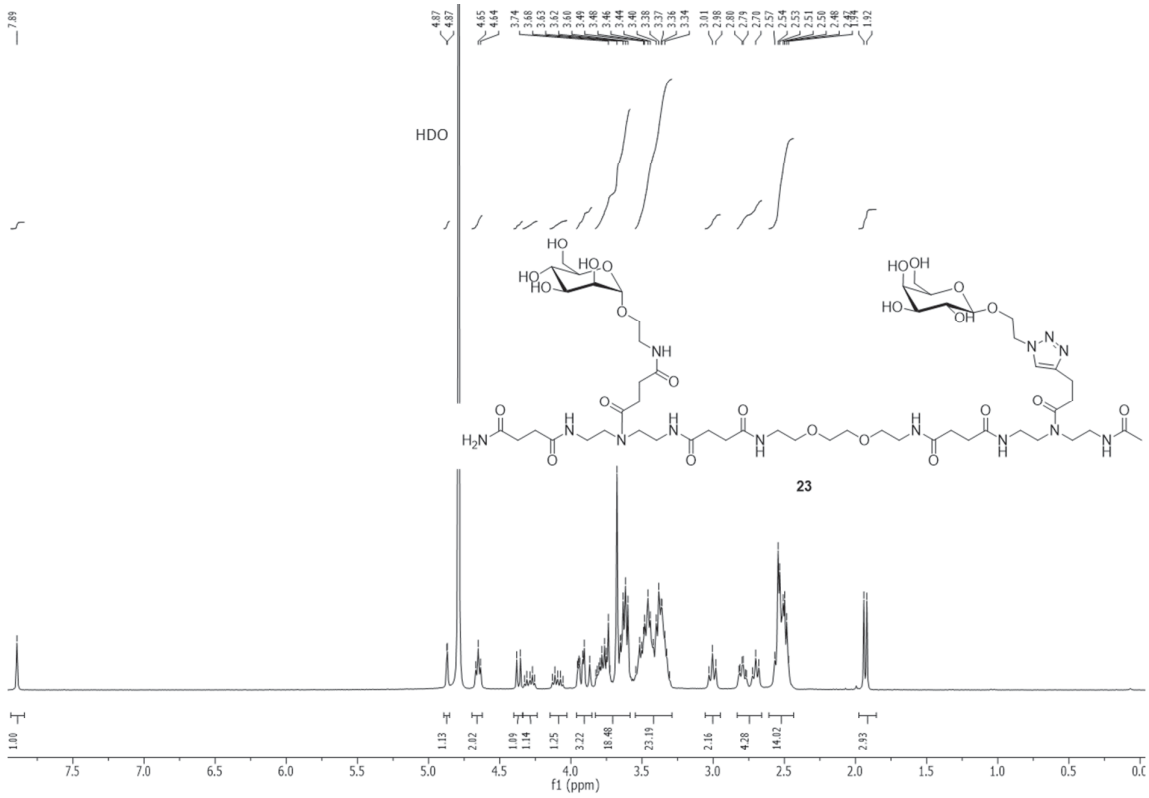

Figure S61: ^{1}H-NMR spectrum of Man(1)-Gal(3)-3 MET **23** (D_2O, 300 MHz).

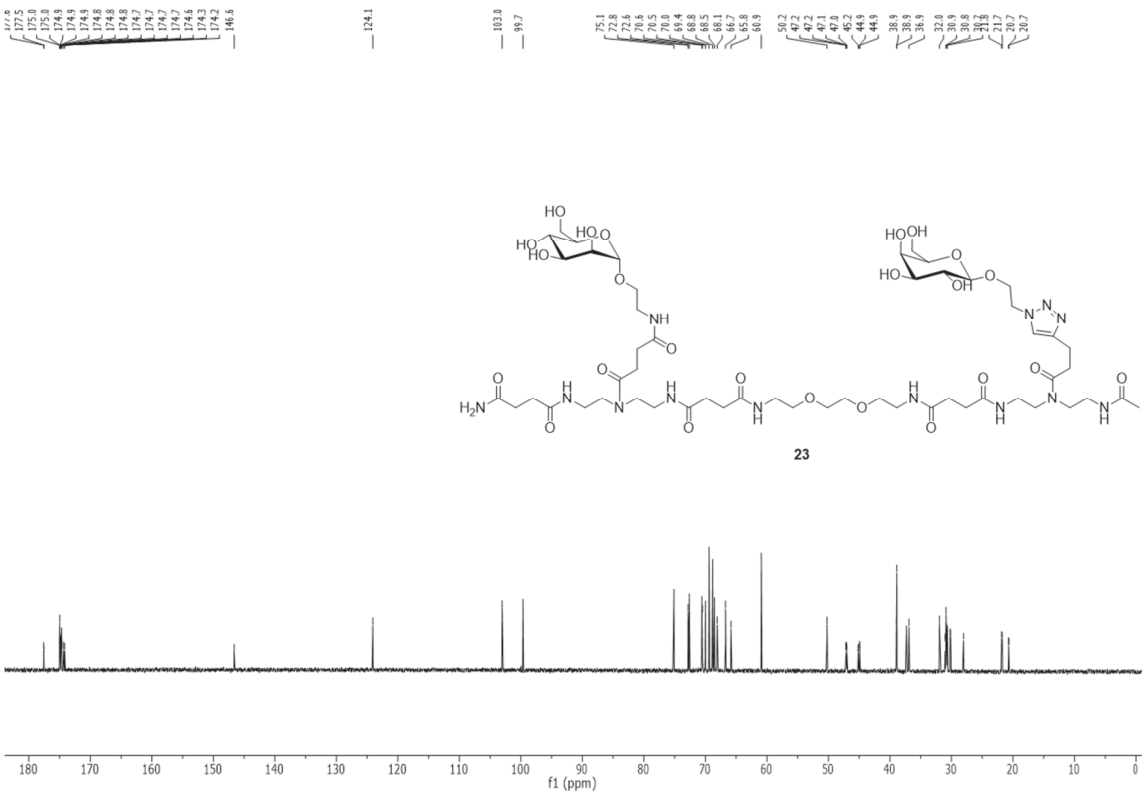

Figure S62: ^{13}C-NMR spectrum of Man(1)-Gal(3)-3 MET **23** (D_2O, 151 MHz).

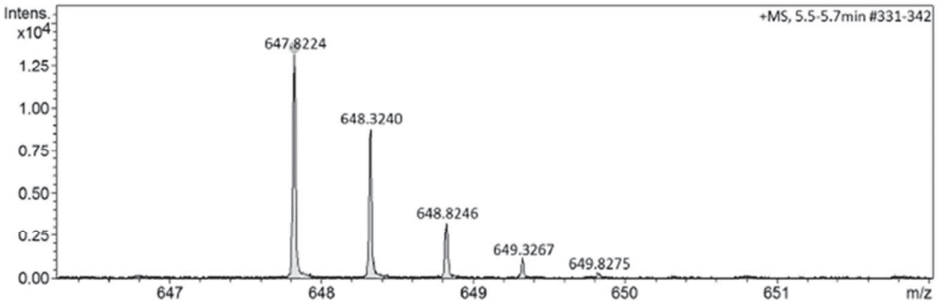

Figure S63: HR-ESI MS spectrum of Man(1)-Gal(3)-3 MET **23** (m/z for $[M+2H]^{2+}$).

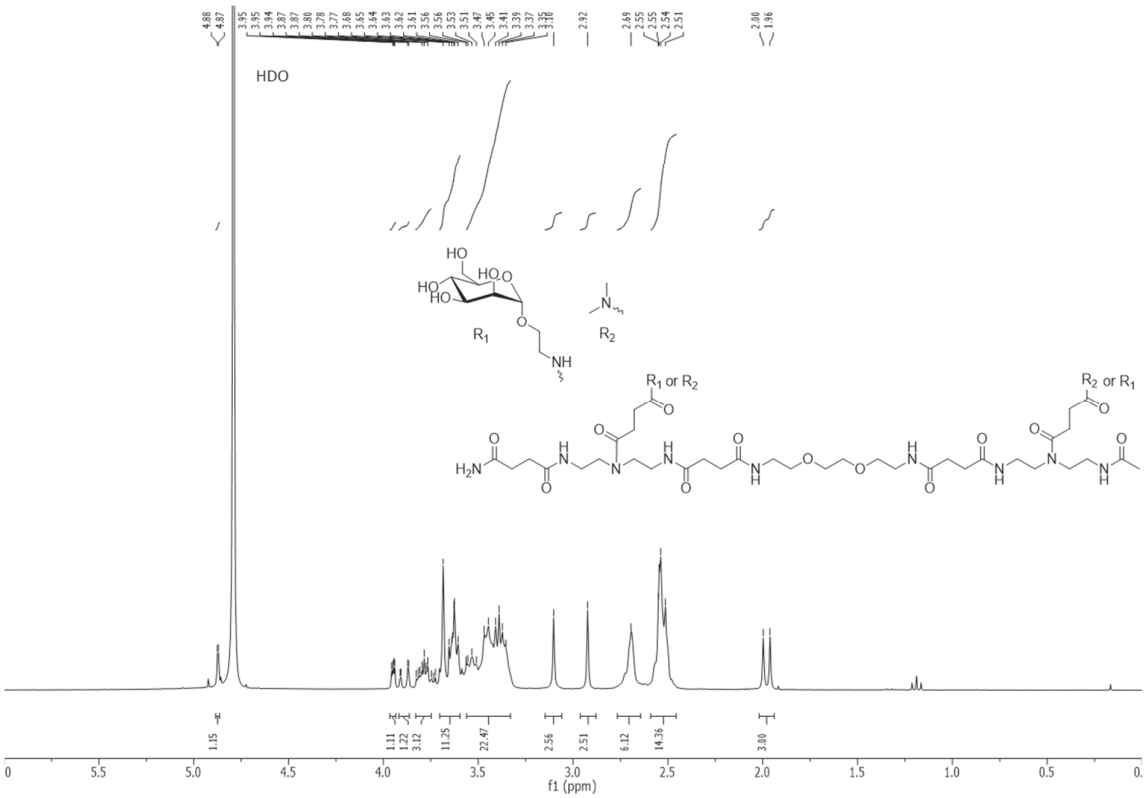

Figure S64: ^{1}H-NMR spectrum of proposed side product **26** (D_2O, 300 MHz).

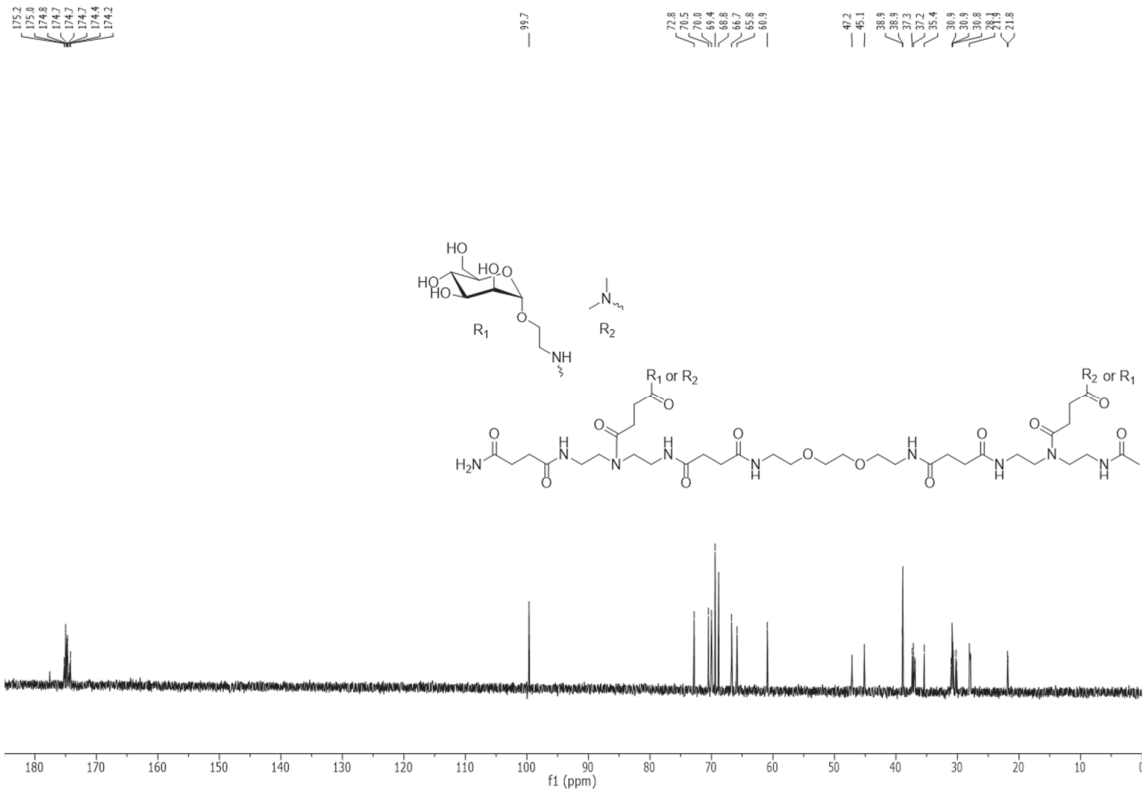

Figure S65: ^{13}C-NMR spectrum of proposed side product **26** (D_2O, 75 MHz).

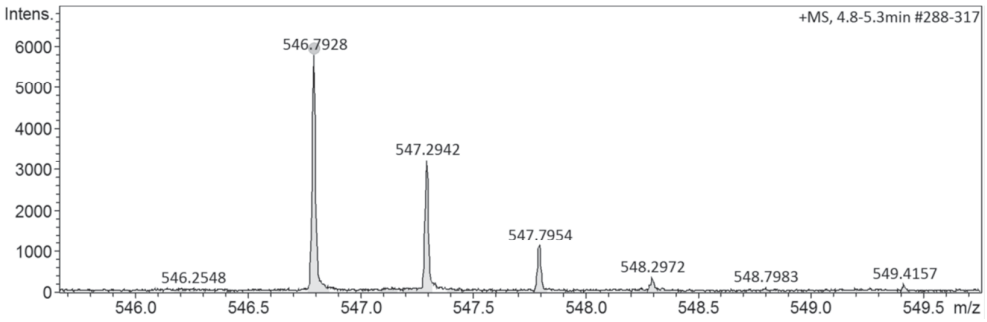

Figure S66: HR-ESI MS spectrum of proposed side product **26** (m/z for $[M+2H]^{2+}$).

2. Effects of Linker and Liposome Anchoring on Lactose-functionalized Glycomacromolecules as Multivalent Ligands for Binding Galectin-3

Authors:	**T. Freichel**, D. Laaf, M. Hoffmann, P. B. Konietzny, V. Heine, R. Wawrzinek, C. Rademacher, N. L. Snyder, L. Elling and L. Hartmann
Journal:	RSC Advances
Issue:	Accepted, 2019, DOI:10.1039/c9ra05497a
Type of paper:	Full Paper
Impact Factor:	3.049 (2017/2018)

1st author contribution:

Collaborative design of structures and binding assays. Synthesis of the building blocks and joined synthesis of carbohydrate derivatives. Synthesis, isolation and analysis of all linear acetylated glucose, galactose and lactose structures except the propyl-linker derivatives of the lactose structures and their shorter counterparts. Synthesis, isolation and analysis of the amine derivatives used for the immobilization on the SPR-senor chip surface. Introduction, development and optimization of the galectin-3 inhibition assay using surface plasmon resonance. Performance and evaluation of the SPR measurements for all glycomacromolecules as well as the liposomes. Visualization and interpretation of the SPR-data. Joined performance of the ELISA-type inhibition measurements. Collaborative visualization and interpretation of the ELISA-data. Collaborative writing of the manuscript.

RSC Advances

PAPER

View Article Online
View Journal | View Issue

Cite this: *RSC Adv.*, 2019, **9**, 23484

Effects of linker and liposome anchoring on lactose-functionalized glycomacromolecules as multivalent ligands for binding galectin-3†

Tanja Freichel,[a] Dominic Laaf,[b] Miriam Hoffmann,[a] Patrick B. Konietzny,[a] Viktoria Heine,[b] Robert Wawrzinek,[c] Christoph Rademacher,[c] Nicole L. Snyder,[d] Lothar Elling[b] and Laura Hartmann*[a]

In this work, we present a bottom-up approach for the synthesis of lactose-functionalized glycomacromolecules and glycofunctionalized liposomes and apply these compounds to investigate their effects of multivalent presentation on binding to galectin-3. Step-wise assembly of tailor-made building blocks on solid supports was used to synthesize a series of oligo(amidoamine) scaffolds that were further conjugated to lactose *via* copper catalyzed 1,3-dipolar cycloaddition. Binding studies with galectin-3 revealed affinities in the micromolar range that increased with increasing carbohydrate valency, and decreased with increasing size and linker flexibility. To further explore their multivalency, selected glycomacromolecules were conjugated to lipids and used in liposomal formulations. Binding studies show a further increase in binding in nanomolar ranges in dependence of both ligand structure and liposomal presentation, demonstrating the power of combining the two approaches.

Received 17th July 2019
Accepted 18th July 2019

DOI: 10.1039/c9ra05497a

rsc.li/rsc-advances

Introduction

Carbohydrate–protein interactions play crucial roles in various biological binding processes such as cell–cell communication and tumor biology.[1] An important family of carbohydrate-recognizing proteins are the galectins (Gal).[2,3] Galectins have been shown to be involved in apoptosis, angiogenesis, cell–cell communication, immune maintenance and cell proliferation.[4–7] There are currently fifteen members of the galectin family, which are further subclassified into three groups: prototype (*e.g.* Gal-1), tandem-repeat (*e.g.* Gal-9) and chimeric (Gal-3).[8] Galectins bind to β-galactoside terminating saccharides, most notably LacNAc (Galβ1-4GlcNAc), through their conserved carbohydrate recognition domain (CRD).[8] The galectin CRD is composed of five binding sites A–E, where C binds the galactose moiety and D the carbohydrate attached at the reducing end of the galactose residue.[2,9] Gal-3, the only chimeric type galectin, is one of the best studied members[4,5,10,11] and is an important target to develop synthetic ligands to better understand the role of Gal-3 in normal and diseased process as well as for the development of new diagnostics and therapeutics.[5]

The natural multivalent ligands for Gal-3 are mostly glycans and glycoproteins such as laminin or fibronectin with *O*- and *N*-linked glycans that often terminate in repeating LacNAc units.[12–15] Given the challenging synthesis of such polysaccharides or glycoproteins, the synthesis of more simplified multivalent glycomimetics as ligands of galectins is gaining attention.[16–18] Multivalent glycomimetics often consist of a synthetic scaffold such as a peptide or polymer presenting multiple copies of a polysaccharide fragment.[18–20] For example, successful implementation of glycomimetics targeting Gal-3 was shown by Becer and co-workers who synthesized a series of glycopolypeptides varying in the spacing and density of carbohydrate ligands.[21] In another example, Kamerling and co-workers used solid phase synthesis to generate glycopeptide libraries to study Gal-3.[22,23] Cloninger and co-workers[18,24] used dendritic scaffolds for the multivalent presentation of carbohydrates and demonstrated their ability to induce Gal-3 aggregation and inhibit cancer cellular aggregation, while Percec and co-workers used glycodendrimers and dendrimersomes to present lactose to different galectins including Gal-1,[25,26] Gal-3 and -4,[27,28] and Gal-8 [26,28,29] to explore their properties. Gabius and Roy evaluated different kinds of glycomimetics from di- to tetra-conjugated lactose-functionalized glycoclusters to non-acontavalent lactoside glycodendrimers and demonstrated their potential in solid phase as well as in cell assays.[30–33] Bonduelle and co-workers used nanoparticles as a platform for the

[a]*Department of Organic and Macromolecular Chemistry, Heinrich-Heine-University Düsseldorf, Universitätsstraße 1, 40225 Düsseldorf, Germany. E-mail: laura.hartmann@hhu.de; Fax: +49-211-81-15840; Tel: +49-211-81-10360*

[b]*Laboratory for Biomaterials, Institute for Biotechnology, Helmholtz-Institute for Biomedical Engineering, RWTH Aachen University, Pauwelsstraße 20, 52074 Aachen, Germany*

[c]*Max Planck Institute of Colloids and Interfaces, Mühlenberg 1, 14424 Potsdam, Germany*

[d]*Department of Chemistry, Davidson College, North Carolina 28035, USA*

† Electronic supplementary information (ESI) available: ^{1}H-NMR, HR-ESI, LCMS, MALDI-TOF. See DOI: 10.1039/c9ra05497a

multivalent presentation of carbohydrates for galectin binding.[34] Additionally, in the group of Elling, the enzymatic build-up of glycans and their subsequent conjugation to bovine serum albumin (BSA) to form so-called neo-glycoproteins was used to demonstrate the effect of multivalency in Gal-3 recognition.[35,36]

Another strategy for a multivalent presentation, which is, to the best of our knowledge unexplored for Gal-3, is the use of surface functionalized liposomes.[37–42] The synthesis of carbohydrate–lipid conjugates and their incorporation into liposomes *via* self-assembly allows for the build-up of multivalent, supramolecular structures, which can be used as ligands, drug- or antigen-delivery systems.[43–47] The use of natural membrane compounds like cholesterol and phosphatidylcholines (*e.g.* DSPC) for the formulation of liposomes can furthermore ensure a higher biocompatibility for biological applications. Thus, the presentation of glycomimetics on the surface of such supramolecular systems can be used for the targeting of proteins or cells for various fundamental and applied applications.[37,48–51]

In this work, we aimed to combine both approaches and show the impact on the binding of multivalent glycomimetics to Gal-3 (Fig. 1). First, we applied our previously introduced solid phase assembly of tailor-made building blocks to obtain monodisperse, sequence-controlled glycooligoamides, so-called precision glycomacromolecules, presenting carbohydrate fragments identified as ligands of Gal-3.[52–56] To test for the influence of the scaffold structure on the lectin binding, glycomacromolecules were synthesized varying the overall valency and distance between individual carbohydrate ligands and in the length of the linker attaching ligands onto the scaffold (Fig. 2). Selected glycomacromolecules were then conjugated to lipids and the resulting ligand–lipid conjugates were used in liposome formulations. With this approach, we incorporate multivalency on two levels: the presentation of multiple lactose ligands along the macromolecular scaffold followed by the multiple presentation of the glycomacromolecules on the liposome (Fig. 1).

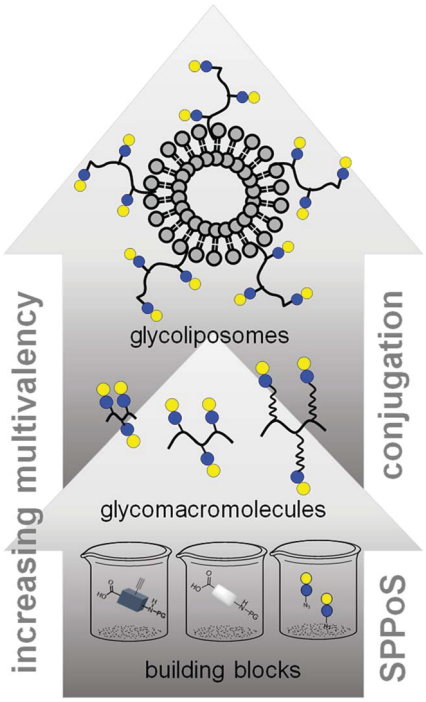

Fig. 1 Schematic representation of assembling glycofunctionalized liposomes using solid phase synthesis of precision glycomacromolecules.

Percec and co-workers used carbohydrate-functionalized dendrimers to incorporate multiple mono- or divalent constructs into liposomes and study the effects on clustered ligand presentation.[25] Ratner and co-workers showed the incorporation of multivalent mannose- and galactose-functionalized polymers into liposomal formulations and the use of such glycopolymer-augmented liposomes to elucidate receptor-mediated uptake in macrophages.[57] While they showed that the use of glycopolymers allowed for higher selectivity and specificity of cellular uptake of the glycoliposomes, they did not compare the effects of multivalent presentation of single ligands *vs.* multivalent glycopolymers on the liposomes. Such 'multivalency of multivalency' glycostructures are well-known in nature, *e.g.* the glycolipids or glycoproteins. Our synthetic platform allows for the systematic build-up of such structures starting from individual building blocks and building to multiple levels of multivalency (Fig. 1). This provides us with model compounds to study whether these two kinds of presentation in the glycomacromolecule–lipid conjugates are simply additive or benefit from additional factors. In this study, the binding to Gal-3 of both glycomacromolecules and glycomacromolecule-functionalized liposomes with variations in the number and spacing of carbohydrate ligands along the scaffold is investigated in inhibition-competition studies using an enzyme-linked immunosorbent inspired-assay (ELISA) and surface plasmon resonance (SPR).

Results and discussion

Synthesis of glycomacromolecules and glycomacromolecule–lipid conjugates

Synthesis of glycomacromolecules **1–10** and **12–16** was accomplished by applying a previously established solid phase polymer strategy (Fig. 2).[52,56,58] In short, building blocks bearing a carboxylic acid and an Fmoc-protected amine group were coupled to an amine functionalized resin using PyBOP and DIPEA for activation. After successful coupling, Fmoc-deprotection with piperidine released the N-terminus of the first building block which could then be used for coupling of the next building block. This stepwise assembly allows for the synthesis of monodisperse, sequence-controlled oligomers. For the synthesis of glycomacromolecules in this study, TDS (triple bond diethylenetriamine succinyl, 1-(fluorenyl)-3,11-dioxo-7-(pent-4-ynoyl)-2-oxa-4,7,10-triazatetra-decan-14-oic acid)[52] was used as an alkyne-functionalized building block for later conjugation with azide-derivatives of different carbohydrate ligands *via* copper(I)-catalyzed alkyne–azide cycloaddition (CuAAC). EDS (ethylene glycol diamine succinyl, 1-(9*H*-fluoren-9-yl)-3,14-dioxo-2,7,10-trioxa-4,13-diazaheptadecan-17-oic acid)[59] was chosen as a spacer

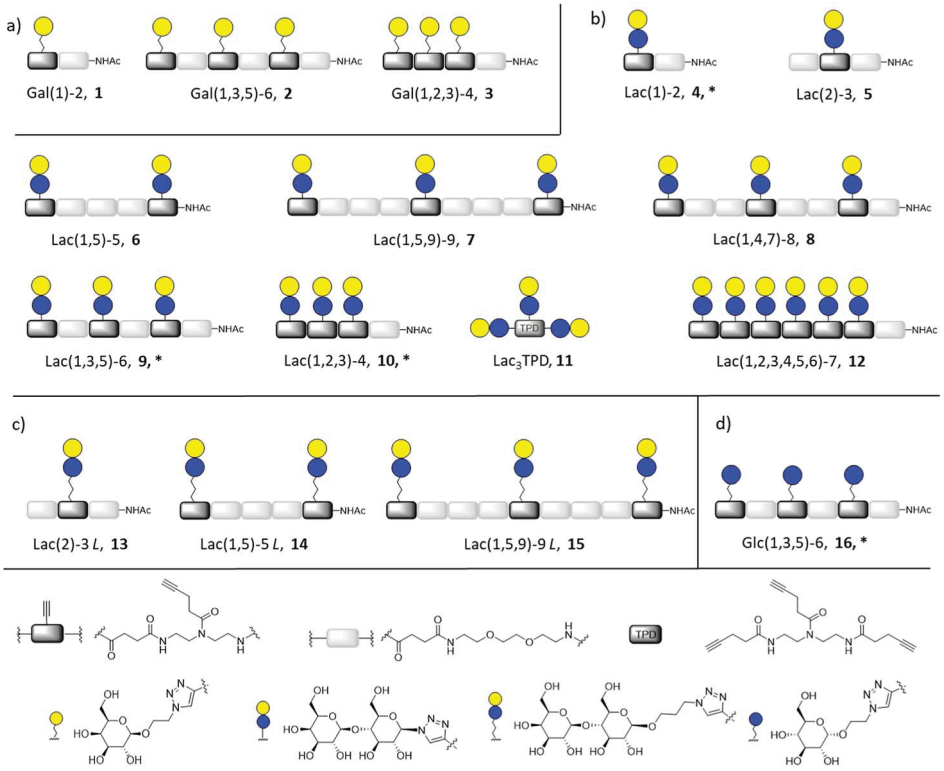

Fig. 2 Overview of synthesized glycomacromolecules: (a) galactose-functionalized structures **1–3**, (b) lactose-functionalized structures **4–12**, (c) propyl lactose-functionalized structures **13–15**, (d) glucose-functionalized structure **16**. Structures denoted with * were synthesized as amine derivatives in addition to the acetyl-capped derivatives.

building block introducing an ethylene glycol motif in the main chain of the glycomacromolecules. Through different combinations of these building blocks, glycomacromolecules with varying numbers of carbohydrate ligands and different spacing between ligands along the oligomeric scaffold were obtained (Fig. 2). β-Galactose (Gal) and β-lactose (Lac) were applied as known binding ligands of Gal-3. To investigate the effect of the linker between the carbohydrate ligand and the oligomeric scaffold, two different lactose-derivatives were conjugated, one with an anomeric azide, and one with a propyl linker terminating in an azide (Fig. 2). Finally, a non-binding α-glucose (Glc) residue was used to prepare glucose-functionalized glycomacromolecules as negative controls. All carbohydrate ligands were conjugated on solid support using previously reported conditions for CuAAC.[60] De-*O*-acetylation of the carbohydrate residues under Zemplén conditions and cleavage from solid support gave the final glycomacromolecules.[61] All structures were then purified by ion exchange and preparative HPLC to obtain final structures with high purities ≥ 95% (determined by UV 214 nm signal of RP-HPLC) (see ESI†).

In contrast to glycomacromolecules **1–10** and **12–16**, compound **11** was prepared in solution. Diethylenetriamine was treated with 4-pentynoyl chloride resulting in the precursor TPD **18** (tripentynoic acid diethylene triamine, *N*,*N*-bis(2-(pent-4-ynamido)ethyl)pent-4-ynamide) (Fig. 2). This was followed by conjugation of an azido-lactose analog *via* CuAAC (Scheme S1†). Global deprotection using Zemplén transesterification, followed by neutralization with Amberlite IR120 resin and

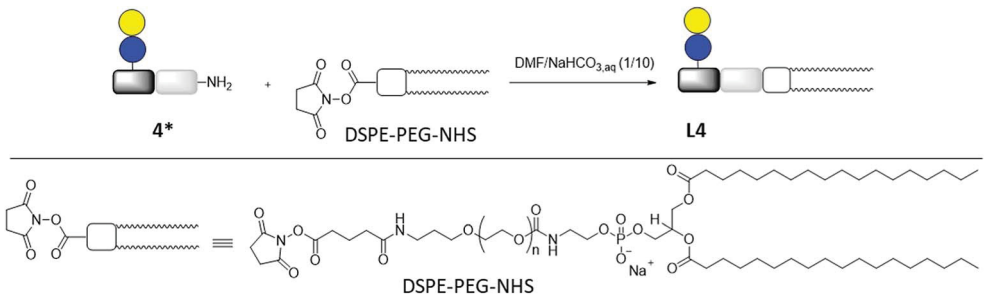

Fig. 3 Synthesis of lipid-conjugate **L4** through the reaction of DSPE-PEG-NHS and glycomacromolecule Lac(1)-2 (**4***).

Table 1 MALDI-TOF-MS and ^{1}H-NMR analytical data for the glycomacromolecule–lipid-conjugates **L4**, **L9**, **L10** and **L16**

	MALDI-TOF-MS[a]		
Glycomacromolecule–lipid-conjugate	MW cal. for $[M + Na]^+$	m/z found	Conversion[b] [%]/yield[c] [%]
L4	$C_{173}H_{330}N_{11}O_{73}PNa$ 3786.5	3787.8	66/58
L9	$C_{243}H_{446}N_{27}O_{107}PNa$ 5511.3	5511.6	56/44
L10	$C_{223}H_{410}N_{23}O_{99}PNa$ 5051.8	5052.4	66/69
L16	$C_{231}H_{428}N_{27}O_{95}PNa$ 5158.0	5158.7	62/35

[a] MALDI-TOF-MS measurements were performed using positive ion mode. Molecular weights were calculated for the monitored maximum peak with a PEG repetition unit of 44. [b] Conversion ratio of conjugated lipid was determined by ^{1}H-NMR *via* integration of the terminal methyl groups of the lipid chains signal normalized to the anomeric proton of the carbohydrate. [c] Determined by balance weight considering the conversion.

preparative HPLC yielded Lac_3TPD **11** with a purity ≥ 95%, determined by RP-HPLC. All final products were analyzed using ^{1}H-NMR spectroscopy, analytical HPLC coupled with ESI-MS and HR-MS analysis (for more information see ESI†). Nomenclature of the final glycomacromolecules includes information on the type and position of the carbohydrate residue, as well as the overall valency of the oligomer. For example, Lac(1)-2, **4**, represents a monovalent structure bearing a Lac ligand on the first position of a dimeric structure and Lac(1,5)-5 L, **14**, is a divalent structure containing propyl linked (L) Lac in position 1 and 5 of a pentameric scaffold.

For the glycomacromolecule–lipid conjugation and later functionalization of the sensor surface for SPR measurements, amine functionalized glycoconjugates **4***, **9***, **10*** and **16*** were synthesized. For these derivatives, CuAAC was performed on scaffolds containing a terminal Fmoc group instead of the usual acetyl group. This was, followed by Fmoc-cleavage with piperidine and deprotection of the carbohydrates. After cleavage, the amine functionalized glycomacromolecules were purified *via* preparative chromatography resulting in purities ≥ 95%, as determined by RP-HPLC (see ESI†).

Lipid conjugation was conducted according to a previously published protocol.[62] Commercially available DSPE-PEG-NHS ester was used as lipid (Fig. 3). The conjugation reaction was performed in a mixture of DMF and $NaHCO_{3\ aq}$ (1/10) overnight. After removal of the solvents, the lipid-conjugates were purified by dialysis against buffer and water. After lyophilization, the products were analyzed by ^{1}H-NMR spectroscopy and MALDI-TOF-MS. The results are summarized in Table 1.

Reaction conversions, equivalent to the ratio of conjugated lipid, were determined by ^{1}H-NMR *via* integration of the terminal methyl groups of the lipid chains normalized to the anomeric proton of the carbohydrate moieties. They were found to be between 56–66%, which could be due to hydrolysis of the NHS-ester group of DSPE-PEG-NHS in aqueous solution. This hypothesis is strengthened by the MALDI-TOF-MS analysis, showing a corresponding MS-signal (see *e.g.* Fig. S69†) of the hydrolysis product of DSPE-PEG-NHS. For liposome formulation, the ratio of conjugated to unconjugated lipids was taken into account in order to obtain similar numbers of carbohydrate ligands per liposome.

Liposome preparation

For the liposome formulation, DSPC was used as the main lipid component with cholesterol as an additive for membrane stabilization through reduction of lipid ordering and increased melting temperatures (Fig. S1†).[63–65] This liposomal formulation is approved by the FDA and therefore regularly used as standard in pharmaceutical research.[66] The glycomacromolecule–lipid conjugates were used in a total quantity of 4.75 mol% in the whole formulation.

Lipid film hydration and extrusion were used for the preparation of the liposomes. Extrusion allowed for size adjustment and homogenization. The liposomes were analyzed with DLS showing diameters (d) of approximately 150 nm and polydispersity indices (PDI) between 0.010–0.039. Vesicles in this PDI-range are termed monodisperse.[67,68] Zeta potentials were measured to verify the negative charge of the surface, which correlates with the successful incorporation of the glycomacromolecule–lipids, and the overall stability of the liposomes. The results of the DLS and zeta potential measurements are summarized in Table 2 and correspond well to comparable systems in literature.[50,62] Measurements were repeated after three months and showed comparable results indicating the stability of the liposomes over time (data not shown).

Considering the incorporated glycomacromolecules could theoretically be presented on the inner or outer surface of the liposomes, the concentration of lactose, which can interact with

Table 2 Dynamic light scattering and zeta potential analysis of the liposomes **L4**, **L9**, **L10** and **L16**

Glycomacromolecule–lipid-conjugate used	Diameter (d)[a] [nm]	PDI[b]	Zeta potential[c] [mV]
L4	156 ± 15	0.010	−23.1 ± 7.6
L9	150 ± 16	0.011	−16.9 ± 8.5
L10	154 ± 29	0.035	−19.6 ± 8.2
L11	146 ± 29	0.039	−16.9 ± 8.5

[a] Diameters (d) were determined by DLS analysis of the liposome solution. [b] PDI were determined *via* Gaussian fit of the DLS curve giving the standard deviation σ and applying PDI = $(\sigma/d)^2$. [c] Zeta potentials were measured with a Zetasizer Nano-Z.

Table 3 Inhibition constants (IC_{50} values), relative inhibitory potencies (RIP), RIP per glycan and inhibitory potencies (IP) for Lac and glycomacromolecules 4–15

Glyco-conjugate	No. of carbohydrate	$IC_{50} \pm SD^a$ [μM]	RIP[b]	RIP/Lac	IP[c] [%]
Lactose	1	159 ± 13	1.0	1.0	—
Lac(1)-2, **4**	1	123 ± 3	1.3	1.3	31
Lac(2)-3, **5**	1	111 ± 4	1.4	1.4	46
Lac(1,5)-5, **6**	2	55 ± 5	2.9	1.5	61
Lac(1,5,9)-9, **7**	3	36 ± 3	4.4	1.5	66
Lac(1,4,7)-8, **8**	3	42 ± 3	3.8	1.3	65
Lac(1,3,5)-6, **9**	3	38 ± 2	4.2	1.4	68
Lac(1,2,3)-4, **10**	3	37 ± 1	4.3	1.4	72
Lac_3-TPD, **11**	3	29 ± 1	5.5	1.8	77
Lac(1,2,3,4,5,6)-7, **12**	6	16 ± 4	9.8	1.6	78
Lac(2)-3 L, **13**	1	133 ± 8	1.2 (0.8*)	1.2	36
Lac(1,5)-5 L, **14**	2	87 ± 3	1.8 (0.6*)	0.9	50
Lac(1,5,9)-9 L, **15**	3	50 ± 2	3.2 (0.7*)	1.1	55

[a] Determined by ELISA-inspired inhibition studies on ASF coated plates. Measurements were performed two times in triplicates. [b] Relative inhibitory potency normalized to IC_{50} value of Lac (159 μM). [c] Reduced IC_{50} experiment determined by SPR inhibition studies with 100 μg mL^{-1} Gal-3 in PBS and 50 μM ligand. Binding signal of blank Gal-3 was set to 100% binding and 0% inhibition, inhibition values reported are referred to Gal-3. *RIP in brackets are the result of a direct comparison of the IC_{50} value of compound **5** to **13**, **6** to **14** and **7** to **15**.

Gal-3 in binding studies, was determined with a lactose-assay kit from BioAssay Systems.[69,70] Here, the use of sterically demanding enzymes allows for the discrimination of the carbohydrates presented on the outer *vs.* the inner surface of the liposomes. Lactase is used to degrade Lac into Glc and Gal and the Gal concentration is determined indicating the concentration of accessible Lac. In contrast to the standard protocol, Lac was not a suitable standard because of the time-dependent behavior of free Lac hydrolysis compared to the conjugated Lac on the liposomes (see Fig. S2†). One reason for the observed discrepancy could be that the lactase converts the free Lac in solution more slowly than the Lac on the liposome surface, which also has been observed for other enzyme–substrate systems.[71] Therefore, Gal was used instead of Lac as an alternative standard. An additional deviation from the protocol involved incubation of the samples with lactase only in assay buffer for 24 hours at 37 °C prior to dye-incubation instead of mixing the sample directly with lactase and dye-reagent simultaneously to achieve full degradation of lactose to its monosaccharides galactose and glucose. To verify the stability of liposomes during the measurements, 20 μL of the liposome–enzyme mixtures were diluted after the assay to a total volume of 1 mL with ultrapure water and measured with DLS. PDI and liposome diameter were in the pre-assay range indicating that the liposomes were stable during the assay (data not shown). Results from this protocol gave the surface concentration of Lac as shown in Table 4. Considering the amount of glycoligand–lipid-conjugate, which was used for the liposome formulation, the percentage of ligand on the liposome surface was calculated to be 94% for both **L4** and **L9** and 66% for **L10**.

Galectin-3 binding studies

Binding of glycomacromolecules and liposomes to Gal-3 was evaluated by an inhibition competition study using an ELISA-inspired assay as previously introduced by Elling and co-workers[72] and commonly used when evaluating the binding of glycomimetic structures to galectins.[73–75] Asialofetuin, a natural multiantennary glycoprotein presenting nine terminal LacNAc residues, was coated onto microplates to enable the binding of Gal-3.[76] Different concentrations of glycomacromolecules were

Table 4 Inhibition constants (IC_{50}-values), relative inhibitory potency (RIP) of the glycomacromolecules 4, 9, 10 and glycomacromolecules functionalized liposomes L4, L9, L10

Glycoconjugate	No. of carbohydrate	$C_{meas.} \pm SD^a$ [μM] ($C_{meas.}/C_{100\%}$ [%])	$IC_{50} \pm SD^b$ [μM]	RIP[c]	$RIP_{ligand/liposome}$[d]
Lac(1)-2, **4**	1	—	123 ± 3	1.3	—
Lac(1,3,5)-6, **9**	3	—	38 ± 2	4.2	—
Lac(1,2,3)-4, **10**	3	—	37 ± 1	4.3	—
Lac(1)-2, **L4**	1	143 ± 19 (94)	12 ± 2	13	10
Lac(1,3,5)-6, **L9**	3	127 ± 18 (94)	1.0 ± 0.1	161	38
Lac(1,2,3)-4, **L10**	3	107 ± 18 (66)	0.3 ± 0.03	482	112

[a] $C_{meas.}$ [μM]: concentration of the glycomacromolecules on the liposome surface determined with the lactose assay (percentage of glycooligomer relative to the theoretical concentration ($C_{oligo}/C_{100\%}$ [%])). [b] Determined by ELISA-inspired inhibition studies on ASF coated plates. Measurements were performed two times in triplicates. [c] Relative inhibitory potency (RIP) normalized to IC_{50} value of lactose (159 μM). [d] RIP of the liposomes compared to the corresponding single ligand in solution.

added to the plates followed by Gal-3 carrying a His (histidine)-tag to achieve a competition event. Residual Gal-3/asialofetuin binding was then determined using a His-tag antibody carrying horseradish peroxidase (HRP) for the conversion of tetramethylbenzidine (TMB). After stopping the reaction by addition of HCl, absorbance was quantified at 640 nm. Inhibition of Gal-3 was determined by observing a decreasing signal in dependence of the ligand concentration.

Plotting of the binding signal of Gal-3 against the ligand concentration gives inhibition curves as shown in Fig. 4a (for more information see ESI†). From these curves, the half maximal inhibition concentrations (IC_{50} values) could be determined. For the relative inhibitory potency (RIP), the obtained IC_{50} values were normalized to the IC_{50} value of non-conjugated Lac. Thus, stronger binding to Gal-3 results in a lower IC_{50} value and a higher RIP. To evaluate effects of valency further, the RIP was normalized to the number of carbohydrates per glycomacromolecule giving the RIP/Lac.

The IC_{50} values and relative inhibitory potencies (RIP) as well as the RIP normalized to carbohydrate moieties for ligands **4–15** are listed in Table 3. Binding studies with galactose structures **1–3** (Fig. S4†) and the negative control **16** (Fig. 3) did not show any significant inhibition. Gal is known to be a poor binder for Gal-3 with K_d values around 10 mM,[77] 50-fold lower compared to the disaccharide Lac with a K_d value of 0.2 mM.[78] Thus, the multivalent presentation of Gal on the macromolecular scaffold did not lead to a sufficient increase in binding to efficiently inhibit Gal-3 in this assay.

In general, a decrease in IC_{50} values and a corresponding increase in RIP values indicates an increase in inhibitory potency and thereby presumably binding affinity. For Lac structures **4–15**, slightly increased inhibitory potencies are observed for glycomacromolecules with increasing valency (number of Lac residues) and decreasing spacing (number of EDS building blocks in between Lac-functionalized building blocks) (Fig. 4b and c). For the trivalent ligands showing the same valency and linker length, the lowest IC_{50} value was observed for the smallest ligand of this series, glycomacromolecule **11**, with 29 ± 1 μM, and the highest IC_{50} value was observed for one of the largest structures, glycomacromolecule **8**, with 42 ± 3 μM. An explanation could be in the sterical and geometrical effects related to the distances between the carbohydrate-epitopes which can have an impact on protein-clustering. Considering the distances of the N-atoms of the three triazoles in the stretched trivalent structures, the smallest structure Lac_3TPD **11** was found to have theoretical

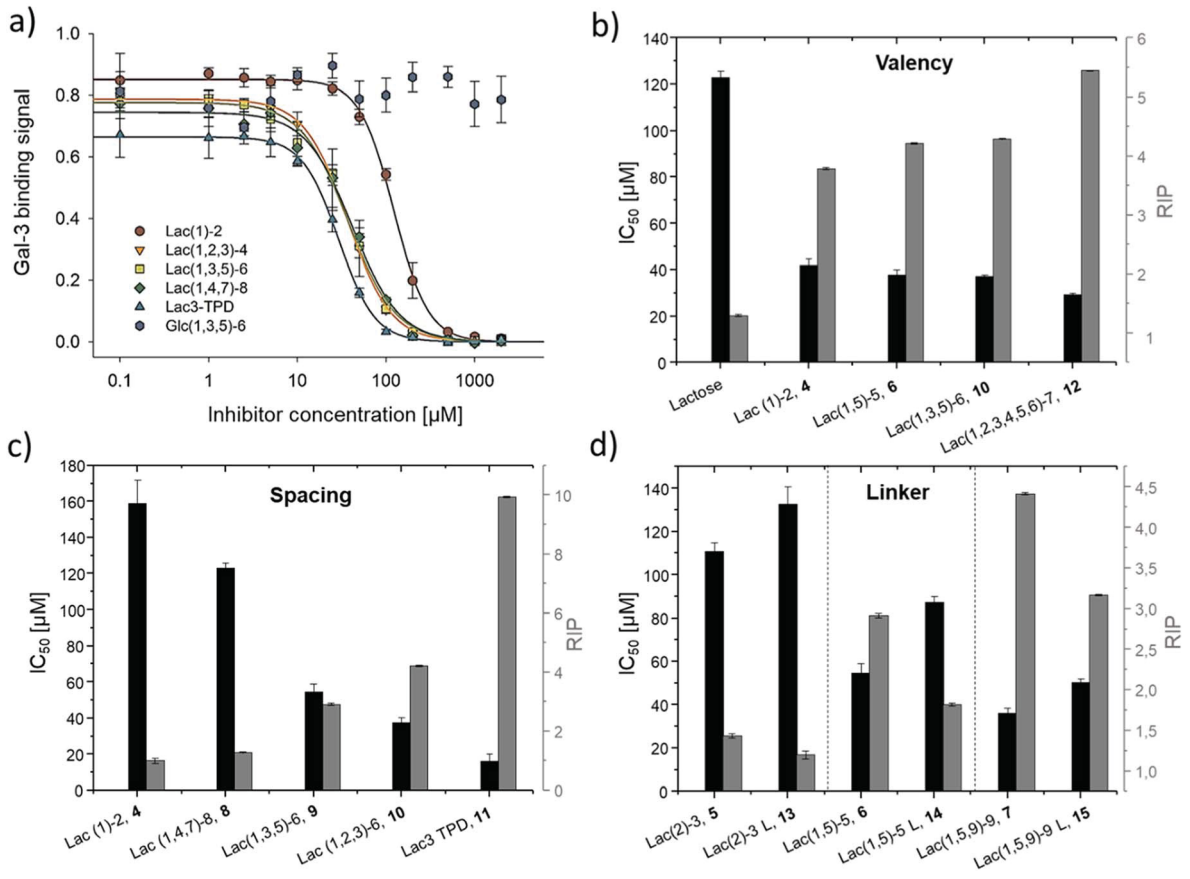

Fig. 4 Results from the inhibition of Gal-3 in an ELISA-inspired assay. (a) Exemplary inhibition curves of the inhibition with structures **4**, **8**, **9**, **10**, **11** and negative control **16**. Values are normalized to the signal of pure Gal-3. (b–d) IC_{50} values [μM] (black) and RIP (grey) for: (b) Lac and glycomacromolecules **4**, **6**, **10** and **12** with increasing valency; (c) glycomacromolecules **4**, **8–11** with decreasing spacing and (d) glycomacromolecules **5–7** and their propyl-Lac counterparts **13–15**. RIP are referenced to the IC_{50} value of lactose.

distances between 8–17 Å, whereas the glycomacromolecule **8** was found to be in a range of 44–87 Å (see ESI Fig. S9 and S10†).

To the best of our knowledge, the distances between the CRDs in oligomeric Gal-3 lattices have not yet been reported, and are likely to vary significantly based on their complexity and flexible geometry.[79] The results of the spacing are strengthened by studying the influence of the linker length and the distance of the triazole moiety from the carbohydrate on the inhibition of Gal-3 as shown in Fig. 4d. When comparing compounds **5–7** and **13–15**, we observe that the introduction of a longer linker between the lactose ligand and oligomer backbone leads to a decrease in binding showing just 0.6–0.8 relative potency when compared to their shorter linker counterparts (Table 3, marked with *). This effect is even more pronounced with the higher valent glycomacromolecules.

We hypothesize the differences in avidity could also be due in part to the triazole motif in the linker participating in hydrophobic interactions in the binding groove of Gal-3. Similar results were found by Nilsson and co-workers where replacing ester or amide bonds through triazoles had an impact on the affinity and specificity towards Gal-3.[80] In addition, the influence of hydrophobic, aromatic residues such as triazole, substituted phenyl and coumaryl methyl on the binding of Gal-3 is well-known from literature and might also effect binding of the glycomacromolecules.[16,33,81–83]

Besides geometrical effects and hydrophobic interactions, entropy can also play an important role where the loss of flexibility due to increased rigidity can have a positive impact on the entropy of the system.[84,85] In this study, Lac_3TPD **11** is assumed to be the most rigid structure showing the highest avidity towards Gal-3 in comparison to the other trivalent systems. Pieters and co-workers performed solid phase inhibition and fluorescence polarization studies on rigidified multivalent lactose ligands where they could see a twofold higher binding of rigidified structures compared to their more flexible counterparts.[19] Furthermore, they could observe a high multivalent effect with increasing valency showing a 300 times higher binding for a tetravalent structure with a IC_{50} value of 0.07 μM compared to the monovalent derivative with an IC_{50} value of 21 μM and free lactose with 300 μM.[19] In our case, the monovalent glycomacromolecules **4** and **5** show only slightly increased binding by a factor of 1.3–1.4 in comparison to free Lac, whereas the highest increase was observed for hexavalent ligand **12** by a factor of about 9–10. Comparing the characteristics of the herein reported glycooligo(amidoamines) and the discussed rigidified lactosidic structures, the more aromatic and thus hydrophobic nature of the structures by Pieters could be the reason for the more distinguished enhancement in binding, caused by participation of the aromatic residues on the binding event as mentioned before.

Overall, looking at all examined structures, the relative increase in inhibition for the glycomacromolecules is comparable to other multivalent constructs of similar valencies from literature, though not as potent as the previously discussed study by Pieters.[19] In another example, Cagnoni and co-workers observed relative potencies of 10 and 6 by presenting dithiogalactose as di- and tetrasaccharides in comparison to the monovalent analogues.[86] The aforementioned glycoclusters synthesized by Gabius and Roy evaluated in a solid-phase assay resulted in IC_{50} values of 165 μM for the divalent structure compared to 62–125 μM for the tetravalent structures. Compared to free lactose with 700 μM, the divalent structure showed an RIP of 4.3 and the tetravalent 5.6–11.2, which is again in the same range or even lower than those reported here from glycooligo(amido amines).[30]

In general, the obtained IC_{50} values of the glycomacromolecules are within the concentration range expected for this type of ELISA-inspired inhibition study on Gal-3. For example, Elling and co-workers reported IC_{50} values between 6 and 42 μM for LacNAc-based di- to heptasaccharides, respectively.[73] Notably, LacNAc is an even better binder for Gal-3 with a K_d of 70 μM.[72]

SPR was used to perform a reduced IC_{50} experiment as a comparable method to support the aforementioned ELISA-inspired assay. Trivalent ligand Lac(1,3,5)-6 (**9***) with a terminal amine group was used for sensor surface functionalization to provide high loading. The experimental conditions were based on the results from the ELISA study. In this case a fixed concentration of Gal-3 (100 μg mL^{-1}) and a fixed concentration of ligands (50 μmol L^{-1}) were used. Comparing Gal-3 binding in presence of the different ligands gives the inhibition potency (IP) at fixed ligand and receptor concentrations. In this context, higher affinity ligands result in a lower Gal-3 binding signal (Fig. 5 and ESI†) and higher IP values (Table 3).

SPR measurements (Fig. 5) support the results and trends observed in the ELISA-inspired assay (Fig. 4). Decreased spacing, *e.g.* going from structure **7** to **11**, led to a slight increase in inhibitory potency from 65% to 77% (Table 3). Structures with the longer propyl-based linker **13–15** again showed lower inhibitory potency compared to derivatives **5–7** with the shorter linker.

Based on these findings, lipid-conjugation was performed with two trivalent ligands with different spacing and overall size (**9*** and **10***) as well as a monovalent glycomacromolecule (**4***). As a negative control, a trivalent Glc-functionalized glycomacromolecule (**16***) of the same sequence as Lac-functionalized ligand (**9***) was included. The inhibitory potency of the liposomes (**L4**, **L9** and **L10**) were studied by the same ELISA-inspired assay previously used for the free ligands (Fig. 4).

To compare results based on the number of Lac ligands available for binding to Gal-3 on the surface of the liposomes, IC_{50} values were normalized to the concentration of Lac as determined by the lactase-assay described above. To further compare the inhibitory potency of the ligands attached to the liposomes *vs.* the free ligands in solution, IC_{50} values were normalized to the IC_{50} value of Lac giving the RIP of the liposomes (Fig. 6).

To better demonstrate and compare the avidity enhancement enabled through the presentation of the glycomacromolecules on the liposomes, the RIPs of the glycomacromolecules were divided by the RIPs of the corresponding liposomes giving the $RIP_{ligand/liposome}$ (Table 4).

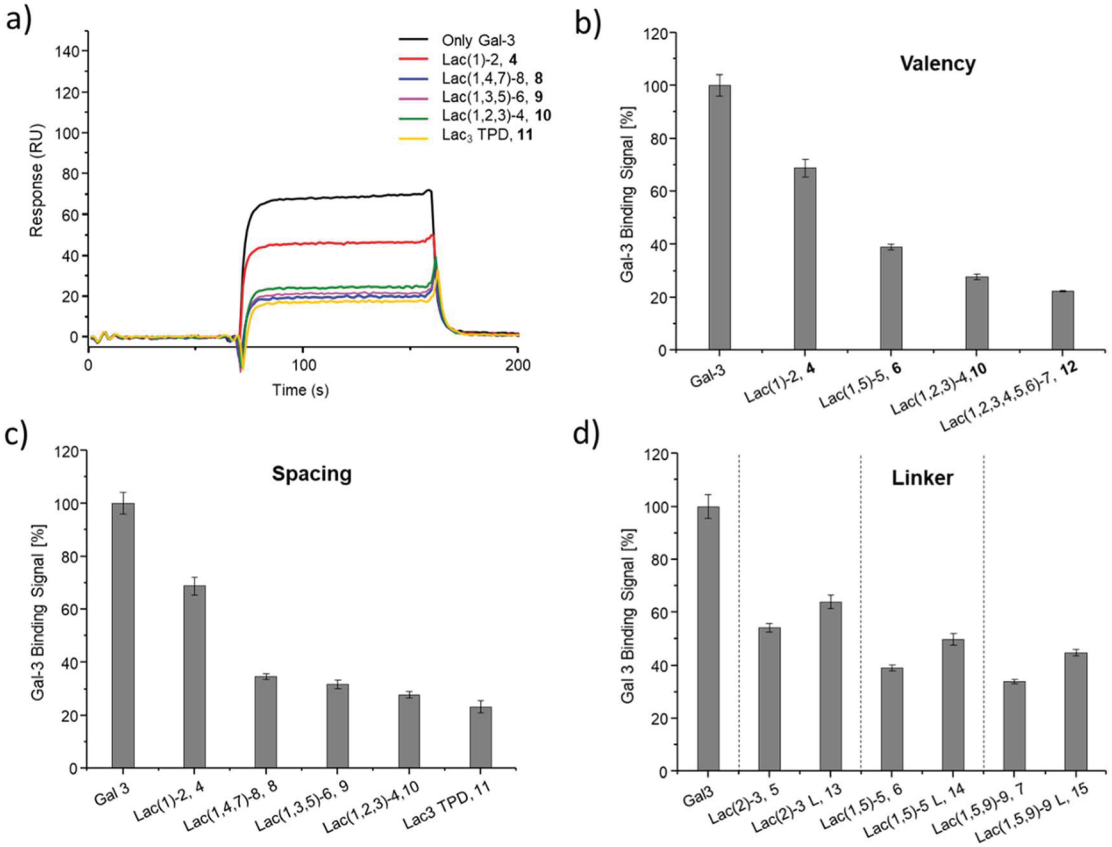

Fig. 5 Results from the reduced IC_{50} SPR inhibition experiment of Gal-3 with samples **4–15**. (a) Exemplary SPR-sensorgrams of only Gal-3 and Gal-3 incubated with macromolecule **4**, **8–11**. (b and c) Gal-3 binding signal ± SD [%] with reference of only Gal-3 signal as 100% binding for (b) glycomacromolecules **4**, **6**, **10** and F with increasing valency; (c) glycomacromolecules **4**, **8–11** with decreasing spacing and (d) glycomacromolecules **5–7** and their propyl Lac counterparts **13–15**. All measurements were performed in triplicates.

Results show the same trends for the different ligands presented on the liposomes in comparison to the free ligands, with the smaller trivalent structure (**L10**) showing a slightly higher inhibition potency than the longer trivalent ligand (**L9**), and trivalent ligands showing higher inhibition potency than the monovalent ligand (**L4**). Negative control **L16** showed no inhibitory effect on Gal-3 binding (Fig. 6).

To support the results of the ELISA, the liposomes were tested in the reduced IC_{50} assay using SPR as previously described for the glycomacromolecules. However, using the same concentration of liposomes as the free glycomacromolecules led to complete inhibition of Gal-3 (data not shown). Reducing the concentration to 10 μM yielded detectable differences in Gal-3 binding (see sensorgrams shown in Fig. 6). Results of the ELISA were again supported with smaller and higher valent structures showing higher binding.

Comparing the IC_{50} values of the liposomes with the corresponding inhibition of the glycomacromolecules revealed that presentation on the liposome surface leads to an increase in inhibitory potencies. For the best binder of the liposomal formulations (**L10**), inhibition potency increases 112-fold from 37 to 0.3 μM in comparison to the free ligand **10**. This is in the order of magnitude for a comparable 'multivalency of multivalency' system from the work of Laaf and co-workers who observed 180 to 350-fold higher inhibition for different saccharides presented in a multivalent fashion on BSA compared to the free saccharide in solution.[35,36] In addition, the glycodendrimers evaluated by Gabius and Roy presenting 90 lactose residues showed IC_{50} values of 0.16 μM compared to 164 μM for the monovalent ligand, resulting in an inhibitory potency of 1025 and 11 per carbohydrate.[31]

Several studies suggest that Gal-3 oligomerizes upon glycan binding through its N-terminal domain,[29,32,87] however, CRD mediated multimerization has also been described.[88–90] With multivalent glycans on cell surfaces, Gal-3 can induce cell–cell interactions, crosslink receptors and even form lattice on cell surfaces.[29,79] Due to the complexity and flexibility of galectin oligomers an increase in inhibitory potential can also point towards the formation of larger aggregates with Gal-3 based on the crosslinking property of galectin oligomers. This has been demonstrated for Gal-3 induced glycodendrimers[24] and glycodendrisomes.[25–29] Lactose was used as relative low affinity glycan and induced aggregation as multivalent ligand through Gal-3 binding. Interesting in our study is that the presentation of lower affinity monovalent ligand **4** and the trivalent ligand **9** on the liposomes (**L4**, **L9**), led to an increase of 10-fold or 38-fold, respectively. This shows that both the multivalency of the glycomacromolecules as, well as the multivalency of the

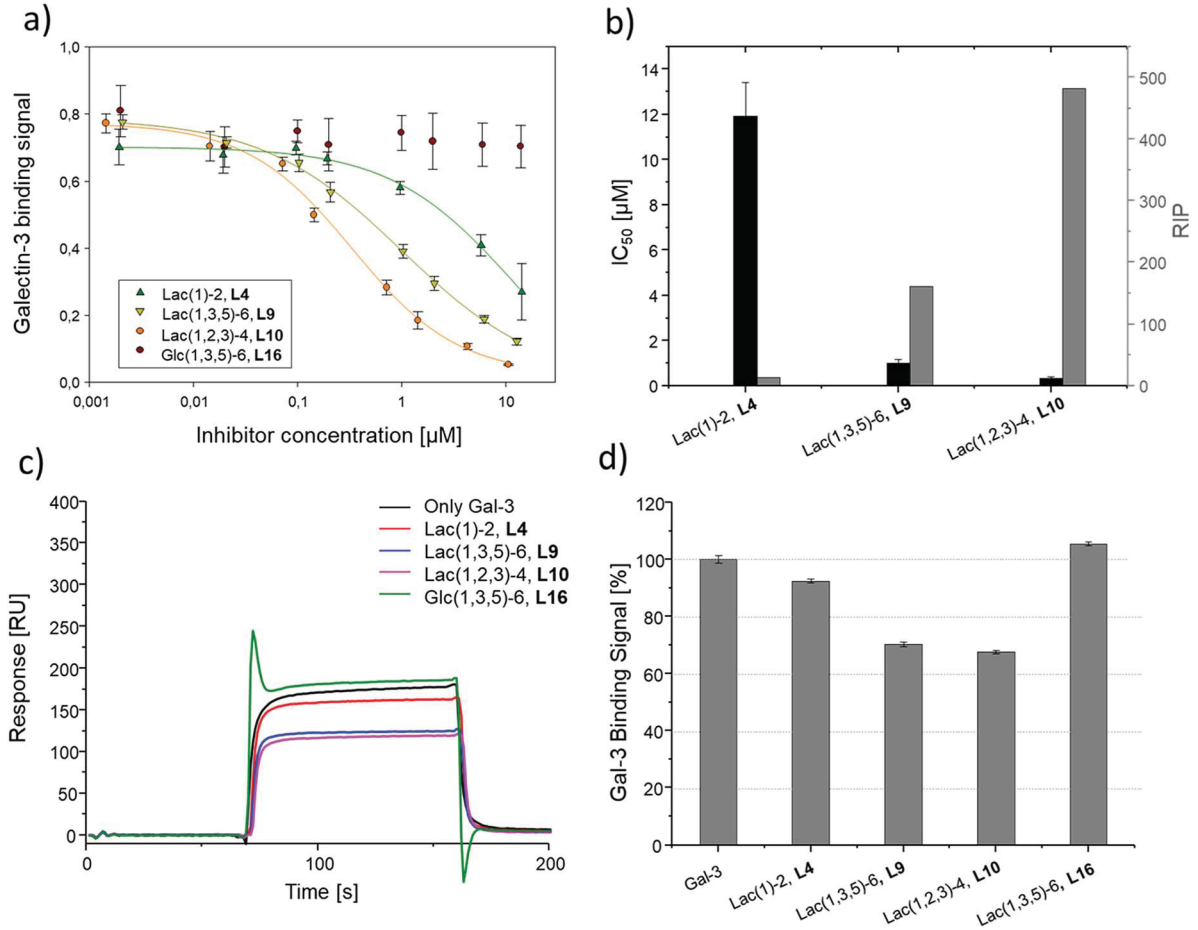

Fig. 6 Results of the inhibition studies of the liposomes **L4**, **L9**, **L10** and **L16**. (a) Inhibition curves of the inhibition of Gal-3 in ELISA-inspired assay. (b) Resulting IC_{50} values and RIP. Results from the reduced IC_{50} SPR inhibition experiment of Gal-3 (100 μg mL^{-1}) and 10 μM of **L4**, **L9**, **L10** and **L16**. (c) Exemplary SPR sensorgrams of only Gal-3 and incubated with **L4**, **L9**, **L10** and **L16**. (d) Gal-3 binding signal ± SD [%] with reference of only Gal-3 signal as 100% binding. All measurements were performed in triplicates.

presentation on the liposomes, contribute to the increased binding of Gal-3. Whether Gal-3 oligomerizes and forms aggregates with multivalent liposomes remains to be studied in future work.

Conclusions

Within this work, we investigated effects of the multivalent presentation of Lac using precision glycomacromolecules in binding to Gal-3. The use of solid phase synthesis allowed for the controlled variation of carbohydrate valency, spacing and linkage on an oligo(amidoamine) scaffold. ELISA-inspired and SPR assays revealed an influence of all three parameters on Gal-3 inhibition giving inhibition constants in the lower μM range. As expected, higher valency leads to higher binding. Surprisingly, decreasing the linker length and overall size of the scaffold also leads to an increase in binding. We partially attribute this to secondary binding interactions of the hydrophobic triazole linkages which are in closer proximity to the lectin for glycomacromolecules with shorter linkers. Further conjugation of selected glycomacromolecules to lipids allowed for additional multivalent presentation on the surface of liposomes, which increased binding and resulted in nM inhibition. However, the presentation of monovalent ligands in the liposomal formulations resulted in a much less pronounced increase in inhibitory potency, showing the importance of multivalency on both length scale, the macromolecular scaffold and liposome decoration, to effectively yield high avidity ligands. Indeed, this is a key feature of many glycoconjugates in nature such as glycolipids or glycoproteins. Our synthetic platform and the approach presented here give straightforward access to the design and synthesis of ligands using 'multivalency of multivalency' effects to achieve high avidity biomimetic ligands and to further study the underlying mechanisms involved in receptor binding and clustering.

Experimental

Materials

All reagents and solvents were used without further purification. Acetic anhydride and sulfonic acid were purchased from VWR chemicals. Piperidine, trifluoro acetic acid, sodium

methoxide, pentynoic acid and sodium diethyldithiocarbamate were purchased from Acros Organics. Dimethylformamide (for peptide synthesis) was purchased from Biosolve. Triisopropylsilane (TIPS) was purchased from Sigma Aldrich. Oxalyl chloride was purchased from Alfa Aesar. HOBt was purchased from Iris Biotech. *N*,*N*-Diisopropylethylamine (DIPEA) and diethylenetriamine were purchased from Carl Roth. Sodium ascorbate, phenol and potassium carbonate were purchased from PanReac AppliChem. Dichloromethane and triethylamine were purchased from Merck. PyBOP was purchased from Fluorochem and $CuSO_4$ anhydrous from Fluka Chemika. Phosphate-buffered saline (PBS) tablets were purchased from Sigma Aldrich and ready-made PBS buffer from Gibco.

Solid phase synthesis was performed on TentaGel® SRAM resin purchased from Rapp Polymere using polypropylene reactors with polyethylene frits closed with Luer-stoppers from MultiSyntech GmbH. Ion exchange resin AG1-X8, quat. ammonium, 100–200 mesh, acetate form was purchased from BioRad and Amberlite IR120 (hydrogen form) from Sigma Aldrich. For the liposomes, 1,2-distearoyl-*sn-glycero*-3-phosphocholine = COATSOME MC-0808® (DSPC), *N*-(methylpolyoxyethylene oxycarbonyl)-1,2-distearoyl-*sn-glycero*-3-phosphoethanolamine sodium salt = SUNBRIGHT DSPE-020CN (DSPE-PEG) and *N*-[*N*′-(succinimidyloxy glutaryl)aminopropylpolyoxyethylene oxycarbonyl]-1,2-distearoyl-*sn-glycero*-3-phosphoethanolamine sodium salt = SUNBRIGHT DSPE-020GS (DSPE-PEG-NHS) were purchased from NOF Europe. Cholesterol was purchased from Sigma Aldrich. Filter supports and a Mini-Extruder Kit were purchased from Avanti Polar Lipids and used with Hamilton-syringes (1000 μL) with polycarbonate membranes, pore sizes 0.1 and 0.2 μm. Slide-A-Lyzer™ Dialysis Cassettes were purchased from Thermo Scientific, ultrapure water was supplied from Invitrogen™ UltraPure™ from FisherScientific. EnzyChrom TM Lactose-Assay Kit was purchased from BioAssay Systems and used together with a Multiskan Go Microplate Spectrophotometer from Thermo Scientific and clear flat-bottom 96-well microplates from Greiner Bio-One.

(2-Azidoethyl)-2,3,4,6-tetra-*O*-acetyl-β-D-galactopyranoside, (2-azidoethyl)-2,3,4,6-tetra-*O*-acetyl-α-D-glucopyranoside and hepta-*O*-acetyl-β-lactosylazide were synthesized following established protocols.[91] Reactions were observed *via* analytical thin layer chromatography, performed on Merck silica gel 60 F254 plates and were visualized with ninhydrin and anisaldehyde staining. ^{1}H-NMR and ^{13}C-NMR spectra were measured on Bruker Avance III 300 or Bruker Avance III 600. Analytical reversed phase HPLC (RP-HPLC) measurements were performed on Agilent Technologies 6120 series coupled with an Agilent quadrupole mass spectrometer. All spectra were measured with solvent A: 95% H_2O, 5% ACN, +0.1% formic acid, and solvent B: 5% H_2O, 95% ACN, +0.1% formic acid with a gradient of 5 to 50% B over 30 min. Purities of the compounds were determined by the integration of the signals absorbing at 214 nm. Preparative RP-HPLC was performed on an Agilent 1200 series. High resolution ESI (HR-ESI) spectra were measured on UHR-QTOF maXis 4G (Bruker Daltonics).

Methods

Solid phase synthesis. Solid phase synthesis of glycooligoamides was performed as reported.[52] General protocols for the solid phase synthesis are described for batch sizes of 0.1 mmol as total loading of the resin. All reactions were performed at room temperature in a reactor with a frit on a shaker.

Resin preparation and Fmoc cleavage. The resin (0.1 mmol, 400 mg, resin loading 0.25 mmol g^{-1}) was transferred into a 10 mL reactor and 5 mL DCM were added to swell the resin for 1 h. After washing the resin 10 times with 5 mL DMF, the Fmoc protecting group was cleaved by adding 5 mL of 25% piperidine in DMF and shaking three times for 10 min. In between the deprotection steps, the resin was washed three times with 5 mL DMF, and after the last deprotection, the resin was washed ten times with 5 mL DMF.

Building block coupling. The building block (0.5 mmol, 5 eq. to total loading of resin) and PyBOP (0.5 mmol, 260 mg, 5 eq.) were dissolved in 3 mL DMF and DIPEA (1 mmol, 0.2 mL, 10 eq.) was added. After flushing the solution with nitrogen for 1 min, the solution was added to the resin and the reaction was shaken for 1–1.5 h. After that, the liquid content was discarded and the resin was washed ten times with 5 mL DMF.

Terminal-NH_2 capping. The resin was treated with 3 mL acetic anhydride two times for 15 min. In between, the resin was washed with 3 mL DMF 3 times. After the last capping step, the resin was washed five times with 5 mL MeOH and five times with 5 mL DMF.

Copper-catalyzed alkyne azide cycloaddition conjugation. Carbohydrate azide derivative (3 eq./alkyne) was dissolved in 2 mL DMF. Separately, $CuSO_4 \cdot 5H_2O$ (50 mol%/alkyne) and sodium ascorbate (50 mol%/alkyne) were each dissolved in 0.2 mL MilliQ water. The carbohydrate solution was first added to the resin, followed by sodium ascorbate and $CuSO_4$. After shaking the reaction mixture overnight, the resin was washed sequentially with 5 mL of DMF, a solution of 0.2 M sodium diethyldithiocarbamate in DMF and water (1/1), water, DMF and DCM until no more color changes were monitored.

Carbohydrate deprotection. The resin was treated two times for 30 min with 5 mL 0.2 M NaOMe in MeOH. In between, the resin was washed three times with 5 mL MeOH, then the resin was washed five times with 5 mL of each MeOH, DMF and DCM.

Macro cleavage. The resin was washed ten times with 5 mL DMF and DCM. A cleavage solution consisting of 5 mL of 95% TFA, 2.5% TIPS and 2.5% DCM was added to the resin, and the reaction mixture was shaken for 1 h. The supernatant was added dropwise to cooled Et_2O (40 mL) to precipitate the product. The mixture was centrifuged, the supernatant was decanted, and the white precipitate was dried under a stream of nitrogen. After dissolving the resulting solid in MilliQ water, the solution was lyophilized.

In solution synthesis of Lac_3TPD 11. 4-Pentynoic acid (37 mmol, 3.6 g, 1 eq.) was dissolved in 90 mL DCM and oxalyl chloride (37 mmol, 3.2 mL, 1 eq.) was added carefully. The reaction was activated by a few drops of DMF and stirred for 1.5 h at room temperature. The resulting 4-pentynoic chloride was purified by fractional distillation.

Diethylenetriamine (3 mmol, 0.3 mL, 1 eq.) was dissolved in 300 mL DCM and 4-pentynoic acid chloride (3 eq.) was added carefully over 30 min. The reaction was stirred for 1 h at room temperature. After adding 100 mL of a saturated $NaHCO_3$ solution, the organic layer was separated, washed two times with 50 mL of saturated $NaHCO_3$ solution and dried over Na_2SO_4. The solvent was removed under reduced pressure and the crude product was recrystallized from ethyl acetate resulting in the desired product **18** as a white solid in yield of 31% (300 mg, 0.87 mmol).

TPD-precursor **18** (0.1 mmol 34 mg, 1 eq.) and azido-lactose (0.45 mmol, 300 mg, 4.5 eq.) were dissolved in 2 mL DMF. Sodium ascorbate (30 mg, 50 mol%/alkyne) and $CuSO_4$ (38 mg, 50 mol%/alkyne) were each dissolved in 0.2 mL H_2O and added to the TPD-lactose solution. The mixture was stirred for 3 d at rt. The reaction mixture was added to 40 mL H_2O to precipitate the product. After centrifugation, the precipitate was redissolved in 1 mL DMF and precipitated in 40 mL H_2O for a second time. The product was deprotected by treating the crude precipitate with 6 mL of 0.2 M NaOMe in MeOH for 1 h. After adding 4 mL H_2O, the solution was neutralized using Amberlite IR120. After filtration and removal of the solvent, the crude product was purified using preparative RP-HPLC. The product was obtained as a white solid with a yield of 50% (73 mg, 0.05 mmol).

Lipid-conjugation. DSPE-PEG-NHS (2 mg, 1 eq.) were dissolved in 100 μL DMF followed by the glycoligands **4***, **9***, **10*** and **16*** (8 eq.) dissolved in 900 μL of 0.1 M $NaHCO_3$ solution and the solution was stirred overnight. After removing the solvents under reduced pressure, the residue was redissolved in 1.5 mL 0.1 M $NaHCO_3$ solution. The solution was dialyzed using Slide-A-Lyzer cassettes with a molecular weight cut-off (MWCO) of 7000 g mol^{-1} first three times for 8–12 h against 0.1 M $NaHCO_3$ and subsequently three times for 8–12 h against water. The sample to solvent ratio was 1 mL to 250 mL up to 1 mL to 550 mL. Yields given in mg relate to the successfully conjugated lipids. The content of unconjugated lipids was quantified *via* ^{1}H-NMR and was excluded in the calculation.

Liposome formulation. Liposomes were prepared by the hydration film extrusion method.[92] The general composition of the liposomes was 57 mol% of DSPC, 38 mol% of cholesterol, 4.75 mol% of DSPE-PEG-ligand and 0.25 mol% DSPE-PEG, or no DSPE-PEG-ligand and 5 mol% DSPE-PEG for an unfunctionalized liposome. For the calculations of the DSPE-PEG-ligand, the effective molar mass was calculated taking into consideration the mixture of conjugated and unconjugated DSPE-PEG-COOH (through partially deactivated NHS) yielded from the conjugation step.

Stock solutions of each 8 mg mL^{-1} DSPE-PEG and DSPE-PEG-ligand in DMSO-d_6, and 20 mg mL^{-1} DSPC and 10 mg mL^{-1} cholesterol in $CDCl_3$ were prepared. The batch for the formulation was calculated for a final total lipid concentration of 3 μmol in 624 μL PBS-buffer (4.81 mM).

All DMSO-dissolved compounds were added to a test tube and the sample was freeze-dried. Then, DSPC and cholesterol were added and the mixture was further dried in a stream of nitrogen and subsequently under high vacuum for 1 h. 624 μL PBS-buffer were added and the test tube was sonicated for four times at 50 °C for 3–4 s, then vortexed and allowed to rest for 30 s. This procedure was repeated until all of the precipitate was suspended.

In the following extrusion step, the extruder was build-up and prepared as described by the supplier. The liposome suspension was taken up with the Hamilton syringe of the mini-extruder kit and was first extruded 30 times through a 0.2 μm filter and then through a 0.1 μm filter. The suspension was allowed to stand for 30 min at room temperature and then stored at 4 °C.

Determination of the lactose concentration on the liposome surface. The determination of lactose-concentration on the liposome surface was conducted with the EnzyChrom™ Lactose-Assay Kit from BioAssay Systems. Changes to the protocol included the following: (i) galactose was used as a standard instead of lactose; (ii) the liposome samples were first incubated with 1 μL lactase in 28.3 μL assay buffer for 24 hours at 37 °C; (iii) following incubation, the standard and liposome samples were treated with 1 μL each of dye reagent and enzyme mix in a total of 56.7 μL assay buffer. Subsequently, all samples were incubated for 30 min at room temperature before the optical density readout. The standards were prepared in Eppendorf tubes to be able to vortex and shortly centrifuge them before application onto the microplate. One stock solution of the lactase in assay buffer as well as enzyme mix plus dye reagent in assay buffer was prepared for all tests of one measurement together, carefully vortexed and subsequently transferred to the microplate.

DLS and zeta potential. Dynamic light scattering (DLS) and zeta potential measurements were performed with 20 μL of the liposome suspension diluted with 980 μL of ultrapure water at 25 °C. DLS was measured on a High Performance Sizer from Malvern Instruments with polystyrene cuvettes and the ALV-correlator software Version 3.0 with a backscattering detector (173°) and 5 measurements per 30 s for each sample. Zeta potential measurements were performed on a Zetasizer Nano Z from Malvern Instruments with DTS1070 capillary cells.

Binding studies

Surface plasmon resonance. The SPR inhibition studies were performed on a CM5 sensor chip on a Biacore X100 from GE Healthcare Life Science. For immobilization, the "Surface Preparation Wizard" for the sensor chip CM5 was used. The functionalization of the two flow cells was performed through an amine-coupling procedure with NHS/EDC (contact time 420 s, flow rate 10 μL min^{-1}). Flow cell 2 (mess cell) was immobilized with 1 mM Lac(1,3,5)-6, **9***, in HBS-P buffer from GE Healthcare with a contact time of 600 s. For flow cell 1 (reference cell) a blank immobilization with ethanolamine was performed according to the software. As running buffer, HBS-P buffer from GE Healthcare was used. The immobilization levels reached 411 RU for flow cell 2 and 186 RU for flow cell 1.

The inhibition assay was performed in a "Custom Assay Wizard-Binding Analysis" in a multi cycle measurement. For the inhibition studies, stock solutions of 200 μg mL^{-1} of Gal-3 and 100 μM for each ligand in PBS buffer (150 mM NaCl, 50 mM NaH_2PO_4, pH 7.5) were prepared. Gal-3 was incubated with each ligand by mixing the solutions of the protein and ligands in

a 1 : 1 ratio, resulting in final concentrations of 100 μg mL^{-1} for Gal-3 and 50 μM for the ligands. The assay was performed with PBS as running buffer using 90 s for association time and 60 s for dissociation time with a flow rate of 10 μL min^{-1} over both flow cells. The cell surface was regenerated by injecting 3 M $MgCl_2$ in MilliQ water for 60 s with a flow rate of 10 μL min^{-1} over the surface after each cycle. Liposomes were measured at concentrations of 10 μM using a stock solution of 20 μM in PBS buffer due to their higher binding affinities to Gal-3.

The report points for the binding event of Gal-3 without and with ligand were taken after 155 s after sensorgram adjustment to baseline. The response unit of only Gal-3 was set as a reference point to 100% binding and 0% inhibition. Inhibition of the glycomacromolecules were referred to the response unit of only Gal-3. All measurements were performed in triplicates.

Enzyme-linked immunosorbent assay (ELISA). Inhibition studies were performed according to an established protocol by Elling and co-workers.[35] Glycoligands **1–16** were measured with final concentrations between 0.1 and 2000 μM and liposomes **L4**, **L9**, **L10** and **L16** with final concentrations calculated according to the results of the Lactose-Assay Kit between 0.002 and 14 μM of the glycoligands.

Conflicts of interest

There are no conflicts to declare.

Acknowledgements

We thank Jan Dirks for his support in synthesizing the H_2SO_4-cat. We acknowledge support by the Heinrich Heine University Duesseldorf. We thank the Boehringer Ingelheim Foundation for financial support through the Plus 3 program and the DFG for support through the large equipment grant INST 208/735-1. L. E. and D. L. gratefully acknowledge financial support by the DFG (project EL 135/12-1).

References

1 D. H. Dube and C. R. Bertozzi, *Nat. Rev. Drug Discovery*, 2005, **4**, 477.
2 H. Leffler, S. Carlsson, M. Hedlund, Y. Qian and F. Poirier, *Glycoconjugate J.*, 2002, **19**, 433–440.
3 P. Nangia-Makker, J. Conklin, V. Hogan and A. Raz, *Trends Mol. Med.*, 2002, **8**, 187–192.
4 A. C. F. Cardoso, L. N. d. S. Andrade, S. O. Bustos and R. Chammas, *Front. Oncol.*, 2016, **6**, 1–12.
5 H. Blanchard, X. Yu, P. M. Collins and K. Bum-Erdene, *Expert Opin. Ther. Pat.*, 2014, **24**, 1053–1065.
6 M. L. Bacigalupo, M. Manzi, G. A. Rabinovich and M. F. Troncoso, *World J. Gastroenterol.*, 2013, **19**, 8831–8849.
7 H. Blanchard, K. Bum-Erdene, M. H. Bohari and X. Yu, *Expert Opin. Ther. Pat.*, 2016, **26**, 537–554.
8 Y.-C. Chan, H.-Y. Lin, Z. Tu, Y.-H. Kuo, S.-T. Hsu and C.-H. Lin, *Int. J. Mol. Sci.*, 2018, **19**, 392.
9 C. T. Öberg, H. Leffler and U. J. Nilsson, *Chimia*, 2011, **65**, 18–23.
10 T. Funasaka, A. Raz and P. Nangia-Makker, *Semin. Cancer Biol.*, 2014, 30–38.
11 K. C. Haudek, K. J. Spronk, P. G. Voss, R. J. Patterson, J. L. Wang and E. J. Arnoys, *Biochim. Biophys. Acta*, 2010, **1800**, 181.
12 K. H. Mayo, in *Galectins and Disease Implications for Targeted Therapeutics*, Am. Chem. Soc., 2012, vol. 1115, pp. 61–77.
13 L. Díaz-Alvarez and E. Ortega, *Mediators Inflammation*, 2017, 9247574.
14 A. Lagana, J. G. Goetz, P. Cheung, A. Raz, J. W. Dennis and I. R. Nabi, *Mol. Cell. Biol.*, 2006, **26**, 3181–3193.
15 J. Ochieng, M. L. Leite-Browning and P. Warfield, *Biochem. Biophys. Res. Commun.*, 1998, **246**, 788–791.
16 V. L. Campo, M. F. Marchiori, L. C. Rodrigues and M. Dias-Baruffi, *Glycoconjugate J.*, 2016, **33**, 853–876.
17 J. M. Cousin and M. J. Cloninger, *Int. J. Mol. Sci.*, 2016, **17**, 1566.
18 A. K. Michel, P. Nangia-Makker, A. Raz and M. J. Cloninger, *ChemBioChem*, 2014, **15**, 2106–2112.
19 I. Vrasidas, S. André, P. Valentini, C. Böck, M. Lensch, H. Kaltner, R. M. J. Liskamp, H.-J. Gabius and R. J. Pieters, *Org. Biomol. Chem.*, 2003, **1**, 803–810.
20 Y. Hou, S. Cao, X. Li, B. Wang, Y. Pei, L. Wang and Z. Pei, *ACS Appl. Mater. Interfaces*, 2014, **6**, 16909–16917.
21 C. Lavilla, G. Yilmaz, V. Uzunova, R. Napier, C. R. Becer and A. Heise, *Biomacromolecules*, 2017, **18**, 1928–1936.
22 S. André, C. E. P. Maljaars, K. M. Halkes, H.-J. Gabius and J. P. Kamerling, *Bioorg. Med. Chem. Lett.*, 2007, **17**, 793–798.
23 C. E. P. Maljaars, S. André, K. M. Halkes, H.-J. Gabius and J. Kamerling, *Anal. Biochem.*, 2008, **378**, 190.
24 C. K. Goodman, M. L. Wolfenden, P. Nangia-Makker, A. K. Michel, A. Raz and M. J. Cloninger, *Beilstein J. Org. Chem.*, 2014, **10**, 1570–1577.
25 S. Zhang, R.-O. Moussodia, C. Murzeau, H.-J. Sun, M. L. Klein, S. Vértesy, S. André, R. Roy, H.-J. Gabius and V. Percec, *Angew. Chem., Int. Ed.*, 2015, **54**, 4036–4040.
26 C. Rodriguez-Emmenegger, Q. Xiao, N. Y. Kostina, S. E. Sherman, K. Rahimi, B. E. Partridge, S. Li, D. Sahoo, A. M. Reveron Perez, I. Buzzaccera, H. Han, M. Kerzner, I. Malhotra, M. Möller, C. J. Wilson, M. C. Good, M. Goulian, T. Baumgart, M. L. Klein and V. Percec, *Proc. Natl. Acad. Sci. U. S. A.*, 2019, **116**, 5376–5382.
27 V. Percec, P. Leowanawat, H.-J. Sun, O. Kulikov, C. D. Nusbaum, T. M. Tran, A. Bertin, D. A. Wilson, M. Peterca, S. Zhang, N. P. Kemat, K. Vargo, D. Moock, E. D. Johnston, D. A. Hammer, D. J. Pochan, Y. Chen, Y. M. Chabre, T. C. Shiao, M. Bergeron-Brleck, S. André, R. Roy, H.-J. Gabius and P. A. Henry, *J. Am. Chem. Soc.*, 2013, **135**, 9055–9077.
28 S. Zhang, Q. Xio, S. E. Sherman, A. Muncan, A. D. M. Rmaos Vincente, Z. Wang, D. A. Hammer, D. Willams, Y. Chen, D. J. Pouchan, S. André, M. L. Klein, H.-J. Gabius and V. Percec, *J. Am. Chem. Soc.*, 2015, **137**, 13334–13344.
29 Q. Xiao, A.-K. Ludwig, C. Romanò, I. Buzzacchera, S. E. Sherman, M. Vetro, S. Vértesy, H. Kaltner, E. H. Reed, M. Möller, C. J. Wilson, D. A. Hammer, S. Oscarson,

M. L. Klein, H.-J. Gabius and V. Percec, *Proc. Natl. Acad. Sci. U. S. A.*, 2018, **115**, E2509–E2518.
30 S. André, B. Liu, H.-J. Gabius and R. Roy, *Org. Biomol. Chem.*, 2003, **1**, 3909–3916.
31 L. Abbassi, Y. M. Chabre, N. Kottari, A. A. Arnold, S. André, J. Josserand, H.-J. Gabius and R. Roy, *Polym. Chem.*, 2015, **6**, 7666–7683.
32 N. Ahmad, H.-J. Gabius, S. André, H. Kaltner, S. Sabesan, R. Roy, B. Liu, F. Macaluso and C. F. Brewer, *J. Biol. Chem.*, 2004, **279**, 10841–10847.
33 S. R. Rauthu, T. C. Shiao, S. André, M. C. Miller, É. Madej, K. H. Mayo, H.-J. Gabius and R. Roy, *ChemBioChem*, 2015, **16**, 126–139.
34 C. Bonduelle, H. Oliveira, C. Gauche, J. Huang, A. Heise and S. Lecommandoux, *Chem. Commun.*, 2016, **52**, 11251–11254.
35 D. Laaf, P. Bojarová, H. Pelantová, V. Křen and L. Elling, *Bioconjugate Chem.*, 2017, **28**, 2832–2840.
36 S. Böcker, D. Laaf and L. Elling, *Biomolecules*, 2015, **5**, 1671.
37 G.-J. Boons, *Expert Rev. Vaccines*, 2010, **9**, 1251–1256.
38 V. P. Torchilin, *Nat. Rev. Drug Discovery*, 2005, **4**, 145.
39 B. S. Pattni, V. V. Chupin and V. P. Torchilin, *Chem. Rev.*, 2015, **115**, 10938–10966.
40 R. Stahn, H. Schäfer, J. Schreiber and M. Brudel, *J. Liposome Res.*, 1995, **5**, 61–73.
41 C. Sandoval-Altamirano, S. A. Sanchez, N. F. Ferreyra and G. Gunther, *Colloids Surf., B*, 2017, **158**, 539–546.
42 R. Zeisig, R. Stahn, K. Wenzel, D. Behrens and I. Fichtner, *Biochim. Biophys. Acta, Biomembr.*, 2004, **1660**, 31–40.
43 C. Kelly, C. Jefferies and S.-A. Cryan, *J. Drug Delivery*, 2011, **2011**, 727241.
44 M. Srinivasarao and P. S. Low, *Chem. Rev.*, 2017, **117**, 12133–12164.
45 N. Jayaraman, K. Maiti and K. Naresh, *Chem. Soc. Rev.*, 2013, **42**, 4640–4656.
46 J. J. Weingart, P. Vabbilisetty and X. L. Sun, *Carbohydrate Nanotechnology*, ed. K. J. Stine, John Wiley & Sons, Inc., 1st edn, 2016.
47 L. Cai, Z. Gu, J. Zhong, D. Wen, G. Chen, L. He, J. Wu and Z. Gu, *Drug Discovery Today*, 2018, **23**, 1126–1138.
48 W. C. Chen, G. C. Completo, D. S. Sigal, P. R. Crocker, A. Saven and J. C. Paulson, *Blood*, 2010, **115**, 4778–4786.
49 N. Kawasaki, J. L. Vela, C. M. Nycholat, C. Rademacher, A. Khurana, N. van Rooijen, P. R. Crocker, M. Kronenberg and J. C. Paulson, *Proc. Natl. Acad. Sci. U. S. A.*, 2013, **110**, 7826–7831.
50 M. S. Macauley, F. Pfrengle, C. Rademacher, C. M. Nycholat, A. J. Gale, A. von Drygalski and J. C. Paulson, *J. Clin. Invest.*, 2013, **123**, 3074–3083.
51 J. Zhu, J. Xue, Z. Guo, L. Zhang and R. E. Marchant, *Bioconjugate Chem.*, 2007, **18**, 1366–1369.
52 D. Ponader, F. Wojcik, F. Beceren-Braun, J. Dernedde and L. Hartmann, *Biomacromolecules*, 2012, **13**, 1845–1852.
53 D. Ponader, P. Maffre, J. Aretz, D. Pussak, N. M. Ninnemann, S. Schmidt, P. H. Seeberger, C. Rademacher, G. U. Nienhaus and L. Hartmann, *J. Am. Chem. Soc.*, 2014, **136**, 2008–2016.
54 C. Gerke, M. F. Ebbesen, D. Jansen, S. Boden, T. Freichel and L. Hartmann, *Biomacromolecules*, 2017, **18**, 787–796.
55 T. Freichel, S. Eierhoff, N. L. Snyder and L. Hartmann, *J. Org. Chem.*, 2017, **82**, 9400–9409.
56 M. Baier, M. Giesler and L. Hartmann, *Chem.–Eur. J.*, 2018, **24**, 1619–1630.
57 J. Chen, H.-N. Son, J. J. Hill, S. Srinivasan, F.-Y. Su, P. S. Stayton, A. J. Convertine and D. M. Ratner, *Nanomedicine*, 2016, **12**, 2031–2041.
58 S. Boden, K. Wagner, M. Karg and L. Hartmann, *Polymers*, 2017, **9**, 716.
59 M. F. Ebbesen, C. Gerke, P. Hartwig and L. Hartmann, *Polym. Chem.*, 2016, **7**, 7086–7093.
60 K. S. Bücher, H. Yan, R. Creutznacher, K. Ruoff, A. Mallagaray, A. Grafmüller, J. S. Dirks, T. Kilic, S. Weickert, A. Rubailo, M. Drescher, S. Schmidt, G. Hansman, T. Peters, C. Uetrecht and L. Hartmann, *Biomacromolecules*, 2018, **19**, 3714–3724.
61 G. Zemplén and E. Pacsu, *Ber. Dtsch. Chem. Ges.*, 1929, **62**, 1613–1614.
62 E.-C. Wamhoff, J. Schulze, L. Bellmann, G. Bachem, F. F. Fuchsberger, J. Rademacher, M. Hermann, B. Del Frari, R. van Dalen, D. Hartmann, N. van Sorge, O. Seitz, P. Stoitzner and C. Rademacher, *ACS Cent. Sci.*, 2019, **5**, 808–820.
63 P. L. Yeagle, *Biochim. Biophys. Acta, Rev. Biomembr.*, 1985, **822**, 267–287.
64 S. Raffy and J. Teissié, *Biophys. J.*, 1999, **76**, 2072–2080.
65 J. Senior and G. Gregoriadis, *Life Sci.*, 1982, **30**, 2123–2136.
66 Y. Barenholz, *J. Controlled Release*, 2012, **160**, 117–134.
67 M. Danaei, M. Dehghankhold, S. Ataei, F. Hasanzadeh Davarani, R. Javanmard, A. Dokhani, S. Khorasani and M. R. Mozafari, *Pharmaceutics*, 2018, **10**, 57.
68 K. N. Clayton, J. W. Salameh, S. T. Wereley and T. L. Kinzer-Ursem, *Biomicrofluidics*, 2016, **10**, 054107.
69 R. I. Jolck, L. N. Feldborg, S. Andersen, S. M. Moghimi and T. L. Andresen, *Adv. Biochem. Eng./Biotechnol.*, 2011, **125**, 251–280.
70 P. Vabbilisetty and X.-L. Sun, *Org. Biomol. Chem.*, 2014, **12**, 1237–1244.
71 I. Taniguchi, K. Akiyoshi and J. Sunamoto, *Macromol. Chem. Phys.*, 1999, **200**, 1386–1392.
72 H. Zhang, D. Laaf, L. Elling and R. J. Pieters, *Bioconjugate Chem.*, 2018, **29**, 1266–1275.
73 L. Bumba, D. Laaf, V. Spiwok, L. Elling, V. Křen and P. Bojarová, *Int. J. Mol. Sci.*, 2018, **19**, 372.
74 M. Wolfenden, J. Cousin, P. Nangia-Makker, A. Raz and M. Cloninger, *Molecules*, 2015, **20**, 7059–7096.
75 P. Sörme, B. Kahl-Knutsson, U. Wellmar, B.-G. Magnusson, H. Leffler and U. J. Nilsson, in *Methods in Enzymology*, Academic Press, 2003, vol. 363, pp. 157–169.
76 T. K. Dam, H.-J. Gabius, S. André, H. Kaltner, M. Lensch and C. F. Brewer, *Biochemistry*, 2005, **44**, 12564–12571.
77 J. Stegmayr, A. Lepur, B. Kahl-Knutson, M. Aguilar-Moncayo, A. A. Klyosov, R. A. Field, S. Oredsson, U. J. Nilsson and H. Leffler, *J. Biol. Chem.*, 2016, **291**, 13318–13334.
78 K. Saraboji, M. Håkansson, S. Genheden, C. Diehl, J. Qvist, U. Weininger, U. J. Nilsson, H. Leffler, U. Ryde, M. Akke and D. T. Logan, *Biochemistry*, 2012, **51**, 296–306.

79 I. R. Nabi, J. Shankar and J. W. Dennis, *J. Cell Sci.*, 2015, **128**, 2213–2219.
80 M. van Scherpenzeel, E. E. Moret, L. Ballell, R. M. J. Liskamp, U. J. Nilsson, H. Leffler and R. J. Pieters, *ChemBioChem*, 2009, **10**, 1724–1733.
81 M. F. Marchiori, D. E. Pires Souto, L. Oliveira Bortot, J. Francisco Pereira, L. T. Kubota, R. D. Cummings, M. Dias-Baruffi, I. Carvalho and V. L. Campo, *Bioorg. Med. Chem.*, 2015, **23**, 3414–3425.
82 J. Tejler, H. Leffler and U. J. Nilsson, *Bioorg. Med. Chem. Lett.*, 2005, **15**, 2343–2345.
83 V. Denavit, D. Lainé, T. Tremblay, J. St-Gelais and D. Giguère, *Trends Glycosci. Glycotechnol.*, 2018, **30**, SE21–SE40.
84 J. M. Fox, M. Zhao, M. J. Fink, K. Kang and G. M. Whitesides, *Annu. Rev. Biophys.*, 2018, **47**, 223–250.
85 C.-e. A. Chang, W. Chen and M. K. Gilson, *Proc. Natl. Acad. Sci. U. S. A.*, 2007, **104**, 1534–1539.
86 A. J. Cagnoni, J. Kovensky and M. L. Uhrig, *J. Org. Chem.*, 2014, **79**, 6456–6467.
87 H. Halimi, A. Rigato, D. Byrne, G. Ferracci, C. Sebban-Kreuzer, L. El Antak and F. Guerlesquin, *PLoS One*, 2014, **9**, e111836.
88 M. Sundqvist, A. Welin, J. Elmwall, V. Osla, U. J. Nilsson, H. Leffler, J. Bylund and A. Karlsson, *J. Leukocyte Biol.*, 2018, **103**, 341–353.
89 R.-Y. Yang, P. N. Hill, D. K. Hsu and F.-T. Liu, *Biochemistry*, 1998, **37**, 4086–4092.
90 A. Lepur, E. Salomonsson, U. J. Nilsson and H. Leffler, *J. Biol. Chem.*, 2012, **287**, 21751–21756.
91 L. Wu and N. S. Sampson, *ACS Chem. Biol.*, 2014, **9**, 468–475.
92 S. Chen, L. Li, C. Zhao and J. Zheng, *Polymer*, 2010, **51**, 5283–5293.

Supporting Information

Effects of Linker and Liposome Anchoring on Lactose-functionalized Glycomacromolecules as Multivalent Ligands for Binding Galectin-3

Tanja Freichel[a], Dominic Laaf [b], Miriam Hoffmann[a], Patrick B. Konietzny[a], Robert Wawrzinek [c],Viktoria Heine[b], Christoph Rademacher [c], Nicole L. Snyder[d], Lothar Elling[b] and Laura Hartmann[a] †

[a] Department of Organic and Macromolecular Chemistry, Heinrich-Heine-University Düsseldorf, Universitätsstraße 1, 40225 Düsseldorf, Germany.

[b] Laboratory for Biomaterials, Institute for Biotechnology and Helmholtz-Institute for Biomedical Engineering, RWTH Aachen University, Pauwelsstraße 20, 52074 Aachen, Germany.

[c] Max Planck Institute of Colloids and Interfaces, Mühlenberg 1, 14476 Potsdam, Germany.

[d] Department of Chemistry, Davidson College, North Carolina 28035, United States.

Corresponding authors: laura.hartmann@hhu.de

Contents

1. Additional information on synthesis of glycomacromolecules and liposome formulation

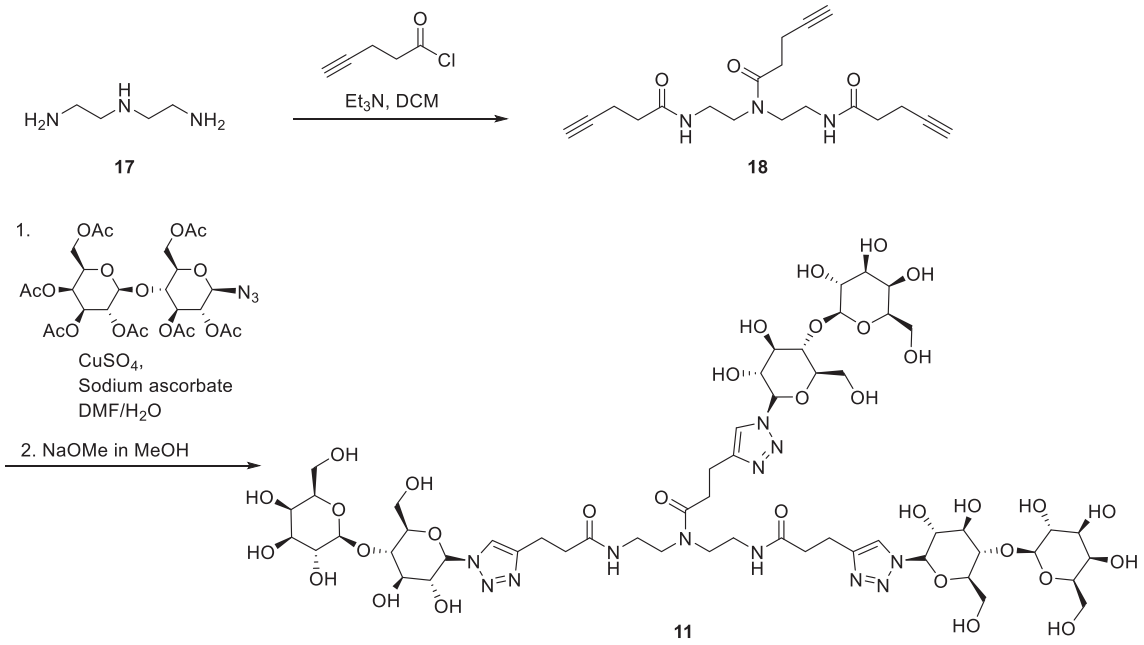

Scheme S 1: Scheme of the synthesis of compound **11**.

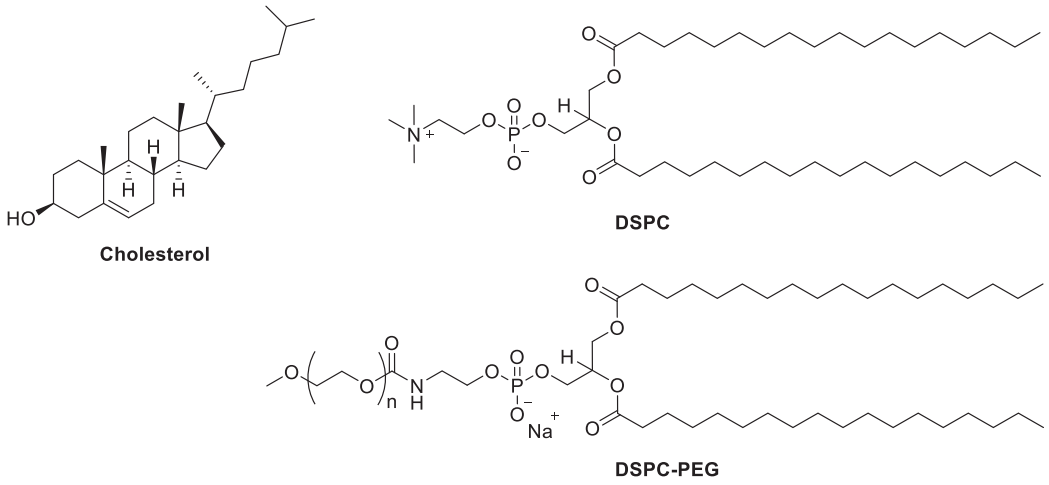

Figure S 1: Components used for the liposome formulation.

1.1. Additional information on the characterization of the functionalization degree of the liposomes

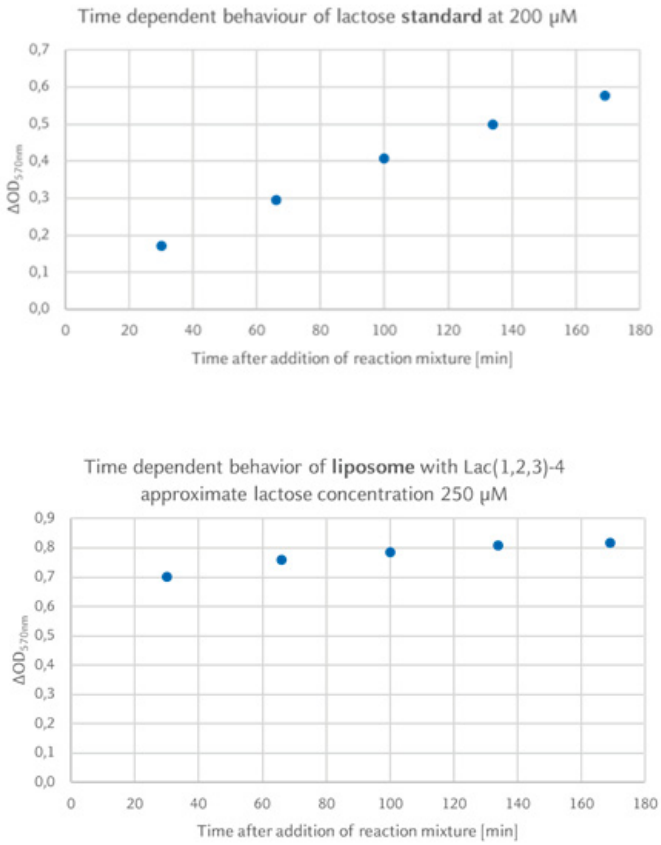

Figure S 2: Results of the Lactose-Assay Kit measuring the time dependent behavior of the absorbent resulting from the conversion of the lactose standard provided by the kit (top) and of the liposome **L10 (bottom)**.

A

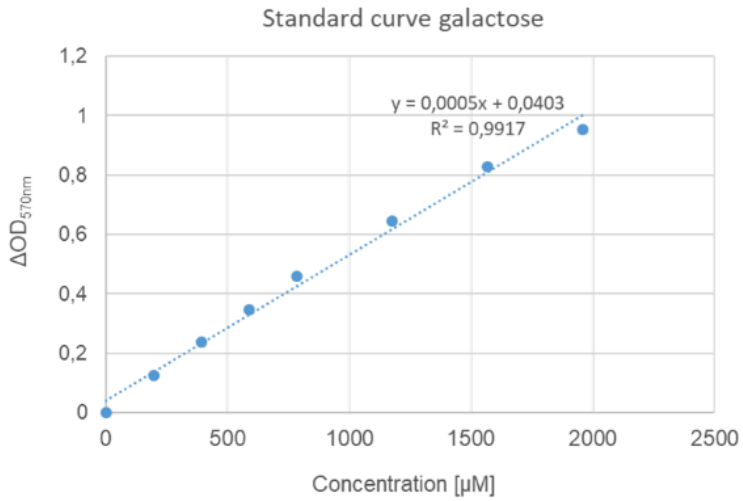

B

Sample	Measured conc. [µM]	Theoretical conc.* [µM]
Liposome L4	143±19	149
Liposome L9	389±53	376
Liposome L10	320±54	447

Figure S 3: Results of the lactose-assay kit: Resulting lactose concentration (B) using the galactose standard curve (A).*calculated from total amount of weighted lipids in consideration of coupling efficiency and for 100 % of lactose-oligomer on outer surface of liposome.

2. Additional information on binding studies of glycomacromolecules

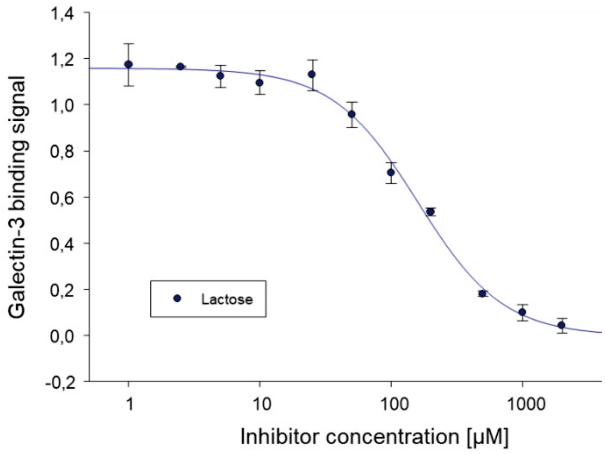

Figure S 4: ELISA inhibition curve of Gal-3 with lactose.

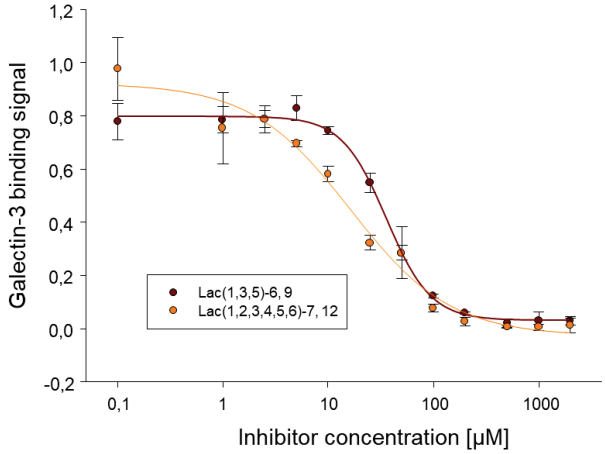

Figure S 5: ELISA inhibition curve of Gal-3 with glycomacromolecules **9** and **12**.

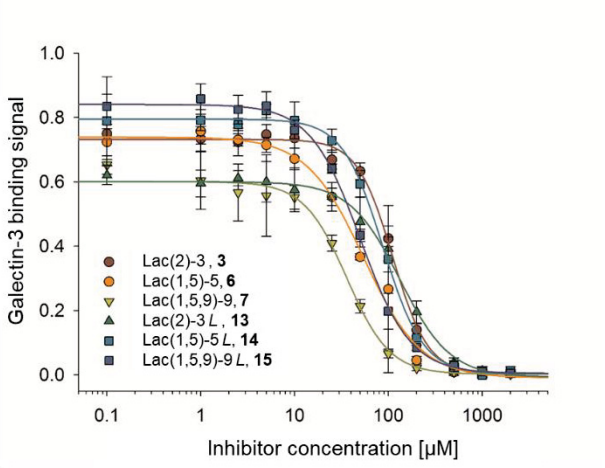

Figure S 6: ELISA inhibition curve of Gal-3 with glycomacromolecules **3,6,7** and **13-15.**

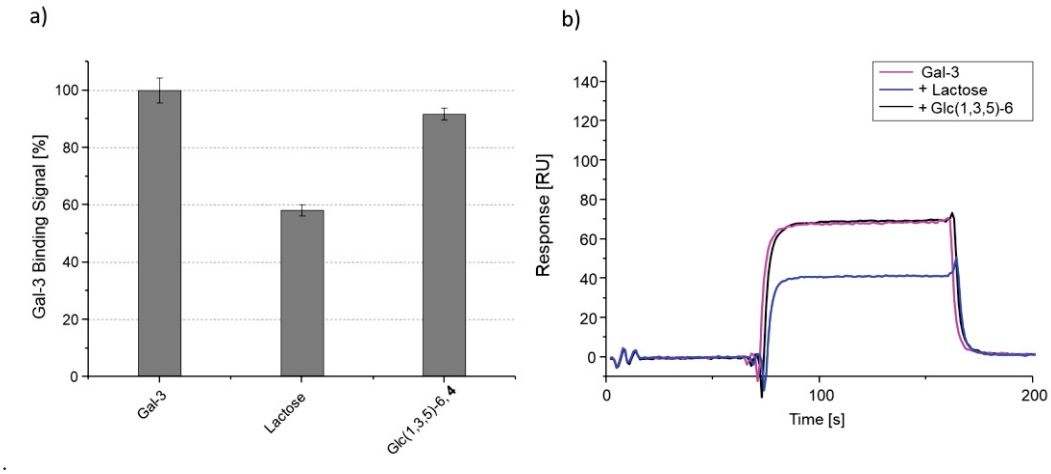

Figure S 7: Results from the SPR inhibition studies of Gal-3 with the controls lactose and Glc(1,3,5)-6, **16**.

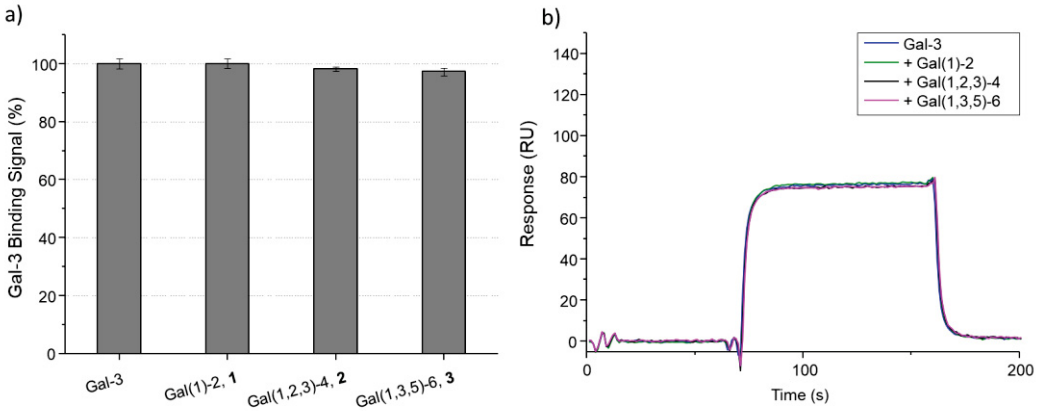

Figure S 8: Results from the SPR inhibition studies of Gal-3 with galactose samples **1, 2** and **3.**

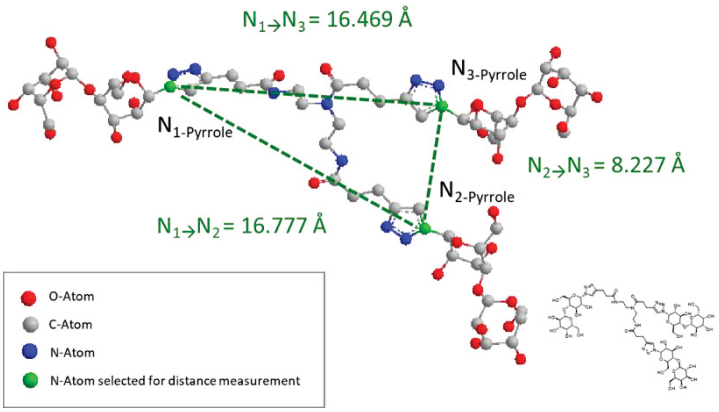

Figure S 9: Chem3D-simulation and measurement of the distances between the three nitrogen-atoms of the triazoles (marked in green) of Lac$_3$TPD **11** after MM2 conformational minimization**.**

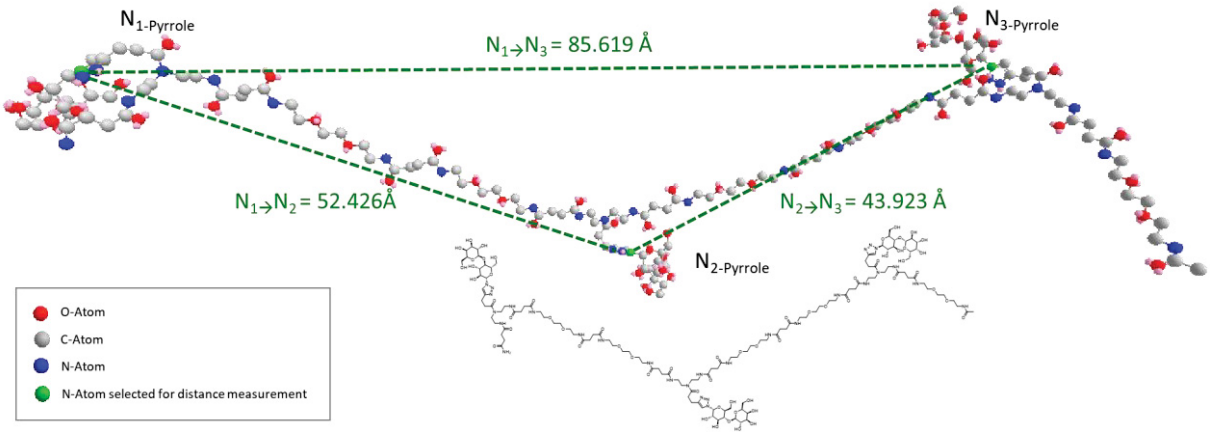

Figure S 10: Chem3D-simulation and measurement of the distances between the three nitrogen-atoms of the triazoles (marked in green) of Lac_3TPD **8** after MM2 conformational minimization**.**

3. Analytical data of glycomacromolecules

3.1. Gal(1)-2, **1**

^{1}H-NMR (300 MHz, Deuterium Oxide) δ [ppm]: 7.90 (s, 1 H, triazole-C*H*), 4.65 (t, J = 5.1 Hz, 2 H, -N-N-C*H*$_2$-), 4.37 (d, J = 7.8 Hz, 1 H, C*H*$_{anomer}$Gal), 4.29 (dt, J = 11.6, 4.8 Hz, 1 H, -C*H*$_{pyranose}$), 4.09 (dt, J = 11.1, 5.2 Hz, 1 H, C*H*$_{pyranose}$), 3.91 (dd, J = 3.4, 1.0 Hz, 1 H, --C*H*$_{pyranose}$), 3.78 – 3.72 (m, 2 H, C*H*$_{pyranose}$), 3.70 – 3.58 (m, 10 H, C*H*$_{pyranose}$, O-C*H*$_2$-), 3.54 – 3.29 (m, 13 H, C*H*$_{pyranose,}$ C=ONH-C*H*$_2$), 3.01 (t, J = 7.1 Hz, 2 H, CH=C-C*H*$_2$), 2.79 (t, J = 7.2 Hz, 2 H, CH=C-CH$_2$-C*H*$_2$), 2.56 – 2.41 (m, 8 H, , NHC=O-C*H*$_2$), 2.00 (s, 3H, -C*H*$_3$). HR-MS (ESI) calc. for $C_{33}H_{59}N_9O_{14}$ $[M+2H]^{2+}$ 402.7085; found 402.7084. Yield: 51 mg (63 %).

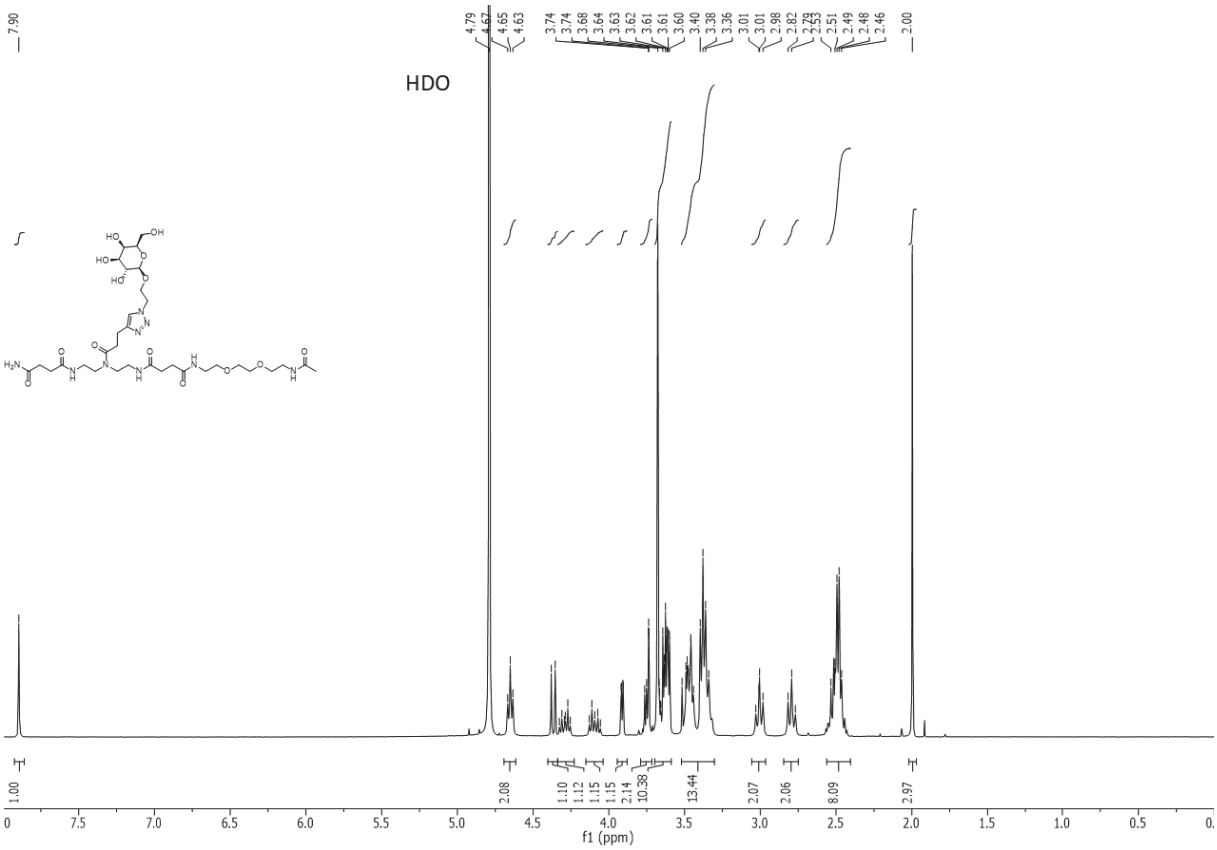

Figure S 11: ^{1}H-NMR spectrum of compound **1.**

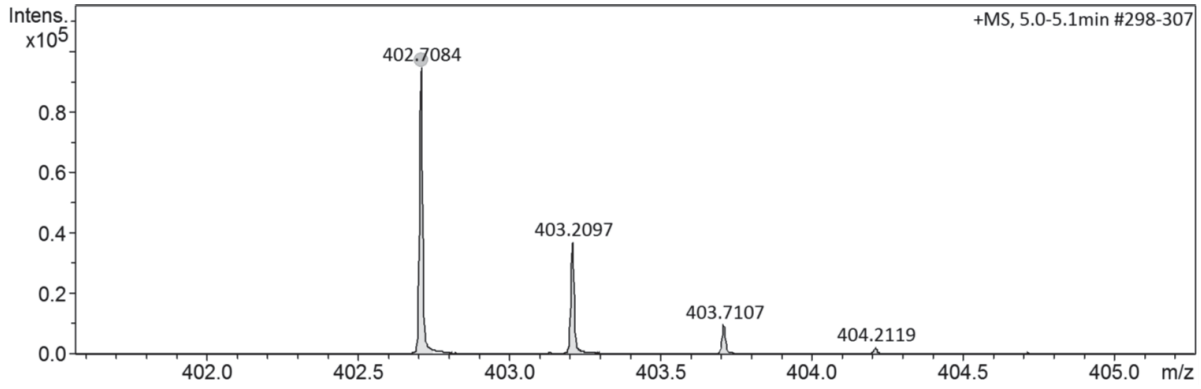

Figure S 12: HR-MS spectrum of compound **1**.

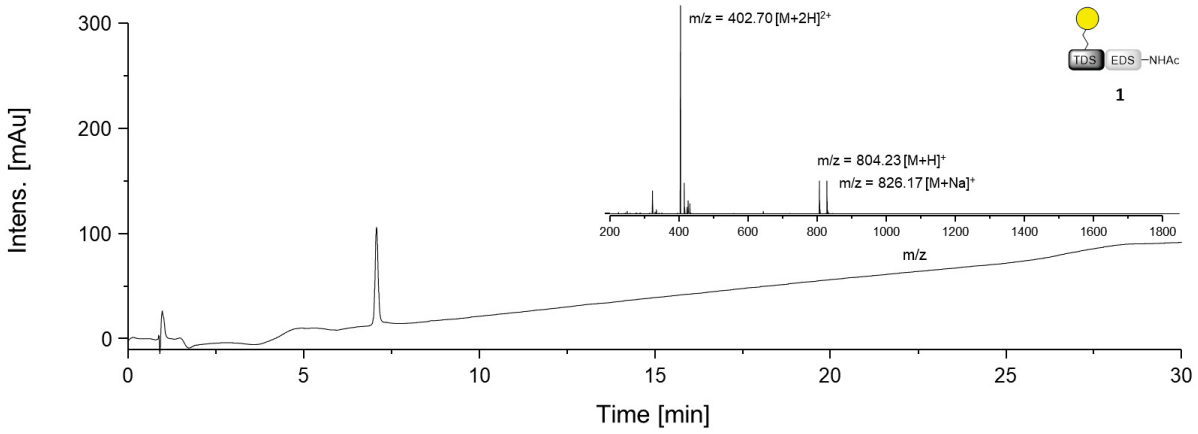

Figure S 13: RP-HPLC and ESI-MS spectrum of compound **1**.

3.2. Gal(1,3,5)-6, **2**

^{1}H-NMR (300 MHz, Deuterium Oxide) δ [ppm]: 7.90 (s, 3 H, triazole-CH), 4.65 (t, J = 5.0 Hz, 6 H, -N-N-C*H*$_2$-), 4.37 (d, J = 7.8 Hz, 3 H, C*H*$_{anomer}$Gal), 4.29 (dt, J = 9.9, 4.8 Hz, 3 H, C*H*$_{pyranose}$), 4.09 (dt, J = 11.0, 5.1 Hz, 3H, C*H*$_{pyranose}$), 3.91 (d, J = 3.3 Hz, 3H, C*H*$_{pyranose}$), 3.78 – 3.71 (m, 6 H, C*H*$_{pyranose}$), 3.70 – 3.56 (m, 30 H, C*H*$_{pyranose}$, O-C*H*$_2$-), 3.53 – 3.30 (m, 39H, C*H*$_{pyranose,}$ C=ONH-C*H*$_2$), 3.00 (t, J = 7.1 Hz, 6 H, CH=C-C*H*$_2$), 2.79 (t, J = 7.2 Hz, 6 H CH=C-CH$_2$-C*H*$_2$), 2.53-2.44 (m, 24 H, NH-C=O-C*H*$_2$-), 2.00 (s, 3H, -C*H*$_3$). HR-MS (ESI) calc. for $C_{95}H_{164}N_{25}O_{40}$ $[M+3H]^{3+}$ 765.0517; found 765.0522. Yield: 119 mg (52 %).

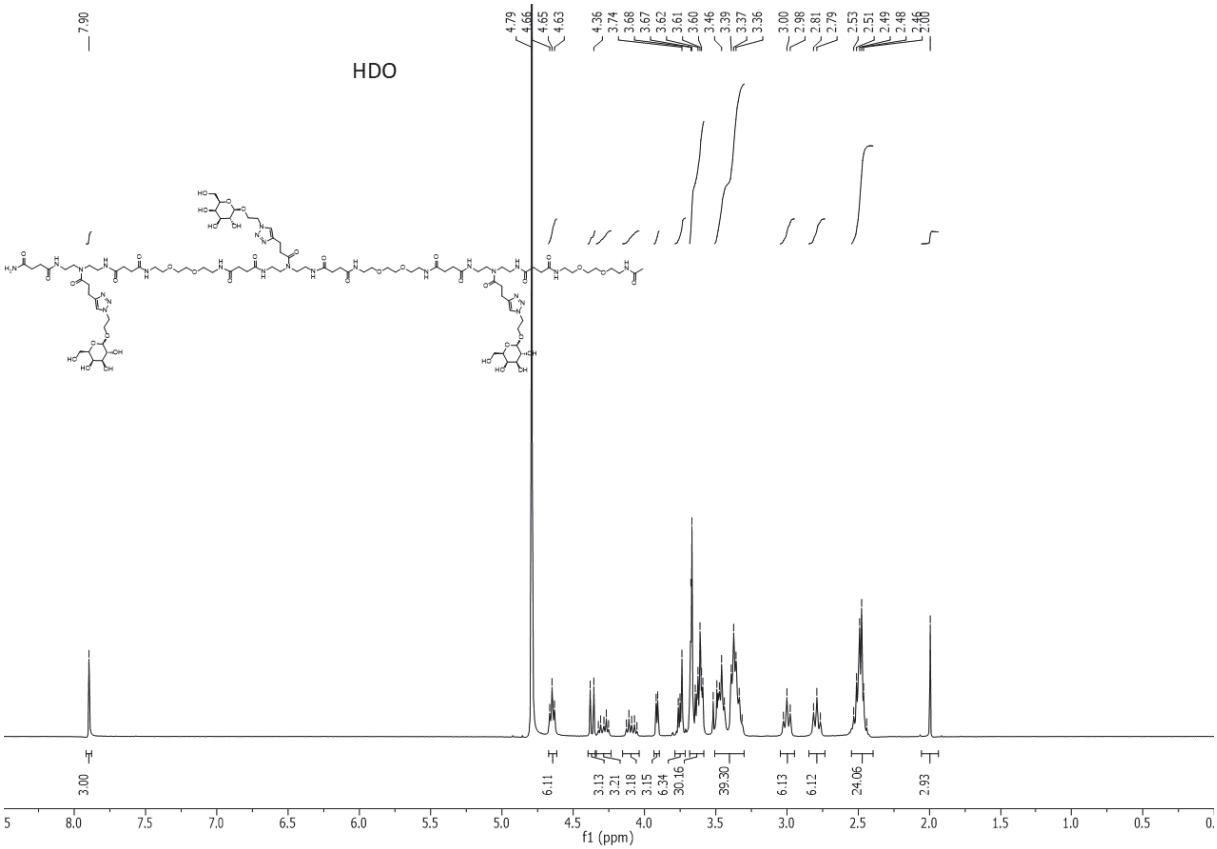

Figure S 14: ^{1}H-NMR spectrum of compound **2.**

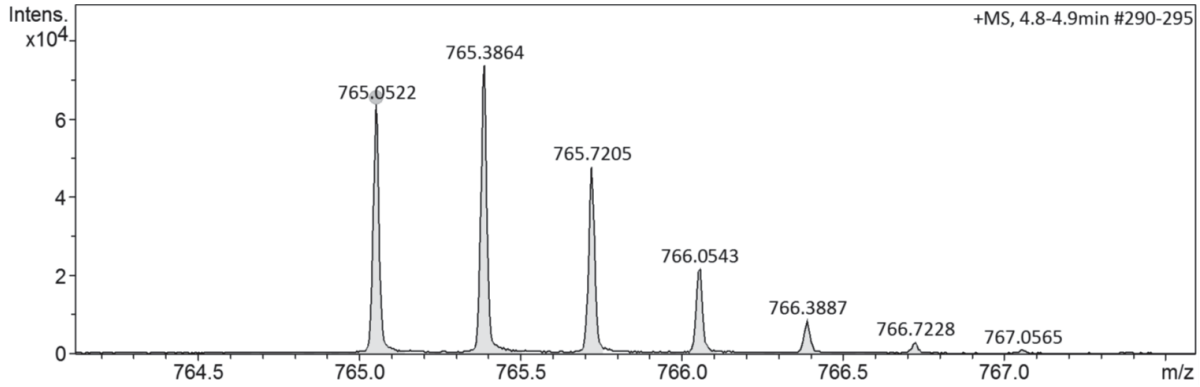

Figure S 15: HR-MS spectrum of compound **2**.

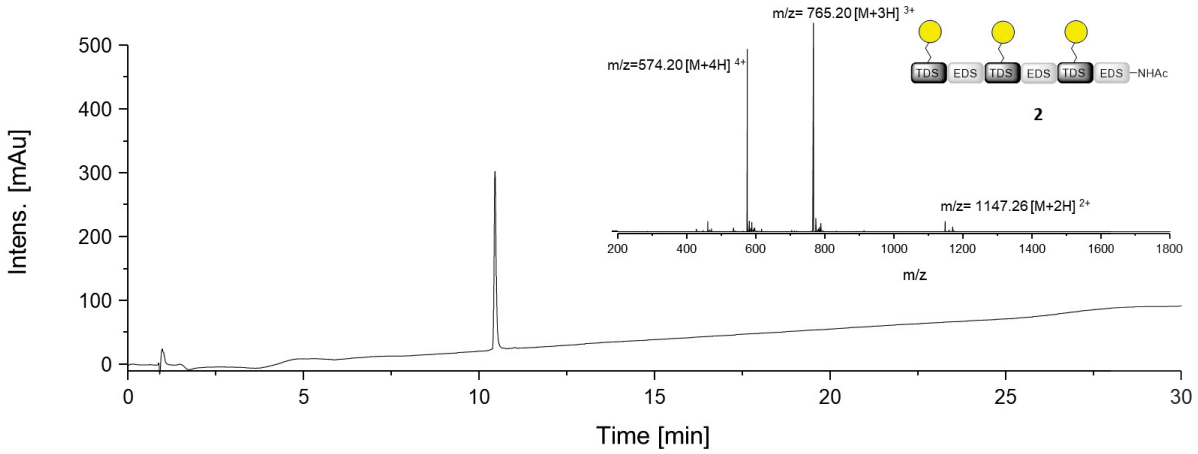

Figure S 16: RP-HPLC and ESI-MS spectrum of compound **2**.

3.3 Gal(1,2,3)-4, **3**

^{1}H-NMR (300 MHz, D_2O) δ [ppm] 7.89 (s, 3H, triazole-C*H*), 4.64 (t, J = 4.7 Hz, 6H, -N-N-CH_2-), 4.37 (d, J = 7.8 Hz, 3H, CH_{anomer}Gal), 4.28 (dt, J = 9.9, 4.7 Hz, 3H, -C$H_{pyranose}$), 4.09 (dt, J = 10.8, 5.0 Hz, 3H, -C$H_{pyranose}$), 3.91 (d, J = 3.0 Hz, 3H, -C$H_{pyranose}$), 3.81 – 3.71 (m, 6H, -C$H_{pyranose}$), 3.70 – 3.58 (m, 15H, C$H_{pyranose}$, O-CH_2-), 3.53 – 3.29 (m, 30H, C$H_{pyranose,}$ C=ONH-CH_2), 3.04 – 2.92 (m, 6H, CH=C-CH_2), 2.78 (t, J = 7.0 Hz, 6H, CH=C-CH$_2$-CH_2), 2.53-2.42 (m, 16H, -N-C=O-CH_2-), 1.99 (s, 3H, -CH_3). HR-MS (ESI) calc. for $C_{75}H_{128}N_{21}O_{32}$ $[M+3H]^{3+}$ 611.6339; found 611.6340. Yield: 90 mg (49 %).

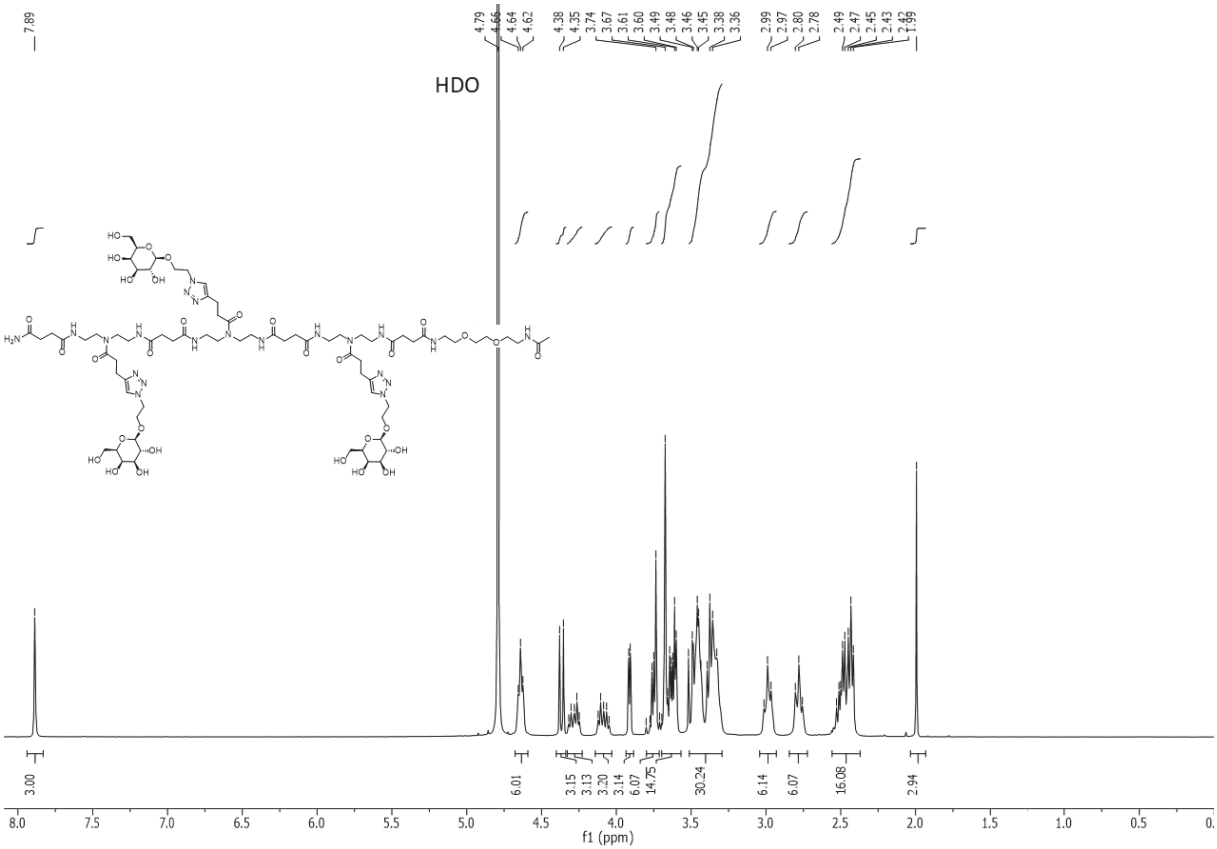

Figure S 17: ^{1}H-NMR spectrum of compound **3.**

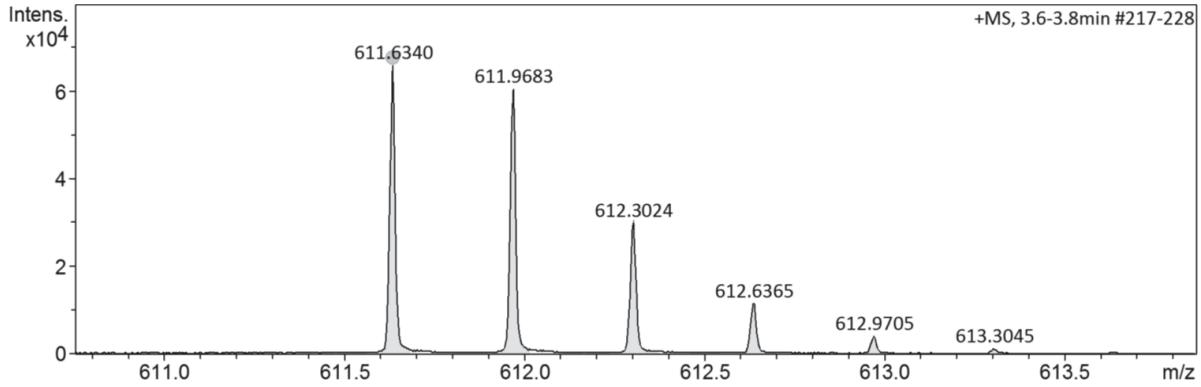

Figure S 18: HR-MS spectrum of compound **3**.

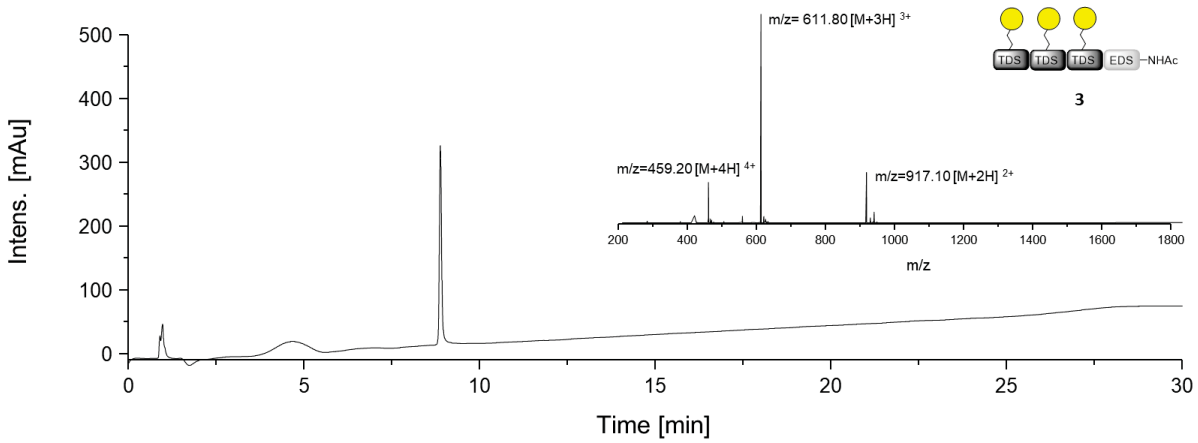

Figure S 19: RP-HPLC and ESI-MS spectrum of compound **3**.

3.4 Lac(1)-2, **4**

^{1}H NMR (300 MHz, Deuterium Oxide) δ [ppm]: 8.05 (s, 1 H, triazole-C*H*), 5.75 (d, J = 9.2 Hz, 1H, CH_{anomer}Glc), 4.52 (d, J = 7.7 Hz, 1H, C$H_{pyranose}$, O-CH_2-), 4.10 – 3.73 (m, 10H, C$H_{pyranose}$, O-CH_2-), 3.72 – 3.57 (m, 10H,), 3.47-3.31 (m 12 H, C=ONH-CH_2), 3.05 (t, J = 7.1 Hz, 2 H, CH=CH-CH_2), 2.82 (t, J = 7.0 Hz, 2 H, CH=CH-CH$_2$-CH_2), 2.58 – 2.43 (m, 8 H, NHC=O-CH_2) , 2.00 (s, 3 H, -CH_3). HR-MS (ESI) calc. for $C_{37}H_{65}N_9O_{18}$ $[M+2H]^{2+}$ 461.7218; found 461.7217. Yield: 51 mg (55 %).

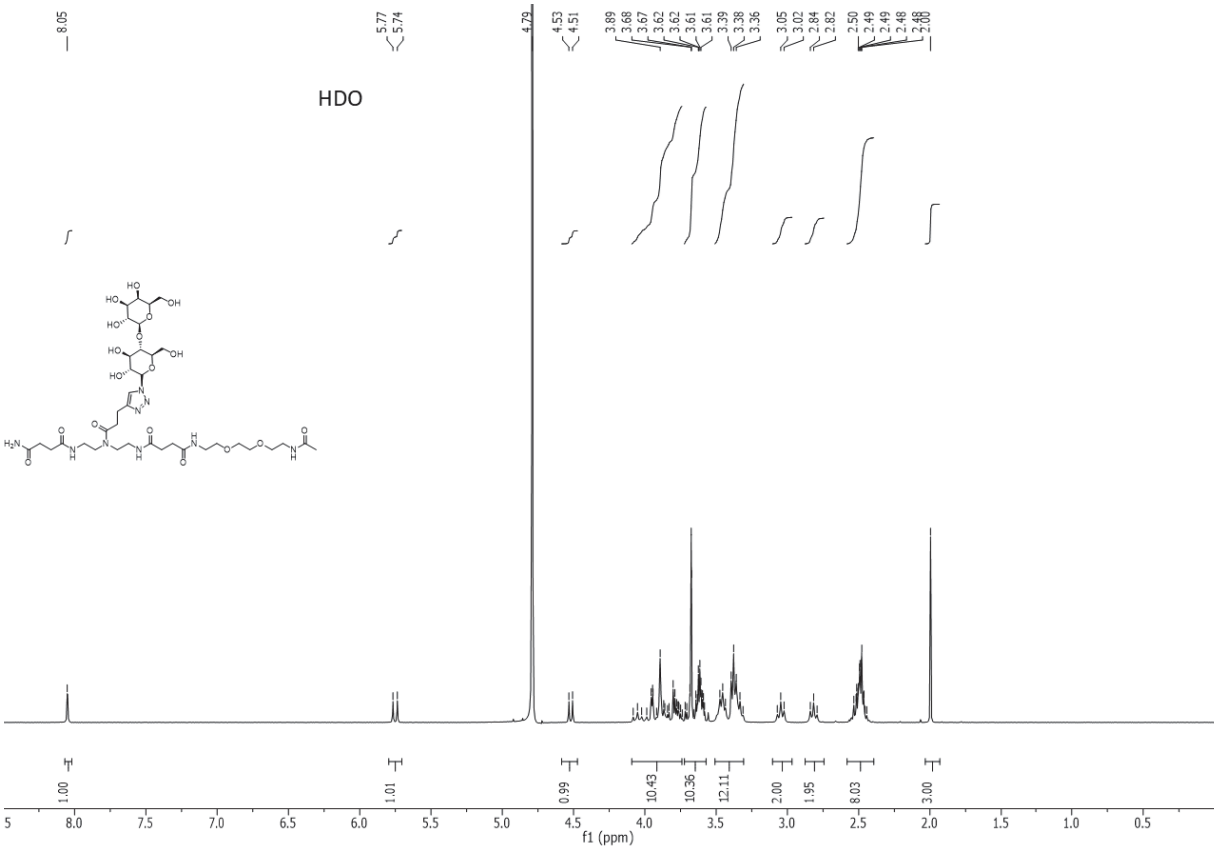

Figure S 20: ^{1}H-NMR spectrum of compound **4.**

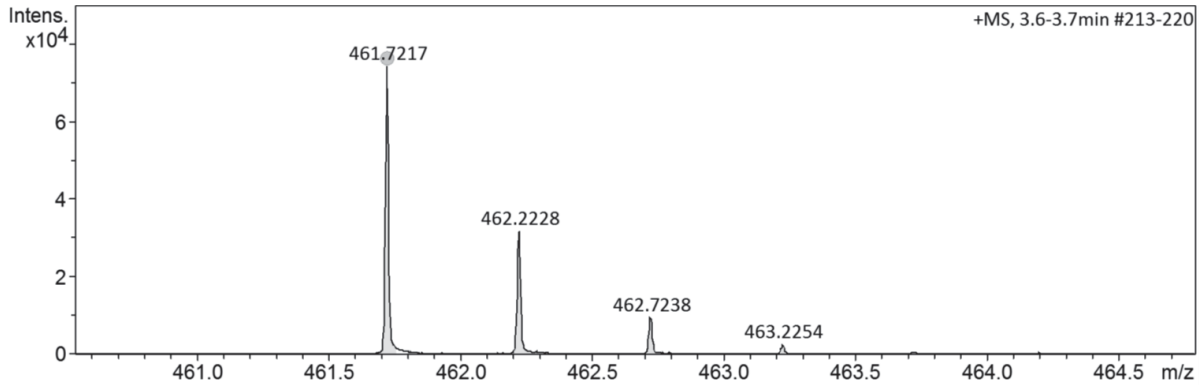

Figure S 21: HR-MS spectrum of compound **4**.

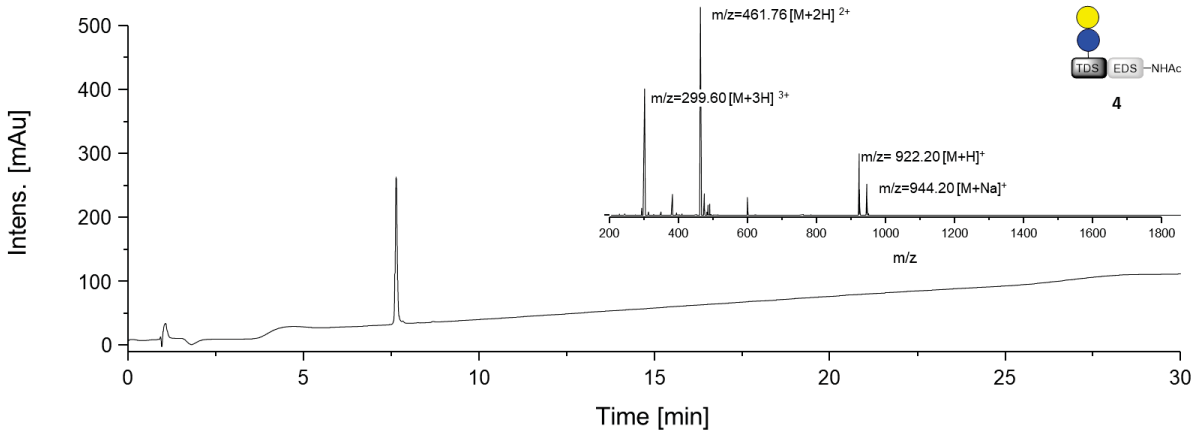

Figure S 22: RP-HPLC and ESI-MS spectrum of compound **4**.

3.5 Lac(1)-2, **4***

^{1}H-NMR (600 MHz, Deuterium Oxide) δ [ppm]: 8.44 (br s, 1H, NH), 8.03 (m, 1H, triazole-C*H*), 5.74 (d, ^{3}J = 9.3 Hz,1H, CH_{anomer}Glc), 4.50 (d, ^{3}J = 7.8 Hz, 1H, CH_{anomer}-Gal), 4.03 (t, ^{3}J = 9.0 Hz, 1H, CH_{pyranose}), 3.97 – 3.55 (m, 19H, O-CH_2-, CH_{pyranose}), 3.45 (m, 4H, C=ONH-CH_2), 3.36 (m, 4H, C=ONH-CH_2), 3.32 (t, 3J = 6.1 Hz, 2H, C=ONH-CH_2), 3.20 (m, 2H, CH_2-NH$_2$), 3.03 (t, ^{3}J = 7.1 Hz, 2H, CH=CH-CH_2), 2.80 (t, ^{3}J = 7.2 Hz, 2H, CH=CH-CH$_2$-CH_2), 2.47 (m, 8H, NHC=O-CH_2). HR-MS (ESI) calc. for $C_{35}H_{63}N_9O_{17}$ $[M+2H]^{2+}$ 440.72; found 440.72. Yield: 48 mg (54 %).

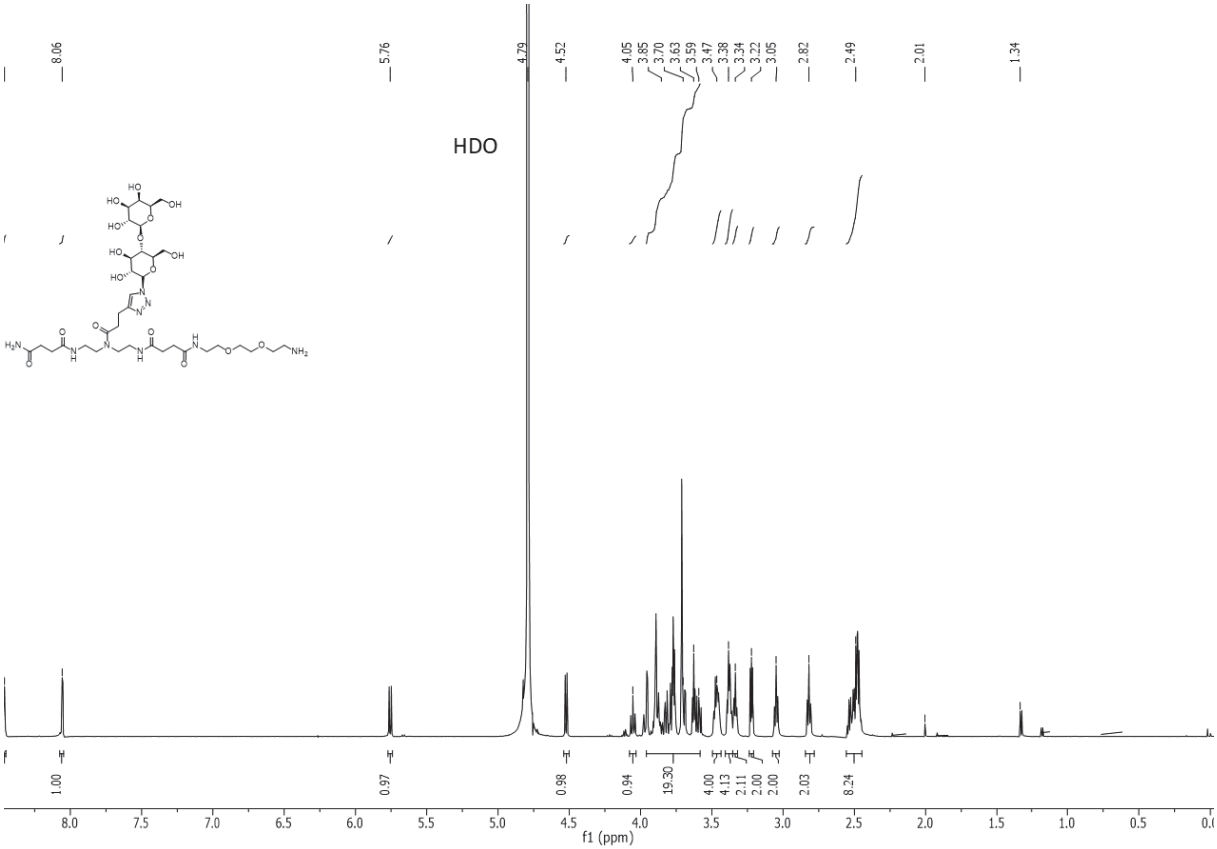

Figure S 23: ^{1}H-NMR spectrum of compound **4*.**

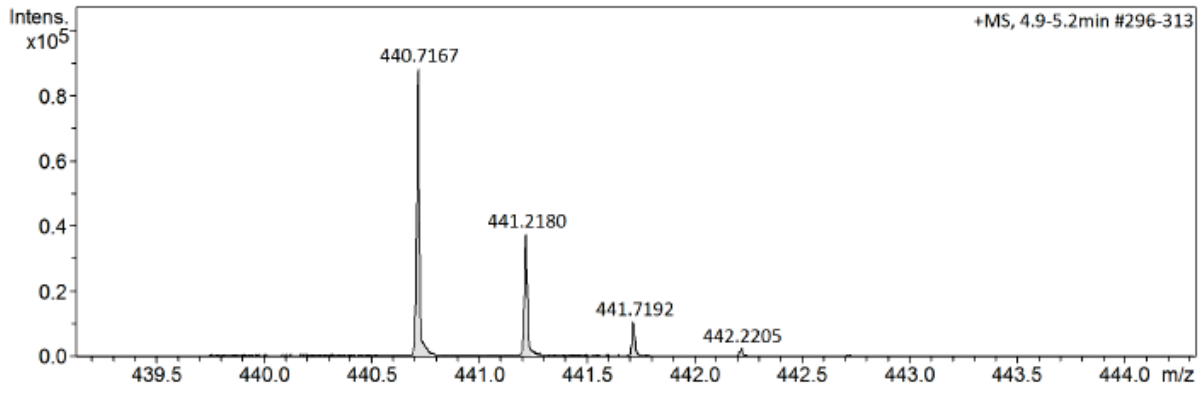

Figure S 24: HR-MS spectrum of compound **4***.

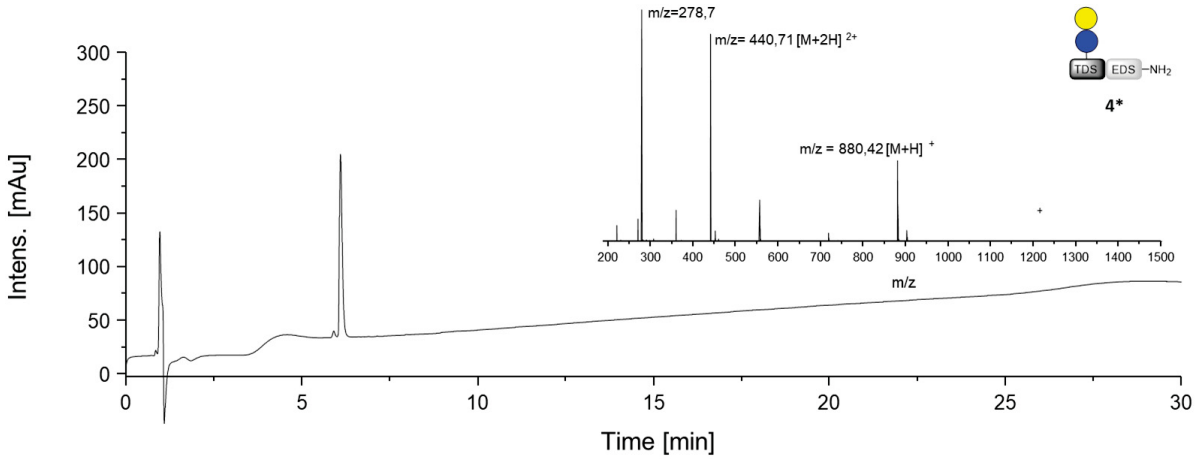

Figure S 25:RP-HPLC and ESI-MS spectrum of compound **4***.

3.6 Lac(2)-3, **5**

^{1}H-NMR (300 MHz, Deuterium Oxide) δ [ppm]: 8.05 (s, 1H, triazole-C*H*); 5.75 (d, ^{3}J = 9.2 Hz, 1H, C*H*$_{\text{anomer}}$Glc), 4.52 (d, ^{3}J = 7.7 Hz, 1H, C*H*$_{anomer}$-Gal), 4.09-3.92 (m, 3H, C*H*$_{\text{pyranose}}$), 3.93-3.82 (m, 4H, C*H*$_{\text{pyranose}}$), 3.81-3.73 (m, 3H, C*H*$_{\text{pyranose}}$), 3.72-3.54 (m, 18H, C*H*$_{\text{pyranose}}$, C*H*$_{2}$ $_{\text{pyranose,}}$ O-C*H*$_{2}$-), 3.51-3.28 (m, 16H, C*H*$_{\text{pyranose,}}$ C=ONH-C*H*$_{2}$), 3.04 (t, ^{3}J = 7.1 Hz, 2H, CH=CH-C*H*$_{2}$), 2.81 (t, ^{3}J = 7.1 Hz, 2H, CH=CH-CH$_{2}$-C*H*$_{2}$), 2.57-2.45 (m, 12H, NHC=O-C*H*$_{2}$), 1.99 (s, 3H, C*H*$_{3}$). HR-MS (ESI): m/z calc. for $C_{47}H_{83}N_{11}O_{22}$ $[M+2H]^{2+}$ 576.7852; found 576.7847. Yield: 267.1 mg (66 %).

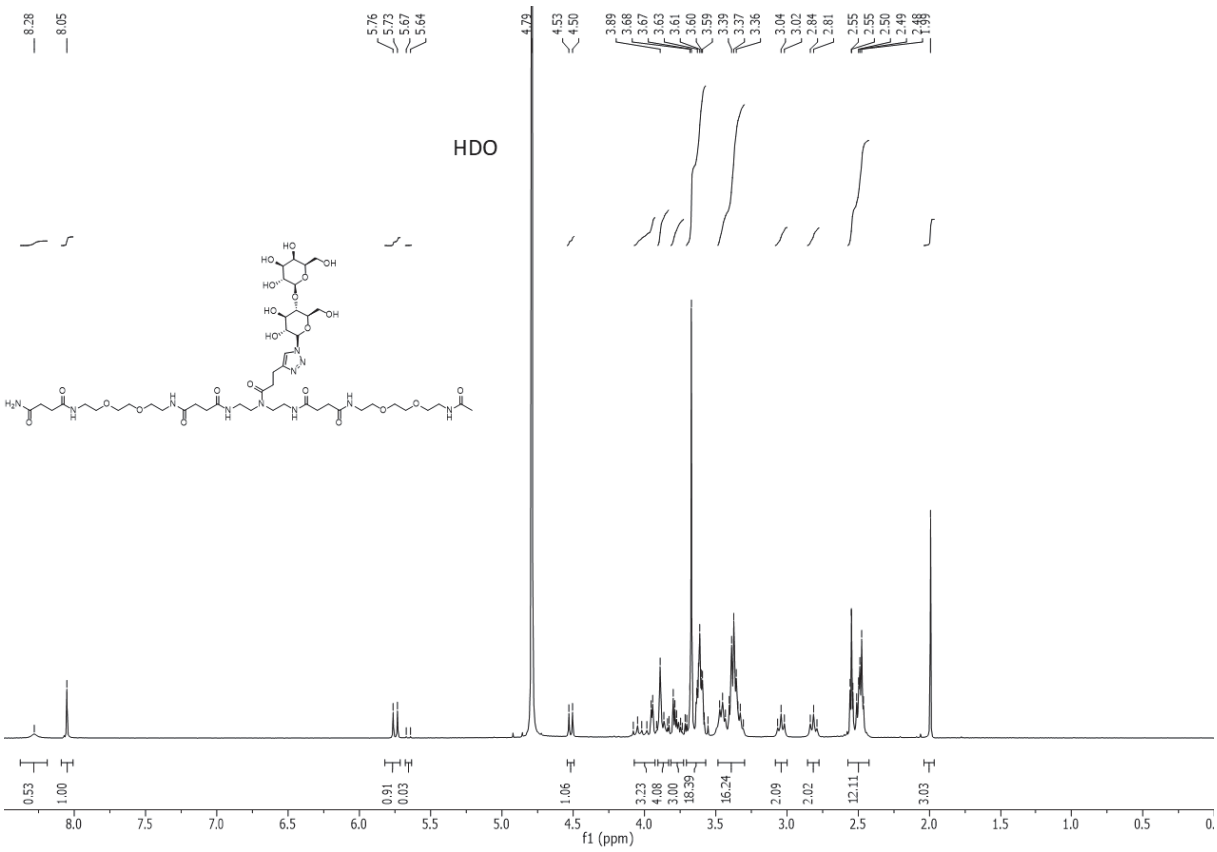

Figure S 26: ^{1}H-NMR spectrum of compound **5**.

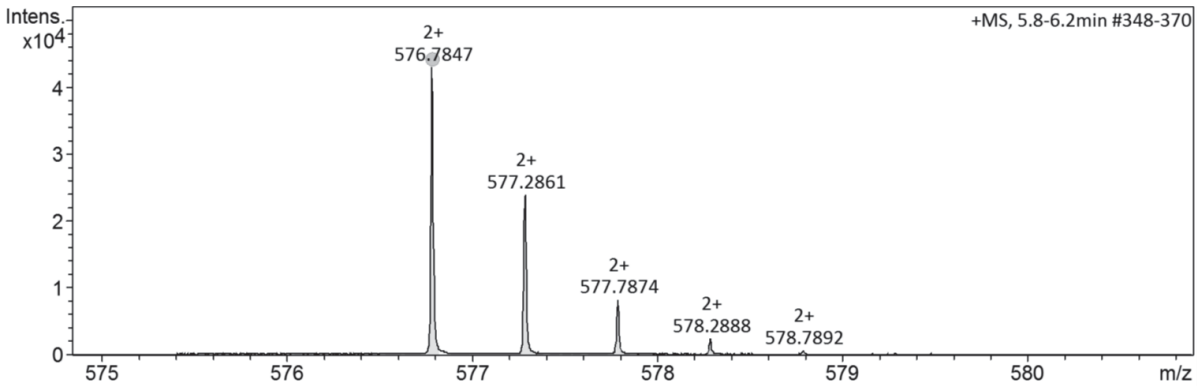

Figure S 27: HR-MS spectrum of compound **5**.

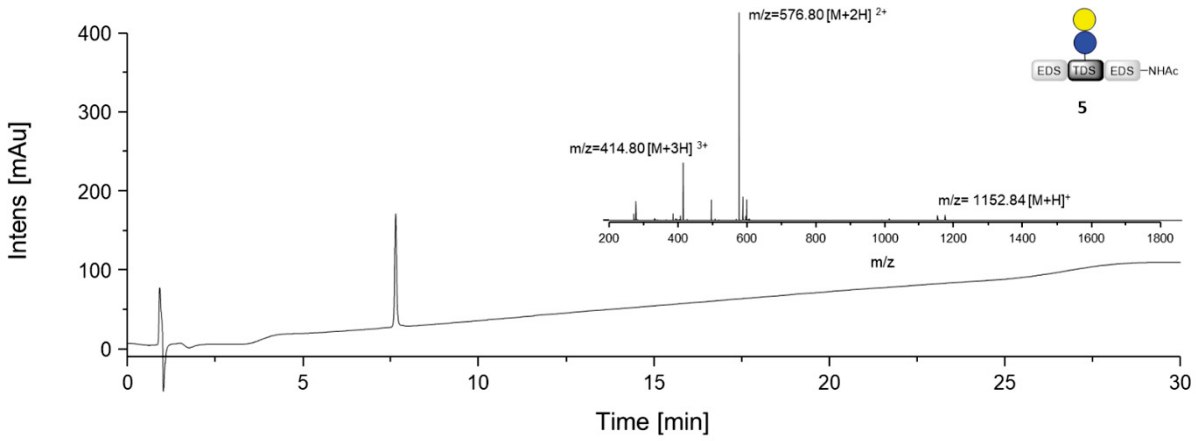

Figure S 28: RP-HPLC and ESI-MS spectrum of compound **5**.

3.7 Lac(1,5)-5, **6**

^{1}H-NMR (300 MHz, Deuterium Oxide) δ [ppm]: 8.05 (s, 2H, triazole-C*H*), 5.75 (d, 2H, ^{3}J = 9.1 Hz, C*H*$_{anomer}$Glc), 4.52 (d, ^{3}J = 7.7 Hz, 2H, C*H*$_{anomer}$-Gal), 4.10-3.73 (m, 18H, C*H*$_{pyranose}$), 3.72-3.54 (m, 30H, C*H*$_{pyranose}$, C*H*$_{2\ pyranose,}$ O-C*H*$_2$-), 3.51-3.29 (m, 28H, C*H*$_{pyranose}$ C=ONH-C*H*$_2$), 3.04 (t, ^{3}J = 7.1 Hz, 4H, CH=CH-C*H*$_2$), 2.81 (t, ^{3}J = 6.5 Hz, 4H, CH=CH-CH$_2$-C*H*$_2$), 2.56-2.44 (m, 20H, NHC=O-C*H*$_2$), 1.94 (s, 1,5H, C*H*$_3$), 1.92 (s, 1,5H, C*H*$_3$). HR-MS (ESI): m/z calc. for $C_{82}H_{142}N_{19}O_{39}$ $[M+3H]^{3+}$ 672.3232; found: 672.3225. Yield: 145.0 mg (28 %).

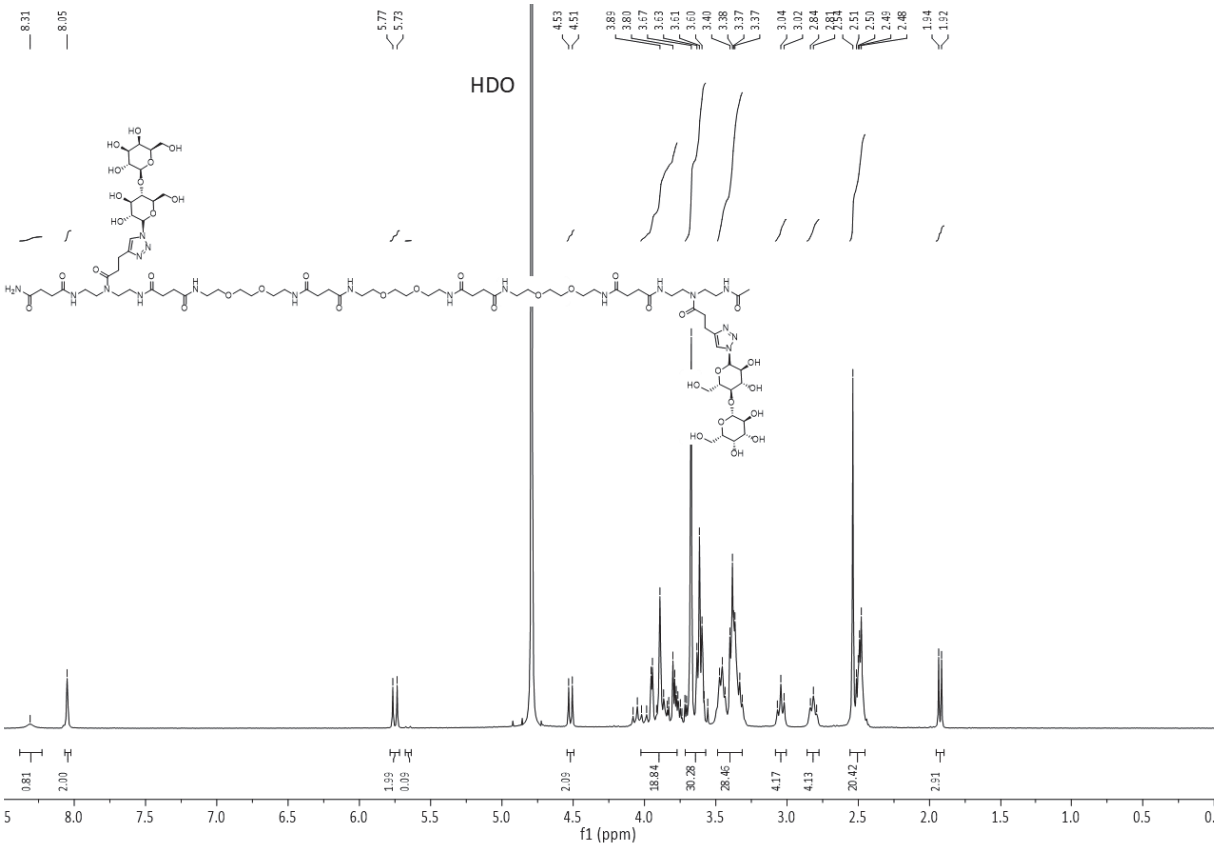

Figure S 29: ^{1}H-NMR spectrum of compound **6**.

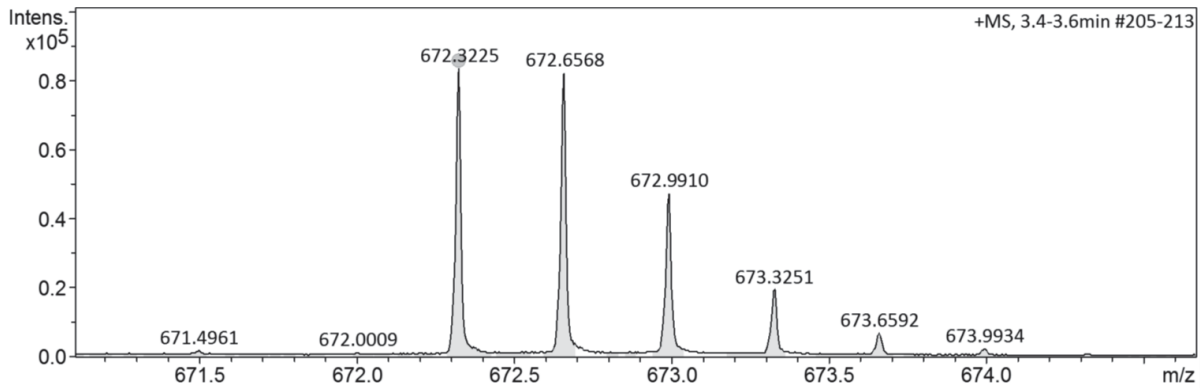

Figure S 30: HR-MS spectrum of compound **6**.

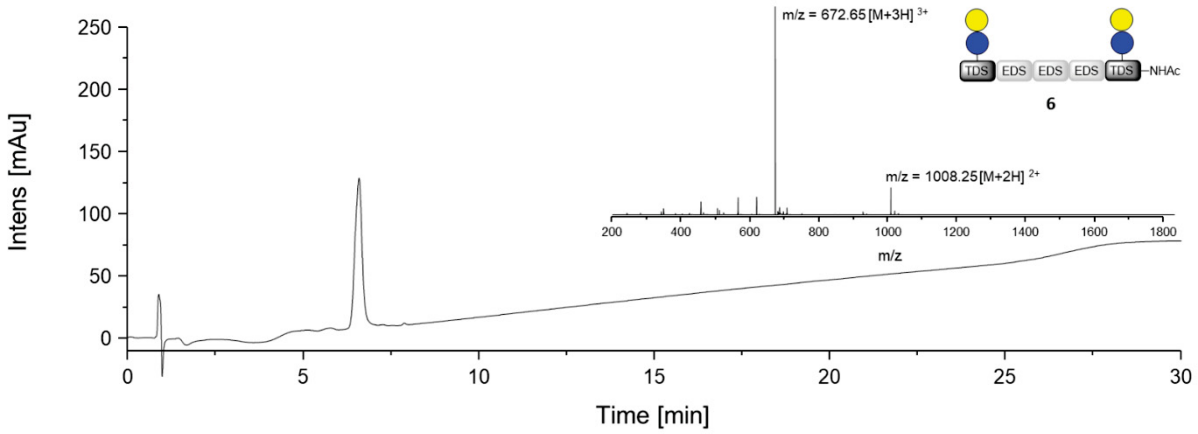

Figure S 31: RP-HPLC and ESI-MS spectrum of compound **6**.

3.8 Lac(1,5,9)-9, **7**

^{1}H-NMR (300 MHz, Deuterium Oxide) δ [ppm]: 8.05 (s, 3H, triazole-C*H*), 5.75 (d, ^{3}J = 9.2 Hz, 3H, C*H*$_{\text{anomer}}$Glc), 4.52 (d, 3H, 3J = 7.7 Hz, C*H*$_{anomer}$-Gal), 4.10-3.92 (m, 8H, C*H*$_{\text{pyranose}}$), 3.92-3.82 (m, 14 H, C*H*$_{\text{pyranose}}$), 3.82-3.73 (m, 6H, C*H*$_{\text{pyranose}}$), 3.72-3.55 (m, 54H, C*H*$_{\text{pyranose}}$, C*H*$_{2\ \text{pyranose,}}$ O-C*H*$_2$-), 3.51-3.28 (m, 50H, C*H*$_{\text{pyranose,}}$ C=ONH-C*H*$_2$), 3.04 (t, ^{3}J = 7.0 Hz, 6H, CH=CH-C*H*$_2$), 2.81 (t, ^{3}J = 7.0 Hz, 6H, CH=CH-CH$_2$-C*H*$_2$), 2.57-2.42 (m, 36H, NHC=O-C*H*$_2$), 1.94 (s, 1,5H, C*H*$_3$), 1.92 (s, 1,5H, C*H*$_3$). HR-MS (ESI): m/z calc. for $C_{137}H_{237}N_{31}O_{64}$ $[M+4H]^{4+}$ 835.1555; found 835.1562. Yield: 76 mg (32 %).

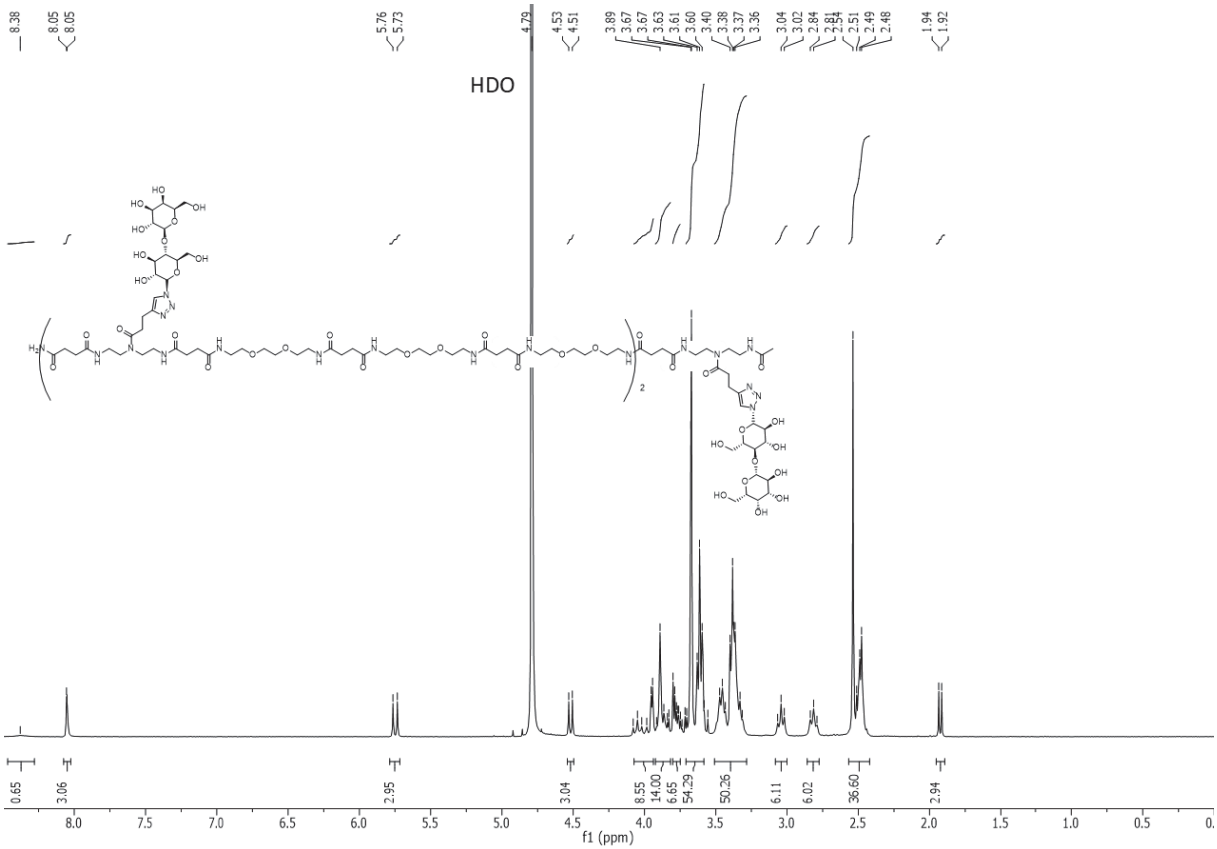

Figure S 32: ^{1}H-NMR spectrum of compound **7.**

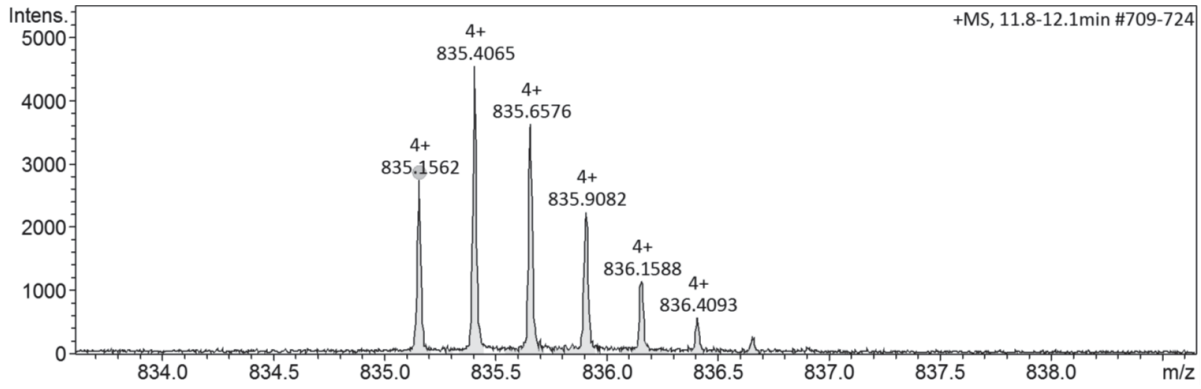

Figure S 33: HR-MS spectrum of compound **7**.

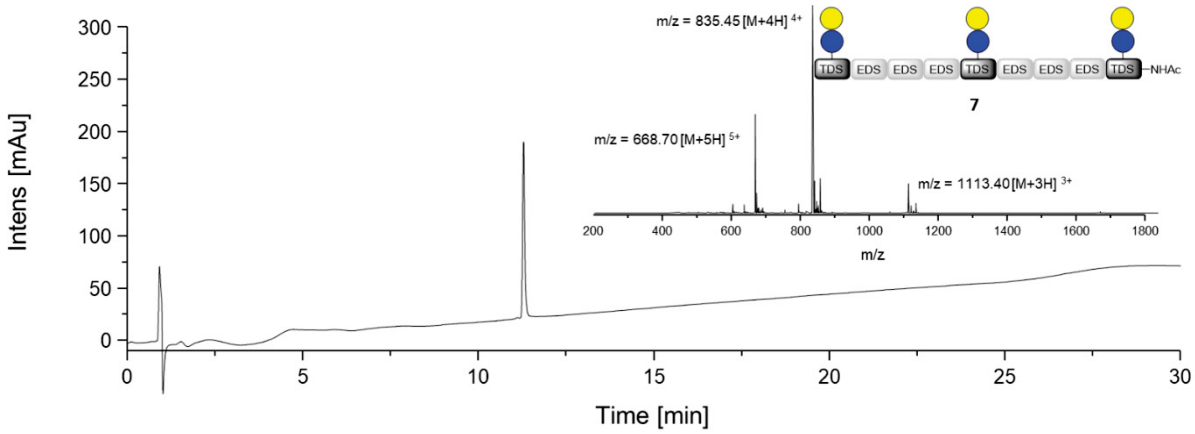

Figure S 34: RP-HPLC and ESI-MS spectrum of compound **7**.

3.9 Lac(1,4,7)-8, **8**

^{1}H-NMR (300 MHz Deuterium Oxide) δ [ppm]: 8.05 (s, 3H, triazole-C*H*), 5.75 (d, ^{3}J = 9.2 Hz, 3H, C*H*$_{anomer}$Glc), 4.52 (d, ^{3}J = 7.6 Hz, 3H, C*H*$_{anomer}$-Gal), 4.11 – 3.53 (m, 77H, C*H*$_{pyranose}$, C*H*$_{2\ pyranose,}$ O-C*H*$_{2}$-), 3.53 – 3.24 (m, 43H, C*H*$_{pyranose}$, C*H*$_{2\ pyranose,}$ C=ONH-C*H*$_{2}$), 3.04 (t, ^{3}J = 7.1 Hz, 6H, CH=CH-C*H*$_{2}$), 2.81 (t, ^{3}J = 7.1 Hz, 6H, CH=CH-CH$_{2}$-C*H*$_{2}$), 2.59 – 2.38 (m, 32H, NHC=O-C*H*$_{2}$), 1.99 (s, 3H, C*H*$_{3}$). HR-MS (ESI) calc. for $C_{127}H_{219}N_{29}O_{60}$ $[M+4H]^{4+}$ 777.6239; found 777.6229. Yield: 107 mg (35 %).

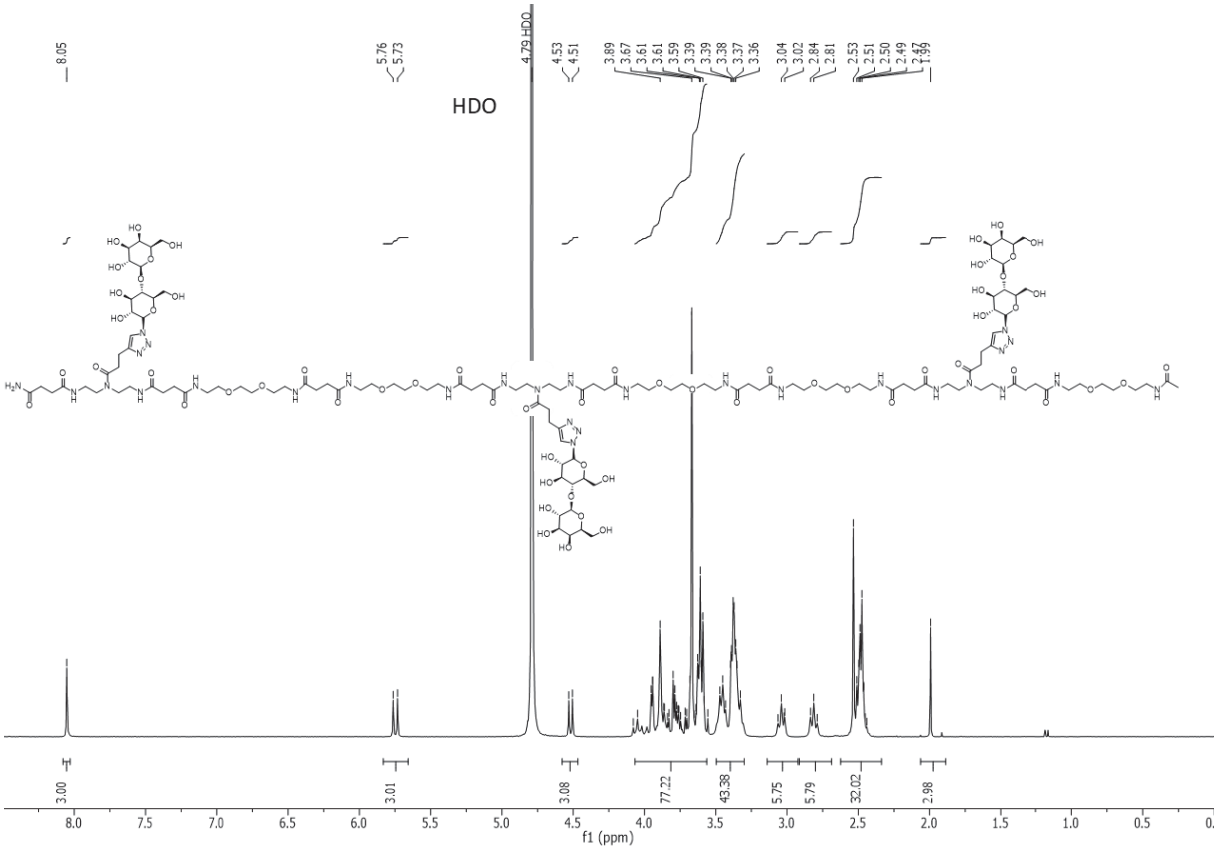

Figure S 35: ^{1}H-NMR spectrum of compound **8.**

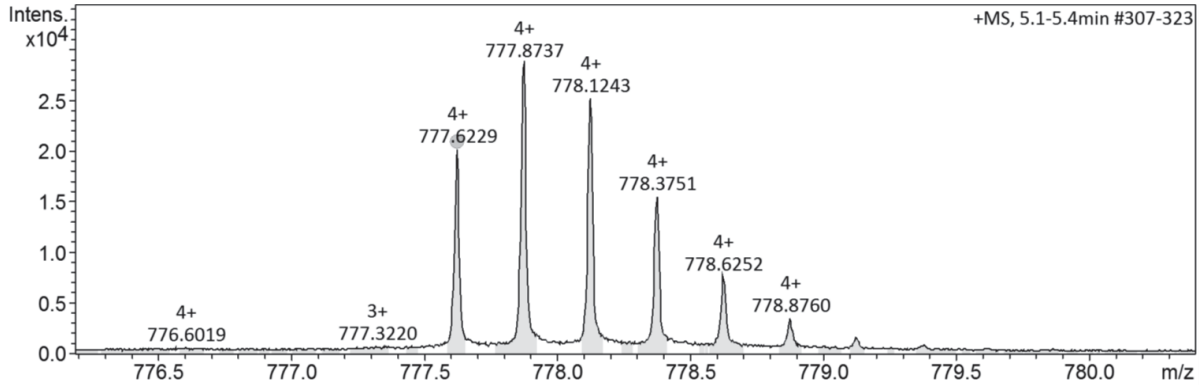

Figure S 36: HR-MS spectrum of compound **8**.

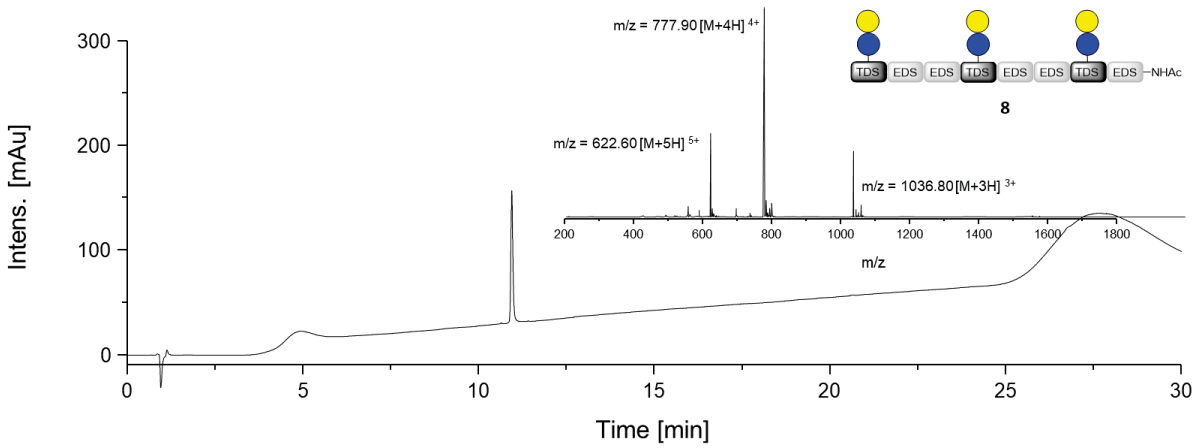

Figure S 37: RP-HPLC and ESI-MS spectrum of compound **8**.

3.10 Lac(1,3,5)-6, **9**

^{1}H-NMR (300 MHz, Deuterium Oxide) δ [ppm]: 8.05 (s, 3H, triazole-C*H*), 5.75 (d, ^{3}J = 9.2 Hz, 3H, C*H*$_{anomer}$Glc), 4.52 (d, ^{3}J = 7.7 Hz, 3H, C*H*$_{anomer}$-Gal), 4.09 – 3.73 (m, 30H, C*H*$_{pyranose}$, C*H*$_{2\ pyranose,}$ O-C*H*$_2$-), 3.73 – 3.55 (m, 30H, C*H*$_{pyranose}$, C*H*$_{2\ pyranose,}$ O-C*H*$_2$-), 3.53 – 3.26 (m, 36H, C*H*$_{pyranose}$, C=ONH-C*H*$_2$), 3.04 (t, ^{3}J = 7.1 Hz, 6H, CH=CH-C*H*$_2$), 2.81 (t, ^{3}J = 7.1 Hz, 6H, CH=CH-CH$_2$-C*H*$_2$), 2.60 – 2.38 (m, 24H, NHC=O-C*H*$_2$), 1.99 (s, 3H, C*H*$_3$). HR-MS (ESI) calc. for $C_{107}H_{182}N_{25}O_{52}$ $[M+3H]^{3+}$ 883.0783; found: 883.0787. Yield: 109 mg (41 %).

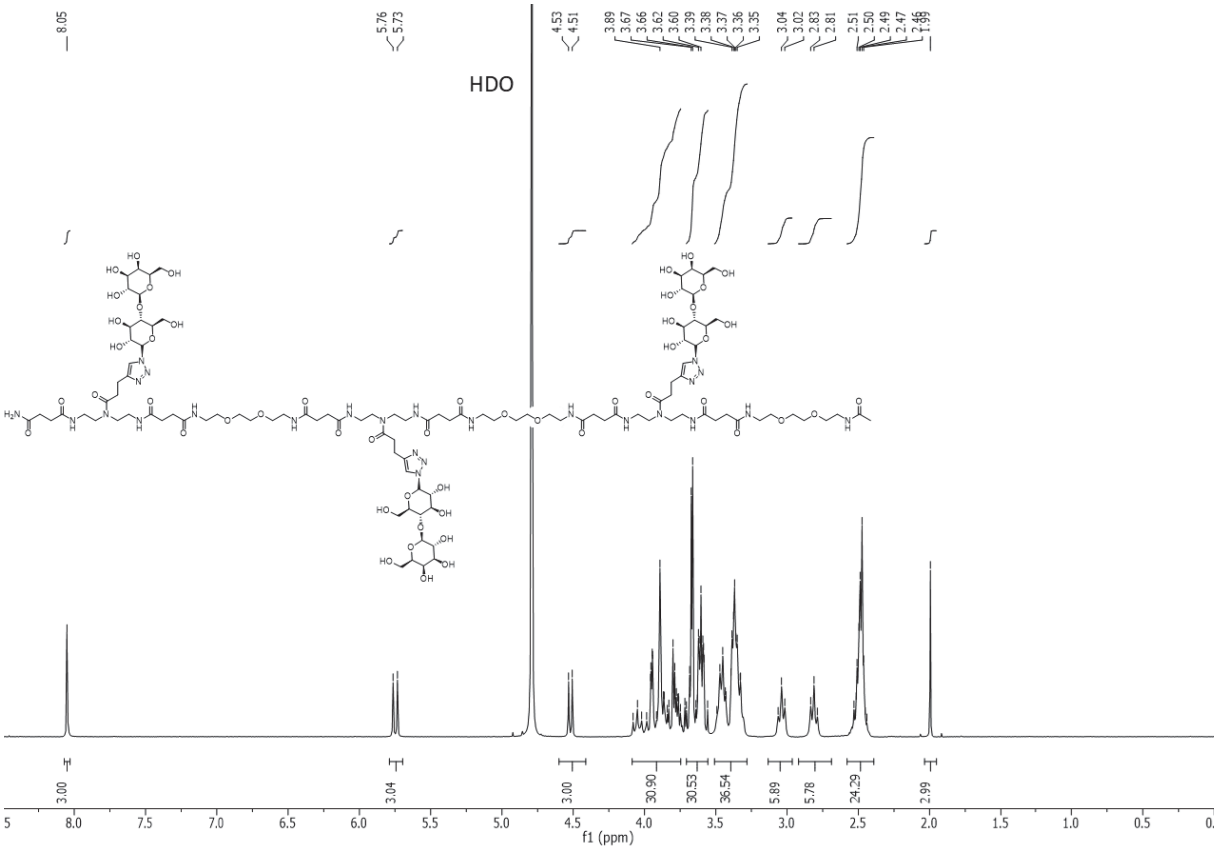

Figure S 38: ^{1}H-NMR spectrum of compound **9.**

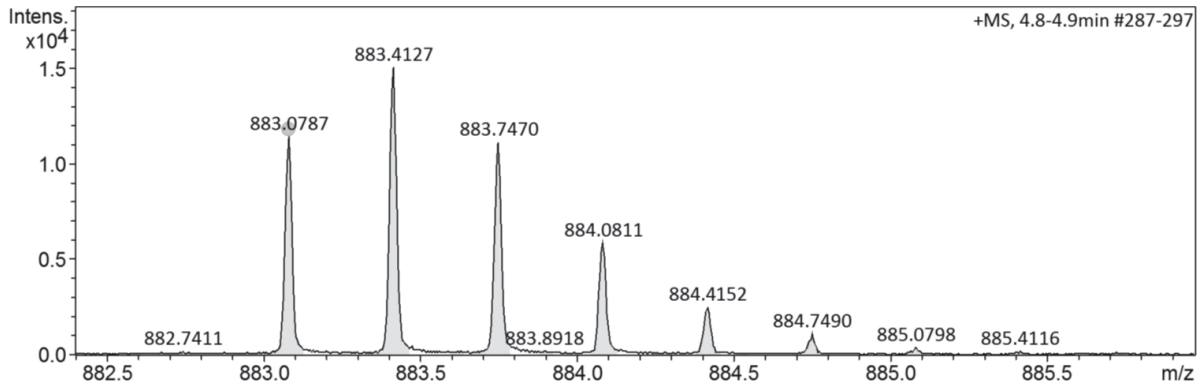

Figure S 39: HR-MS spectrum of compound **9**.

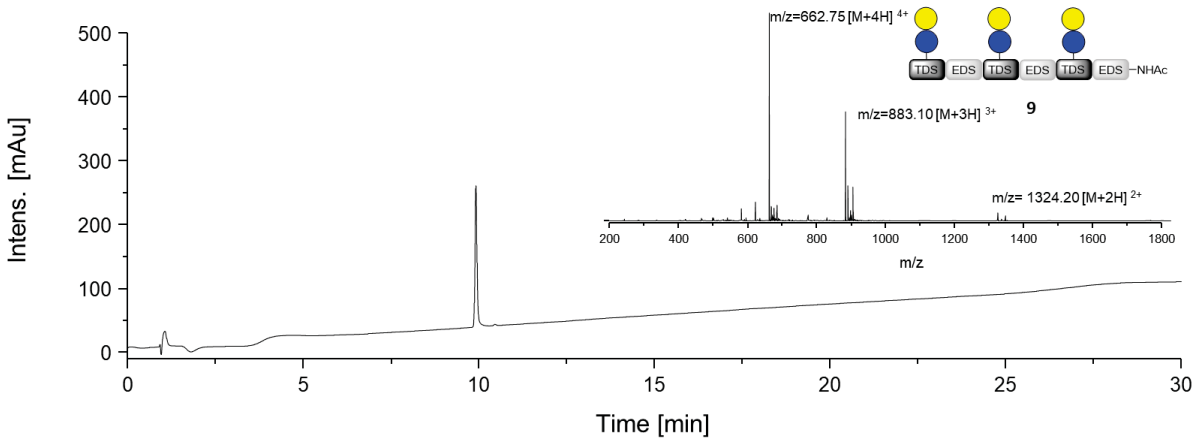

Figure S 40: RP-HPLC and ESI-MS spectrum of compound **9**.

3.11 Lac(1,3,5)-6, **9***

^{1}H-NMR (600 MHz, Deuterium Oxide) δ [ppm]: 8.43 (br s, 2 H, NH), 8.03 (m, 3H, triazole-C*H*), 5.73 (m, 3H, C*H*$_{\text{anomer}}$Glc), 4.50 (d, ^{3}J = 7.8 Hz, 3H, C*H*$_{anomer}$-Gal), 4.03 (t, ^{3}J = 9.1 Hz, 3H, C*H*$_{\text{pyranose}}$), 3.99 – 3.55 (m, 57H, C*H*$_{\text{pyranose}}$, C*H*$_{2\ \text{pyranose,}}$ O-C*H*$_2$-), 3.44 (m, 12 H, C=ONH-C*H*$_2$), 3.33 (m, 22H, C*H*$_{\text{pyranose,}}$ C=ONH-C*H*$_2$), 3.20 (t, ^{3}J = 5.1 Hz, 2 H, C*H*$_2$-NH$_2$), 3.02 (m, 6H, CH=CH-C*H*$_2$), 2.79 (m, 6H, CH=CH-CH$_2$-C*H*$_2$), 2.47 (m, 24 H, NHC=O-C*H*$_2$). HR-MS (ESI) calc. for $C_{105}H_{180}N_{25}O_{51}$ $[M+3H]^{3+}$ 869.07; found: 869.08. Yield: 103 mg (40 %).

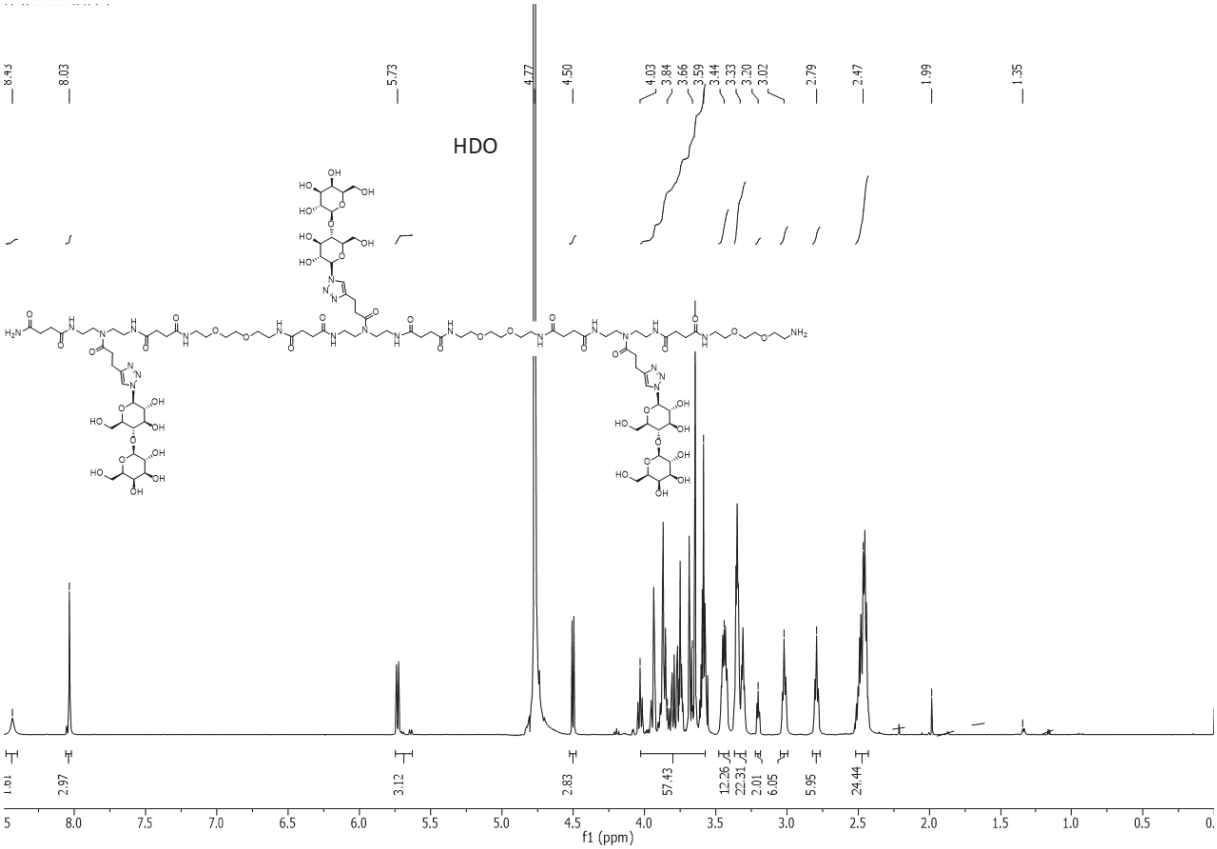

Figure S 41: ^{1}H-NMR spectrum of compound Lac(1,3,5)-6, **9*.**

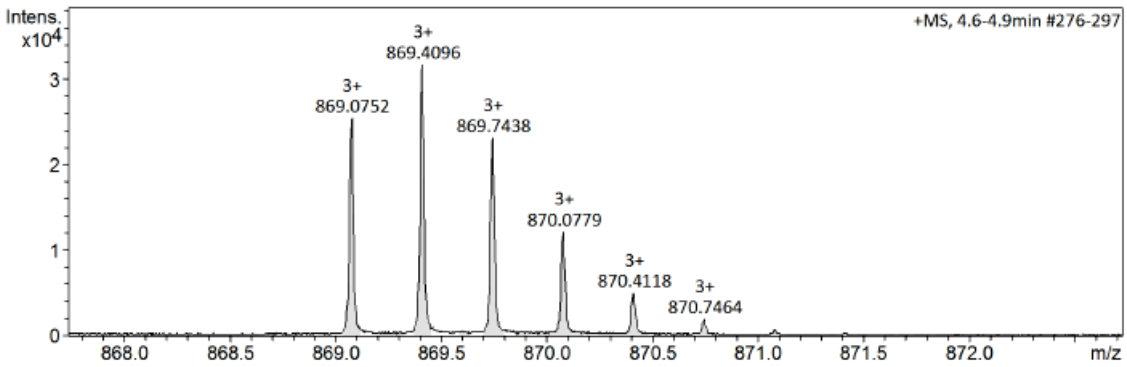

Figure S 42: HR-MS spectrum of compound **9***.

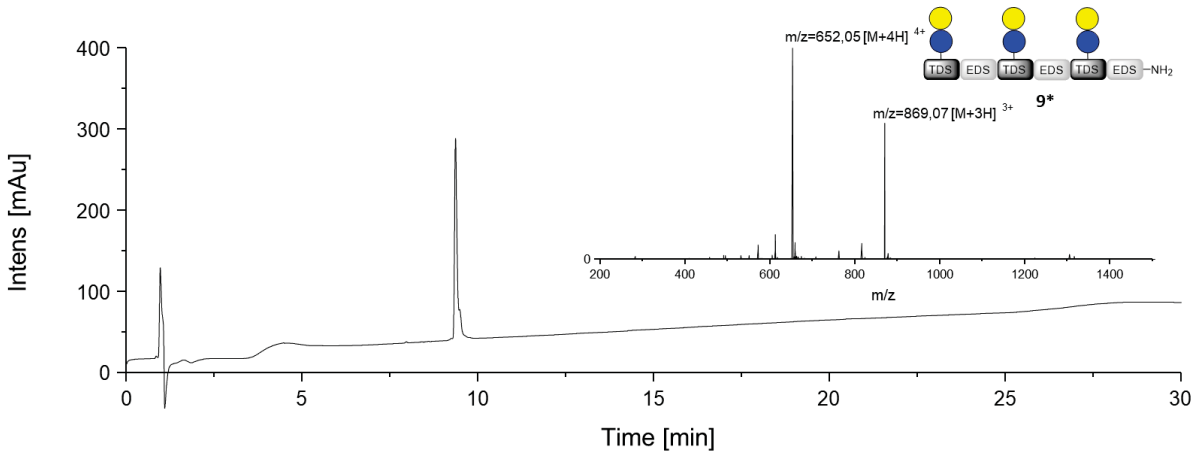

Figure S 43: RP-HPLC and ESI-MS spectrum of compound **9*.**

3.12 Lac(1,2,3)-4, **10**

^{1}H-NMR (300 MHz, Deuterium Oxide) δ [ppm]:8.12 – 7.97 (m, 3H, triazole-C*H*), 5.74 (d, ^{3}J = 9.2 Hz, 3H, C*H*$_{\text{anomer}}$Glc), 4.52 (d, ^{3}J = 7.6 Hz, 3H, C*H*$_{anomer}$-Gal), 4.10 – 3.53 (m, 44H, C*H*$_{\text{pyranose}}$, C*H*$_{2\ \text{pyranose}}$, O-C*H*$_{2}$-), 3.53 – 3.25 (m, 28H, C*H*$_{\text{pyranose}}$, C=ONH-C*H*$_{2}$), 3.12 – 2.93 (m, 6H, CH=CH-C*H*$_{2}$), 2.88 – 2.70 (m, 6H, CH=CH-CH$_{2}$-C*H*$_{2}$), 2.57 – 2.35 (m, 16H, NHC=O-C*H*$_{2}$), 1.99 (s, 3H, C*H*$_{3}$). HR-MS (ESI) calc. for $C_{87}H_{146}N_{21}O_{44}$ $[M+3H]^{3+}$ 729.6605; found 729.6606. Yield: 121 mg (55 %).

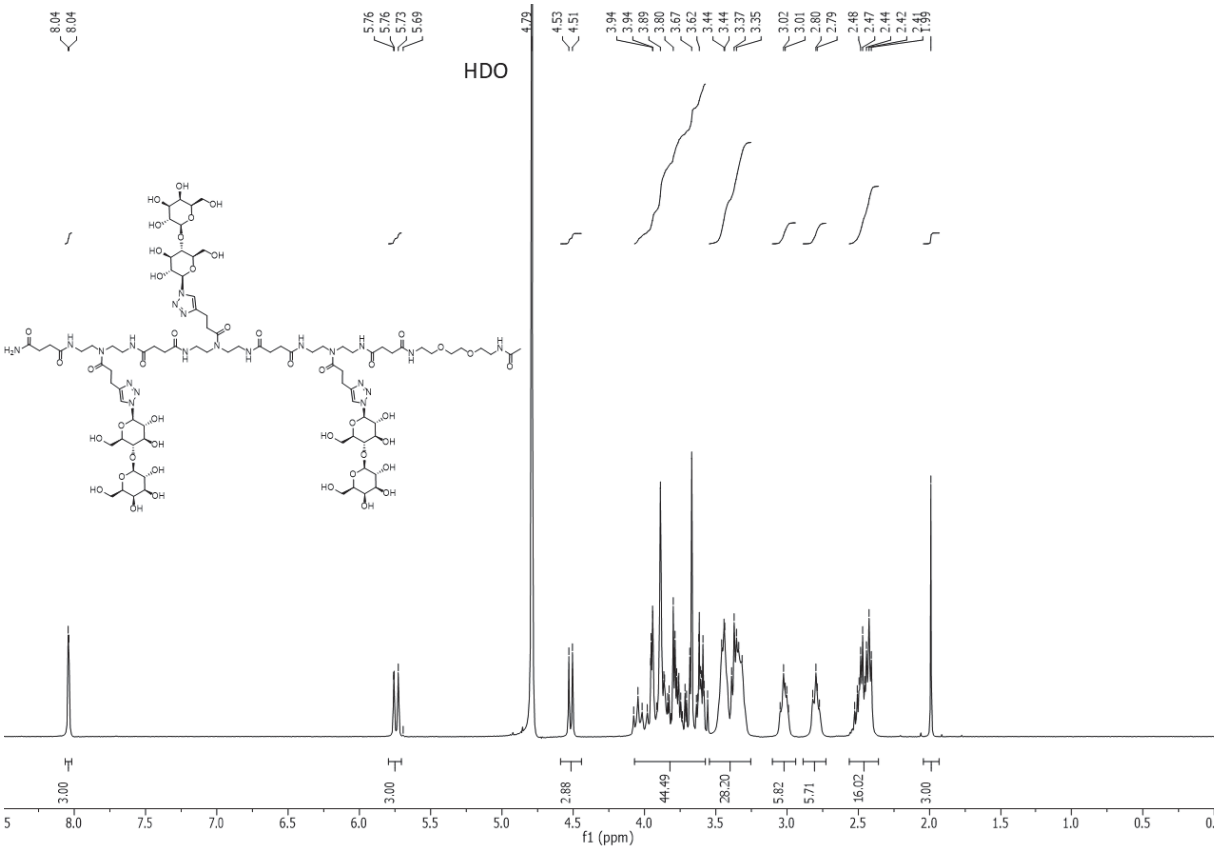

Figure S 44: ^{1}H-NMR spectrum of compound **10.**

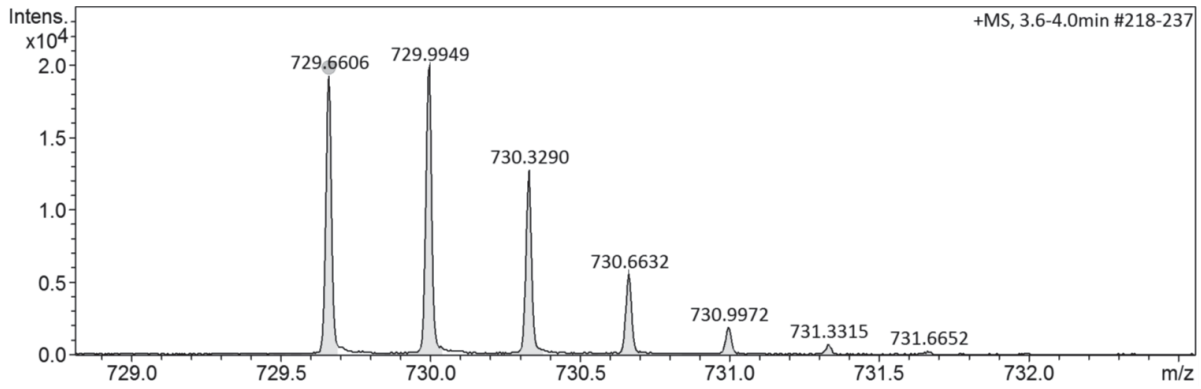

Figure S 45: HR-MS spectrum of compound **10**.

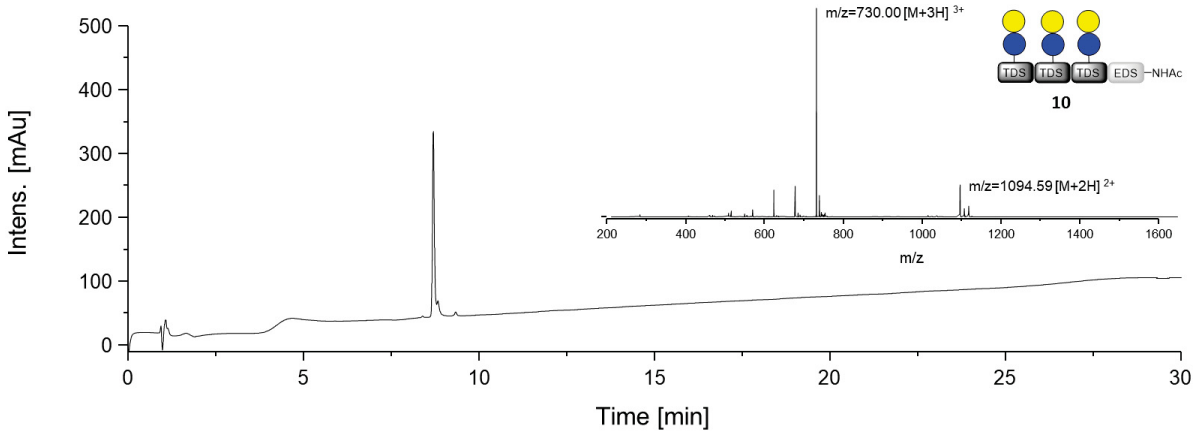

Figure S 46: RP-HPLC and ESI-MS spectrum of compound **10**.

3.13 Lac(1,2,3)-4, **10***

^{1}H-NMR (600 MHz, Deuterium Oxide) δ [ppm]: 8.45 (br s, 1H, NH), 8.02 (m, 3H, triazole-C*H*), 5.74 (m, 3H, C*H*$_{\text{anomer}}$Glc), 4.50 (d, ^{3}J = 7.8 Hz, 3H, C*H*$_{\textit{anomer}}$-Gal), 4.03 (m, 3 H, C*H*$_{\text{pyranose}}$), 3.96 – 3.55 (m, 41H, C*H*$_{\text{pyranose}}$, C*H*$_{2\ \text{pyranose}}$, O-C*H*$_2$-), 3.43 (m, 12H, C=ONH-C*H*$_2$), 3.33 (m, 14H, C=ONH-C*H*$_2$), 3.20 (m, 2H, C*H*$_2$-NH$_2$), 3.01 (m, 6H, CH=CH-C*H*$_2$), 2.78 (m, 6H, CH=CH-CH$_2$-C*H*$_2$), 2.45 (m, 16H, NHC=O-C*H*$_2$). HR-MS calc. for $C_{85}H_{144}N_{21}O_{43}$ $[M+3H]^{3+}$ 715.66; found: 715.66. Yield: 97 mg (45 %).

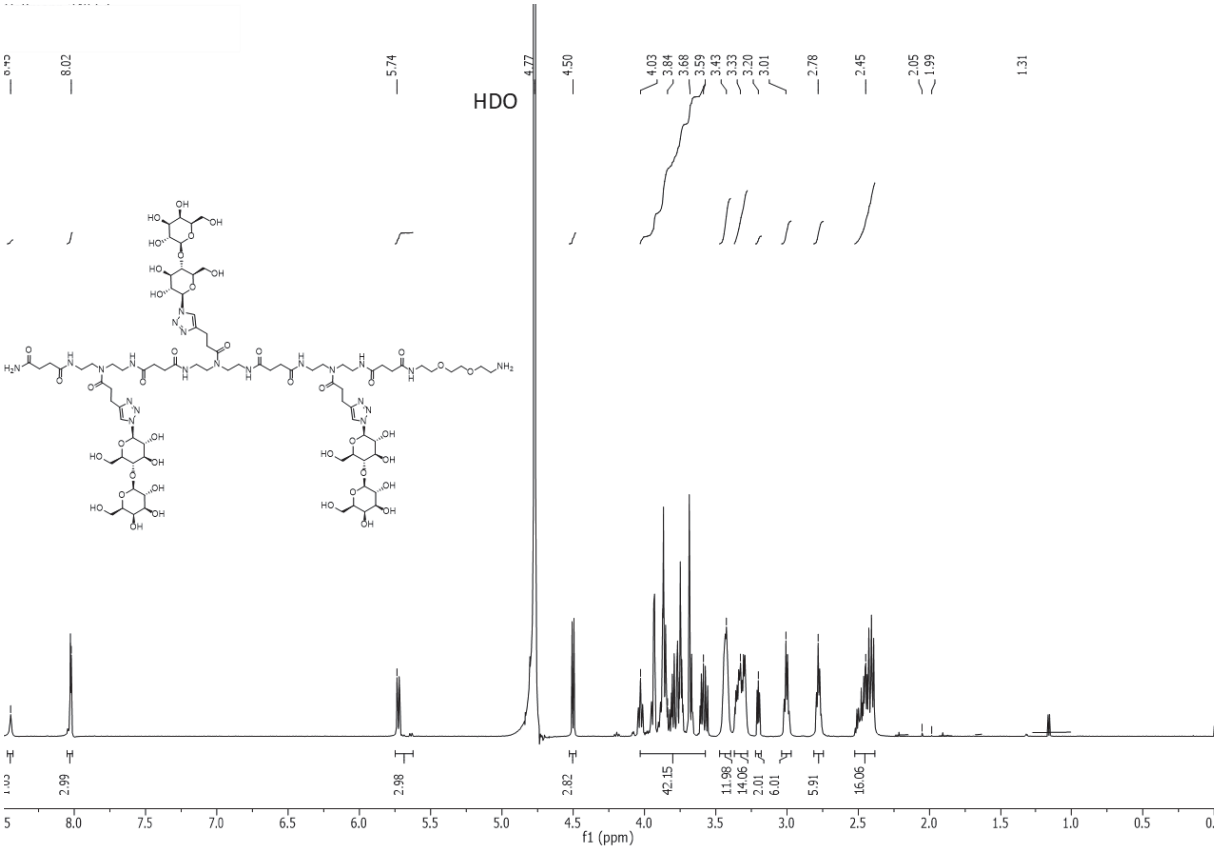

Figure S 47: ^{1}H-NMR spectrum of compound **10*.**

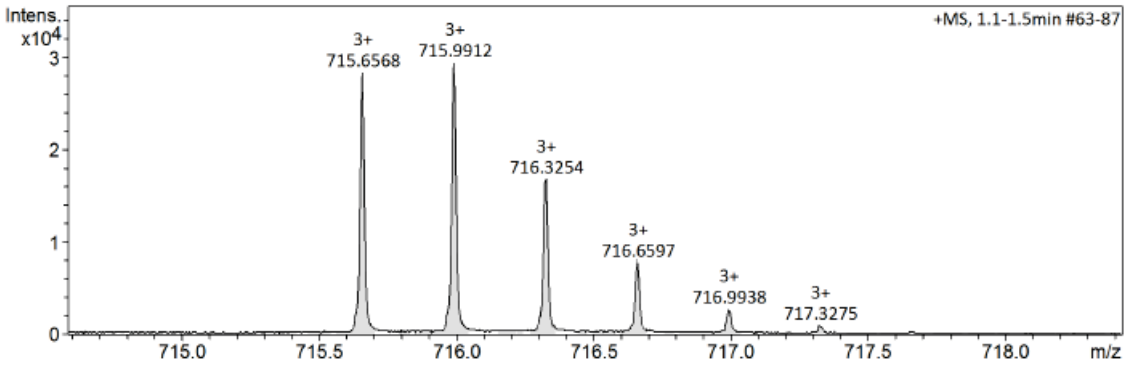

Figure S 48: HR-MS spectrum of compound **10***.

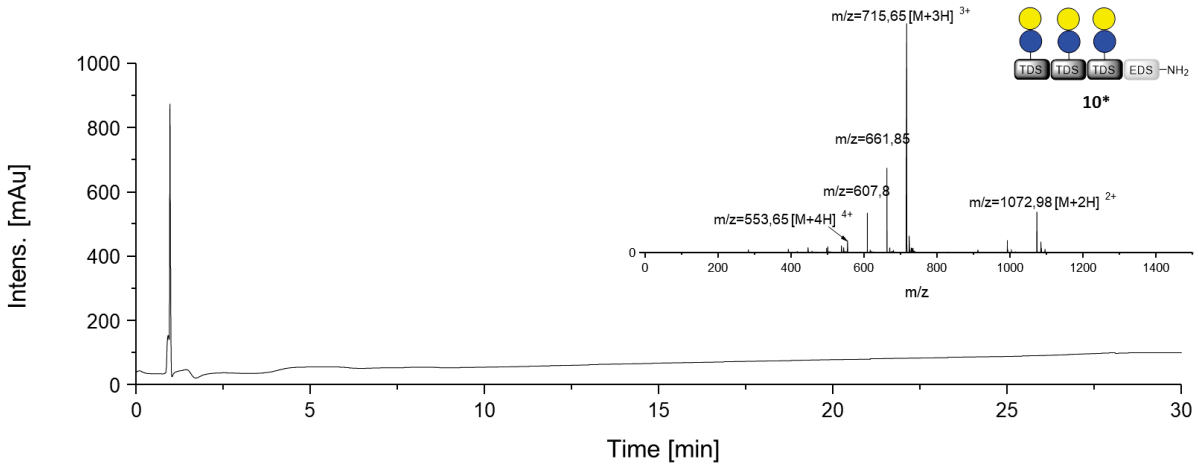

Figure S 49: RP-HPLC and ESI-MS spectrum of compound **10***.

3.14 Lac_3TPD, **11**

^{1}H NMR (300 MHz, Deuterium Oxide) δ [ppm]: 8.03 (s, 2H, triazole-C*H*), 8.00 (s, 1H, triazole-C*H*), 5.77 – 5.68 (m, 3H, CH_{anomer}Glc), 4.52 (d, ^{3}J = 7.7 Hz, 3H, CH_{anomer}-Gal), 4.04 (t, ^{3}J = 8.6 Hz, 3H, C$H_{pyranose}$), 3.99 – 3.73 (m, 27H), 3.69 (dd, ^{3}J = 10.0, 3.3 Hz, 3H, C$H_{pyranose}$), 3.59 (dd, ^{3}J = 10.0, 7.6 Hz, 3H, C$H_{pyranose}$), 3.38 – 3.21 (m, 8H, C=ONH-CH_2), 3.07 – 2.92 (m, 6H, CH=CH-CH_2), 2.71 (t, ^{3}J = 7.1 Hz, 2H, CH=CH-CH$_2$-CH_2), 2.65 – 2.51 (m, 4H, CH=CH-CH$_2$-CH_2). HR-MS (ESI) calc. for $C_{55}H_{90}N_{12}O_{33}$ $[M+2H]^{2+}$ 723.2861; found 723.2859. Yield: 73 mg (50 %).

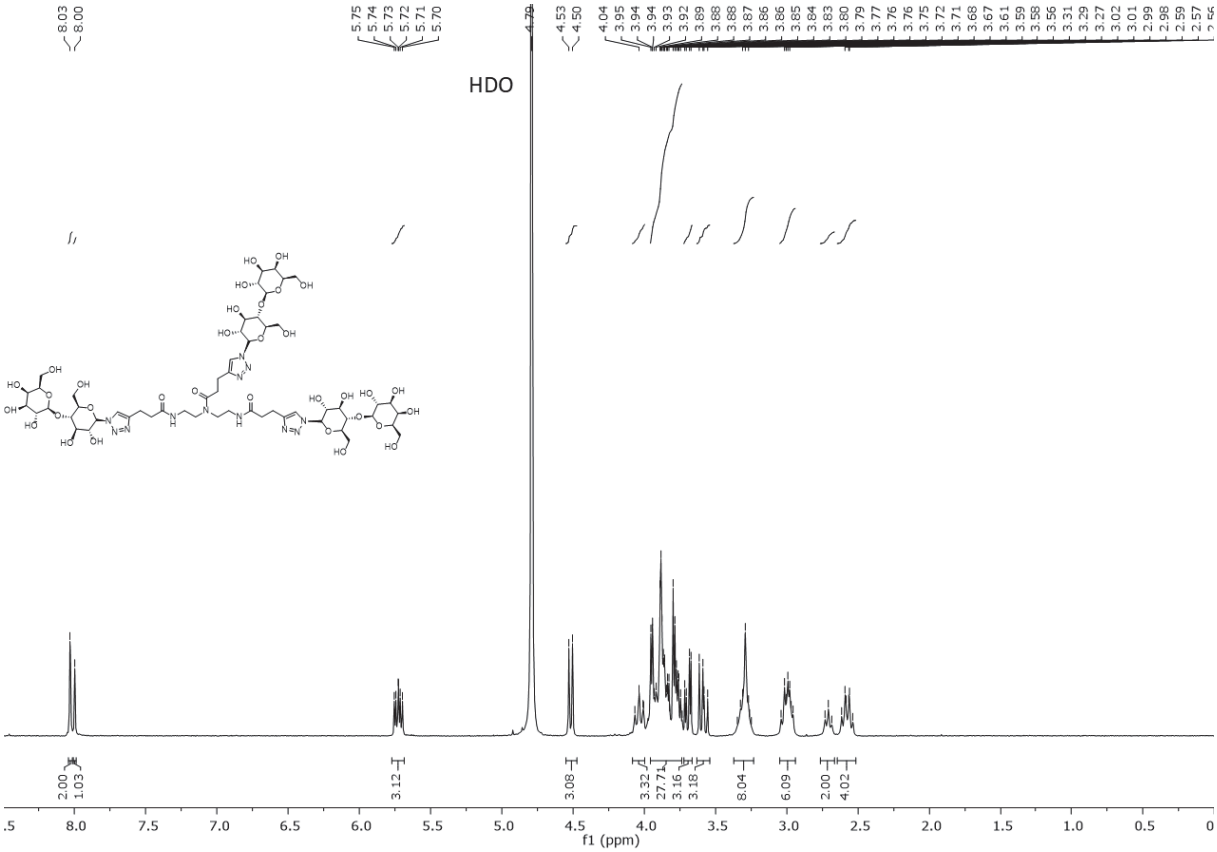

Figure S 50: ^{1}H-NMR spectrum of compound **11.**

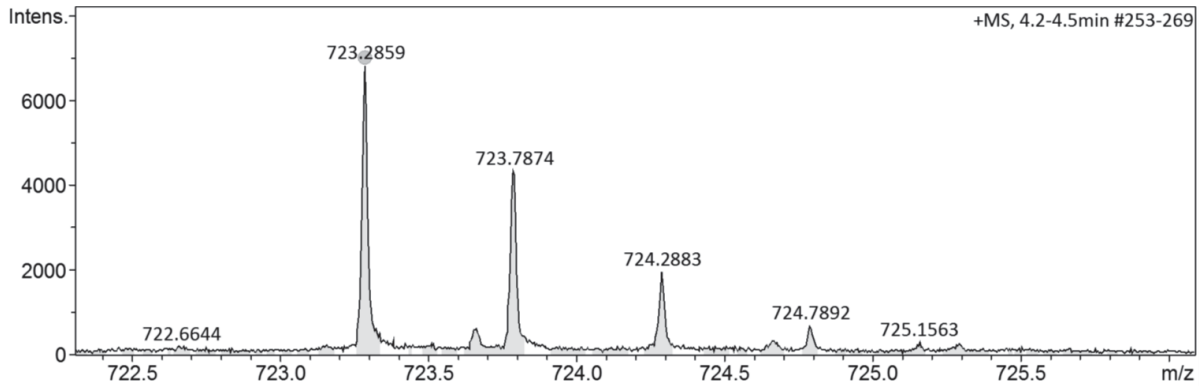

Figure S 51: HR-MS spectrum of compound **11**.

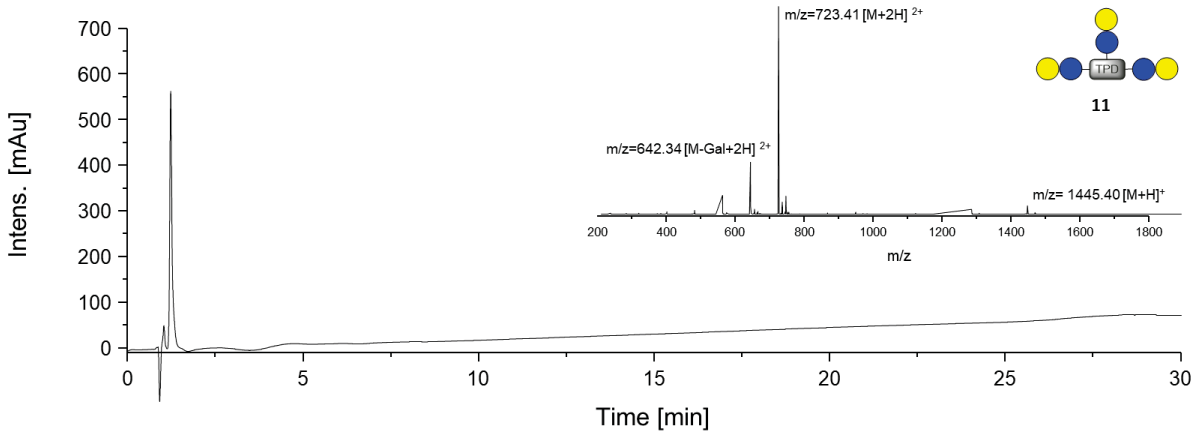

Figure S 52: RP-HPLC and ESI spectrum of compound **11.**

3.15 Lac(1,2,3,4,5,6)-7, **12**

^{1}H-NMR (300 MHz, Deuterium Oxide) δ [ppm]: 8.04 (m, 6H, triazole-CH), 5.74 (d, J = 9.2 Hz, 6H, C*H*$_{anomer}$Glc), 4.52 (d, J = 7.6 Hz, 6H, C*H*$_{anomer}$-Gal), 4.10 – 3.74 (m, 62H, C*H*$_{pyranose}$, O-C*H*$_2$-), 3.72 – 3.54 (m, 20H, C*H*$_{\text{pyranose}}$, C*H*$_{2\ \text{pyranose,}}$ O-C*H*$_2$-), 3.50 – 3.27 (m, 50H, C=ONH-C*H*$_2$), 3.04-2.98 (m, 12H, CH=CH-C*H*$_2$), 2.85 – 2.72 (m, 12H, CH=CH-CH$_2$-C*H*$_2$), 2.52-2.41 (m, 28H, NHC=O-C*H*$_2$), 1.99 (s, 3H, C*H*$_3$). HR-MS (ESI+) m/z calc. for $C_{162}H_{267}N_{39}O_{83}$ $[M+4H]^{4+}$ 1021.6962; found 1021.6962. Yield: 235.1 mg (55 %).

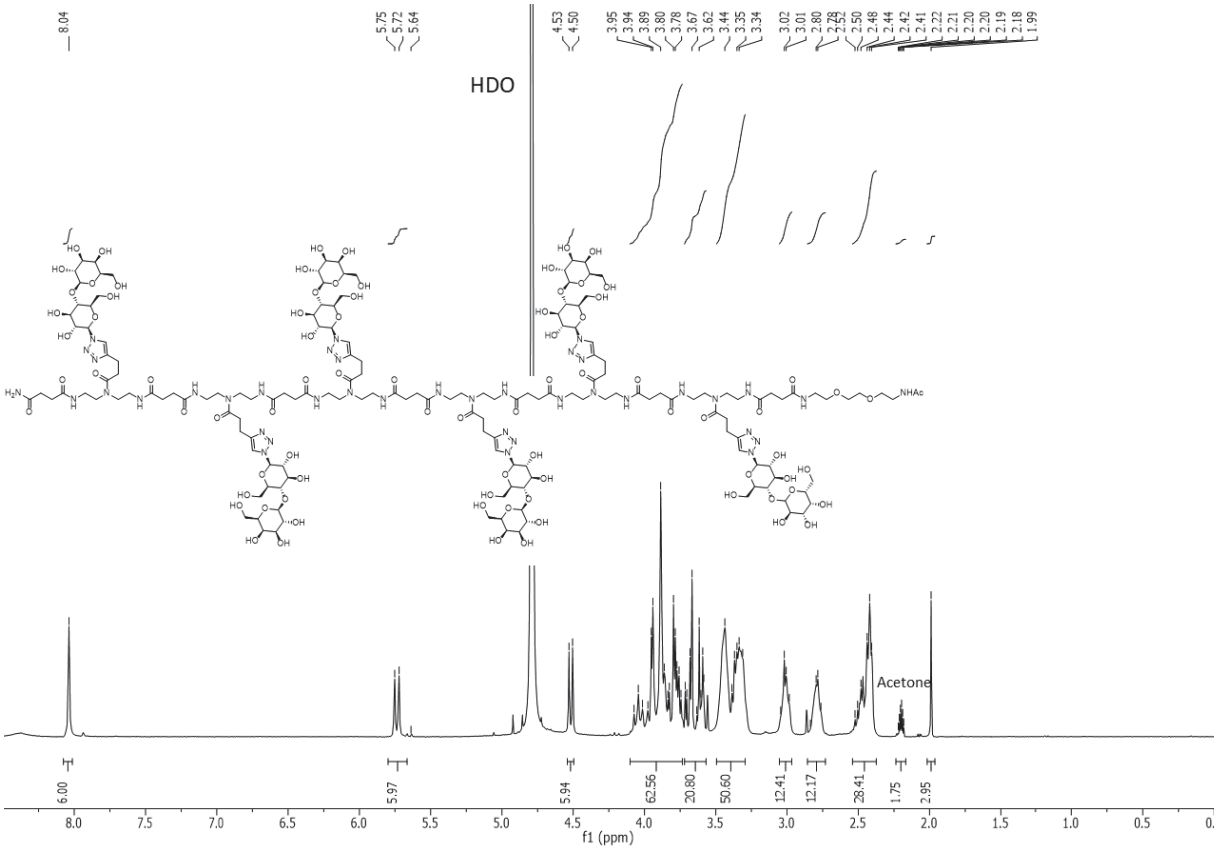

Figure S 53: ^{1}H-NMR spectrum of compound **12.**

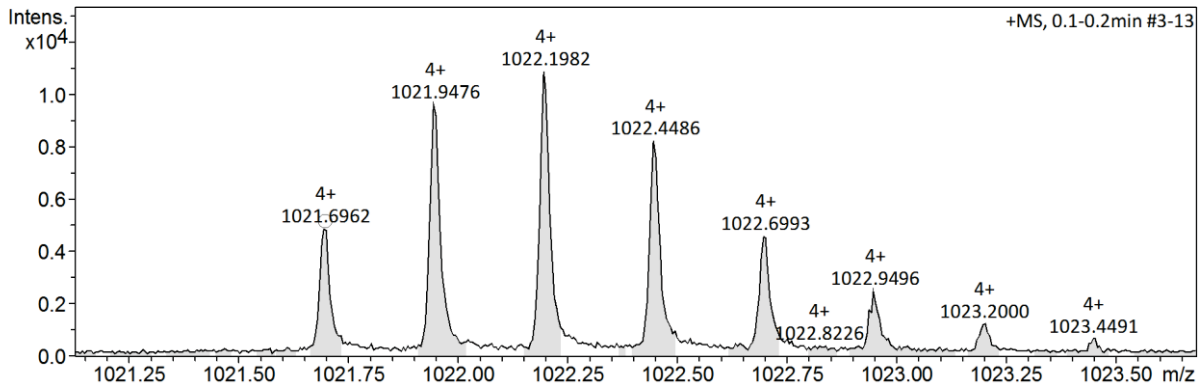

Figure S 54: HR-MS spectrum of compound **12**.

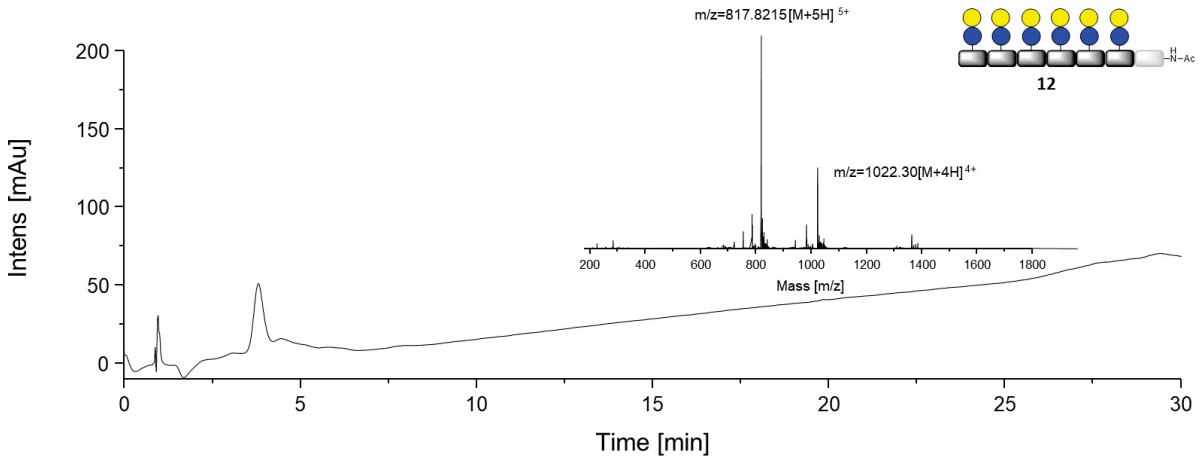

Figure S 55: RP-HPLC and ESI spectrum of compound **12.**

3.16 Lac(2)-3 L, **13**

^{1}H-NMR (300 MHz, Deuterium Oxide) δ [ppm]:7.84 (s, 1H, triazole-C*H*), 4.53 (t, 2H, ^{3}J = 6.8 Hz, , O-C*H*$_2$-), 4.46 (2x d, 2H, ^{3}J ≈ 7.7 Hz , ^{3}J ≈ 7.7 Hz, C*H*$_{anomer}$Glc, C*H*$_{anomer}$-Gal), 4.01-3.70 (m, 7H, C*H*$_{pyranose}$), 3.70-3.51 (m, 22H, O-C*H*$_2$- , C*H*$_{pyranose,}$ -N-N-C*H*$_2$-), 3.50-3.29 (m, 17, C=ONH-C*H*$_2$, C*H*$_{pyranose}$), 3.00 (t, ^{3}J = 7.0 Hz, 2H, CH=CH-C*H*$_2$), 2.79 (t, ^{3}J = 7.1 Hz, 2H, CH=CH-CH$_2$-C*H*$_2$), 2.57-2.43 (m, 12H, NHC=O-C*H*$_2$), 2.21 (p, 2H, ^{3}J = 6.6 Hz, CH$_2$-C*H*$_2$-CH$_2$), 1.99 (s, 3H, C*H*$_3$). HR-MS (ESI): m/z calc. for $C_{50}H_{89}N_{11}O_{23}$ $[M+2H]^{2+}$ 605.8061; found 605.8072. Yield: 235.1 mg (55 %).

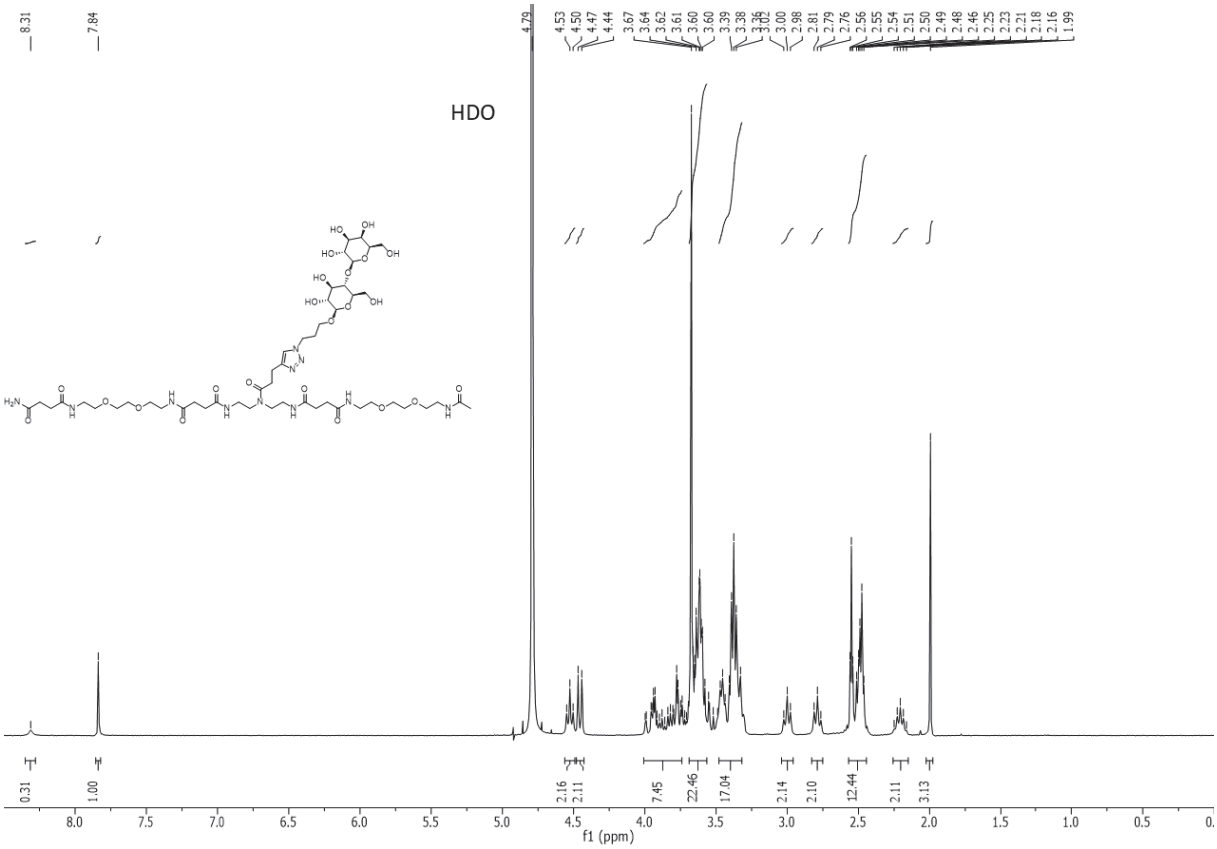

Figure S 56: ^{1}H-NMR spectrum of compound **13.**

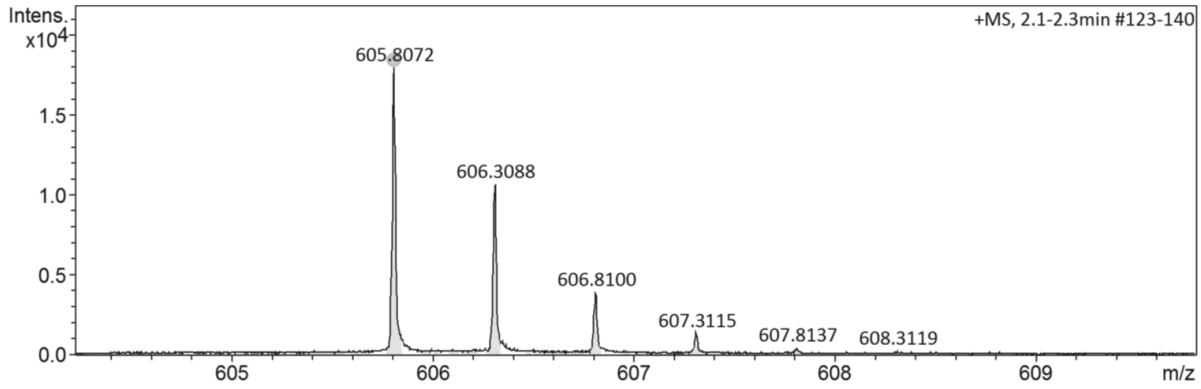

Figure S 57: HR-MS spectrum of compound **13**.

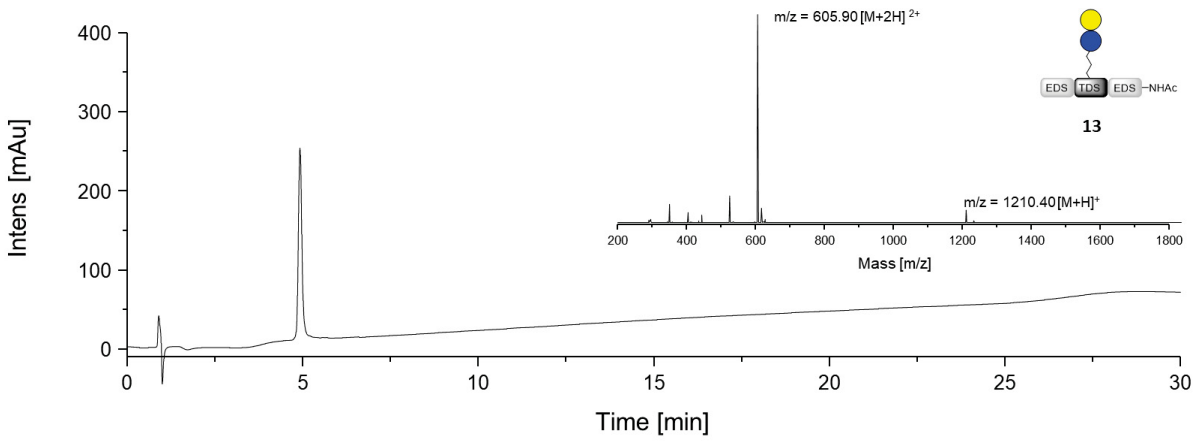

Figure S 58: RP-HPLC and ESI spectrum of compound **13**.

3.17 Lac(1,5)-5 L, **14**

^{1}H-NMR (300 MHz, Deuterium Oxide) δ [ppm]:7.84 (s, 2H, triazole-C*H*), 4.53 (t, ^{3}J = 6.8 Hz, 4H, O-C$H_{2\text{propyl}}$), 4.46 (m, 4 H, CH_{anomer}Glc, CH_{anomer}-Gal), 4.01-3.70 (m, 13H, CH_{pyranose}), 3.70-3.51 (m, 37H, O-CH_2-, C$H_{\text{pyranose,}}$ -N-N-CH_2-), 3.50-3.29 (m, 30H, C=ONH-C$H_{2,}$ CH_{pyranose}), 3.00 (t, ^{3}J = 7.0 Hz, 4H, CH=CH-CH_2), 2.79 (t, 4H, CH=CH-CH$_2$-CH_2), 2.56-2.45 (m, 20H, NHC=O-CH_2), 2.21 (m, 4H, CH$_2$-CH_2-CH$_2$), 1.94 (s, 1.5H, CH_3), 1.91 (s, 1.5H, CH_3). HR-MS (ESI): m/z calc. for $C_{88}H_{154}N_{19}O_{41}$ $[M+3H]^{3+}$ 711.0178; found 711.0183. Yield: 120.7 mg (23 %).

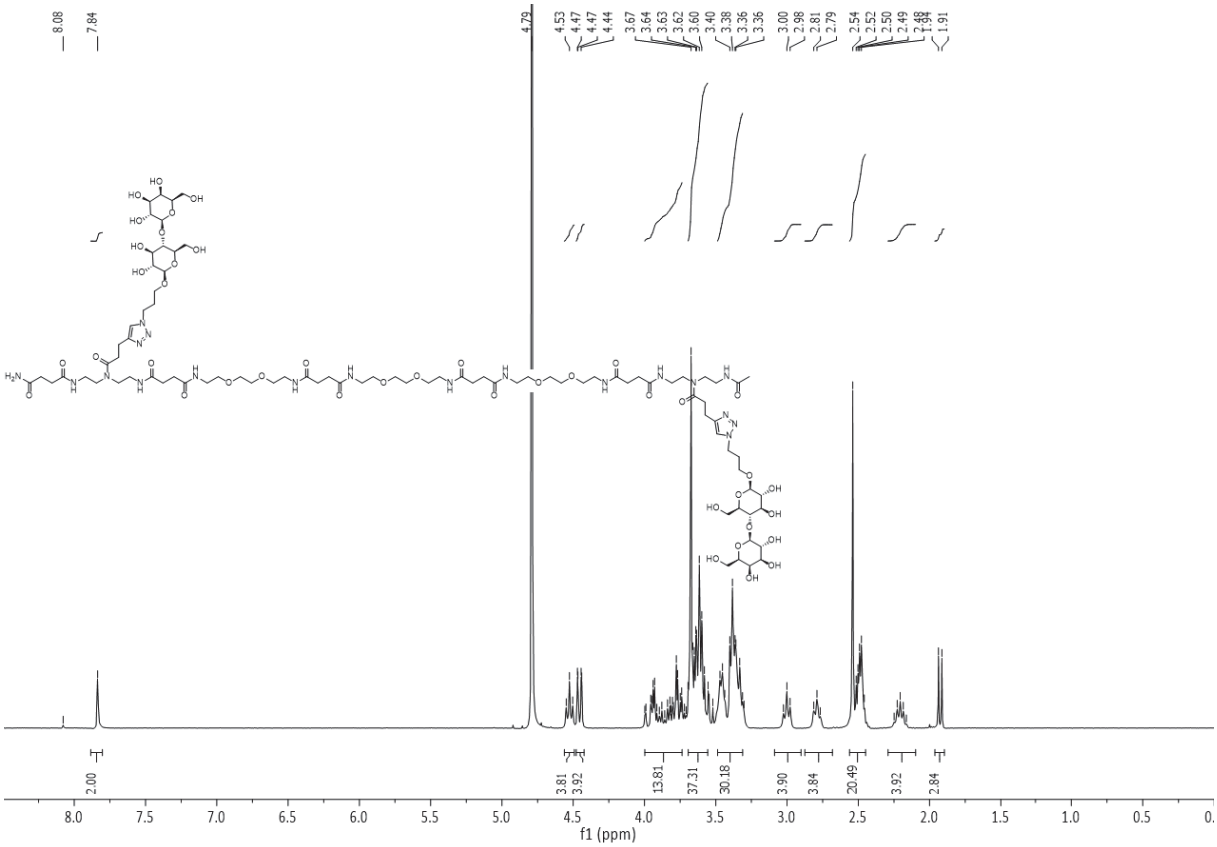

Figure S 59: ^{1}H-NMR spectrum of compound **14.**

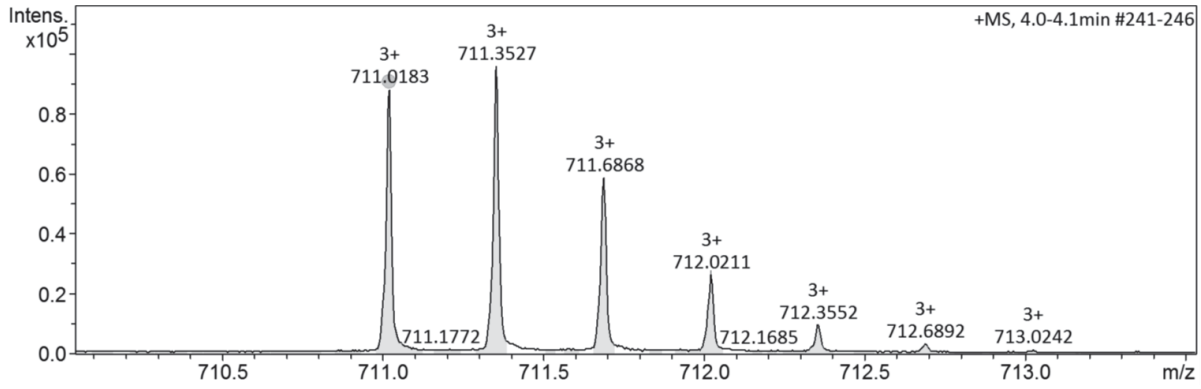

Figure S 60: HR-MS spectrum of compound **14**.

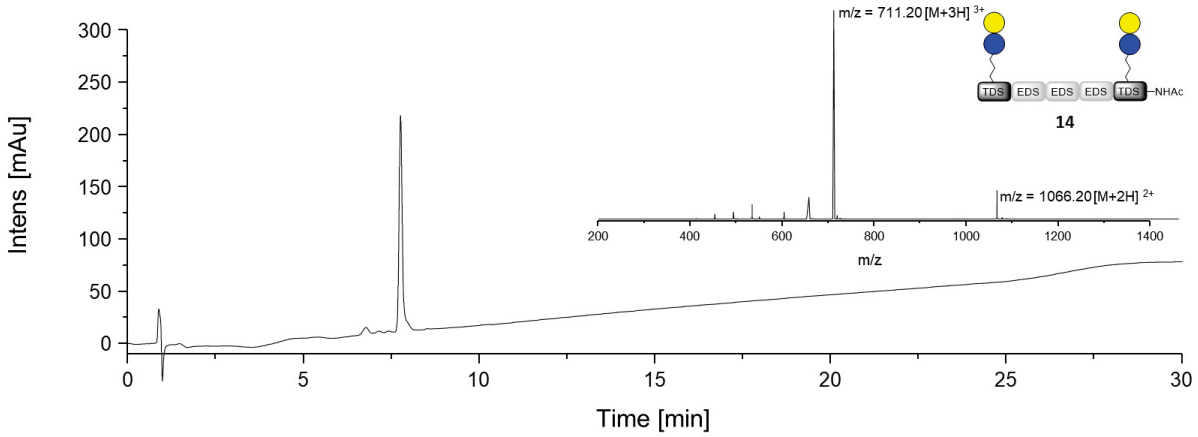

Figure S 61: RP-HPLC and ESI-MS spectrum of compound **14**.

3.18 Lac(1,5,9)-9 L, **15**

^{1}H-NMR (300 MHz, Deuterium Oxide) δ [ppm]:7.84 (s, 3H, triazole-C*H*), 4.53 (t, ^{3}J = 6.8 Hz, 6H, O-C$H_{2\text{propyl}}$-), 4.46 (m, 6H, CH_{anomer}Glc, CH_{anomer}-Gal), 4.01-3.70 (m, 20H, CH_{pyranose}), 3.70-3.51 (m, 66H, O-CH_2-, CH_{pyranose}, -N-N-CH_2-), 3.50-3.30 (m, 52H, CH_{pyranose}, C=ONH-CH_2), 3.00 (t, ^{3}J = 6.9 Hz, 6H, CH=CH-CH_2), 2.79 (t, ^{3}J = 7.0 Hz, 6H, CH=CH-CH_2-CH_2), 2.56-2.45 (m, 36H, NHC=O-CH_2), 2.21 (m, 6H, CH_2-CH_2-CH_2), 1.94 (s, 1.5H, CH_3), 1.91 (s, 1.5H, CH_3). HR-MS (ESI): m/z calc. for $C_{146}H_{255}N_{31}O_{67}$ $[M+4H]^{4+}$ 878.6869; found 878.6877. Yield: 69.9 mg (22 %).

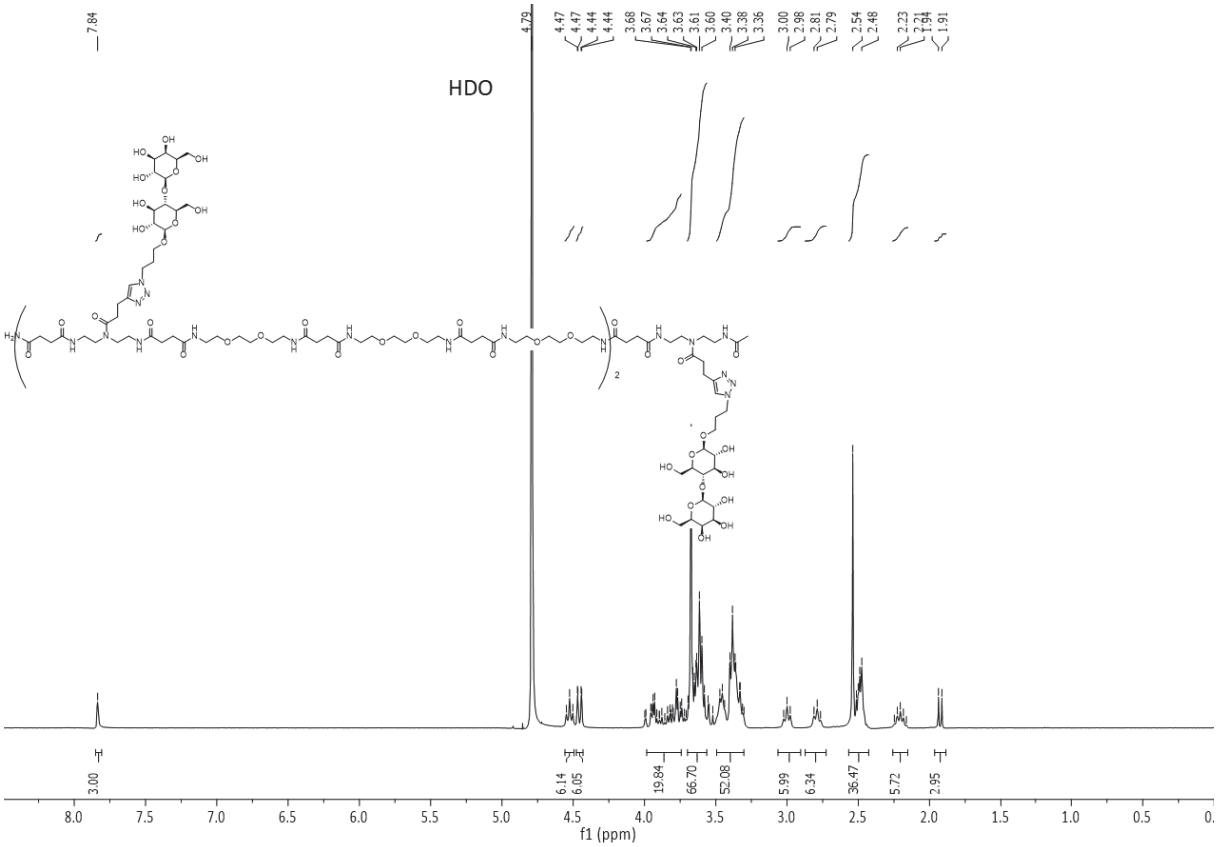

Figure S 62: ^{1}H-NMR spectrum of compound **15.**

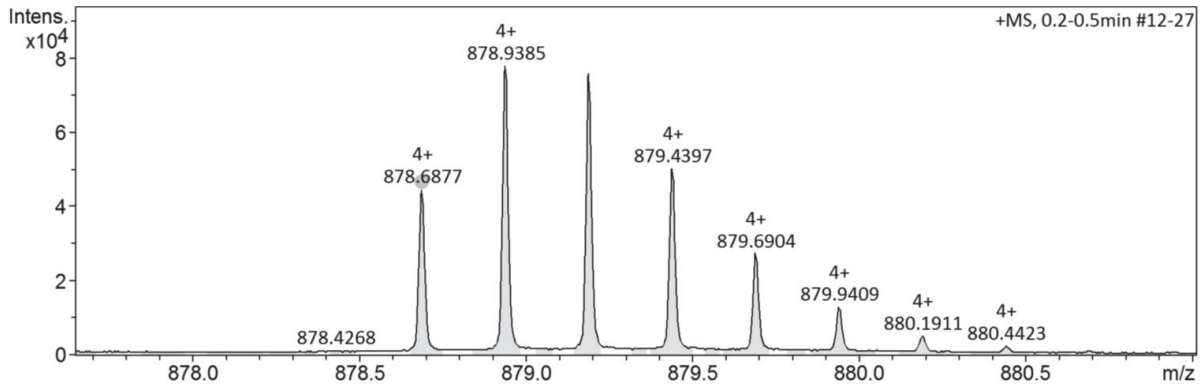

Figure S 63: HR-MS spectrum of compound **15**.

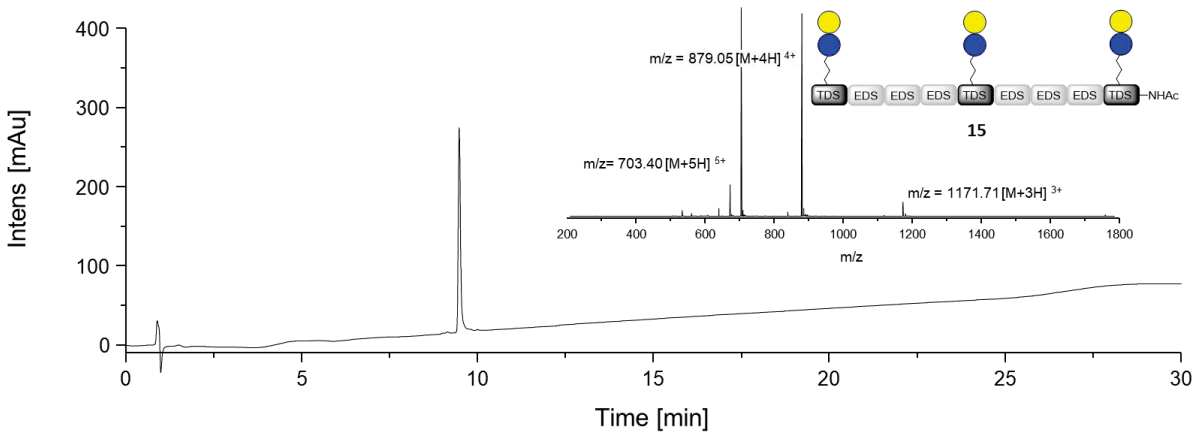

Figure S 64: RP-HPLC and ESI-MS spectrum of compound **15**.

3.19 Glc(1,3,5)-6, **16**

^{1}H-NMR (300 MHz, D_2O) δ [ppm]7.93 – 7.87 (m, 3H, triazole-C*H*), 4.88 (d, J = 3.4 Hz, 2.7H, CH_{anomer}Glc), 4.72 –4.59 (m, 6H, -N-N-CH_2), 4.43 (d, J = 7.9 Hz, 0.3H, CH_{anomer}Glc), 4.16 – 4.02 (m, 3H, O-CH_2-), 4.00 – 3.86 (m, 3H, O-CH_2-), 3.73 – 3.56 (m, 33H, O-CH_2-, C=ONH-CH_2, C$H_{pyranose}$), 3.55 – 3.43 (m, 17H, O-CH_2-), 3.42 – 3.30 (m, 27H, CH_2-NH_2), 3.00 (t, J = 7.3 Hz, 6H, CH=C-CH_2), 2.92 – 2.74 (m, 9H, CH=C-CH_2-CH_2), 2.58 – 2.42 (m, 24H, NHC=O-CH_2), 2.00 (s, 3H, -CH_3). HR-MS (ESI) calc. for $C_{95}H_{164}N_{25}O_{40}$ $[M+3H]^{3+}$ 765.0517; found 765.0527. Yield: 110 mg (48 %).

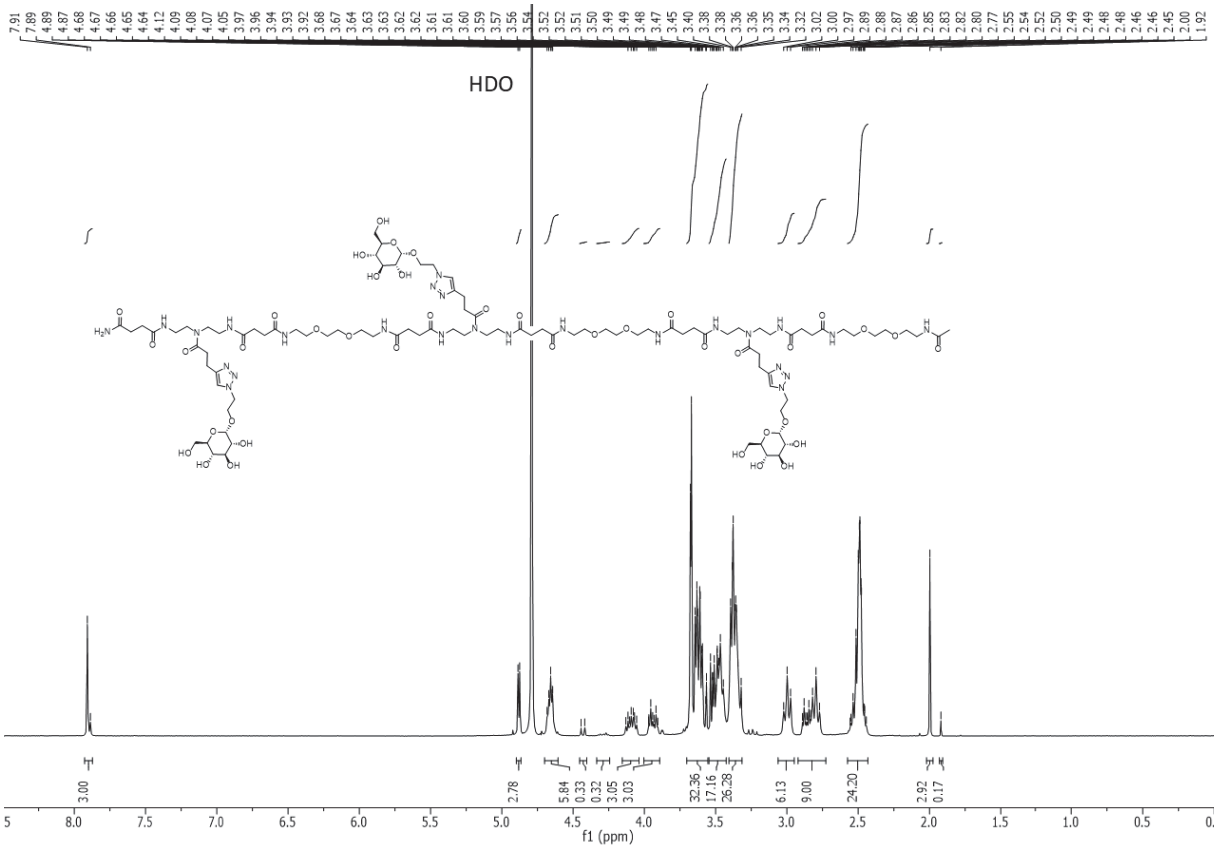

Figure S 65: ^{1}H-NMR spectrum of compound **16.**

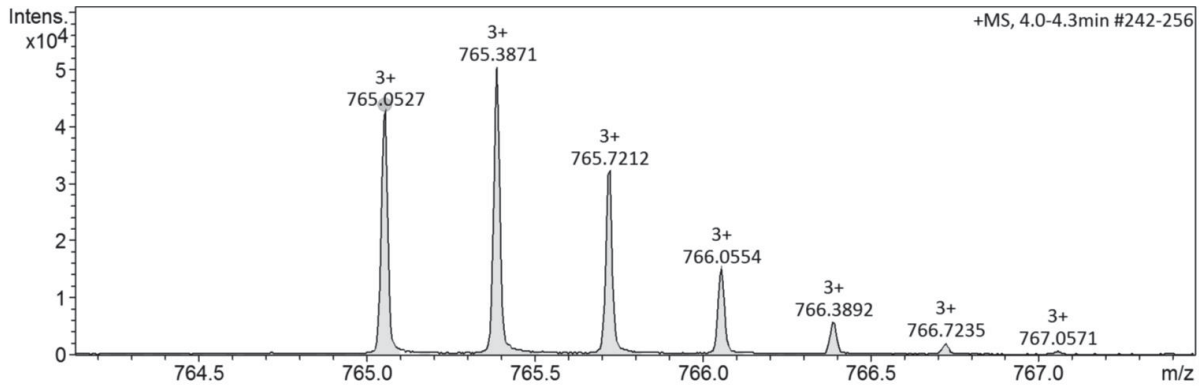

Figure S 66: HR-MS spectrum of compound **16**.

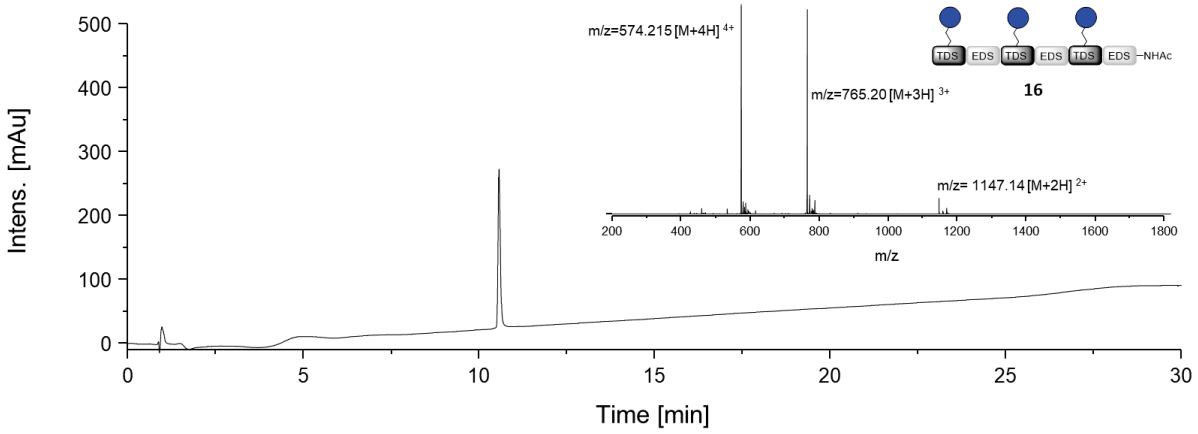

Figure S 67*:* RP-HPLC and ESI-MS spectrum of compound **16**.

3.20 Glc(1,3,5)-6, **16***

^{1}H-NMR (600 MHz, Deuterium Oxide) δ [ppm]: 8.46 (br s. 1 H. NH). 7.88 (m, 3H, triazole-C*H*), 4.80 (m, 3H, CH_{anomer}Glc), 4.64 (m, 6H, -N-N-CH_2-), 4.41 (d, $^{3}J_{HH}$ = 7.9 Hz, 0.6H, CH_{anomer}Glc), 4.07 (m, 3H, O-CH_2-), 3.91 (m, 3H, O-CH_2-), 3.75 (dd, $^{3}J_{HH}$ = 5.6; 4.6 Hz, 2H, O-CH_2-), 3.69 (s, 4H, O-CH_2-), 3.65 (s, 8H, O-CH_2-), 3.63 – 3.28 (m, 59H, O-CH_2-, C=ONH-CH_2, C$H_{pyranose}$), 3.21 (m, 2H, CH_2-NH_2), 2.98 (m, 6H, CH=C-CH_2), 2.87– 2.75 (m, 9H, CH=C-CH_2-CH_2), 2.48 (m, 24H, NHC=O-CH_2). ESI-MS m/z calc. for $C_{93}H_{162}N_{25}O_{39}$ $[M+3H]^{3+}$ 751.04. found: 751.25. Yield: 86 mg (38 %).

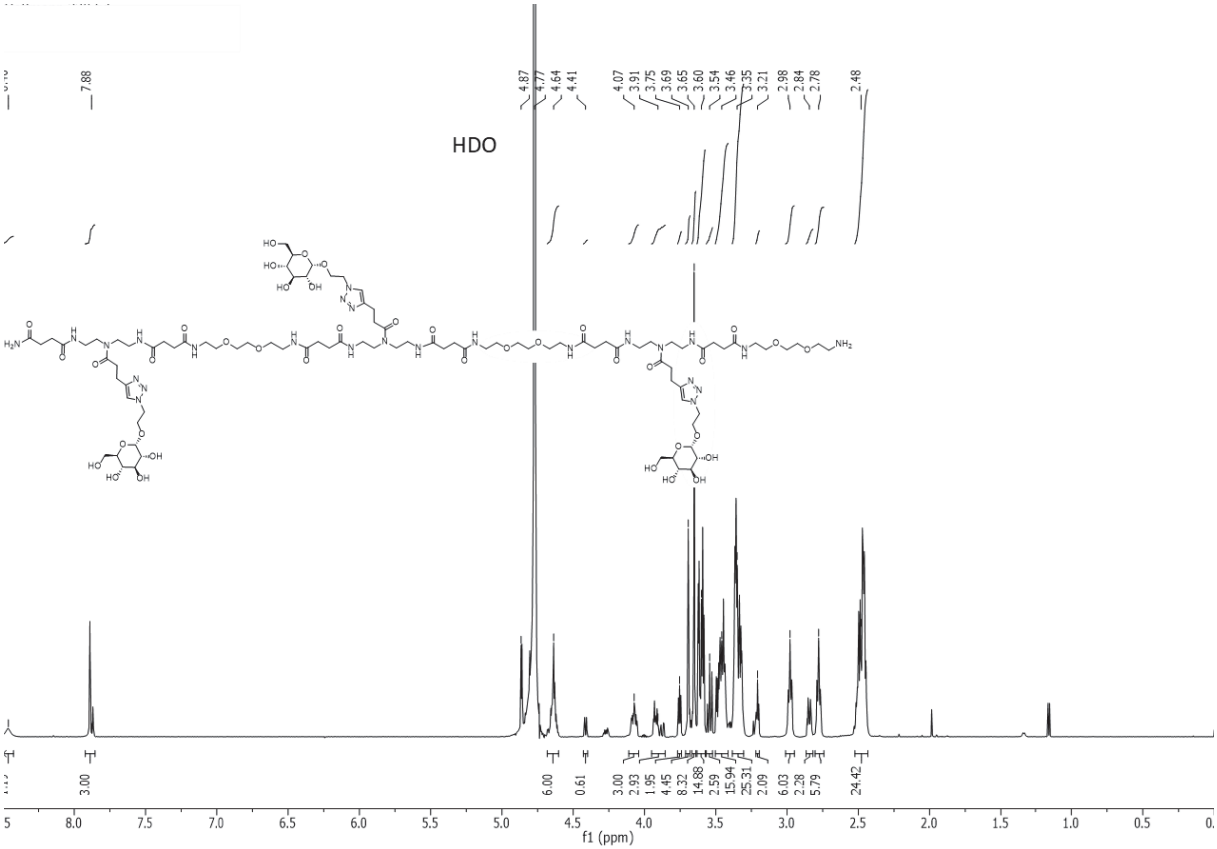

Figure S 68: ^{1}H-NMR spectrum of compound **16*.**

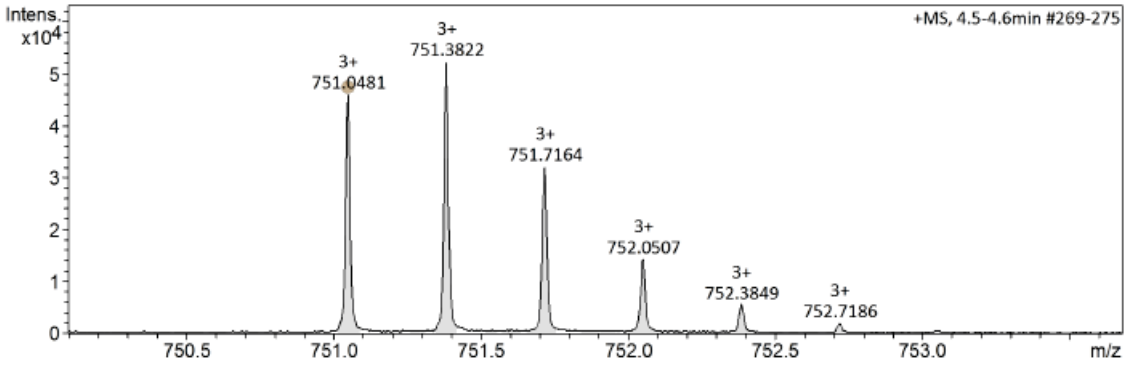

Figure S 69: HR-MS spectrum of compound **16***.

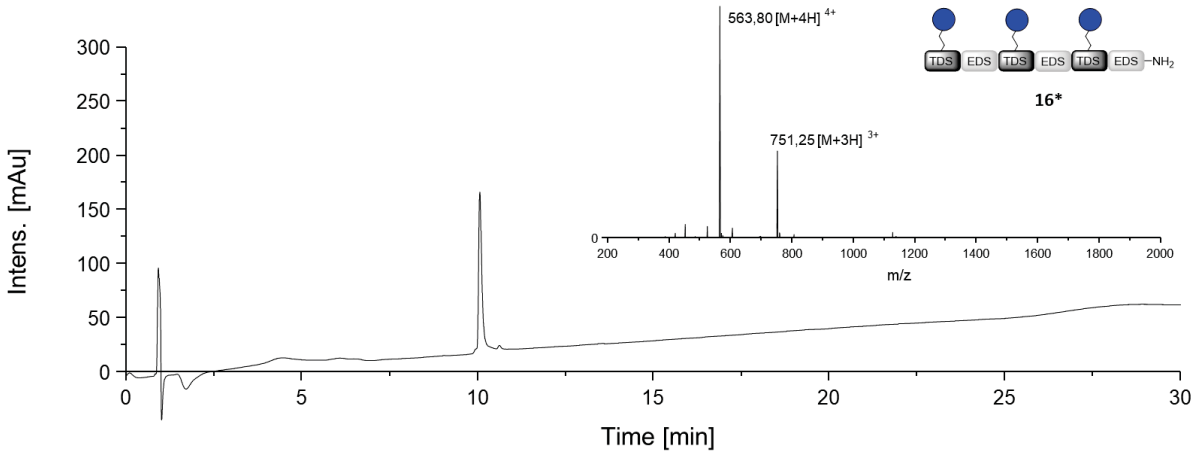

Figure S 70*:* RP-HPLC and ESI-MS spectrum of compound **16***.

4. Analytical data for glycomacromolecule-lipid conjugates

4.1. Lac(1)-2-PEG-DSPE-conjugate, **L4**

Yield: 2.01 mg (58 %). Conversion: 66 %. MALDI-TOF-MS calc. for $C_{173}H_{330}N_{11}O_{73}PNa$ $[M+Na]^+$ 3786.5; found: 3787.8.

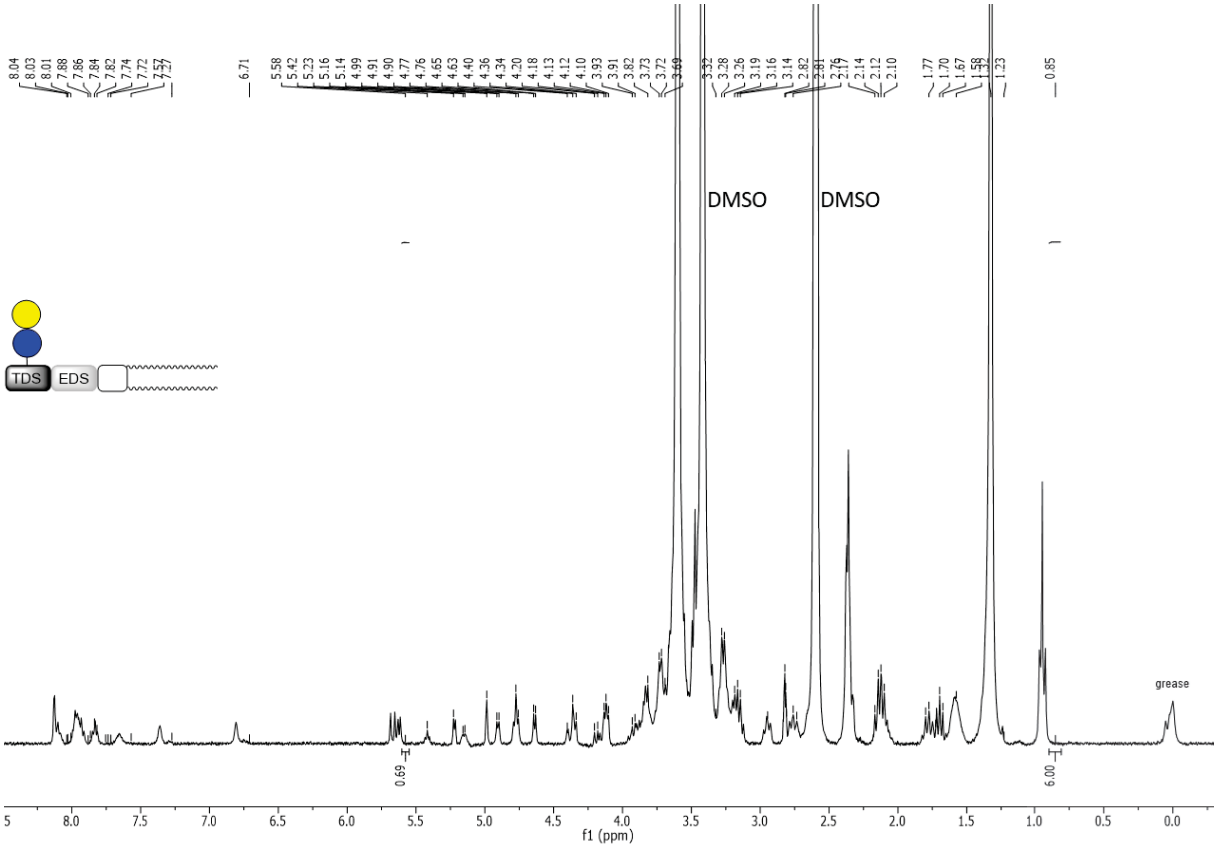

Figure S 71: ^{1}H-NMR spectrum of compound **L4**.

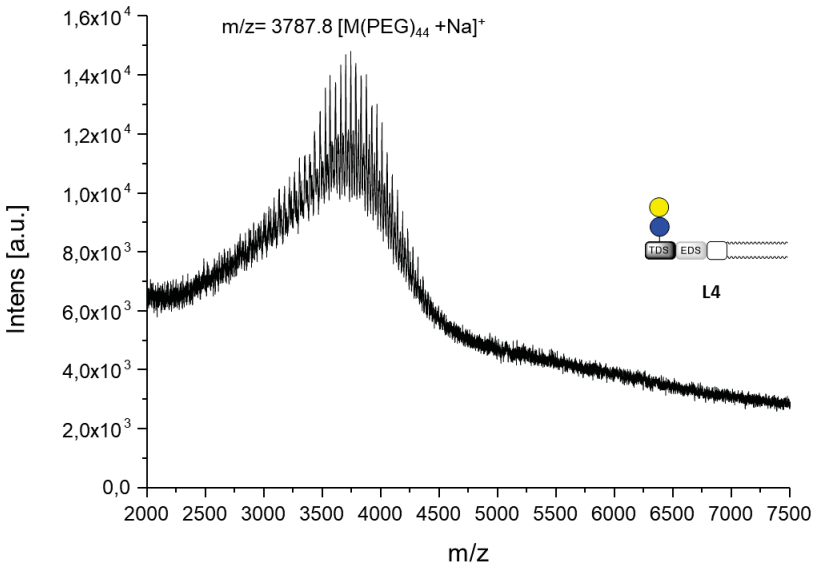

Figure S 72: MALDI-TOF-MS-spectrum of compound **L4**.

4.2. Lac(1,3,5)-6-PEG-DSPE-conjugate, **L9**

Yield: 2.26 mg (44 %). Conversion: 56 %. MALDI-TOF-MS calc. für $C_{243}H_{446}N_{27}O_{107}PNa$ $[M+Na]^+$ 5511.3; found: 5511.6.

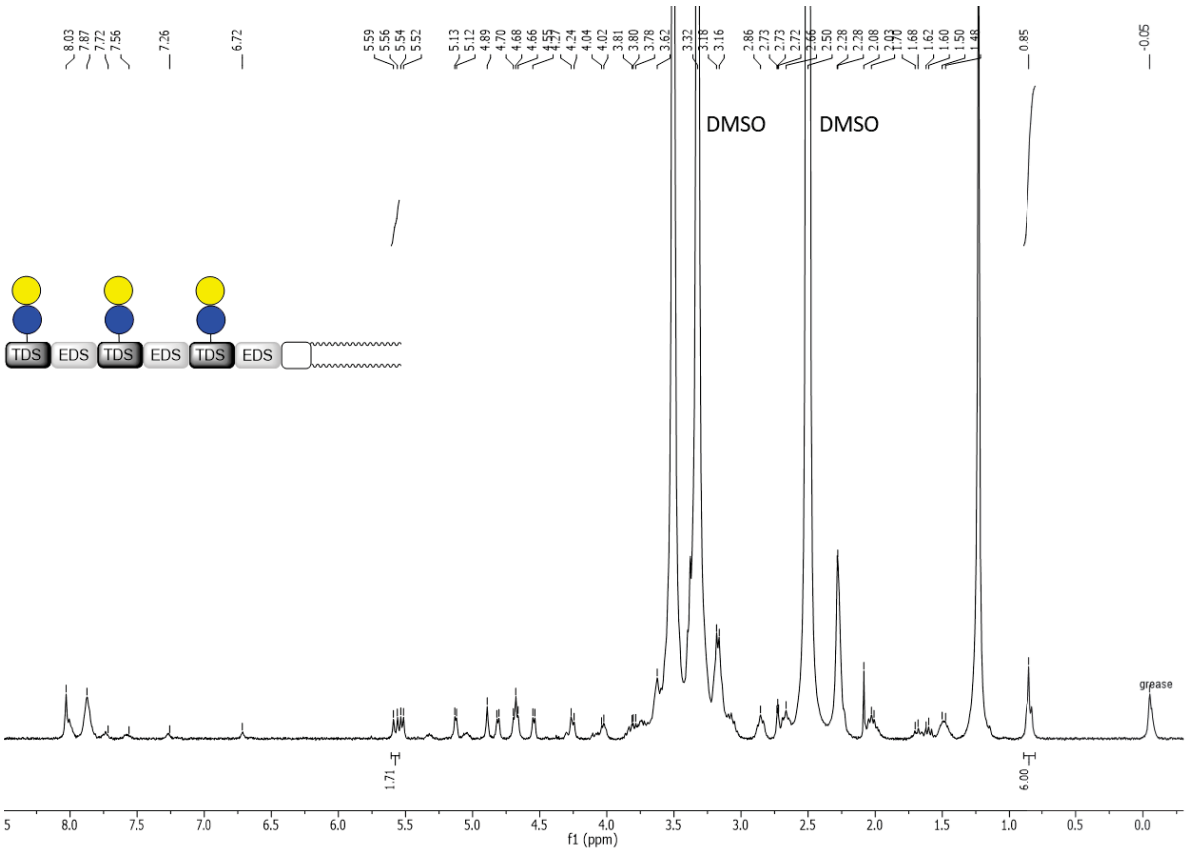

Figure S 73: ^{1}H-NMR spectrum of compound **L9.**

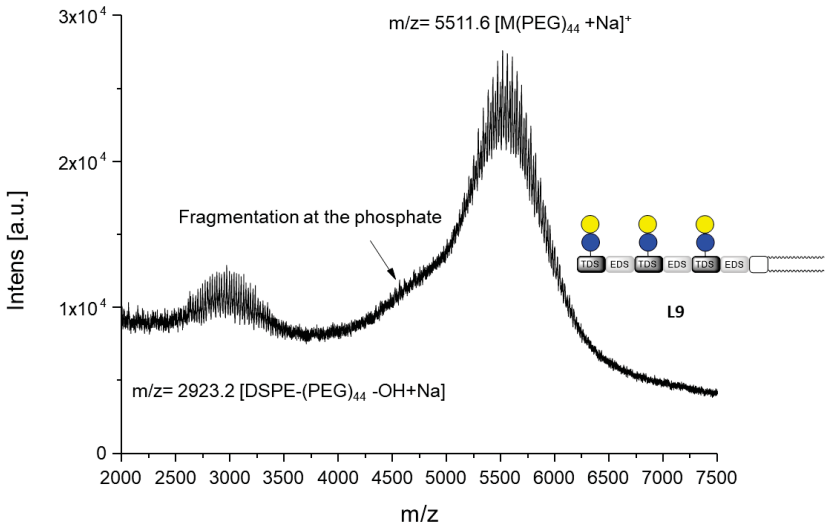

Figure S 74: MALDI-TOF-MS-spectrum of compound **L9**.

4.3. Lac(1,2,3)-4-PEG-DSPE-conjugate, **L10**

Yield: 3.00 mg (69 %). Conversion: 66 %. MALDI-TOF-MS calc. for $C_{223}H_{410}N_{23}O_{99}PNa$ $[M+Na]^+$ 5051.8; found 5052.5.

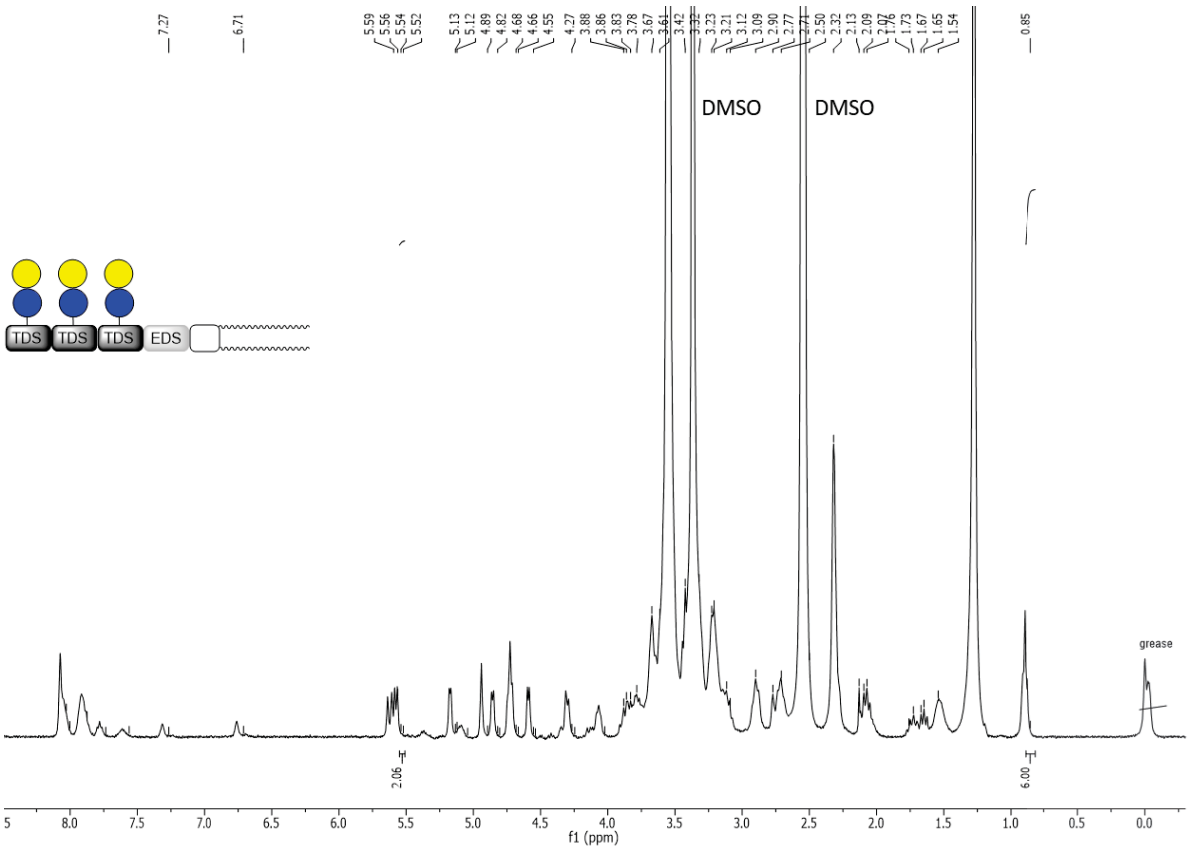

Figure S 75: ^{1}H-NMR spectrum of compound **L10.**

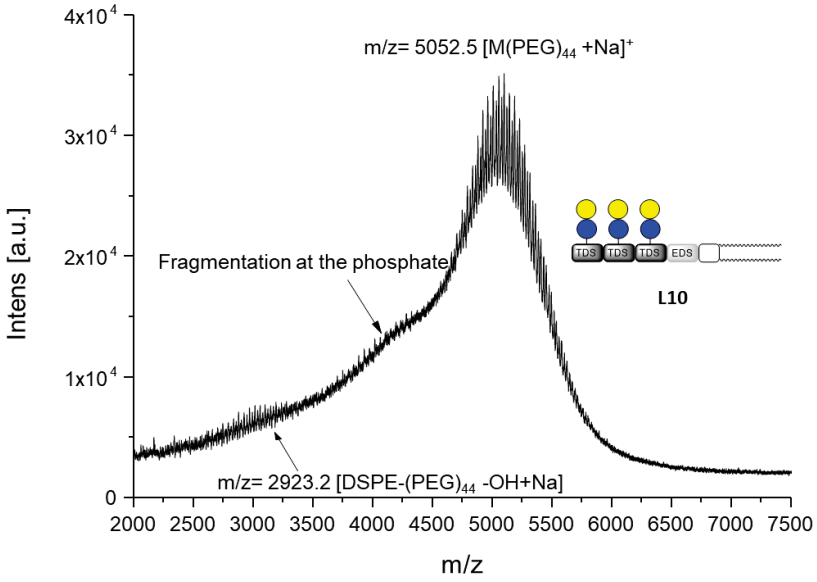

Figure S 76: MALDI-TOF-MS-spectrum of compound **L10**.

4.4. Glc(1,3,5)-6-PEG-DSPE-conjugate**, L16**

Yield: 1.54 mg (35 %). Conversion: 62 % (as determined by ^{1}H-NMR). MALDI-TOF-MS calc. for $C_{231}H_{428}N_{27}O_{95}PNa$ $[M+Na]^{+}$ 5158.0; found: 5158.7.

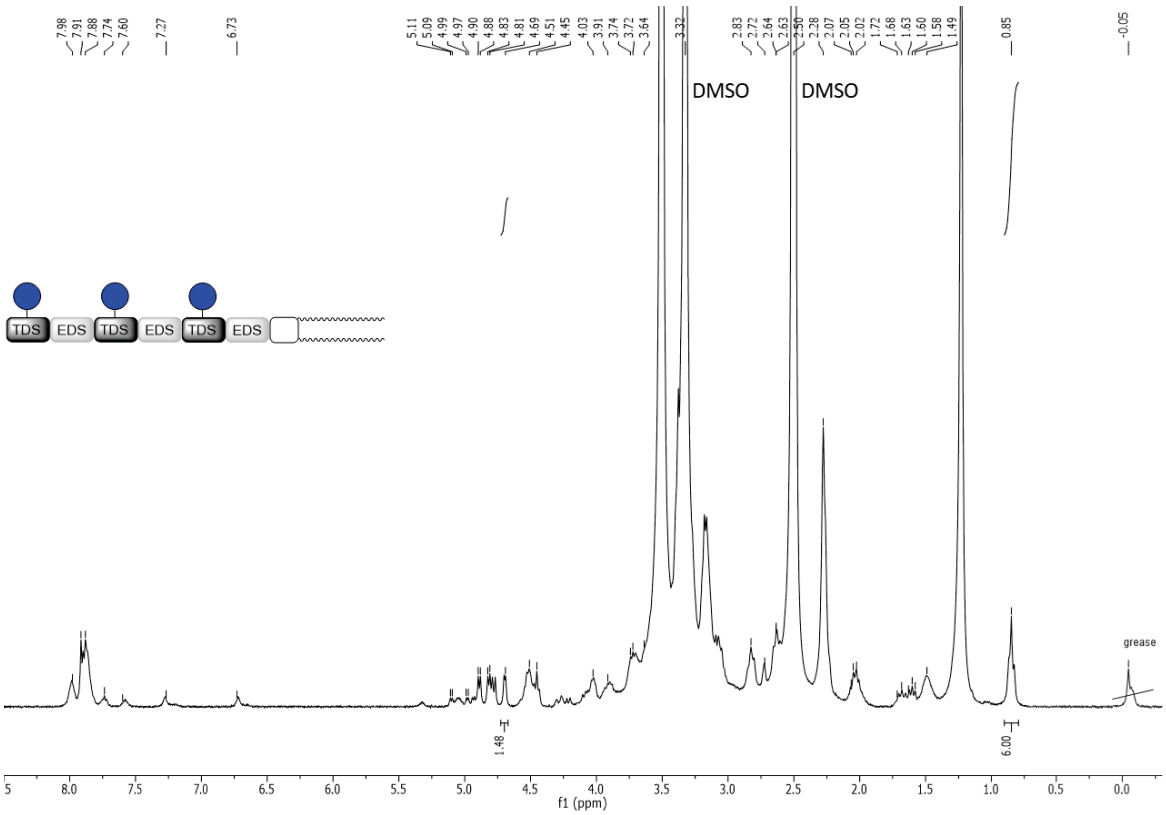

Figure S 77: ^{1}H-NMR spectrum of compound **L16.**

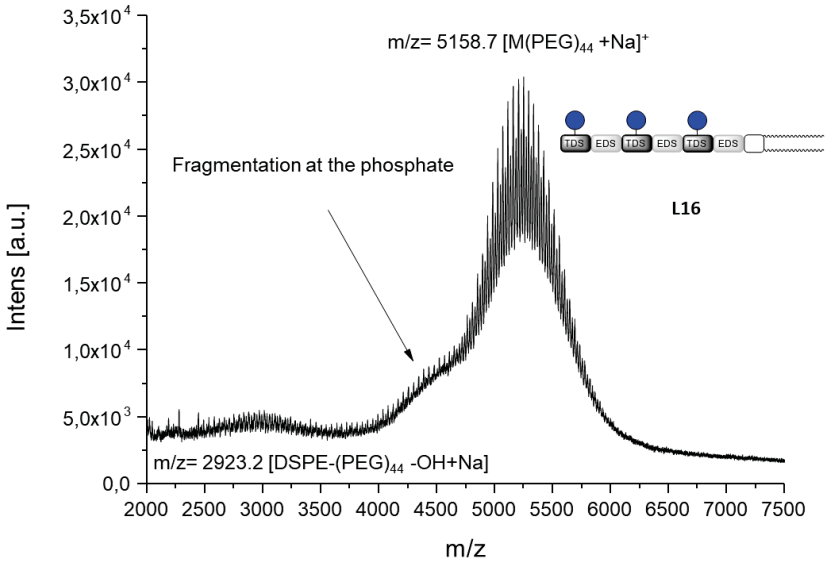

Figure S 78: MALDI-TOF-MS-spectrum of compound **L16.**

5. Analytical data of liposomes

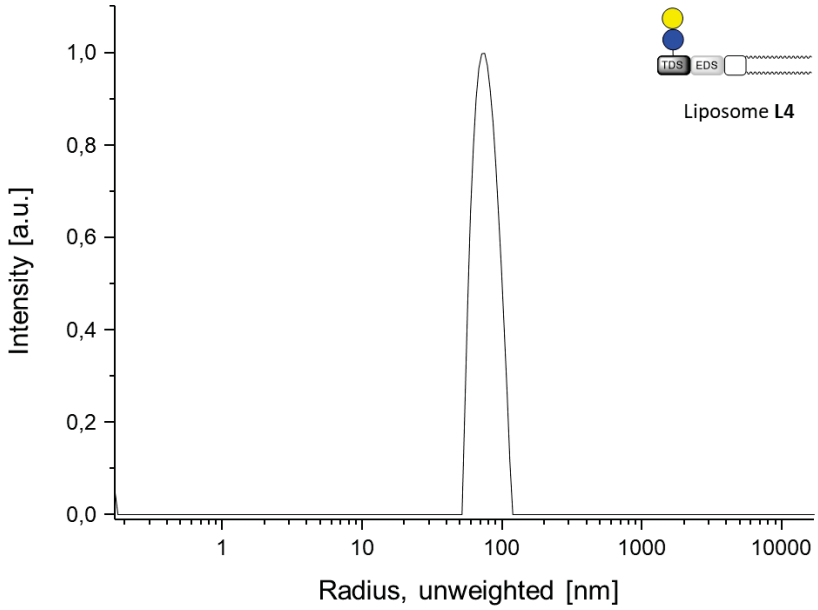

Figure S 79: Exemplary DLS spectrum of **liposome L4.**

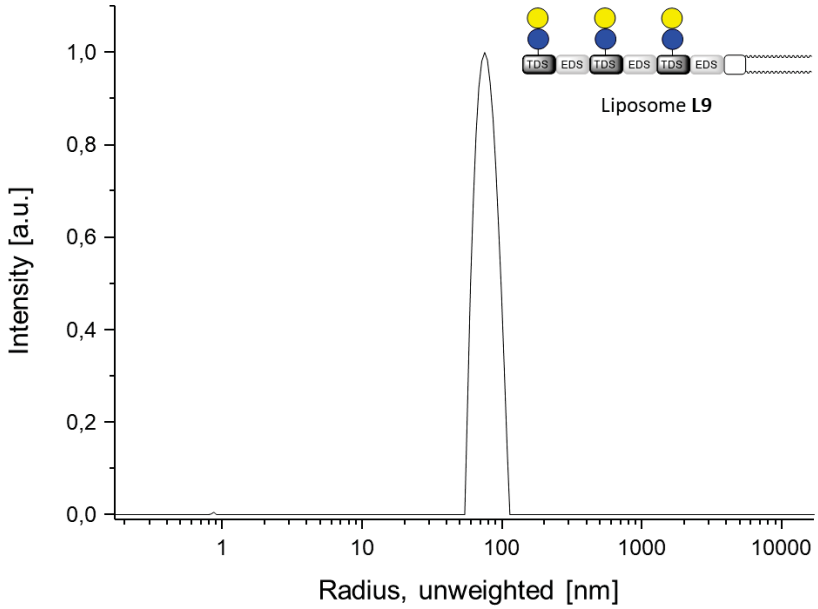

Figure S 80: Exemplary DLS spectrum of **liposome L9.**

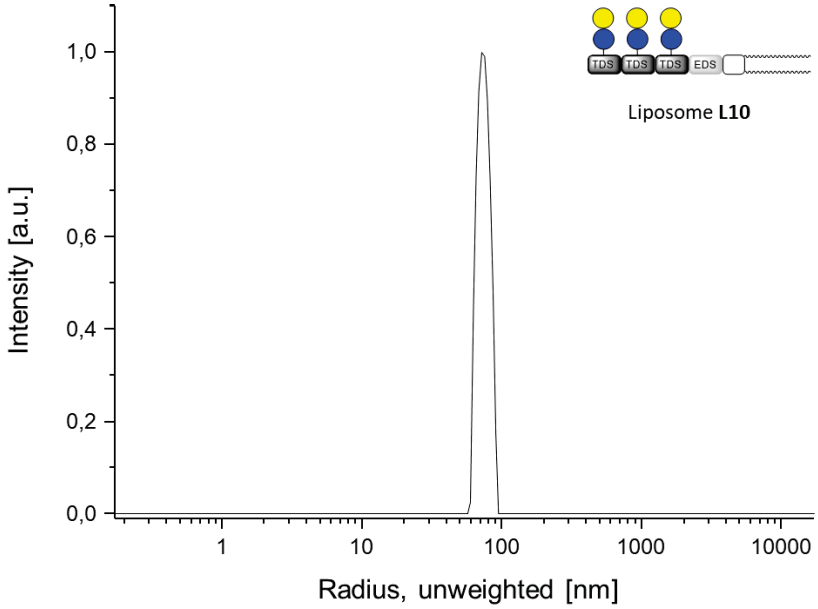

Figure S 81: Exemplary DLS spectrum of **liposome L10.**

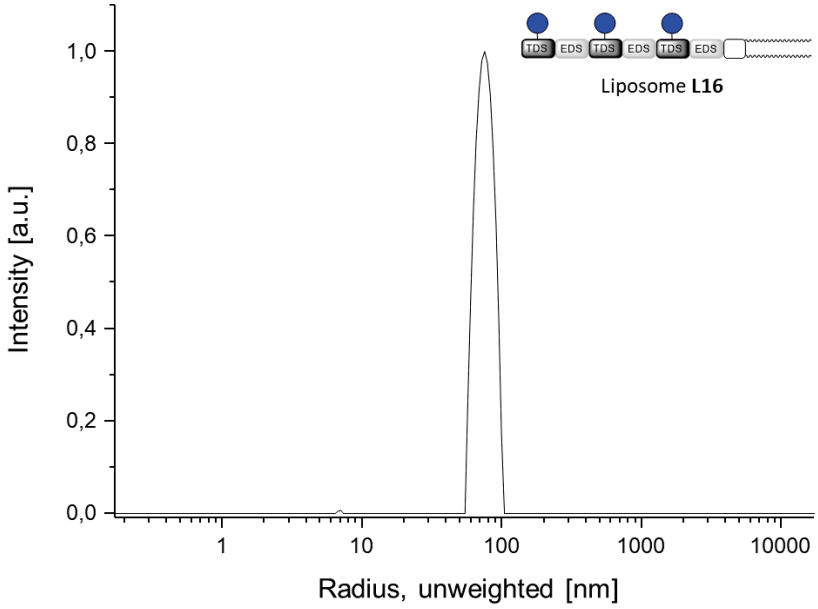

Figure S 82: Exemplary DLS spectrum of **liposome L16.**

3. Sequence-defined Heteroglycomacromolecules Bearing Sulfated and Sulfonated Non-Glycosidic Moieties Selectively Bind Galectin-3 and Delay Wound Healing of a Galectin-3 Positive Tumor Cell Line

Authors:	**T. Freichel**, V. Heine, D. Laaf, E. E. Mackintosh, S. Sarafova, L. Elling, N. L. Snyder and L. Hartmann
Issue	In preparation
Type of paper:	Communication

1st author contribution:

Collaborative design of structures, binding assays and cell studies. Synthesis of all building block and carbohydrate building blocks. Development and optimization of the synthesis, isolation and purification of the heteroglycomacromolecules as acetylated-, amine- and FITC-derivatives, including the use of an orthogonal conjugation approach. Analysis of all glycomacromolecules. Development, performance, visualization and interpretation of the SPR-measurements. Joined performance of the ELISA-type assays. Visualization and interpretation of the obtained data supported by coauthors. Optimization and performance of tissue culturing of the tumor cell lines. Optimization and performance of the cell studies including flow cytometry, MTT-assay and wound healing assays. Joined performance of fluorescence microscopy. Writing of the first manuscript draft and collaborative finalization of the manuscript.

Sequence-defined Heteroglycomacromolecules Bearing Sulfated and Sulfonated Non-Glycosidic Moieties Selectively Bind Galectin-3 and Delay Wound Healing of a Galectin-3 Positive Tumor Cell Line

Tanja Freichel[a], Viktoria Heine[b], Dominic Laaf[b], Eleanor E. Mackintosh[c], Sophia Sarafova[c], Lothar Elling[b], Nicole L. Snyder* [c], and Laura Hartmann* [a]

[a] T. Freichel, Prof. Dr. L. Hartmann*, Heinrich-Heine University Düsseldorf, Institute of Organic and Macromolecular Chemistry, Universitätsstraße 1, 40225 Düsseldorf, Germany.

[b] Dr. D. Laaf, Prof. Dr. L. Elling, RWTH Aachen, RWTH Aachen University, Laboratory for Biomaterials, Institute for Biotechnology and Helmholtz-Institute for Biomedical Engineering, Pauwelsstr. 20, 52074 Aachen, Germany.

[c] Prof. Dr. S. Sarafova, Prof. Dr. N. L. Snyder*, Davidson College. Chemistry Department, Davidson, NC 28035, U.S.

ABSTRACT: Within this work, we introduce a new class of sequence-defined heteromultivalent glycomacromolecules bearing both lactose residues and non-glycosidic moieties with the goal of addressing secondary binding sites in the carbohydrate recognition domain of galectin-3. Galectins, a family of β-galactoside-binding proteins, are known to play crucial roles in different signaling pathways involved in tumor biology. Thus, research has focused on the design and synthesis of galectin targeting ligands for use as diagnostic markers or potential therapeutics. Heteromultivalent glycomacromolecules provide for the development of ligands with high avidity and specificity, which we demonstrate by combining the concepts of multivalency and the introduction of non-glycosidic moieties bearing either neutral, amine or sulfonated/sulfated groups. Enzyme linked immunosorbent assay and surface plasmon resonance studies were performed with the aforementioned glycomacromolecules, demonstrating a positive impact of the sulfonated/sulfated non-glycosidic moieties on galectin-3 binding but not on galectin-1 binding. Furthermore, selected compounds were tested on galectin-3 positive MCF 7 breast cancer cells, resulting in a selective biological effect in wound closure assays.

Many processes in tumorigenesis are the result of dysregulated protein expression and the presentation of abnormal glycan motifs on the cell surface. [1-3] One family of proteins known to be involved in tumor biology are the galectins. Galectins consist of a conserved carbohydrate recognition domain that is known to bind β-galactoside terminating glycans such as those terminating in lactose (Lac) or poly *N*-acetyl-lactosamine (LacNAc). Galectin-3 (Gal-3) is the only chimeric galectin within the galectin family, and contains a proline-rich *N*-terminal domain which can self-oligomerize into pentameric lectin lattices.[4, 5] Gal-3 is normally found in the nucleus and cytoplasm, but can also be secreted and can interact with glycoproteins on cell surfaces. Gal-3 has been shown to play an important role in tumor metastasis and migration.[2, 6, 7] For example, monoclonal anti-galectin-3 antibodies and synthetic glycoamines were successfully used to inhibit lung metastasis and breast cancer metastasis in mouse models, respectively.[2, 8, 9] Based on these findings, a significant number of studies have been devoted to the synthesis and design of Gal-3 ligands for use as diagnostic markers or potential therapeutics.[5, 10-12] In an effort to enhance Gal-3-carbohydrate ligand interactions, several different strategies have been explored. One example involves the multivalent presentation of carbohydrate residues on macromolecular scaffolds as described by Gabius and Pieters,[13, 14] Gabius and Roy,[15, 16] Elling,[17] Cloninger,[18, 19] Lecommandoux[20] and Wang.[21, 22] This approach takes advantage of the ability of Gal-3 to oligomerize in the presence of multivalent ligands leading to an effective increase in binding avidity.[23, 24] Other studies using monovalent carbohydrates have revealed that the introduction of non-glycosidic moieties can enhance the affinity of ligands targeting Gal-3.[25-27] For example, Nilsson and co-workers demonstrated that galactose derivatives containing aldoximes with different aromatic residues at the anomeric center could serve as LacNAc-mimetics with increased affinity.[11] As another example, TD139, a small molecule Gal-3 ligand bearing non-glycosidic moieties, is currently in clinical trials for treating idiopathic pulmonary fibrosis (IPF).[28] In addition to non-glycosidic moieties, it has also been demonstrated, that sulfation patterns can be used to attenuate the affinity and selectivity of ligands for Gal-3.[5, 29-32] For example, Nilsson

and Leffler revealed that by combining sulfation and incorporating non-glycosidic moieties increased binding to Gal-3 could be achieved, from a K_d value of 5900 µM for the unsubstituted methyl galactoside to 2800 µM for the 2-*O*-sulfated and 87 µM for the 3-*O*-methylbenzamido- and 2-*O*-sulfated derivative.[33, 34] Thus the combination of all three approaches, multivalency, sulfation and non-glycosidic moieties, via the use of heteromultivalent glycomacromolecules provides an attractive platform for the development of high avidity and specificity ligands [35-37], but to the best of our knowledge has not yet been applied for targeting Gal-3.

Herein, we report the solid phase polymer synthesis (SPPoS) of a library of sequence-defined lactose-based glycooligo(amidoamines) bearing non-glycosidic, sulfonated and sulfated moieties as selective ligands of Gal-3. The resulting heteromultivalent glycomacromolecules were evaluated for binding to Gal-3 and Gal-1 using enzyme-linked immunosorbent assay (ELISA). Results from ELISA studies revealed that glycomacromolecules bearing lactose and sulfate or sulfonate groups selectively bound Gal-3 over Gal-1. Binding studies with Gal-3 were then confirmed surface-plasmon resonance (SPR) studies.

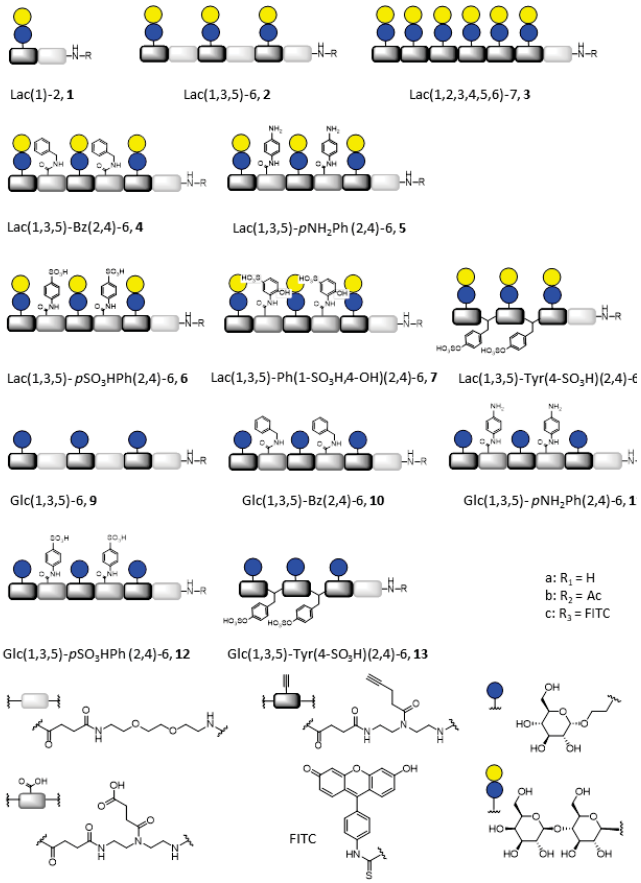

Scheme 1. Overview of synthesized structures.

The best ligands were then applied to a wound healing assay using Gal-3 positive human cancer cells, demonstrating their selective ability to interfere with tumor cell migration. Lactose-based glycomacromolecules **1-8** were prepared as potential selective ligands for Gal-3 and glucose derivatives **9-13** as non-binding controls (Scheme 1). SPPoS uses tailor-made building blocks for the stepwise assembly of monodisperse, sequence-defined oligo(amidoamines) on solid support by applying standard Fmoc-peptide coupling protocols. The building blocks used in this study include TDS (triple bond diethylenetriamine succinyl, 1-(fluorenyl)-3,11-dioxo-7-(pent-4-ynoyl)-2-oxa-4,7,10-triazatetra-decan-14-oic acid)[38] for introducing an alkyne moiety in the side chain that can be used for site-selective conjugation of azido-functionalized carbohydrates via copper-catalyzed azide-alkyne cycloaddition (CuAAC), MDS (methyl succinyl diethylenetriamine succinyl, 1-(9H-fluoren-9-yl)-7-(4-methoxy-4-oxobutanoyl)-3,11-dioxo-2-oxa-4,7,10-triazatetradecan-14-oic acid)[39] for introducing a carboxylic group in the side chain for conjugation via amide coupling, and EDS (ethylene glycol diamine succinyl, 1-(9H-fluoren-9-yl)-3,14-dioxo-2,7,10-trioxa-4,13-diazaheptadecan-17-oic acid)[40] for introducing an ethylene glycol motif in the main chain. Homomultivalent glycomacromolecules **1-3,** and **9** were synthesized according to previously established methods using TDS and EDS (see SI p.8-28 and p.50-56) and vary in the number of glycosidic residues.[38, 41] With the exception of **1** and **3**, which were designed to represent mono- and higher valent analogs respectively, all heteromultivalent glycomacromolecules carry three glycosidic residues and two non-glycosidic moieties, and were designed to be similar in length and molecular weight for better comparison in binding studies.

Heteromultivalent glycomacromolecules were synthesized by replacing the EDS building blocks of compound **2** with MDS.[39] The carboxylic side chain of the MDS building block and the alkyne moiety of the TDS building block enabled orthogonal post-modification of the scaffolds via amine coupling and CuAAC, respectively. As non-glycosidic moieties, aryl-residues bearing different amine or sulfonic acid functionalities were used.[42] Sulfonic acid functionalities were used instead of sulfates because of their inherent stability. Glycomacromolecules were synthesized with different end-functionalities: free (subgroup a) and capped amine (subgroup b) or FITC-conjugated derivatives (subgroup c) for different studies (Scheme 1).

Final glycomacromolecules were deprotected, cleaved from the resin, purified by ion-exchange chromatography, and preparative RP-HPLC, and isolated with purities > 90 % (as determined by RP-HPLC analysis) (see SI Figures S29-S49; S57-S76).

Table 1. Results of the inhibition-competition binding studies of glycomacromolecules 1b-8b to Gal-1 and Gal-3 in the ELISA-type assay and Gal-3 in SPR measurements.

Glycomacromolecule	Carbohydrate residues	Gal-1 IC_{50}±SD [μM] [a]	RIP_{Gal-1} [b]	Gal-3 IC_{50}±SD [μM] [a]	RIP_{Gal-3}[b]	Gal-3 IP[%][c]
Lactose	1	420 ± 94	1.0	159 ± 13	1	-
1b	1	296 ± 70	1.4	123 ± 3	1.3	31 ± 3
2b	3	55 ± 12	7.6	38 ± 2	4.2	68 ± 2
3b	6	64 ± 5	6.5	16 ± 4	9.9	78 ± 0.5
4b	3	105 ± 14	4.0	25 ± 1	6.3	73 ± 3
5b	3	134 ± 22	3.1	22 ± 2	7.4	75 ± 3
6b	3	100 ± 21	4.2	16 ± 1	9.9	79 ± 3
7b	3	127 ± 19	3.3	15 ± 0.3	10.5	81 ± 2
8a/b	3	89 ±18	4.7	14 ± 1	11.4	78 ± 0.4

[a] IC_{50} values were determined in ELISA-type inhibition studies for Gal-1 and Gal-3 binding to asialofetuin. Measurements were performed two times in triplicates. Results for Gal-3 were confirmed by SPR experiments at one fixed concentration of ligands and Gal-3 (see SI). [b] Relative inhibitory potency (RIP): Calculated referring to the IC_{50}-value of lactose. [c] Inhibitory potency (IP) resulting from the SPR inhibition studies were calculated relative to the binding signal of pure Gal-3 to the glycomacromolecule **2a** functionalized SPR-surface as a 100 % binding signal and 0 % IP.

For Lac(1,3,5)-Ph(1-SO_3H,4-OH)(2,4)-6, **7**, attachment of the non-glycosidic sidechain after carbohydrate conjugation as described above was unsuccessful, potentially due to steric hindrance of the lactose residues. Therefore, the synthetic route was altered to reverse the amide and CuAAC coupling steps. This strategy resulted in the desired product after deprotection, cleavage and purification (see SI Figure S57-S60). Furthermore, shorter sulfated heterostructures **8** and **13** were synthesized using Fmoc-L-Tyr(4-SO_3H)-OH instead of the MDS building block, applying standard protocols giving the desired products after deprotection, cleavage and purification.

To investigate the binding avidities of the heteromultivalent glycomacromolecules as selective ligands for Gal-3, competitive-inhibition binding studies were performed testing the ability to competitively inhibit the binding of Gal-3 to the glycoprotein asialofetuin (ELISA). These results were compared to similar studies with Gal-1 to determine selectivity differences between these two galectins. Gal-1 was selected for these studies because of the similarities in their carbohydrate recognition domains (CRD) as well as their significant but unique roles in tumor metastasis and transformation. ELISA gives the half-maximum inhibitory concentration (IC_{50}) of each ligand as a measure of avidity towards Gal-3 or Gal-1. Lower IC_{50}-values thus correspond to higher avidity (Table 1).

In general, homomultivalent structures show similar binding (Gal-1) or an increase in binding (Gal-3) with increasing valency. However, when comparing trivalent homomultivalent glycomacromolecule **2b** lacking aromatic residues with trivalent heteromultivalent analogs **4b-8b** bearing aromatic residues, binding to Gal-1 decreased while binding to Gal-3 increase. For better comparison, IC_{50}-values were normalized to the IC_{50}-value of lactose giving the relative inhibitory potential (Table 1: RIP). Heteromultivalent glycomacromolecule ligands containing aromatic residues and three lactose units (**4b-8a/b**) showed decreased binding with Gal-1 by a factor of 1.5 to 2–fold in comparison to **2b**. In contrast, binding to Gal-3 increased by a factor of 1.5 to 3–fold. The latter observation is likely due to hydrophobic interactions in the binding site of the CRD of Gal-3 and is in accordance with the aforementioned studies on aromatic residues and their participation in a Gal-3 binding event.[43] The Gal-3 CRD of consists of five different subunits A-E; lactose is known to bind within subunits C and D, whereby subunits A, B and E serve as potential secondary bindings sites.[44,45]

Notably, significant increases in binding were observed for glycomacromolecules bearing sulfonated (**6b** and **7b**) and sulfated (**8b**) aromatic moieties in binding studies with Gal-

3. These results were further confirmed by SPR assays conducted with the heteromultivalent glycomacromolecules and Gal-3 using lactose glycomacromolecule **2a** for comparison.[27] For SPR experiments, a fixed concentration of Gal-3 and a ligand was used to determine the inhibitory potencies (IP) of the ligand as a value for avidity. A higher IP caused by the same ligand concentration would correspond to higher avidity (Table 1). The higher avidity of the sulfonated and sulfated derivatives (**6b**-**8b**) is in accordance with studies investigating the influence of negatively charged glycans on Gal-3 binding showing higher affinities in comparison to uncharged glycans.[29, 31, 32] When further normalizing the RIP onto the number of binding motifs for Gal-3, counting both carbohydrates and non-glycosidic moieties, we see that replacing carbohydrate ligands of **3b** with non-glycosidic motifs results in conjugates with similar (**6b**) or even higher (**7b** and **8b**) overall avidity. However, when replacing the binding carbohydrate ligands (lactose) with a non-binding carbohydrate ligand (glucose, **9b**-**13b**), we see no inhibition in both ELISA and SPR studies (see SI Figure S111 -S113) showing that the lactose is required for binding to Gal-3 and only the specific combination of lactose and sulfonated or sulfated non-glycosidic motifs leads to higher avidity ligands.

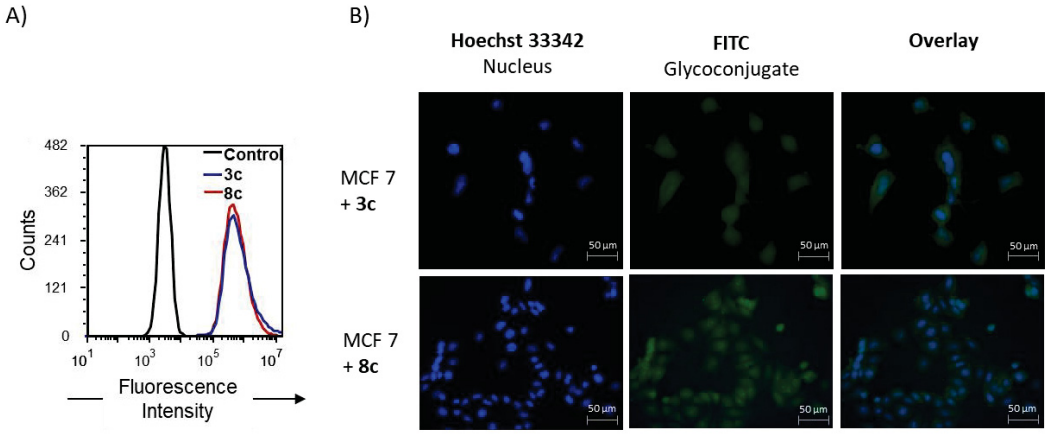

Figure 1. Interaction and localization studies of FITC-derivatives **3c** and **8c** on MCF 7 cells. A) Flow cytometry histogram of the FITC-channel for blank cells and cells stained with 200 µM **3c** (red) and **8c** (blue). B) Fluorescence images of MCF 7 cells stained with 200 µM **3c** and **8c** (3 hours at 37°C) and as references Hoechst 33342 staining for nucleus localization

To further investigate the effect of glycomacromolecules as ligands of Gal-3 in functions of cells overexpressing the Gal-3 receptor, *in vitro* cell studies were performed using human breast cancer cell line MCF 7 (known to overexpress Gal-3) and epithelial cell line HEK 293 (control with no Gal-3 receptors).[46] Immunostaining of untreated live cells confirmed that only MCF 7 cells have cell surface expression of Gal-3 and neither cell line has cell surface expression of Gal-1, a galectin with similar binding properties (Figures S114). Internal staining of fixed, permeabilized MCF 7 cells resulted in higher level of Gal-3 staining, demonstrating that a substantial intracellular reserve of Gal-3 is present in these cells (Figure S114). In contrast, HEK 293 has a substantially lower expression of intracellular Gal-3 that is notably less than the intracellular expression of Gal-1.

As a prerequisite for further testing, cell toxicity of glycomacromolecules selected for cell experiments (**1-3**, **6**, **8-9**,**12-14**) was determined via MTT cell viability assay. Results demonstrated no detectable differences in viability between the vehicle control and cells treated with the glycomacromolecules after 48 h incubation (Figure S115 /116). To test the general ability of glycomacromolecules to interact with the cells, flow cytometry studies were performed using FITC-conjugated derivatives **1c-3c, 6c, 8c, 9c, 12c, 13c** at two different concentrations. After fixation of the cells, analysis of stained cells via flow cytometry showed a dose dependent staining for both cell lines for all compounds (Figure S117/118). The lack of a significant difference in the mean-FITC values suggests non-selective uptake rather than selective uptake (Figure 1A). Fluorescence microscopy was then performed to analyze localization of the glycomacromolecules. Exemplary comparison of compounds **3c** (**3b** as best homomultivalent binder) and **8c** (**8b** as best heteromultivalent binder) shows a general staining of both cell lines (Figure 1B, for HEK 293 see SI). However, for compound **8c**, there appears to be a stronger enrichment of fluorescence around the nucleus in comparison to the cytosol. A similar pattern was observed for cells stained with **6c**, **12c** and **13c** (Figure S119-S123) and

seems to be related to the presence of the aryl sulfonated/sulfated side chains. One possible explanation for this finding is that the negative charge of the sulfonic acids might lead to an attractive interaction with positively charged nucleoporins.[47] However, at this point, it is not possible to differentiate between an enrichment on or in the nucleus.

Since the tested glycomacromolecules showed no cytotoxic behavior and positive uptake into cells, we decided to study their influence on cell migration, which is known to be mediated by Gal-3. This was accomplished by performing a wound closure assay as described by Dion and coworkers[48, 49] using compounds **1a-3a**, **6a**, **8a-9a** and **12-14a** representing the direct precursor of the FITC derivatives. Cells were cultivated as a monolayer and a "wound field" was created (Figure 2A). Cells were then incubated with the glycomacromolecules, and the width of the wound field was observed under an inverted microscope. The distance analysis at different time points was used to create a wound closure curve (Figure 2B). In this model, ligand binding to Gal-3 is expected to result in a reduction in wound closure over time.

Indeed, we observed different effects on wound closure for the different glycomacromolecules (Figure S124-133; Table S1-S3). Generally, glucose functionalized glycomacromolecules resulted in a slightly faster wound closure.[50] In comparison, the lactose-derivatives led to a delayed wound closure, especially sulfonic acid derivatives **6a** and sulfated **8a**. For example, after 48 h compound **8a** differed with 57 ± 5 % almost 20 % from the corresponding glucose derivative **13a** showing 76 ± 5 % closure (Table S2).

These results are in agreement with similar studies on other ligand systems targeting lectins involved in cell migration.[42, 48, 49, 51] For example, Dion and co-workers observed a delay in wound healing of around 20 % for the treatment of keratinocytes with lactosamine based (2-naphthyl)methyl compounds inspired by TD139, which is currently in clinical trials.[28, 48, 49] Ramen and co-workers achieved a delay of 20-30 % through the incubation of MCF 7 cells with a nucleoside analogue addressing RNA helicase.[51]

To examine the effects of sustained exposure of the glycomacromolecules on the MCF 7 cells, we performed a "dosing" study by introducing additional aliquots of glycomacromolecules **6a**, **8a**, **12a** and **13a** after 12, 24, 36 and 48 h giving in total an additional 100 mol% (Figure 2b). In this experiment, the differences in wound closure were even more significant, yielding delays of 53 ± 7 % for **8a** compared to 80 ± 4 % for **13a** after 48 h (Figure S127, S133 and Table S3) indicating a dose specific response. The same experiments were repeated on the HEK 293 cell line. However, no significant difference in the migration was observed in comparison to the vehicle control (Figure S128-131). Therefore, we concluded that glycomacromolecule ligands with higher inhibition potentials in the ELISA and SPR studies also showed stronger effects in the migration assay for Gal-3 positive cells. Again we find that replacing carbohydrate ligands with sulfonated/sulfated non-glycosidic motifs results similar or even stronger effects (comparing **3a** and **8a**). Negative controls replacing lactose by glucose side chains, showed no effects in similar studies, confirming that it is the combination of carbohydrate and non-glycosidic motifs that enables high avidity and selective binding.

In conclusion, we introduced the synthesis of heteromultivalent lactose-functionalized glycomacromolecules bearing non-glycosidic moieties as side chains. These structures were successfully tested as inhibitors of Gal-3 using ELISA and SPR studies showing increased selectivity and avidity can be achieved through combination of both, glycosidic- and non-glycosidic, especially sulfonated or sulfated motifs. The same trend was observed in wound closure studies using a Gal-3 positive MCF 7 breast-cancer cell line where the most significant biological effect was achieved for structures shown to have the highest inhibition of Gal-3. Based on these findings, future studies will explore the possibility of using heteromultivalent glycomacromolecules in lectin-based drug targeting applications, and will further study their effects on cell migration.

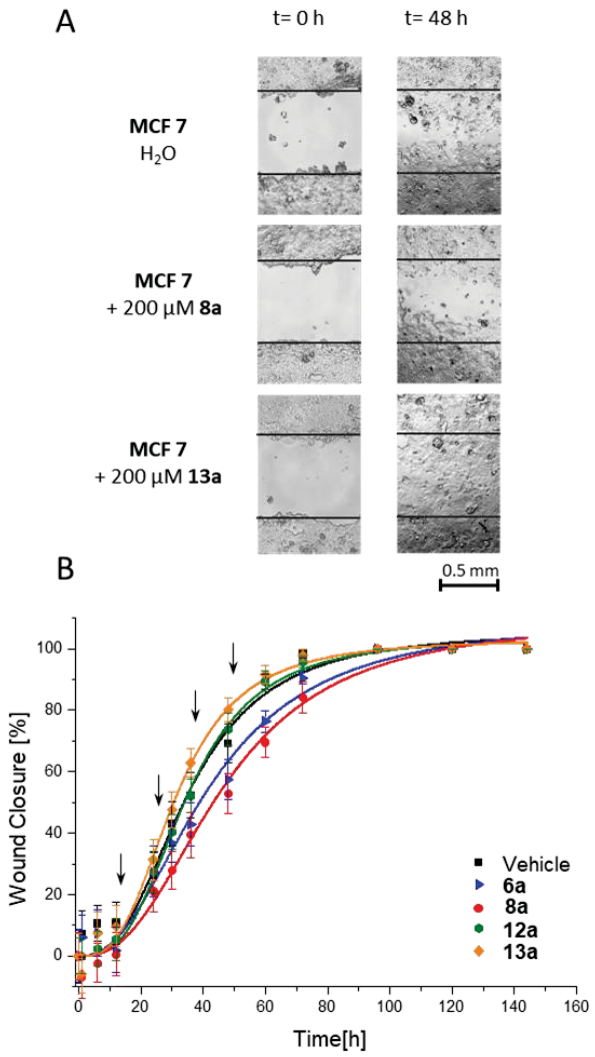

Figure 2. Wound healing experiment of MCF 7. A. Exemplary images of the wound area at time point t=0h and t=48 h for MCF 7 treated with the vehicle control H_2O (top), lactose structure **8a** (middle) and corresponding glucose structure **13a** (bottom). B. Results of the time dependent wound closure for dosing tests with compounds **6a**,**8a**,**12a** and **13a**. (for more data see SI S124-S133)

ASSOCIATED CONTENT

Supporting Information

The Supporting Information is available free of charge on the ACS Publications website. Experimental details and analytical data are presented in the supporting information. File type: PDF.

AUTHOR INFORMATION

Corresponding Author

Prof. Dr. Laura Hartmann
Heinrich-Heine University Düsseldorf
Institute of Organic and Macromolecular Chemistry
Universitätsstraße 1, 40225 Düsseldorf, Germany
E-mail: Laura.Hartmann@hhu.de.

Present Addresses

[a] T. Freichel, Prof. Dr. L. Hartmann*
Heinrich-Heine University Düsseldorf
Institute of Organic and Macromolecular Chemistry
Universitätsstraße 1, 40225 Düsseldorf, Germany

[b] Dr. D. Laaf, Prof. Dr. L. Elling
RWTH Aachen
RWTH Aachen University, Laboratory for Biomaterials, Institute for Biotechnology and Helmholtz-Institute for Biomedical Engineering, Pauwelsstr. 20, 52074 Aachen, Germany

[c] Prof. Dr. S. Sarafova, Prof. Dr. N. L. Snyder*
Davidson College
Chemistry Department
Davidson, NC 28035, U.S.

Notes

The authors declare no competing financial interests.

ACKNOWLEDGMENT

The authors thank the Boehringer-Ingelheim-Foundation for support through the 'Perspektivenprogramm Plus3'. T.F. would like to thank Junior Scientist and International Researcher Center (JUNO) at Heinrich-Heine University for support through the StayConnected@HHU program. N.L.S would like to thank the NIH for partial support through an NIH-R15 award (1R15GM119067-01) and an NSF-MRI award (1624377). The authors thank Nika Fendler for her support in tissue culturing. D.L., V.H. and L.E acknowledge support by the Deutsche Forschungsgemeinschaft DFG through the collaborative research center SFB 985 "Functional microgels and microgel systems" (project C3) and DFG project EL 135/12-1.

REFERENCES

[1] P. M. Pereira, W. Rizvi, N. V. S. D. K. Bhupathiraju, N. Berisha,R. Fernandes, J. P. C. Tomé, C. M. Drain, *Bioconjugate Chem.*, **2018**, 29, 306-315.
[2] C. A. Duckworth, S. E. Guimond, P. Sindrewicz, A. J. Hughes, N. S. French, L.-Y. Lian, E. A. Yates, D. M. Pritchard, J. M. Rhodes, J. E. Turnbull, L.-G. Yu, *Oncotarget*, **2015**, 6, 23671-23687.
[3] D. H. Dube, C. R. Bertozzi, *Nat. Rev. Drug Discovery*, **2005**, 4, 477.
[4] K. C. Haudek, K. J. Spronk, P. G. Voss, R. J. Patterson, J. L. Wang, E. J. Arnoys, *Biochim. Biophys. Acta*, **2010**, 1800, 181.
[5] L. Ballell, M. van Scherpenzeel, K. Buchalova, R. M. J. Liskamp, R. J. Pieters, *Org. Biomol. Chem.*, **2006**, 4, 4387-4394.
[6] A. C. F. Cardoso, L. N. d. S. Andrade, S. O. Bustos, R. Chammas, *Front. Oncol.* **2016**, 6, 1-12.
[7] T. Funasaka, A. Raz, P. Nangia-Makker, *Semin. Cancer Biol.*, **2014**, 0, 30-38.
[8] P. Nangia-Makker, V. Hogan, Y. Honjo, S. Baccarini, L. Tait, R. Bresalier, A. Raz, *J. Natl. Cancer Inst.*, **2002**, 94, 1854-1862.

[9] F.-T. Liu, G. A. Rabinovich, *Nat. Rev. Cancer*., **2005**, 5, 29.
[10] V. L. Campo, M. F. Marchiori, L. C. Rodrigues, M. Dias-Baruffi *Glycoconjugate J*., **2016**, 33, 853-876.
[11] J. Tejler, H. Leffler, U. J. Nilsson, *Bioorg. Med. Chem. Lett.,* **2005**, 15, 2343-2345.
[12] H. Blanchard, X. Yu, P. M. Collins, K. Bum-Erdene, *Expert Opin. Ther. Pat.,* **2014**, 24, 1053-1065.
[13] I. Vrasidas, S. André, P. Valentini, C. Böck, M. Lensch, H. Kaltner, R. M. J. Liskamp, H.-J. Gabius, R. J. Pieters, *Org. Biomol. Chem.,* **2003**, 1, 803-810.
[14] S. André, R. J. Pieters, I. Vrasidas, H. Kaltner, I. Kuwabara, F.-T. Liu, R. M. J. Liskamp, H.-J. Gabius *ChemBioChem*., **2001**, 2, 822-830.
[15] S. André, B. Liu, H.-J. Gabius, R. Roy, *Org. Biomol. Chem.,* **2003**, 1, 3909-3916.
[16] L. Abbassi, Y. M. Chabre, N. Kottari, A. A. Arnold, S. André, J. Josserand, H.-J. Gabius, R. Roy, *Polym Chem.*, **2015**, 6, 7666-7683.
[17] L. Bumba, D. Laaf, V. Spiwok, L. Elling, V. Křen, P. Bojarová, *Int. J. Mol. Sci.,* **2018**, 19, 372.
[18] C. K. Goodman, M. L. Wolfenden, P. Nangia-Makker, A. K. Michel, A. Raz, M. J. Cloninger, *Beilstein J. Org. Chem.,* **2014**, 10, 1570-1577.
[19] A. K. Michel, P. Nangia-Makker, A. Raz, M. J. Cloninger, *ChemBioChem.,* **2014**, 15, 2106-2112.
[20] C. Bonduelle, H. Oliveira, C. Gauche, J. Huang, A. Heise, S. Lecommandoux, *Chem. Commun.,* **2016**, 52, 11251-11254.
[21] H. Wang, W. Huang, J. Orwenyo, A. Banerjee, G. R. Vasta, L.-X. Wang, *Bioorg. Med. Chem.,* **2013**, 21, 2037-2044.
[22] J. H. Ennist, H. R. Termuehlen, S. P. Bernhard, M. S. Fricke, M. J. Cloninger, *Bioconjugate Chem.,* **2018**, 29, 4030-4039.
[23] C. Boscher, J. W. Dennis, I. R. Nabi, *Curr. Opin. Cell Biol.,* **2011**, 23, 383-392.
[24] T. K. Dam, H.-J. Gabius, S. André, H. Kaltner, M. Lensch, C. F. Brewer, *Biochemistry*. **2005**, 44, 12564-12571.
[25] C. T. Öberg, H. Leffler, U. J. Nilsson, *CHIMIA,* **2011**, 65, 18-23.
[26] T. Delaine, I. Cumpstey, L. Ingrassia, M. L. Mercier, P. Okechukwu, H. Leffler, R. Kiss, U. J. Nilsson, *J. Med. Chem.,* **2008**, 51, 8109-8114.
[27] H. Zhang, D. Laaf, L. Elling, R. J. Pieters, *Bioconjugate Chem*., **2018**, 29, 1266-1275.
[28] A. Mackinnon, L. Nicol, J. Walker, P. Ford, H. Schambye, A. Pederson, U. Nilsson, H. Leffler, T. Thomas, D. Francombe, J. Simpson, M. Gibbons, T. M. Maher, *A24. IPF: CLINICAL STUDIES, THERAPEUTICS, AND MORE,* **2017,** A7560-A7560.
[29] Q. Xiao, A.-K. Ludwig, C. Romanò, I. Buzzacchera, S. E. Sherman, M. Vetro, S. Vértesy, H. Kaltner, E. H. Reed, M. Möller, C. J. Wilson, D. A. Hammer, S. Oscarson, M. L. Klein, H.-J. Gabius, V. Percec, *Proc. Natl. Acad. Sci.,* **2018**, 115, E2509-E2518.
[30] H. Tateno, A. Mori, N. Uchiyama, R. Yabe, J. Iwaki, T. Shikanai, T. Angata, H. Narimatsu, J. Hirabayashi, *Glycobiology*, **2008**, 18, 789-798.
[31] M. L. Talaga, N. Fan, A. L. Fueri, R. K. Brown, P. Bandyopadhyay, T. K. Dam *Biochemistry*. **2016**, 55, 4541-4551.
[32] S. R. Stowell, C. M. Arthur, P. Mehta, K. A. Slanina, O. Blixt, H. Leffler, D. F. Smith, R. D. Cummings, *J. Biol. Chem.*, **2008**, 283, 10109-10123.
[33] C. T. Öberg, H. Leffler, U. J. Nilsson, *J. Med. Chem.,* **2008**, 51, 2297-2301.
[34] C. T. Öberg, A.-L. Noresson, H. Leffler, U. J. Nilsson, *Chem. Eur. J.,* **2011**, 17, 8139-8144.
[35] L. E. Wilkins, N. Badi, F. Du Prez, M. I. Gibson, *ACS Macro Lett*., **2018**, 7, 1498-1502.
[36] H.-A. Tran, P. I. Kitov, E. Paszkiewicz, J. M. Sadowska, D. R. Bundle, *Org. Biomol. Chem.,* **2011**, 9, 3658-3671.
[37] M. W. Jones, L. Otten, S. J. Richards, R. Lowery, D. J. Phillips, D. M. Haddleton, M. I. Gibson, *Chem. Sci*., **2014**, 5, 1611-1616.
[38] D. Ponader, F. Wojcik, F. Beceren-Braun, J. Dernedde, L. Hartmann, *Biomacromolecules*. **2012**, 13, 1845-1852.
[39] T. Freichel, S. Eierhoff, N. L. Snyder, L. Hartmann, *J. Org. Chem.,* **2017**, 82, 9400-9409.
[40] M. F. Ebbesen, C. Gerke, P. Hartwig, L. Hartmann, *Polym. Chem*., **2016**, 7, 7086-7093.
[41] D. Ponader, P. Maffre, J. Aretz, D. Pussak, N. M. Ninnemann, S. Schmidt, P. H. Seeberger, C. Rademacher, G. U. Nienhaus, L. Hartmann, *J. Am. Chem. Soc.,* **2014**, 136, 2008-2016.
[42] J. Brunetti, L. Depau, C. Falciani, M. Gentile, E. Mandarini, G. Riolo, P. Lupetti, A. Pini, L. Bracci, *Sci. Rep*., **2016**, 6, 27174.
[43] S. R. Rauthu, T. C. Shiao, S. André, M. C. Miller, É. Madej, K. H. Mayo, H.-J. Gabius, R. Roy, *ChemBioChem*., **2015**, 16, 126-139.
[44] V. Denavit, D. Lainé, T. Tremblay, J. St-Gelais, D. Giguère, *Trends Glycosci. Glycotechnol.*, **2018**, 30, SE21-SE40.
[45] K. L. Hudson, G. J. Bartlett, R. C. Diehl, J. Agirre, T. Gallagher, L. L. Kiessling, D. N. Woolfson, *J. Am. Chem. Soc.,* **2015**, 137, 15152-15160.
[46] P. S. R. Arun Satelli, Prem K. Gupta, Paul R. Lockman, Kalkunte S. Srivenugopal, U. Subrahmanyeswara Rao, *Oncology*., **2008**, 19, 587-594.
[47] A. Goryaynov, W. Yang, *PLOS ONE*, **2014**, 9, e88792.
[48] D. Johann, D. Frédérique, S. Nataliya, A. Tamara, L. Annie, V. Mireille, T. Charles, D. Christophe, P. Françoise, G. Cyrille, *ChemBioChem*., **2017**, 18, 782-789.
[49] D. Johann, A. Tamara, S. Nataliya, D. Samir, L. Annie, D. Frédérique, V. Mireille, T. Charles, P. Françoise, T. Stéphane, D. Christophe, T. Hiroaki, H. Jun, G. Cyrille, *ChemBioChem*., **2017**, 18, 2428-2440.
[50] X. Chen, L. Hui, D. A. Foster, C. M. Drain, *Biochemistry*, **2004**, 43, 10918-10929.
[51] M. Xie, F. Vesuna, M. Botlagunta, G. M. Bol, A. Irving, Y. Bergman, R. S. Hosmane, Y. Kato, P. T. Winnard, V. Raman, *Oncotarget*, **2015**, 6, 29901-2991.

Supporting Information

Sequence-defined Heteroglycomacromolecules Bearing Sulfated and Sulfonated Non-Glycosidic Moieties Selectively Bind Galectin-3 and Delay Wound Healing of a Galectin-3 Positive Tumor Cell Line

Tanja Freichel[a], Viktoria Heine[b], Dominic Laaf[b], Eleanor E. Mackintosh[c], Sophia Sarafova[c], Lothar Elling[b], Nicole L. Snyder* [c], and Laura Hartmann* [a]

ABSTRACT: Within this work, we introduce a new class of sequence-defined heteromultivalent glycomacromolecules bearing both lactose residues and non-glycosidic moieties with the goal of addressing secondary binding sites in the carbohydrate recognition domain of galectin-3. Galectins, a family of β-galactoside-binding proteins, are known to play crucial roles in different signaling pathways involved in tumor biology. Thus, research has focused on the design and synthesis of galectin targeting ligands for use as diagnostic markers or potential therapeutics. Heteromultivalent glycomacromolecules provide for the development of ligands with high avidity and specificity, which we demonstrate by combining the concepts of multivalency and the introduction of non-glycosidic moieties bearing either neutral, amine or sulfonated/sulfated groups. Enzyme linked immunosorbent assay and surface plasmon resonance studies were performed with the aforementioned glycomacromolecules, demonstrating a positive impact of the sulfonated/sulfated non-glycosidic moieties on galectin-3 binding but not on galectin-1 binding. Furthermore, selected compounds were tested on galectin-3 positive MCF 7 breast cancer cells, resulting in a selective biological effect in wound closure assays. DOI: 10.1002/anie.2016XXXXX

[a] T. Freichel, Prof. Dr. L. Hartmann*
Heinrich-Heine University Düsseldorf
Institute of Organic and Macromolecular Chemistry
Universitätsstraße 1, 40225 Düsseldorf, Germany
E-mail: Laura.Hartmann@hhu.de

[b] Dr. D. Laaf, Prof. Dr. L. Elling
RWTH Aachen
RWTH Aachen University, Laboratory for Biomaterials, Institute for Biotechnology and Helmholtz-Institute for Biomedical Engineering,
Pauwelsstr. 20, 52074 Aachen, Germany

[c] Prof. Dr. S. Sarafova, Prof. Dr. N. L. Snyder*
Davidson College
Chemistry Department
Davidson, NC 28035, U.S.
E-mail: nisnyder@davidson.edu

Table of Contents

Figures

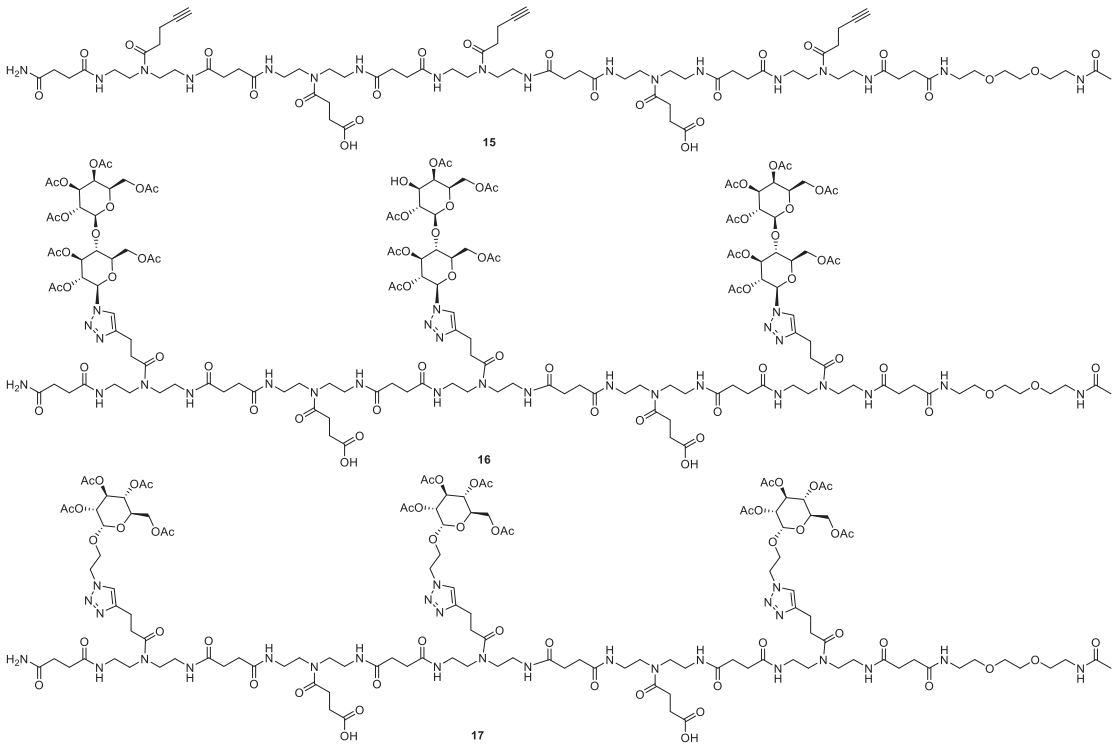

Figure S 1: Precursors for the synthesis of the heteroglycoconjugates.

Experimental Procedures

Synthesis of Glycomacromolecules

General Methods

Acetic anhydride was purchased from VWR chemicals. Piperidine, trifluoro acetic acid, sodium methoxide, *N*-Boc phenylenediamine 4-pentynoic acid and sodium diethyldithiocarbamte were purchased from Acros Organics. Dimethylformamide (for peptide synthesis) was purchased from Biosolve. 3-Amino-4-hydroxy benzene-sulfonic acid and TIPS were purchased from Sigma Aldrich. 4-Amino benzene sulfonic acid was purchased from J&K, benzylamine, oxalyl chloride from Alfa Aesar. HOBt was purchased from Iris Biotech. DIPEA and diethylenetriamine were purchased from Carl Roth, lithium hydroxide, sodium ascorbate and potassium carbonate from PanReac AppliChem. DCM and triethyleneamine were purchased from Merck. HATU was purchased from Abcr. PyBOP from Fluorochem and $CuSO_4$ anhydrous from Fluka Chemika. Fmoc-L-Tyr(4-SO_3H)-OH was purchased from Iris Biotech GmbH. Solid phase synthesis was performed on TentaGel®SRam resin purchased from Rapp Polymere using polypropylene reactors with polyethylene frits closed with luerstoppers from MultiSyntech GmbH. Building blocks TDS, EDS and MDS were synthesized as reported earlier. (2-Azidoethyl)-2,3,4,6-tetra-O-acetyl-β-D-galactopyranoside, (2-Azidoethyl)-2,3,4,6-tetra-O-acetyl-α-D-glucosepyranoside and 2,3,4,6-tetra-O-acetyl-α-D-glucosepyranoside were synthesized as known from literature.[1] Reactions were monitored via analytical thin layer chromatography, performed on Merck silica gel 60 F254 plates and were visualized with ninhydrin staining. All reagents and solvents were used without further purification.

^{1}H-NMR and ^{13}C-NMR spectra were measured on Bruker Avance III 300 or Bruker Avance III 600. Analytic reversed phase HPLC (RP-HPLC) measurements were performed on Agilent Technologies 6120 series coupled with an Agilent Quadrupol mass spectrometer. All spectra were measured with solvent A: 95 % H_2O, 5 % ACN, 0.1 % formic acid, and solvent B: 5 % H_2O, 95 % ACN, 0.1 % formic acid with a gradient of 5 to 50 % B in 30 min. Purities of the compounds were determined by the integrations of the signals given through the absorption at 214 nm. Preparative RP-HPLC was performed on an Agilent 1200 series. High resolution ESI (HR-ESI) spectra were measured on UHR-QTOF maXis 4G (Bruker Daltonics).

Solid Phase Synthesis

General protocols for the solid phase synthesis are described for batch sizes of 0.1 mmol resin. All reactions were performed at room temperature in a polypropylene syringe reactor with a frit on a shaker.

A: Resin preparation and Fmoc cleavage
0.1 mmol resin (800 mg, resin loading 0.25 mmol/g,) were transferred into a 10 ml reactor and 5 ml DCM were added to swell the resin for 1 h. After washing the resin 10 times with 5 ml DMF, Fmoc was cleaved by adding 5 ml of 25 % piperidine in DMF three times for 10 min. In between the deprotection steps, the resin was washed three times with 5 ml DMF, and after the last deprotection, the resin was washed ten times with 5 ml DMF.

B: Building block and amino acid coupling
0.5 mmol building block (5 eq) and 260 mg PYBOP (0.5 mmol, 5 eq) were dissolved in 3 ml DMF and 0.2 ml DIPEA (1 mmol, 10 eq) were added. After flushing the solution with nitrogen for 1 min, the solution was added to the resin and the reaction was shaken for 1-1.5 h. After that, the liquid content was discarded, and the resin was washed ten times with 5 ml DMF.

C: Terminal-NH_2 capping
The resin was treated with 3 ml acetic anhydride for two times 15 min. In between, the resin was washed with DMF. After the last capping step, the resin was washed five times with 5 ml MeOH and five times with 5 ml DMF.

D: Deprotection of carboxylic side chain[2]
For conditioning, the resin was washed ten times with 5 ml of THF/H_2O (1/1). For deprotection, the resin was treated two times for one hour with 5 ml 0.2 M LiOH in THF/H_2O (1/1). In between, the resin was washed three times with 5 ml THF/H2O (1/1). After deprotection, the resin was washed alternately five times with each 5 ml of H_2O, DMF and DCM.

E: Carbohydrate conjugation-CuAAC
Azido carbohydrate derivatives (3 eq /alkyne group) were dissolved in 2 ml DMF. Separately, $CuSO_4$ (50 mol% /alkyne) and sodium ascorbate (50 mol% /alkyne) were each dissolved in 0.2 ml MilliQ water. The carbohydrate solution was first added to the resin, followed by sodium ascorbate and $CuSO_4$. After shaking the reaction mixture over night, the resin was washed

sequentially with 5 ml of DMF, a solution of 0.2 M sodium diethyldithiocarbamte in DMF and water (1/1), water, DMF and DCM until no more color changes were observable after the treatment with the diethyldithiocarbamte solution.

F: Side chain coupling
F.1 Coupling with HATU: 0.6 mmol of the amine residue (3 eq/acid) and 0.6 mmol HATU (3 eq/acid) were each dissolved in 1.5 ml DMF. 0.4 ml DIPEA (2 mmol, 10 eq/acid) were added to HATU and the reaction mixture was added to the resin. After a 15 min preactivation of the resin, the amine was added and the reaction was shaken for 1.5 h.
F.2 Coupling with PyBOP: 0.6 mmol of the amine residue (3 eq/acid) was dissolved in 1.5 ml DMF/DCM (1/1). 0.6 mmol PyBOP (3 eq/acid) and 0.6 mmol HOBt (3 eq/acid) were dissolved in 1.5 ml DMF/DCM(1/1) and 0.4 ml DIPEA (2 mmol, 10 eq/acid) were added. The reaction mixture was added to the resin, and after a 15 min preactivation, the amine was added and the reaction was shaken for 1.5 h.

G: Carbohydrate deprotection
The resin was treated two times for 30 min with 5 ml 0.2 M NaOMe in MeOH. In between, the resin was washed with three times with 5 ml MeOH. At the end, the resin was washed with each five times with 5 ml of MeOH, DMF and DCM.

H: Macro cleavage
The resin was washed ten times with 5 ml DMF and DCM. A cleavage solution (5 ml) consisting of 95 % TFA, 2.5 % TIPS and 2.5 % DCM was then added, and the reaction was shaken for 1 h. The supernatant was added dropwise to cooled Et_2O (40 ml) to precipitate the product. The mixture was centrifuged, the supernatant was decanted, and the white precipitate was dried under a stream of nitrogen. The resulting solid was dissolved in water and lyophilized.

I: TFA removal
TFA-removal was performed with a AG1-X8, quarternary ammonium, 100-200 mesh, acetate form resin from BioRad according to a protocol by Roux et al.[3] A 1.6 M acetic acid solution was prepared by diluting 23 mL acetic acid in 227 mL water and a 0.16 M solution by diluting 2.3 ml acidic acid in 247.7 ml water. For 100 mg sample, 1000 mg of the ion exchange resin were used. The resin was activated by washing three times with 10 mL of the 1.6 M acetic acid solution, followed by three times with 10 mL of the 0.16 M acetic acid solution. The sample was dissolved in 10 ml water and the solution was loaded to the resin into the syringe. The syringe was shaken for 1 h. The supernatant was recovered, and the resin was washed three times with 2 ml water. The combined water phases were loaded onto new, freshly activated resin and shaken for 1 h. The supernatant was collected, and the resin was washed three times with 2 ml water. The combined liquid phases were lyophilized to obtain the crude product as a white solid.

For the acetyl-capped heteroderivatives, precursor scaffold **15** (Figure S5) *N*-terminus was capped with acetic anhydride followed by deprotection of the carboxylic side chain with lithium hydroxide in THF/H_2O. In the next step, precursor **15** was conjugated with either a protected 2,3,6,2',3',4',6'-hepta-*O*-acetyl-β-lactosyl azide (for **4-6**) or 2-azidoethyl 2,3,4,6-tetra-*O*-acetyl-α-D-glucopyranoside (for **10-12**) resulting in **16** and **17**, respectively (Figure S1). After splitting each batch into three equal aliquots, the non-glycosidic motifs benzylamine (-Bz), *N*-Boc phenylenediamine (-*p*NH_2Ph), and 4-amino benzene sulfonic acid (-*p*SO_3HPh), were coupled to the carboxylic side chains using HATU and DIPEA.

For the amine and FITC derivatives, the Fmoc group of the last EDS building block remained until the end of the solid phase assembly. Since the basic deprotection conditions for the MDS-sidechain could result in loss of Fmoc groups, Boc protected β-alanine was used as final building block for structures **6a,c** and **12a,c**. FITC conjugation was performed in solution on purified glycomacromolecules as reported privously[4], and the corresponding FITC conjugates were repurified by preparative chromatography.

Glycomacromolecules were used as isolated after precipitation, TFA removal and preparative purification. All samples have purities higher 90 % (see RP-HPLC spectra below), however, they contain small amounts of deletion sequences that are individually assigned and quantified in the according HPLC spectra (see below). The ESI-MS-spectrum of the main peak is given, but the analysis of each individual peak is not further shown.

Binding Studies

Enzyme-linked immunosorbent assay (ELISA) inspired inhibition studies

ELISA-type inhibition studies were performed according to an already established protocol by Elling and coworkers.[5] Inhibition of Gal-3 binding to asialofetuin was investigated for glycoligands **1b-13b** with final concentrations between 0.1 and 2000 µM. All measurements and performed two times in triplicates.

SPR-inhibition studies

The SPR-inhibition studies were performed on a lactose-functionalized CM5 senor chip on a Biacore X100 from GE Healthcare Life Science. The lactose-functionalized CM5 chip was prepared using the "surface preparation wizard" for the sensor chip CM5. An amine-coupling procedure with NHS/EDC (contact time 420 s, flow rate 10 µL/min) was used for the functionalization of the two flow cells.

Therefore, flow cell 1, as reference cell was blank immobilized with ethanolamine according to the software. For flow cell 2 (mess cell) 1 mM Lac(1,3,5)-6, **2a**, in HBS-P buffer from GE Healthcare was used with a contact time of 600 s. As running buffer, HBS-P buffer from GE Healthcare was used. The immobilization levels reached were 411 RU for flow cell 2 and 186 RU for flow cell 1.

The inhibition assay was performed in a "Custom Assay Wizard-Binding Analysis" in a multi cycle measurement. For the inhibition studies, stock solutions of 100 µM of each ligand and 200 µg/mL of Gal-3 both in PBS buffer (150 mM NaCl, 50 mM NaH_2PO_4, pH 7.5) were prepared. Gal-3 was incubated with each ligand by mixing the solutions of the protein and ligands in a 1:1 ratio, resulting in final concentrations of 100 µg/mL for Gal-3 and 50 µM for the ligands. PBS was used as running buffer during the measurements choosing an association time of 90 s and a dissociation time of 60 s with a flow rate of 10 µL/min over both flow cells. For regeneration of the cell surface, 3 M $MgCl_2$ in MilliQ water was injected for 60 s with a flow rate of 10 µL/min after each cycle.

The evaluation was performed using the evaluation software provided by GE Healthcare. The response unit of the Gal-3 binding event without and after incubation with the ligands was taken 155 s after start of the sample injection. The response unit (RU) for only Gal-3 represents the 100 % binding and 0% inhibition event. The value of the inhibition with the glycomacromolecules were referred to the response unit of only Gal-3. All measurements were performed in triplicates.

Cell based assays

Cell lines and tissue culturing

Tissue culture was performed in a SterilGARD® III Advance SG 603 laminar flow hood from Baker Company. Cell cultures were observed using a Zeiss Axiovert 25 inverted microscope. All cell lines and culture media were purchased from ATCC. Cell line HEK-293 (#CRL-1573) was grown in Eagle's Minimum Essential Medium (EMEM) (# 30-2003) and supplemented with 10 % of FBS and 1 % Pen/Strep. Cell line MCF7 (ATCC® HTB-22) was cultured in EMEM with 0.1 mg/ml insulin, 10 % of FBS and 1 % Pen/Strep. Cells were cultured in 75 cm^2 tissue culture flask from TPP at 37 °C and 5 % CO_2 in a CO_2 water jacketed incubator 3110 from Scientific Inc. Once weekly, the medium was changed and the trypsinization of confluent cells was performed with trypsin-EDTA solution from ATCC (#30-2101) for subculturing as recommended by the supplier. Cell counting was performed with a 2 %-trypan-blue solution in PBS from VWR and disposable hemacytometers from Incyto C-chip™.

Galectin-antibody analysis with flow cytometry

Human galectin-1 biotinylated antibody, human galectin-3 biotinylated antibody and goat IgG biotinylated antibody as isotype control were purchased from R&D systems (#BAF1152, BAF1154 and BAF108).

For surface staining, cells were suspended at $5 \cdot 10^6$ cells/ml in DPBS buffer containing 0.1 % w/w BSA and 0.1 % w/w sodium azide. 100 µL of the cell suspension (500,000 cells) were incubated with 3 µL of human BD Fc block (#564220) from BD biosciences for 10 min at room temperature. Without washing in between, either 3 µL of the biotinylated human galectin antibodies or the isotype control (each 0.5 µg/ µL stock solution) were added and the cells were incubated for an additional 1 h on ice. After that, the cells were washed three times with cooled PBS+ buffer (containing BSA and sodium azide) by centrifugation at 780 rpm and 4 °C for 5 min, followed by resuspension of the pellet in PBS. After the last centrifugation step, the cell pellet was resuspended in 100 µL of PBS+ and the cells were stained with 10 µL of a 0.002 ug/ml solution of Streptavidin-PE conjugate for 20 min at room temperature. The cells were washed three time with on ice cooled PBS+, followed by the resuspension of the cell pellet in 300 µL of PBS+ buffer for the flow cytometry measurements using an the Accuri C6 flow cytometer. For intracellular staining, the cells were fixed before staining using a Fixation/Permeabilization Solution Kit from BD Bioscience. Therefore, a cell pellet of 500,000 cells was suspended in 1 ml Fix/Perm. Solution provided by the kit for 20 min on ice. Cells were washed 3 times with 1 ml BD Perm/Wash™ Buffer. After that, the staining was performed as described for the surface staining using permeabilization buffer for the washing steps in between to ensure permeability. A total of 100,000 cells were counted with a medium flow rate. Evaluation of the FACS result were performed with the FCS Express 4 program.

Studies of FITC-conjugated glycooligomers using flow cytommetry

The entire procedure was performed while avoiding light exposure to the samples. 500,000 cells in 90 µL were seeded into 96-well plates. 10 uL of FITC conjugated derivatives of the glycoconjugates, prepared as 2000 µM and 1000 µM stock solutions in water, were added to the cells resulting in a total volume of 100 µL containing 200 µM and 100 uM of the ligands, respectively. After incubation of the cells for 3 h at 37 °C and 5 % CO_2, the content of each well was transferred to a centrifuge tube and the well was washed one time with 200 µL PBS, which was afterwards transferred to the same corresponding centrifuge tube. After washing the cells 3 times with 1 mL PBS buffer, the cells were fixed with 100 µL of a Cytofix solution for 20 min on ice. Fixed cells were washed three times with 1 ml PBS+ before measuring with an Accuri 6 flow cytometer. 20,000 cells were collected with a slow flow rate of 14 uL/min. In between samples, two washing steps were performed at a high flow rate of 66 µL/min for one minute, the first of which involved a bleach solution containing 4% of hypochlolrite, followed by MilliQ water. A slow flow rate and the washing steps were needed to avoid clogging the system.

Fluorescence microscopy

Cells were grown on 24 mm cover slips (# 229174) in 6-well plates (#229106) purchased from Celltreat. Cover slips were first coated with a 0.01% poly-L-lysine solution from Sigma Aldrich for 5 min, followed by three washing steps with sterile MilliQ water. Cover slips were transferred into 6-well-plates and allowed to dry at room temperature for 2 h.

The cells lines were trypsinized, counted, centrifuged and resuspended to a final concentration of 70.000 cells/ml in the corresponding total growth medium. Next, 3 ml of the cell suspension were transferred to each well. The cells were grown on the cover slips for 2 days at 37°C at 5 % CO_2.

The staining procedure was performed in petri dishes (60 mm x 15 mm) from Fisher Brand. After removing the cell medium, the cover slips were carefully washed twice with prewarmed PBS. Staining was performed after fixation of the adherent cells with 1 ml of 3.7 % formaldehyde solution in PBS for 10 min at room temperature. The cover slips were washed again with prewarmed PBS and transferred into small petri dishes for the permeabilization with a solution of 0.1 % Tween 20 in PBS for 5 min at room temperature. The cover slips were washed two more times with PBS and transferred into a new clean petri dish for staining.

First, the staining with FITC-labeled glycoconjugates was performed. Cover slips were freed from buffer and incubated with 200 µL of 200 µM FITC-labeled glycoconjugate solution for 3 hours at 37°C and 5% CO_2. The supernatant was removed, and the cover slips were washed 3 times with PBS. As a negative control, the glycoconjugate staining was skipped. The next step was the reference staining.

For reference staining Hoechst 33342 (#H1399) staining for the nucleus an Alexa Fluor™ 647 Phalloidin (#A22287) staining for actin were used; both were purchased from Invitrogen. The dilutions were prepared as recommended by supplier:100 mg of 33342 Hoechst was dissolved in 10 ml deionized H_2O. 5 µL of 33342 Hoechst stock solution was further diluted in 10 mL PBS (1:2000 ratio). The content of the Alexa Fluor ™ 647 Phalloidin vial was dissolved in 1.5 ml methanol and further diluted by mixing 5 µL of the phalloidin stock solution in 200 µL PBS. For staining, the cover slips were freed from buffer and 200 µL of phalloidin-staining and 200 µL of Hoechst staining solution were simultaneously added on the cover slips and co-incubated for 40 min at room temperature. The supernatant was removed and the cover slips were washed 3 times with PBS. TrueBlack® Lipofuscin autofluorescence quencher from Biotium (#23007) was diluted by mixing 50 µL of the 20 x stock solution in 1 mL 70 % ethanol right before usage. The cover slips were coated with the dilution for 30 sec. After that, the cover slip was washed carefully 3 times with PBS buffer, freed from an excess of liquid by dapping on dust free tissue and flipped onto glass slides for microscopy, using one drop of ProLong™ Gold as antifade mountant (#P10144). Fluorescence microscopy was performed with an Olympus DP80 coupled with Prior Scientific Launches L200S fluorescence illumination system.

MTT cell viability assay

An MTT Assay Kit was purchased from Abcam (#ab211091). Cells were seeded into 96-well plates with a volume of 90 µL/well and 40,000 cells for the HEK 293 cell line and 30,000 cells for the MCF 7 cell line in complete growth medium. 10 µL of amine-derivatives of the glycoconjugates, prepared as 2000 µM stock solutions in water were added to the cells resulting in a total volume of 100 µL containing 200 µM of the ligands. After incubation of the cells for 48 h at 37 °C and 5 % CO_2, the plates were centrifuged at 1000 rpm, 4 °C for 5 min. 60 µL of the supernatant were carefully removed, followed by the addition of 50 µL PBS and 50 µL MTT reagent. After incubation for 3 hours at 37 °C and 5 % CO_2 the plates were centrifuged and 75 µL of the supernatant were removed. The purple precipitation was than dissolved by adding 200 µL of DMSO to each well and shaking the plate for 3 hours at room temperature covered with aluminum foil. The plates were read out with a Synergy H1 microplate reader from Biotek at 590 nm without a lid.

Migration Assay

Cells were seeded at 400,000 cells/well in 12-well plates with a final volume of 1 ml cell culture medium. Cells were grown for 48 h until a dense monolayer was reached. A wound field was created with a 10 µL pipet tip using a line on the back of the plate as guide. After creation of the wound field, the medium was removed and replaced by 360 µL total growth medium and 40 µL of a 2000 µM glycoconjugate or lactose solution in MiliQ water resulting in a final glycoconjugate concentration of 200 µM. For the unstained control, 400 µL complete growth medium and for the vehicle control 360 µL complete growth medium and 40 µL of MiliQ water were added. For the dosing experiments, an extra 30 µL of complete growth medium and 10 µL of the 2000 µM glycomacromolecule solution was added after 12, 24, 36 and 48 h. For the migration experiments, the amine-derivatives of the glycomacromolecules were used, as the direct precursor of the FITC-derivatives, used in the other cell studies.

Pictures were taken with a Nikon Eclipse TS100 using a Nikon E Plan 4x 0.10 ∞ /WD 30 Microscope Objective and coupled with a Nikon ELWD 0.3/OD75 condenser. Distances of the wound field were analyzed with the free software ImageJ.

Results and Discussion

Analytics Glycomacromolecules

Lac(1)-2–NH_2, **1a**

^{1}H NMR (300 MHz, Deuterium Oxide) δ [ppm]: 7.98 – 7.94 (m, 1H, triazole-C*H*), 5.66 (d, *J* = 9.2 Hz, 1H CH_{anomer}Glc), 4.43 (d, *J* = 7.7 Hz, 1H, CH_{anomer}-Gal), 4.02 – 3.45 (m, 20H, C$H_{pyranose}$, C$H_{2\ pyranose,}$ O-CH_2-), 3.44 – 3.20 (m, 10H, C=ONH-CH_2), 3.13 (t, *J* = 5.0 Hz, 2H,CH_2-NH_2), 2.96 (t, *J* = 7.0 Hz, 2H, CH=CH-CH_2), 2.73 (t, *J* = 7.0 Hz, 2H, CH=CH-CH_2-CH_2), 2.50 – 2.34 (m, 8H, NHC=O-CH_2).

^{13}C NMR (75 MHz, Deuterium Oxide) δ [ppm]: 188.64, 175.21, 175.03, 87.38, 77.88, 77.55, 75.63, 72.73, 72.15, 71.17, 69.66, 69.07, 68.79, 66.72, 61.30, 60.24, 45.16, 41.31, 39.32, 39.05, 37.10, 32.07, 31.17, 31.16, 31.00, 30.85, 30.48.

HR MS (ESI$^+$) *m/z* calc. for $C_{35}H_{63}N_9O_{17}$ $[M+2H]^{2+}$ 440.72; found 440.72. Yield: 48 mg (54 %).

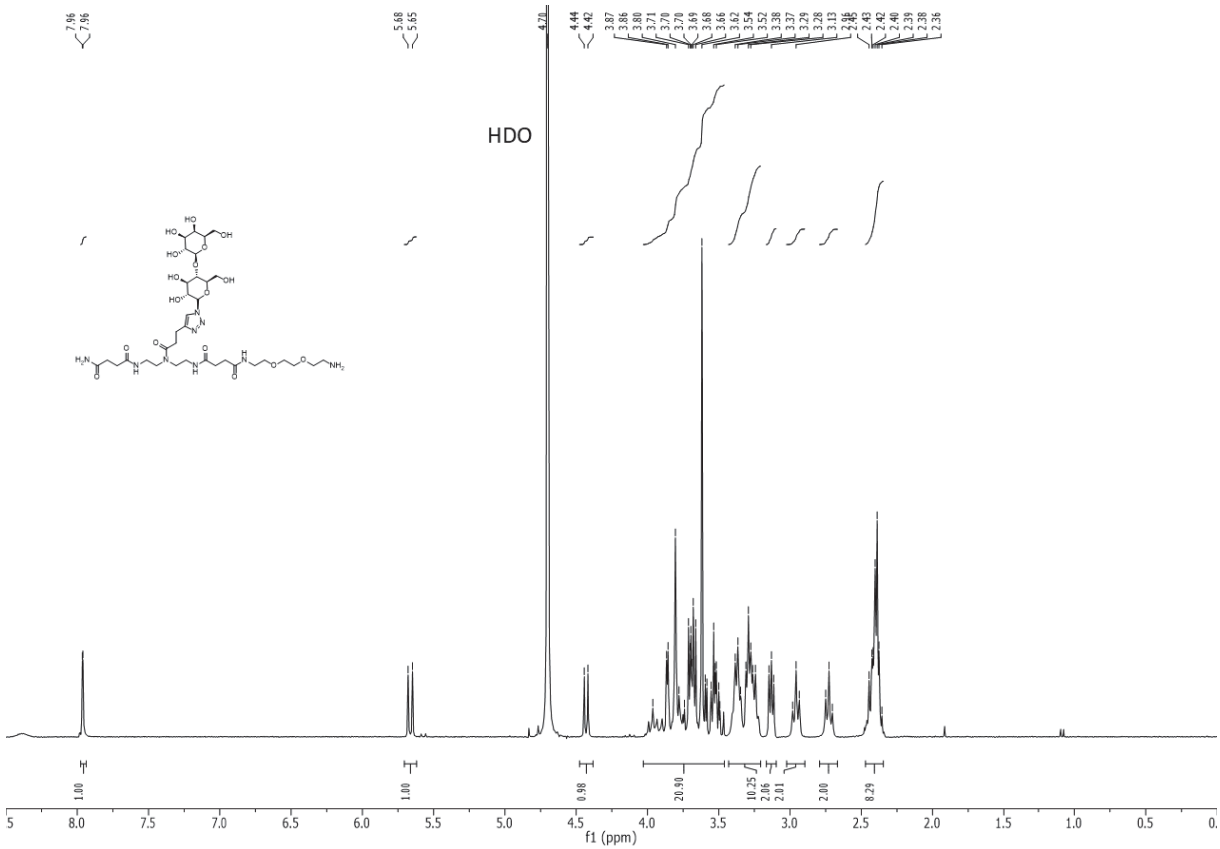

Figure S 2: ^{1}H NMR spectrum of compound **1a.**

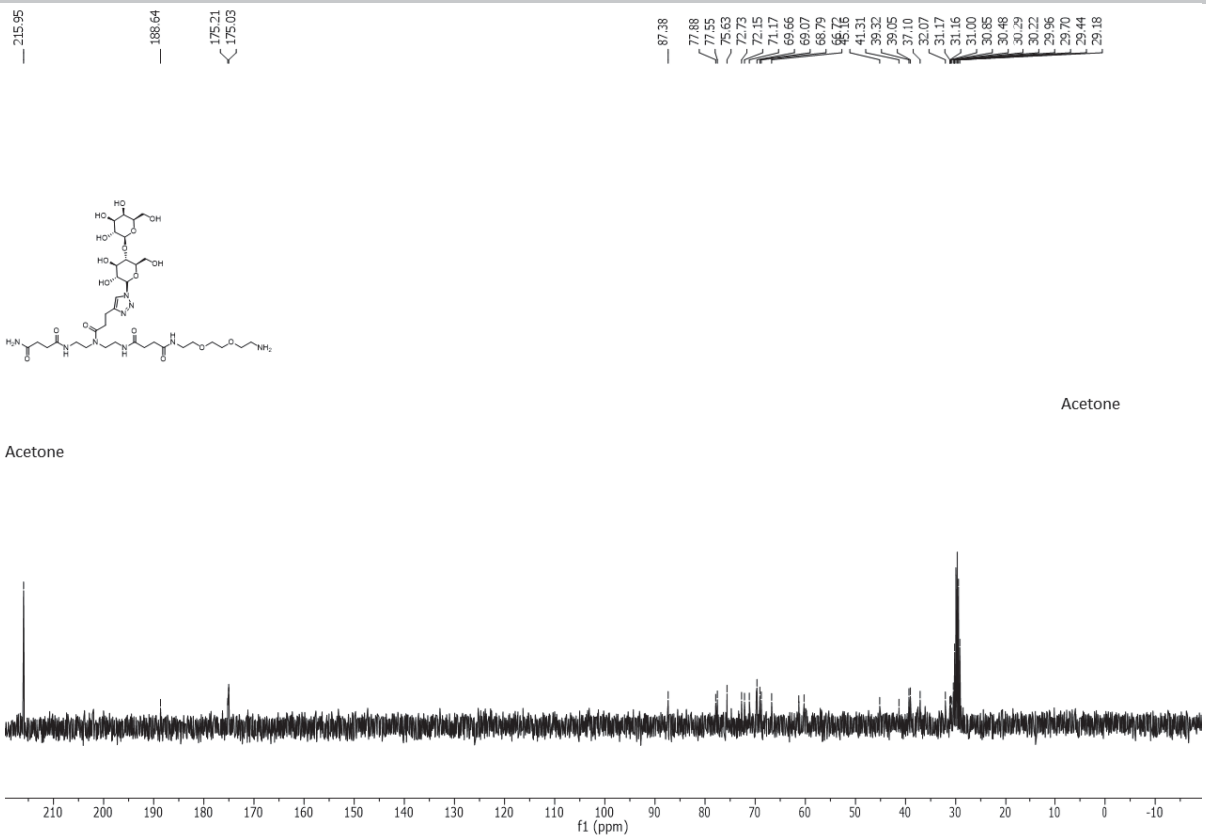

Figure S 3: ^{13}C NMR spectrum of compound **1a.**

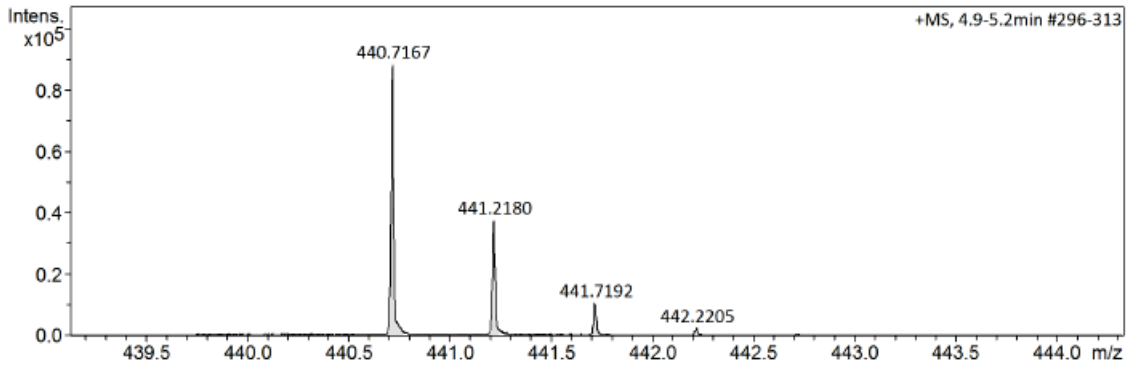

Figure S 4: HR-MS spectrum of compound **1a.**

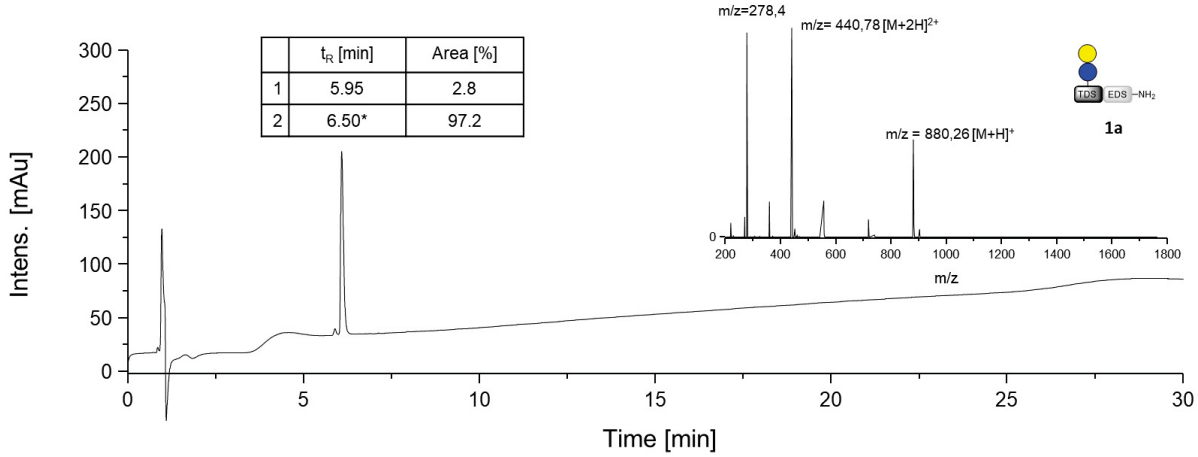

Figure S 5: RP-HPLC chromatogram and ESI$^+$-MS spectrum of compound **1a.** Retention time t_R [min] and area [%] of the peaks are given. ESI-MS spectrum of the main peak (*) is shown.

Lac(1)-2–Ac, **1b**

^{1}H-NMR (300 MHz, Deuterium Oxide) δ [ppm]: 8.05 (s, 1 H, triazole-C*H*,), 5.75 (d, J = 9.2 Hz, 1H, CH_{anomer}Glc), 4.52 (d, J = 7.7 Hz, 1H, CH_{anomer}-Gal), 4.10 – 3.73 (m, 10H, C$H_{pyranose}$, C$H_{2\ pyranose,}$ O-CH_2-), 3.72 – 3.57 (m, 10H, C$H_{pyranose}$, C$H_{2\ pyranose,}$ O-CH_2-), 3.47-3.31 (m 12 H, C=ONH-CH_2), 3.05 (t, J = 7.1 Hz, 2H, CH=CH-CH_2), 2.82 (t, J = 7.0 Hz, 2H, - CH=CH-CH_2-CH_2), 2.58 – 2.43 (m, 8H, NHC=O-CH_2) , 2.00 (s, 3H, -CH_3).

^{13}C-NMR (75 MHz, Deuterium Oxide) δ [ppm]: 176.64, 174.15, 173.97, 173.89, 173.80, 173.37, 146.24, 121.71, 102.05, 86.31, 76.81, 76.46, 74.55, 73.71, 71.66, 71.09, 70.10, 68.56, 67.93, 67.72, 65.16, 60.23, 58.89, 46.28, 44.13, 38.11, 38.05, 36.44, 36.02, 30.98, 29.99, 29.79, 29.36, 20.97, 19.80.

HR MS (ESI^{+}) *m/z* calc. for $C_{37}H_{65}N_9O_{18}$ $[M+2H]^{2+}$ 461.7218; found 461.7217. Yield: 51 mg (55 %).

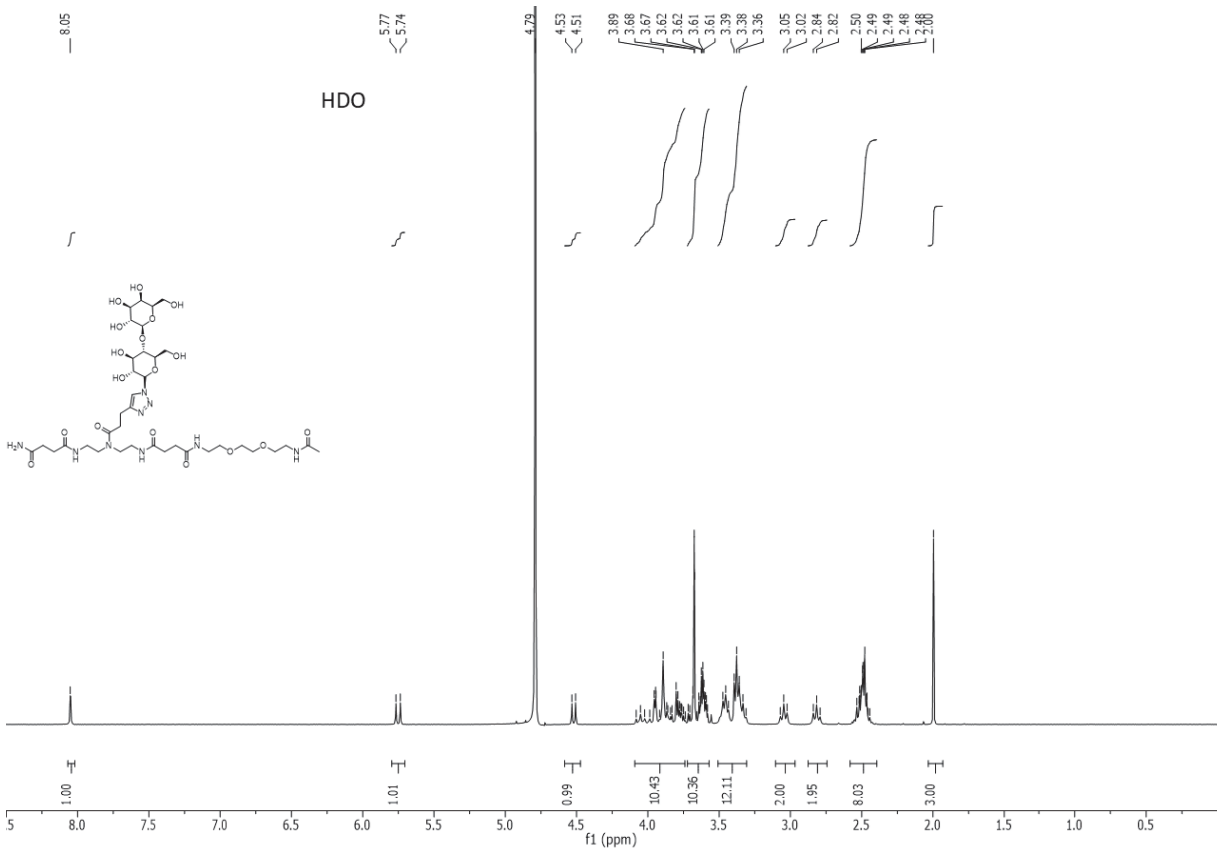

Figure S 6: ^{1}H-NMR spectrum of compound **1b.**

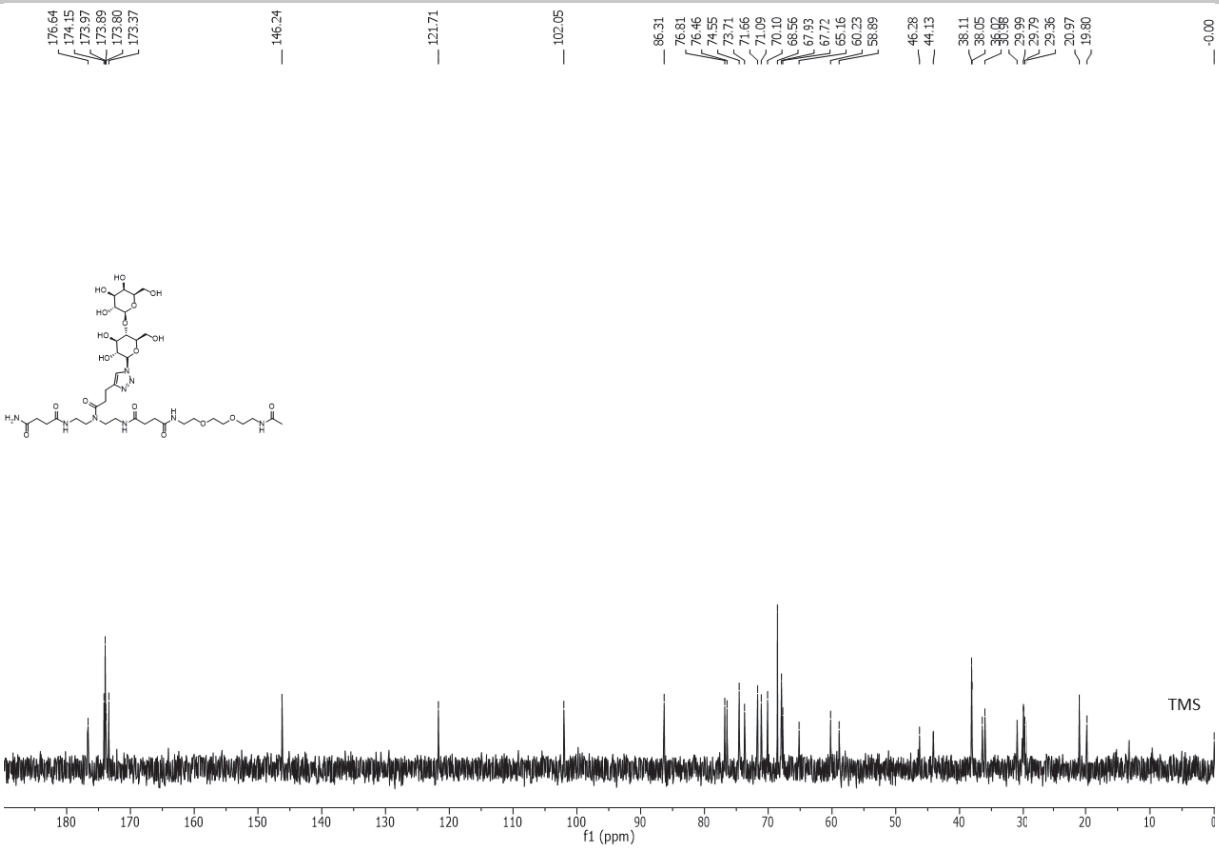

Figure S 7: ^{13}C-NMR spectrum of compound **1b.**

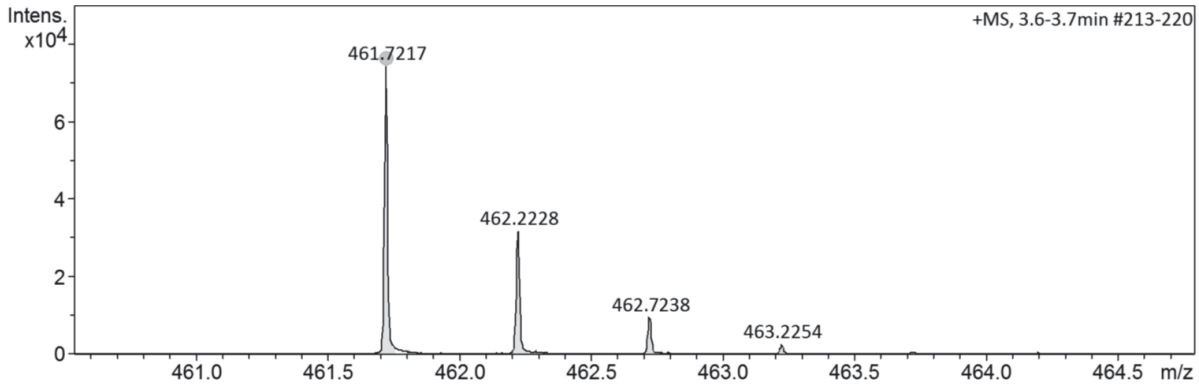

Figure S 8: HR-MS spectrum of compound **1b.**

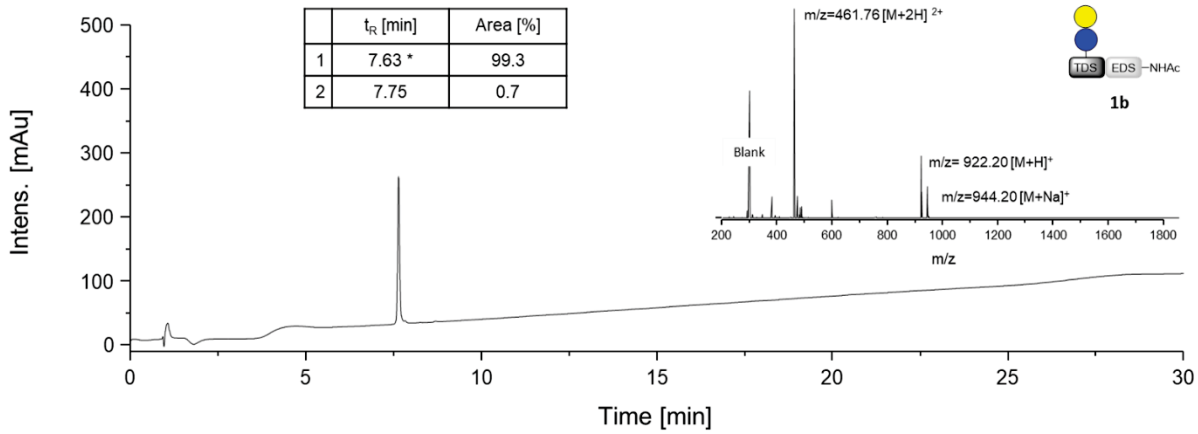

	t_R [min]	Area [%]
1	7.63 *	99.3
2	7.75	0.7

Figure S 9: RP-HPLC chromatogram and ESI$^+$-MS spectrum of compound **1b.** Retention time t_R [min] and area [%] of the peaks are given. ESI-MS spectrum of the main peak (*) is shown.

Lac(1)-2-FITC, **1c**

^{1}H NMR (300 MHz, Deuterium Oxide) δ [ppm]: 8.21 – 7.88 (m, 3H; FITC-C*H,* triazole-C*H*), 7.65 (s, 1H, FITC-C*H,*), 7.11 – 6.43 (m,6, FITC-C*H*), 5.68 (d, *J* = 8.9 Hz, 1H, CH_{anomer}Glc), 4.49 (d, *J* = 7.3 Hz, 1H, CH_{anomer}-Gal), 4.12 – 3.11 (m, 32H, C$H_{pyranose}$, C$H_{2\ pyranose,}$ O-CH_2-, C=ONH-CH_2), 3.00 – 2.82 (m, 2H, CH=CH-CH_2), 2.78 – 2.58 (m, 2H, CH=CH-CH$_2$-CH_2), 2.53 – 2.14 (m, 8H, NHC=O-CH_2).

HR MS (ESI$^+$) *m/z* calc. for $C_{54}H_{62}N_{24}O_{12}S$ $[M+2H]^{2+}$ 635.2344; found 635.2344. Yield: 11 mg (56 %).

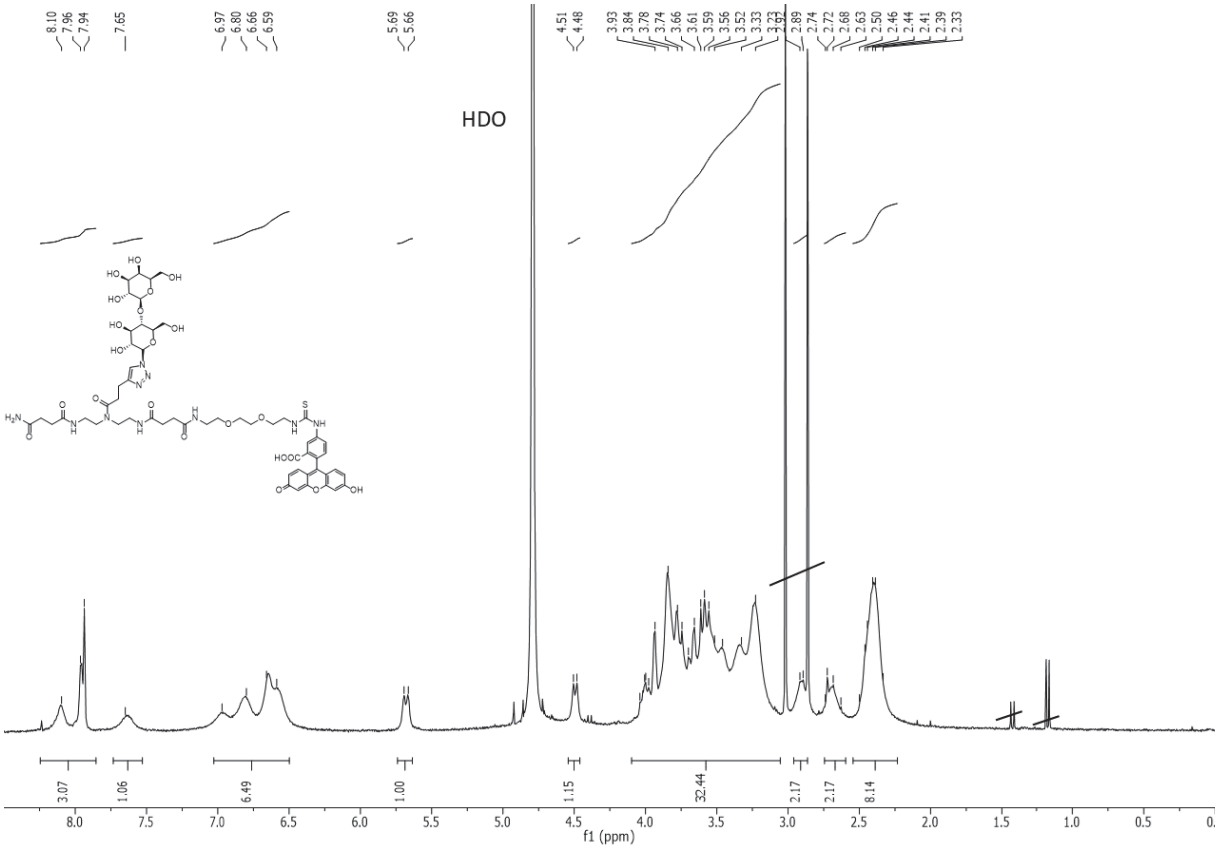

Figure S 10: ^{1}H-NMR spectrum of compound **1c**.

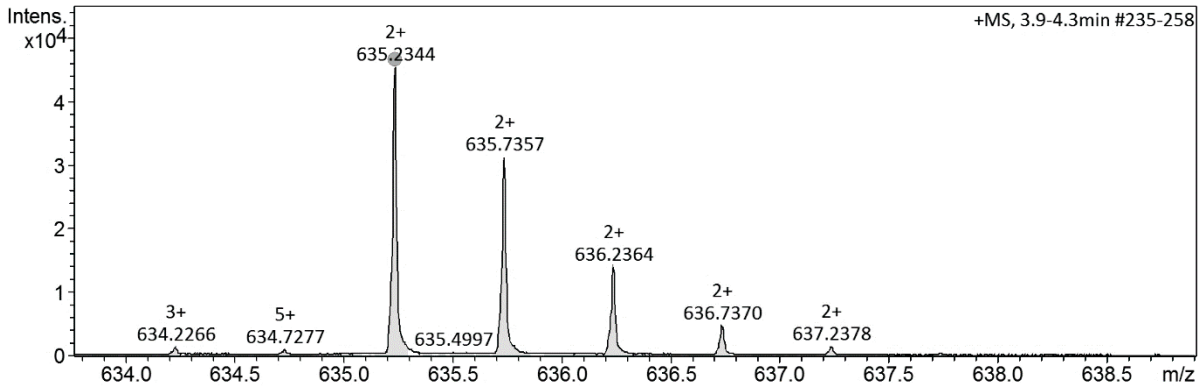

Figure S 11: HR-MS spectrum of compound **1c.**

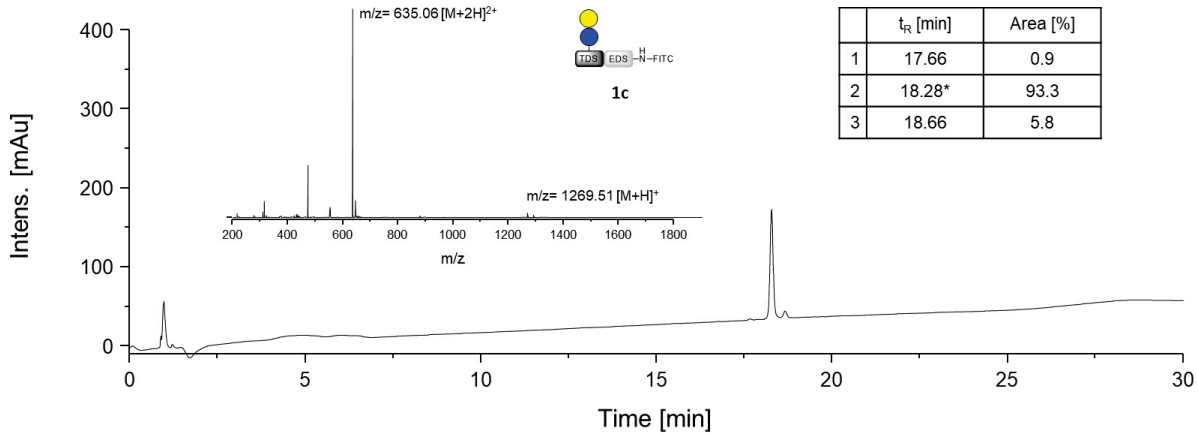

	t_R [min]	Area [%]
1	17.66	0.9
2	18.28*	93.3
3	18.66	5.8

Figure S 12: RP-HPLC chromatogram and ESI$^+$-MS spectrum of compound **1c.** Retention time t_R [min] and area [%] of the peaks are given. ESI-MS spectrum of the main peak (*) is shown.

Lac(1,3,5)-6–NH_2, **2a**

^{1}H NMR (300 MHz, Deuterium Oxide) δ [ppm]: 8.05 (s, 3H, triazol-C*H*), 5.75 (d, *J* = 9.2 Hz, 3H, CH_{anomer}Glc), 4.52 (d, *J* = 7.7 Hz, 3H, CH_{anomer}Gal), 4.11 – 3.54 (m, 60H, C$H_{pyranose}$, C$H_{2\ pyranose,}$ O-CH_2-), 3.54 – 3.28 (m, 34H, C$H_{pyranose,}$, C=ONH-CH_2), 3.26 – 3.18 (m, 2H, CH_2-NH_2), 3.04 (t, *J* = 6.9 Hz, 6H, CH=CH-CH_2), 2.81 (t, *J* = 6.9 Hz, 6H, CH=CH-CH_2-CH_2), 2.48 (h, *J* = 6.6 Hz, 24H, NHC=O-CH_2).

^{13}C NMR (75 MHz, Deuterium Oxide) δ [ppm]: 175.19, 175.00, 174.92, 174.83, 170.60, 147.30, 122.78, 103.15, 87.41, 77.90, 77.58, 75.65, 74.82, 72.76, 72.18, 71.19, 69.79, 69.66, 69.07, 68.81, 66.62, 61.31, 59.98, 47.34, 45.20, 39.33, 39.14, 37.53, 37.11, 32.07, 31.24, 31.08, 20.90.

HR-MS (ESI$^+$) *m/z* calc. for $C_{105}H_{180}N_{25}O_{51}$ $[M+3H]^{3+}$ 869.07; found: 869.08. Yield: 103 mg (40 %).

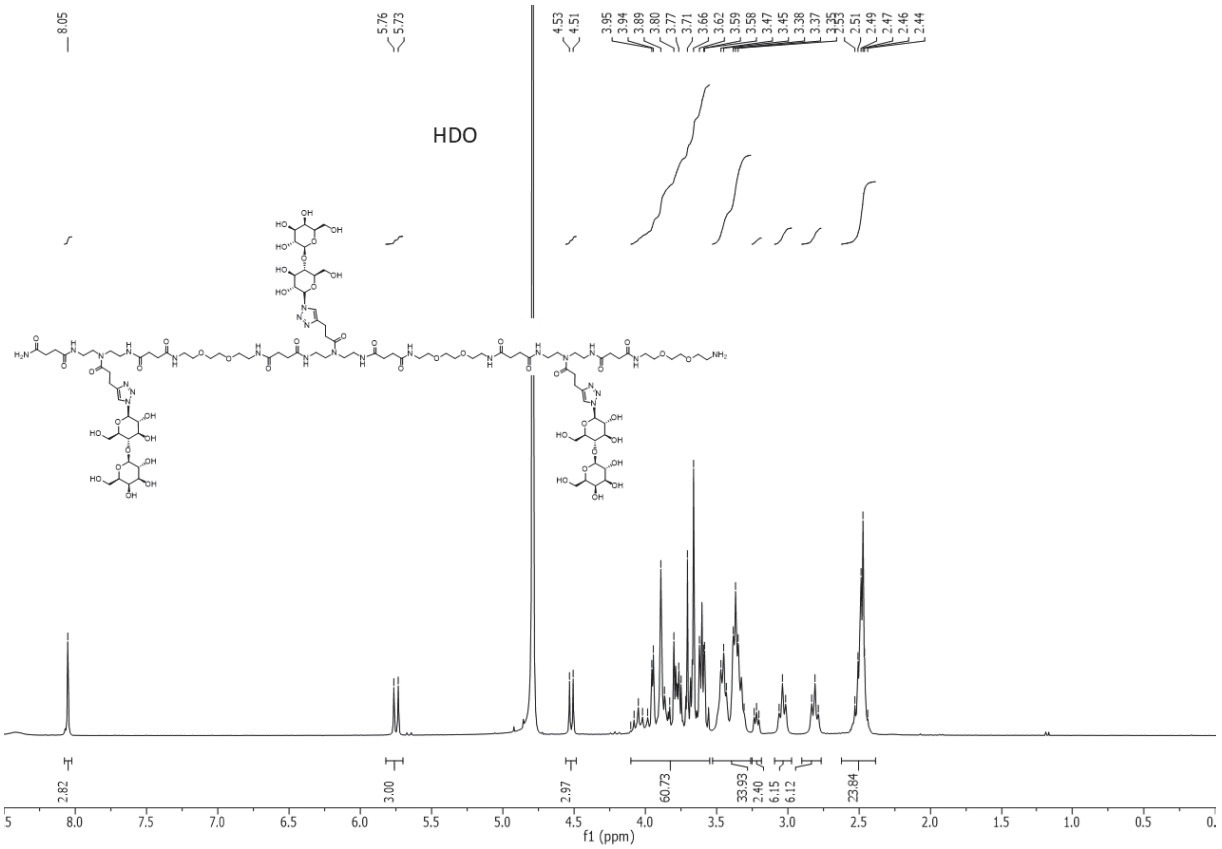

Figure S 13: ^{1}H-NMR spectrum of compound **2a**.

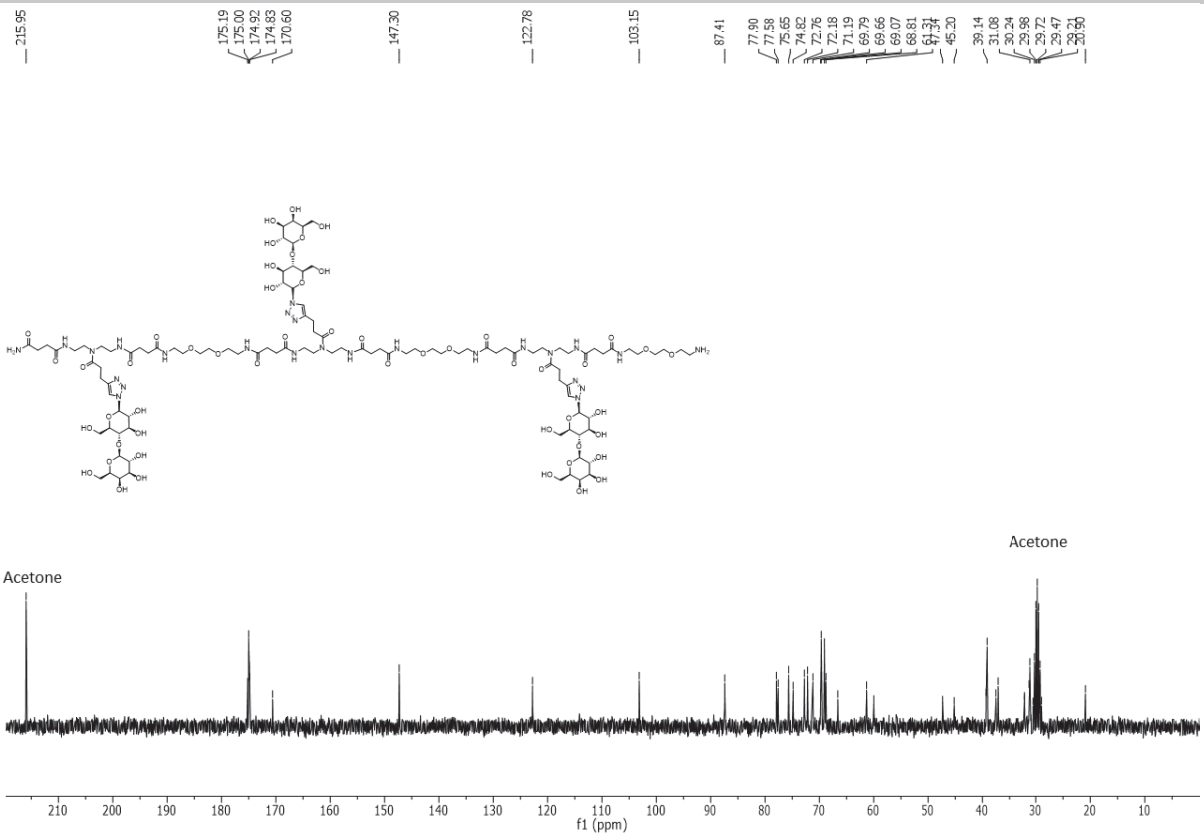

Figure S 14: ^{13}C-NMR spectrum of compound **2a**.

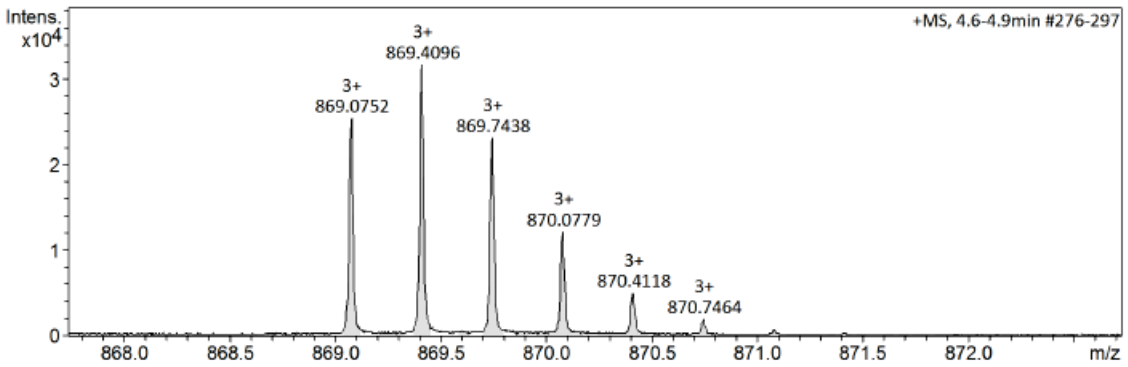

Figure S 15: HR-MS spectrum of compound **2a.**

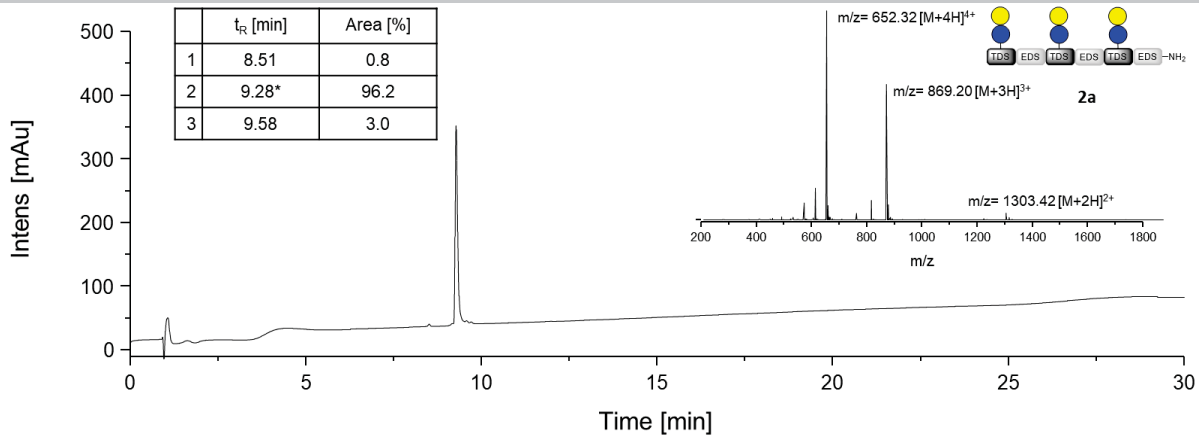

	t_R [min]	Area [%]
1	8.51	0.8
2	9.28*	96.2
3	9.58	3.0

Figure S 16: RP-HPLC chromatogram and ESI$^+$-MS spectrum of compound **2a.** Retention time t_R [min] and area [%] of the peaks are given. ESI-MS spectrum of the main peak (*) is shown.

Lac(1,3,5)-6–Ac, **2b**

^{1}H-NMR (300 MHz, Deuterium Oxide) δ [ppm]: 8.05 (s, 3H, triazole-C*H*), 5.75 (d, J = 9.2 Hz, 3H, CH_{anomer}Glc), 4.52 (d, J = 7.7 Hz, 3H, CH_{anomer}-Gal), 4.13 – 3.56 (m, 60H, C$H_{pyranose}$, C$H_{2\ pyranose}$, O-CH_2-), 3.53 – 3.26 (m, 36H, C$H_{pyranose}$, C$H_{2\ pyranose}$, NHC=O-CH_2), 3.04 (t, J = 7.1 Hz, 6H, CH=CH-CH_2), 2.81 (t, J = 7.1 Hz, 6H, CH=CH-CH_2-CH_2), 2.60 – 2.38 (m, 24H, NHC=O-CH_2), 1.99 (s, 3H, CH_3).

^{13}C NMR (75 MHz Deuterium Oxide) δ [ppm]: 174.43, 174.24, 174.17, 174.08, 146.53, 122.02, 102.38, 86.64, 77.13, 76.80, 74.87, 74.05, 71.98, 71.42, 70.42, 68.88, 68.30, 68.04, 60.54, 59.22, 46.57, 44.42, 38.43, 38.37, 36.76, 36.34, 31.29, 30.48, 30.36, 30.27, 21.29, 20.13.

HR-MS (ESI$^+$) *m/z* calc. for $C_{107}H_{182}N_{25}O_{52}$ $[M+3H]^{3+}$ 883.0783; found: 883.0787. Yield: 109 mg (41 %).

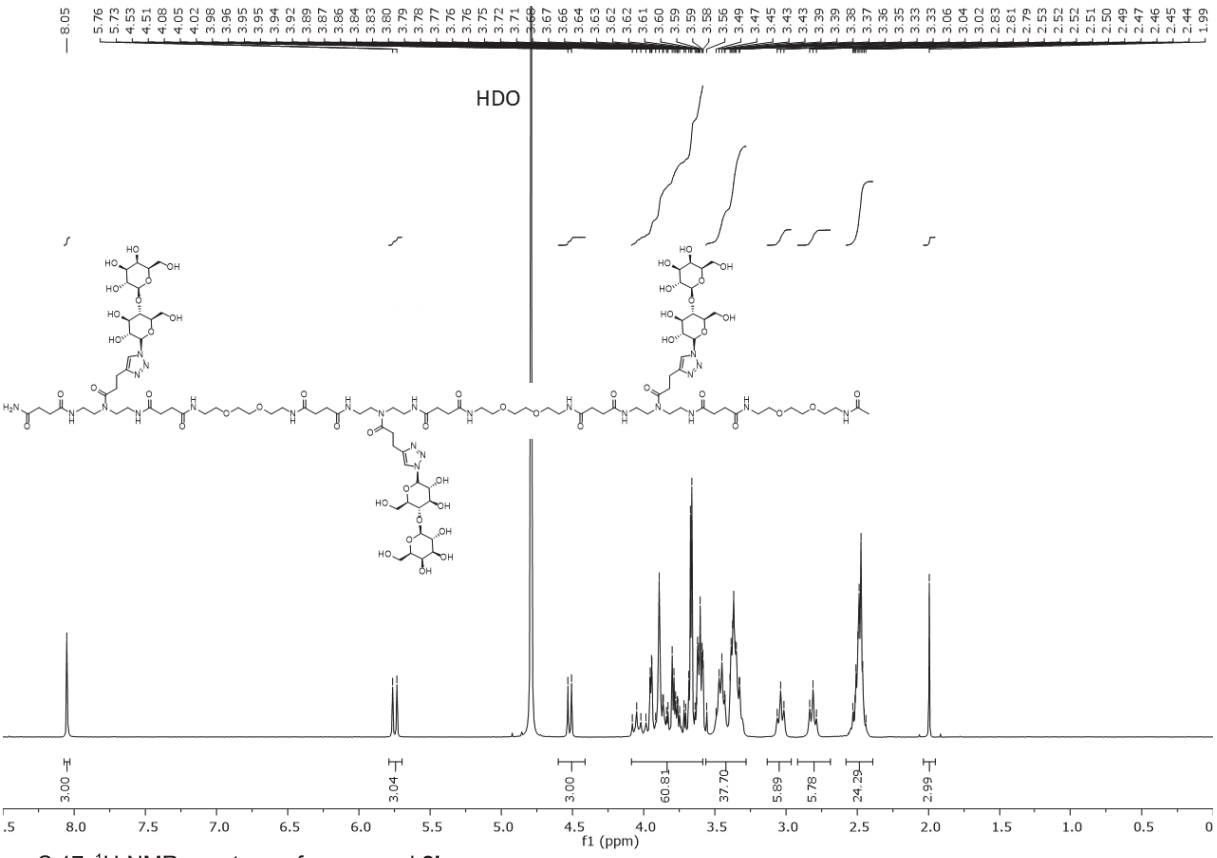

Figure S 17: ^{1}H-NMR spectrum of compound **2b.**

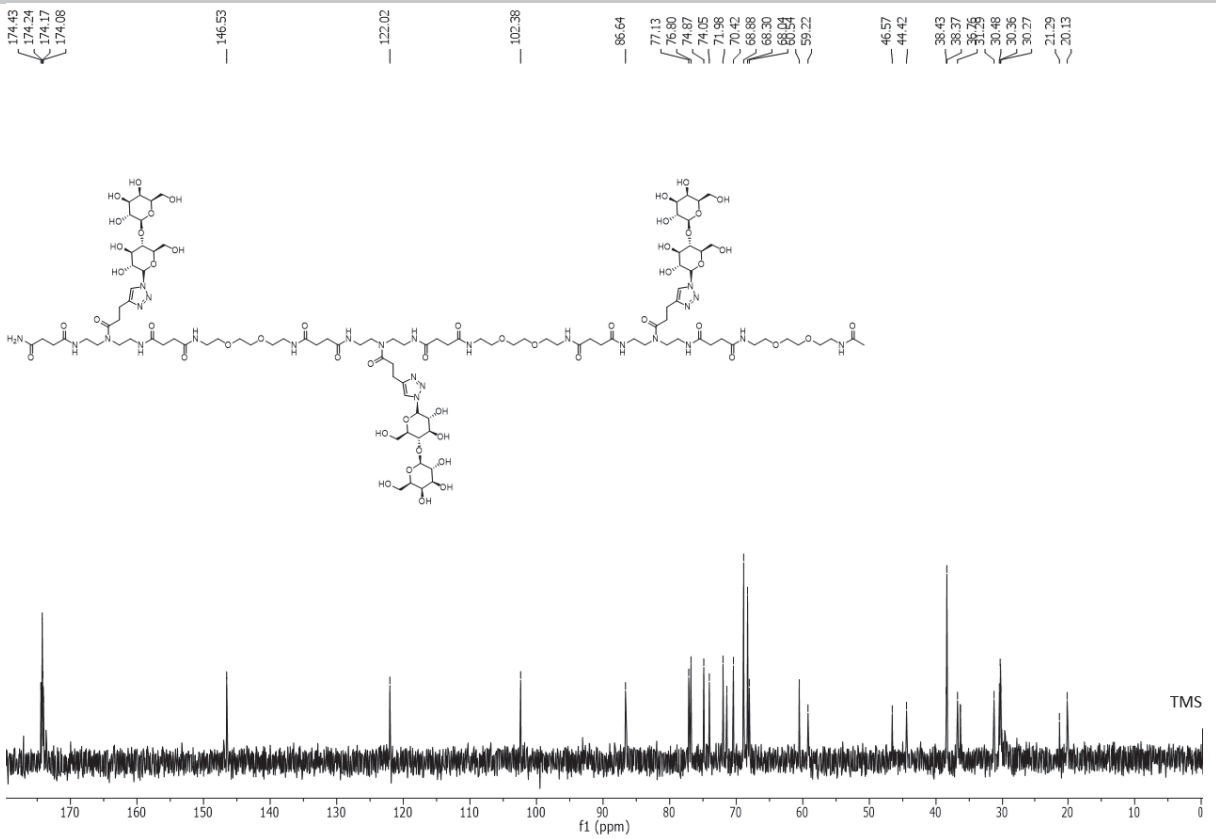

Figure S 18: ^{13}C-NMR spectrum of compound **2b**.

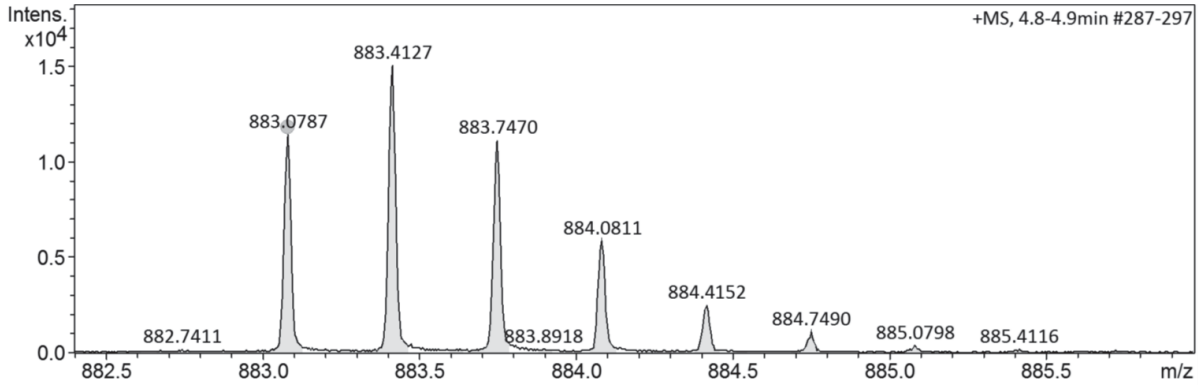

Figure S 19: HR-MS spectrum of compound **2b.**

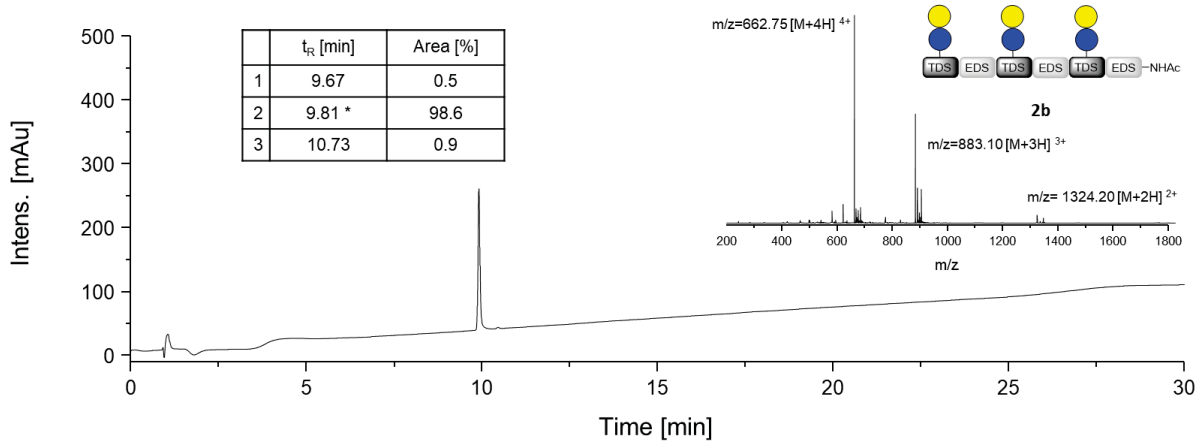

	t_R [min]	Area [%]
1	9.67	0.5
2	9.81 *	98.6
3	10.73	0.9

Figure S 20: RP-HPLC chromatogram and ESI$^+$-MS spectrum of compound **2b.** Retention time t_R [min] and area [%] of the peaks are given. ESI-MS spectrum of the main peak (*) is shown.

Lac(1,3,5)-6–FITC, **2c**

^{1}H NMR (600 MHz, Deuterium Oxide) δ [ppm]: 8.12 (s, 1H, FITC-C*H*), 8.07 – 7.95 (m, 3H, triazole-C*H*), 7.70 (s, 1H, FITC-C*H*), 7.07 (s, 1H, FITC-C*H*), 6.90 (s, 2H, FITC-C*H*), 6.79 (s, 2H, FITC-C*H*), 6.67 (d, *J* = 8.8 Hz, 2H, FITC-C*H*), 5.77 – 5.66 (m, 3H, CH_{anomer}-Glc), 4.55 – 4.46 (m, 3H, CH_{anomer}-Gal), 4.07 – 3.99 (m, 3H, C$H_{pyranose}$), 3.97 – 3.79 (m, 20H, C$H_{pyranose}$, C$H_{2\ pyranose}$, O-CH_2-), 3.79 – 3.51 (m, 40H, C$H_{pyranose}$, C$H_{2\ pyranose}$, O-CH_2-, C=ONH-CH_2), 3.48 – 3.20 (m, 34H, C$H_{pyranose}$, C=ONH-CH_2), 3.07 – 2.89 (m, 6H, CH=CH-CH_2), 2.83 – 2.66 (m, 6H, CH=CH-CH$_2$-CH_2), 2.53 – 2.34 (m, 24H, NHC=O-CH_2).

^{13}C NMR (151 MHz, Deuterium Oxide) δ [ppm]: 177.48, 174.58, 146.96, 122.47, 102.92, 87.18, 77.65, 77.39, 75.40, 74.58, 72.52, 71.94, 70.94, 69.40, 68.81, 68.56, 61.06, 59.76, 47.10, 45.01, 38.89, 37.30, 36.88, 31.76, 31.00, 30.88, 30.83, 30.77, 30.21, 30.08, 20.64.

HR-MS (ESI^{+}) *m/z* calc. for $C_{126}H_{191}N_{26}O_{56}S$ $[M+3H]^{3+}$ 998.7534; found 998.7514. Yield: 21 mg (60 %).

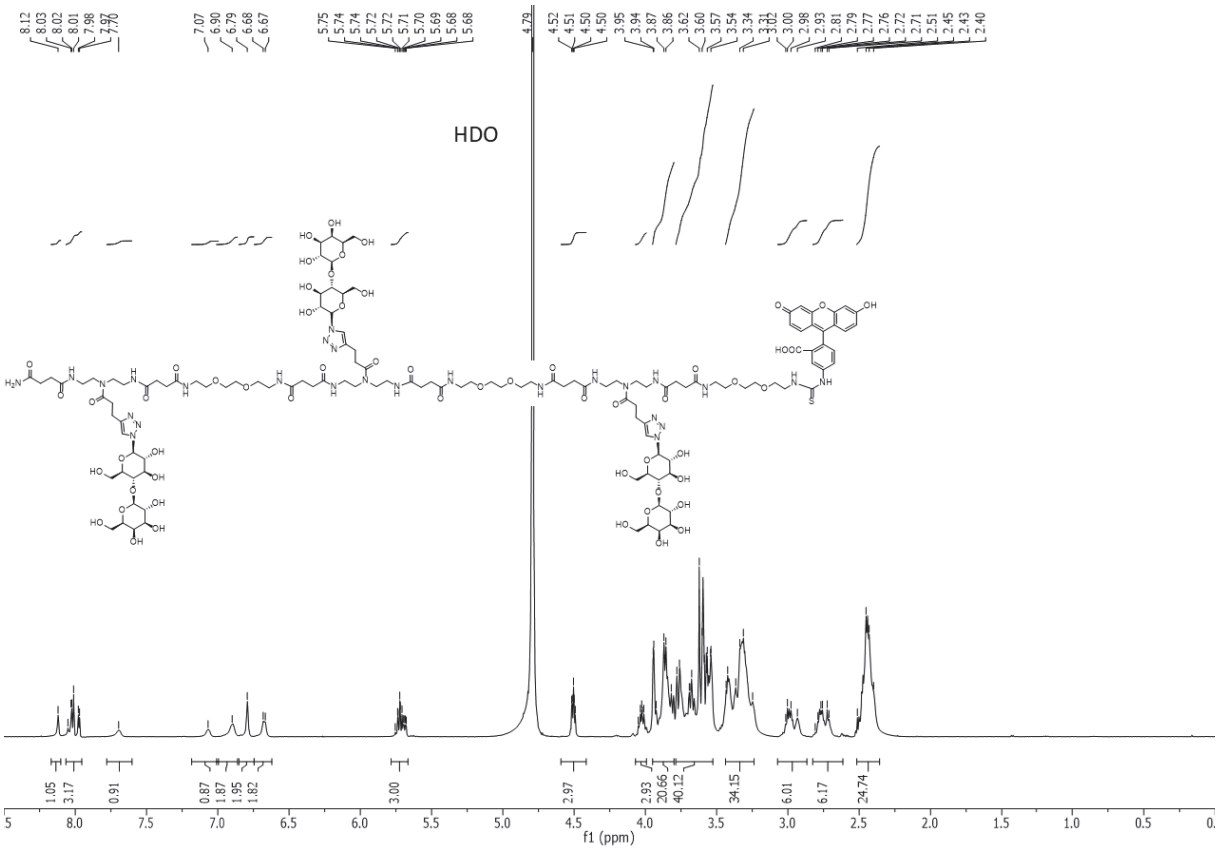

Figure S 21: ^{1}H-NMR spectrum of compound **2c.**

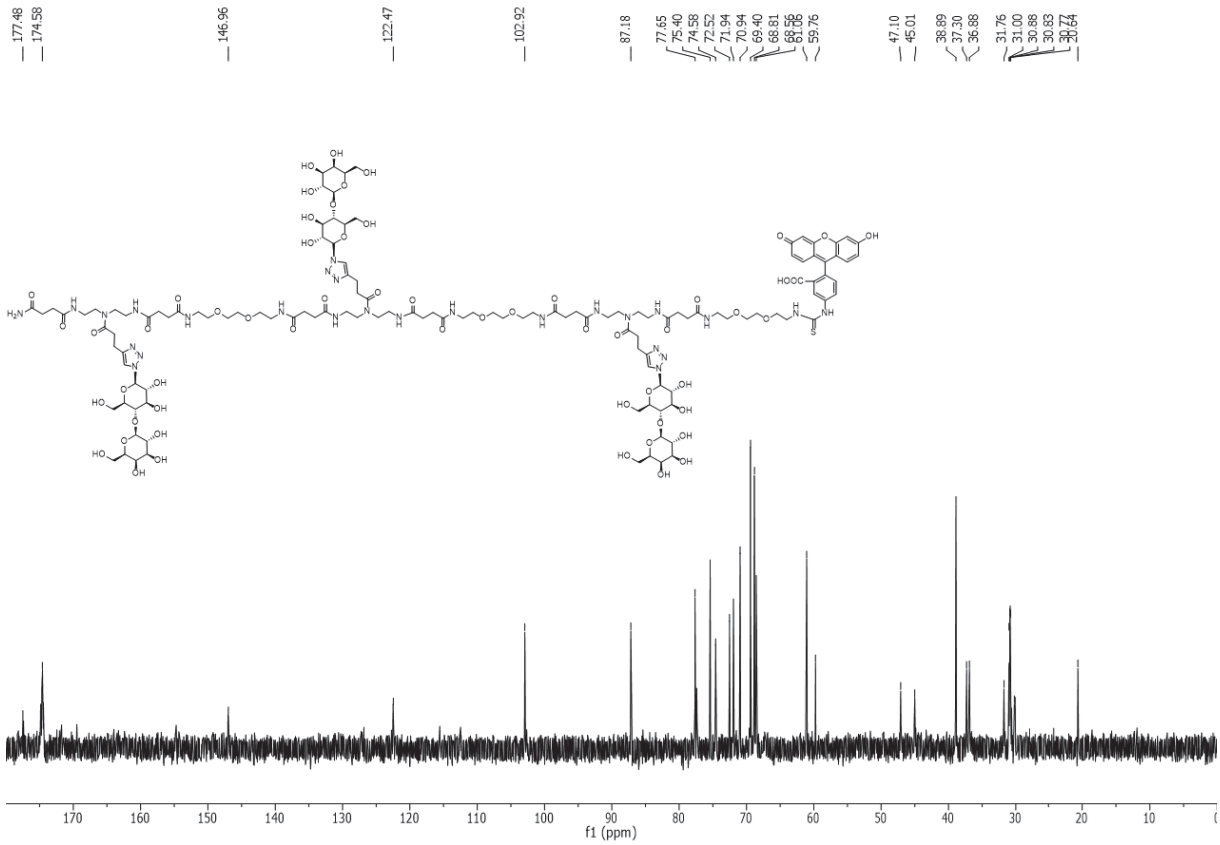

Figure S 22: ^{13}C-NMR spectrum of compound **2c**.

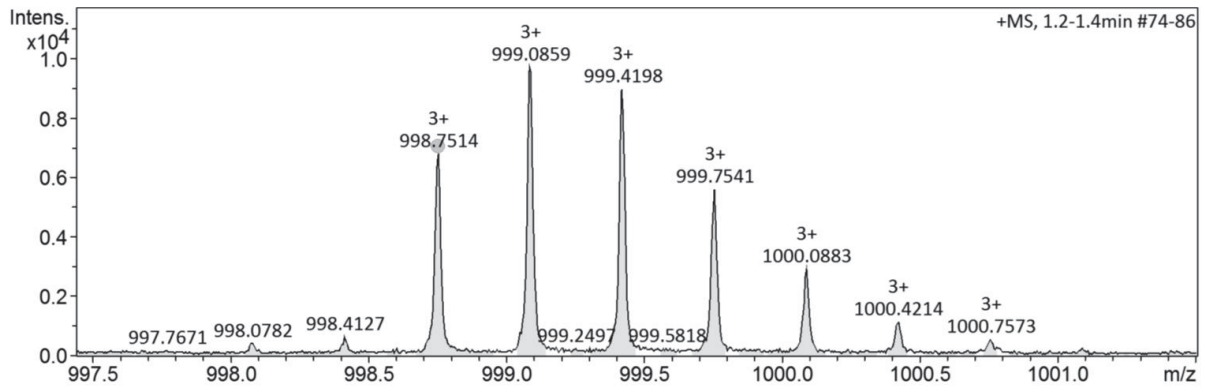

Figure S 23: HR-MS spectrum of compound **2c.**

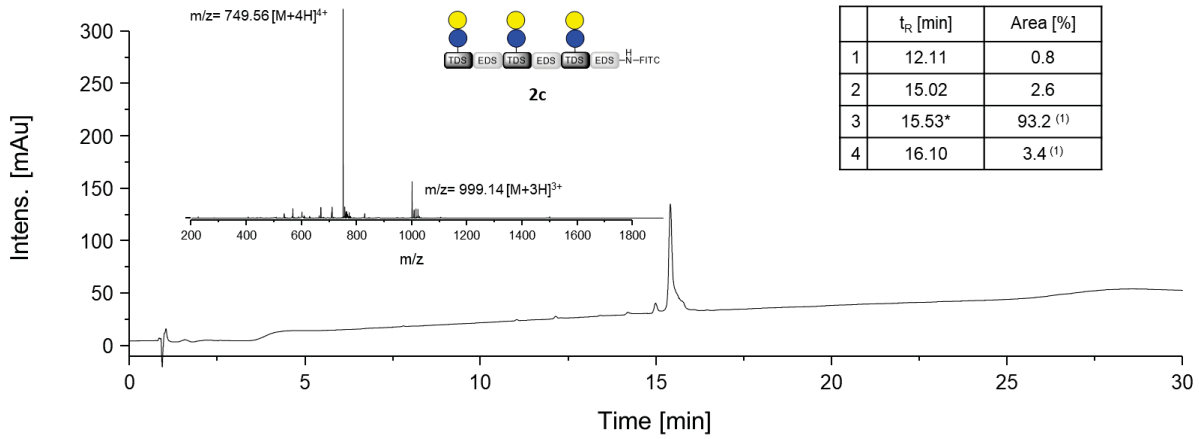

	t_R [min]	Area [%]
1	12.11	0.8
2	15.02	2.6
3	15.53*	93.2 (1)
4	16.10	3.4 (1)

Figure S 24: RP-HPLC chromatogram and ESI$^+$-MS spectrum of compound **2c**. Retention time tR [min] and area [%] of the peaks are given. ESI-MS spectrum of the main peak (*) is shown. (1) Peaks with the same m/z.

Lac(1,2,3,4,5,6)-7–NH_2, **3a**

^{1}H NMR (300 MHz, Deuterium Oxide) δ [ppm]: 8.05 – 8.01 (m, 6H, triazole-C*H*), 5.74 (d, *J* = 9.2 Hz, 6H, CH_{anomer}Glc), 4.52 (d, *J* = 7.6 Hz, 4H, CH_{anomer}-Gal), 4.09 – 3.82 (m, 44H, C$H_{pyranose}$, O-CH_2-), 3.82 – 3.54 (m, 36H, C$H_{pyranose}$, C$H_{2\ pyranose}$, O-CH_2-), 3.52 – 3.27 (m, 50H, C=ONH-CH_2), 3.24 – 3.19 (m, 2H, CH_2-NH_2), 3.07 – 2.95 (m, 12H, CH=CH-CH_2), 2.85 – 2.73 (m, 12H, CH=CH-CH_2-CH_2), 2.56 – 2.37 (m, 28H, NHC=O-CH_2).

^{13}C NMR (126 MHz, Deuterium Oxide) δ [ppm]: 173.92, 146.27, 121.70, 102.13, 86.36, 76.86, 76.77, 74.59, 73.82, 71.78, 71.15, 70.18, 67.79, 65.08, 60.24, 59.06, 46.29, 44.15, 38.32, 38.04, 36.54, 36.12, 31.01, 30.18, 30.06, 30.01, 29.89, 19.89, 13.27.

HR-MS (ESI$^+$) *m/z* calc. for $C_{160}H_{265}N_{39}O_{82}$ [M+4H] $^{4+}$ 1011.1936; found 1011.1945.Yield: 174 mg (43 %).

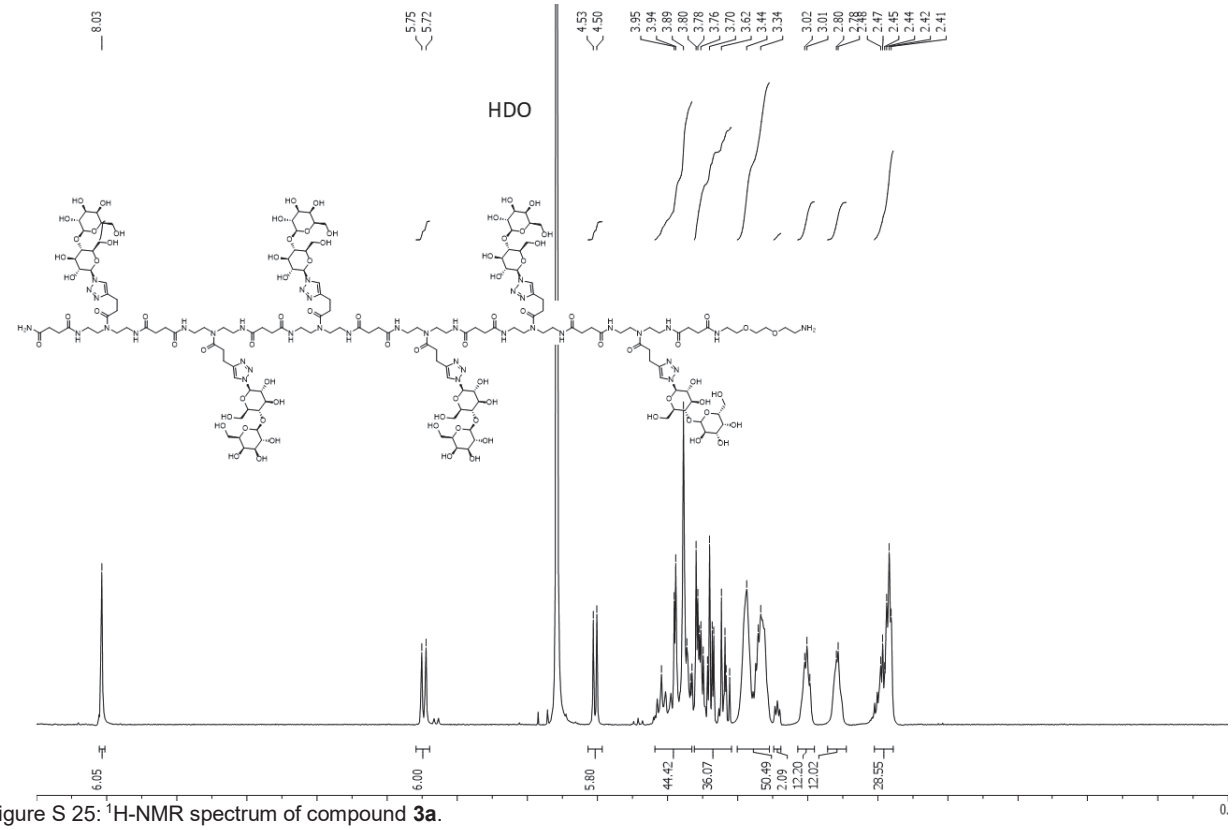

Figure S 25: ^{1}H-NMR spectrum of compound **3a**.

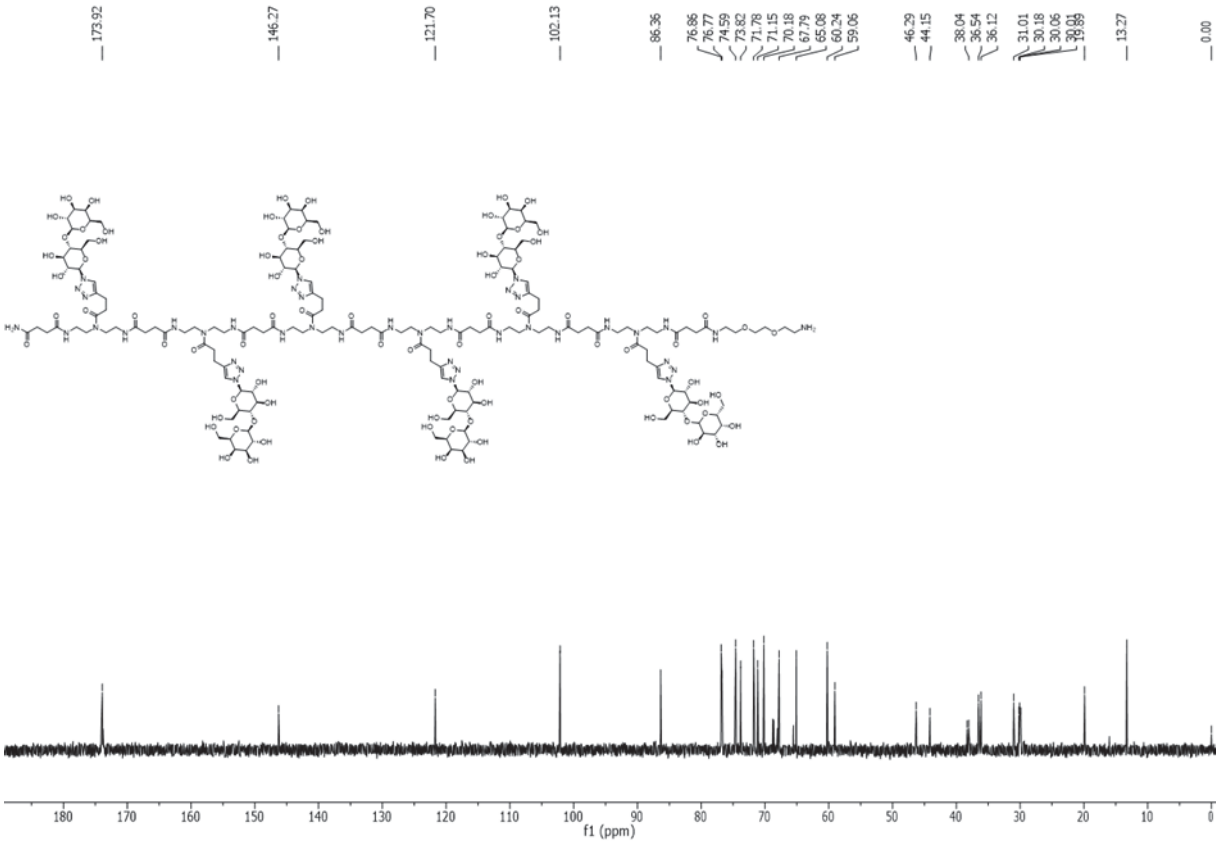

Figure S 26: ^{13}C-NMR spectrum of compound **3a**.

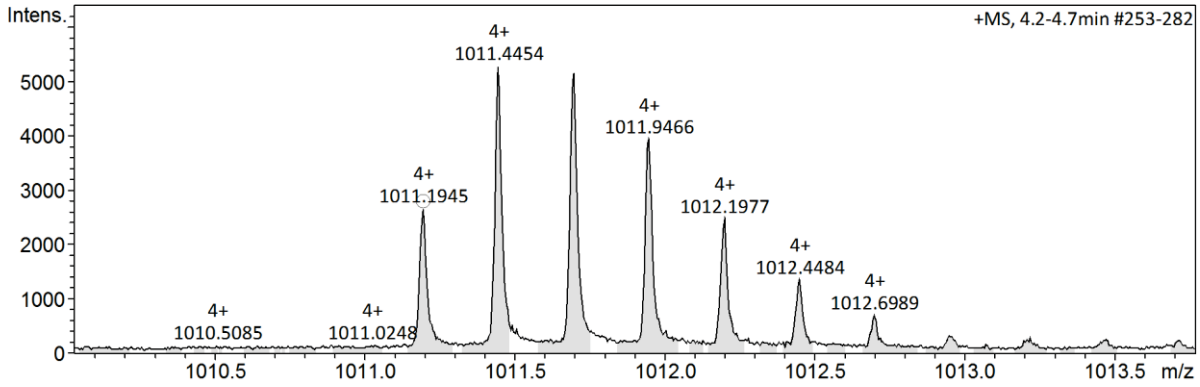

Figure S 27: RP-HPLC chromatogram and ESI$^+$-MS spectrum of compound **3a.**

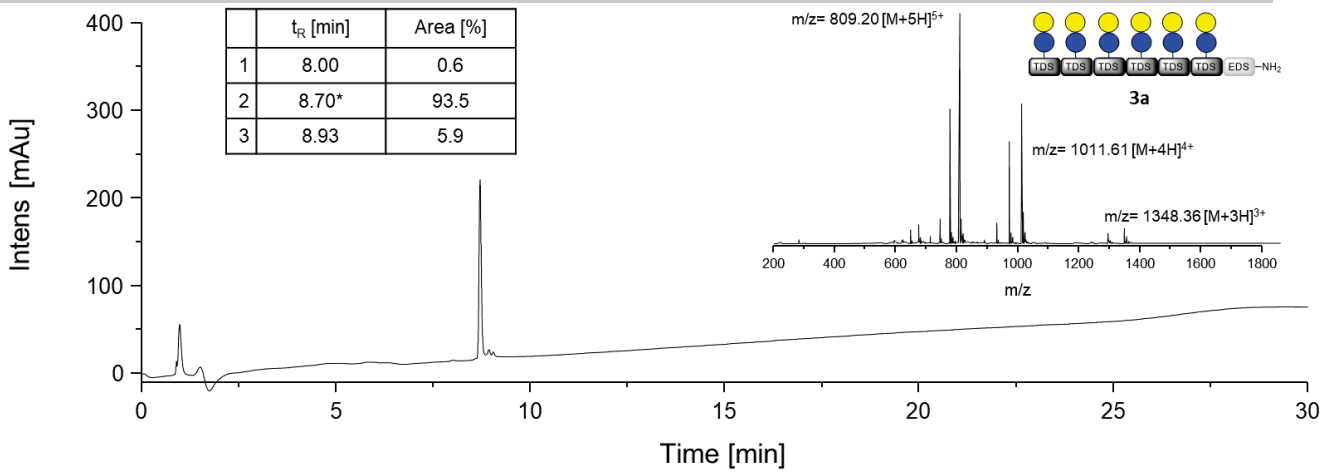

	t_R [min]	Area [%]
1	8.00	0.6
2	8.70*	93.5
3	8.93	5.9

Figure S 28: RP-HPLC chromatogram and ESI$^+$-MS spectrum of compound **3a.** Retention time t_R [min] and area [%] of the peaks are given. ESI-MS spectrum of the main peak (*) is shown.

Lac(1,2,3,4,5,6)-7–NHAc, **3b**

^{1}H NMR (600 MHz, Deuterium Oxide) δ [ppm]:8.04 (m, 6H, triazole-C*H*), 5.74 (d, J = 9.2 Hz, 6H, C*H*$_{anomer}$Glc), 4.52 (d, J = 7.6 Hz, 6H, C*H*$_{anomer}$-Gal), 4.10 – 3.74 (m, 62H, CH$_{pyranose}$, O-CH2-), 3.72 – 3.54 (m, 20H, CH$_{pyranose}$, C*H*$_{2\ pyranose}$, O-C*H*$_2$-), 3.50 – 3.27 (m, 50H, C=ONH-C*H*$_2$), 3.04-2.98 (m, 12H, CH=CH-C*H*$_2$), 2.85 – 2.72 (m, 12H, CH=CH-CH$_2$-C*H*$_2$), 2.52-2.41 (m, 28H, NHC=O-C*H*$_2$), 1.99 (s, 1H, C*H*$_3$).

^{13}C NMR (151 MHz, Deuterium Oxide) δ [ppm]: 215.59, 174.62, 174.05, 146.95, 122.42, 102.80, 87.07, 77.55, 77.24, 75.29, 74.47, 72.41, 71.84, 70.85, 69.29, 68.46, 60.96, 59.64, 46.96, 44.80, 38.84, 37.16, 36.75, 31.70, 30.67, 30.15, 29.89, 29.63, 29.37, 29.11, 28.85, 28.60, 20.56.

HR-MS (ESI^{+}) *m/z* calc. for $C_{162}H_{267}N_{39}O_{83}$ [M+4H] $^{4+}$ 1021.6962; found 1021.6962. Yield: 235.1 mg (55 %).

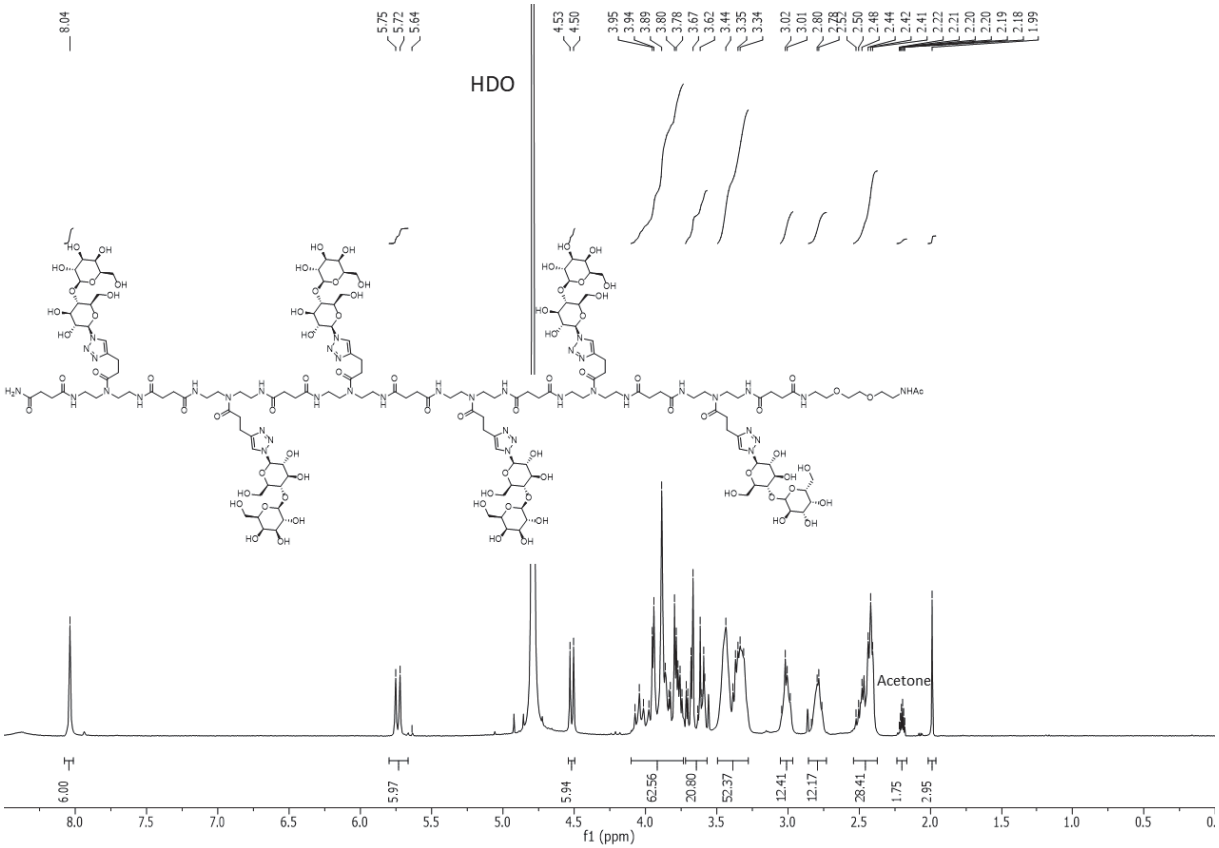

Figure S 29: ^{1}H-NMR spectrum of compound **3b**.

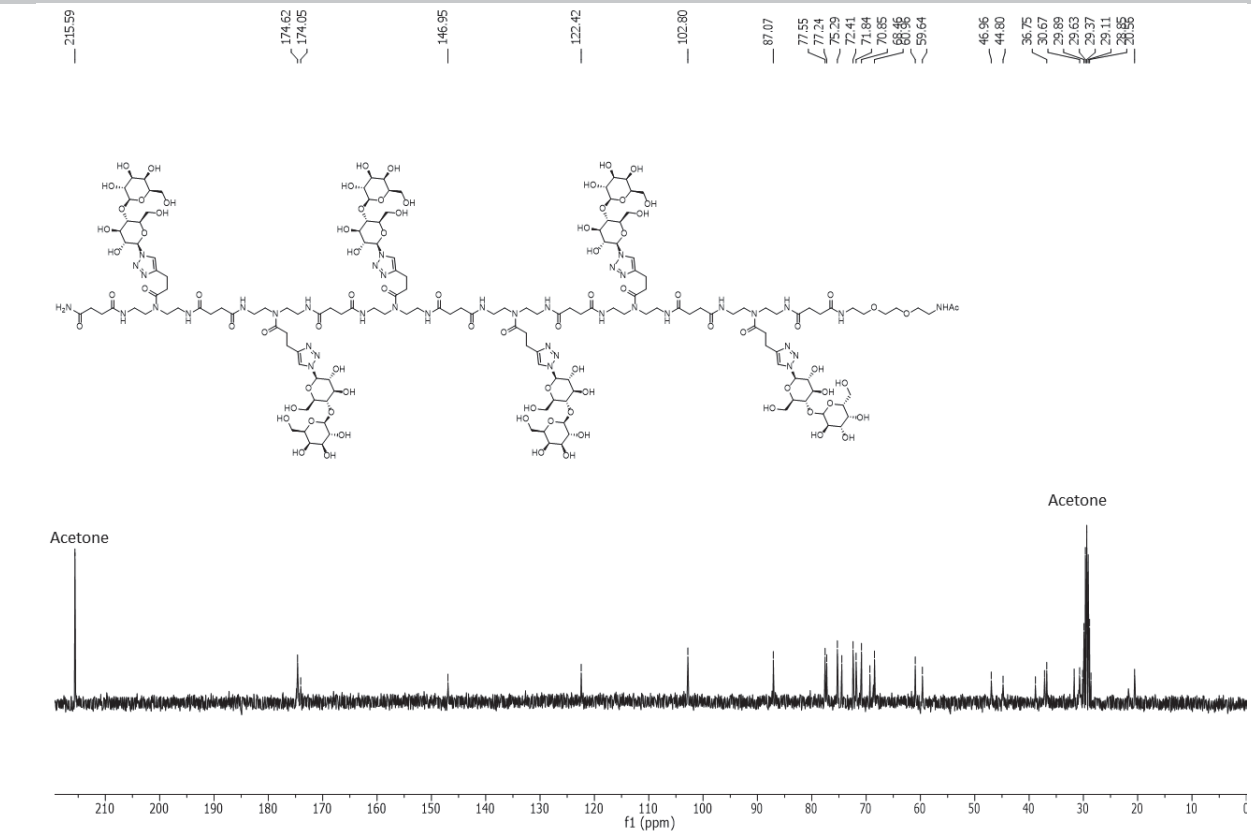

Figure S 30: ^{13}C-NMR spectrum of compound **3b**.

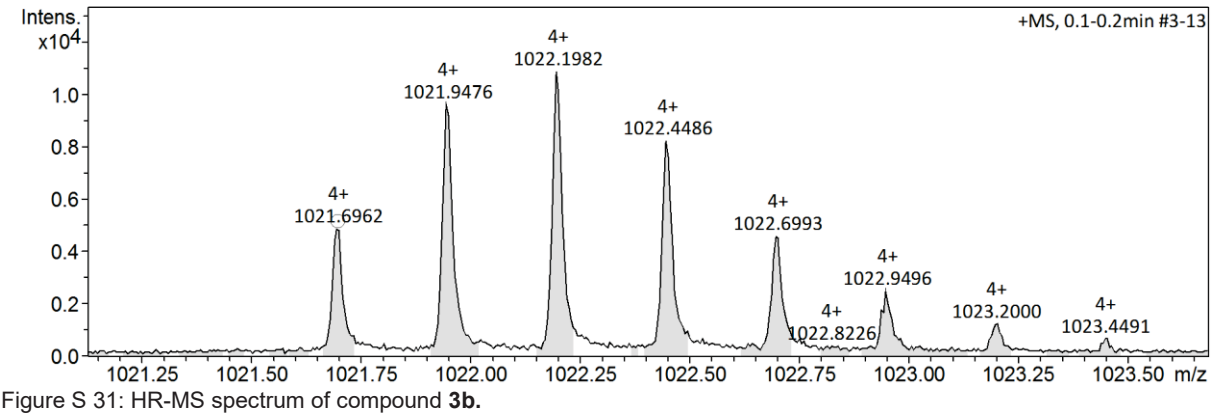

Figure S 31: HR-MS spectrum of compound **3b.**

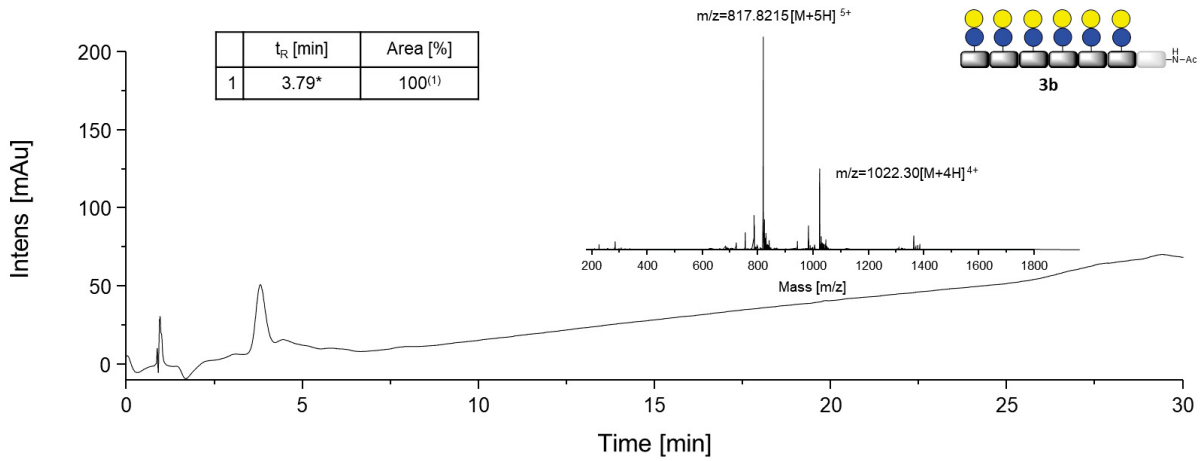

Figure S 32: RP-HPLC chromatogram and ESI$^+$-MS spectrum of compound **3b.** Retention time t_R [min] and area [%] of the peaks are given. ESI-MS spectrum of the main peak (*) is shown.

Lac(1,2,3,4,5,6)-7–FITC, **3c**

^{1}H NMR (600 MHz, Deuterium Oxide) δ [ppm]: δ 8.11 (s, 1H, FITC-C*H*), 8.08 – 7.93 (m, 6H, triazole-C*H*), 7.71 (s, 1H, FITC-C*H*), 7.15 (d, *J* = 6.5 Hz, 1H, FITC-C*H*), 6.93 (d, *J* = 7.0 Hz, 2H, FITC-C*H*), 6.86 (s, 2H, FITC-C*H*), 6.71 (d, *J* = 7.0 Hz, 2H, FITC-C*H*), 5.79 – 5.66 (m, 6H, CH_{anomer}Glc), 4.58 – 4.44 (m, 6H, CH_{anomer}-Gal), 4.07 – 3.54 (m, 80H, CH_{pyranose}, C$H_{2\ \text{pyranose,}}$ O-CH_2-), 3.51 – 3.18 (m, 52H, CH_{pyranose}, C=ONH-CH_2), 3.07 – 2.89 (m, 12H, CH=CH-CH_2), 2.85 – 2.65 (m, 12H, CH=CH-CH$_2$-CH_2), 2.55 – 2.32 (m, 28H, NHC=O-CH_2).

^{13}C NMR (151 MHz, Deuterium Oxide) δ [ppm]: 174.61, 146.99, 122.46, 102.92, 87.17, 77.64, 77.39, 75.39, 74.57, 72.51, 71.94, 70.94, 68.55, 61.05, 59.76, 47.06, 44.95, 37.28, 36.87, 31.75, 30.79, 30.61, 20.64.

HR-MS (ESI^{+}) *m/z* calc. for $C_{182}H_{276}N_{38}O_{88}S$ $[M+4H]^{4+}$ 1108.4497; found 1108.4503. Yield: 15 mg (33 %).

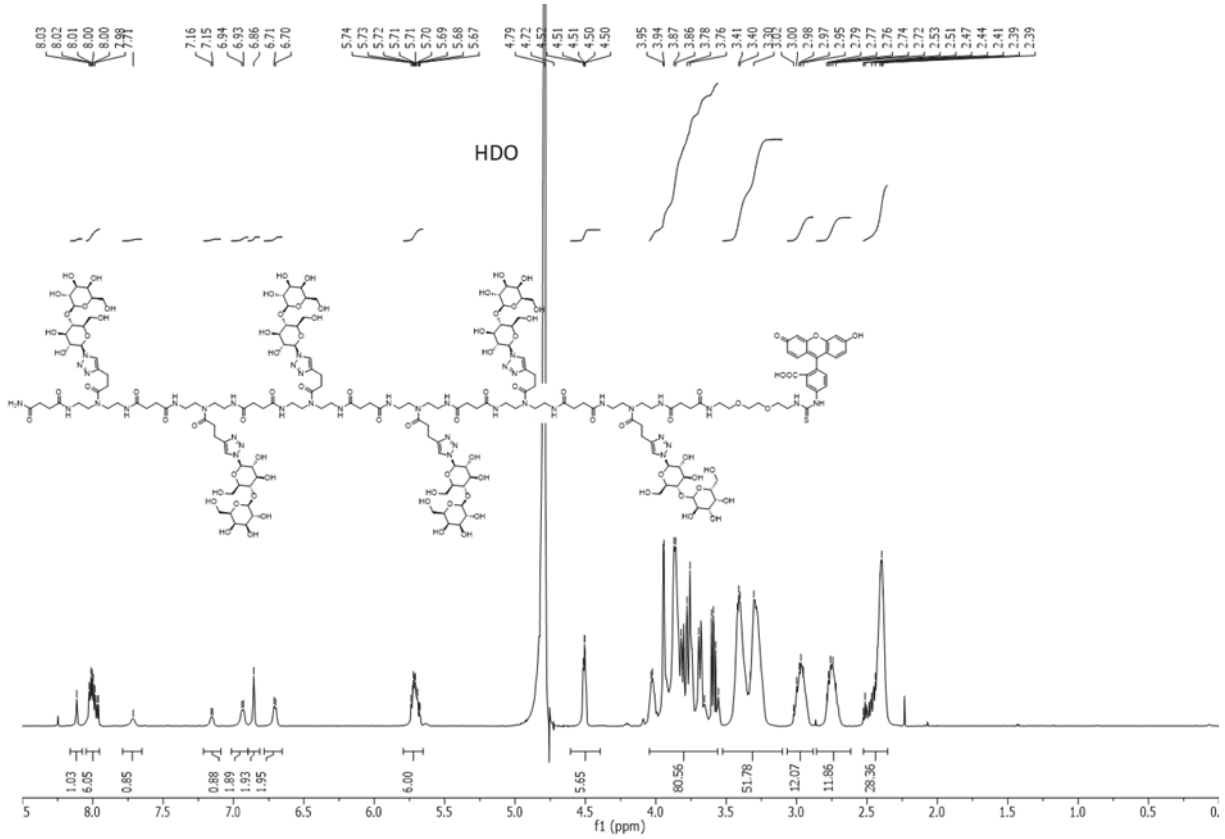

Figure S 33: ^{1}H-NMR spectrum of compound **3c**.

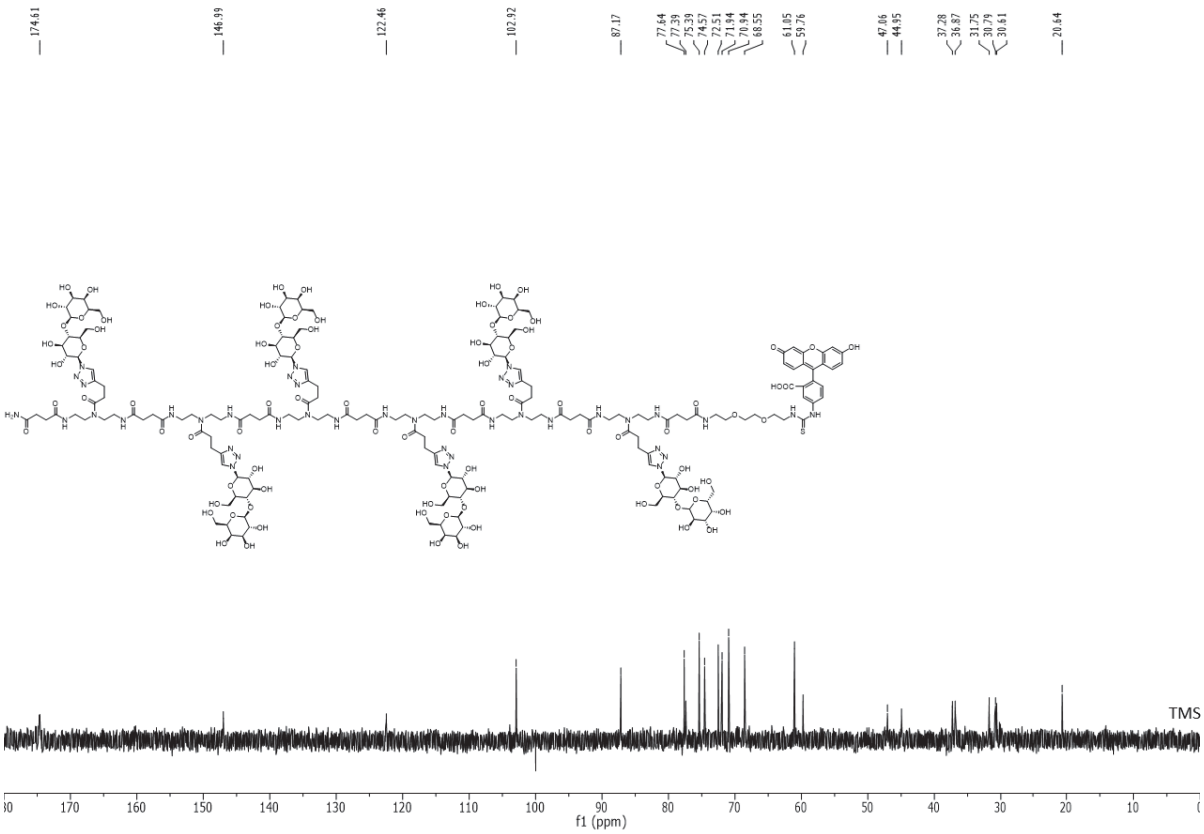

Figure S 34: ^{13}C-NMR spectrum of compound **3c**.

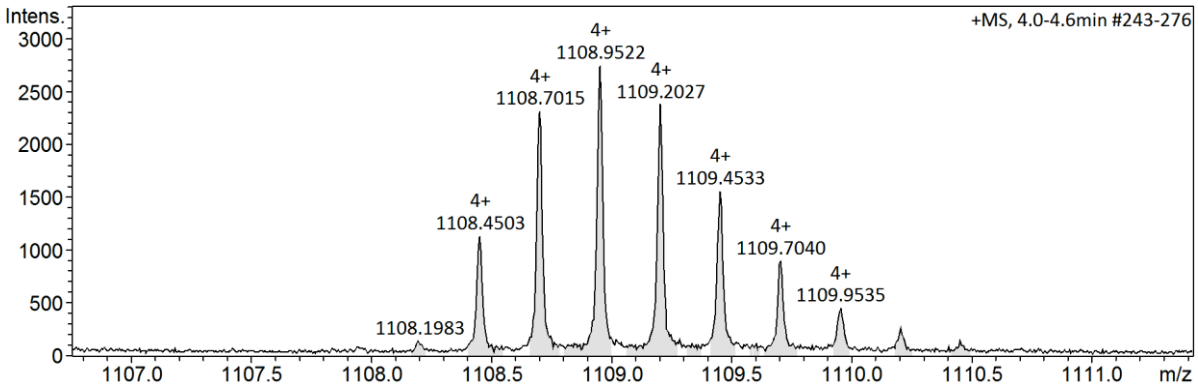

Figure S 35**:** HR-MS spectrum of compound **3c.**

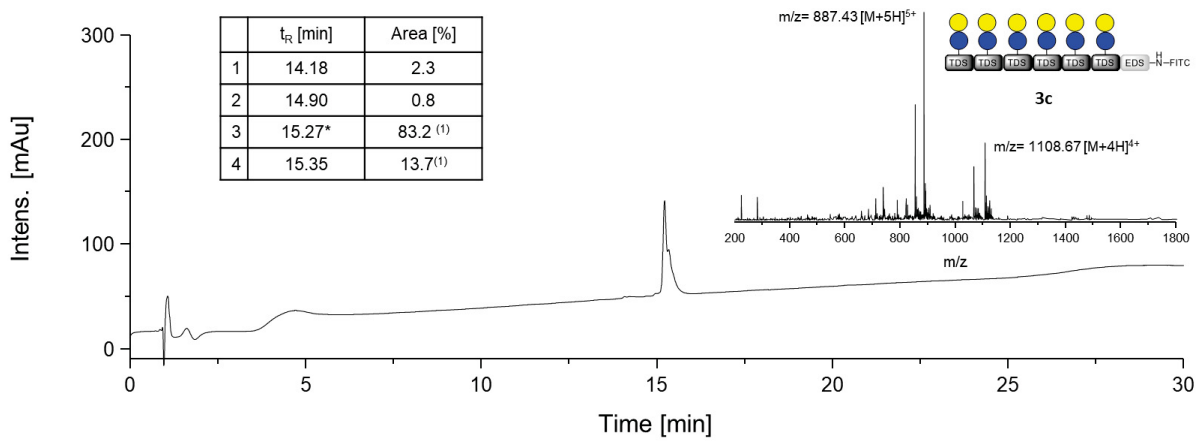

	t_R [min]	Area [%]
1	14.18	2.3
2	14.90	0.8
3	15.27*	83.2 (1)
4	15.35	13.7(1)

Figure S 36: RP-HPLC chromatogram and ESI$^+$-MS spectrum of compound **3c.** Retention time t_R [min] and area [%] of the peaks are given. ESI-MS spectrum of the main peak (*) is shown. (1) Peaks show the same m/z.

Lac(1,3,5)-Bz(2,4)-6–Ac, **4b**

^{1}H NMR (300 MHz, Deuterium Oxide) δ [ppm]: 8.05 – 8.00 (m, 3H, triazole-C*H*), 7.41 – 7.25 (m, 10H, aromatic-C*H*), 5.79 – 5.68 (m, 3H, CH_{anomer}Glc), 4.56 – 4.46 (m, 2H, C$H_{anomerGal}$), 4.35 (s, 4H, aromatic C$H_{2,}$), 4.12 – 3.53 (m, 48H, C$H_{pyranose}$, C$H_{2\ pyranose,}$ O-CH_2-), 3.52 – 3.22 (s, 44H, C$H_{pyranose}$,C=ONH-CH_2), 3.08 – 2.95 (m, 6H, CH=CH-CH_2), 2.84 – 2.73 (m, 6H, CH=CH-CH_2-CH_2), 2.73 – 2.34 (m, 34H, C$H_{pyranose}$, NHC=O-CH_2), 1.99 (s, 3H, CH_3).

^{13}C NMR (126 MHz, Deuterium Oxide) δ [ppm]: 173.96, 173.91, 173.79, 146.27, 137.37, 127.92, 126.54, 126.34, 121.70, 102.14, 86.36, 76.86, 76.77, 74.59, 73.82, 71.79, 71.15, 70.17, 68.61, 68.01, 67.97, 67.78, 65.08, 60.23, 59.05, 46.32, 46.24, 44.21, 42.11, 38.16, 38.11, 36.55, 36.50, 36.13, 30.99, 30.25, 30.19, 30.13, 30.08, 30.03, 29.91, 29.47, 29.34, 27.35, 21.05, 19.88, 13.28.

HR MS (ESI$^+$) *m/z* calc. for $C_{125}H_{198}N_{29}O_{52}$ $[M+3H]^{3+}$ 979.1241 found 979.1237. Yield: 104 mg (35 %).

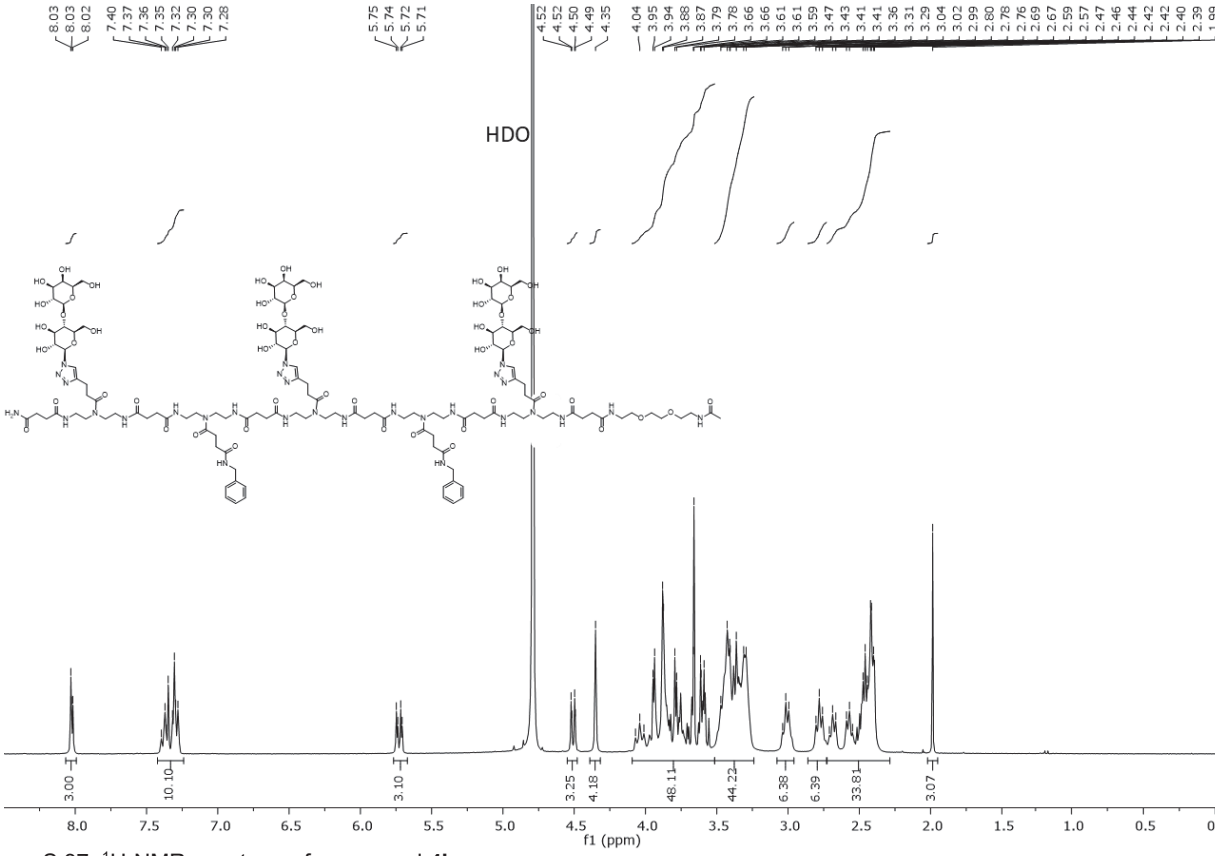

Figure S 37: ^{1}H-NMR spectrum of compound **4b**.

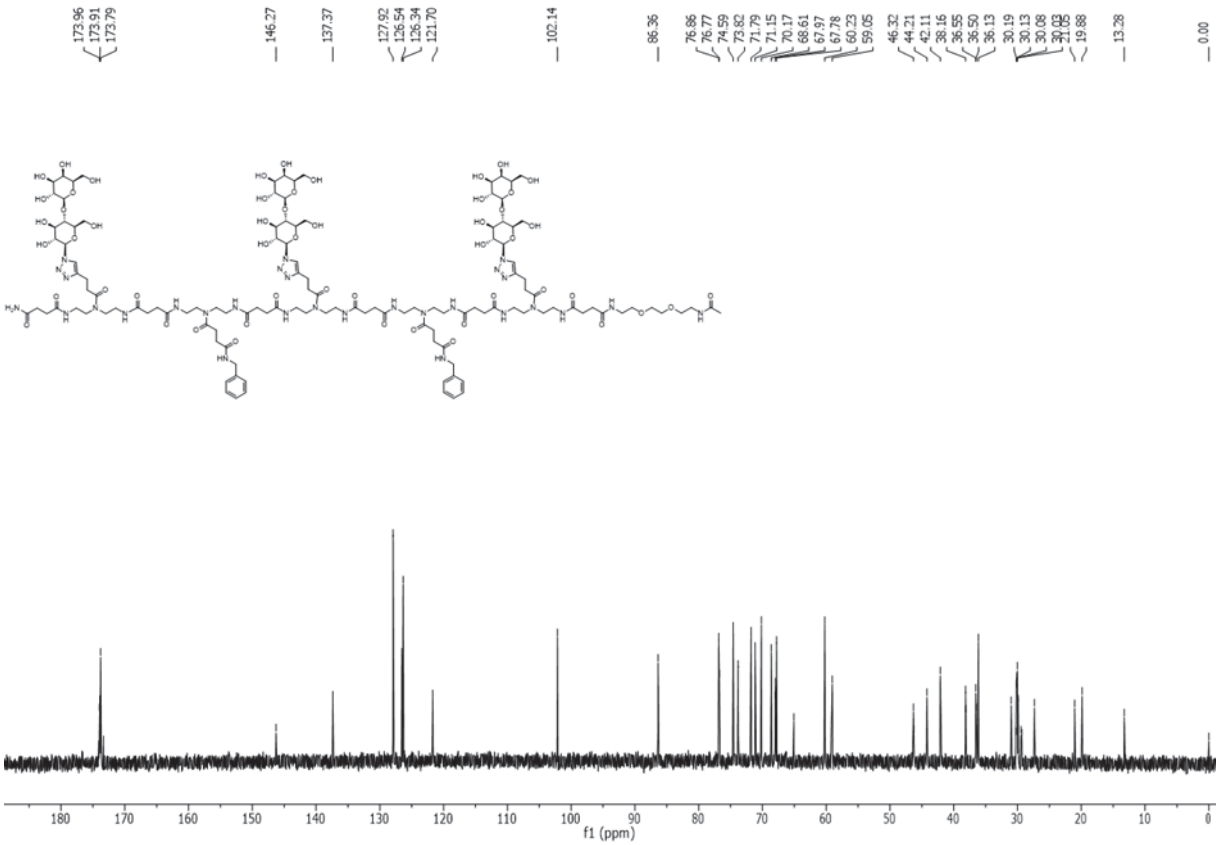

Figure S 38: ^{13}C-NMR spectrum of compound **4b**.

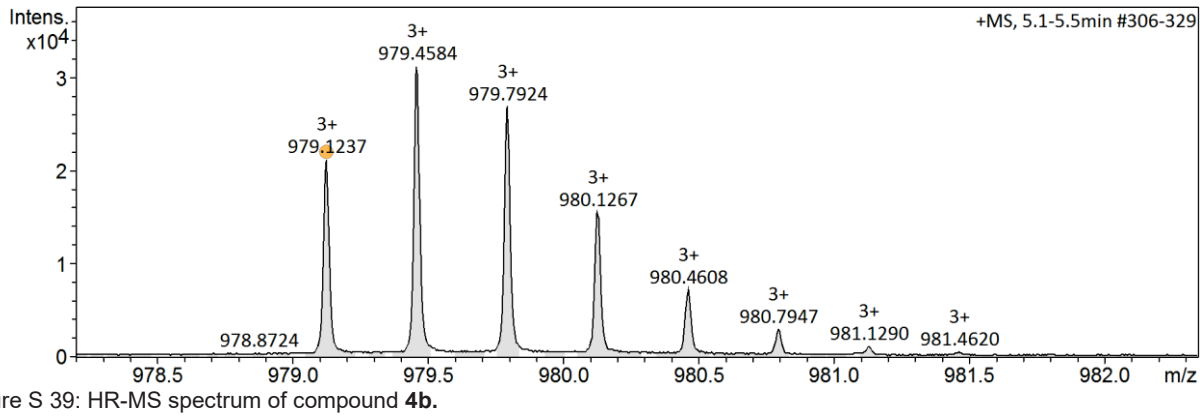

Figure S 39: HR-MS spectrum of compound **4b.**

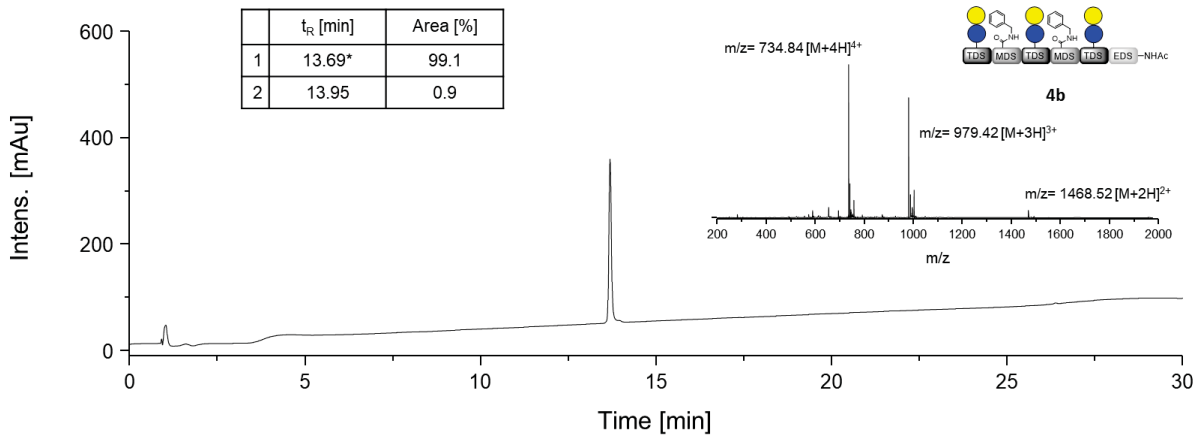

Figure S 40: RP-HPLC chromatogram and ESI$^+$-MS spectrum of compound **4b.** Retention time t_R [min] and area [%] of the peaks are given. ESI-MS spectrum of the main peak (*) is shown.

Lac(1,3,5)-*p*NH_2Ph(2,4)-6–Ac, **5b**

^{1}H NMR (300 MHz, Deuterium Oxide) δ [ppm]: 8.09 – 7.97 (m, 3H, triazole-CH), 7.23 (d, J = 8.4 Hz, 4H, aromatic C*H*), 6.87 (d, J = 8.4 Hz, 4H, aromatic C*H*), 5.79 – 5.68 (m, 3H, CH_{anomer}Glc), 4.55 – 4.45 (m, 3H, CH_{anomer}Gal), 4.11 – 3.57 (m, 46H, C$H_{pyranose}$, CH_2 $_{pyranose,}$ O-CH_2-), 3.56 – 3.23 (m, 46H, C$H_{pyranose}$,C=ONH-CH_2), 3.08 – 2.93 (m, 6H, CH=CH-CH_2), 2.85 – 2.59 (m, 15H, CH=CH-CH$_2$-CH_2, C$H_{pyranose}$), 2.55 – 2.30 (m, 24H, C$H_{pyranose,}$ NHC=O-CH_2), 1.99 (s, 3H, CH_3).

^{13}C NMR (126 MHz, Deuterium Oxide) δ [ppm]: 173.91, 146.26, 122.48, 121.70, 116.63, 102.14, 86.36, 76.86, 76.78, 74.60, 73.83, 71.79, 71.15, 70.18, 68.61, 68.01, 67.97, 67.79, 60.24, 59.06, 46.33, 44.22, 38.16, 38.11, 36.55, 36.21, 36.14, 30.99, 30.09, 29.94, 27.29, 21.06, 19.89, 13.28.

HR-MS (ESI$^+$) *m/z* calc. for $C_{123}H_{197}N_{31}O_{52}$ $[M+4H]^{4+}$ 735.0925; found 735.0917. Yield: 110 mg (38 %).

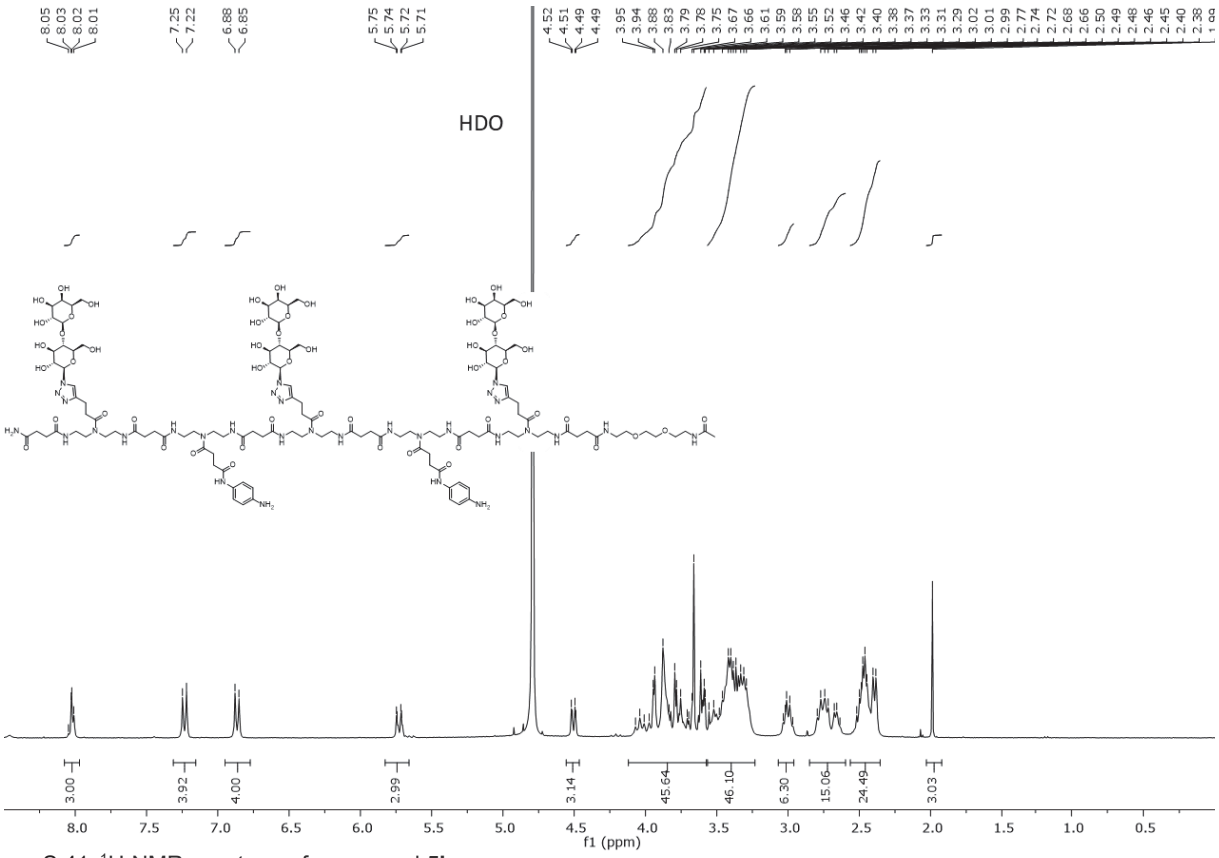

Figure S 41: ^{1}H-NMR spectrum of compound **5b**.

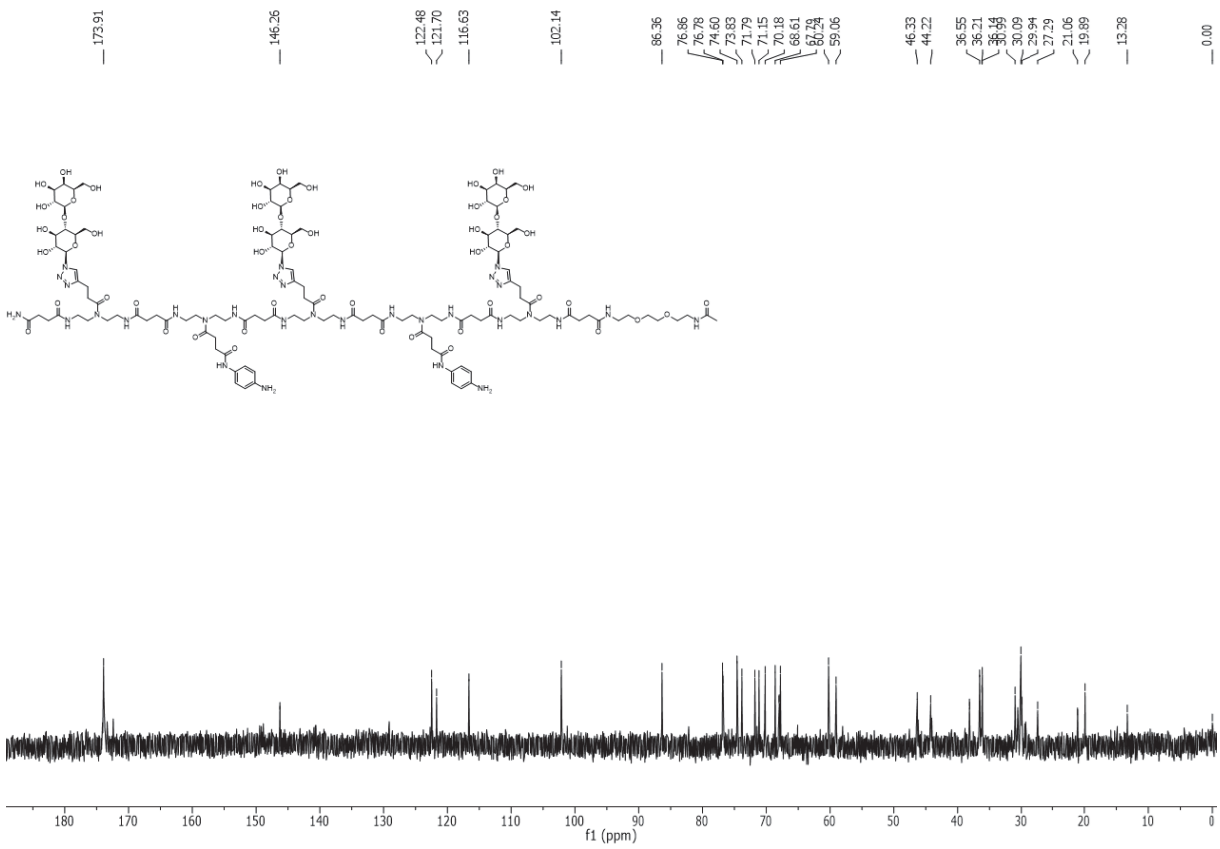

Figure S 42: ^{13}C-NMR spectrum of compound **5b**.

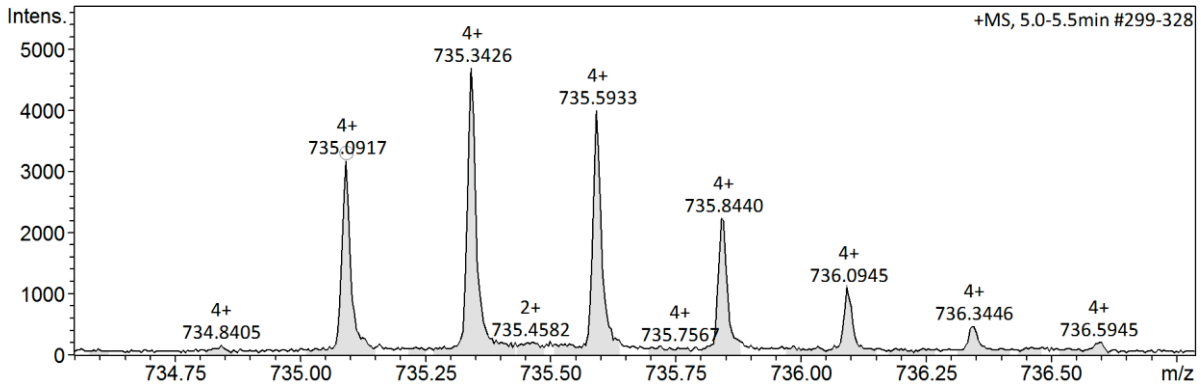

Figure S 43: HR-MS spectrum of compound **5b.**

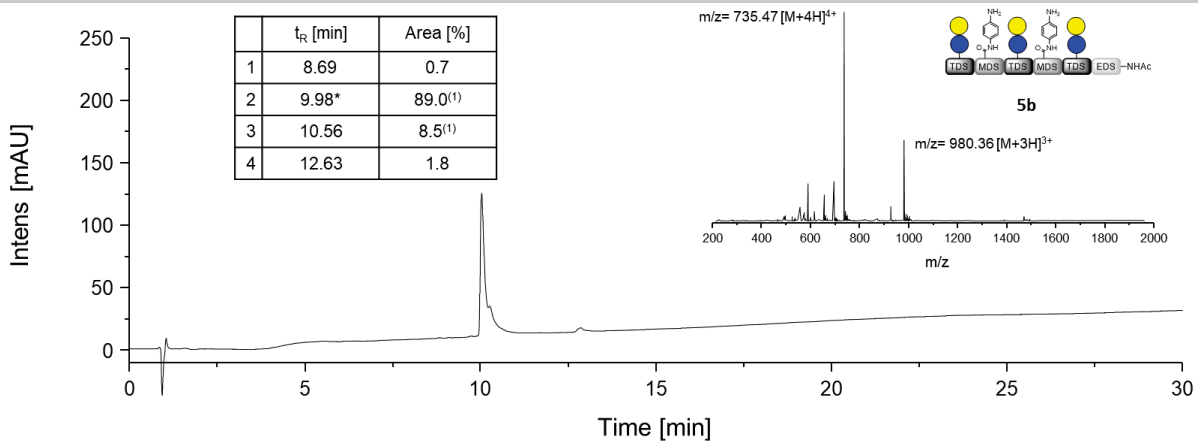

	t_R [min]	Area [%]
1	8.69	0.7
2	9.98*	89.0(1)
3	10.56	8.5(1)
4	12.63	1.8

Figure S 44: RP-HPLC chromatogram and ESI$^+$-MS spectrum of compound **5b.** Retention time t_R [min] and area [%] of the peaks are given. ESI-MS spectrum of the main peak (*) is shown. (1) Peaks with the same m/z.

Lac(1,3,5)-*p*SO_3H Ph(2,4)-6–NH_2, **6a**

^{1}H NMR (300 MHz, Deuterium Oxide) δ [ppm]: 8.06 – 7.98 (m, 3H, triazole-C*H*), 7.76 (d, J = 8.7 Hz, 4H, aromatic C*H*), 7.57 (d, J = 8.6 Hz, 4H, aromatic C*H*), 5.79 – 5.67 (m, 3H, CH_{anomer}-Glc), 4.56 – 4.45 (m, 3H, CH_{anomer}-Gal), 4.10 – 3.70 (m, 30H, C$H_{pyranose}$, C$H_{2\ pyranose}$, O-CH_2-), 3.68 – 3.20 (m, 60H, C$H_{pyranose}$, C=ONH-CH_2, CH_2-NH_2), 3.11 – 2.91 (m, 6H, CH=CH-CH_2), 2.85 – 2.62 (m, 16H, CH=CH-CH_2-CH_2, NHC=O-CH_2), 2.55 – 2.31 (m, 24H, NHC=O-CH_2).

^{13}C NMR (151 MHz, Deuterium Oxide) δ [ppm]:173.90, 173.90, 173.76, 172.58, 171.31, 146.24, 139.24, 137.54, 125.68, 121.71, 119.55, 102.06, 86.32, 76.80, 76.52, 74.55, 73.74, 71.69, 71.13, 70.13, 68.54, 67.97, 67.88, 67.75, 60.23, 58.93, 48.46, 46.24, 44.12, 38.04, 36.43, 36.03, 34.87, 31.06, 30.92, 30.69, 29.99, 29.89, 29.80, 26.95, 19.81.

HR MS (ESI$^+$) *m/z* calc. for $C_{124}H_{197}N_{30}O_{58}S_2$ $[M+3H]^{3+}$ 1032.7604 found; 1032.7593. Yield: 27 mg (10 %).

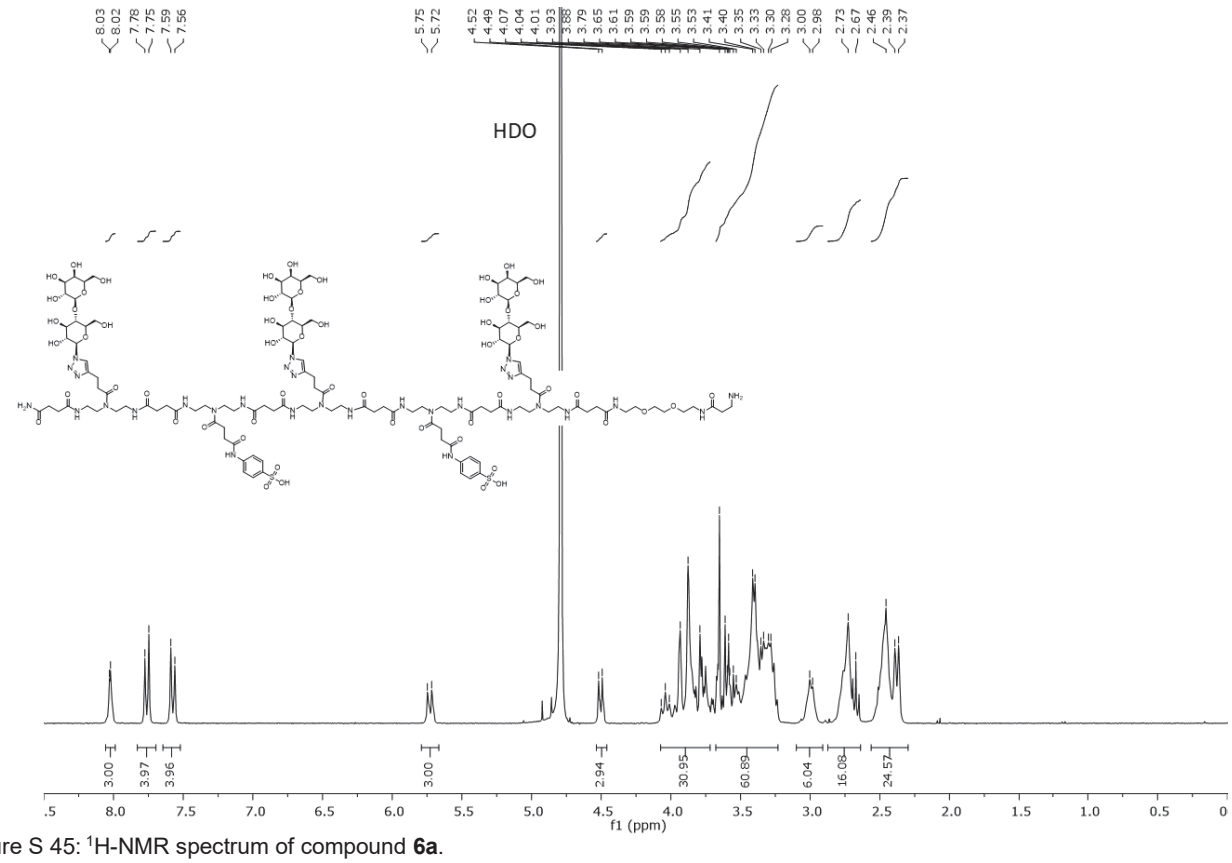

Figure S 45: ^{1}H-NMR spectrum of compound **6a**.

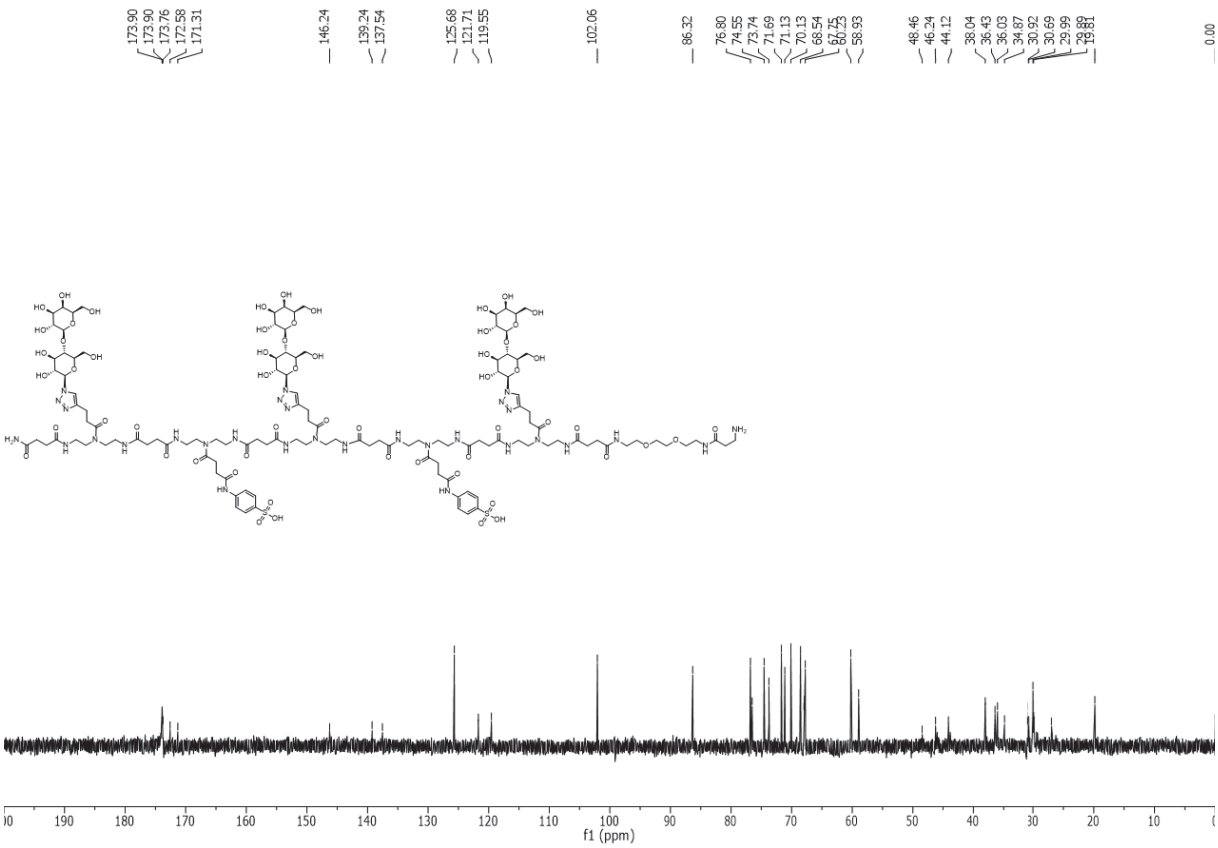

Figure S 46: ^{13}C-NMR spectrum of compound **6a**.

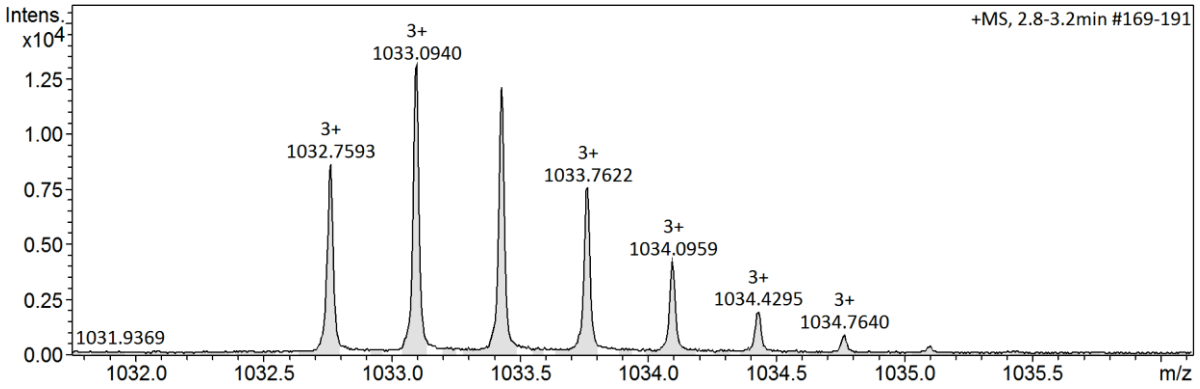

Figure S 47: HR-MS spectrum of compound **6a.**

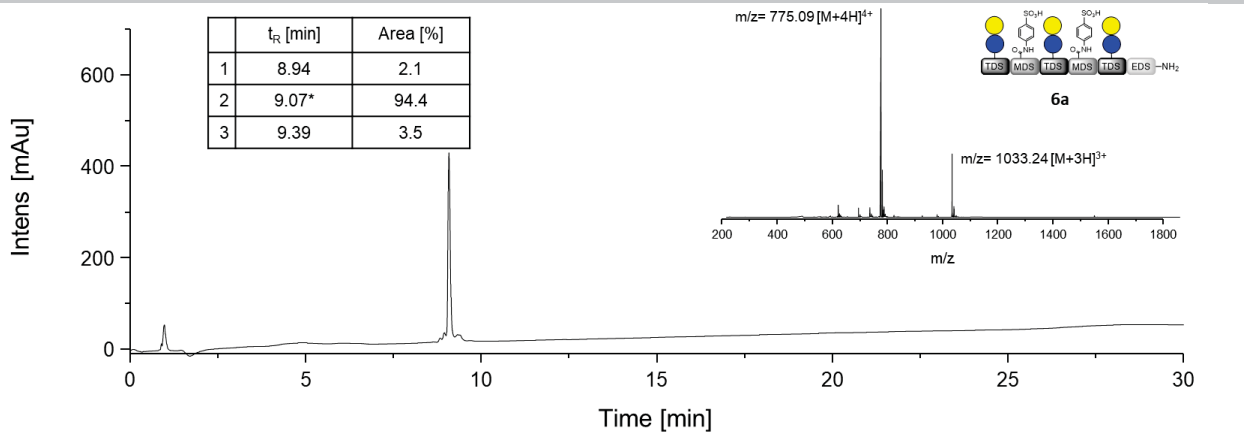

	t_R [min]	Area [%]
1	8.94	2.1
2	9.07*	94.4
3	9.39	3.5

Figure S 48: RP-HPLC chromatogram and ESI$^+$-MS spectrum of compound **6a.** Retention time t_R [min] and area [%] of the peaks are given. ESI-MS spectrum of the main peak (*) is shown.

Lac(1,3,5)-*p*SO_3H Ph(2,4)-6–Ac, **6b**

^{1}H NMR (300 MHz, Deuterium Oxide) δ [ppm]: 8.09 – 7.96 (m, 3H, triazole-C*H*), 7.76 (d, J = 8.7 Hz, 4H, aromatic C*H*), 7.58 (d, J = 8.5 Hz, 4H, aromatic C*H*), 5.86 – 5.60 (m, 3H, CH_{anomer}-Glc), 4.58 – 4.43 (m, 3H, CH_{anomer}-Gal), 4.12 – 3.97 (m, 3H, C$H_{pyranose}$), 3.97 – 3.49 (m, 45H, C$H_{pyranose}$, C$H_{2\ pyranose}$, O-CH_2-), 3.49 – 3.22 (m, 40H, C=ONH-CH_2), 3.11 – 2.90 (m, 6H, CH=CH-CH_2), 2.84 – 2.65 (m, 14H, CH=CH-CH_2-CH_2,), 2.58 – 2.32 (m, 24H, NHC=O-CH_2), 1.99 (s, 3H).

^{13}C NMR (126 MHz, Deuterium Oxide) δ [ppm]:173.90, 146.27, 141.84, 139.20, 125.72, 121.74, 119.67, 102.13, 86.37, 76.86, 76.76, 74.57, 73.80, 71.78, 71.15, 70.17, 68.60, 67.96, 67.79, 65.08, 60.22, 59.06, 46.33, 46.12, 44.23, 44.02, 38.17, 38.11, 36.54, 36.21, 36.14, 31.00, 30.79, 30.10, 27.07, 21.05, 19.87, 13.27.

HR S (ESI$^+$) *m/z* calc. for $C_{123}H_{194}N_{29}O_{58}S_2$ $[M+3H]^{3+}$ 1023.0849, found; 1023.0848. Yield: 23 mg (10 %).

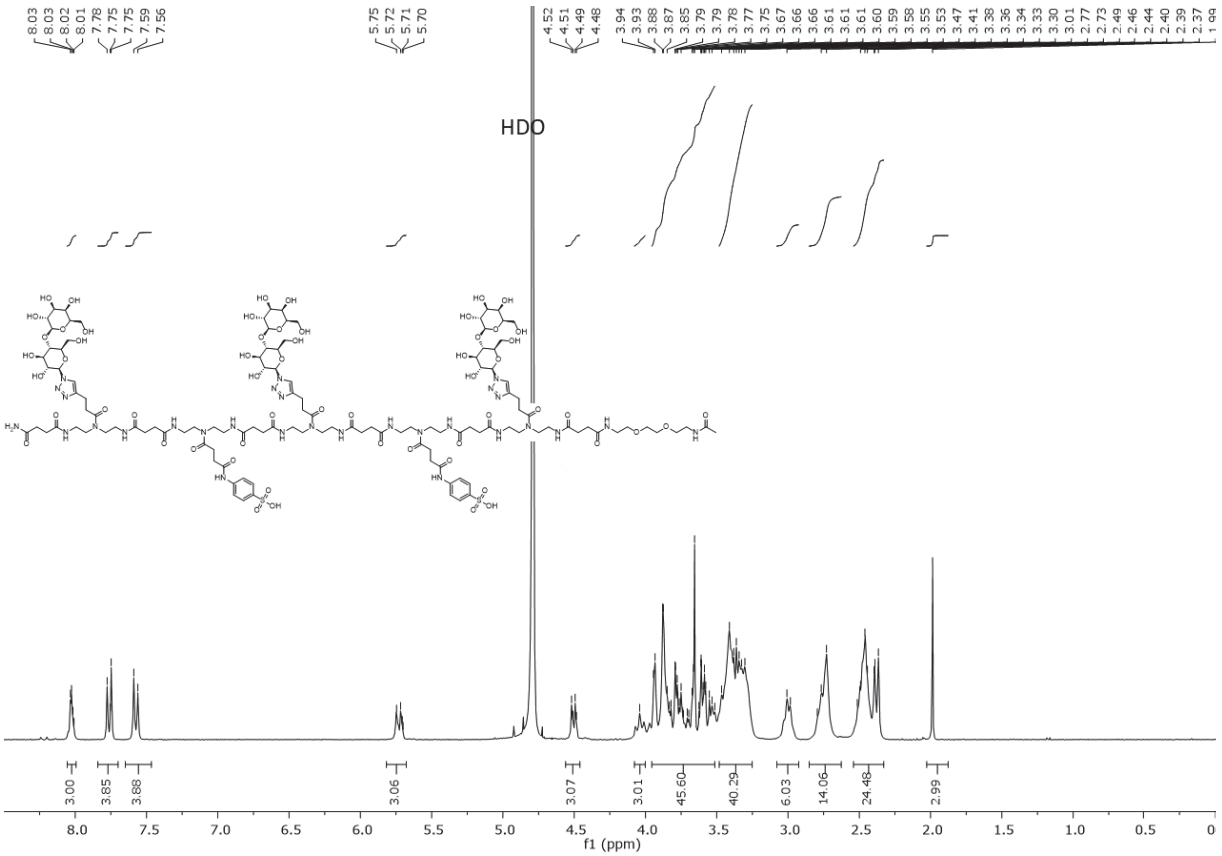

Figure S 49: ^{1}H-NMR spectrum of compound **6b.**

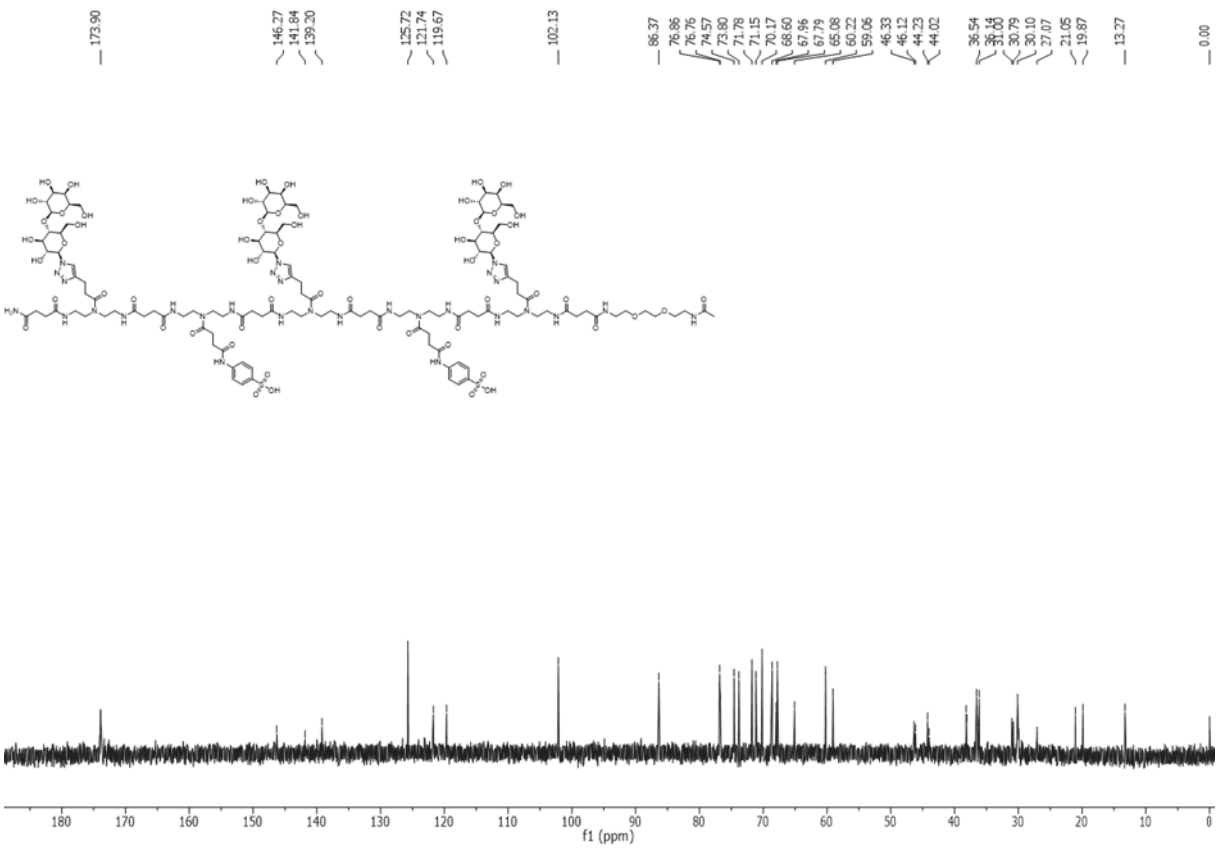

Figure S 50: ^{13}C-NMR spectrum of compound **6b**.

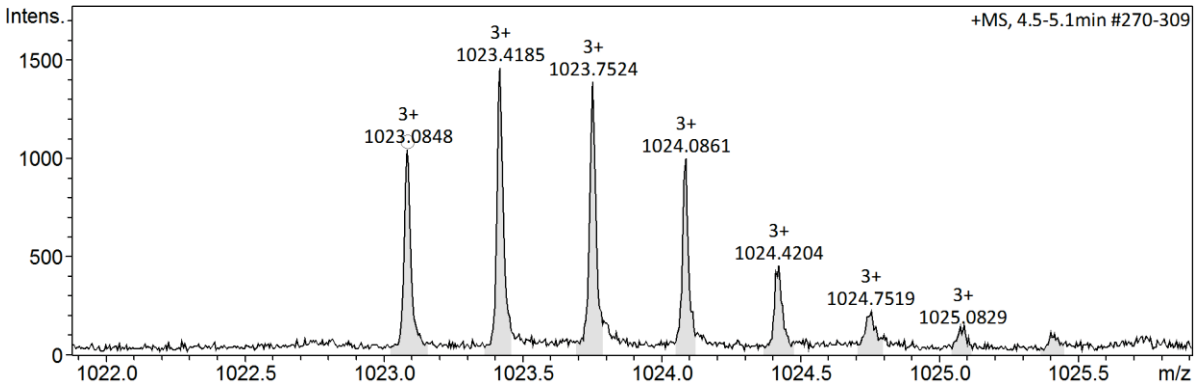

Figure S 51: HR-MS spectrum of compound **6b.**

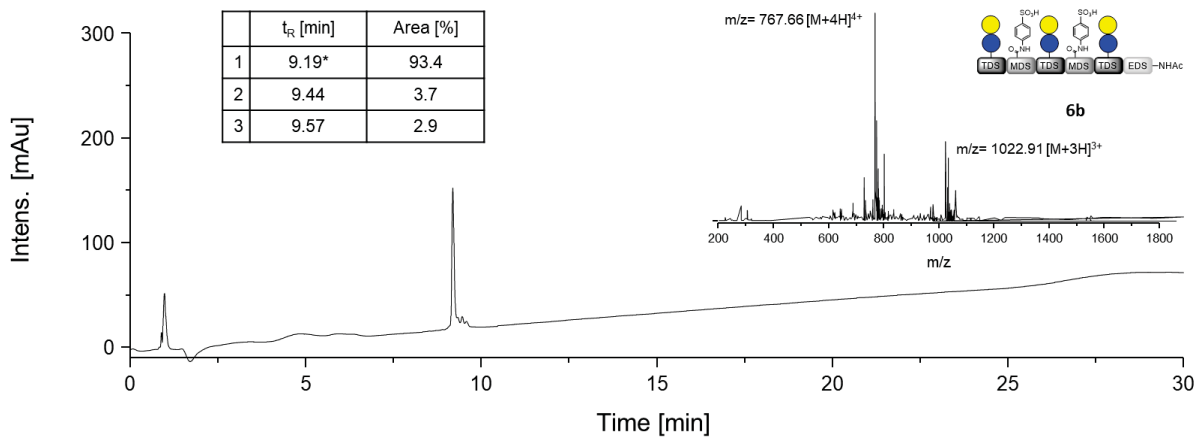

	t_R [min]	Area [%]
1	9.19*	93.4
2	9.44	3.7
3	9.57	2.9

Figure S 52: RP-HPLC chromatogram and ESI$^+$-MS spectrum of compound **6b.** Retention time t_R [min] and area [%] of the peaks are given. ESI-MS spectrum of the main peak (*) is shown.

Lac(1,3,5)-*p*SO_3H Ph(2,4)-6–FITC, **6c**

^{1}H NMR (300 MHz, Deuterium Oxide) δ [ppm]: 8.08 – 7.95 (m, 3H, triazole-C*H*), 7.79 – 7.65 (m, 4H, aromatic C*H*), 7.62 – 7.49 (m, 4H, aromatic C*H*), 7.33 – 7.19 (m, 2H, FITC-C*H*), 6.76 – 6.62 (m, 2H, FITC-C*H*), 5.78 – 5.66 (m, 3H, CH_{anomer}-Glc), 4.55 – 4.46 (m, CH_{anomer}-Gal), 4.12 – 3.56 (m, 45H, C$H_{pyranose}$, CH_2 $_{pyranose,}$ O-CH_2-), 3.56 – 3.16 (m, 45H, C$H_{pyranose,}$ C=ONH-C$H_{2,}$ CH_2-NH_2), 3.07 – 2.91 (m, 6H, CH=CH-CH_2), 2.82 – 2.60 (m, 17 H, CH=CH-CH_2-C$H_{2,}$ NHC=O-CH_2), 2.55 – 2.17 (m, 23H, NHC=O-CH_2).

^{13}C NMR (75 MHz, Deuterium Oxide) δ [ppm]: 174.96, 174.92, 174.79, 167.78, 126.73, 103.13, 93.57, 87.39, 77.87, 77.84, 77.60, 77.58, 75.60, 74.78, 72.73, 72.18, 71.17, 69.69, 69.65, 69.61, 69.55, 68.99, 68.77, 66.77, 61.28, 59.99, 47.08, 45.95, 45.15, 44.24, 37.50, 37.45, 37.23, 37.18, 37.08, 31.21, 31.13, 31.10, 31.05, 20.90.

HR MS (ESI$^+$) *m/z* calc. for $C_{146}H_{209}N_{29}O_{64}S_3$ $[M+4H]^{4+}$ 872.0783, found; 872.0800. Yield: 7 mg (36 %).

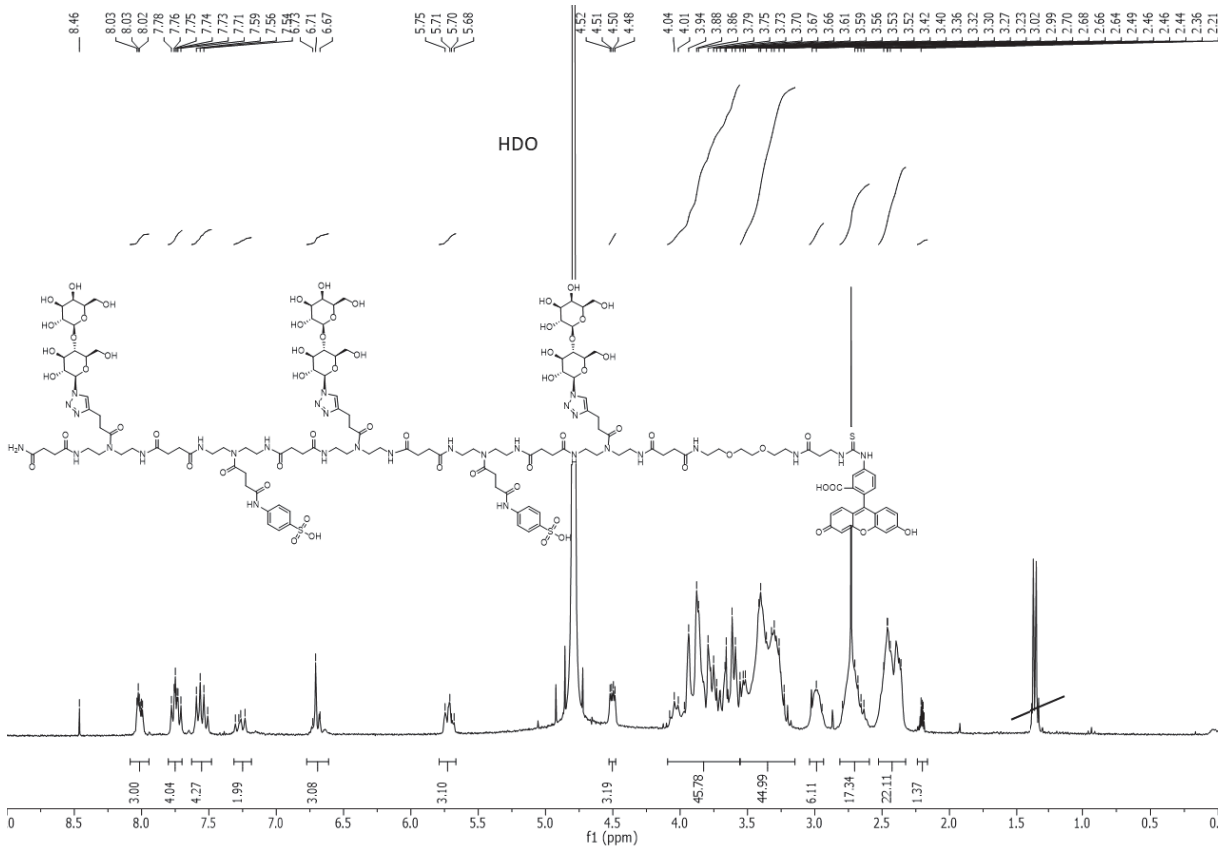

Figure S 53: ^{1}H-NMR spectrum of compound **6c.**

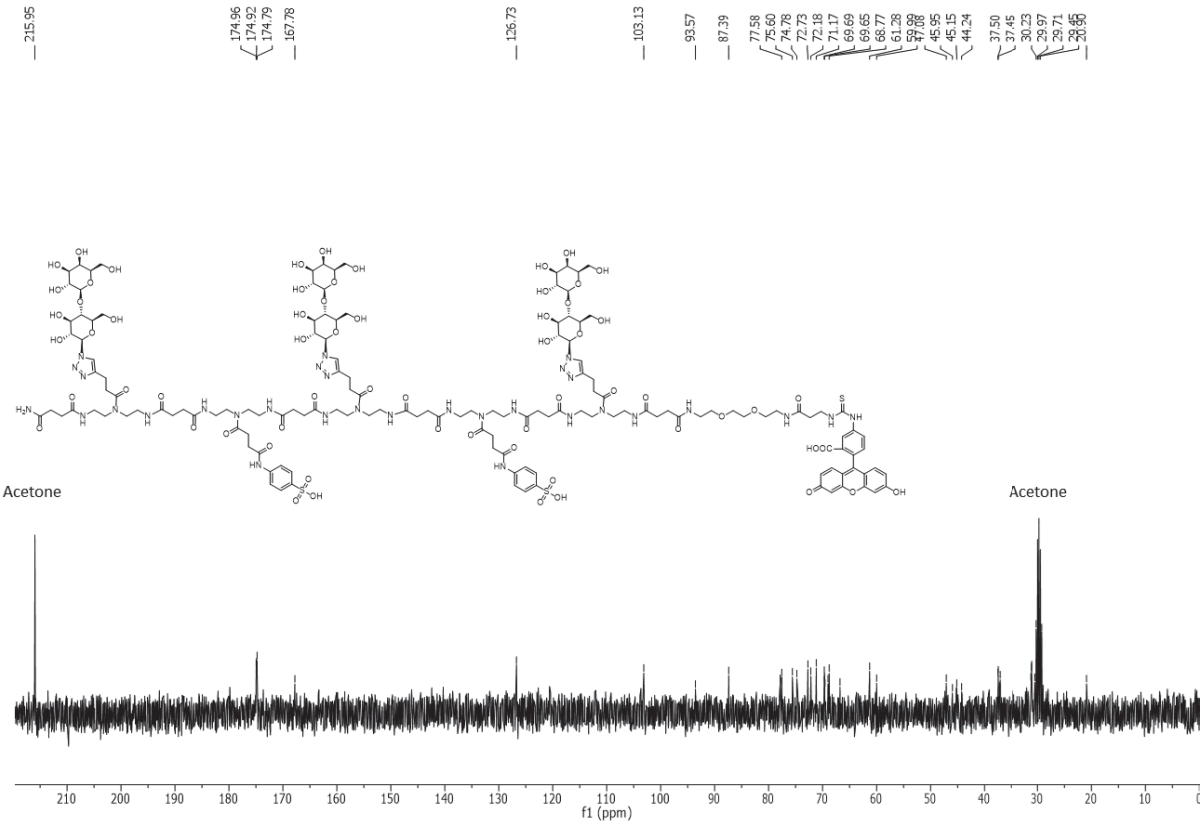

Figure S 54: ^{13}C-NMR spectrum of compound **6c**.

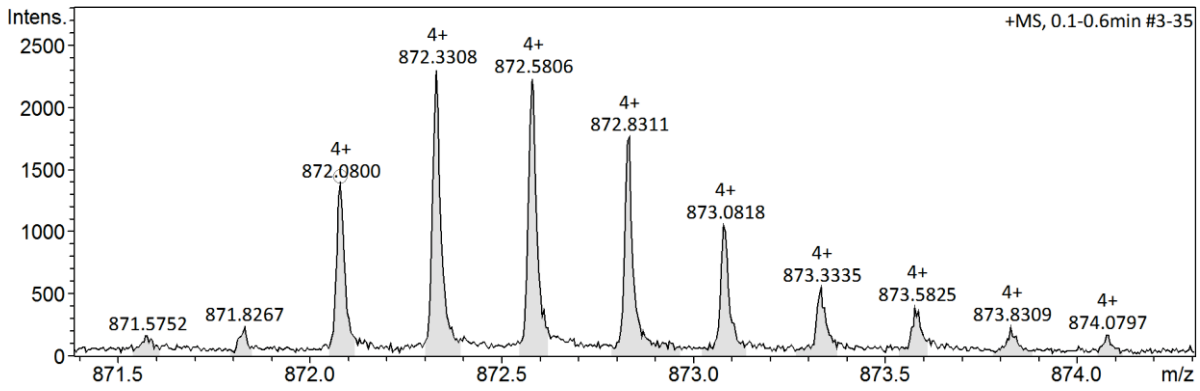

Figure S 55: HR-MS spectrum of compound **6c.**

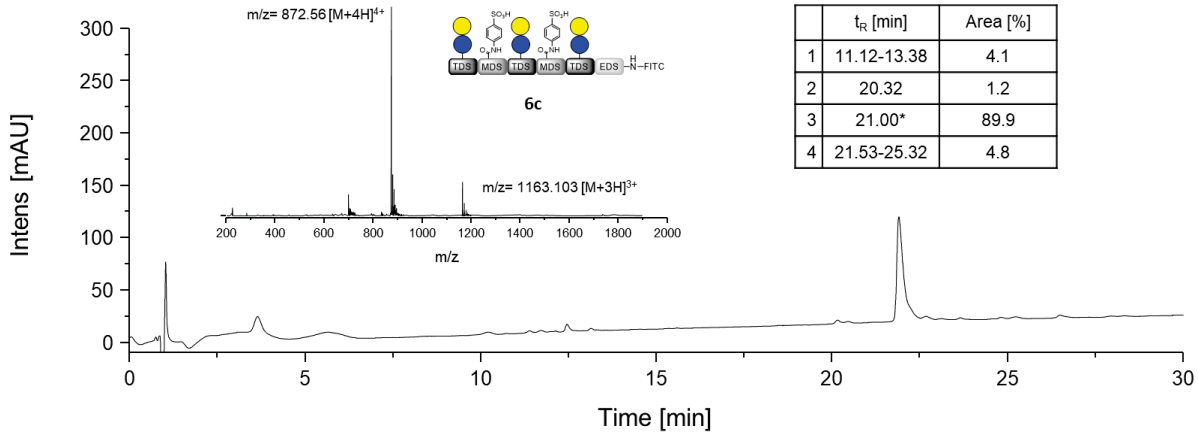

	t_R [min]	Area [%]
1	11.12-13.38	4.1
2	20.32	1.2
3	21.00*	89.9
4	21.53-25.32	4.8

Figure S 56: RP-HPLC chromatogram and ESI$^+$-MS spectrum of compound **6c.** Retention time t_R [min] and area [%] of the peaks are given. ESI-MS spectrum of the main peak (*) is shown.

Lac(1,3,5)-(1-SO_3H,4-OH)Ph(2,4)-6–Ac, **7b**

^{1}H NMR (300 MHz, Deuterium Oxide) δ [ppm]: 8.09 – 7.91 (m, 3H, triazole-C*H*), 7.53 (dd, J = 8.5, 2.2 Hz, 2H, aromatic C*H*), 7.03 (d, J = 8.5 Hz, 2H, aromatic C*H*), 5.81 – 5.63 (m, 3H, CH_{anomer}-Glc), 4.58 – 4.40 (m, 3H, CH_{anomer}-Gal), 4.13 – 3.68 (m, 38H, C$H_{pyranose,}$ C$H_{2\ pyranose,}$ O-CH_2-), 3.68 – 3.17 (m, 52H, C$H_{pyranose,}$ C=ONH-C$H_{2,}$), 3.10 – 2.89 (m, 6H, CH=CH-CH_2), 2.83 – 2.62 (m, 14H, CH=CH-CH_2-C$H_{2,}$ NHC=O-CH_2), 2.59 – 2.30 (m, 24H,), 1.99 (s, 3H,CH_3).

^{13}C NMR (126 MHz, Deuterium Oxide) δ [ppm]: 173.89, 121.71, 115.45, 102.11, 86.34, 76.84, 76.74, 74.56, 73.83, 71.82, 71.18, 70.20, 68.58, 67.95, 67.83, 65.07, 60.25, 59.09, 56.65, 44.22, 38.15, 36.53, 30.95, 30.11, 19.85, 16.01, 13.27.

HR MS (ESI$^+$) *m/z* calc. for $C_{123}H_{194}N_{29}O_{60}S_2$ $[M+3H]^{3+}$ 1033.7482, found; 1033.7487. Yield: 20 mg (9 %).

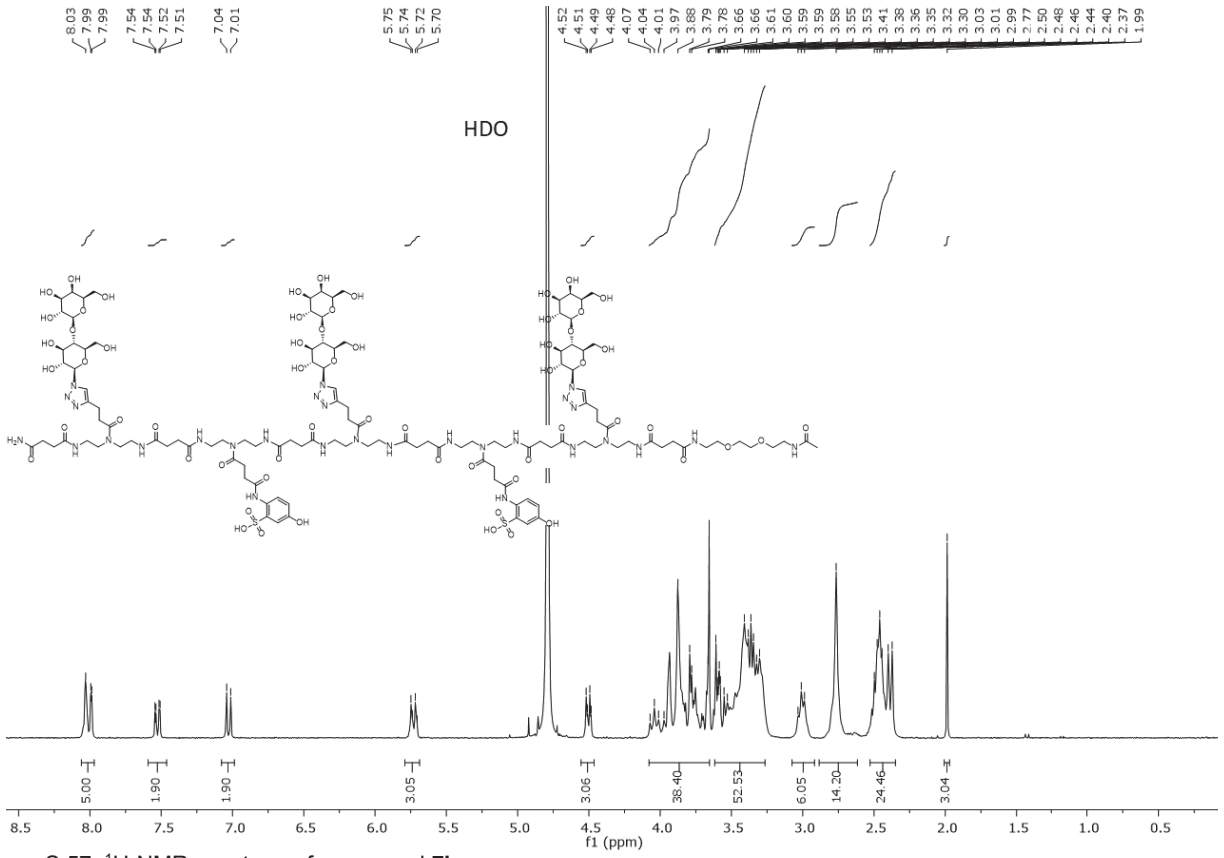

Figure S 57: ^{1}H-NMR spectrum of compound **7b**.

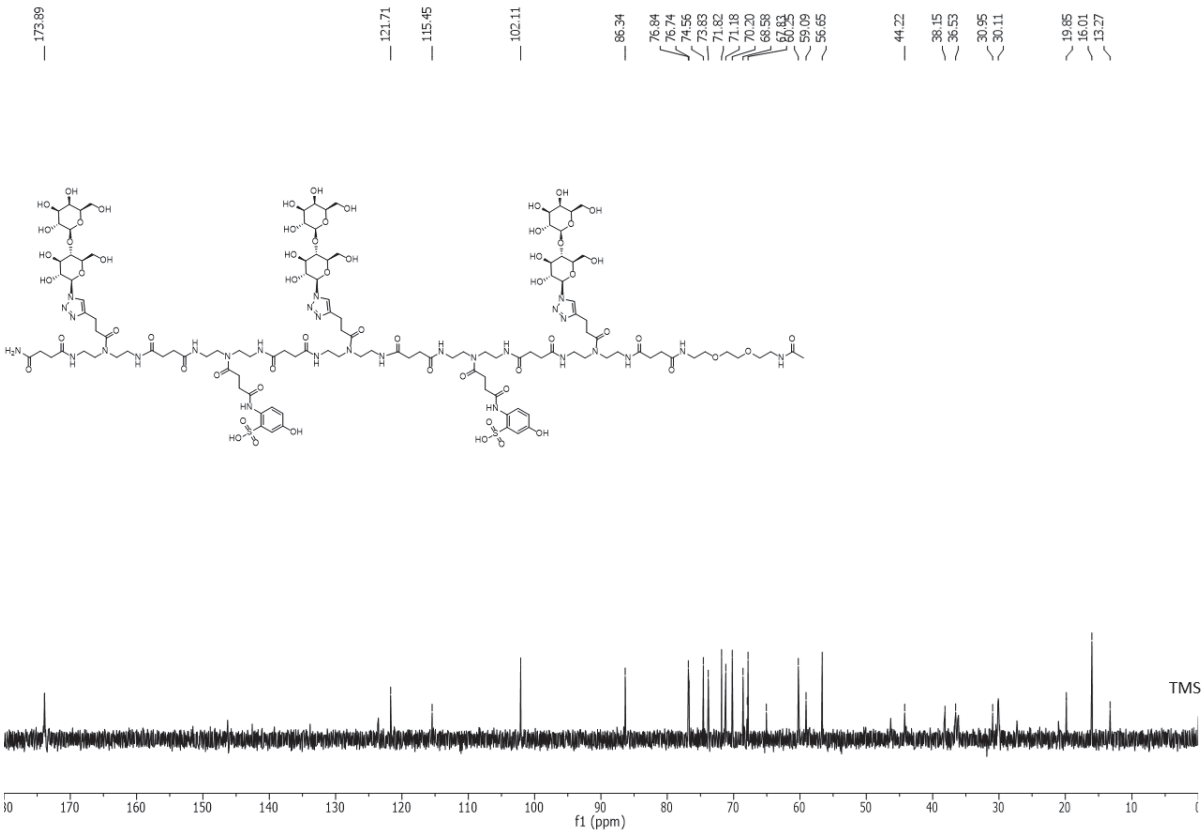

Figure S 58: ^{13}C-NMR spectrum of compound **7b**.

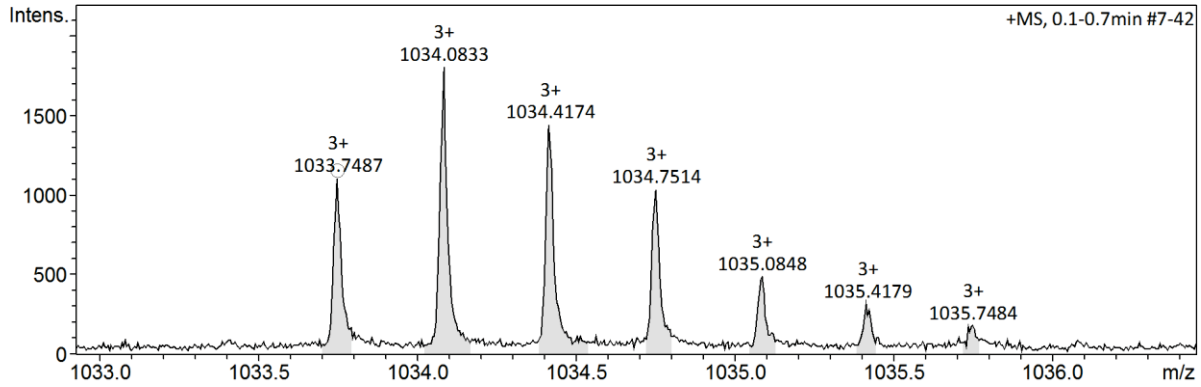

Figure S 59: HR-MS spectrum of compound **7b.**

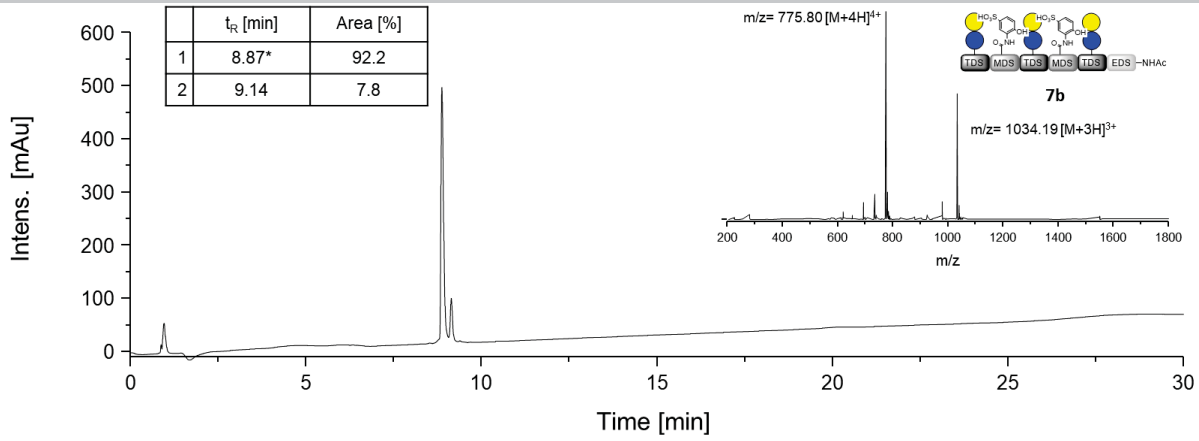

Figure S 60: RP-HPLC chromatogram and ESI$^+$-MS spectrum of compound **7b.** Retention time t_R [min] and area [%] of the peaks are given. ESI-MS spectrum of the main peak (*) is shown.

Lac(1,3,5)-Tyr(4-SO_3H)(2,4)-6–NH_2, **8a**

^{1}H NMR (600 MHz, Deuterium Oxide) δ [ppm]: 8.08 – 7.98 (m, 3H, triazole-C*H*), 7.29 – 7.20 (m, 6H, aromatic C*H*), 7.20 – 6.81 (m, 2H, aromatic C*H*), 5.75-5,72 (m, 3H, CH_{anomer}-Glc), 4.54 – 4.48 (m, 3H, CH_{anomer}-Gal), 4.07 – 3.56 (m, 52H, Tyr C*H,* C$H_{pyranose}$, C$H_{2\ pyranose,}$ O-CH_2-), 3.44- 3.20 (m, 32H, C$H_{pyranose,}$ C=ONH-C$H_{2,}$ Tyr CH_2), 3.13 –2.72 (m, 20H, CH=CH-CH_2-C$H_{2,}$ NHC=O-CH_2), 2.54 – 2.25 (m, 18H, NHC=O-CH_2).

^{13}C NMR (75 MHz, Deuterium Oxide) δ [ppm]: 175.09, 174.95, 174.71, 174.62, 173.28, 150.50, 147.35, 130.57, 122.74, 121.73, 103.19, 87.40, 77.88, 75.59, 74.84, 72.82, 72.21, 71.21, 69.81, 69.67, 69.08, 68.83, 66.57, 61.24, 60.12, 47.52, 45.29, 39.38, 39.10, 37.60, 37.19, 32.04, 31.14, 30.98, 30.44, 20.91.

HR MS (ESI$^+$) *m/z* calc. for $C_{103}H_{162}N_{23}O_{53}S_2$ $[M+3H]^{3+}$ 877.6704; found 877.6701.

Yield: 82 mg (31 %).

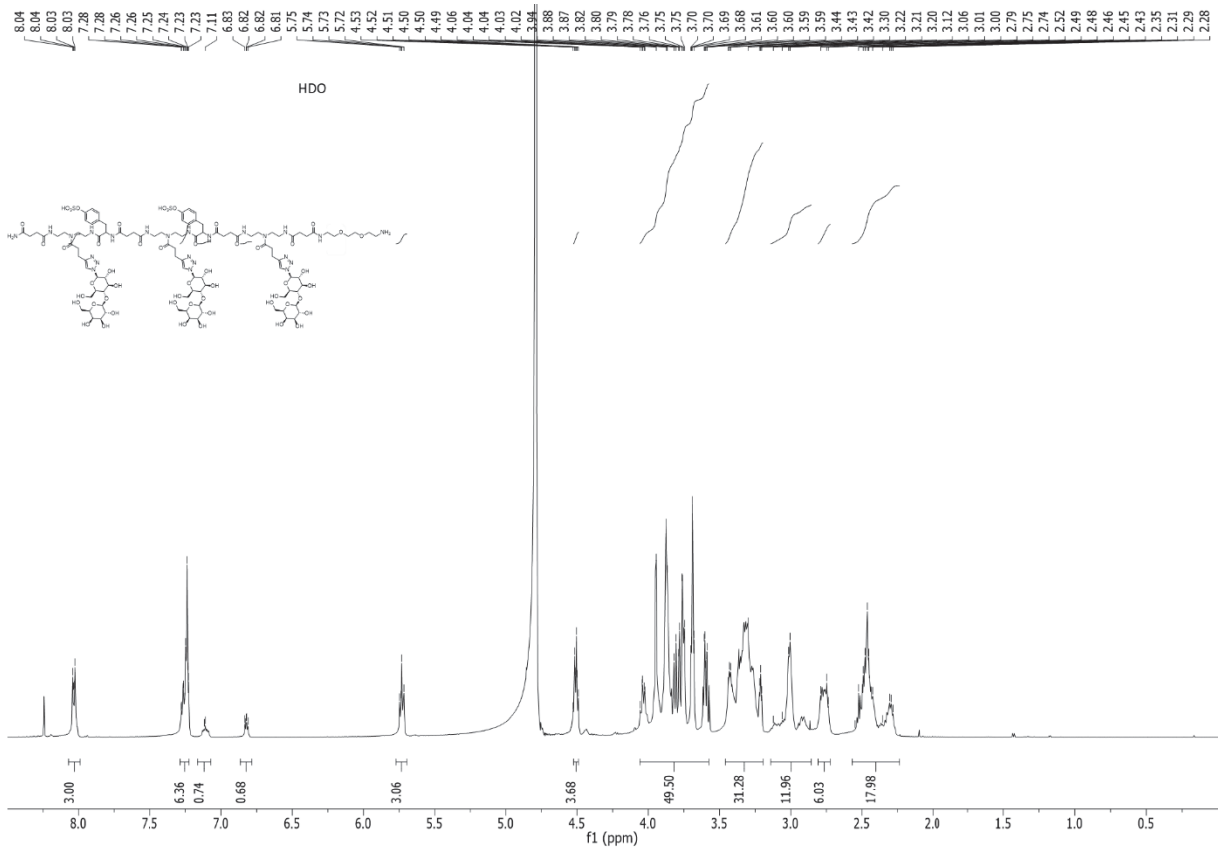

Figure S 61: ^{1}H-NMR spectrum of compound **8a**.

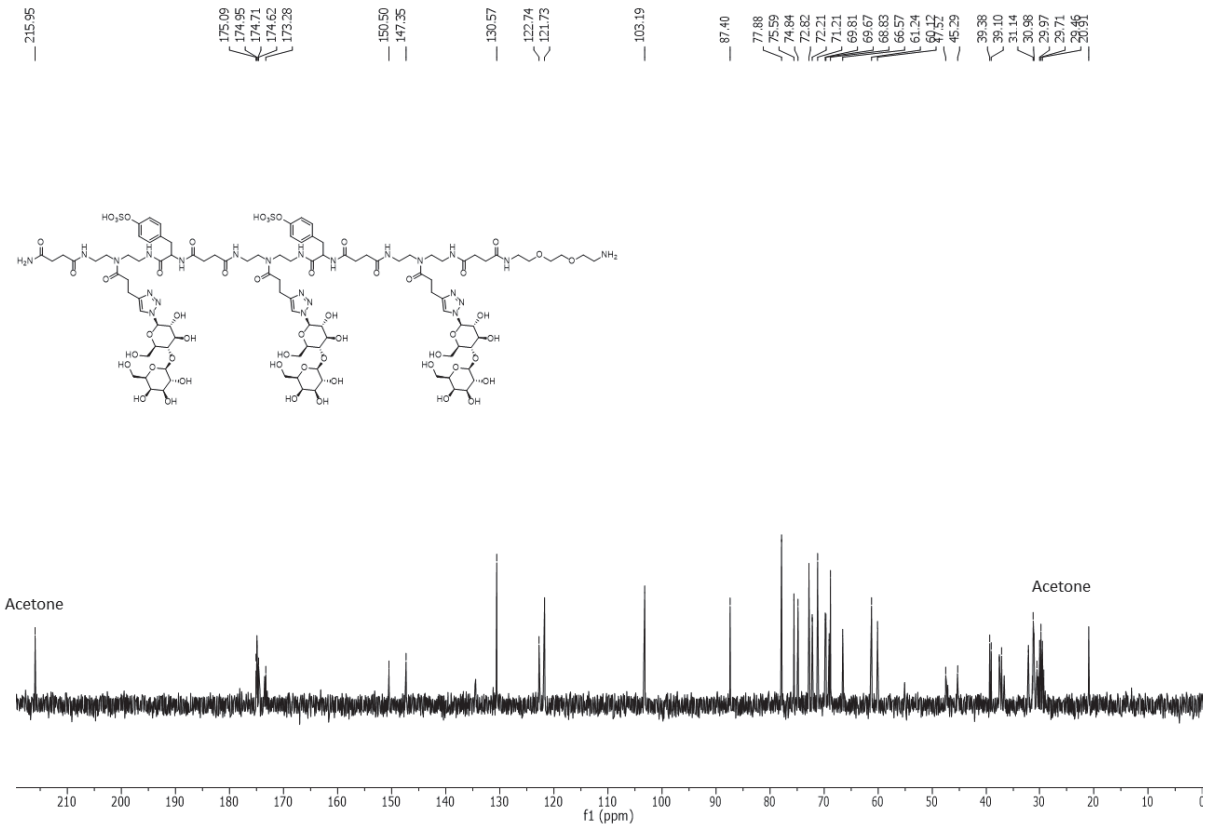

Figure S 62: ^{13}C-NMR spectrum of compound **8a.**

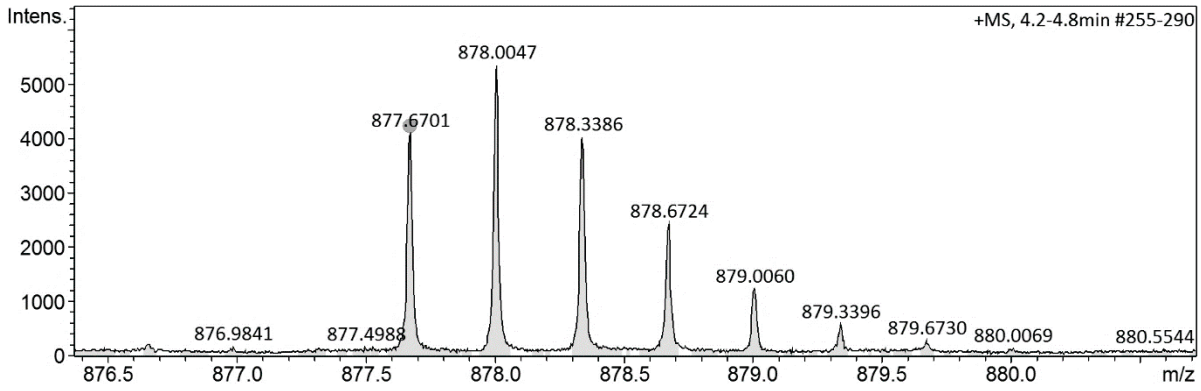

Figure S 63: HR-MS spectrum of compound **8a.**

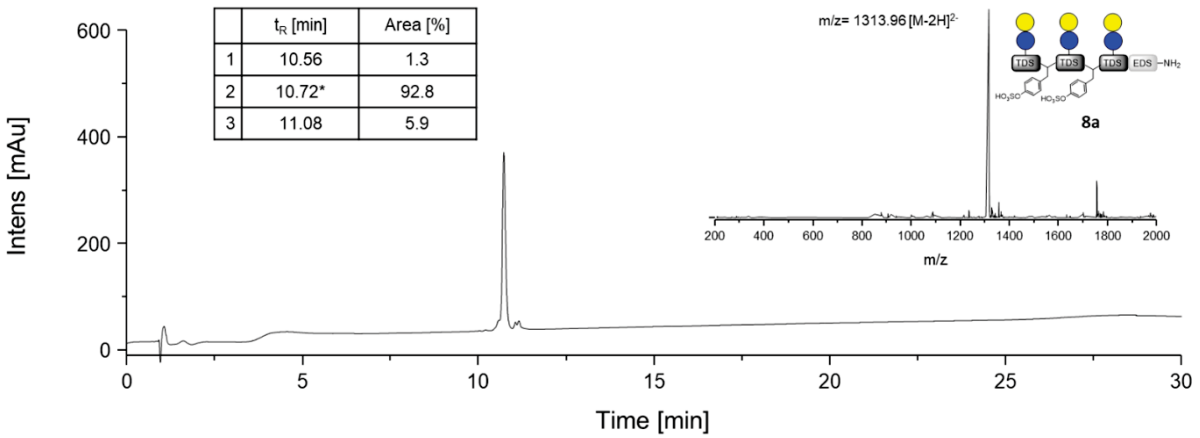

Figure S 64: RP-HPLC chromatogram and ESI$^+$-MS spectrum of compound **8a.** Retention time t_R [min] and area [%] of the peaks are given. ESI-MS spectrum of the main peak (*) is shown.

Lac(1,3,5)-Tyr(4-SO_3H)(2,4)-6–FITC, **8c**

^{1}H NMR (300 MHz, Deuterium Oxide) δ [ppm]: 8.07 – 7.89 (m, 4H, triazole-C*H*), 7.71 – 7.57 (m, 1H, FITC-C*H*) 7.31 – 7.14 (m, 8H, phenyl-C*H,* FITC-*CH*), 7.14 – 6.96 (m, 2H, FITC-*CH*), 6.86 – 6.58 (m, 2H, FITC-*CH*), 5.75-5,63 (m, 3H, CH_{anomer}-Glc), 4.53 – 4.49 (m, 3H, CH_{anomer}-Gal), 4.08 – 3.53 (m, 49H, Tyr C*H,* C$H_{pyranose}$, C$H_{2\ pyranose,}$ O-CH_2-), 3.49 – 3.15 (m, 29H, C$H_{pyranose,}$ C=ONH-C$H_{2,}$ Tyr CH_2), 3.11 – 2.83 (m, 10H, CH=CH-CH_2-C$H_{2,}$ NHC=O-CH_2), 2.82 – 2.65 (m, 6H, CH=CH-CH_2-CH_2), 2.55 – 2.23 (m, 16H, NHC=O-CH_2).

^{13}C NMR (75 MHz, Deuterium Oxide) δ [ppm]:175.11, 175.00, 174.97, 174.90, 174.90, 174.74, 174.65, 174.58, 173.52, 150.53, 147.36, 147.28, 131.07, 130.59, 122.76, 122.66, 122.63, 121.75, 113.48, 103.35, 103.23, 87.44, 77.91, 75.62, 74.87, 72.86, 72.25, 71.25, 69.84, 69.81, 69.71, 69.12, 68.87, 66.61, 61.27, 60.17, 55.24, 55.19, 55.18, 55.15, 47.56, 47.48, 47.42, 47.20, 47.17, 47.13, 45.44, 45.38, 45.34, 45.32, 45.28, 39.42, 39.25, 39.14, 37.63, 37.61, 37.58, 37.45, 37.42, 37.23, 36.77, 36.75, 36.57, 32.08, 32.06, 32.03, 31.33, 31.26, 31.18, 31.01, 30.92, 30.90, 30.60, 30.48, 20.95.

HR MS (ESI$^+$) *m/z* calc. for $C_{124}H_{173}N_{24}O_{58}S_3$ $[M+3H]^{3+}$ 1007.3490 found 1007.3480. Yield: 5 mg (32 %).

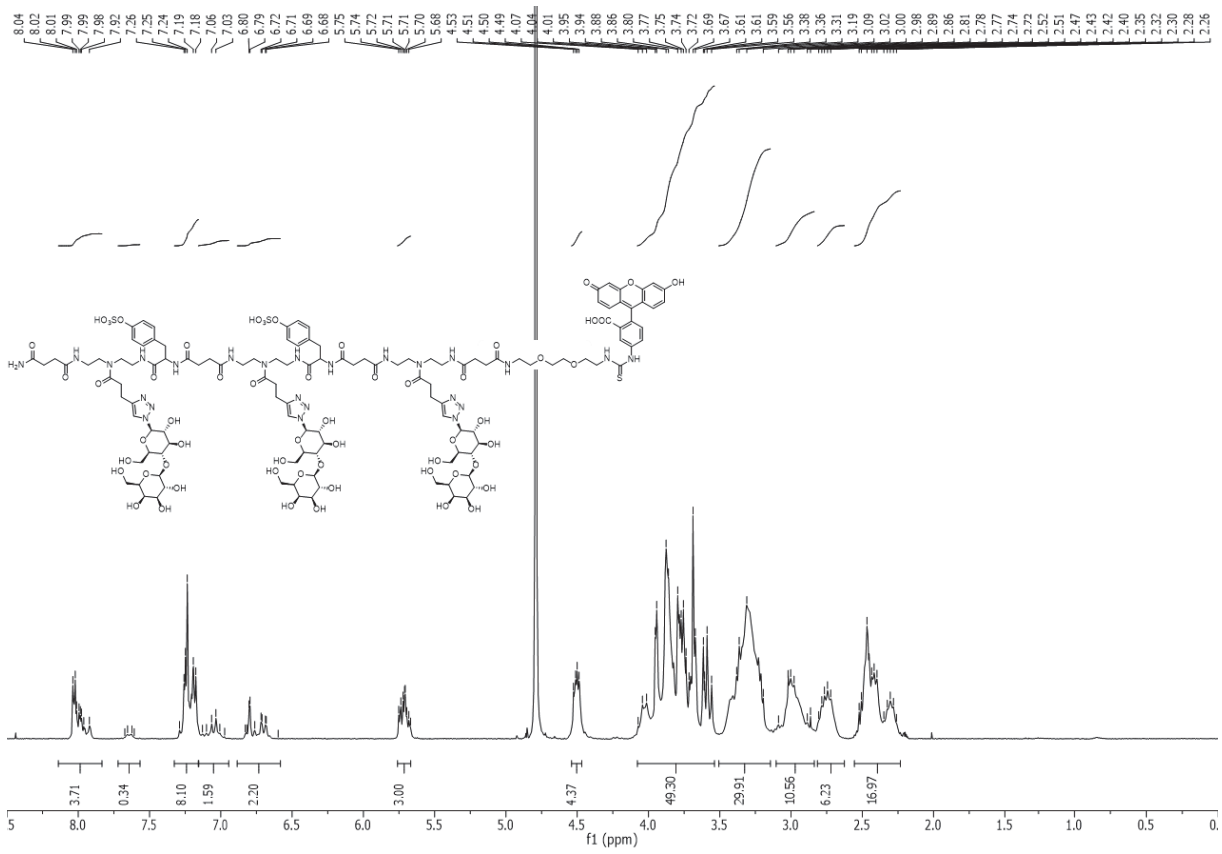

Figure S 65: ^{1}H-NMR spectrum of compound **8c.**

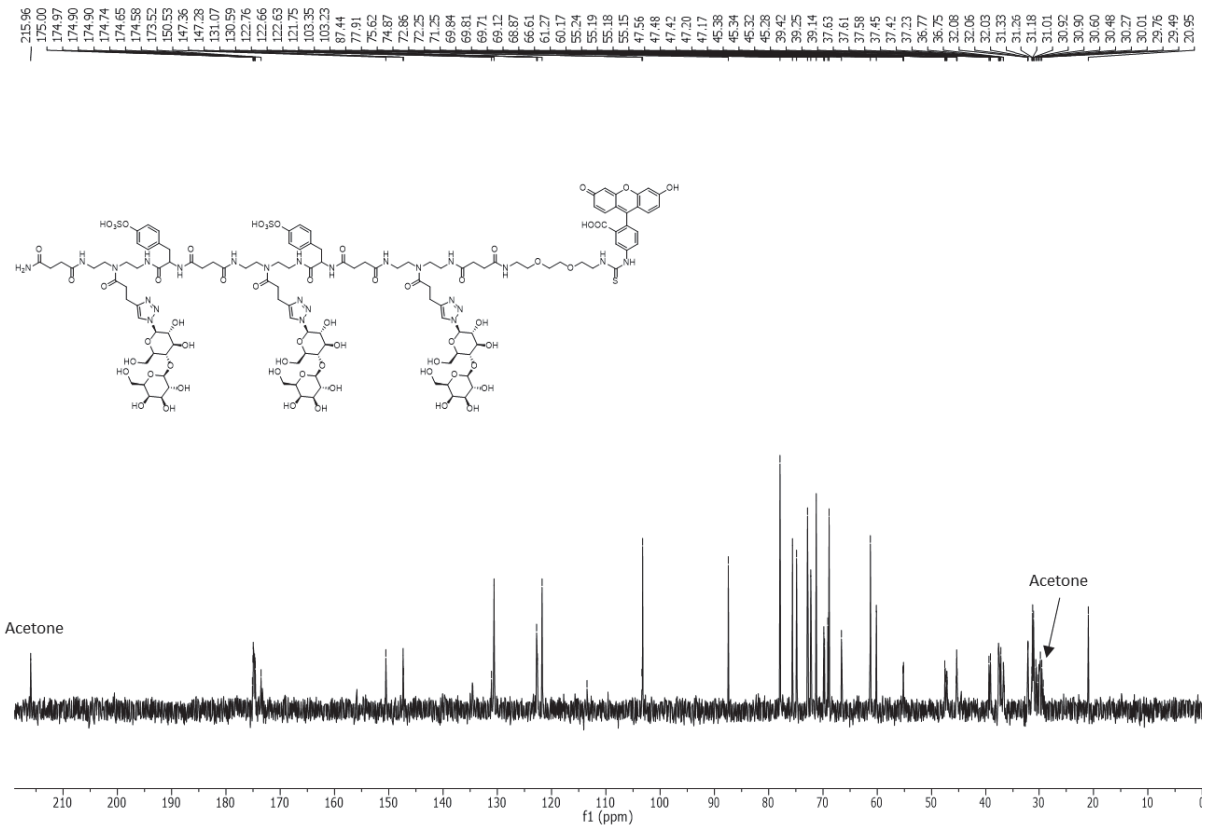

Figure S 66: ^{13}C-NMR spectrum of compound **8c**.

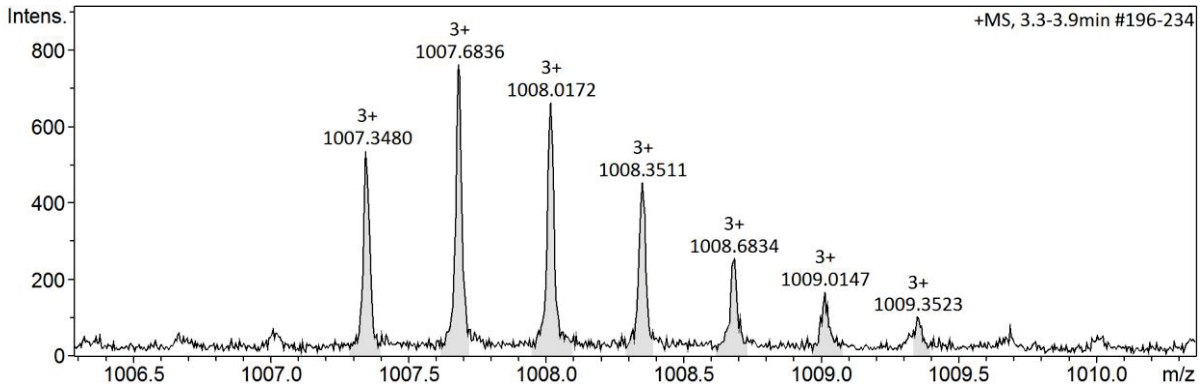

Figure S 67: HR-MS spectrum of compound **8c.**

Glc(1,3,5)-6–NH_2, **9a**

^{1}H-NMR (600 MHz, Deuterium Oxide) δ [ppm]: 8.46 (br s. 1 H. NH). 7.88 (m, 3H, triazole-C*H*), 4.80 (m, 3H, CH_{anomer}Glc), 4.64 (m, 6H, -N-N-CH_2-), 4.41 (d, ^{3}JHH = 7.9 Hz, 0.6H. CH_{anomer}Glc). 4.07 (m, 3H, O-CH_2-), 3.91 (m, 3H, O-CH_2-), 3.75 (dd, 3J = 5.6; 4.6 Hz, 2H, O-CH_2-), 3.69 (s, 4H, O-CH_2-), 3.65 (s, 8H, O-CH_2-, C$H_{pyranose}$), 3.63 – 3.28 (m, 59H, O-CH_2-, C=ONH-CH_2, C$H_{pyranose}$), 3.21 (m, 2H, CH_2-NH_2), 2.98 (m, 6H, CH=C-CH_2), 2.87– 2.75 (m, 9H, C$H_{pyranose}$,, CH=C-CH_2-CH_2), 2.48 (m, 24H, NHC=O-CH_2).

^{13}C NMR (75 MHz, Deuterium Oxide) δ [ppm]: 177.79, 175.18, 175.04, 175.01, 174.94, 174.85, 171.24, 147.07, 124.31, 102.74, 98.20, 76.20, 75.89, 73.23, 73.18, 72.04, 71.42, 69.85, 69.81, 69.68, 69.32, 69.10, 68.42, 66.73, 66.12, 60.39, 50.23, 47.39, 45.27, 39.36, 39.16, 39.09, 37.57, 37.15, 32.23, 31.28, 31.15, 31.11, 31.03, 30.52, 20.90.

HR MS (ESI$^+$) *m/z* calc. for $C_{93}H_{162}N_{25}O_{39}$ $[M+3H]^{3+}$ 751.04. found 751.25. Yield: 86 mg (38 %).

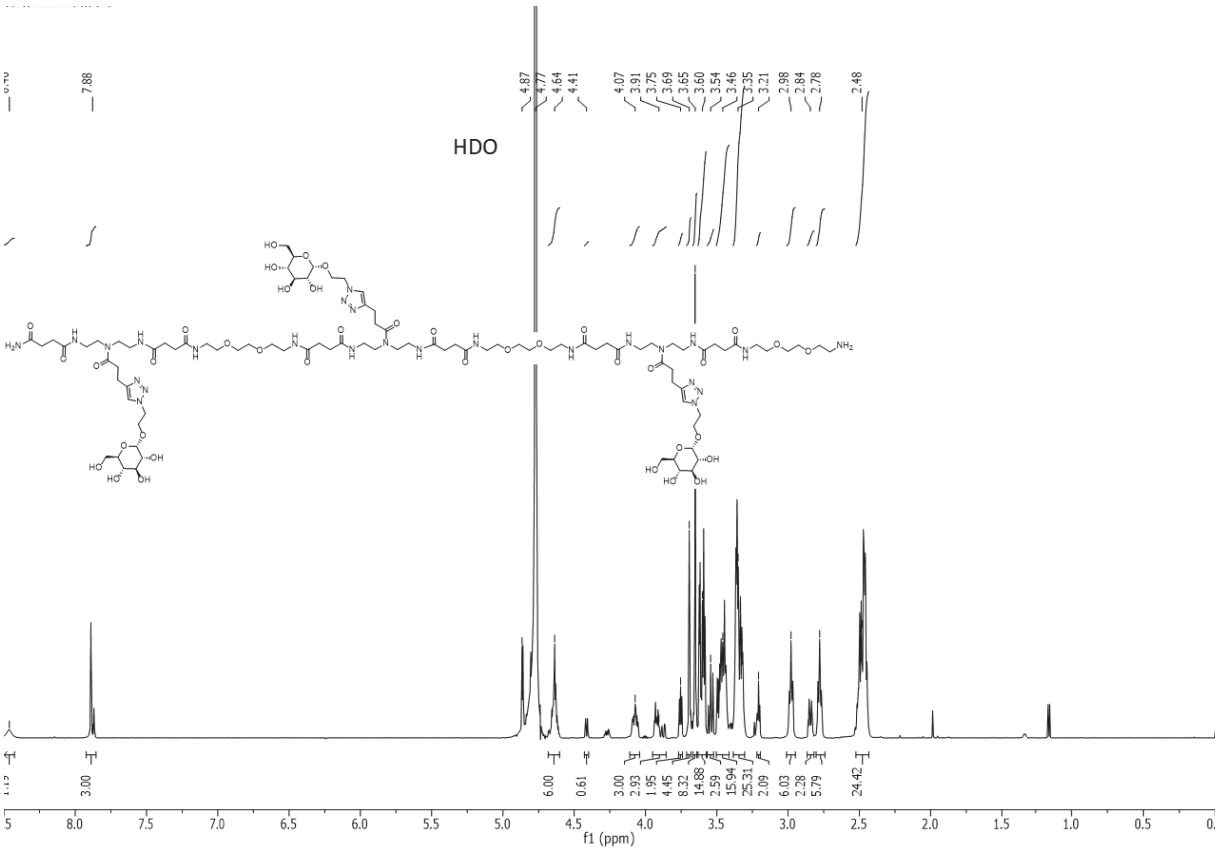

Figure S 68: ^{1}H-NMR spectrum of compound **9a.**

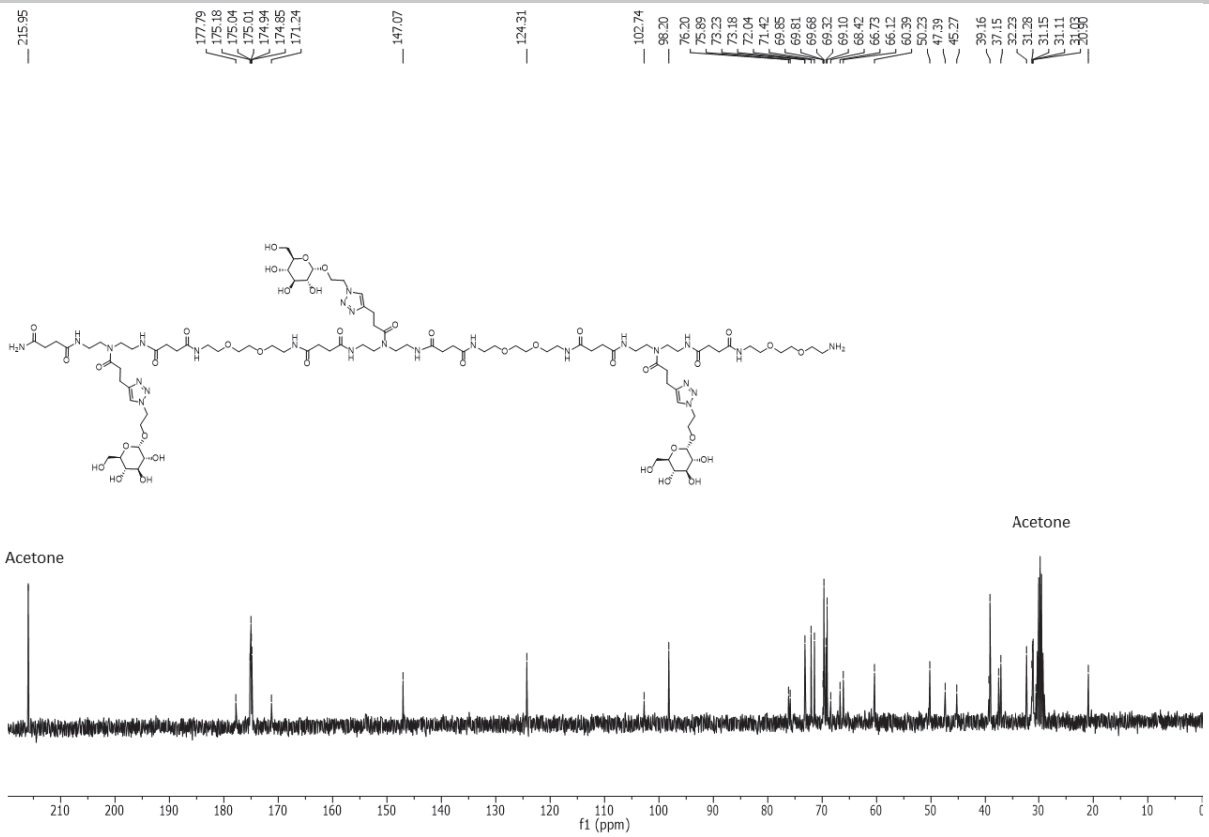

Figure S 69: ^{13}C-NMR spectrum of compound **9a**.

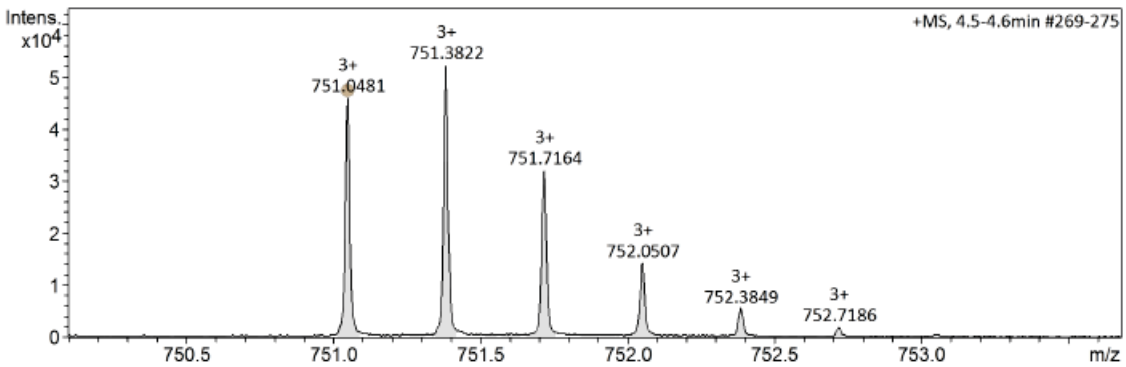

Figure S 70: HR-MS spectrum of compound **9a**.

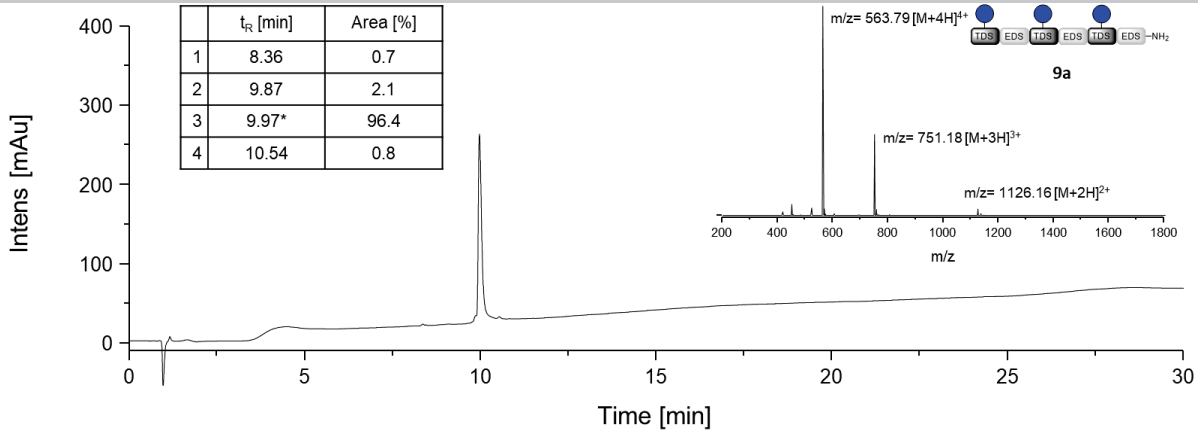

	t_R [min]	Area [%]
1	8.36	0.7
2	9.87	2.1
3	9.97*	96.4
4	10.54	0.8

Figure S 71: RP-HPLC chromatogram and ESI$^+$-MS spectrum of compound **9a.** Retention time t_R [min] and area [%] of the peaks are given. ESI-MS spectrum of the main peak (*) is shown.

Glc(1,3,5)-6–Ac, **9b**

^{1}H NMR (300 MHz, Deuterium Oxide) δ [ppm]: 7.91 (s, 3H, triazole-CH), 4.88 (d, J = 3.4 Hz, 3H, C*H*$_{anomer}$Glc), 4.71 – 4.61 (m, 6H, -N-N-CH2-), 4.15 – 4.03 (m, 3H, C*H*$_{pyranose}$), 3.99 – 3.89 (m, 3H, C*H*$_{pyranose}$), 3.74 – 3.55 (m, 35H, CH-Glc, -O-C*H*$_2$), 3.54 – 3.43 (m, 18H, -O-C*H*$_2$, C*H*$_{pyranose}$), 3.42 – 3.30 (m, 30H, -NH-C*H*$_2$-), 3.00 (t, J = 7.3 Hz, 6H, CH=C-C*H*$_2$), 2.91 – 2.74 (m, 9H, C*H*$_{pyranose}$, NH-C=O-C*H*$_2$-), 2.58 – 2.42 (m, 28H, NH-C=O-C*H*$_2$-), 2.00 (s, 3H, C*H*$_3$).

^{13}C NMR (75 MHz, Deuterium Oxide) δ [ppm]: 173.96, 173.82, 173.78, 173.72, 173.63, 145.83, 123.07, 96.96, 71.94, 70.80, 70.19, 68.44, 68.08, 67.86, 67.80, 64.89, 59.14, 48.99, 46.13, 44.05, 37.92, 36.34, 35.91, 31.00, 30.05, 29.88, 29.80, 20.85, 19.66.

HR MS (ESI^{+}) *m/z* calc. for $C_{95}H_{164}N_{25}O_{40}$ $[M+3H]^{3+}$ 765.0517; found 765.0527. Yield: 110 mg (48 %).

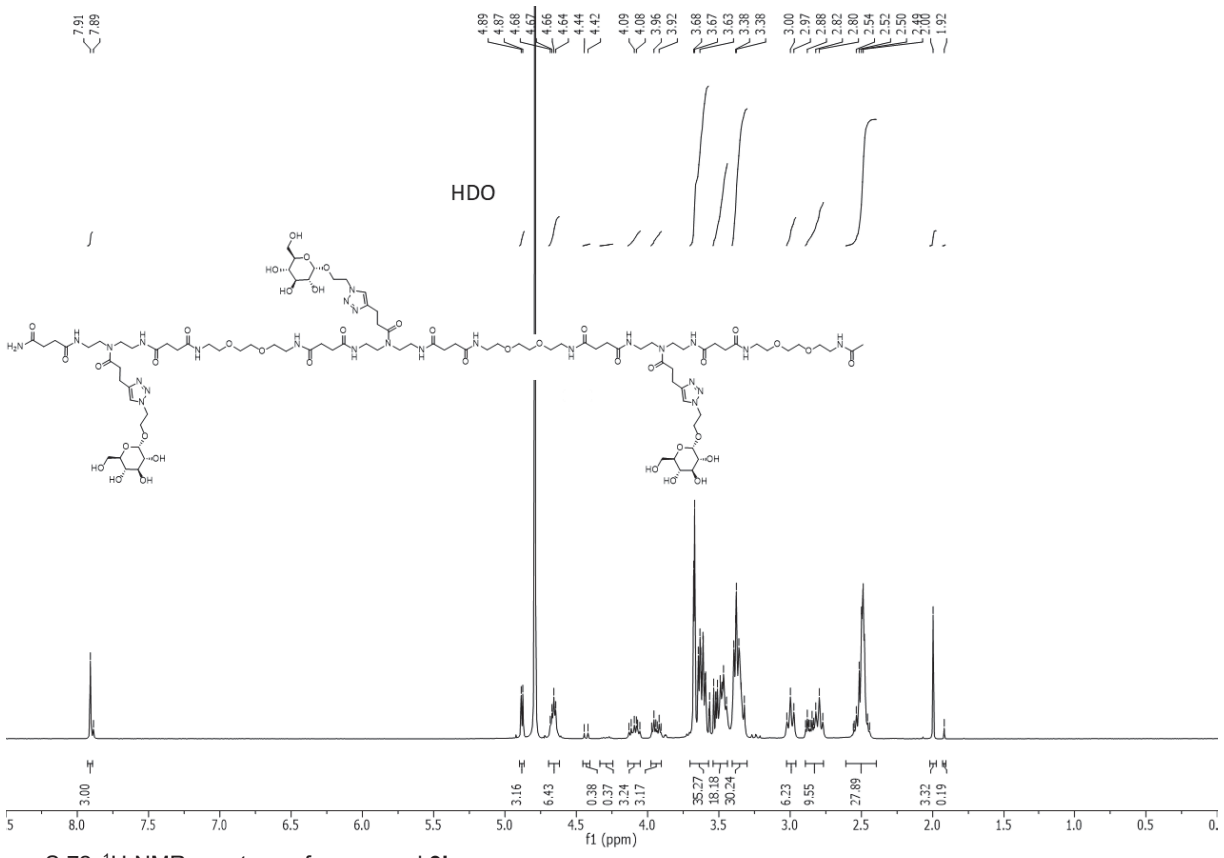

Figure S 72: ^{1}H-NMR spectrum of compound **9b.**

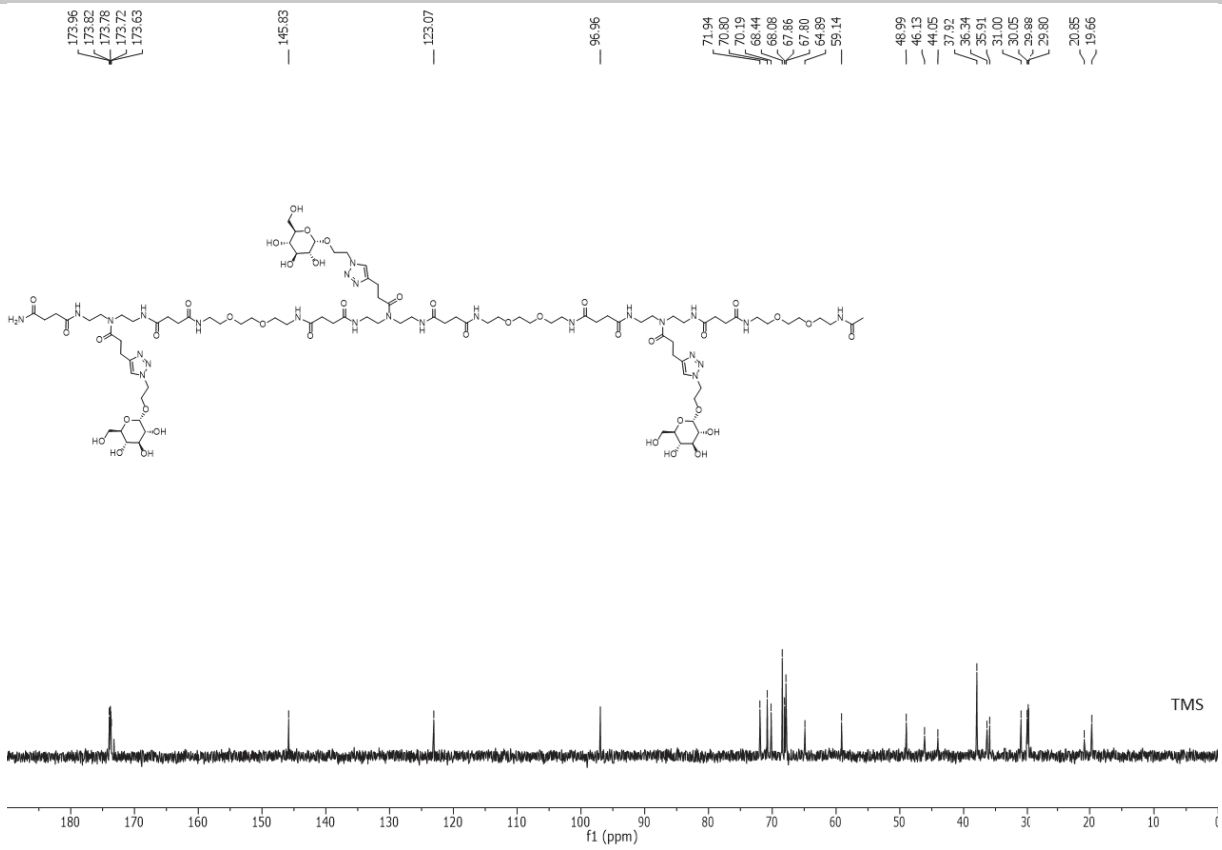

Figure S 73: ^{13}C-NMR spectrum of compound **9b**.

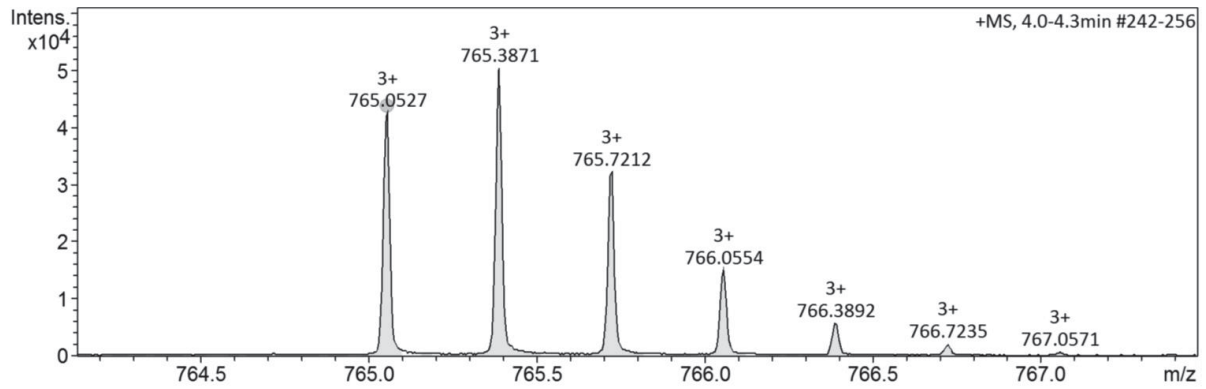

Figure S 74: HR-MS spectrum of compound **9b.**

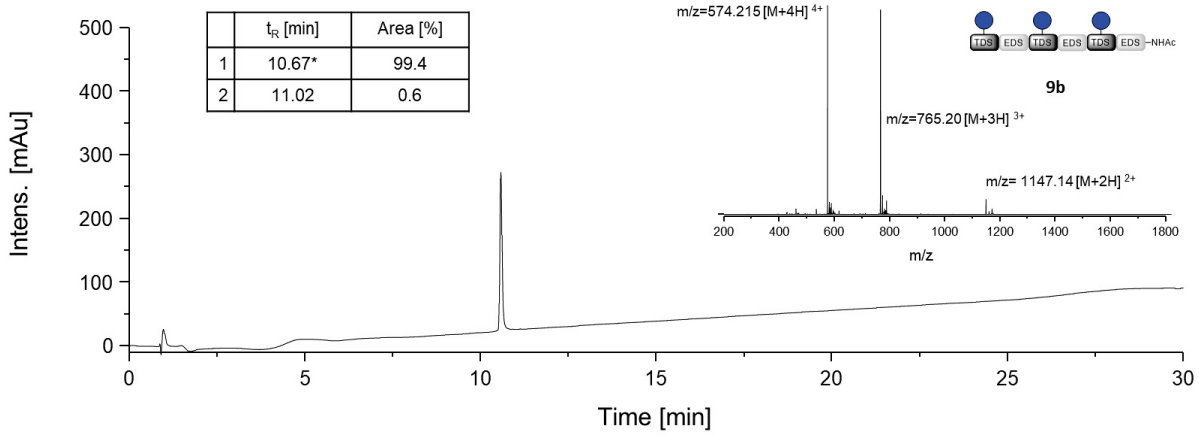

Figure S 75: RP-HPLC chromatogram and ESI$^+$-MS spectrum of compound **9b.** Retention time t_R [min] and area [%] of the peaks are given. ESI-MS spectrum of the main peak (*) is shown.

Glc(1,3,5)-6–FITC, **9c**

^{1}H NMR (300 MHz, Deuterium Oxide) δ [ppm]: 8.02 (s, 1H, FITC-C*H*), 7.91 – 7.76 (m, 3H, triazole-C*H*), 7.64 (d, *J* = 7.1 Hz, 1H, FITC-C*H*), 7.01 (d, *J* = 7.5 Hz, 1H, FITC-C*H*), 6.80 – 6.64 (m, 4H, FITC-C*H*), 6.57 (d, *J* = 8.7 Hz, 2H, FITC-C*H*), 4.88 – 4.84 (m, 3H, CH_{anomer}Glc), 4.66 – 4.52 (m, 6H, -N-N-CH_2-), 4.13 – 3.96 (m, 3H, C$H_{pyranose}$), 3.96 – 3.82 (m, 3H, C$H_{pyranose}$), 3.79 – 3.48 (m, 38H, C$H_{pyranose}$, CH_2 $_{pyranose,}$ O-CH_2-), 3.48 – 3.22 (m, 40H, C$H_{pyranose,}$ C=ONH-CH_2), 3.02 – 2.82 (m, 8H, C$H_{pyranose,}$ CH=CH-CH_2), 2.80 – 2.64 (m, 6H, CH=CH-CH$_2$-CH_2), 2.54 – 2.36 (m, 24H, NHC=O-CH_2).

^{13}C NMR (75 MHz, Deuterium Oxide) δ [ppm]: 175.10, 174.79, 174.69, 141.29, 131.57, 124.21, 98.20, 73.18, 72.04, 71.43, 69.67, 69.32, 69.09, 66.11, 60.38, 47.39, 46.04, 45.32, 44.48, 39.15, 37.58, 37.15, 37.12, 31.26, 31.11, 31.04, 20.90.

HR MS (ESI^{+}) *m/z* calc. for $C_{114}H_{173}N_{26}O_{44}S$ $[M+3H]^{3+}$ 880.7268; found 880.7260. Yield: 15 mg (42 %).

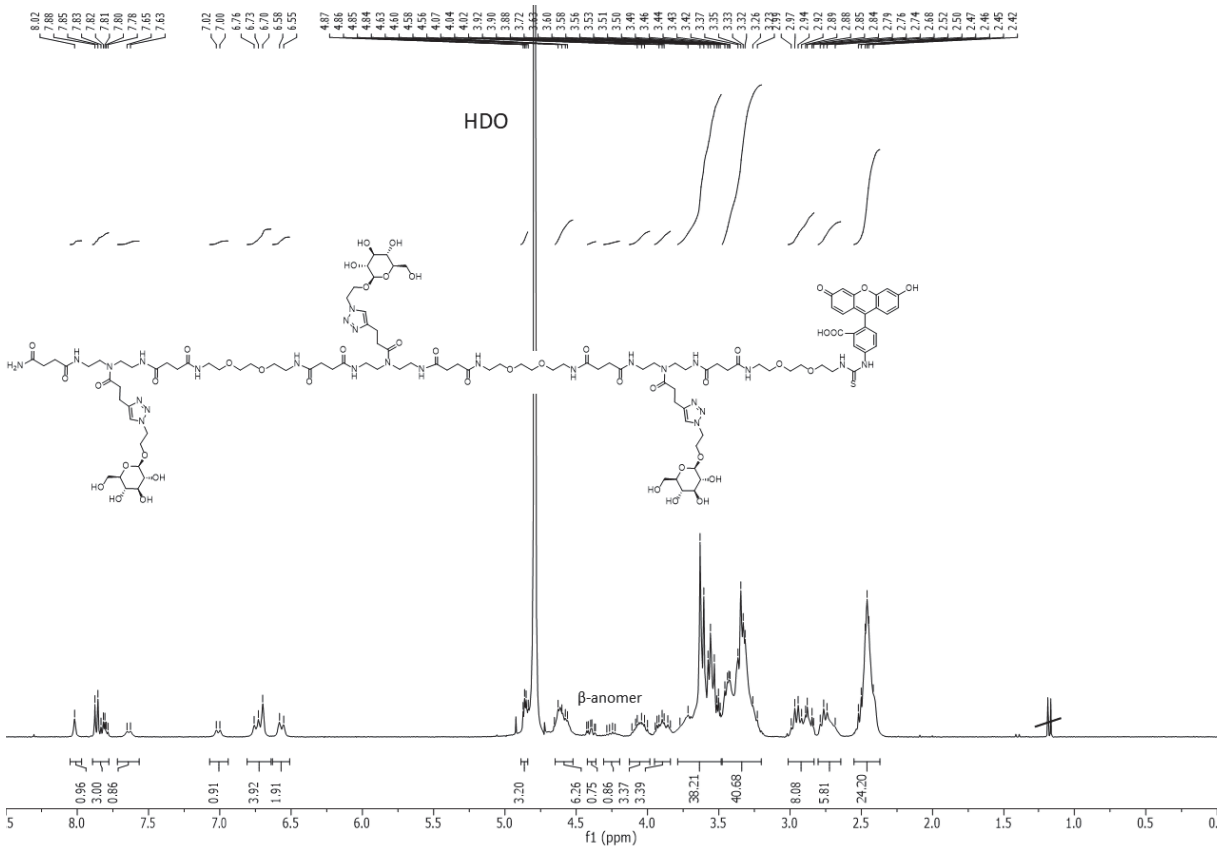

Figure S 76: ^{1}H-NMR spectrum of compound **9c**.

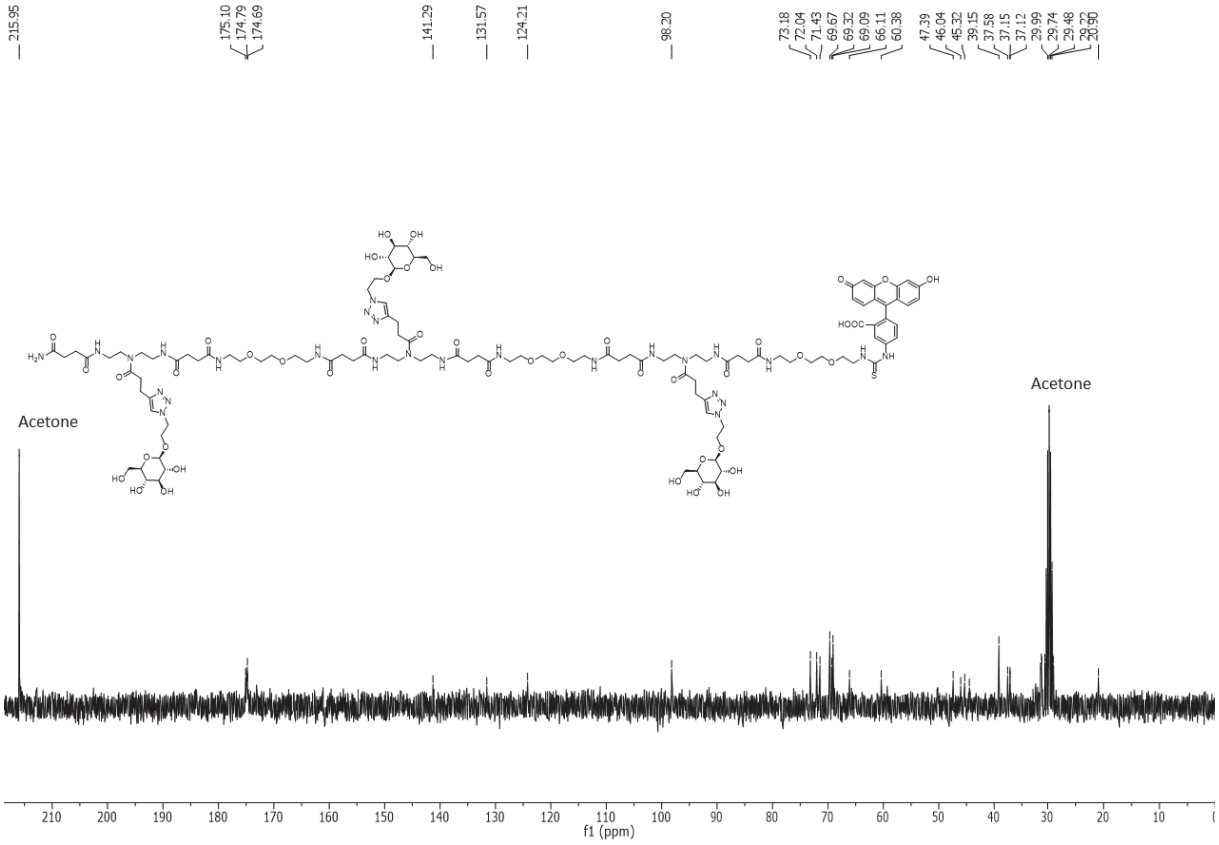

Figure S 77: ^{13}C-NMR spectrum of compound **9c**.

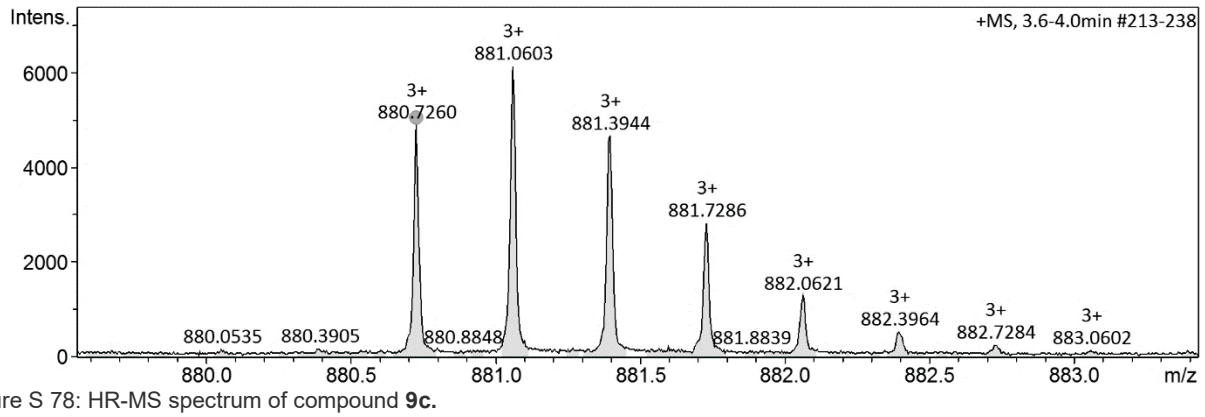

Figure S 78: HR-MS spectrum of compound **9c.**

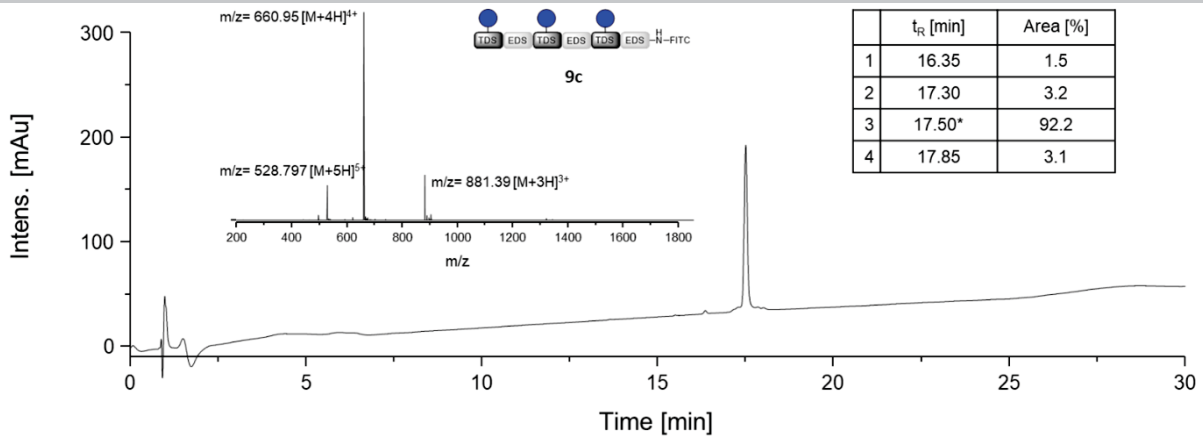

	t_R [min]	Area [%]
1	16.35	1.5
2	17.30	3.2
3	17.50*	92.2
4	17.85	3.1

Figure S 79: RP-HPLC chromatogram and ESI$^+$-MS spectrum of compound **9c.** Retention time t_R [min] and area [%] of the peaks are given. ESI-MS spectrum of the main peak (*) is shown.

Glc(1,3,5)-Bz(2,4)-6–Ac, **10b**

^{1}H NMR (300 MHz, Deuterium Oxide) δ [ppm]: 7.94 – 7.82 (m, 3H, triazole-CH), 7.44 – 7.24 (m, 10H, aromatic-C*H*), 4.90 – 4.85 (m, 3H, CH_{anomer}Glc), 4.68 – 4.56 (m, 6H, -N-N-C*H2*-), 4.35 (s, 4H, aromatic CH_2), 4.14 – 4.01 (m, 3H, C$H_{pyranose}$), 3.97 – 3.84 (m, 3H, C$H_{pyranose}$), 3.68 – 3.57 (m, 15H, C$H_{pyranose}$, O-CH_2-), 3.55 – 3.26 (m, 53H, C$H_{pyranose}$ C=ONH-CH_2), 3.04 – 2.92 (m, 6H, CH=C-CH_2), 2.90 – 2.81 (m, 3H, C$H_{pyranose}$), 2.81 – 2.66 (m, 10H, NH-C=O-CH_2-), 2.62 – 2.38 (m, 28H, NH-C=O-CH_2-), 1.99 (s, 3H, -CH_3).

^{13}C NMR (126 MHz, Deuterium Oxide) δ [ppm]: 173.97, 173.91, 173.79, 146.00, 137.36, 127.89, 126.52, 126.32, 123.14, 97.20, 72.16, 71.02, 70.39, 68.61, 68.36, 68.01, 67.97, 65.08, 59.42, 49.13, 46.33, 44.28, 42.10, 38.16, 38.11, 36.56, 36.13, 31.15, 30.19, 30.12, 30.07, 30.03, 29.92, 27.35, 21.04, 19.85, 0.00.

HR MS (ESI$^+$) *m/z* calc. for $C_{113}H_{180}N_{29}O_{40}$ $[M+3H]^{3+}$ 861.0975; found 861.0978. Yield: 81 mg (31 %).

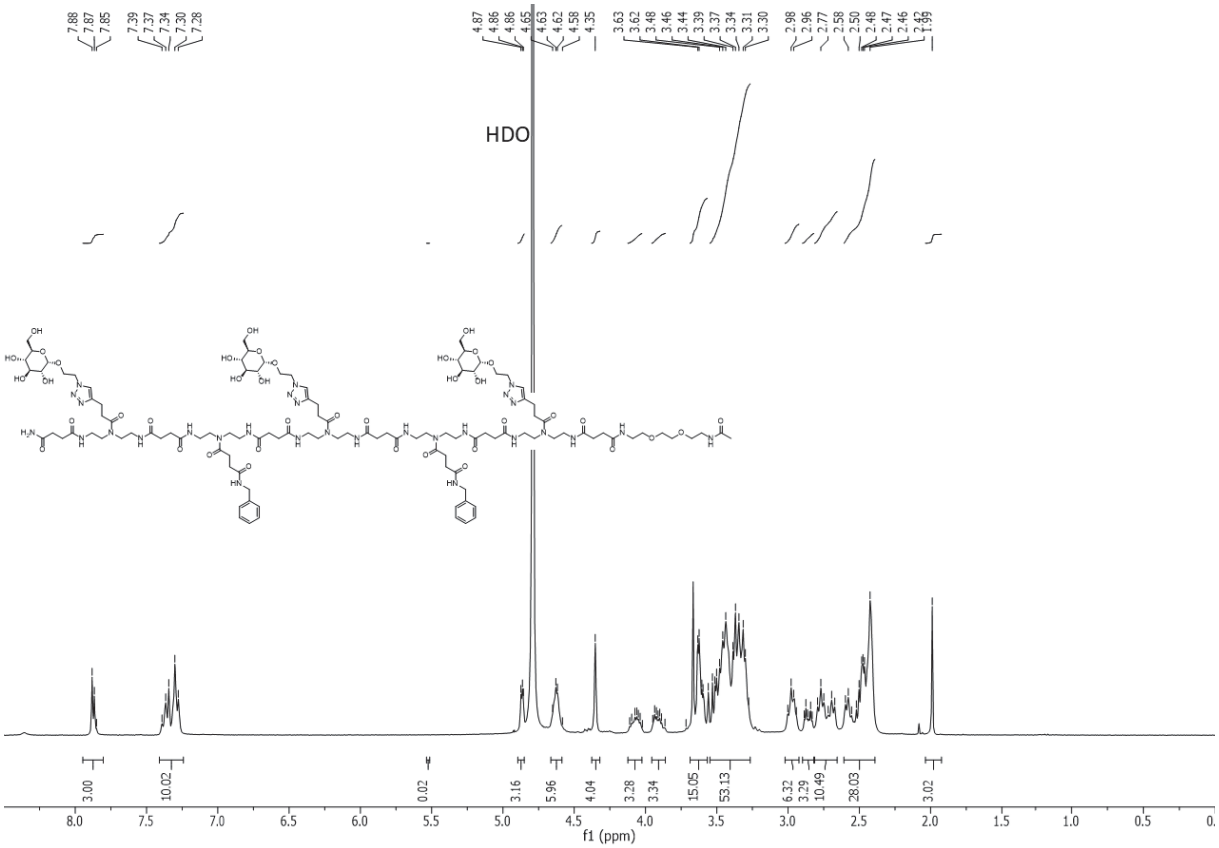

Figure S 80: ^{1}H-NMR spectrum of compound **10b.**

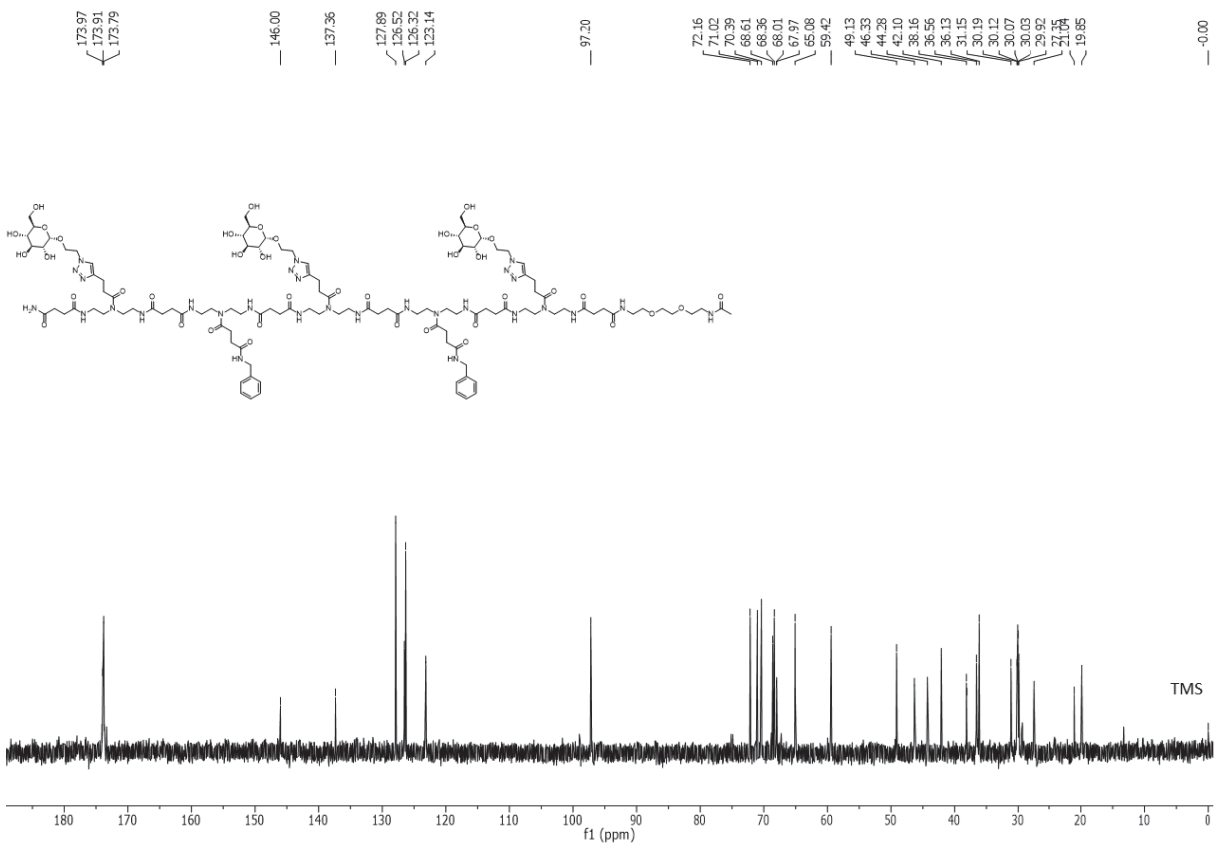

Figure S 81: ^{13}C-NMR spectrum of compound **10b.**

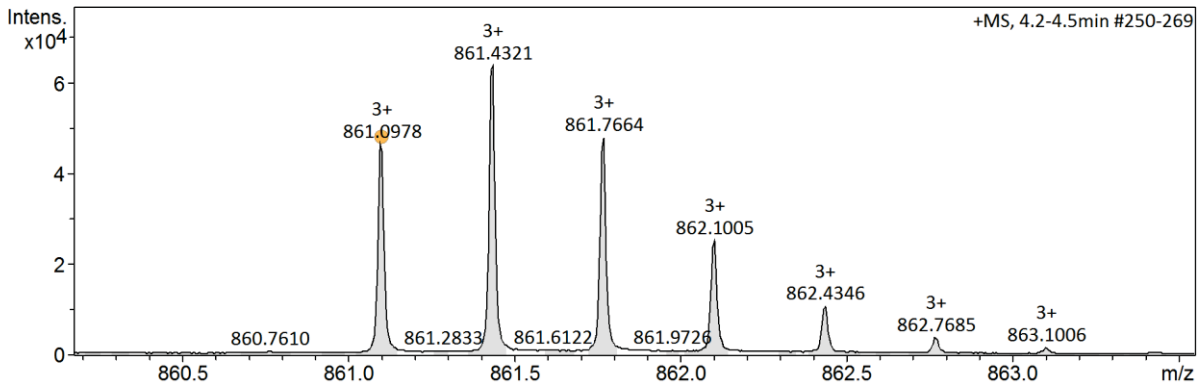

Figure S 82: HR-MS spectrum of compound **10b.**

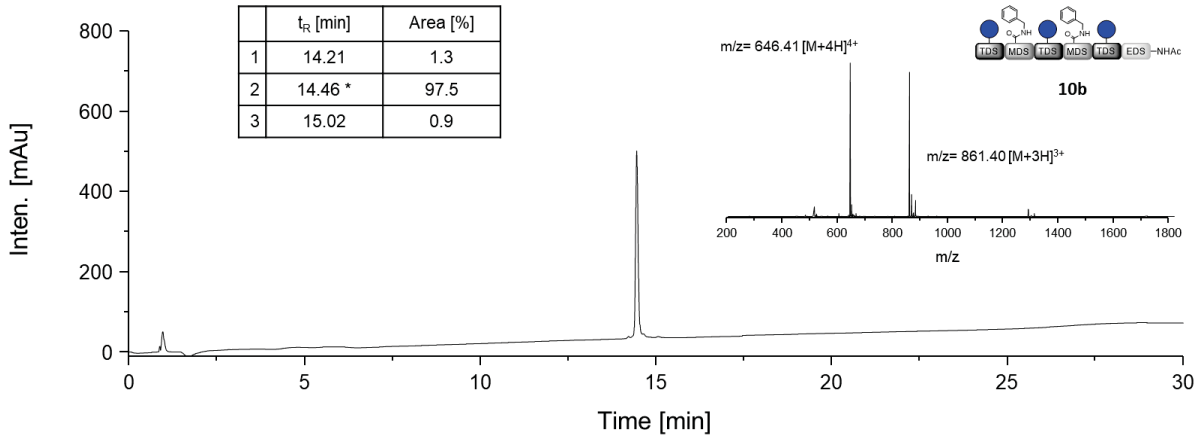

	t_R [min]	Area [%]
1	14.21	1.3
2	14.46 *	97.5
3	15.02	0.9

Figure S 83: RP-HPLC chromatogram and ESI$^+$-MS spectrum of compound **10b.** Retention time t_R [min] and area [%] of the peaks are given. ESI-MS spectrum of the main peak (*) is shown.

Glc(1,3,5)-*p*NH_2Ph(2,4)-6–Ac, **11b**

^{1}H NMR (300 MHz, Deuterium Oxide) δ [ppm]: 7.95 – 7.80 (m, 3H, triazole-CH), 7.22 (d, J = 8.5 Hz, 4H, aromatic-C*H*), 6.85 (d, J = 8.2 Hz, 4H, aromatic-C*H*), 4.89 – 4.84 (m, 3H, CH_{anomer}Glc), 4.69 – 4.56 (m, 6H, -N-N-CH_2-), 4.13 – 4.00 (m, 3H, C$H_{pyranose}$), 3.96 – 3.85 (m, 3H, C$H_{pyranose}$), 3.70 – 3.58 (m, 14H, C$H_{pyranose}$, O-CH_2-), 3.58 – 3.25 (m, 53H, C$H_{pyranose}$ C=ONH-CH_2), 3.02 – 2.91 (m, 6H, CH=C-CH_2), 2.89 – 2.81 (m, 3H, C$H_{pyranose}$), 2.81 – 2.61 (m, 14H, -N-C=O-CH_2-), 2.56 – 2.35 (m, 24H, NH-C=O-CH_2-), 1.99 (s, 3H, -CH_3).

^{13}C NMR (75 MHz, Deuterium Oxide) δ [ppm]: 175.53, 175.34, 175.27, 175.18, 174.77, 147.64, 123.13, 103.49, 87.75, 78.24, 77.91, 75.99, 75.15, 73.09, 72.53, 71.53, 69.99, 69.41, 69.36, 69.15, 66.58, 61.65, 60.33, 47.67, 45.54, 39.54, 39.48, 37.87, 37.45, 32.41, 31.59, 31.42, 30.80, 22.40, 21.24, 14.66.

HR MS (ESI$^+$) *m/z* calc. for $C_{111}H_{178}N_{31}O_{40}$ $[M+3H]^{3+}$ 861.7610; found 861.7597. Yield: 84 mg (33 %).

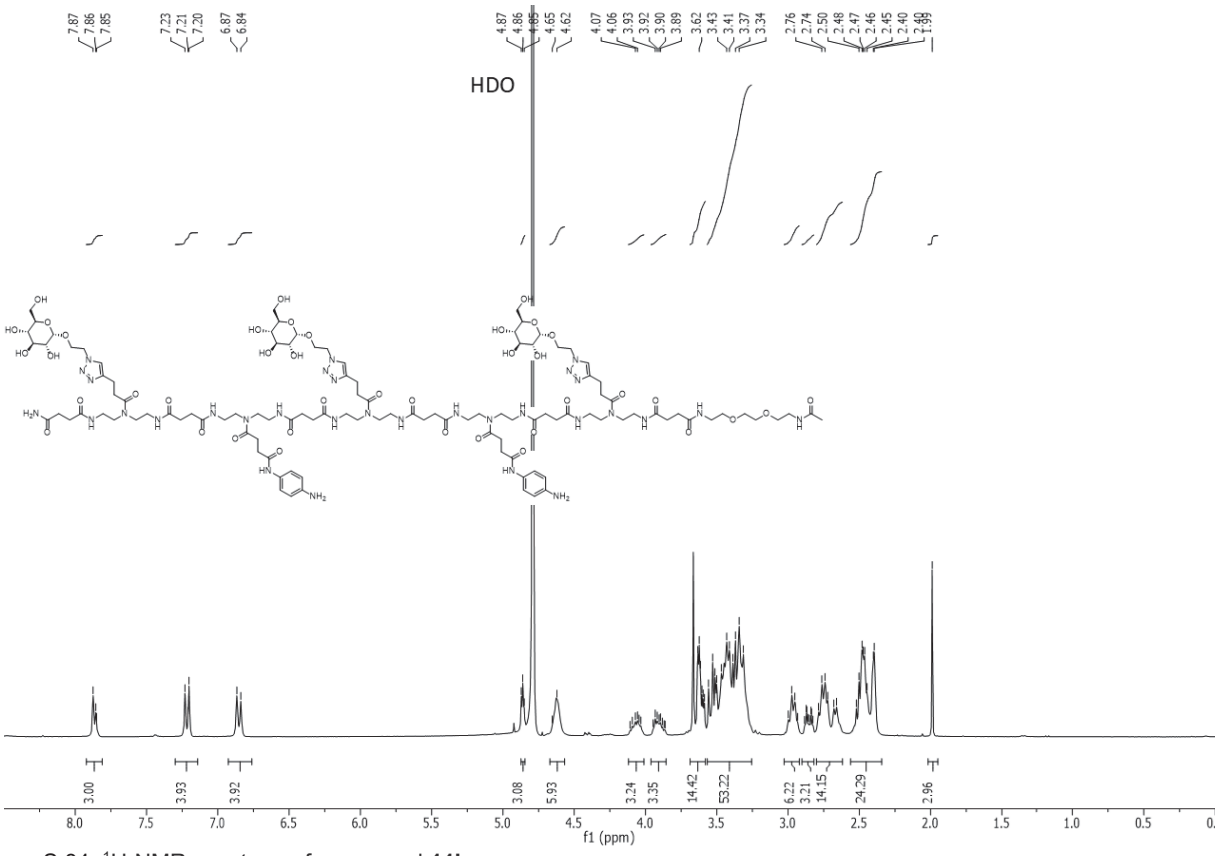

Figure S 84: ^{1}H-NMR spectrum of compound **11b.**

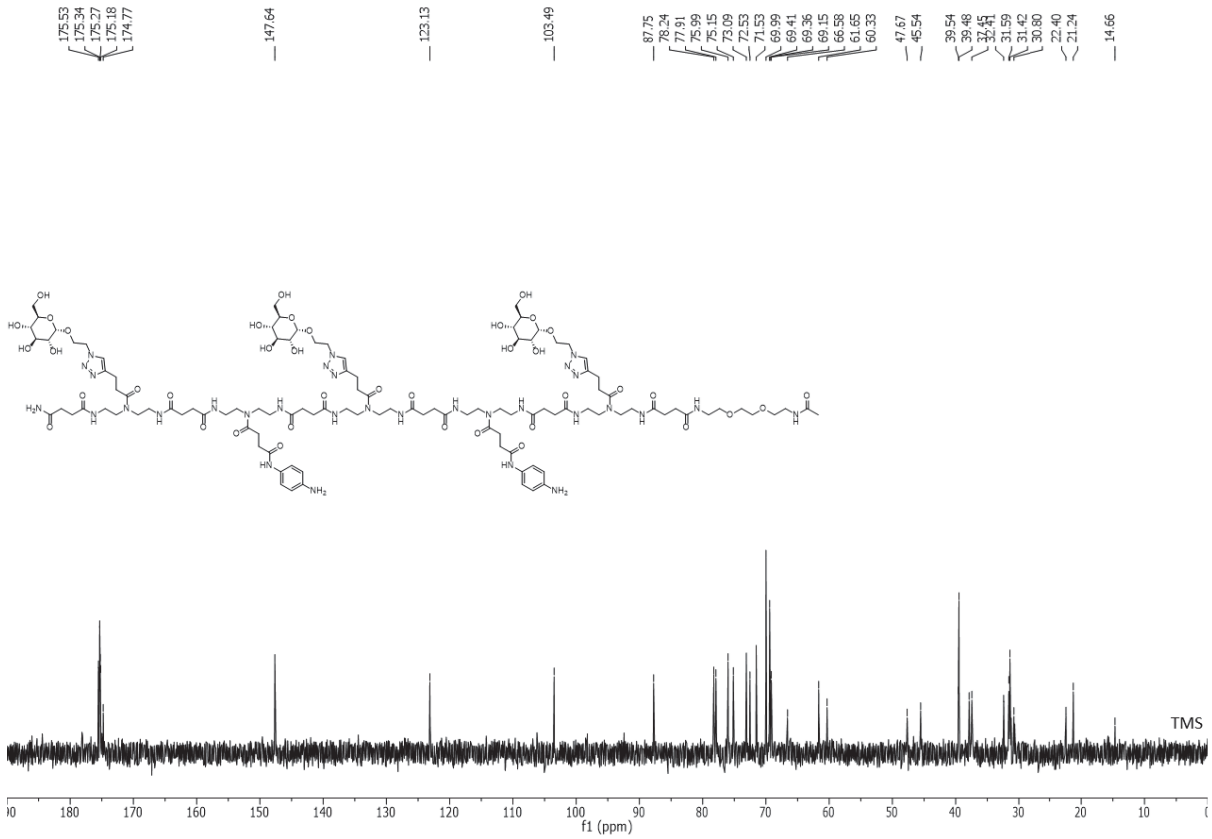

Figure S 85: ^{13}C-NMR spectrum of compound **11b.**

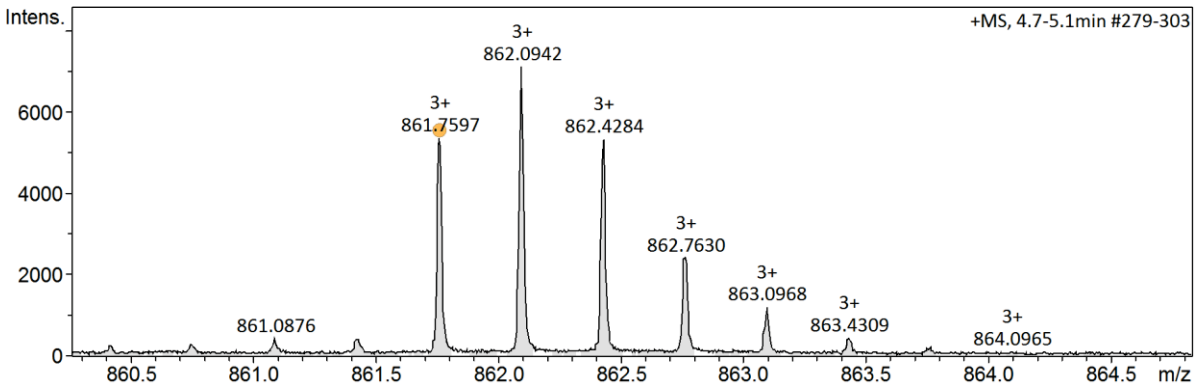

Figure S 86: HR-MS spectrum of compound **11b.**

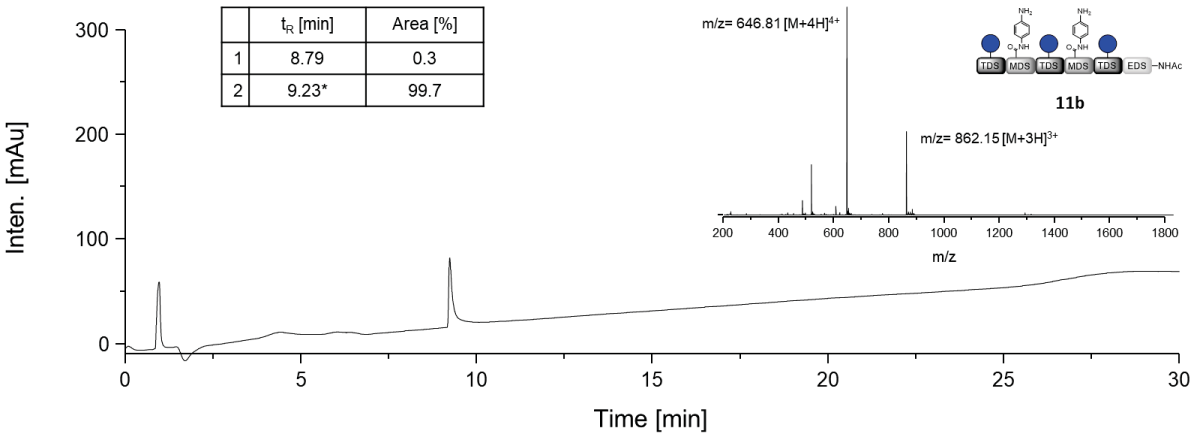

Figure S 87: RP-HPLC chromatogram and ESI$^+$-MS spectrum of compound **11b.** Retention time t_R [min] and area [%] of the peaks are given. ESI-MS spectrum of the main peak (*) is shown.

Glc(1,3,5)-*p*SO_3H Ph(2,4)-6–NH_2, **12a**

^{1}H NMR (300 MHz Deuterium Oxide) δ [ppm]: 8.26 (br s, 1H, NH), 7.93 – 7.84 (m, 3H, triazole-C*H*), 7.75 (d, *J* = 8.6 Hz, 4H, aromatic-C*H*), 7.56 (d, *J* = 8.6 Hz, 4H, aromatic-C*H*), 4.89 – 4.84 (m, 3H, CH_{anomer}Glc), 4.69 – 4.55 (m, 6H,-N-N-CH_2), 4.12 – 4.00 (m, 3H, C$H_{pyranose}$), 3.97 – 3.83 (m, 3H, C$H_{pyranose}$), 3.69 – 3.52 (m, 23H, C$H_{pyranose}$, CH_2 $_{pyranose,}$ O-CH_2-), 3.50 – 3.22 (m, 47H, C$H_{pyranose}$, CH_2 $_{pyranose,}$ C=ONH-CH_2, CH_2-NH_2), 3.03 – 2.91 (m, 6H, CH=CH-CH_2), 2.91 – 2.82 (m, 3H, C$H_{pyranose}$), 2.81 – 2.64 (m, 16H, CH=CH-CH_2-CH_2, NH-C=O-CH_2), 2.57 – 2.32 (m, 24H, NH-C=O-CH_2).

^{13}C NMR (75 MHz, Deuterium Oxide) δ [ppm]: 174.68, 140.06, 138.34, 126.46, 120.30, 97.90, 72.89, 71.74, 71.14, 69.36, 69.03, 65.82, 60.09, 49.94, 45.03, 38.86, 36.88, 35.69, 31.89, 30.84, 20.62.

HR MS (ESI$^+$) *m/z* calc. for $C_{112}H_{179}N_{30}O_{46}S_2$ $[M+3H]^{3+}$ 914.7338; found 914.7332. Yield: 30 mg (15 %).

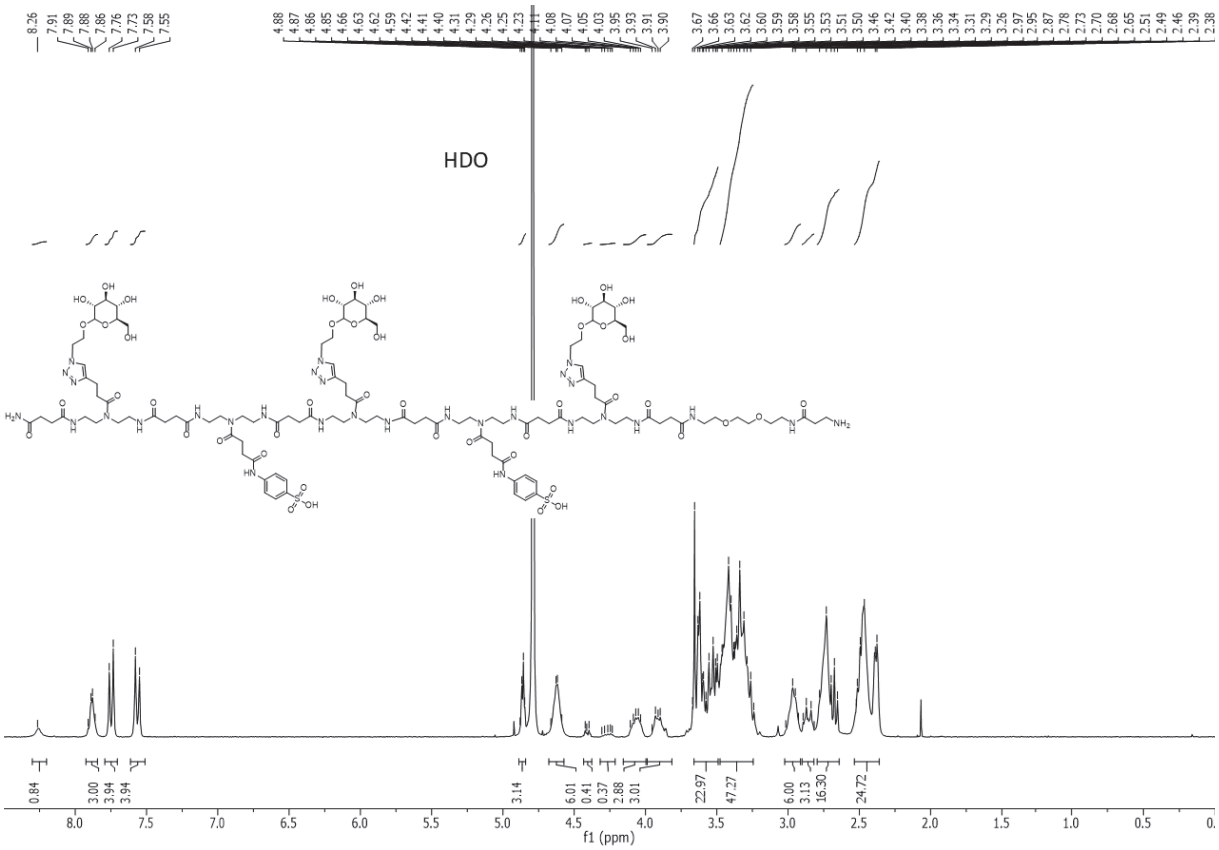

Figure S 88: ^{1}H-NMR spectrum of compound **12a.**

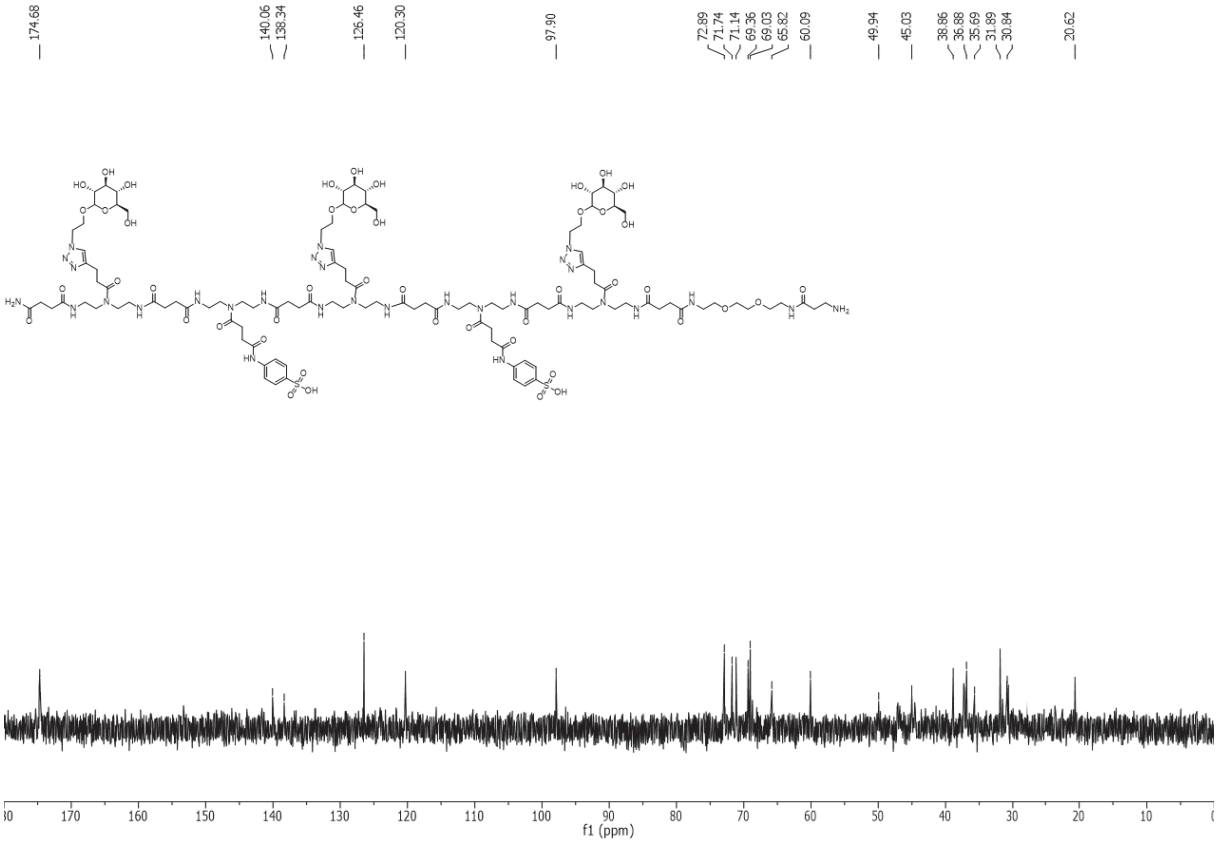

Figure S 89: ^{13}C-NMR spectrum of compound **12a.**

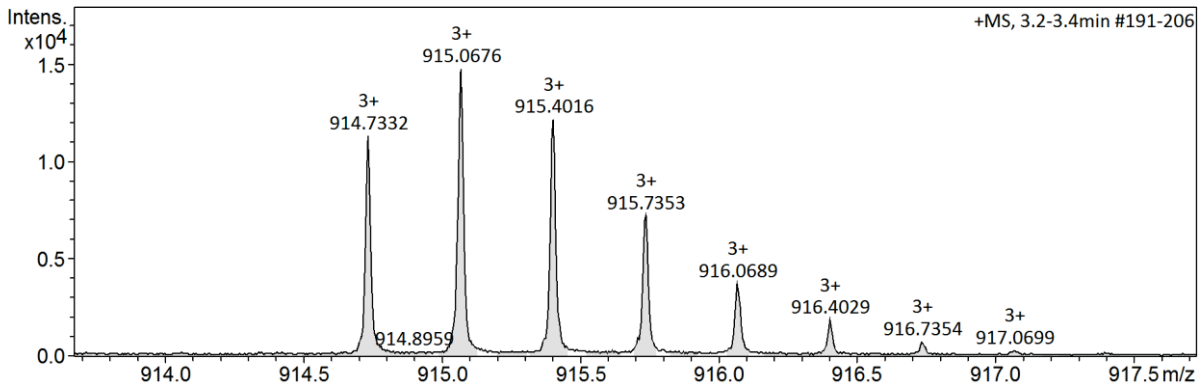

Figure S 90: HR-MS spectrum of compound **12a.**

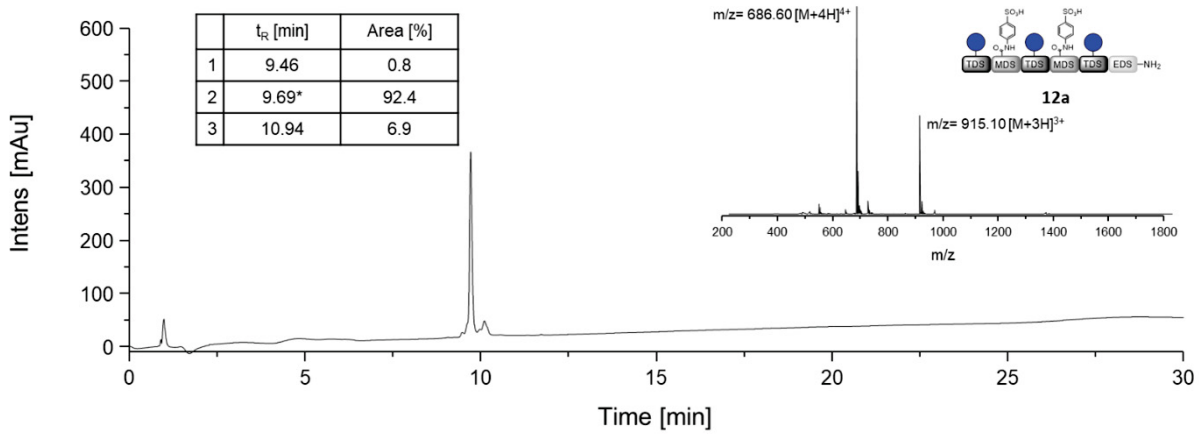

	t_R [min]	Area [%]
1	9.46	0.8
2	9.69*	92.4
3	10.94	6.9

Figure S 91: RP-HPLC chromatogram and ESI$^+$-MS spectrum of compound **12a.** Retention time t_R [min] and area [%] of the peaks are given. ESI-MS spectrum of the main peak (*) is shown.

Glc(1,3,5)-*p*SO_3H Ph(2,4)-6–Ac, **12b**

^{1}H NMR (300 MHz, Deuterium Oxide) δ [ppm]: δ 7.93 – 7.82 (m, 3H, triazole-C*H*), 7.75 (d, *J* = 8.5 Hz, 4H, aromatic-C*H*), 7.57 (d, *J* = 8.5 Hz, 4H, aromatic-C*H*), 4.88 – 4.84 (m, 3H, CH_{anomer}Glc), 4.69 – 4.56 (m, 6H, N-N-CH_2-), 4.12 – 4.00 (m, 3H, C$H_{pyranose}$), 3.97 – 3.85 (m, 3H, C$H_{pyranose}$), 3.69 – 3.58 (m, 36H, C$H_{pyranose}$, O-CH_2-), 3.57 – 3.24 (m, 59H, O-CH_2-, C=ONH-CH_2, C$H_{pyranose}$), 3.03 – 2.91 (m, 6H, CH=C-CH_2), 2.90 – 2.81 (m, 4H, C$H_{pyranose}$), 2.80 – 2.68 (m, 14H, C$H_{pyranose}$ CH=C, -CH_2-CH_2), 2.55 – 2.34 (m, 26H, NHC=O-CH_2), 1.99 (s, 3H, CH_3).

^{13}C NMR (126 MHz, Deuterium Oxide) δ [ppm]: 174.05, 173.89, 125.69, 119.61, 99.01, 97.19, 72.16, 71.00, 70.40, 68.60 68.36, 67.96, 65.08, 59.42, 49.15, 46.34, 44.28, 38.16, 38.11, 36.56, 36.22, 36.15, 31.13, 30.10, 21.04, 19.85, 13.27.

HR MS (ESI$^+$) *m/z* calc. for $C_{111}H_{176}N_{29}O_{46}S_2$ [M+3H]$^{3+}$ 905.0583; found 905.0574. Yield: 23 mg (9 %).

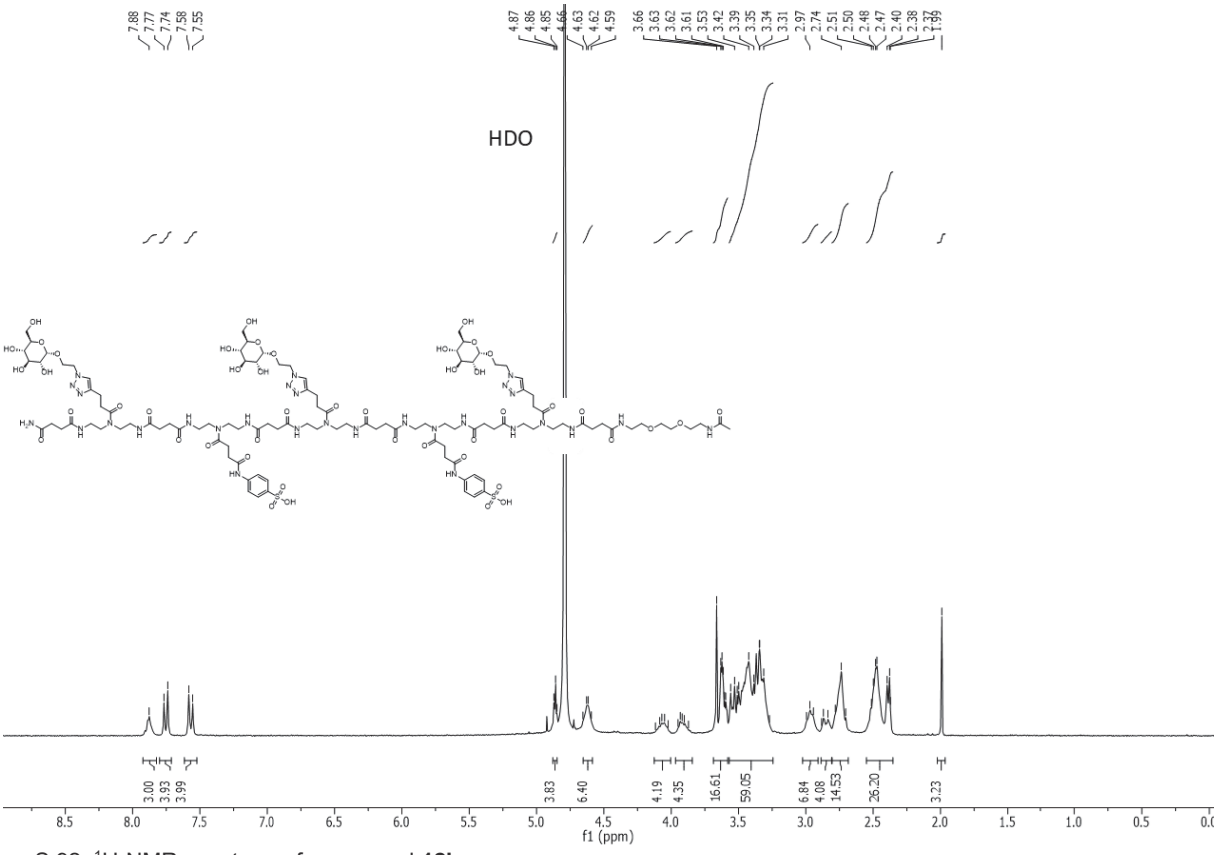

Figure S 92: ^{1}H-NMR spectrum of compound **12b.**

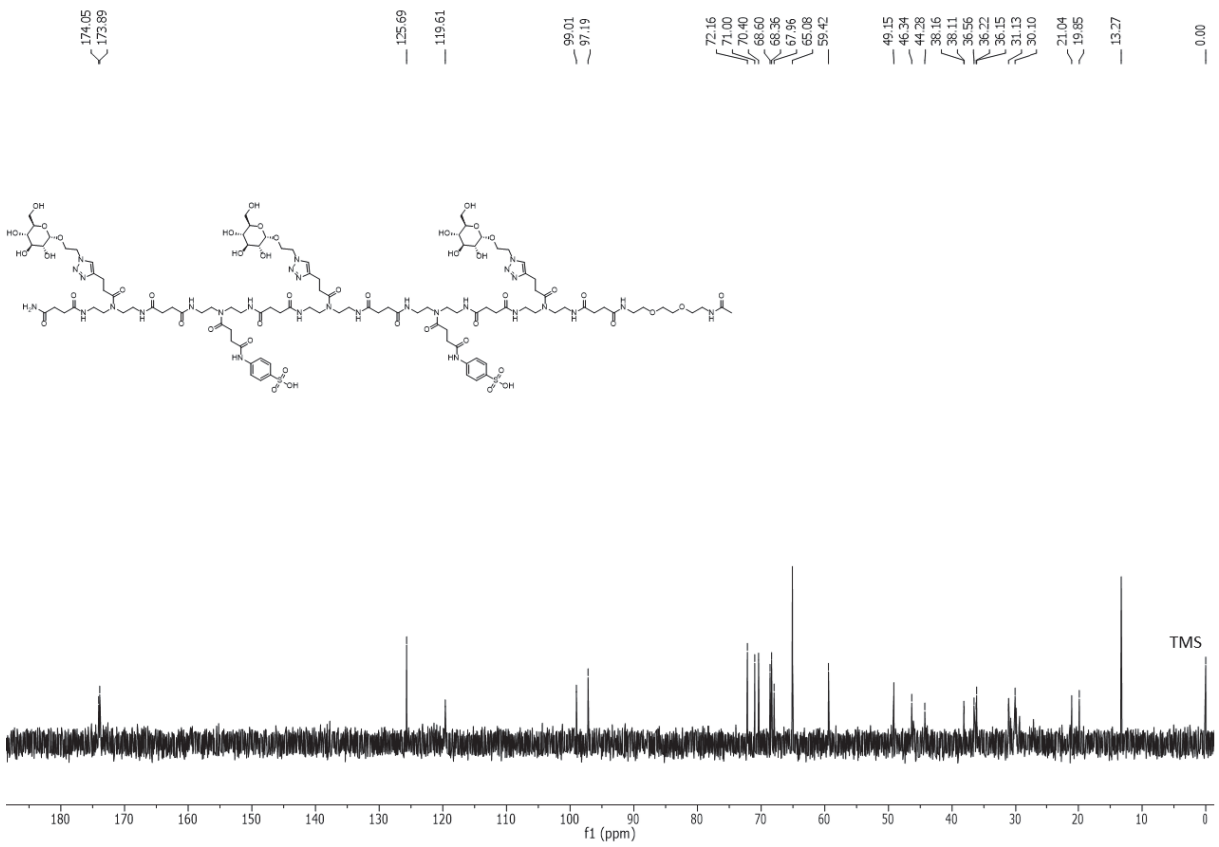

Figure S 93: ^{13}C-NMR spectrum of compound **12b**.

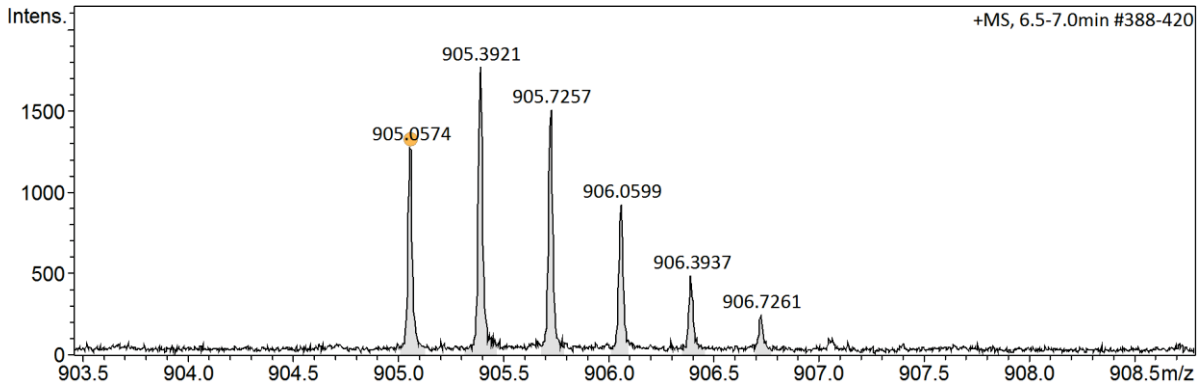

Figure S 94: HR-MS spectrum of compound **12b.**

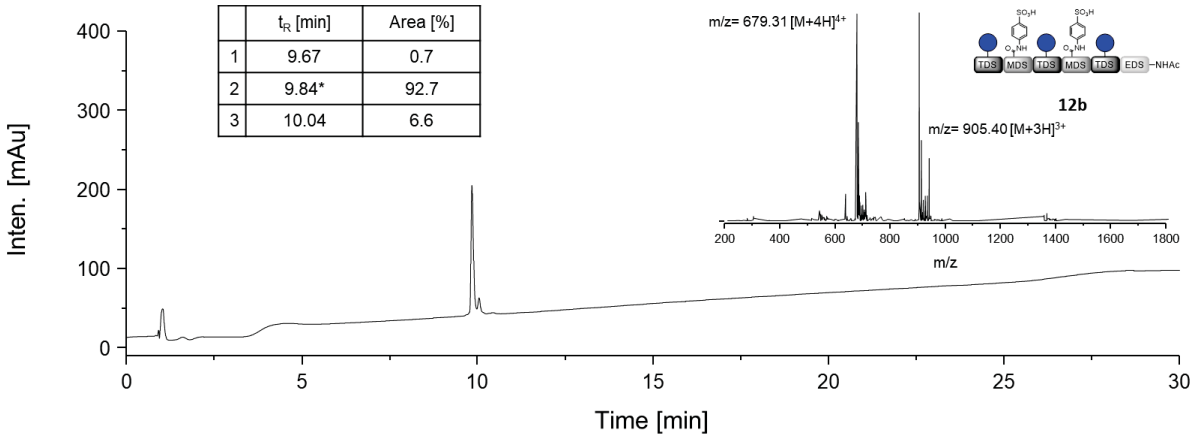

	t_R [min]	Area [%]
1	9.67	0.7
2	9.84*	92.7
3	10.04	6.6

Figure S 95: RP-HPLC chromatogram and ESI$^+$-MS spectrum of compound **12b.** Retention time t_R [min] and area [%] of the peaks are given. ESI-MS spectrum of the main peak (*) is shown.

Glc(1,3,5)-*p*SO_3H Ph(2,4)-6–FITC, **12c**

^{1}H NMR (300 MHz Deuterium Oxide) δ [ppm]: 7.92 – 7.80 (m, 3H, triazole-C*H*), 7.80 – 7.63 (m, 5H, aromatic-C*H,* FITC C*H*), 7.62 – 7.47 (m, aromatic-C*H,* FITC C*H*), 7.32 – 7.15 (m, 1H, FITC C*H*), 6.74 – 6.53 (m, 2H, FITC C*H*), 4.89 – 4.84 (m, 3H, CH_{anomer}Glc), 4.66 – 4.54 (m, 6H ,-N-N-CH_2), 4.13 – 3.98 (m, 3H, C$H_{pyranose}$), 3.96 – 3.83 (m, 3H, C$H_{pyranose}$), 3.69 – 3.23 (m, 23H, C$H_{pyranose}$, CH_2 $_{pyranose,}$ O-CH_2, C=ONH-CH_2), 3.03 – 2.65 (m, 28H, CH=CH-CH_2-CH_2, NH-C=O-CH_2), 2.55 – 2.33 (m, 26H, NH-C=O-CH_2).

^{13}C NMR (75 MHz, Deuterium Oxide) δ [ppm]: 174.92, 147.00, 140.31, 126.70, 124.21, 120.53, 98.14, 73.12, 71.97, 71.39, 69.27, 66.06, 60.33, 50.15, 47.34, 45.27, 39.09, 37.49, 37.44, 37.13, 37.11, 35.95, 32.16, 31.09, 30.48, 20.85.

HR MS (ESI$^+$) *m/z* calc. for $C_{133}H_{191}N_{31}O_{51}S_3$ $[M+4H]^{4+}$ 783.5611; found 783.5627. Yield: 9 mg (33 %).

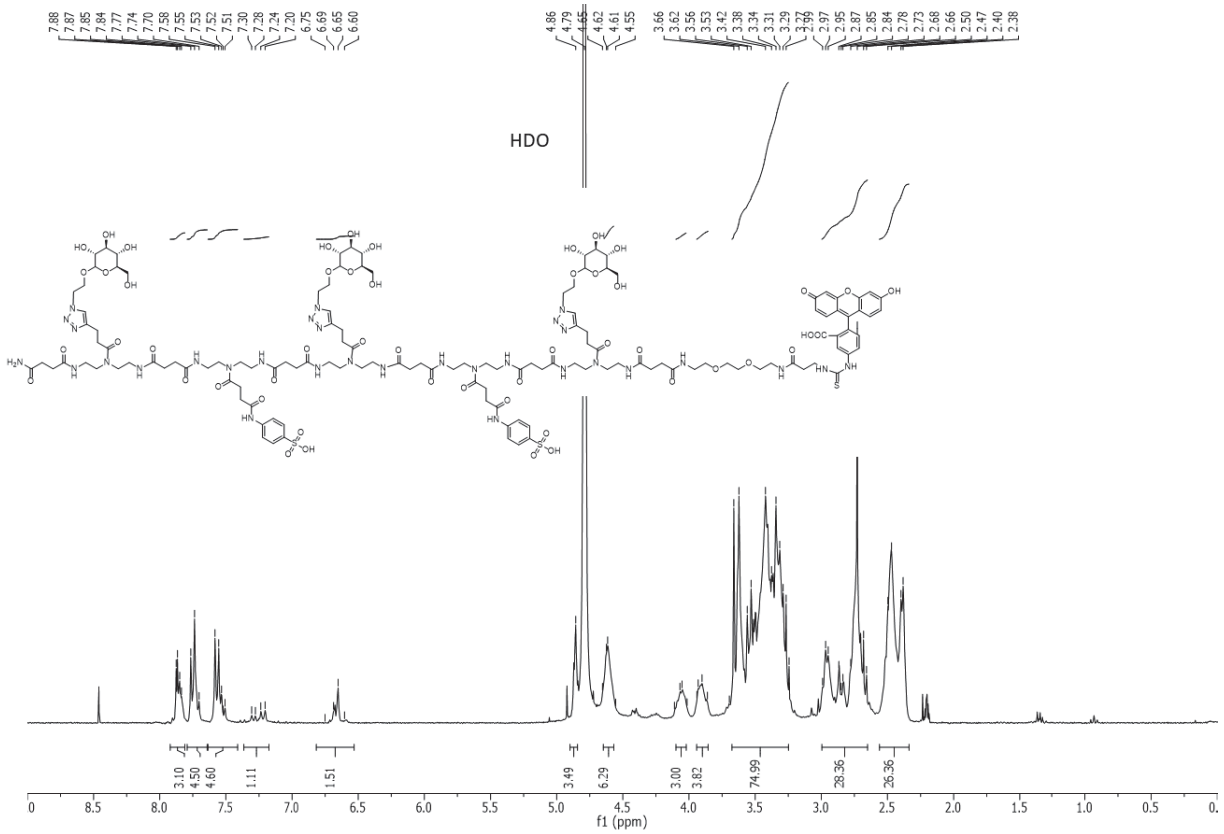

Figure S 96: ^{1}H-NMR spectrum of compound **12c.**

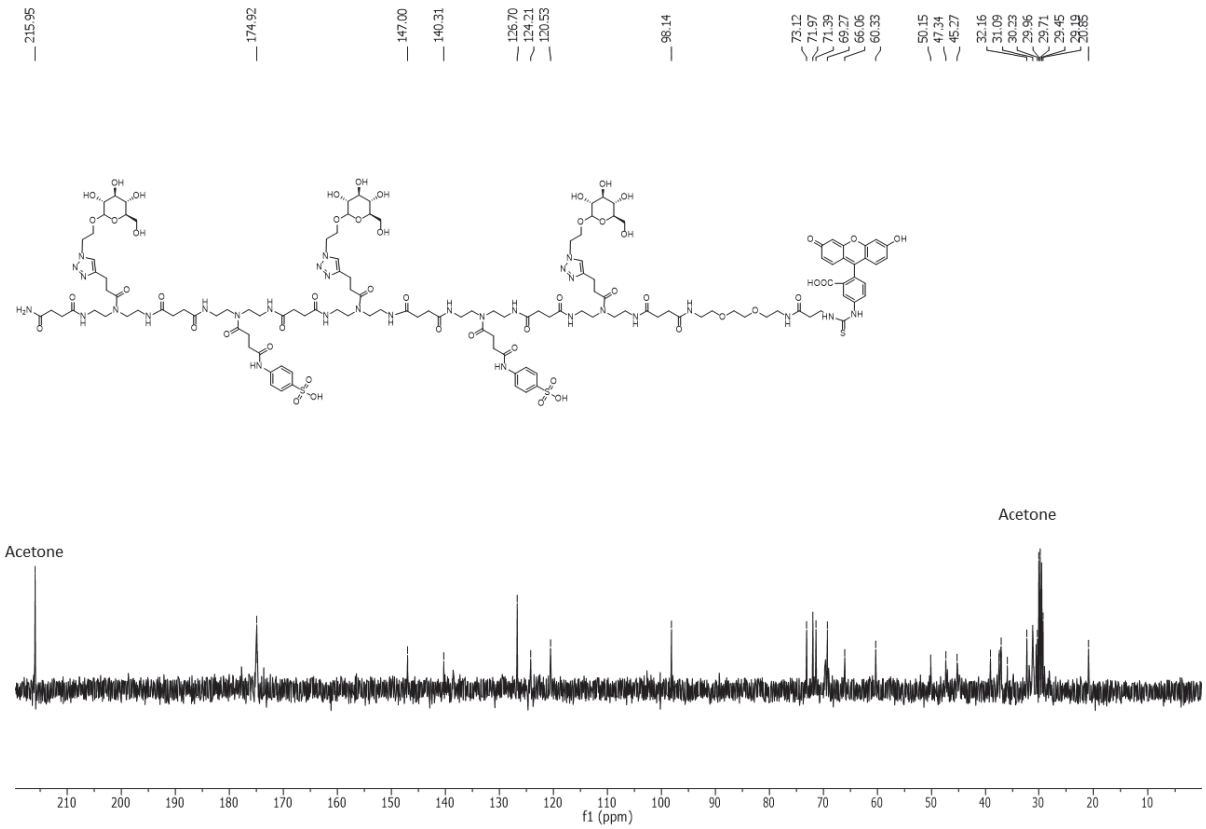

Figure S 97: ^{13}C-NMR spectrum of compound **12c.**

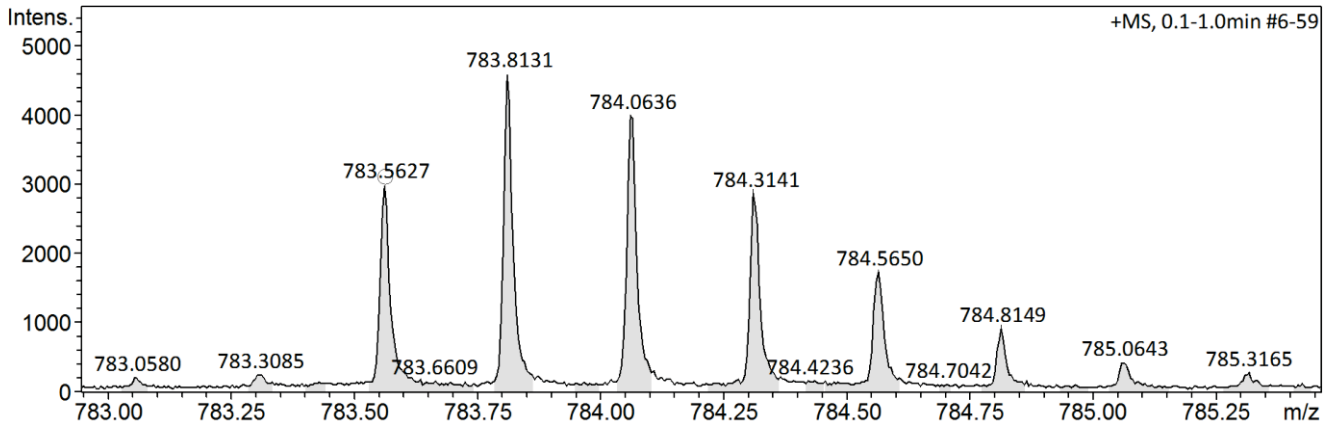

Figure S 98: HR-MS spectrum of compound **12c.**

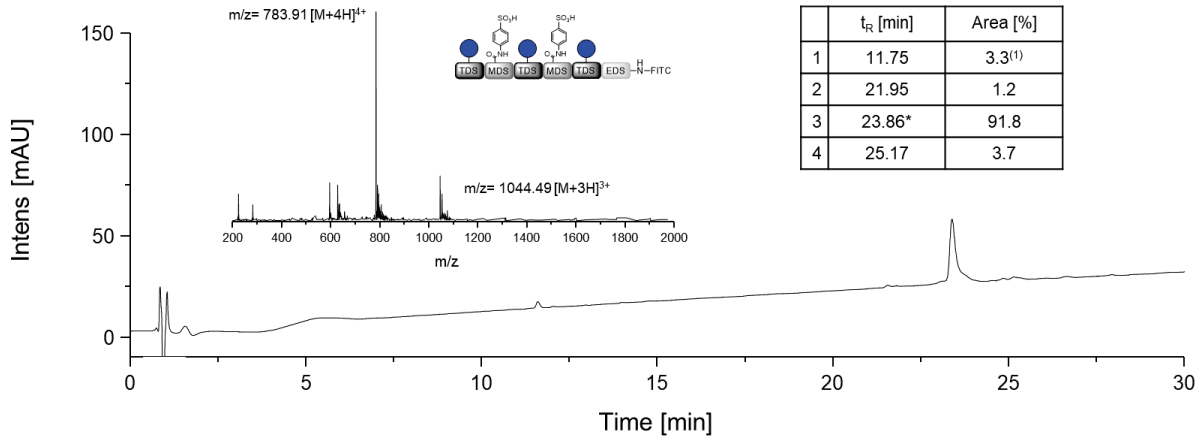

	t_R [min]	Area [%]
1	11.75	3.3(1)
2	21.95	1.2
3	23.86*	91.8
4	25.17	3.7

Figure S 99: RP-HPLC chromatogram and ESI$^+$-MS spectrum of compound **12c.** Retention time t_R [min] and area [%] of the peaks are given. ESI-MS spectrum of the main peak (*) is shown. (1) Unconjugated starting material.

Glc(1,3,5)-Tyr(4-SO_3H)(2,4)-6–NH_2, **13a**

^{1}H NMR (600 MHz, Deuterium Oxide) δ [ppm]: 7.95 – 7.87 (m, 3H, triazole-C*H*), 7.29 – 7.19 (m,8H, aromatic C*H*), 4.90 – 4.85 (m, 3H, CH_{anomer}Glc), 4.68 – 4.57 (m, 6H,-N-N-CH_2), 4.55 – 4.48 (m, 3H, C$H_{pyranose}$), 4.12 – 4.04 (m, 3H, C$H_{pyranose}$), 3.96 – 3.86 (m, 3H, C$H_{pyranose}$), 3.78 – 3.74 (m, 2H, O-CH_2-), 3.71 – 3.54 (m, 14H, Tyr C*H,* C$H_{pyranose}$, CH_2 $_{pyranose,}$ O-CH_2-), 3.51 – 3.19 (m, 36H, O-CH_2-, C=ONH-C$H_{2,}$ C$H_{pyranose}$), 3.11 – 2.85 (m, 14H, CH_2-NH_2, CH=C-C$H_{2,}$ C$H_{pyranose,}$), 2.80 – 2.72 (m, 6H, CH=CH-CH_2-C$H_{2,}$), 2.55 – 2.40 (m, 12H, NH-C=O-CH_2), 2.36 – 2.27 (m, 4H, NH-C=O-CH_2).

HR MS (ESI$^+$) *m/z* calc. for $C_{91}H_{144}N_{23}O_{41}S_2$ $[M+3H]^{3+}$ 759.6438; found 759.6430. Yield: 82 mg (36 %).

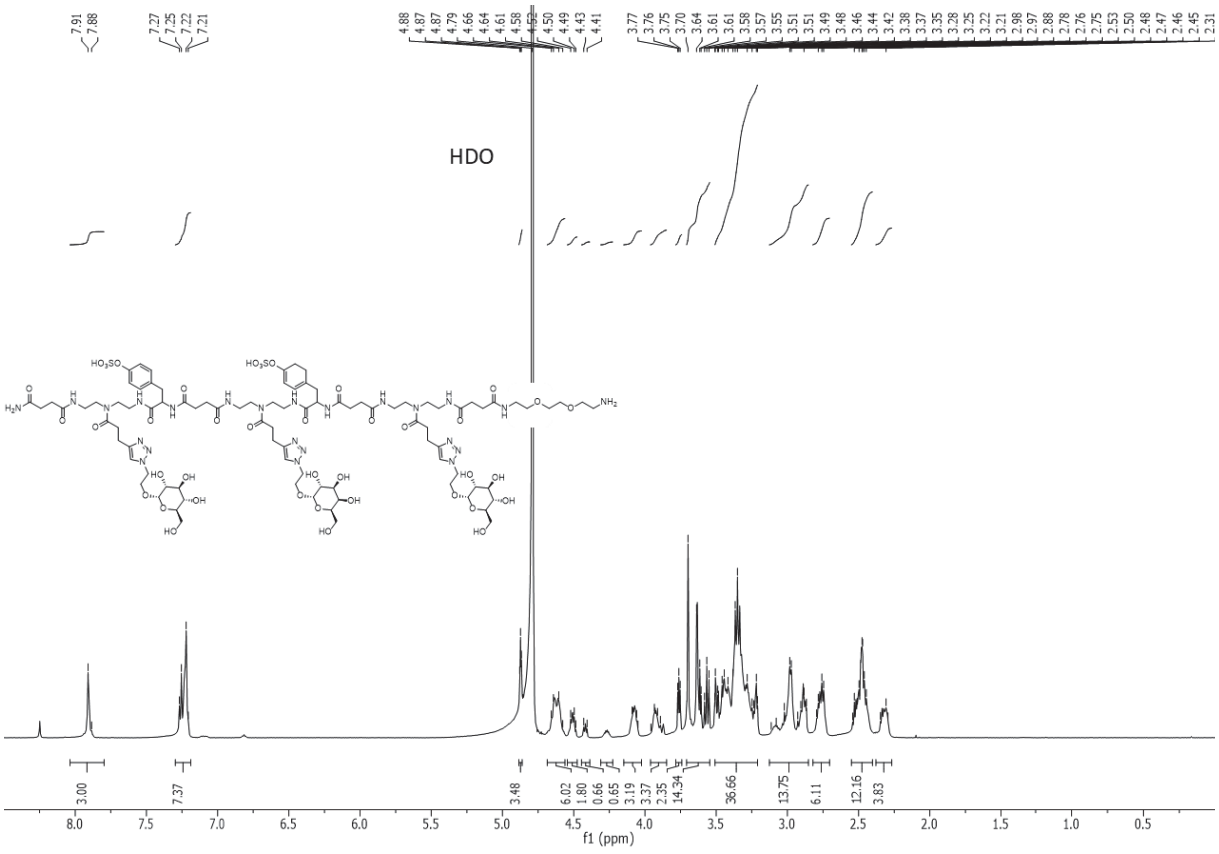

Figure S 100: ^{1}H-NMR spectrum of compound **13a.**

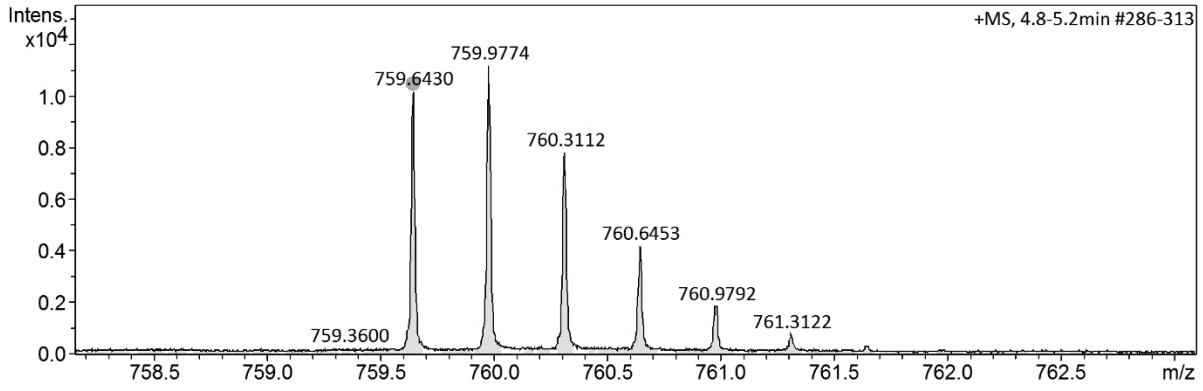

Figure S 101: HR-MS spectrum of compound **13a.**

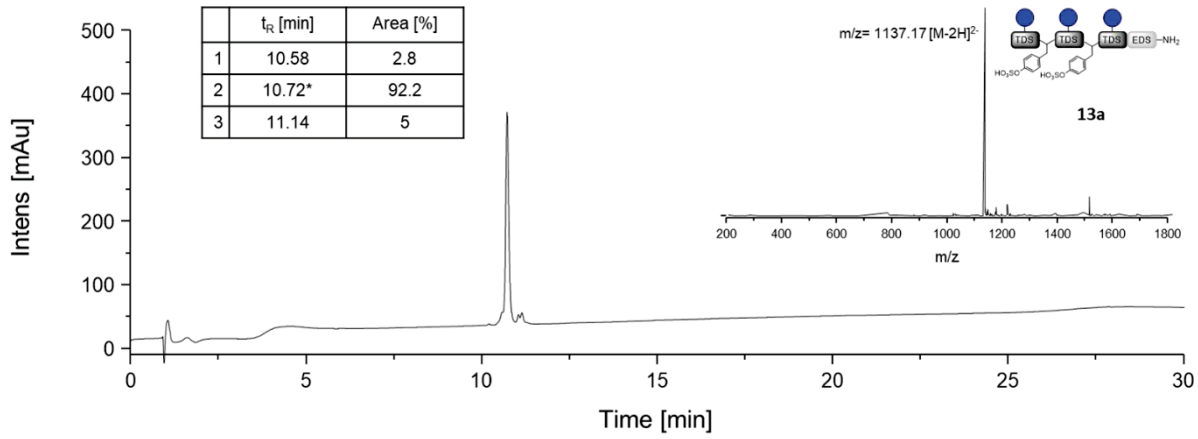

	t_R [min]	Area [%]
1	10.58	2.8
2	10.72*	92.2
3	11.14	5

Figure S 102: RP-HPLC chromatogram and ESI$^-$-MS spectrum of compound **13a**. Retention time t_R [min] and area [%] of the peaks are given. ESI-MS spectrum of the main peak (*) is shown.

Glc(1,3,5)-Tyr(4-SO_3H)(2,4)-6–FITC,**13c**

^{1}H NMR (300 MHz, Deuterium Oxide) δ [ppm]: 7.89 – 7.77 (m, 4H, triazole-C*H,* FITC C*H*), 7.70 – 7.58 (m, 1H, FITC C*H*), 7.31 – 7.14 (m, 9H, aromatic C*H*, FITC C*H*), 6.82 – 6.67 (m, 4H, FITC C*H*), 4.88 – 4.84 (m, 3H, CH_{anomer}Glc), 4.64 – 4.53 (m, 1H), 4.12 – 3.98 (m, m, 3H, C$H_{pyranose}$), 3.95 – 3.13 (m, 55H, Tyr C*H,* Tyr CH_2*,* C$H_{pyranose}$, CH_2 pyranose, O-CH_2-, C=ONH-CH_2,), 3.02 – 2.81 (m, 14H,, CH=C-CH_2*,* C$H_{pyranose}$), 2.79 – 2.63 (m, 6H, CH=CH-CH_2-CH_2), 2.56 – 2.24 (m, 16H, NH-C=O-CH_2).

^{13}C NMR (75 MHz, Deuterium Oxide) δ [ppm]: 215.95, 174.91, 174.74, 166.67, 158.04, 150.42, 148.46, 146.96, 138.65, 130.53, 124.15, 121.72, 98.17, 73.14, 71.97, 71.43, 69.77, 69.29, 69.28, 66.11, 60.32, 54.57, 50.13, 47.10, 37.54, 37.13, 32.16, 31.11, 30.89, 20.83.

HR MS (ESI$^+$) *m/z* calc. for $C_{112}H_{155}N_{24}O_{46}S_3$ $[M+3H]^{3+}$ 889.3224; found 889.3218. Yield: 5 mg (25 %).

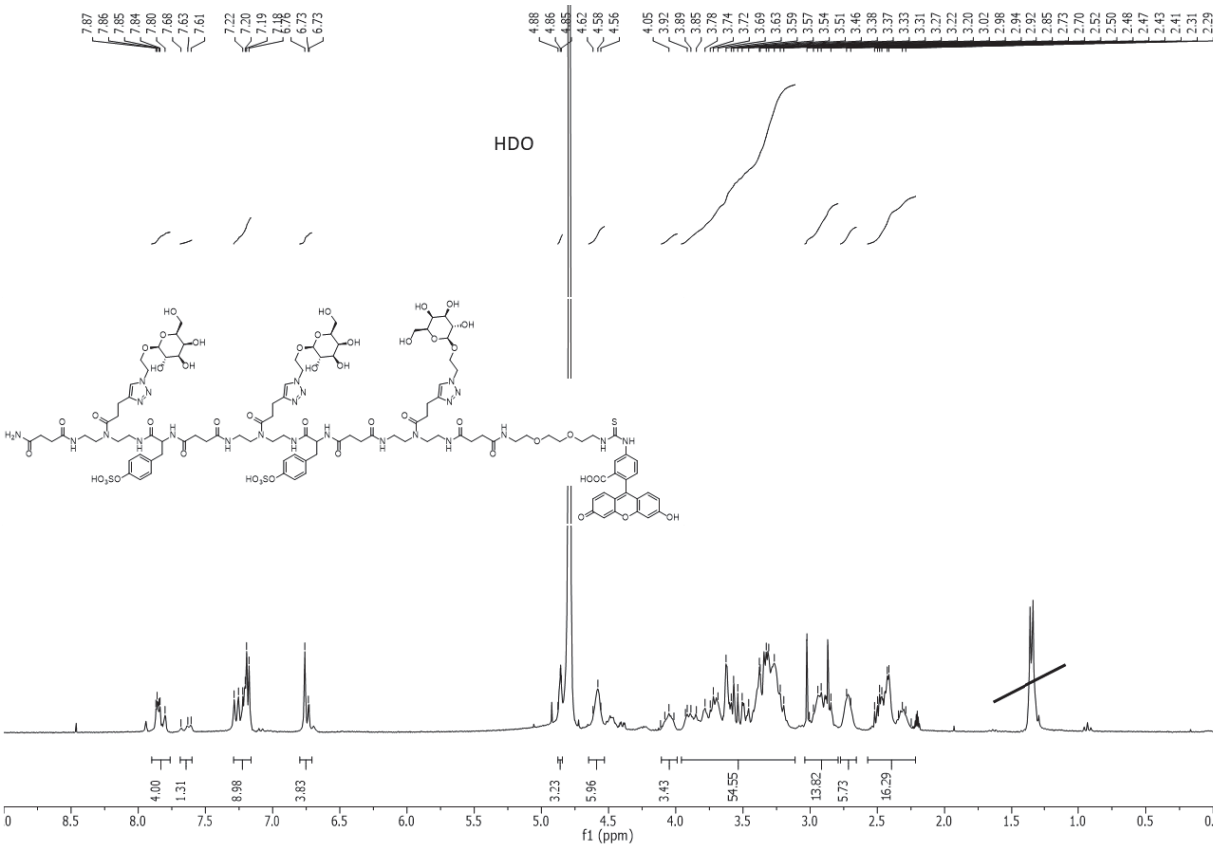

Figure S 103: ^{1}H-NMR spectrum of compound **13c.**

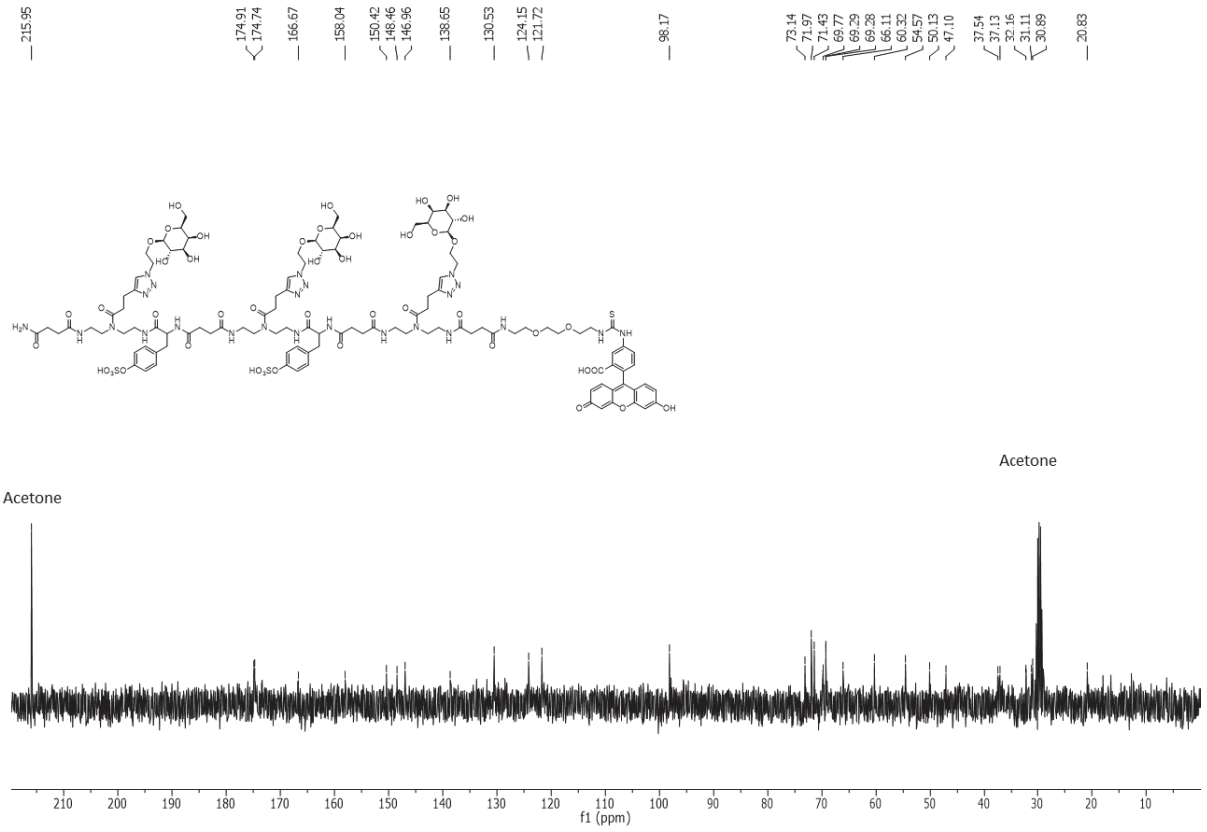

Figure S 104: ^{13}C-NMR spectrum of compound **13c**.

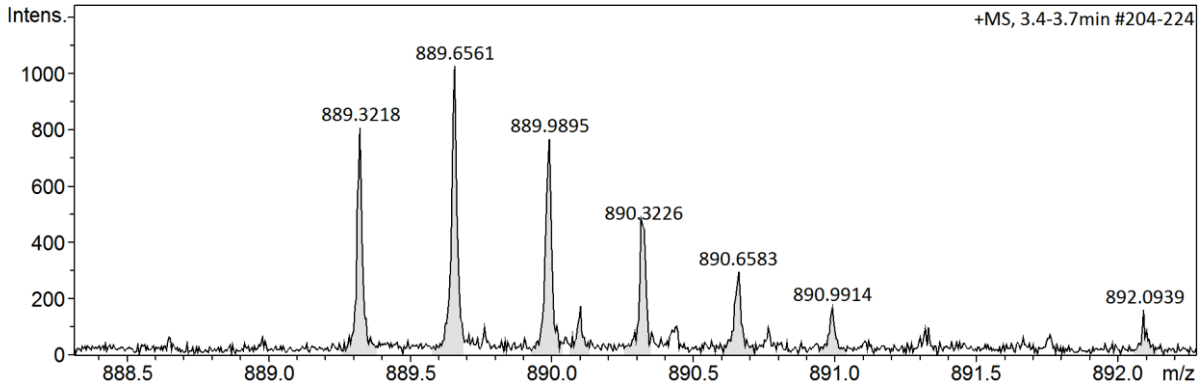

Figure S 105: HR-MS spectrum of compound **13c.**

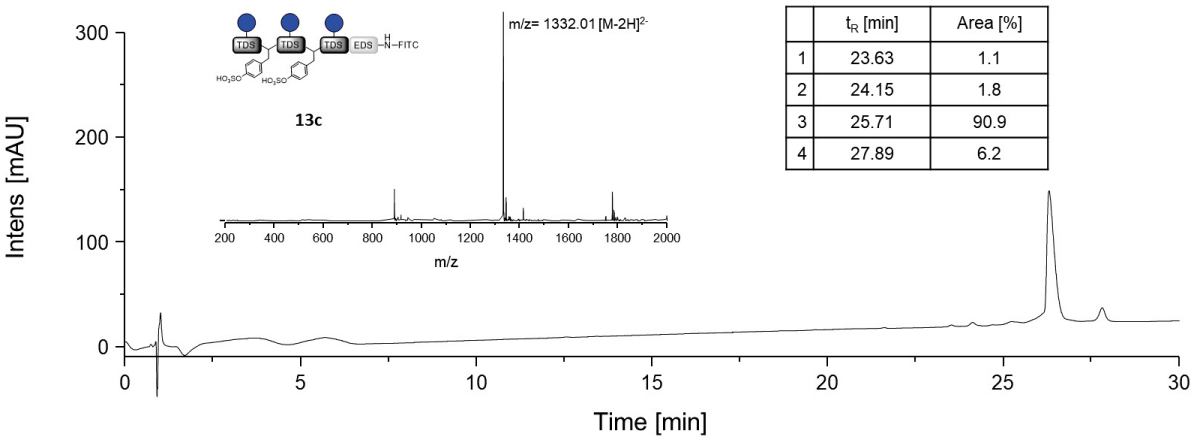

	t_R [min]	Area [%]
1	23.63	1.1
2	24.15	1.8
3	25.71	90.9
4	27.89	6.2

Figure S 106: RP-HPLC chromatogram and ESI$^+$-MS spectrum of compound **13c.** Retention time t_R [min] and area [%] of the peaks are given. ESI-MS spectrum of the main peak (*) is shown.

EDS-FITC, **14**

^{1}H NMR (300 MHz, Deuterium Oxide) δ [ppm]: 8.34 (s, 1H, , FITC-C*H*), 7.83 (s, 1H), 7.39 (s, 1H, FITC-C*H* H), 6.88 (s, 2H, , FITC-C*H*), 6.39 (d, J = 29.0 Hz, 4H, , FITC-C*H*), 3.75 – 3.10 (m, 14H), 3.02 – 2.88 (m, 2H), 2.49 – 2.16 (m, 4H).

^{13}C NMR (75 MHz, Deuterium Oxide) δ [ppm]: 215.96, 175.75, 174.69, 170.78, 69.89, 69.84, 69.06, 39.45, 36.97, 31.13, 31.04, 30.90, 30.25, 29.99, 29.73, 29.47, 29.21.

HR MS (ESI^{+}) *m/z* calc. for $C_{33}H_{39}N_5O_9S$ $[M+2H]^{2+}$ 340.6229; found 340.6233.

Yield: 56 mg (82 %).

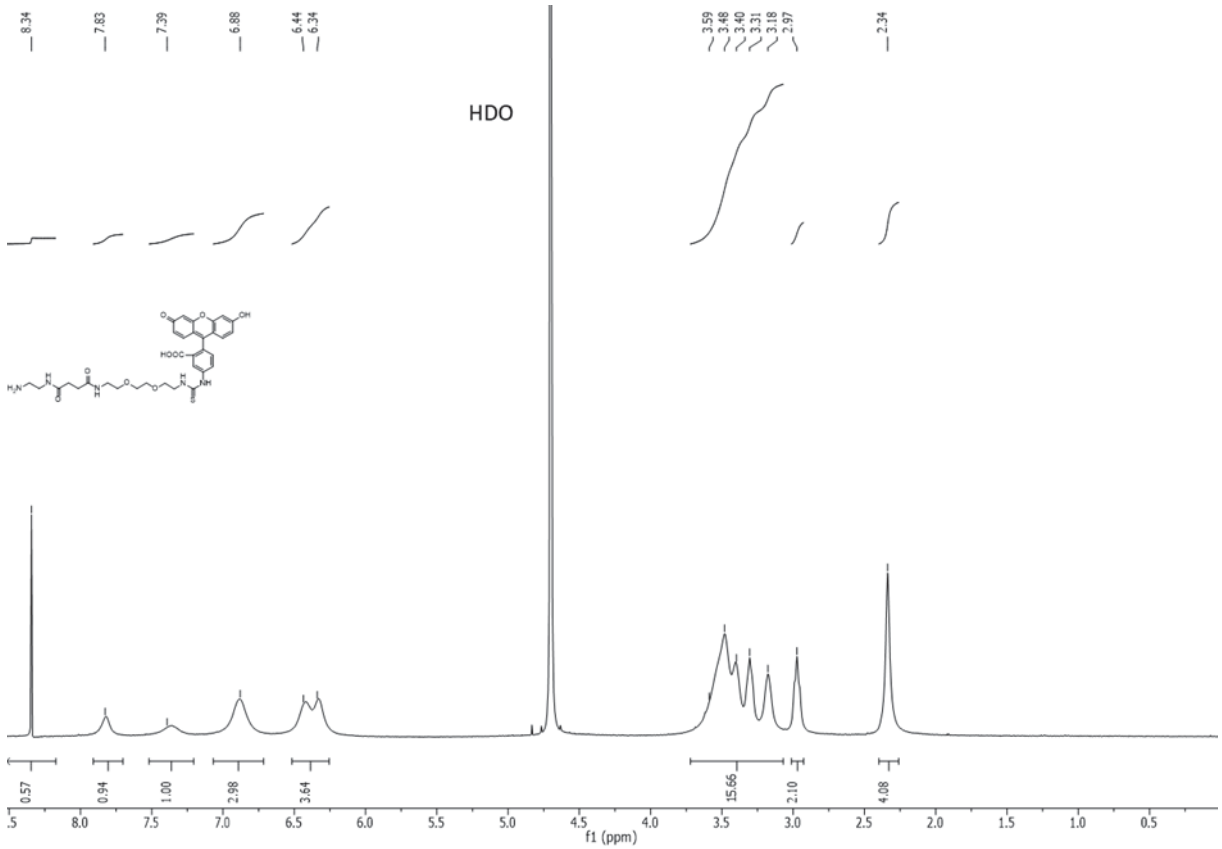

Figure S 107: ^{1}H-NMR spectrum of compound **14.**

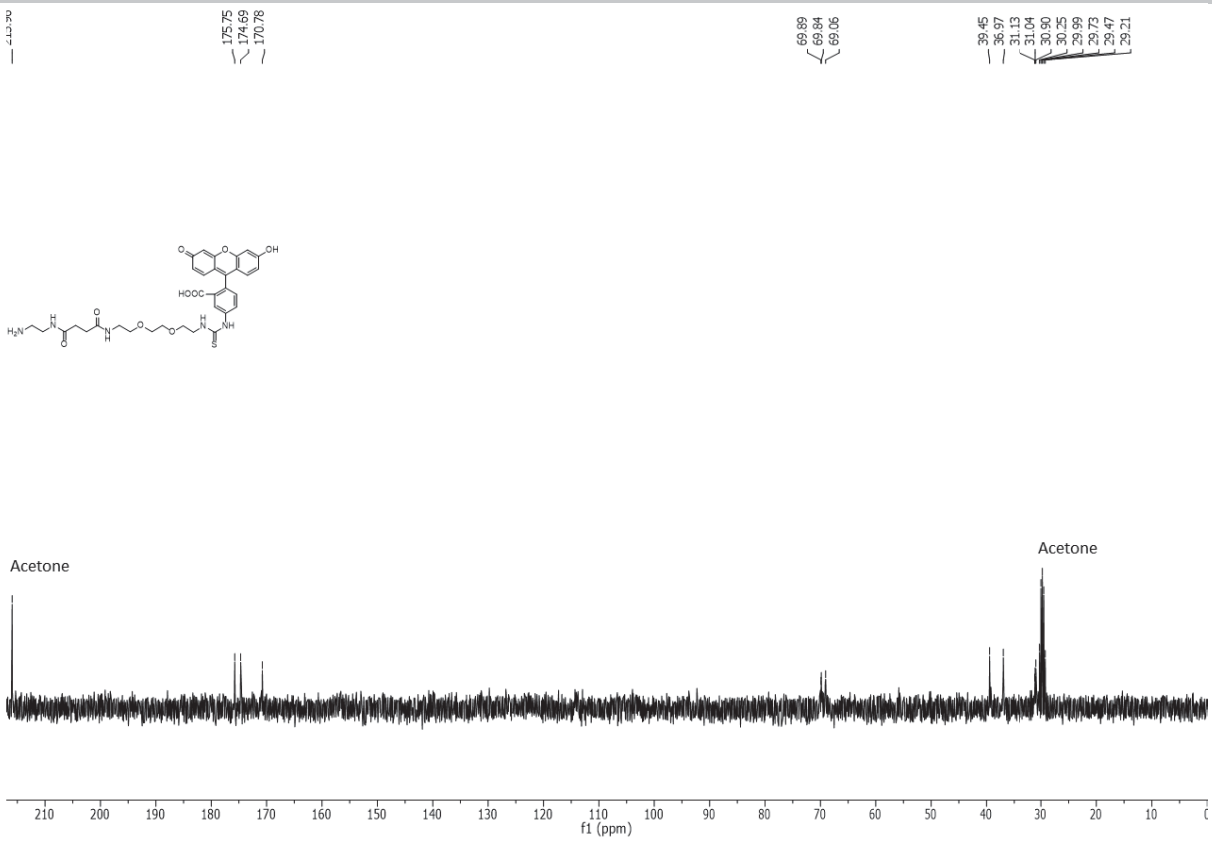

Figure S 108: ^{13}C-NMR spectrum of compound **14.**

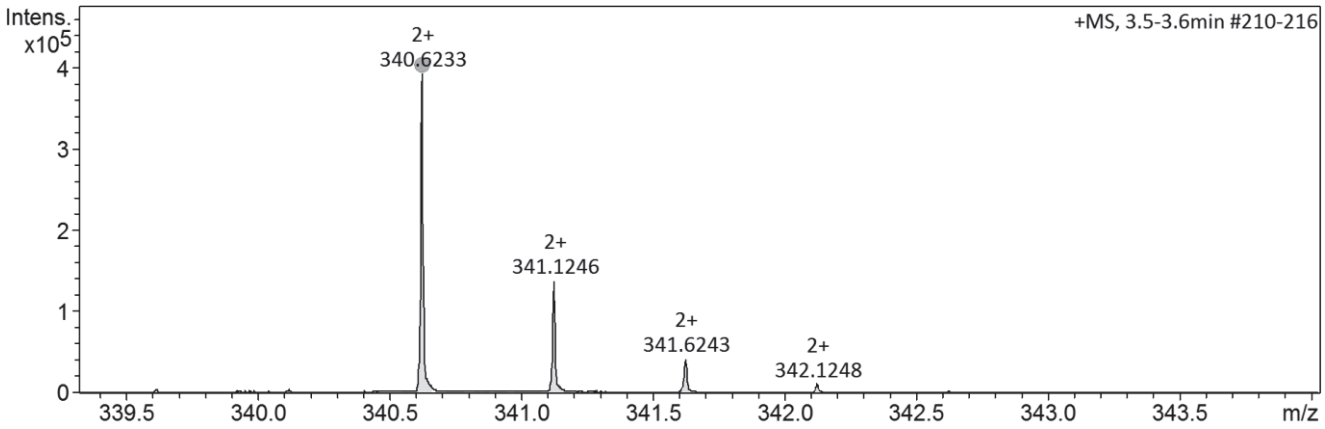

Figure S 109: HR-MS spectrum of compound **14.**

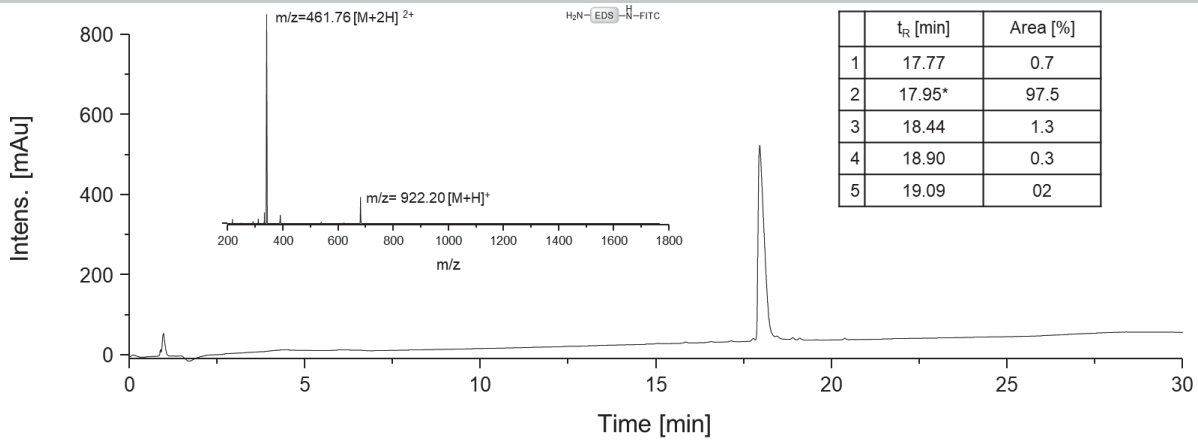

	t_R [min]	Area [%]
1	17.77	0.7
2	17.95*	97.5
3	18.44	1.3
4	18.90	0.3
5	19.09	02

Figure S 110: RP-HPLC chromatogram and ESI$^+$-MS spectrum of compound **14.** Retention time t_R [min] and area [%] of the peaks are given. ESI-MS spectrum of the main peak (*) is shown.

Results Binding Studies

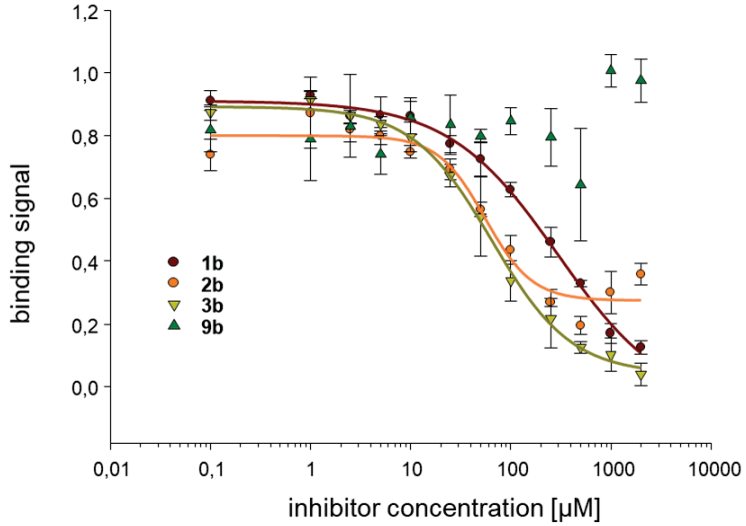

Figure S 111: Inhibition curves of the inhibition competition ELISA-type assays of Gal-1 with compounds **1b-3b** and 9**b**.

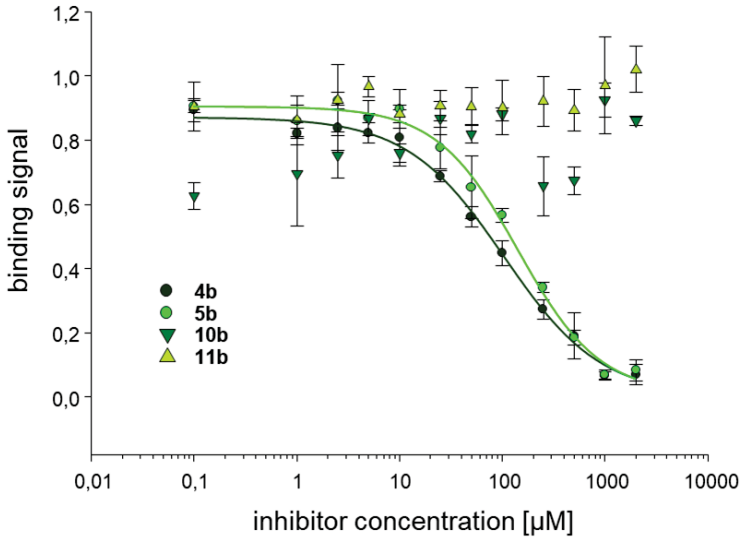

Figure S 112: Inhibition curves of the inhibition competition ELISA-type assays of Gal-1 with compounds **4b-5b** and 10**b-11b**.

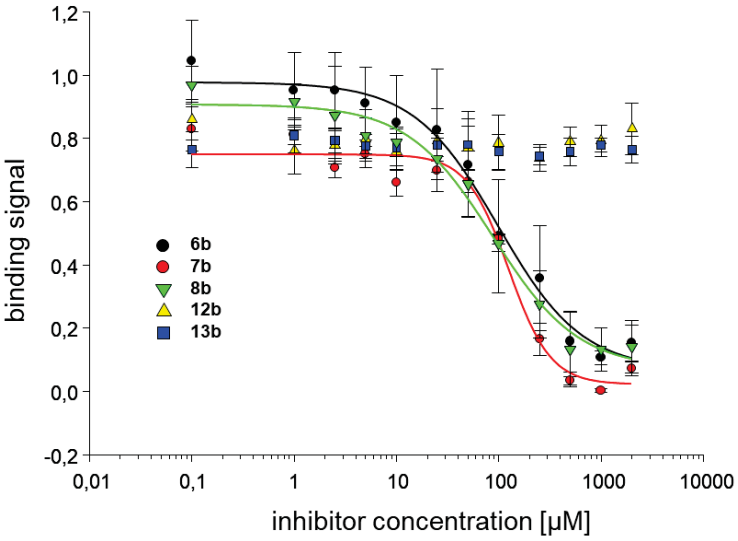

Figure S 113: Inhibition curves of the inhibition competition ELISA-type assays of Gal-1 with compounds **6b-8b** and **12b-13b**.

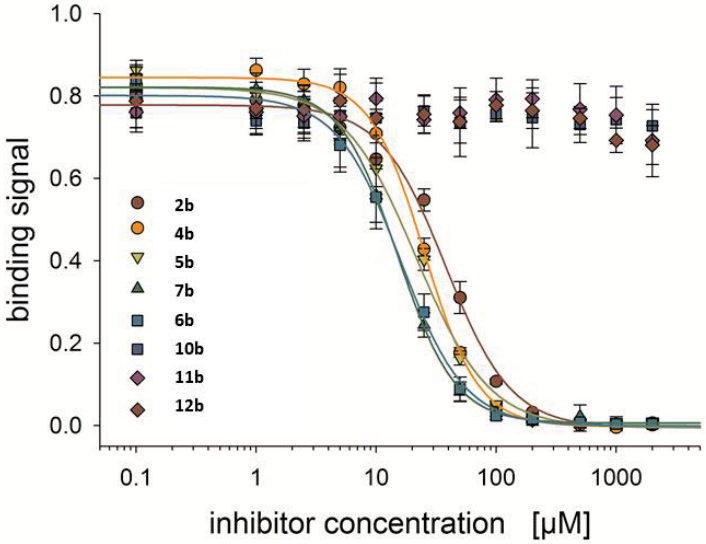

Figure S 114: Inhibition curves of the inhibition competition ELISA-type assays of Gal-3 with compounds **2b,4b-7b** and **10b-12b**.

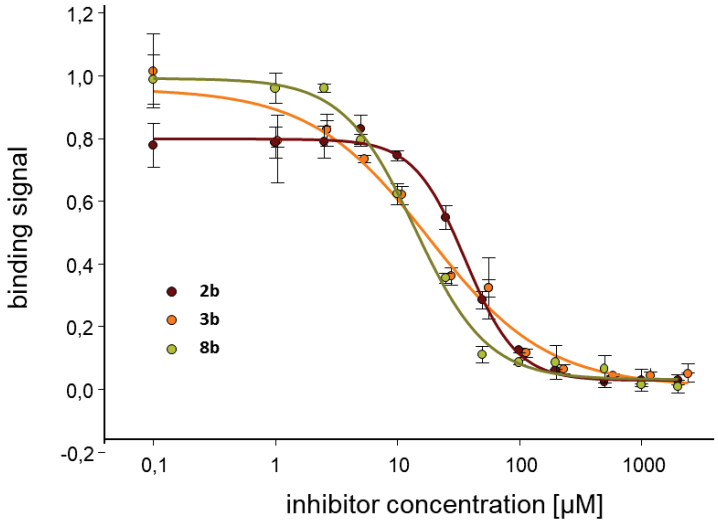

Figure S 115: Inhibition curves of the inhibition competition ELISA-type assays of Gal-3 with compounds **2b,3b** and **8b.**

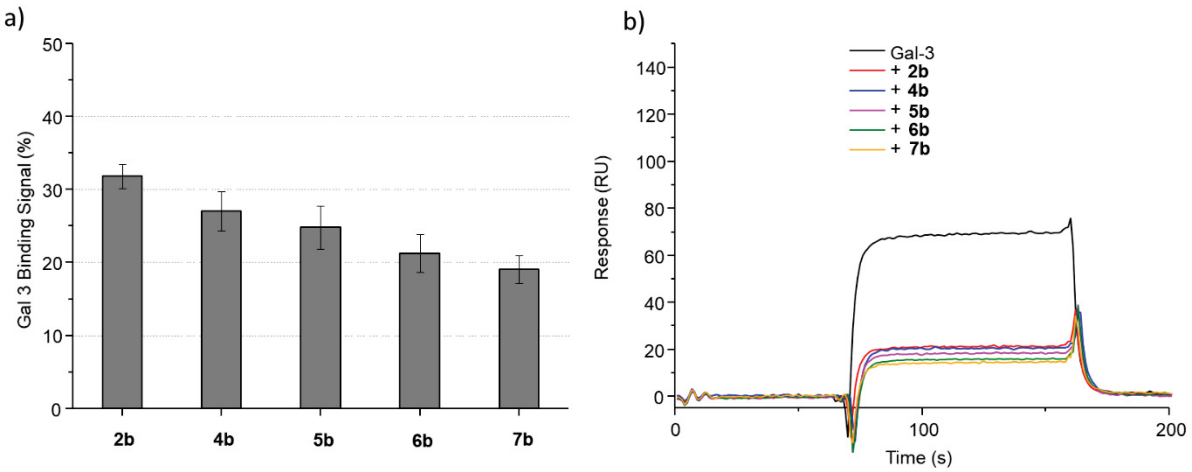

Figure S 116: Results from the SPR inhibition studies of Gal-3 and samples **2b**,**4b-7b**. Values are calculated regarding the signal of Gal-3 as 100 % binding signal.

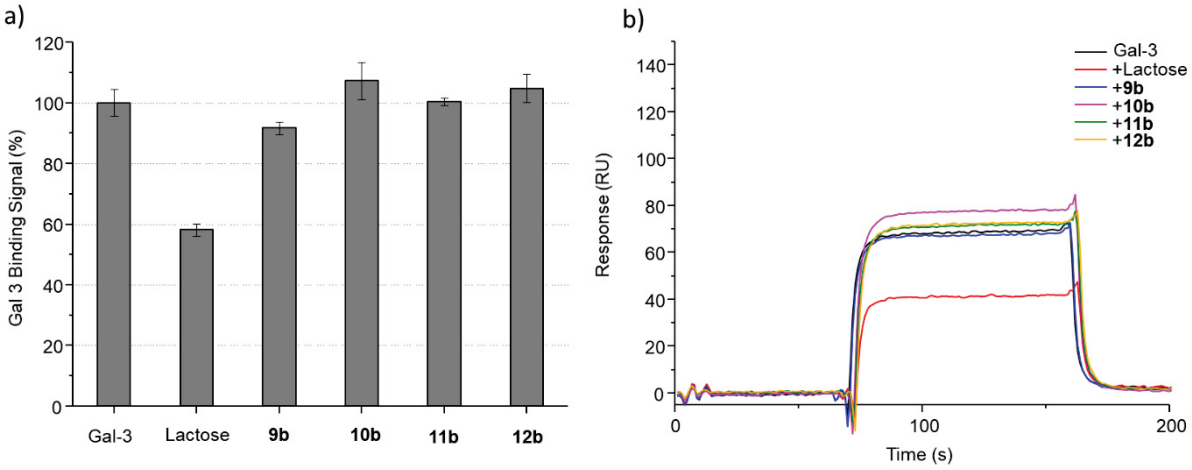

Figure S 117: Results from the SPR inhibition studies of Gal-3 with lactose as control and samples **9b-12b**. Values are calculated regarding the signal of Gal-3 as 100 % binding signal.

Results Cell Assays

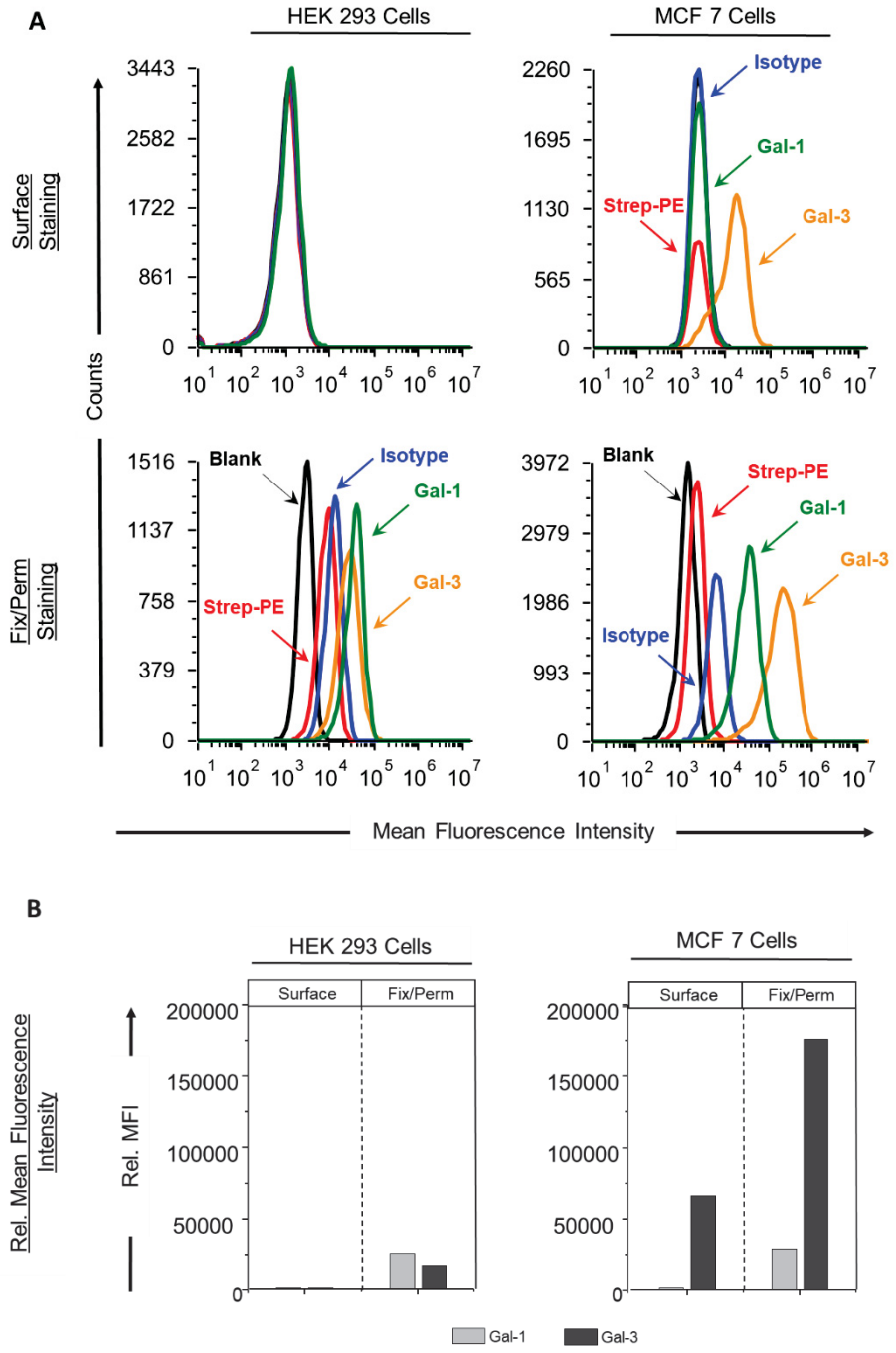

Figure S 118: Flow cytometry of the antibody staining of HEK 293 and MCF 7 cells. A. Histogram of the mean fluorescence intensity (MFI) of the surface staining and intracellular staining after fixation and permeabilization (Fix/Perm.) using biotinylated anti-bodies and PE-conjugated streptavidin. Unstained (black), streptavidin-PE (red), isotype control (blue), anti-Gal-3 (yellow) and anti-Gal-1(green). B. Relative mean fluorescence of the Gal-3 staining on the surface and after fixation and permeabilization. Values are MFI of Gal-1 or Gal-3 subtracted by the MFI of the isotype control.

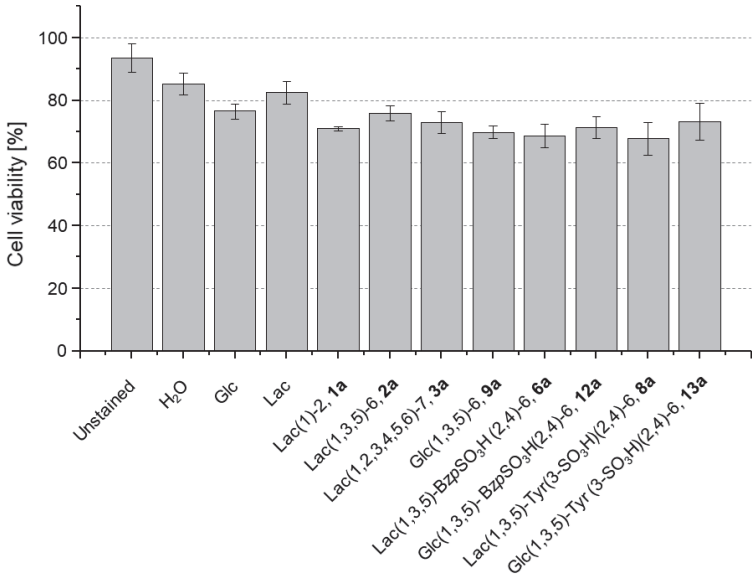

Figure S 119: Results of the MTT cell viability assay for the HEK 293 cell line. Measurements were performed two times in triplicates.

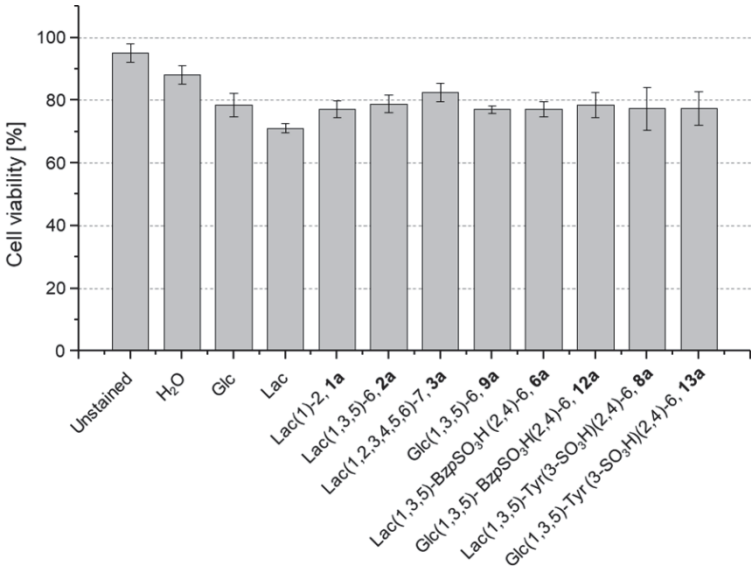

Figure S 120: Results of the MTT cell viability assay for MCF 7 cell line. Measurements were performed two times in triplicates.

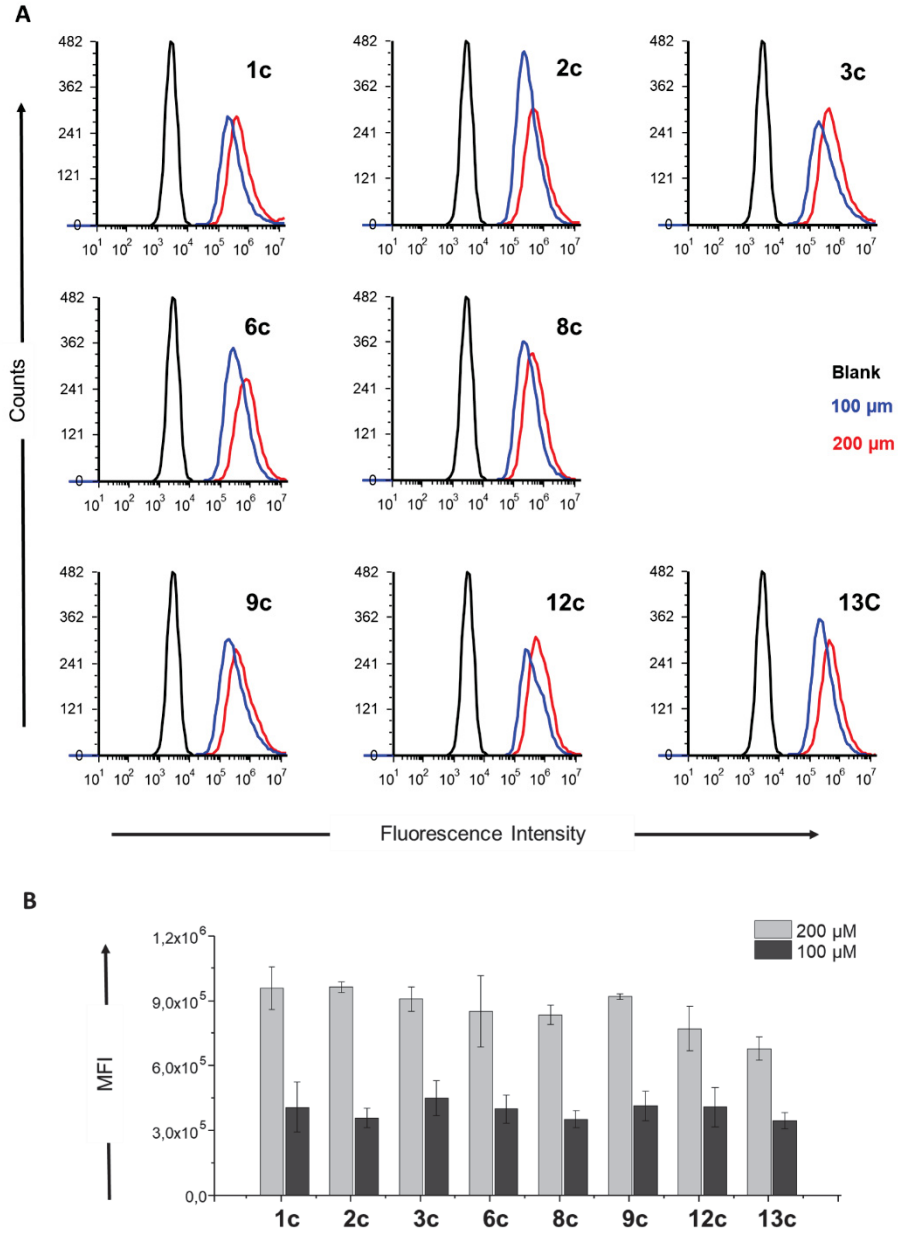

Figure S 121: Results of the uptake studies of the MCF 7 cells for glycomacromolecules **1-3c, 6c, 8c, 9c, 12c, 13c**. A. Histograms of the flow measurements showing the mean fluorescence intensity (MFI) of unstained cells and cells incubated with FITC-labeled glycomacromolecules at final concentrations of 100 and 200 µM. B. Comparison of the MFI-values for the different glycomacromolecules. Measurements were performed in duplicates.

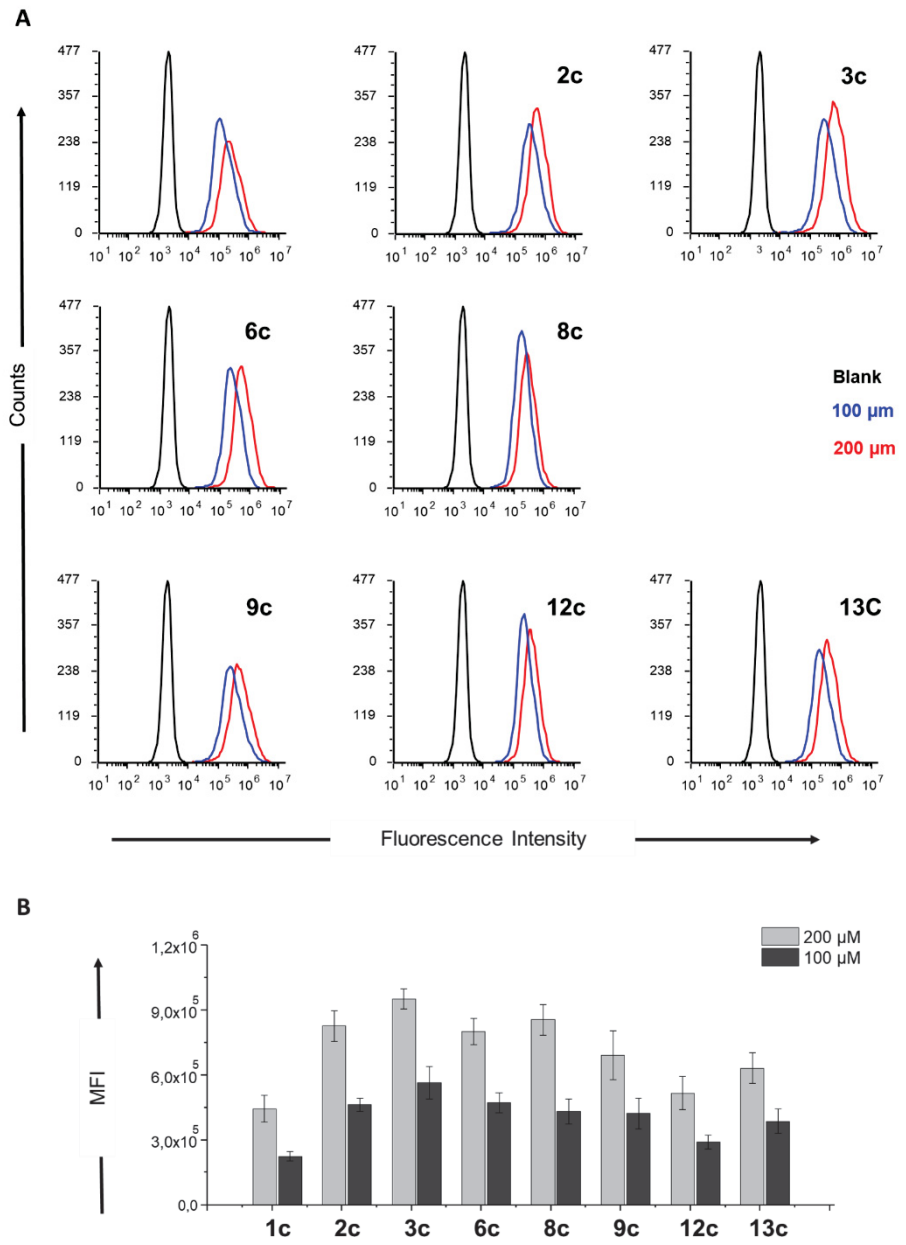

Figure S 122: Results of the uptake studies of HEK 293 cells for glycomacromolecules **1-3c, 6c, 8c, 9c, 12c, 13c**. A. Histograms of the flow measurements showing the mean fluorescence intensity (MFI) of unstained cells and cells incubated with FITC-labeled glycomacromolecules at a final concentration of 100 and 200 µM. B. Comparison of the MFI-values for the different glycomacromolecules. Measurements were performed in duplicates.

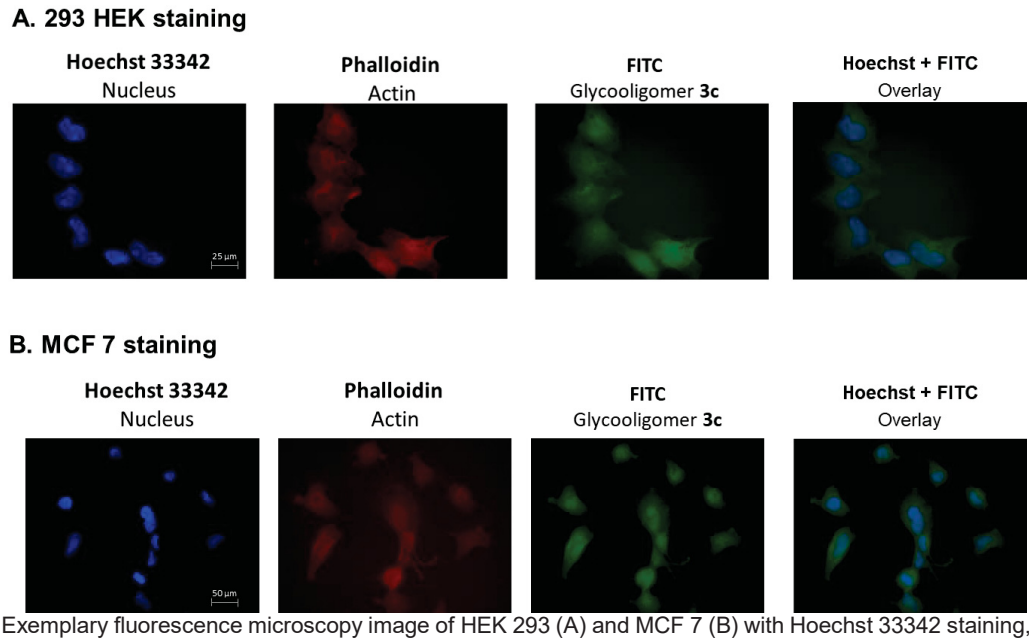

Figure S 123: Exemplary fluorescence microscopy image of HEK 293 (A) and MCF 7 (B) with Hoechst 33342 staining, Phalloidin staining and glycocoligomer **3c**.

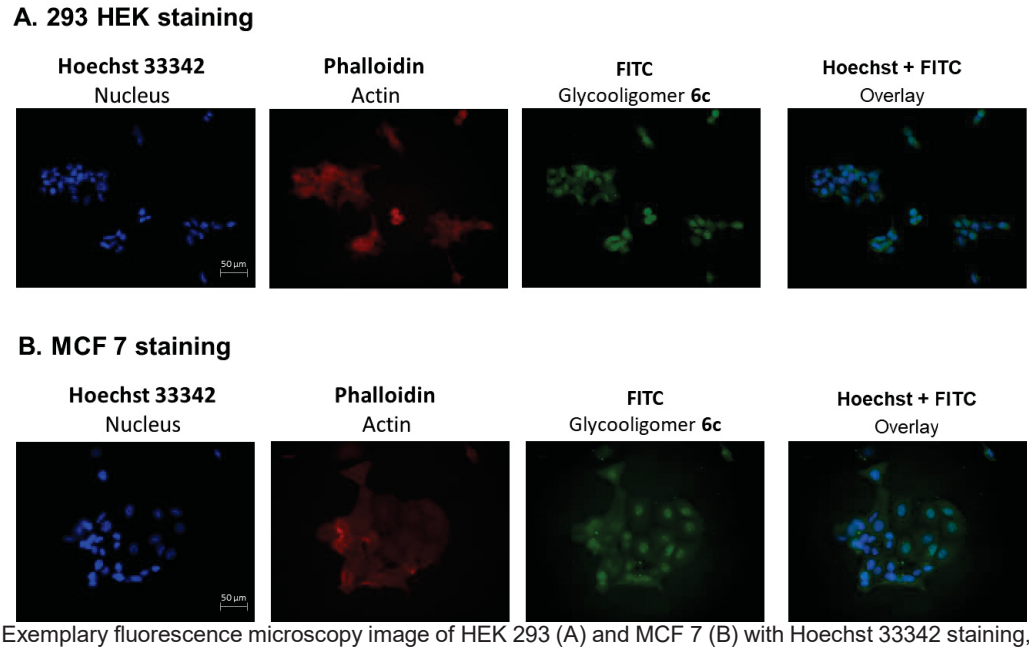

Figure S 124: Exemplary fluorescence microscopy image of HEK 293 (A) and MCF 7 (B) with Hoechst 33342 staining, Phalloidin staining and glycocoligomer **6c**.

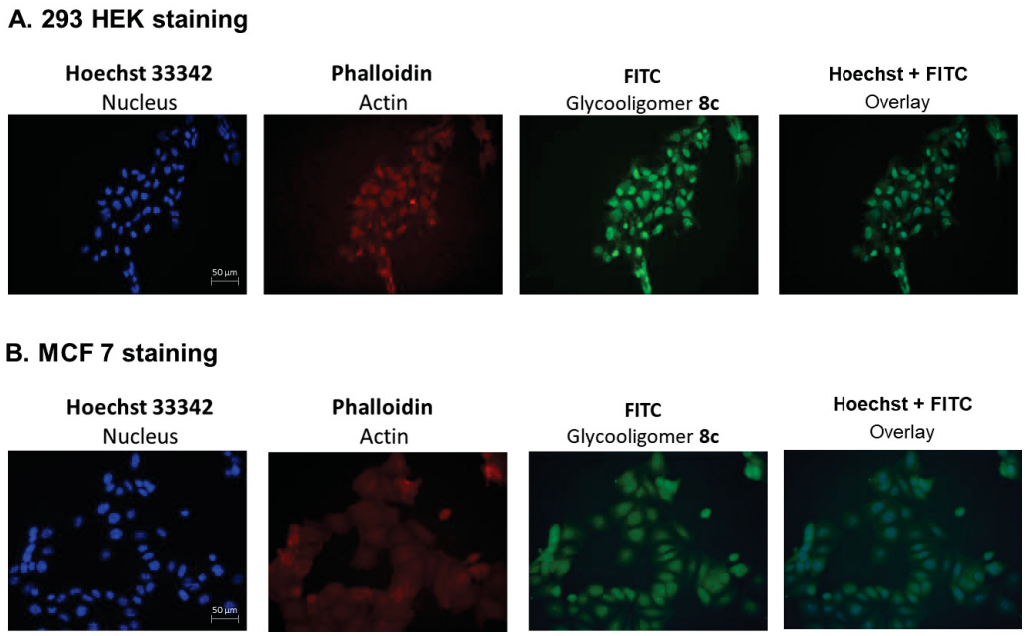

Figure S 125: Exemplary fluorescence microscopy image of HEK 293 (A) and MCF 7 (B) with Hoechst 33342 staining, Phalloidin staining and glycocoligomer **8c**.

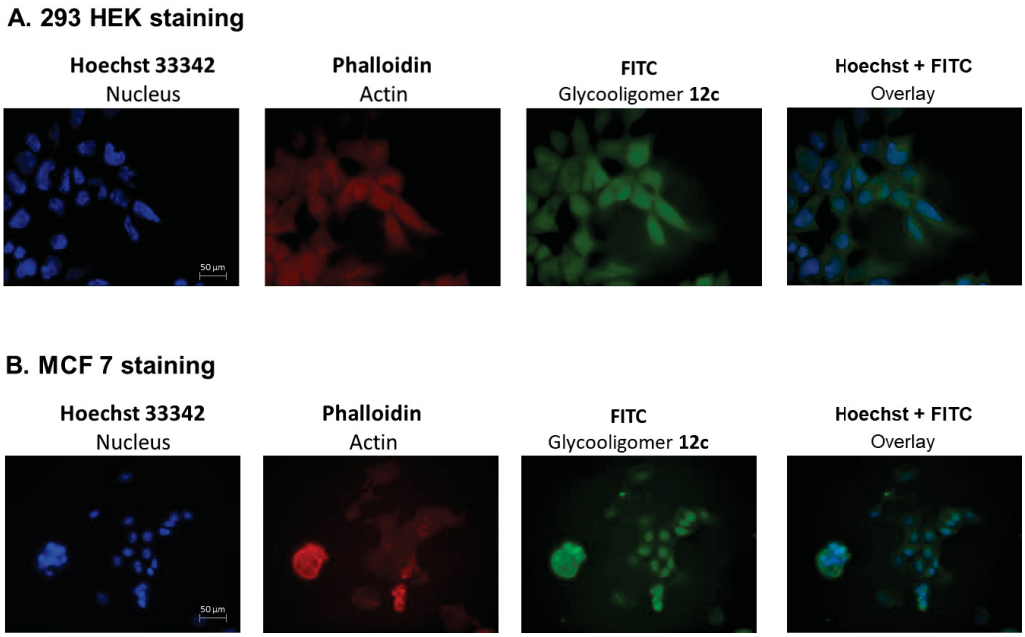

Figure S 126: Exemplary fluorescence microscopy image of HEK 293 (A) and MCF 7 (B) with Hoechst 33342 staining, Phalloidin staining and glycocoligomer **12c**.

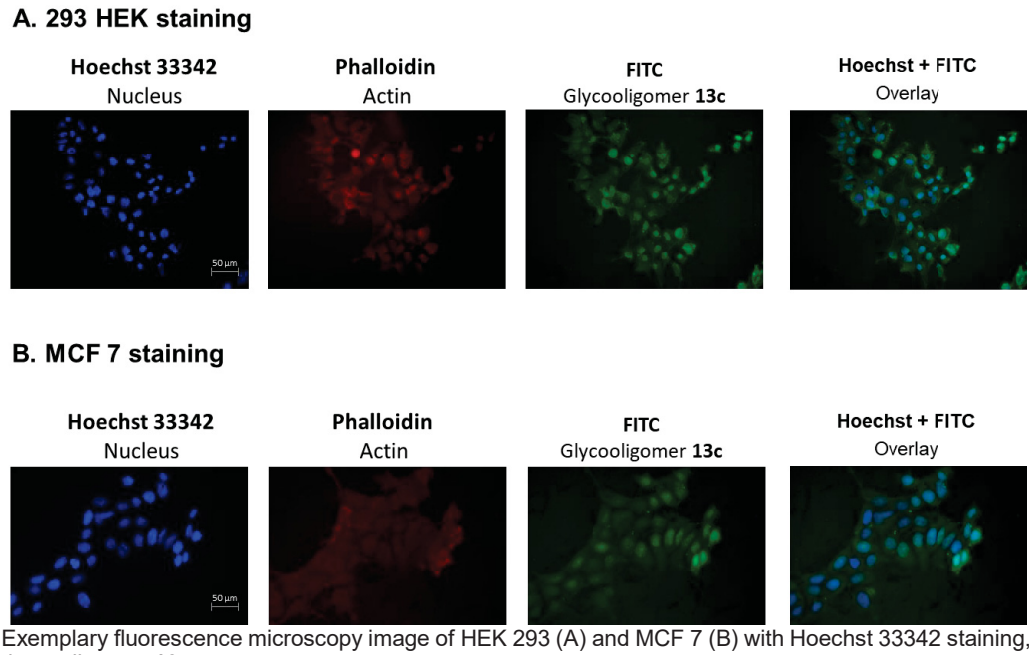

Figure S 127: Exemplary fluorescence microscopy image of HEK 293 (A) and MCF 7 (B) with Hoechst 33342 staining, Phalloidin staining and glycocoligomer **13c**.

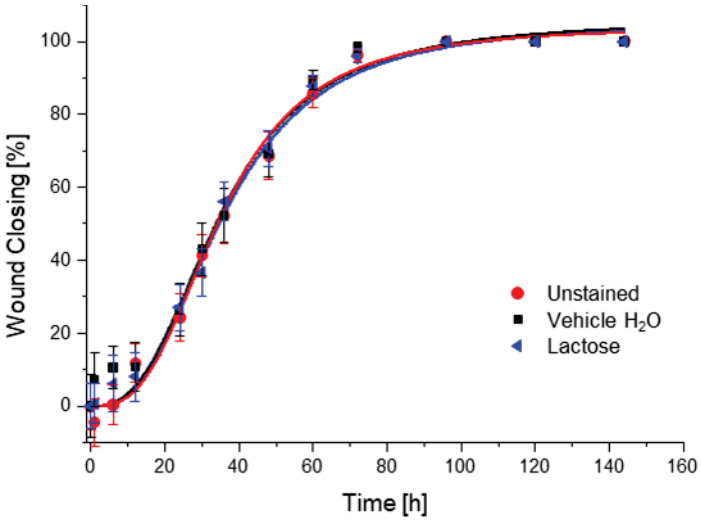

Figure S 128: Results of the migration of assays of MCF7: Untreated (red), vehicle control with H_2O (black) and treated with lactose (blue).

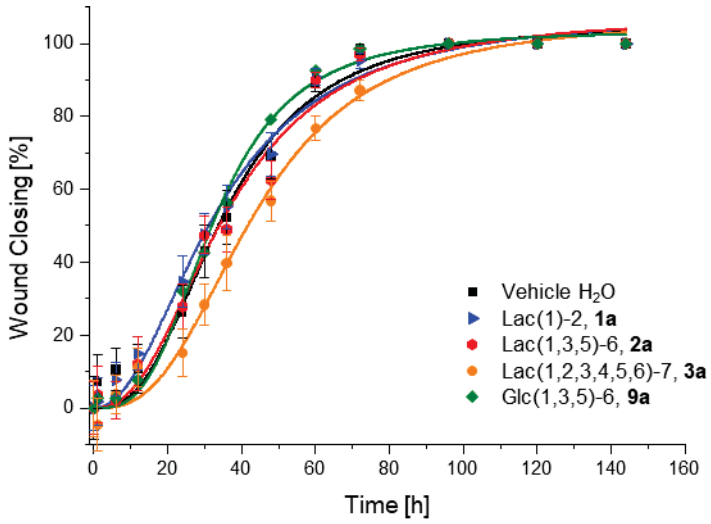

Figure S 129: Results of the migration of assays of MCF7 treated with the vehicle control H_2O (black) and compounds **1a** (blue), **2a** (red), **3a** (orange) and **9a** (green).

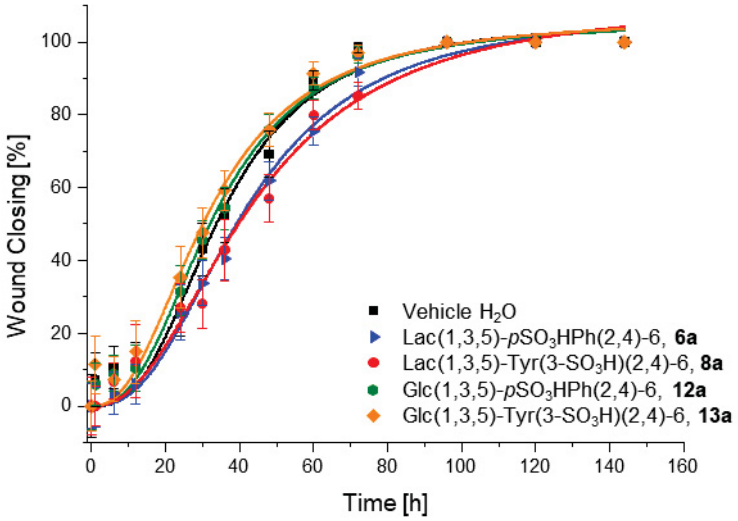

Figure S 130: Results of the migration of assays of MCF7 treated with the vehicle control H_2O (black) and compounds **6a** (blue), **8a** (red), **12a** (green) and **13a** (orange).

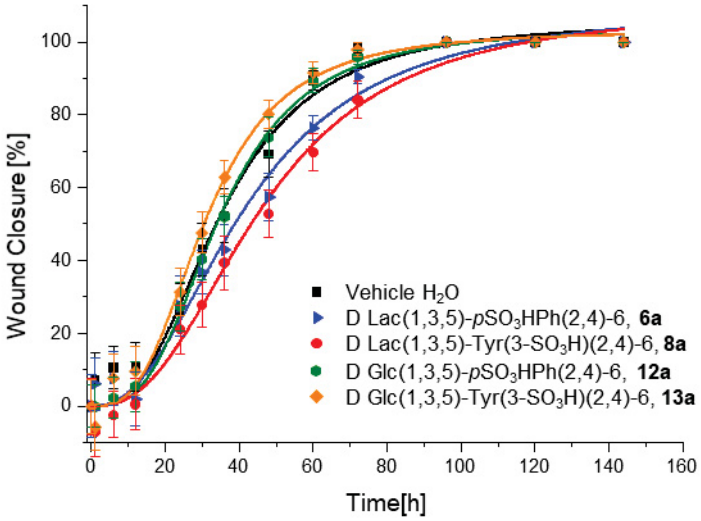

Figure S 131: Results of the migration of assays of MCF7 treated with the vehicle control H_2O (black) and compounds **6a** (blue), **8a** (red), **12a** (green) and **13a** (orange) in a dosing experiment giving extra doses after 12,24,36 and 48 h.

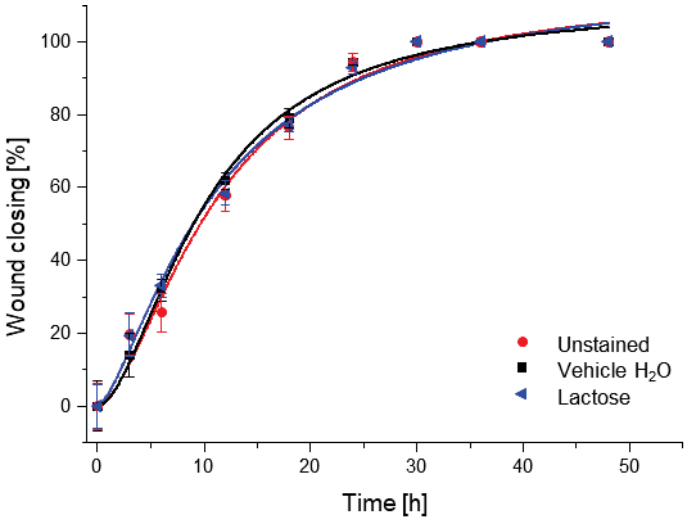

Figure S 132: Results of the migration of assays of HEK 293: Untreated (red), vehicle control with H_2O (black) and treated with lactose (blue).

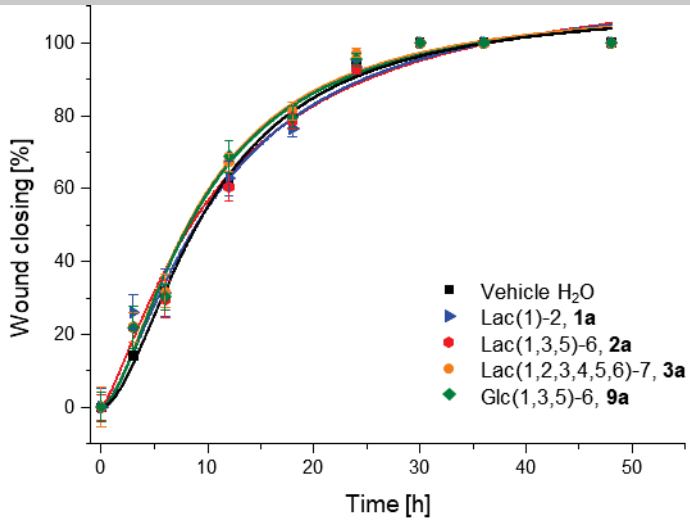

Figure S 133: Results of the migration of assays of HEK 293 treated with the vehicle control H_2O (black) and compounds **1a** (blue), **2a** (red), **3a** (orange) and **9a** (green).

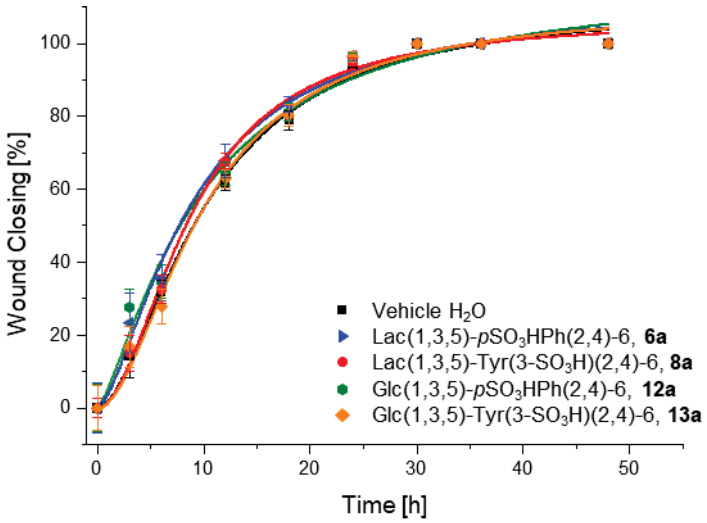

Figure S 134: Results of the migration of assays of HEK 293 treated with the vehicle control H_2O (black) and compounds **6a** (blue), **8a** (red), **12a** (green) and **13a** (orange).

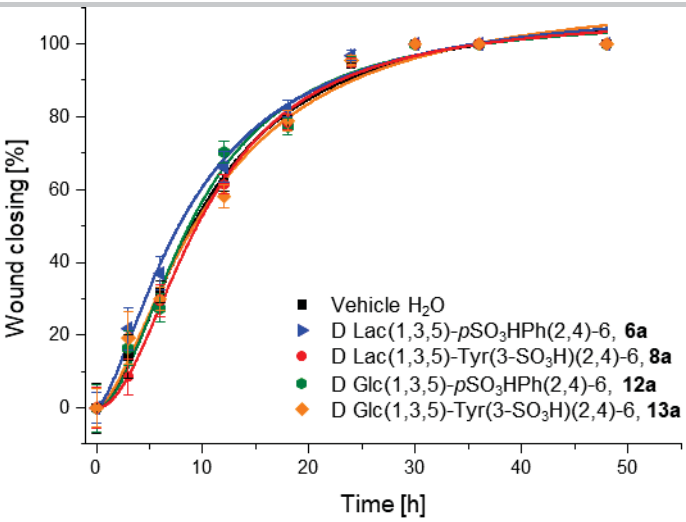

Figure S 135: Results of the migration of assays of HEK 293 treated with the vehicle control H_2O (black) and compounds **6a** (blue), **8a** (red), **12a** (green) and **13a** (orange) in a dosing experiment giving extra doses after 12,24,36 and 48 h.

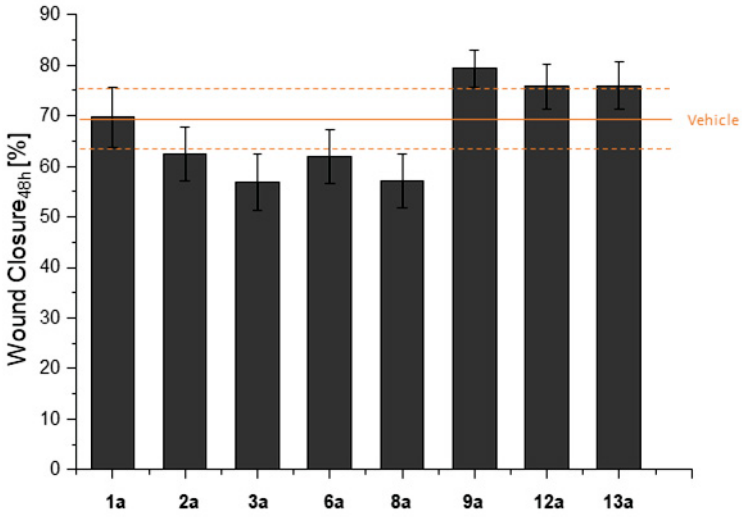

Figure S 136: Comparison of the woundc closure± SD [%] of the MCF 7 cells after 48 h. Vehicle control (orange line) and SD (dotted line).

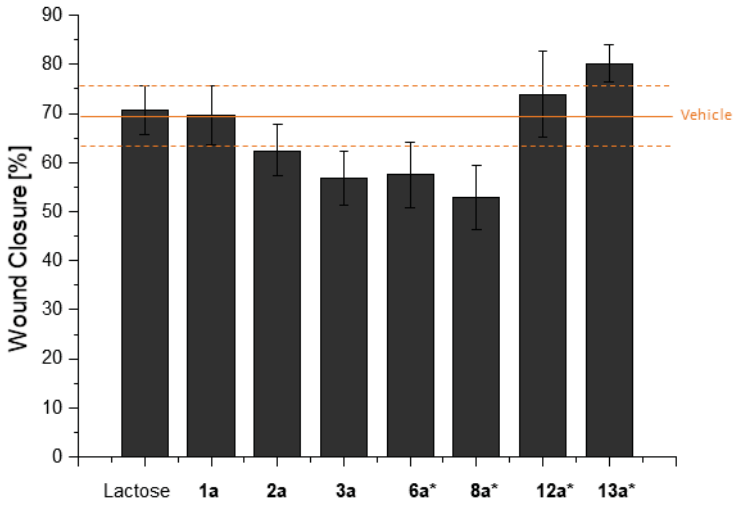

Figure S 137: Comparison of the woundc closure± SD [%] of the MCF 7 cells after 48 h. Vehicle control (orange line) and SD (dotted line). The results of the compounds marked with * are from dosing experiments.

Table S1. Percentage wound closure after 48 h for MCF 7 migration treated with glycoconjugates **1a-3a, 9a** and controls.

Glycoconjugate	Wound closure $_{48\,h}$ + SD [%] [a]
Unstained	69 ± 6
Vehicle Control	69 ± 6
Lactose	71 ± 5
Lac(1)-2, **1a**	70 ± 6
Lac(1,3,5)-6, **2a**	62 ± 5
Lac(1,2,3,4,5,6)-7, **3a**	57 ± 5
Glc(1,3,5)-6, **9a**	79 ± 4

[a] Wound closure with the standard deviation SD [%] was calculated refereeing the distance of the woundfield at time point 48 h to the woundfield at time point 0h. Woundfield distance at 0h was set to 0 % wound closure. Distance value for one timepoint is the average of 25 different distance measurements using an ImageJ software.

Table S2. Percentage wound closure after 48 h for MCF 7 migration treated with glycoconjugates **6a, 8a, 12a** and **13a.**

Glycoconjugates	Wound closure $_{48\,h}$ + SD [%] [a]
Vehicle Control	69 ± 6
Lac(1,3,5)-*p*SO_3HPh(2,4)-6, **6a**	62 ± 5
Lac(1,3,5)-Tyr(3-SO_3H)(2,4)-6, **8a**	57 ± 5
Glc(1,3,5)-*p*SO_3HPh(2,4)-6, **12a**	76 ± 4
Glc(1,3,5)-Tyr(3-SO_3H)(2,4)-6, **13a**	76 ± 5

[a] Wound closure with the standard deviation SD [%] was calculated refereeing the distance of the woundfield at time point 48 h to the woundfield at time point 0h. Woundfield distance at 0h was set to 0 % wound closure. Distance value for one timepoint is the average of 25 different distance measurements using an ImageJ software.

Table S3. Percentage wound closure after 48 h for MCF 7 migration treated with glycoconjugates **6a, 8a, 12a** and **13a** in dosing experiments, giving extra doses after **12, 24,36,48 h.**

Glycoconjugates	Wound closure $_{48\,h}$ + SD [%] [a]
Vehicle Control	69 ± 6
Dosing Lac(1,3,5)-*p*SO_3HPh(2,4)-6, **6a**	58 ± 7
Dosing Lac(1,3,5)-Tyr(3-SO_3H)(2,4)-6, **8a**	53 ± 7
Dosing Glc(1,3,5)-*p*SO_3HPh(2,4)-6, **12a**	74 ± 8
Dosing Glc(1,3,5)-Tyr(3-SO_3H)(2,4)-6, **13a**	80 ± 4

[a] Wound closure with the standard deviation SD [%] was calculated refereeing the distance of the woundfield at time point 48 h to the woundfield at time point 0h. Woundfield distance at 0h was set to 0 % wound closure. Distance value for one timepoint is the average of 25 different distance measurements using an ImageJ software.

Author Contributions

Tanja Freichel synthesized all building blocks and glycooligomers, performed the SPR measurements and cell studies, assisted with the ELISA measurements and drafted the article. Dominic Laaf designed and performed the ELISA measurements in collaboration with Tanja Freichel and Viktoria Heine. Sophia Sarafova assisted with the design of the flow cytometry assays. Lothar Elling provided analytical methods and assisted with the analysis of binding study data. Nicole L. Snyder and Laura Hartmann conceived the project, contributed to the analysis, discussion and interpretation of the data and finalized the article.

References

[1] L. Wu, N. S. Sampson, *ACS Chemical Biology* **2014**, *9*, 468-475.
[2] T. Freichel, S. Eierhoff, N. L. Snyder, L. Hartmann, *The Journal of Organic Chemistry* **2017**, *82*, 9400-9409.
[3] S. Roux, E. Zékri, B. Rousseau, M. Paternostre, J.-C. Cintrat, N. Fay, *Journal of Peptide Science* **2008**, *14*, 354-359.
[4] I. Joachim, S. Rikker, D. Hauck, D. Ponader, S. Boden, R. Sommer, L. Hartmann, A. Titz, *Organic & Biomolecular Chemistry* **2016**, *14*, 7933-7948.
[5] L. Bumba, D. Laaf, V. Spiwok, L. Elling, V. Křen, P. Bojarová, *International Journal of Molecular Sciences* **2018**, *19*, 372.

References

[1] A. Hölemann, P. H. Seeberger *Curr. Opin. Biotechnol.*. **2004**, 15, 615-622.
[2] M. M. Fuster, J. D. Esko *Nat. Rev. Cancer*. **2005**, 5, 526-542.
[3] L. A. Smets, W. P. van Beek *Biochim. Biophys. Acta, Rev. Cancer*. **1984**, 738, 237-249.
[4] B. G. Davis *Chem. Rev.*. **2002**, 102, 579-602.
[5] P. Nangia-Makker, J. Conklin, V. Hogan, A. Raz *Trends Mol. Med.*. **2002**, 8, 187-192.
[6] H. Ghazarian, B. Idoni, S. B. Oppenheimer *Acta Histochem.*. **2011**, 113, 236-247.
[7] K. Murayama, E. J. Nichols, S. B. Levery, W. G. Carter, S.-I. Hakomori *Glycoconjugate J.*. **1984**, 1, 155-169.
[8] E. Gorelik, U. Galili, A. Raz *Cancer Metastasis Rev.*. **2001**, 20, 245-277.
[9] C. Boscher, J. W. Dennis, I. R. Nabi *Curr. Opin. Cell Biol.*. **2011**, 23, 383-392.
[10]F. Liesche, A. C. Kölbl, M. Ilmer, S. Hutter, U. Jeschke, U. Andergassen *Medicine Reports*. **2016**, 13, 4309-4314.
[11] C. J. Thibodeaux, C. E. Melançon, 3rd, H.-w. Liu *Angew Chem Int Ed Engl*. **2008**, 47, 9814-9859.
[12] R. M. Wilson, S. J. Danishefsky *J. Am. Chem. Soc.*. **2013**, 135, 14462-14472.
[13] K. Saraboji, M. Håkansson, S. Genheden, C. Diehl, J. Qvist, U. Weininger, U. J. Nilsson, H. Leffler, U. Ryde, M. Akke, D. T. Logan *Biochemistry*. **2012**, 51, 296-306.
[14] C. Müller, G. Despras, T. K. Lindhorst *Chem. Soc. Rev.*. **2016**, 45, 3275-3302.
[15] R. J. Pieters *Org. Biomol. Chem.*. **2009**, 7, 2013-2025.
[16] D. J. Diestler, E. W. Knapp *The Journal of Physical Chemistry C*. **2010**, 114, 5287-5304.
[17] M. Mammen, S.-K. Choi, G. M. Whitesides *Angew. Chem., Int. Ed.*. **1998**, 37, 2754-2794.
[18] M. Gómez-García, J. M. Benito, R. Gutiérrez-Gallego, A. Maestre, C. O. Mellet, J. M. G. Fernández, J. L. J. Blanco *Org. Biomol. Chem.*. **2010**, 8, 1849-1860.
[19] M. Weber, A. Bujotzek, R. Haag *J. Phys. Chem.*. **2012**, 137, 054111.
[20] S. Cecioni, A. Imberty, S. Vidal *Chem. Rev.*. **2015**, 115, 525-561.
[21] V. Wittmann *Curr. Opin. Chem. Biol.*. **2013**, 17, 982-989.
[22] E. Hochuli, W. Bannwarth, H. Döbeli, R. Gentz, D. Stüber *Bio/Technology*. **1988**, 6, 1321-1325.
[23] B. R. Caré, H. A. Soula *BMC Syst. Biol.*. **2011**, 5, 48-48.
[24] J. Rao, J. Lahiri, R. M. Weis, G. M. Whitesides *J. Am. Chem. Soc.*. **2000**, 122, 2698-2710.
[25] D. Pussak, D. Ponader, S. Mosca, T. Pompe, L. Hartmann, S. Schmidt *Langmuir*. **2014**, 30, 6142-6150.
[26] D. Ponader, P. Maffre, J. Aretz, D. Pussak, N. M. Ninnemann, S. Schmidt, P. H. Seeberger, C. Rademacher, G. U. Nienhaus, L. Hartmann *J. Am. Chem. Soc.*. **2014**, 136, 2008-2016.
[27] L. E. Wilkins, N. Badi, F. Du Prez, M. I. Gibson *ACS Macro Lett.*. **2018**, 7, 1498-1502.
[28] M. W. Jones, L. Otten, S. J. Richards, R. Lowery, D. J. Phillips, D. M. Haddleton, M. I. Gibson *Chemical Science*. **2014**, 5, 1611-1616.
[29] M. L. Wolfenden, M. J. Cloninger *Bioconjugate Chem.*. **2006**, 17, 958-966.
[30] M. I. García-Moreno, F. Ortega-Caballero, R. Rísquez-Cuadro, C. Ortiz Mellet, J. M. García Fernández *Chem. - Eur. J.*. **2017**, 23, 6295-6304.
[31] C. Ortiz Mellet, J.-F. Nierengarten, J. M. García Fernández *J. Mater. Chem. B*. **2017**, 5, 6428-6436.
[32] C. Pifferi, B. Thomas, D. Goyard, N. Berthet, O. Renaudet *Chemistry*. **2017**, 23, 16283-16296.

[33] M. Gómez-García, J. M. Benito, D. Rodríguez-Lucena, J.-X. Yu, K. Chmurski, C. Ortiz Mellet, R. Gutiérrez Gallego, A. Maestre, J. Defaye, J. M. García Fernández *J. Am. Chem. Soc.*. **2005**, 127, 7970-7971.
[34] M. Fukuda *Biol. Pharm. Bull.*. **2012**, 35, 1622-1625.
[35] M.-M. Wei, Y.-S. Wang, X.-S. Ye *Med. Res. Rev.*. **2018**, 38, 1003-1026.
[36] E. Dabelsteen *J. Pathol.*. **1996**, 179, 358-369.
[37] L. Veillon, C. Fakih, H. Abou-El-Hassan, F. Kobeissy, Y. Mechref *ACS Chem. Neurosci.*. **2018**, 9, 51-72.
[38] R. Roy, T. C. Shiao, K. Rittenhouse-Olson *Braz. J. Pharm. Sci.*. **2013**, 49, 85-108.
[39] T. Buskas, P. Thompson, G.-J. *Chem. Commun. (Cambridge, U. K.)*. **2009**, 5335-5349.
[40] G. Ragupathi, D. M. Coltart, L. J. Williams, F. Koide, E. Kagan, J. Allen, C. Harris, P. W. Glunz, P. O. Livingston, S. J. Danishefsky *Proc. Natl. Acad. Sci.*. **2002**, 99, 13699-13704.
[41] S. F. Slovin, G. Ragupathi, C. Musselli, C. Fernandez, M. Diani, D. Verbel, S. Danishefsky, P. Livingston, H. I. Scher *Cancer Immunol. Immunother.*. **2005**, 54, 694-702.
[42] S. F. Slovin, S. J. Keding, G. Ragupathi *Immunol. Cell Biol.*. **2005**, 83, 418-428.
[43] C. Bies, C.-M. Lehr, J. F. Woodley *Adv. Drug Delivery Rev.*. **2004**, 56, 425-435.
[44] L. Cai, Z. Gu, J. Zhong, D. Wen, G. Chen, L. He, J. Wu, Z. Gu *Drug Discovery Today*. **2018**, 23, 1126-1138.
[45] V. L. Campo, M. F. Marchiori, L. C. Rodrigues, M. Dias-Baruffi *Glycoconjugate J.*. **2016**, 33, 853-876.
[46] A. C. F. Cardoso, L. N. d. S. Andrade, S. O. Bustos, R. Chammas *Front. Oncol.*. **2016**, 6, 1-12.
[47] C. A. Duckworth, S. E. Guimond, P. Sindrewicz, A. J. Hughes, N. S. French, L.-Y. Lian, E. A. Yates, D. M. Pritchard, J. M. Rhodes, J. E. Turnbull, L.-G. Yu *Oncotarget*. **2015**, 6, 23671-23687.
[48] A. Lagana, J. G. Goetz, P. Cheung, A. Raz, J. W. Dennis, I. R. Nabi *Mol. Cell. Biol.*. **2006**, 26, 3181-3193.
[49] A. K. Michel, P. Nangia-Makker, A. Raz, M. J. Cloninger *Chembiochem*. **2014**, 15, 2106-2112.
[50] Y. Takenaka, T. Fukumori, A. Raz *Glycoconjugate J.*. **2002**, 19, 543-549.
[51] D. Compagno, F. M. Jaworski, L. Gentilini, G. Contrufo, I. G. Perez, M. T. Elola, N. Pregi, G. A. Rabinovich, D. J. Laderach *Curr. Mol. Med.*. **2014**, 14, 630-651.
[52] I. R. Nabi, J. Shankar, J. W. Dennis *J. Cell Sci.*. **2015**, 128, 2213-2219.
[53] N. Ahmad, H.-J. Gabius, S. André, H. Kaltner, S. Sabesan, R. Roy, B. Liu, F. Macaluso, C. F. Brewer *J. Biol. Chem.*. **2004**, 279, 10841-10847.
[54] E. M. Rapoport, O. V. Kurmyshkina, N. V. Bovin *Biochemistry (Moscow)*. **2008**, 73, 393-405.
[55] V. Denavit, D. Lainé, T. Tremblay, J. St-Gelais, D. Giguère *Trends Glycosci. Glycotechnol.*. **2018**, 30, SE21-SE40.
[56] H. Blanchard, X. Yu, P. M. Collins, K. Bum-Erdene *Expert Opin. Ther. Pat.*. **2014**, 24, 1053-1065.
[57] J. Seetharaman, A. Kanigsberg, R. Slaaby, H. Leffler, S. H. Barondes, J. M. Rini *J. Biol. Chem.*. **1998**, 273, 13047-13052.
[58] C. T. Öberg, H. Leffler, U. J. Nilsson *CHIMIA Int. J. Chem.*. **2011**, 65, 18-23.
[59] P. Sörme, P. Arnoux, B. Kahl-Knutsson, H. Leffler, J. M. Rini, U. J. Nilsson *J. Am. Chem. Soc.*. **2005**, 127, 1737-1743.

[60] M. F. Marchiori, D. E. Pires Souto, L. Oliveira Bortot, J. Francisco Pereira, L. T. Kubota, R. D. Cummings, M. Dias-Baruffi, I. Carvalho, V. L. Campo *Bioorg. Med. Chem.*. **2015**, 23, 3414-3425.
[61] S. G. Gouin, J. M. García Fernández, E. Vanquelef, F.-Y. Dupradeau, E. Salomonsson, H. Leffler, M. Ortega-Muñoz, U. J. Nilsson, J. Kovensky *ChemBioChem*. **2010**, 11, 1430-1442.
[62] S. R. Rauthu, T. C. Shiao, S. André, M. C. Miller, É. Madej, K. H. Mayo, H.-J. Gabius, R. Roy *ChemBioChem*. **2015**, 16, 126-139.
[63] J. Tejler, H. Leffler, U. J. Nilsson *Bioorg. Med. Chem. Letters*. **2005**, 15, 2343-2345.
[64] P. Sörme, B. Kahl-Knutsson, M. Huflejt, U. J. Nilsson, H. Leffler *Anal. Biochem.*. **2004**, 334, 36-47.
[65] Y.-C. Chan, H.-Y. Lin, Z. Tu, Y.-H. Kuo, S.-T. Hsu, C.-H. Lin *Int. J. Mol. Sci.*. **2018**, 19, 392.
[66] T. Delaine, I. Cumpstey, L. Ingrassia, M. L. Mercier, P. Okechukwu, H. Leffler, R. Kiss, U. J. Nilsson *J. Med. Chem.*. **2008**, 51, 8109-8114.
[67] A. Mackinnon, L. Nicol, J. Walker, P. Ford, H. Schambye, A. Pederson, U. Nilsson, H. Leffler, T. Thomas, D. Francombe, J. Simpson, M. Gibbons, T. M. Maher in *TD139, A Novel Inhaled Galectin-3 Inhibitor for the Treatment of Idiopathic Pulmonary Fibrosis (IPF). Results from the First in (IPF) Patients Study, Vol.*, pp.A7560-A7560.
[68] J. Brunetti, L. Depau, C. Falciani, M. Gentile, E. Mandarini, G. Riolo, P. Lupetti, A. Pini, L. Bracci *Sci. Rep.*. **2016**, 6, 27174.
[69] Q. Xiao, A.-K. Ludwig, C. Romanò, I. Buzzacchera, S. E. Sherman, M. Vetro, S. Vértesy, H. Kaltner, E. H. Reed, M. Möller, C. J. Wilson, D. A. Hammer, S. Oscarson, M. L. Klein, H.-J. Gabius, V. Percec *Proc. Natl. Acad. Sci.*. **2018**, 115, E2509-E2518.
[70] H. Tateno, A. Mori, N. Uchiyama, R. Yabe, J. Iwaki, T. Shikanai, T. Angata, H. Narimatsu, J. Hirabayashi *Glycobiology*. **2008**, 18, 789-798.
[71] S. R. Stowell, C. M. Arthur, P. Mehta, K. A. Slanina, O. Blixt, H. Leffler, D. F. Smith, R. D. Cummings *The J. Biol. Chem.*. **2008**, 283, 10109-10123.
[72] C. T. Öberg, H. Leffler, U. J. Nilsson *J. Med. Chem.*. **2008**, 51, 2297-2301.
[73] C. T. Öberg, A.-L. Noresson, H. Leffler, U. J. Nilsson *Chem. - Eur. J.*. **2011**, 17, 8139-8144.
[74] M. L. Talaga, N. Fan, A. L. Fueri, R. K. Brown, P. Bandyopadhyay, T. K. Dam *Biochemistry*. **2016**, 55, 4541-4551.
[75] C. Bonduelle, H. Oliveira, C. Gauche, J. Huang, A. Heise, S. Lecommandoux *Chem. Commun.*. **2016**, 52, 11251-11254.
[76] A. J. Cagnoni, J. Kovensky, M. L. Uhrig *J. Org. Chem.*. **2014**, 79, 6456-6467.
[77] T. K. Dam, H.-J. Gabius, S. André, H. Kaltner, M. Lensch, C. F. Brewer *Biochemistry*. **2005**, 44, 12564-12571.
[78] C. K. Goodman, M. L. Wolfenden, P. Nangia-Makker, A. K. Michel, A. Raz, M. J. Cloninger *Beilstein J. Org. Chem.*. **2014**, 10, 1570-1577.
[79] D. Laaf, P. Bojarová, H. Pelantová, V. Křen, L. Elling *Bioconjugate Chem.*. **2017**, 28, 2832-2840.
[80] H. Wang, W. Huang, J. Orwenyo, A. Banerjee, G. R. Vasta, L.-X. Wang *Bioorg. Med. Chem.*. **2013**, 21, 2037-2044.
[81] M. Wolfenden, J. Cousin, P. Nangia-Makker, A. Raz, M. Cloninger *Molecules*. **2015**, 20, 7059-7096.
[82] H. Zhang, D. Laaf, L. Elling, R. J. Pieters *Bioconjugate Chem.*. **2018**, 29, 1266-1275.
[83] S. André, R. J. Pieters, I. Vrasidas, H. Kaltner, I. Kuwabara, F.-T. Liu, R. M. J. Liskamp, H.-J. Gabius *ChemBioChem*. **2001**, 2, 822-830.

[84] L. Bumba, D. Laaf, V. Spiwok, L. Elling, V. Křen, P. Bojarová *Int. J. Mol. Sci.*. **2018**, 19, 372.
[85] J. H. Ennist, H. R. Termuehlen, S. P. Bernhard, M. S. Fricke, M. J. Cloninger *Bioconjugate Chem.*. **2018**, 29, 4030-4039.
[86] S. André, B. Liu, H.-J. Gabius, R. Roy *Org. Biomol. Chem.*. **2003**, 1, 3909-3916.
[87] L. Abbassi, Y. M. Chabre, N. Kottari, A. A. Arnold, S. André, J. Josserand, H.-J. Gabius, R. Roy *Polym Chem-Uk*. **2015**, 6, 7666-7683.
[88] S. Böcker, D. Laaf, L. Elling *Biomolecules*. **2015**, 5, 1671.
[89] O. Oyelaran, J. C. Gildersleeve *Curr. Opin. Chem. Biol.*. **2009**, 13, 406-413.
[90] Richard D. Cummings, J. M. Pierce *Chem. Biol.*. **2014**, 21, 1-15.
[91] A. Bernardi, J. Jiménez-Barbero, A. Casnati, C. De Castro, T. Darbre, F. Fieschi, J. Finne, H. Funken, K.-E. Jaeger, M. Lahmann, T. K. Lindhorst, M. Marradi, P. Messner, A. Molinaro, P. V. Murphy, C. Nativi, S. Oscarson, S. Penadés, F. Peri, R. J. Pieters, O. Renaudet, J.-L. Reymond, B. Richichi, J. Rojo, F. Sansone, C. Schäffer, W. B. Turnbull, T. Velasco-Torrijos, S. Vidal, S. Vincent, T. Wennekes, H. Zuilhof, A. Imberty *Chem. Soc. Rev.*. **2013**, 42, 4709-4727.
[92] C. Gerke, M. Ebbesen, D. Jansen, S. Boden, T. Freichel, L. Goodwin, F. Pieper, A. C. de la Calle, S. Schmidt, L. Hartmann *Abstracts of Papers of the American Chemical Society*. **2017**, 254.
[93] V. Ladmiral, E. Melia, D. M. Haddleton *Eur. Polym. J.*. **2004**, 40, 431-449.
[94] S. G. Spain, M. I. Gibson, N. R. Cameron *J. Polym. Sci., Part A: Polym. Chem.*. **2007**, 45, 2059-2072.
[95] E. Fernandez-Megia, J. Correa, I. Rodríguez-Meizoso, R. Riguera *Macromolecules*. **2006**, 39, 2113-2120.
[96] W. B. Turnbull, J. F. Stoddart *Rev. Mol. Biotechnol.*. **2002**, 90, 231-255.
[97] B. E. Collins, J. C. Paulson *Curr. Opin. Chem. Biol.*. **2004**, 8, 617-625.
[98] M. Abellán Flos, M. I. García Moreno, C. Ortiz Mellet, J. M. García Fernández, J.-F. Nierengarten, S. P. Vincent *Chem. - Eur. J.*. **2016**, 22, 11450-11460.
[99] S. Zhou, P. Trochimczyk, L. Sun, S. Hou, H. Li *Curr. Org. Chem.*. **2016**, 20, 1490-1501.
[100] E.-C. Wamhoff, J. Schulze, L. Bellmann, G. Bachem, F. F. Fuchsberger, J. Rademacher, M. Hermann, B. Del Frari, R. van Dalen, D. Hartmann, N. van Sorge, O. Seitz, P. Stoitzner, C. Rademacher *bioRxiv*. **2018**.
[101] G.-J. Boons *Expert Rev Vaccines*. **2010**, 9, 1251-1256.
[102] N. Jayaraman, K. Maiti, K. Naresh *Chem. Soc. Rev.*. **2013**, 42, 4640-4656.
[103] S. Boden, K. Wagner, M. Karg, L. Hartmann *Polymers*. **2017**, 9, 716.
[104] K. Sakurai, Y. Hatai, A. Okada *Chemical Science*. **2016**, 7, 702-706.
[105] I. Sinaida, R. Susanna, M. Anne, K. Katharina, B. Sophia, F. Claudia, L. T. K., W. Marcus, H. Laura *Macromol. Biosci.*. **2017**, 17, 1700198.
[106] F. Jacobi, A. Camaleño de la Calle, S. Boden, A. Grafmüller, L. Hartmann, S. Schmidt *Biomacromolecules*. **2018**, 19, 3479-3488.
[107] C. Gerke, M. F. Ebbesen, D. Jansen, S. Boden, T. Freichel, L. Hartmann *Biomacromolecules*. **2017**, 18, 787-796.
[108] D. Ponader, F. Wojcik, F. Beceren-Braun, J. Dernedde, L. Hartmann *Biomacromolecules*. **2012**, 13, 1845-1852.
[109] M. Baier, M. Giesler, L. Hartmann *Chem. - Eur. J.*. **2018**, 24, 1619-1630.
[110] T. Freichel, S. Eierhoff, N. L. Snyder, L. Hartmann *J. Org. Chem.*. **2017**, 82, 9400-9409.
[111] F. Wojcik, S. Lel, A. G. O'Brien, P. H. Seeberger, L. Hartmann *Beilstein J. Org. Chem.*. **2013**, 9, 2395-2403.

[112] R. B. Merrifield *J. Am. Chem. Soc.*. **1963**, 85, 2149-2154.
[113] E. Fischer, E. Fourneau *Ber. Dtsch. Chem. Ges.*. **1901**, 34, 2868-2877.
[114] M. Bergmann, L. Zervas *Ber. Dtsch. Chem. Ges. .A and B*. **1932**, 65, 1192-1201.
[115] V. d. Vigneaud, C. Ressler, C. J. M. Swan, C. W. Roberts, P. G. Katsoyannis, S. Gordon *J. Am. Chem. Soc.*. **1953**, 75, 4879-4880.
[116] R. B. Merrifield in Automated Peptide Synthesis, Springer Berlin Heidelberg, City, **1966**, pp.1-13.
[117] R. S. Hodges, R. B. Merrifield *Anal. Biochem.*. **1975**, 65, 241-272.
[118] V. K. Sarin, S. B. H. Kent, J. P. Tam, R. B. Merrifield *Anal. Biochem.*. **1981**, 117, 147-157.
[119] R. A. Houghten *Proc. Natl. Acad. Sci.*. **1985**, 82, 5131-5135.
[120] S. C. Miller, T. S. Scanlan *J. Am. Chem. Soc.*. **1998**, 120, 2690-2691.
[121] G. Sabatino, A. M. Papini *Curr Opin Drug Discov Devel*. **2008**, 11, 762-770.
[122] T. I. Al-Warhi, H. M. A. Al-Hazimi, A. El-Faham *J. Saudi Chem. Soc.*. **2012**, 16, 97-116.
[123] V. Mäde, S. Els-Heindl, A. G. Beck-Sickinger *Beilstein J. Org. Chem.*. **2014**, 10, 1197-1212.
[124] D. s. M. M. Jaradat *Amino Acids*. **2018**, 50, 39-68.
[125] J. M. Palomo *RSC Adv.*. **2014**, 4, 32658-32672.
[126] G. B. Fields, R. L. Noble *Int. J. Pept. Protein Res.*. **1990**, 35, 161-214.
[127] A. Isidro-Llobet, M. Álvarez, F. Albericio *Chem. Rev.*. **2009**, 109, 2455-2504.
[128] P. T. Shelton, K. J. Jensen in *Linkers, Resins, and General Procedures for Solid-Phase Peptide Synthesis,* Humana Press, Totowa, NJ, **2013**, pp.23-41.
[129] J. Alsina, F. Albericio *Pept. Sci.*. **2003**, 71, 454-477.
[130] K. Barlos, D. Gatos, J. Kallitsis, G. Papaphotiu, P. Sotiriu, Y. Wenqing, W. Schäfer *Tetrahedron Lett.*. **1989**, 30, 3943-3946.
[131] O. Luna, J. Gomez, C. Cárdenas, F. Albericio, S. Marshall, F. Guzmán *Molecules*. **2016**, 21, 1542.
[132] C. A. G. N. Montalbetti, V. Falque, *ChemInform*, **2005,**61,10827-10852.
[133] Y. S. Klausner, M. Bodansky *Synthesis*. **1972**, 1972, 453-463.
[134] E. Valeur, M. Bradley *Chem. Soc. Rev.*. **2009**, 38, 606-631.
[135] J. Coste, E. Frerot, P. Jouin *J. Org. Chem.*. **1994**, 59, 2437-2446.
[136] L. A. Carpino, A. El-Faham, F. Albericio *Tetrahedron Lett.*. **1994**, 35, 2279-2282.
[137] W. König, R. Geiger *Chem. Ber.*. **1970**, 103, 788-798.
[138] L. A. Carpino, H. Imazumi, A. El-Faham, F. J. Ferrer, C. Zhang, Y. Lee, B. M. Foxman, P. Henklein, C. Hanay, C. Mügge, H. Wenschuh, J. Klose, M. Beyermann, M. Bienert *Angew. Chem., Int. Ed.*. **2002**, 41, 441-445.
[139] R. B. Merrifield *Science*. **1965**, 150, 178-185.
[140] R. Frank *J. Immunol. Methods*. **2002**, 267, 13-26.
[141] S. L. Pedersen, K. J. Jensen in *Instruments for Automated Peptide Synthesis*, Humana Press, Totowa, NJ, **2013**, pp.215-224.
[142] D. Riester, K.-H. Wiesmüller, D. Stoll, R. Kuhn *Anal. Chem.*. **1996**, 68, 2361-2365.
[143] G. G. Smith, T. Sivakua *J. Org. Chem.*. **1983**, 48, 627-634.
[144] P. D'Arrigo, D. Arosio, L. Cerioli, D. Moscatelli, S. Servi, F. Viani, D. Tessaro *Tetrahedron: Asymmetry*. **2011**, 22, 851-856.
[145] P. Li, Y.-L. Yin, D. Li, S. Woo Kim, G. Wu *Br. J. Nutr.*. **2007**, 98, 237-252.
[146] Y. Junya, A. Ayatoshi, T. Kenji *Curr. Rheumatol. Rev.*. **2009**, 5, 252-258.
[147] A. Boeijen, J. van Ameijde, R. M. J. Liskamp *J. Org. Chem.*. **2001**, 66, 8454-8462.

[148] M.-A. Poupart, D. R. Cameron, C. Chabot, E. Ghiro, N. Goudreau, S. Goulet, M. Poirier, Y. S. Tsantrizos *J. Org. Chem.*. **2001**, 66, 4743-4751.
[149] A. G. M. Barrett, A. J. Hennessy, R. L. Vézouët, P. A. Procopiou, P. W. Seale, S. Stefaniak, R. J. Upton, A. J. P. White, D. J. Williams *J. Org. Chem.*. **2004**, 69, 1028-1037.
[150] E. Biron, J. Chatterjee, H. Kessler *Org. Lett.*. **2006**, 8, 2417-2420.
[151] D. M. Rothman, M. E. Vazquez, E. M. Vogel, B. Imperiali *J. Org. Chem.*. **2003**, 68, 6795-6798.
[152] B. M. Zeglis, F. Emmetiere, N. Pillarsetty, R. Weissleder, J. S. Lewis, T. Reiner *ChemistryOpen*. **2014**, 3, 48-53.
[153] K. G. Varnava, V. Sarojini *Chem. - Asian J.*. **2019**, 14, 1088-1097.
[154] G. Barany, R. B. Merrifield *J. Am. Chem. Soc.*. **1977**, 99, 7363-7365.
[155] C.-H. Wong, S. C. Zimmerman *Chem. Commun.*. **2013**, 49, 1679-1695.
[156] F. Wojcik, S. Mosca, L. Hartmann *J. Org. Chem.*. **2012**, 77, 4226-4234.
[157] L. Hartmann, E. Krause, M. Antonietti, H. G. Börner *Biomacromolecules*. **2006**, 7, 1239-1244.
[158] F. Wojcik, A. G. O'Brien, S. Götze, P. H. Seeberger, L. Hartmann *Chem. - Eur. J.*. **2013**, 19, 3090-3098.
[159] C. Gerke, F. Jacobi, L. E. Goodwin, F. Pieper, S. Schmidt, L. Hartmann *Macromolecules*. **2018**, 51, 5608-5619.
[160] I. Joachim, S. Rikker, D. Hauck, D. Ponader, S. Boden, R. Sommer, L. Hartmann, A. Titz *Org. Biomol. Chem.*. **2016**, 14, 7933-7948.
[161] D. Ponader, S. Igde, M. Wehle, K. Märker, M. Santer, D. Bléger, L. Hartmann *Beilstein J. Org. Chem.*. **2014**, 10, 1603-1612.
[162] C. D. Hein, X.-M. Liu, D. Wang *Pharm. Res.*. **2008**, 25, 2216-2230.
[163] C. E. Hoyle, C. N. Bowman *Angew. Chem., Int. Ed.*. **2010**, 49, 1540-1573.
[164] H. C. Kolb, K. B. Sharpless *Drug Discovery Today*. **2003**, 8, 1128-1137.
[165] R. Huisgen *Angew. Chem., Int. Ed. in English*. **1963**, 2, 565-598.
[166] N. J. Agard, J. A. Prescher, C. R. Bertozzi *J. Am. Chem. Soc.*. **2004**, 126, 15046-15047.
[167] B. T. Worrell, J. A. Malik, V. V. Fokin *Science (New York, N.Y.)*. **2013**, 340, 457-460.
[168] M. Baier, J. L. Ruppertz, M. M. Pfleiderer, B. S. Blaum, L. Hartmann *Chem. Commun.*. **2018**, 54, 10487-10490.
[169] H. Staudinger, J. Meyer *Helv. Chim. Acta*. **1919**, 2, 635-646.
[170] E. Saxon, J. I. Armstrong, C. R. Bertozzi *Org. Lett.*. **2000**, 2, 2141-2143.
[171] B. L. Nilsson, R. J. Hondal, M. B. Soellner, R. T. Raines *J. Am. Chem. Soc.*. **2003**, 125, 5268-5269.
[172] J. P. Malkinson, R. A. Falconer, I. Toth *J. Org. Chem.*. **2000**, 65, 5249-5252.
[173] M. Köhn, R. Breinbauer *Angew. Chem., Int. Ed.*. **2004**, 43, 3106-3116.
[174] H.-A. Tran, P. I. Kitov, E. Paszkiewicz, J. M. Sadowska, D. R. Bundle *Org. Biomol. Chem.*. **2011**, 9, 3658-3671.
[175] R. S. Loka, M. S. McConnell, H. M. Nguyen *Biomacromolecules*. **2015**, 16, 4013-4021.
[176] J. L. Jiménez Blanco, C. Ortiz Mellet, J. M. García Fernández *Chem. Soc. Rev.*. **2013**, 42, 4518-4531.
[177] J.-M. Lehn *Chem. - Eur. J.*. **1999**, 5, 2455-2463.
[178] O. Ramström, J.-M. Lehn *ChemBioChem*. **2000**, 1, 41-48.
[179] O. Ramström, S. Lohmann, T. Bunyapaiboonsri, J.-M. Lehn *Chem. - Eur. J.*. **2004**, 10, 1711-1715.
[180] B. Thomas, M. Fiore, I. Bossu, P. Dumy, O. Renaudet *Beilstein J. Org. Chem.*. **2012**, 8, 421-427.

[181] G. C. Daskhan, C. Pifferi, O. Renaudet *ChemistryOpen*. **2016**, 5, 477-484.
[182] B. Thomas, M. Fiore, G. C. Daskhan, N. Spinelli, O. Renaudet *Chem. Commun.*. **2015**, 51, 5436-5439.
[183] L. Xue, X. Xiong, K. Chen, Y. Luan, G. Chen, H. Chen *Polym Chem-Uk*. **2016**, 7, 4263-4271.
[184] J. Katajisto, T. Karskela, P. Heinonen, H. Lönnberg *J. Org. Chem.*. **2002**, 67, 7995-8001.
[185] P. Reuther, Master Thesis, University Duesseldorf, **2017**.
[186] I. Vrasidas, S. André, P. Valentini, C. Böck, M. Lensch, H. Kaltner, R. M. J. Liskamp, H.-J. Gabius, R. J. Pieters *Org. Biomol. Chem.*. **2003**, 1, 803-810.
[187] H. Blanchard, K. Bum-Erdene, M. H. Bohari, X. Yu *Expert Opin. Ther. Pat.*. **2016**, 26, 537-554.
[188] D. Johann, D. Frédérique, S. Nataliya, A. Tamara, L. Annie, V. Mireille, T. Charles, D. Christophe, P. Françoise, G. Cyrille *ChemBioChem*. **2017**, 18, 782-789.
[189] D. Johann, A. Tamara, S. Nataliya, D. Samir, L. Annie, D. Frédérique, V. Mireille, T. Charles, P. Françoise, T. Stéphane, D. Christophe, T. Hiroaki, H. Jun, G. Cyrille *ChemBioChem*. **2017**, 18, 2428-2440.
[190] M. Xie, F. Vesuna, M. Botlagunta, G. M. Bol, A. Irving, Y. Bergman, R. S. Hosmane, Y. Kato, P. T. Winnard, V. Raman *Oncotarget*. **2015**, 6, 29901-29913.
[191] N. Bertleff-Zieschang, J. Bechold, C. Grimm, M. Reutlinger, P. Schneider, G. Schneider, J. Seibel *ChemBioChem*. **2017**, 18, 1477-1481.
[192] I. Cumpstey, E. Salomonsson, A. Sundin, H. Leffler, U. J. Nilsson *Chem. - Eur. J.*. **2008**, 14, 4233-4245.
[193] L. R. Prost, J. C. Grim, M. Tonelli, L. L. Kiessling *ACS Chem. Biol.*. **2012**, 7, 1603-1608.
[194] X. Chen, L. Hui, D. A. Foster, C. M. Drain *Biochemistry*. **2004**, 43, 10918-10929.
[195] T. J. Dougherty, C. J. Gomer, B. W. Henderson, G. Jori, D. Kessel, M. Korbelik, J. Moan, Q. Peng *J. Natl. Cancer Inst.*. **1998**, 90, 889-905.

Appendix

1. List of Abbreviations

Arg	Arginine
ASF	Asialofetuin
Asn	Asparagine
BADS	beznyl azide diethylenetriamine succinic acid
BOP	(Benzotriazol-1-yloxy)tris(dimethylamino)phosphonium hexafluorophosphate
CFG	Consortium for Functional Glycomics
CRD	Carbohydrate recognition domain
CuAAC	Copper-catalyzed azide-alkyne cycloaddition
DBF	Dibenzofulvene
DCM	Dichlormethane
DDS	Drug delivery system
DDS	Double bond diethylenetriamine succinic acid
DIC	Diisopropylcarbodiimide
DIC	Diisopropylcarbodiimid
DIPEA	Diisoproylethylamine
DMF	*N*,*N*-Dimethylformamide
DMSO	Dimethylsulfoxide
e.g.	Exempli gratia (for example)
EDC	1-Ethyl-3-(3-dimethylaminopropyl)carbodiimide
EDS	Ethylene glycol diamine succinic acid
ELISA	Enzyme-Linked immunosorbent assay
et al.	Et alii (and other)
Fmoc	9- Fluorenylmethoxycarbonyl
FSC	Forward scattered
Gal-3	Galectin-3
Glu	Glutamic acid
HATU	O-(7-Azabenzotriazol-1-yl)-N,N,N′,N′-tetramethyluronium-hexafluorphosphat
His	Histidine
HOBt	1-Hydroxybenzotriazole
HRP	Horseradish peroxidase
kDa	Kilo Dalton
Lac	Lactose
LacNAc	N-Acetyllactosamine
MDS	Methyl succinyl diethylenetriamine succinic acid
MTT	Methyl-thiazolyl-tetrazolium
NADH	Nicotinamide adenine dinucleotide hydrogen
NDS	Norbonene diethylenetriamine succinic acid
NHS	N-Hydroxysuccinimide
Ni-NTA	Nickel - nitrilotriacetic acid
ODS	Octyl diamine succinic acid

PyBOP	Benzotriazol-1-yl-oxytripyrrolidinophosphonium hexafluorophosphate
RU	Response unit
SDS	Short diamine succinic acid
SPR	Surface plasmon resonance
SSC	Sideward scattered
STF	Sialylated Thomson-Friedenreich
STn	Sialylated Thomson-nouveau
TACA	Tumor-associated carbohydrate antigens
TDG	Thiodigalactoside
TDS	Triple bond diethylenetriamine succinic acid
TF	Thomson-Friedenreich
TMB	Tetramethylbenzidine
Tn	Thomson-nouveau
Try	Tyrosine

2. List of Figures

Acknowledgments

Mein erster Dank geht an Prof. Dr. Laura Hartmann, für die Möglichkeit in Ihrer Arbeitsgruppe ein neues, interessantes und vielversprechendes Themengebiet der Chemie kennenzulernen und dort meine Dissertation anzufertigen. Ich danke Ihr für die Bereitstellung des interesanten Themas, für das einhergende Vertrauen und die zahlreichen produktiven Gespräche. Gleichzeitig danke ich Ihr für die Möglichkeit der Eigenständigkeit und die Verwirklichung eigener Ideen. Sie hat sowohl auf persönlicher als auch fachlicher Ebene einen großen Anteil an der Umsetzung und Erfolg dieser Arbeit. Des Weiteren danke ich Ihr für die Möglichkeit und das damit verbundene Vertrauen, einen Forschungsaufenthalt in Davidson, North Carolina, USA wahrzunhemen.

Prof. Dr. Jörg Pietruszka danke ich sehr für die Übernahme der Zweitkorrektur meiner Arbeit.

Ein weiterer besonderer Dank richtet sich an Prof. Dr. Nicole L. Snyder. Sie war über die Jahre nich nur als Kooperationspartnerin, sondern auch als Gastprofessorin, während meines Forschungsaufenthaltes in Davidson durch Ihre Expertise und Motivation am Gelingen dieser Arbeit beteiligt. Ich danke Ihr für die Zeit und Hingabe, besonders während meiner Zeit in Davidson.

Des Weiteren möchte ich dem Team von Prof. Dr. Laura Hartmann danken. Dabei geht ein besonderer Dank an Frau Dr. Monir Tabatabai, Frau Stephanie Scheelen sowie Frau Michaela Kitza, welche durch Ihre Hilfsbereitschaft und Fürsorge zum reibungslosen Verlauf der Promotion beigetragen haben. Des Weiteren danke ich ebenfalls Frau Sonja Coors, Frau Birgit Ohler, Frau Maria Breuer und Frau Viola Schürmanns für Ihre Hilfe.

Ein besonderer Dank geht an Luca Ceasar, Miriam Hoffmann und Patrick Konietzny, welche durch ihre hervorragende Arbeit im Zuge ihrer Bachelor bzw Masterarbeiten, nicht nur fachlich, sondern auch auf persönlicher Ebene zum Gelingen dieser Arbeit beigetragen haben.

Ein weiterer Dank geht an die gesamte Gruppe, insbesondere an meine sehr wertgeschätzen Laborkollegen Kira Neuhaus, Miriam Hoffmann, Patrick Konietzny, Mischa Baier und Katharina Bücher und an das sehr lustige Büro mit Lukas Fischer, Dana Itskalov und Kira Neuhaus. Auch die Anfangszeit mit Katharina Bücher, Alexander Strzelczyk, Alberto Alberto Camaleño de la Calle, Hanqing Wang möchte ich nicht missen. Des Weiteren Danke ich allen für die legendären Klassenfahrten und lustige Grillfeiern, die es so gab. Ein klasse Team. Ein besonderer Dank geht

zudem an das SPR-Team mit Sophia Boden und Markus Giesler. Nicht zu vergessen sind natürlich Tanja Paul, Christoph Gerke und alle Mädels.

Ein großer Dank, geht an alle die, die mir im Zuge meines Forschungsaufenthalts am Davidson College in North Carolina geholfen haben. Zunächst möchte ich dem "Junior Scientist and International Researcher Center "(JUNO) für die finanzielle Unterstützung im Zuge Forscher Alumni Programm - StayConnected@HHU danken. Neben Laura Hartmann und Nicole Snyder für die Möglichkeit, geht mein größter Dank an Prof. Dr. Sophia Sarafova, welche durch Ihre Expertise in biologischen Fragestellungen einen wesentlichen Anteil am Gelingen der Zellstudien hatte. Der zweite Dank geht an Nika Fendler, die mir in meiner Zeit am Davidson College nicht nur mit den Zellen geholfen hat, sondern auch Privat das Leben am Davidson College zeigte. Auch möchte ich hier die Chance nutzen, Julia Meisel erstens für Ihre Arbeit am Staudinger Projekt und zweitens für die schöne Zeit in Davidson zu danken.

Ebenfalls danke ich der Gruppe von Prof. Dr. Lothar Elling der RWTH Aachen für die erfolgreiche Kooperation. Mein besonderer Dank gilt dabei Dominic Laaf für die angenehme und produktive Zusammenarbeit, ebenso wie Viktria Heine.

Für die schriftliche Ausarbeitung der Veröffentlichungen und das Korrekturlesen der Dissertation geht des Weiteren ein besonderer Dank an: Nicole Snyder, Lukas Fischer, Miriam Hoffmann, Stephen Hill, Patrick Konietzny und Katharina Schettle.

Zu guter Letzt geht mein größter Dank an meine Familie, insbesondere meine Eltern und mein Schwesterherz, auf deren Unterstützung und Rückhalt ich stets bauen konnte. Ohne euch hätte ich nie zu der Person werden können, die ich heute bin und auch nie das erreichen können, was ich erreicht habe. Ein nicht minderer Dank geht an meine Oma, welche mich ebenfalls stets unterstützt und so viel Stolz und Vertrauen in mich gesteckt hat. Ebenfalls danke ich meinen Schwager, meinen Paten, Onkeln, Tanten und meinen Cousinen. Ebenfalls danke ich meinen Freunden und den Menschen, die mich in den letzten Jahren begleitet, motiviert, unterstützt und mir beigestanden haben.